Novel Ferrocene-based Phosphine Ligands for Earth-Abundant Metal-Catalysed Asymmetric Hydrogenation

by

Liyao Zeng

UNIVERSITY OF BIRMINGHAM

A thesis submitted to the
University of Birmingham
For the degree of
DOCTOR OF PHILOSOPHY

School of Chemistry
College of Engineering and Physical Sciences
University of Birmingham
December 2021

Abstract

Transition metal-catalysed homogeneous asymmetric hydrogenation has been developed as one of the most efficient and atom-economical methods for the synthesis of chiral molecules. In this field, thousands of chiral phosphine ligands have been reported, with ferrocene as one of privileged ligand scaffolds because of its unique electronic and steric properties. In recent years, earth-abundant metal-catalysed asymmetric hydrogenation has attracted much attention in order to handle the high supply risk of precious metals, however, with slow progress due to the lack of effective chiral ligands. This thesis mainly aims to contribute to the development in asymmetric hydrogenation catalysed by earth-abundant first-row metals (e.g. manganese, iron, cobalt, nickel, copper etc), by designing and synthesizing novel ferrocene-based chiral multidentate phosphine ligands. As a result, a series of highly reactive and enantioselective multidentate phosphine ligands have been developed, including novel ferrocene-based tridentate PNP ligands for manganese catalysis, novel ferrocene-based secondary phosphine oxide ligands Fc-SPO for cobalt catalysis and others. The PNP ligands have been proven highly efficient for manganese-catalysed asymmetric hydrogenation of simple ketones, giving excellent enantioselectivities (92%~99% ee for aryl alkyl ketones) as well as high efficiencies (TON up to 2000). The Fc-SPO ligands have been successfully applied for cobalt-catalysed asymmetric hydrogenation of diaryl ketones, providing high yields (up to 99%) and good enantioselectivities (up to 92% ee). In addition to multidentate phosphine ligands, this thesis briefly introduces another ligand design strategy towards transition metal-catalysed asymmetric hydrogenation, involving noncovalent interaction-assisted ferrocenyl phosphine ligands.

The second aim of the Mn-PNP complex mentioned above is used as a novel redox-switchable catalyst for the asymmetric hydrogenation of acetophenone. Switching between two iron oxidation states of the ferrocene unit was found to have a significant effect on the catalytic reactivity, with the process chemically reversible. Furthermore, an attempt on the development of novel DNA-organometallic

hybrid phosphine ligands for DNA-based asymmetric catalysis has been performed by incorporating a small ferrocenyl phosphine molecule into the DNA backbone. Despite phosphine oxidation issue, the resulting ferrocenyl phosphine oxide-modified strands could still successfully form DNA duplexes, which widens the range of bio-organometallic nucleic acid systems that can be made.

Thesis outline

Chapter 1 reviews the development of chiral phosphine ligands in transition metal-catalysed asymmetric hydrogenation, including ferrocene-based chiral phosphine ligands. And earth-abundant metal catalysis is introduced in detail.

Chapter 2 presents the synthesis of a family of ferrocene-based chiral tridentate PNP ligands and their successfully applications for manganese-catalysed asymmetric hydrogenation of simple ketones with high enantioselectivities (92%~99% ee for aryl alkyl ketones) as well as high efficiencies (TON up to 2000). Manganese intermediates involved in the catalytic cycle were analysed, with DFT calculation carried out to help understand the chiral induction model. This chapter (page 50 – 192) is adapted with permission from {*ACS Catalysis* **2020**, 10, 23, 13794 – 13799}. Copyright {2020} American Chemical Society. Liyao Zeng is the first author and performed all the synthesis and catalysis studies. Huaxin Yang and Menglong Zhao are acknowledged for their preparations of compound **2**, **3a**, **4a** and PNP ligand **5a** in large scales (up to 20 g) using my synthesis procedures (Scheme 2.1). Dr Jialin Wen is acknowledged for performing the computational modelling studies.

Chapter 3 describes the preparation of novel ferrocene-based secondary phosphine oxide Fc-SPO ligands and their successfully applications for cobalt-catalysed asymmetric hydrogenation of diaryl ketones with high yields (up to 99%) and good enantioselectivities (up to 92% ee).

Chapter 4 introduces two ligand design strategies towards transition metal-catalysed asymmetric hydrogenation, including noncovalent interaction-assisted ferrocenyl phosphine ligands and multidentate phosphine ligands. Ligand examples designed based on each approach are summarized.

Chapter 5 addresses the ferrocene-based manganese complexes Mn-PNP as redox-switchable catalysts for the asymmetric hydrogenation of acetophenone. Switching between two iron oxidation states of the ferrocene unit was found to have a significant effect on the catalytic reactivity, with the process chemically reversible.

Chapter 6 involves efforts to develop a new type of DNA-organometallic hybrid scaffold for asymmetric catalysis, via the incorporation of a small ferrocenyl phosphine monomer into the DNA phosphate backbone. Despite phosphine oxidation issue, the resulting ferrocenyl phosphine oxide-modified strands could still successfully form DNA duplexes, which widens the range of bio-organometallic nucleic acid systems that can be made.

Abbreviations

Ac	Acetyl	AH	Asymmetric hydrogenation
aq.	Aqueous	ar	Aryl
ATH	Asymmetric transfer hydrogenation		
BDan	1,8-Diaminonaphthalatoboryl	Bn	Benzyl
BPin	Pinacolatoboryl	Bu	Butyl
c	Concentration	Calcd	Calculated
cat.	Catalyst	CBS	Corey-Bakshi-Shibata
CD	Circular dichroism	conc.	Concentrated
Conv.	Conversion	Cp	Cyclopentadienyl
CV	Cyclic voltammogram		
d	Doublet	DCE	Dichloroethane
DCM	Dichloromethane	DFT	Density functional theory
DIBAL	Diisobutylaluminium hydride	DIPEA	Diisopropylamine
DMAP	4,4-Dimethylaminopyridine	DMF	Dimethylformamide
DMSO	Dimethylsulfoxide	DMT	Dimethoxytrityl
DNA	Deoxyribonucleic acid		
e.e.	Enantiomeric excess	EI	Electrospray ionisation
eq.	Equivalent	ESI	Electrospray ionisation
Et	Ethyl	EtOAc	Ethyl acetate
Fc	Ferrocene		
GC	Gas chromatography		
HFIP	Hexafluoroisopropanol	HPLC	High performance liquid chromatography
HRMS	High-resolution mass spectrometry		

IR	Infrared		
m	Multiplet	Me	Methyl
m.p.	Melting point	MS	Mass spectrometry
MTBE	Methyl tert-butyl ether		
n-BuLi	*n*-Butyllithium	NMR	Nuclear magnetic resonance
ODN	Oligonucleotide	OTf	Trifluoromethanesulfonate
Ox.	Oxidant		
PE	Petroleum	Ph	Phenyl
ppm	Parts per million	PNP	Phosphorus-nitrogen-phosphorus
Pr	Propyl		
q	Quartet		
Red.	Reductant	RSC	Redox switchable catalysis
rac.	Racemic	rt	Room temperature
s	Singlet	sat.	Saturated
SPO	Secondary phosphine oxide		
t	Triplet	TBDPS	*tert*-butyldiphenylsilyl
t-BuLi	*tert*-Butyllithium	TEA	Triethylamine
TFA	Trifluoroacetic acid	TFE	Trifluoroethanol
THF	Tetrahydrofuran	TMEDA	Tetramethylethylenediamine
TMS	Trimethylsilyl	Tol	Toluene
TON	Turnover number		
UV	Ultraviolet		
XRD	X-ray diffraction		

Acknowledgements

Firstly, huge thanks to Prof Xumu Zhang and Prof Jim Tucker for giving me the opportunity to undertake the joint PhD programme between SUSTech and Birmingham! Xumu, thanks for your showing me how to be a true scientist. Your model will always remind me to do beautiful and useful chemistry. Jim, thanks for your teaching me how to be a true professor. I have learnt a lot in experiments, critical thinking and English writing under your patient guidance. And your sincere encouragement keeps me optimistic and confident. Special thanks also to Dr Jialin Wen for detailed guidance and help in experiments, DFT study and paper writing, without whom my first paper would not be published successfully.

Thank you to the past and present members of the Zhang group. Thanks to Dr Genqian Chen, Dr Qin Yin, Dr Yingjun Li, Dr Shaotao Bai, and Mrs Hongqi Tao for your support and help. Thanks to Dr Yanan Duan, Dr Lean Hu, Dr Shaoke Zhang, Dr Xiaoyong Du, Dr Jianfei Yu, Dr Longsheng Zheng, Dr Zengjin Dai and Dr Wei Fang for your useful advice in the lab. Thanks to Dr Fanping Huang for your help in XRD studies. Thanks to Huaxin Yang and Heng Wang for your help in synthesis. Thanks to Fuhao Zhang for your advice in organic synthesis, I will miss our discussions during our PhD life and wish you also get the PhD degree soon. Special thanks to the undergraduate Menglong Zhao for your help in the last three years, it has been a pleasant journey to explore science with you and wish you receive the best PhD offer soon.

Thank you to the past and present members of the Tucker group. Thanks to Dr Media Ismail, Dr Huy Nguyen, Dr Francia Allabush, Dr Klaudia Englert, Dr Edward Wilkinson, Dr Georgina Leck, Dr Charlotte Farrow, Marium, Yifeng, Jake and Aldrich for your kindly help. Thanks to Jack for your help in electrochemistry. And thanks to Dr Georgia Orton from the Neil Champness group for your

help in spectroelectrochemistry. It has been a pleasure to work with all of you, and wish you all the best in the future.

Thanks to all the members of the SUSTech Baseball Team. Fighting together with you in baseball games has been a memorable experience.

Sincere thanks to my family for your love and support all the time. Thanks to my mom, brother Songyao and sister Xianyuan, I love you so much. Special thanks to my aunt Youtao and uncle Xugang for your looking after me since I was 14 years old. Uncle Xugang is like my father as well as my best friend, and we have kept a long chatting once a week for 10 years since I left Akesu city. Thanks to younger brother Haohao and little sister Jingjing for your company when I was a teenager, please forgive my absence in your growing during the last 10 years, I love you. From Xinjiang to Beijing, to Tomsk, to Seoul, to Shenzhen and to Birmingham, I have grown up to be a real man. I feel so lucky to receive countless love and support from my family, and I wish you all healthy and happy everyday.

Finally, I would like to say thanks to my wife Leilei. We met exactly at the starting point of my PhD training in 2017. At that time, you went to Newcastle for your master project while I did the first-year study in Birmingham. Every Friday I would be very excited to catch a coach of National Express to see you, and you would prepare a delicious dinner to wait for me. Then in 2018 we went back to SUSTech, Shenzhen, and you have been living with me ever since. Thank God you said yes to marry me at the outside theatre of SUSTech on the first day of 2020, and then we applied for a marriage certificate on Dec 17th of the same year. Thank you my dear, I would not have accomplished the PhD project without your sweet company and strong support, and half of this thesis should be attributed to you. Promise you we will have a lovely wedding after I obtain the PhD degree. I love you!

Table of Contents

Chapter 1 Introduction

1.1 Asymmetric hydrogenation

1.1.1 Overview

Asymmetric hydrogenation (AH) is a fundamental chemical reaction, converting prochiral compounds comprised of unsaturated double bonds (C=C, C=O, C=N etc.) to chiral products.[1] In principle, AH catalysis can be homogeneous[2-3] or heterogeneous[4]; in this thesis the focus is on homogeneous AH. Enabling high stereocontrol for a broad range of target chiral compounds and employing hydrogen gas as a green reductant, transition metal-catalysed AH has been developed as one of the most efficient and atom-economical methods for the synthesis of chiral molecules.[5] Meanwhile, AH has been applied widely in industry for preparing optically pure fine chemicals such as pharmaceuticals, agrochemicals, flavours, and fragrances.[6] In 2001, Knowles and Noyori won the Nobel Prize in chemistry for their transcendent contributions in the field of AH.[7-8]

The initial cases of the homogeneous AH were reported by Knowles[9] and Horner[10] et al. respectively in 1968, using optically-active monodentate tertiary phosphines to replace triphenylphosphine of the Wilkinson's catalyst $[RhCl(PPh_3)_3]$[11] in rhodium-catalysed AH of alkenes, providing up to 15% ee for the products (Scheme 1.1). Although low enantioselectivities were obtained, the pioneering work inspired other groups to develop more efficient chiral phosphine ligands for the AH.

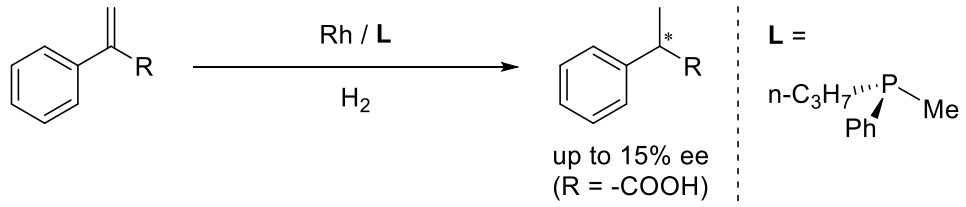

Scheme 1.1 The first homogeneous AH reported by Knowles and Horner et al

In 1971, Kagan et al made a breakthrough in the field of AH via the synthesis of a C_2-symmetric diphosphine ligand **DIOP**, providing high enantioselectivities for rhodium-catalysed AH of dehydro

amino acids and enamides (Scheme 1.2).[12-13] In 1975, the Knowles group at Monsanto established another important C_2-symmetric diphosphine ligand **DIPAMP**, affording excellent enantioselectivity (up to 96% ee) for rhodium-catalysed AH of α-acetamidoacrylic acids.[14-16] This ligand was then applied successfully for the industrial synthesis of L-DOPA, a chiral drug used against Parkinson's disease.[17]

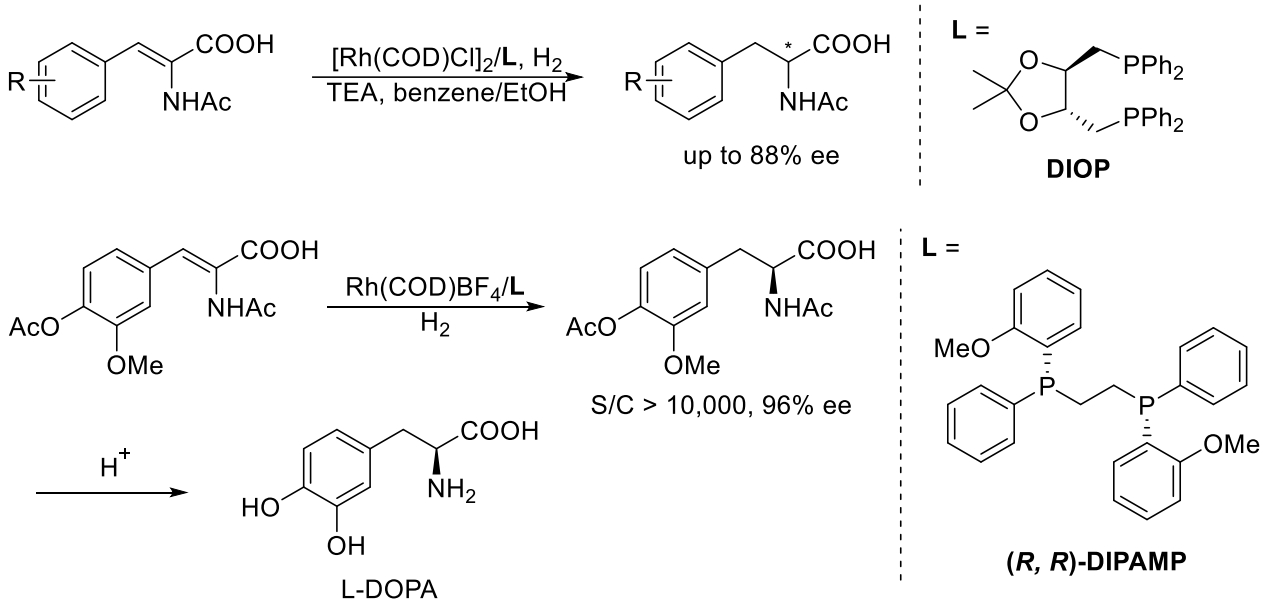

Scheme 1.2 **DIOP** and **DIPAMP** ligands for Rh-catalyzed AH

In addition to **DIOP** and **DIPAMP** ligands, some other chiral phosphine ligands (**CAMP**,[18] **CHIRALPHOS**,[19-20] **PROPHOS**,[21] **BPPM**,[22] **CBD**[23] etc) were also developed for AH in the 1970s (Figure 1.1). However, these reports mainly focused only on rhodium-catalysed reactions with limited substrates composed of unsaturated amino acids and their derivatives.

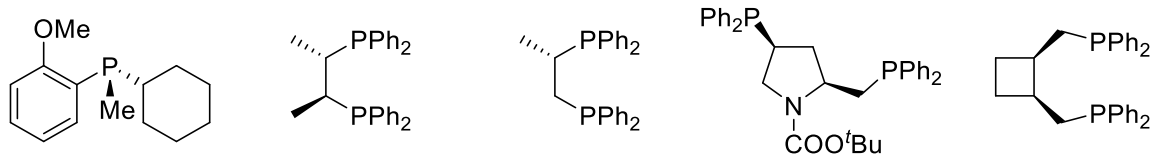

(*S*)-CAMP **(*S,S*)-CHIRAPHOS** **(*S*)-PROPHOS** **(*S,S*)-BPPM** **(*R,R*)-CBD**

Figure 1.1 Representative chiral phosphine ligands developed in the 1970s

In the 1980s, another landmark ligand **BINAP**[24] and its corresponding ruthenium complexes were developed by Noyori et al, which were applied successfully for the ruthenium-catalysed AH of a variety of substrates, giving excellent reactivities and enantioselectivities (Figure 1.2).[25-26]

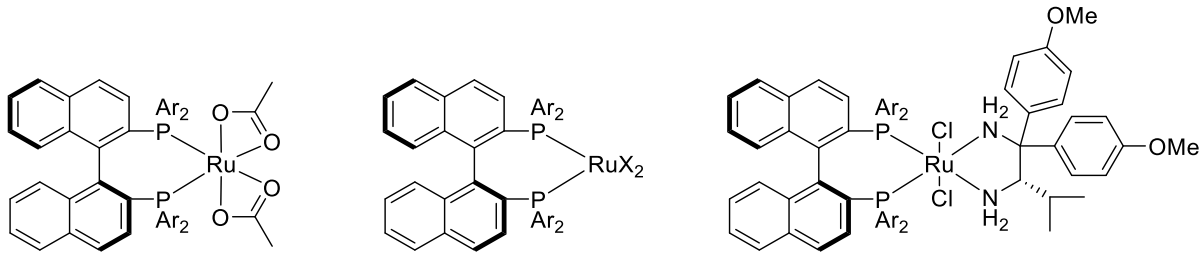

Ru(OAc)$_2$[(*S*)-BINAP] **RuX$_2$[(*S*)-BINAP]** **(trans)-RuCl$_2$[(*S*)-BINAP][(*S*)-daipen]**

Figure 1.2 Ru-**BINAP** complexes reported by Noyori et al.

Ru(OAc)$_2$/**BINAP** complexes showed supreme performances in the AH of various functionalized olefins, including N-acyl-1-alkylidenetetrahydroisoquinolines, allylic and homoallylic alcohols and unsaturated carboxylic acids (Scheme 1.3),[27-29] while the halogen-containing RuX$_2$/**BINAP** complexes were highly efficient catalysts for the AH of functionalized ketones (Scheme 1.4).[30-31] In 1995, they made another breakthrough in this area via the discovery of a unique Ru-**BINAP**-diamine catalyst system. This was found to be highly efficient for the AH of simple ketones including aromatic, heteroaromatic, and olefinic ketones (Scheme 1.5).[32] Surprisingly, the Ru/**BINAP**/Daipen complex could catalyse the AH of acetophenone with millions of turnover numbers, displaying tremendous prospects and potential for industrial use.

a. AH of N-acyl-1 -alkylidenetetrahydroisoquinolines

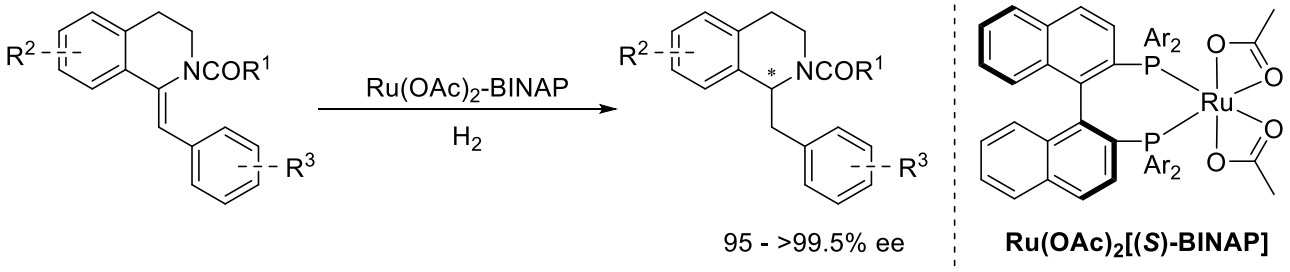

b. AH of allylic and homoallylic alcohols

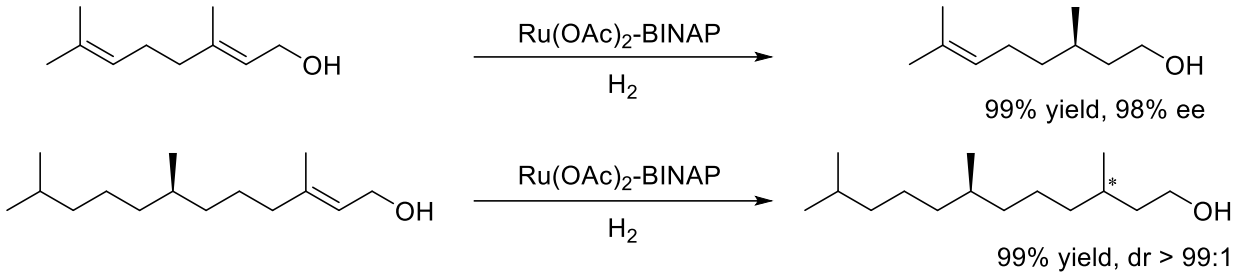

c. AH of unsaturated carboxylic acids

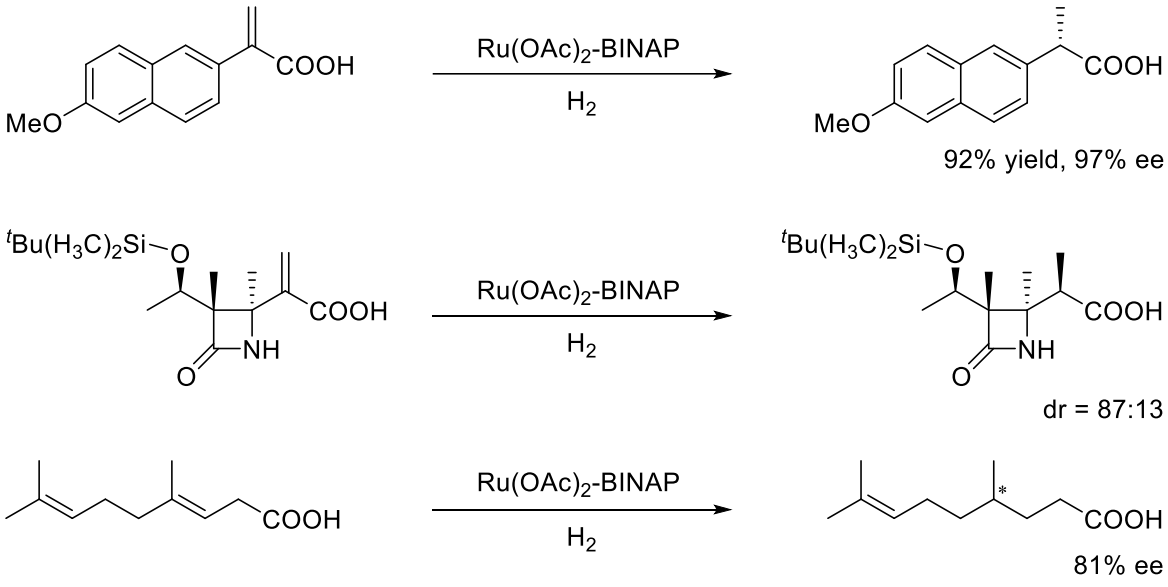

Scheme 1.3 $Ru(OAc)_2$/**BINAP** complexes catalyzed the AH of functionalized olefin

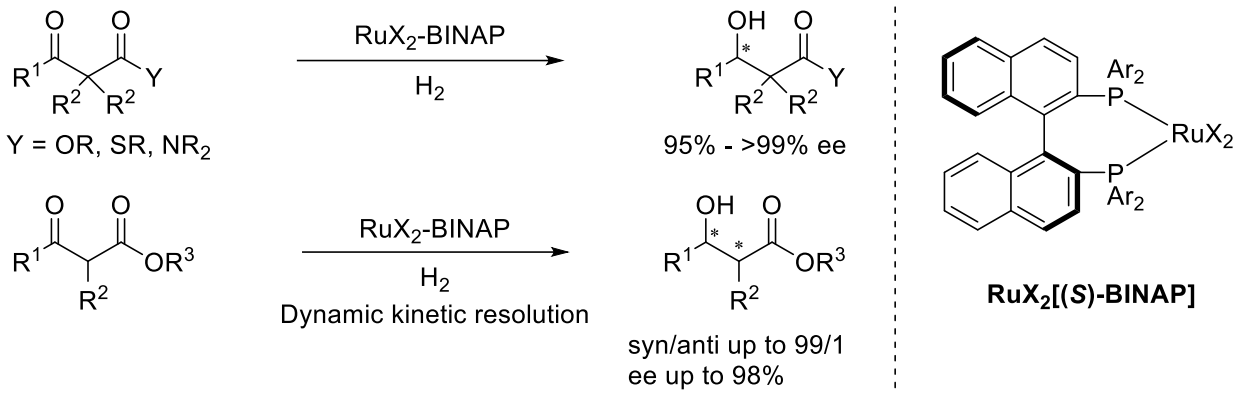

Scheme 1.4 RuX_2/**BINAP** complexes catalyzed the AH of functionalized ketones

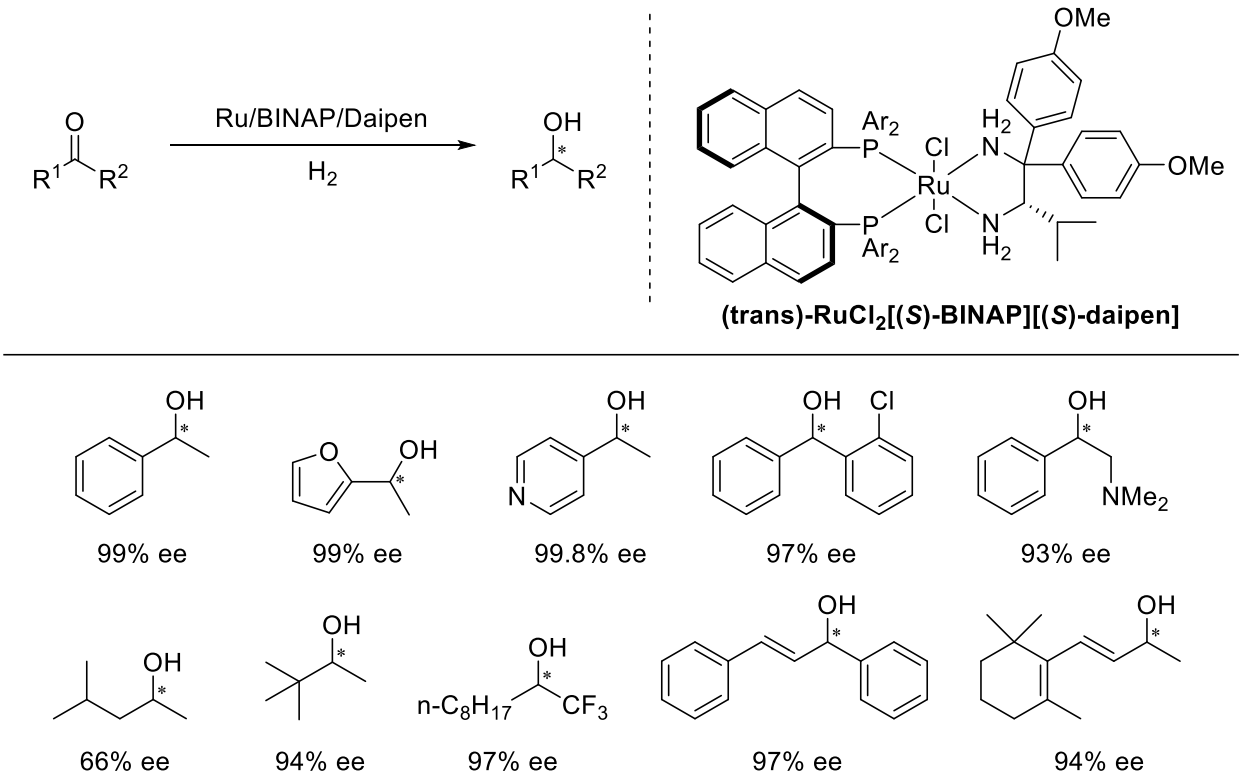

Scheme 1.5 Ru/**BINAP**/diamine complexes catalyzed the AH of simple ketones

The tremendous success of **BINAP** ligands in AH encouraged other groups to develop other efficient axially chiral diphosphine ligands, including **BICHEP**,[33] **Segphos**,[34] **Cn-TunaPhos**,[35] **NaPhePHOS**,[36] **P-Phos**[37] etc (Figure 1.3).

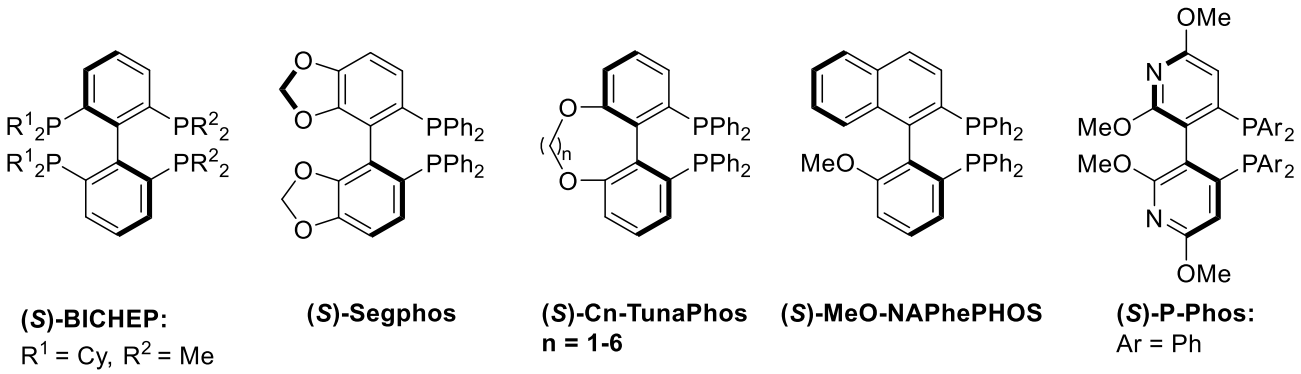

Figure 1.3 Selected axially chiral diphosphine ligands

Over the past decades, transition metal-catalysed AH has been studied in depth. In addition to those ligands mentioned above, large numbers of other types of chiral phosphine ligands have been developed within academia and industry.[38] Some representative ligands are summarized in Figure 1.4.

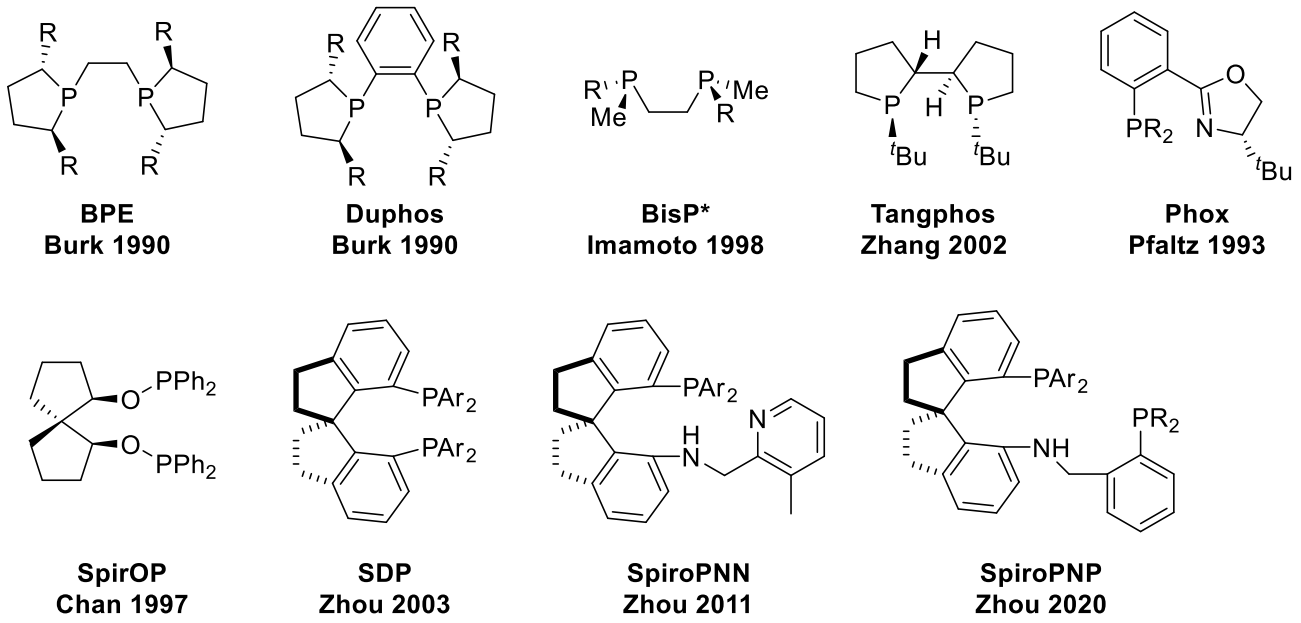

Figure 1.4 Representative chiral phosphine ligands for AH

In the early 1990s, Burk et al reported a new series of electron-rich chiral diphospholane ligands **BPE** and **Duphos**, exhibiting extremely high efficiencies for the AH of various substrates containing *α*-

(acylamino)acrylic acids, enamides, enol acetates, β-keto esters, α,β-unsaturated carboxylic acids and itaconic acids (Scheme 1.6).[39-40] These results significantly expanded the substrate scope of Rh-catalyzed AH.

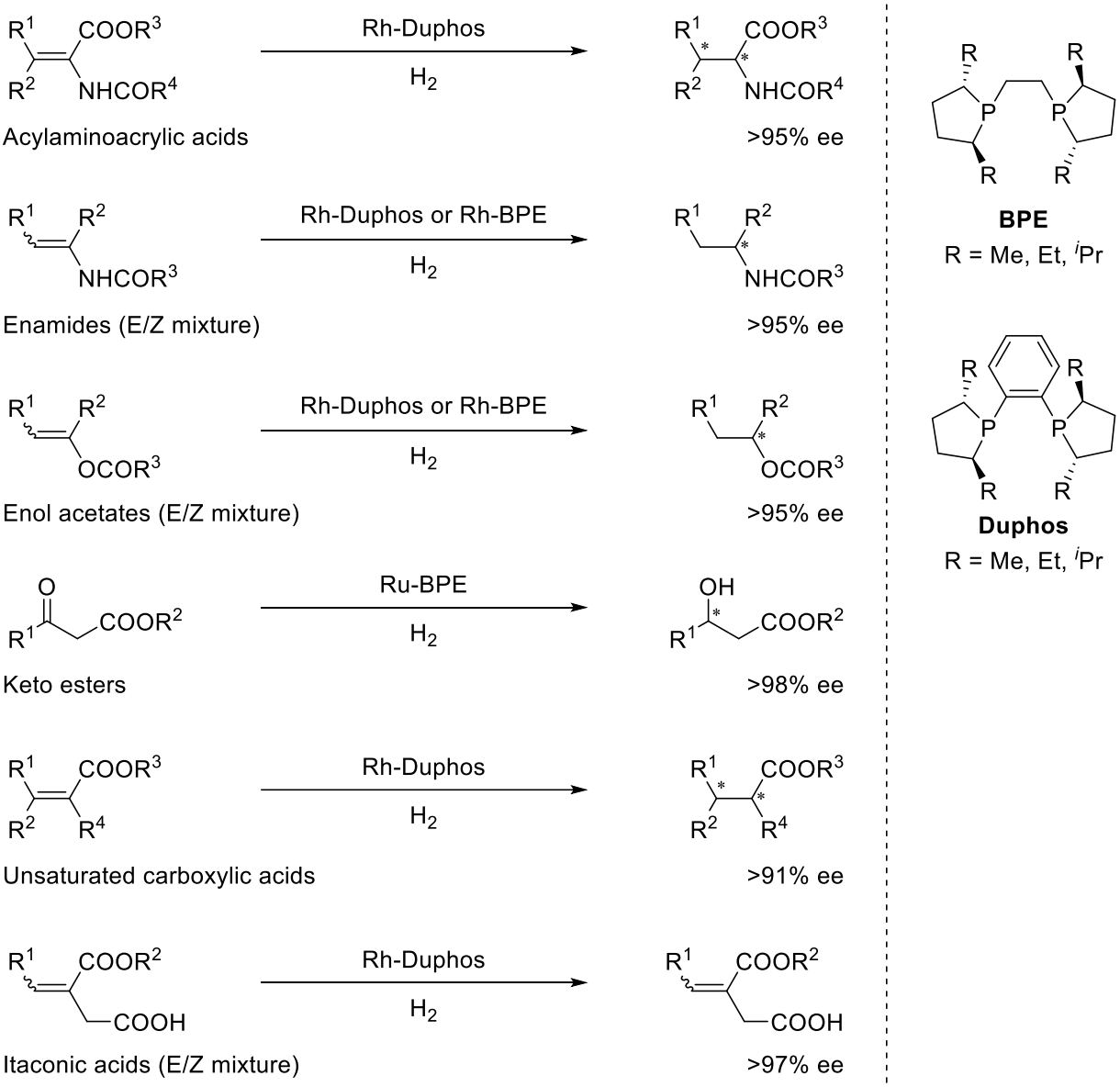

Scheme 1.6 Applications of **BPE** and **Duphos** ligands for AH

The **DIPAMP** ligand developed by Knowles in the 1970s was the first P-chiral diphosphine ligand efficient for AH, suggesting unique enantio-induction of the P-chiral diphosphine ligands. However, the development of this type of ligand went slowly due to the difficulties in ligand synthesis, its

unstable configuration and gradual racemization at high temperatures. Until 1998, Imamoto and co-workers introduced a new group of P-chiral diphosphine ligands **BisP***, showing significant reactivities and enantioselectivities in the AH of *α*-(acylamino)acrylic acids, enamides, (*E*)-*β*-(acylamino)-acrylates and *α*,*β*-unsaturated-*α*-acyloxyphosphonates (Scheme 1.7).[41-45]

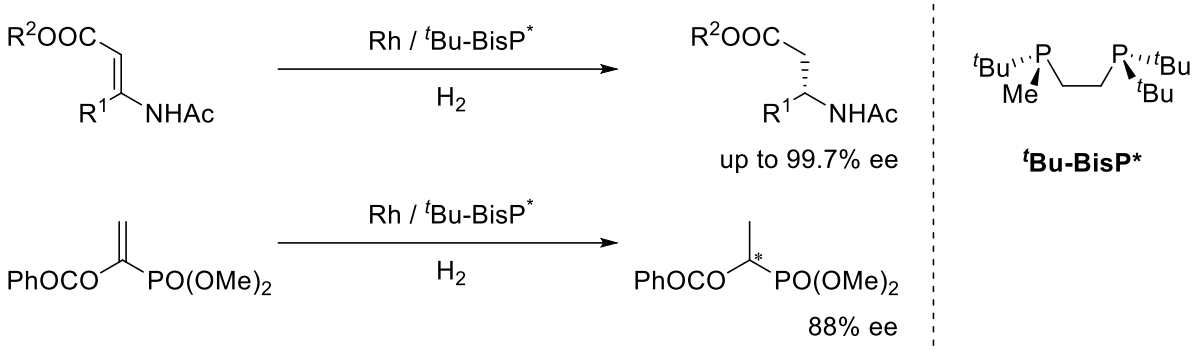

Scheme 1.7 Applications of **BisP*** ligand for AH

Based on the discovery of the **BisP*** ligands, Zhang et al. developed another famous P-chiral diphosphine ligand, **Tangphos** (Scheme 1.8).[46] This ligand has a rigid structure scaffold, embodying two chiral carbon centers and two chiral phosphorus centers. Metal-**Tangphos** complex made a great distinction between different steric groups because of the high steric hindrance of the *tert*-butyl group, becoming a very efficient catalyst for the Rh-catalyzed AH of a series of functionalized alkenes.[47-48]

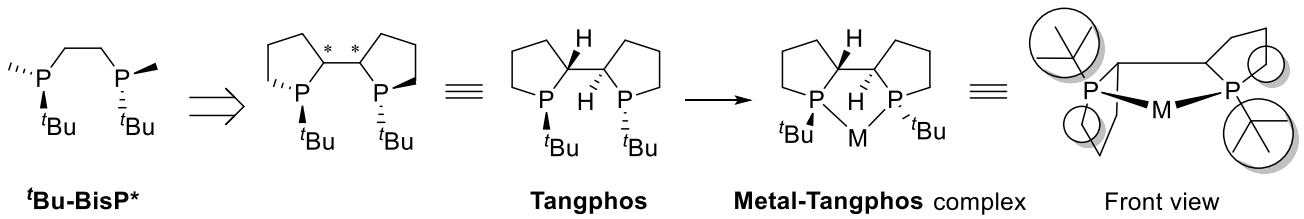

Scheme 1.8 Ligand design of **Tangphos**

Subsequently, the Zhang group reported a family of **Tangphos**-type ligands such as **Duanphos**,[49] **Zhangphos**[50] and **Binapine**[51] (Figure 1.5). Some of them are now commercially available. Tang et al. described the synthesis of chiral bisdihydrobenzooxaphosphole ligands **BIPOP**.[52]

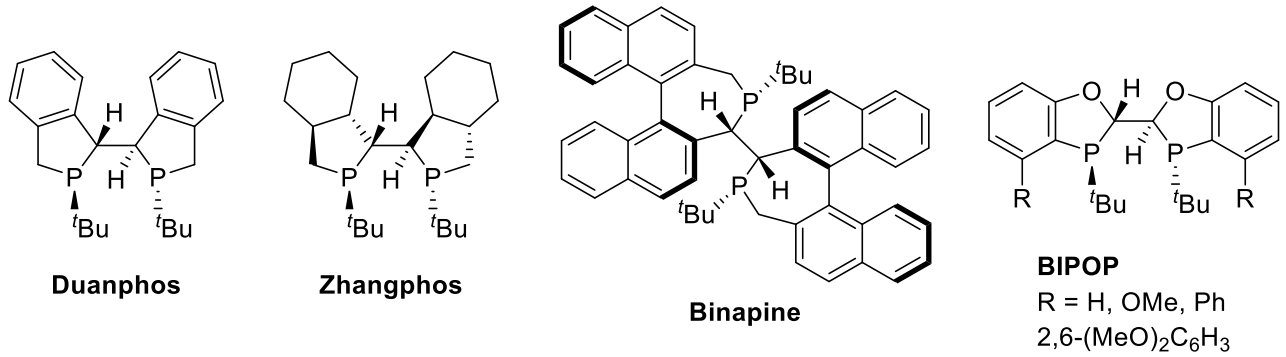

Figure 1.5 Selected **Tangphos**-type ligands

The efficient AH of functionalized alkenes by chiral rhodium or ruthenium complexes can be largely explained by metal coordination from the directing groups of substrates. Unfunctionalized alkenes that lack these directing groups are not efficiently hydrogenated by such catalyst systems, which was a significant challenge before the 1990s. Pfaltz et al introduced chiral PN compound **Phox**[53-54] ligands and their corresponding iridium complexes, affording excellent reactivities and enantioselectivities in the AH of unfunctionalized alkenes such as (*E*)-1,2-diphenyl-1-propene (Scheme 1.9).[55-57]

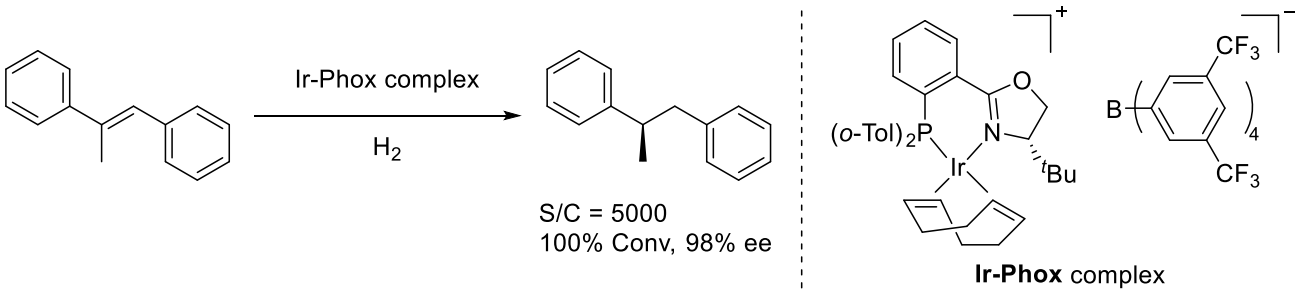

Scheme 1.9 Ir-**Phox** complex for the AH of (*E*)-1,2-diphenyl-1-propene

Since the first chiral spirocyclic diphosphinite ligand **SpirOP**[58] was reported by Chan et al in 1997, the chiral spiro backbone has shown to be one of the most powerful ligand scaffolds for AH, on account of its total rigidity. In 2003, Zhou et al synthesized a landmark chiral spiro diphosphine ligand **SDP** based on 1,1'-spirobiindane scaffold, and the corresponding Ru-**SDP**-diamine complexes were reported to afford high reactivities (up to 100,000 TON) and excellent enantioselectivities (up to 99.5% ee) for the AH of simple ketones (Scheme 1.10).[59] Later, they found that Ru-**SDP**-diamine complexes were also very efficient catalysts for the AH of racemic α-substituted carbonyl compounds via dynamic kinetic resolution.[60-61] In 2011, a set of new chiral spiro tridentate ligand **SpiroPNN** was developed by Zhou et al, providing extremely high efficiencies in the Ir-catalyzed AH of ketones. The Ir-**SpiroPNN** complexes catalyzed the AH of aryl alkyl ketones with up to 99.9% ee and up to 4,550,000 TON.[62] To the best of our knowledge, this amazing result is the best catalytic efficiency for a homogenous asymmetric reaction so far. Furthermore, this iridium system also possesses highly catalytic abilities for the AH of β-ketoesters, offering up to 1,230,000 TON.[63] In 2020, the same group made another significant breakthrough in the AH of dialkyl ketones. This type of ketone bears two sterically and electronically similar alkyl groups, causing a huge and long-standing challenge in distinguishing prochiral centres or faces for controlling the stereoselectivity. Inspired by previous biocatalytic reduction of ketones, Zhou et al designed and synthesized the chiral spiro tridentate ligand **SpiroPNP**. The Ir-**SpiroPNP** catalysts were endowed with crowded and narrow chiral pockets, giving excellent enantioselectivities in the AH of various dialkyl ketones.[64]

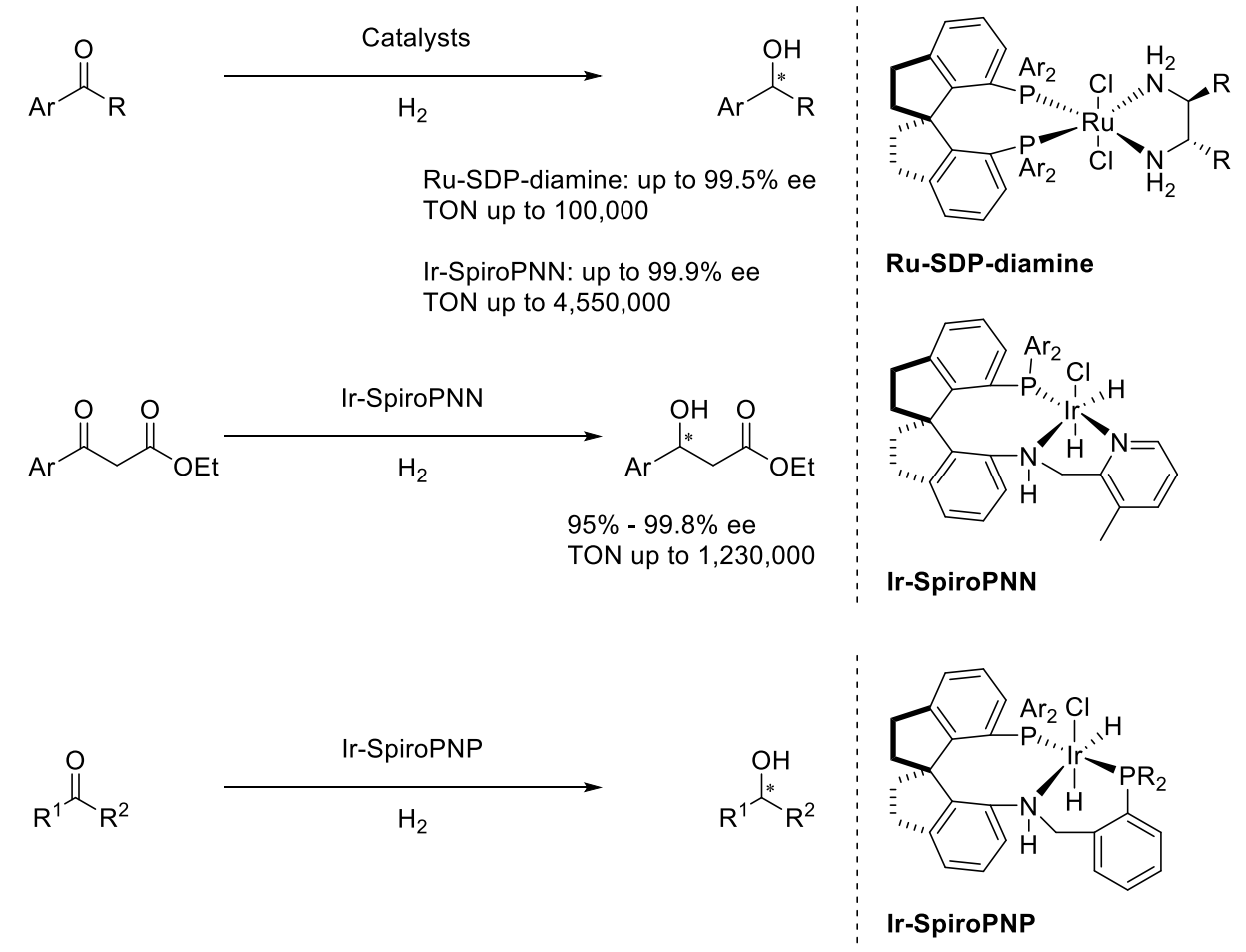

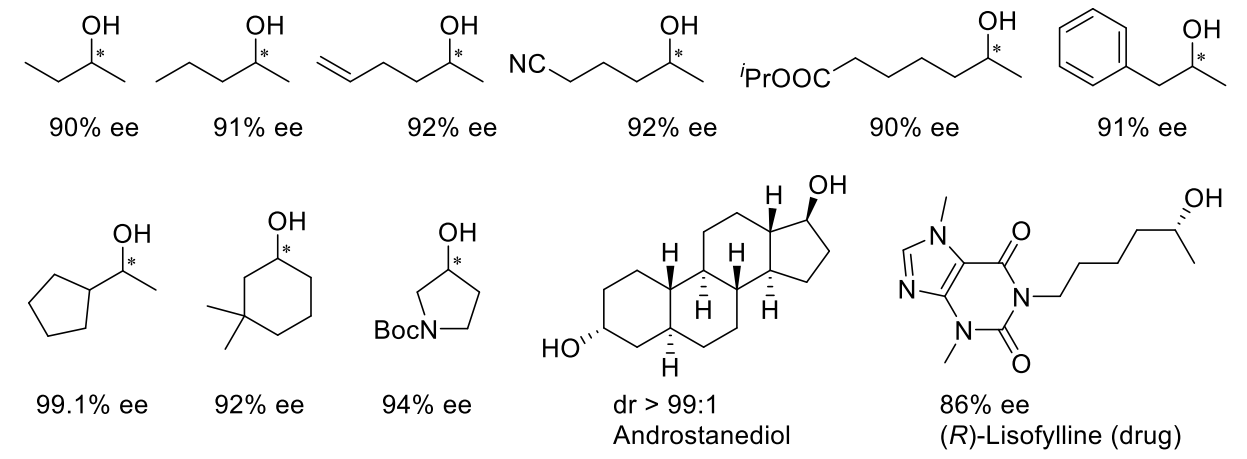

Scheme 1.10 Applications of chiral spiro phosphine ligands for AH

1.1.2 Chiral ferrocenyl phosphine ligands

Since its discovery in the 1950s with its distinctive sandwich geometry,[65] ferrocene and its derivatives have become important starting materials in organometallic chemistry.[66-67] Ferrocene is regarded as

a privileged ligand scaffold for asymmetric catalysis because of its outstanding properties, including high thermal stability and air stability, adequate rigidity and steric bulkiness, planar chirality, and electronic contributions.[68] Basically, all kinds of substituted ferrocene can be readily synthesized by introducing various groups onto the electron-rich cyclopentadienyl rings of ferrocene. As a result, a great variety of ferrocene-based chiral phosphine ligands have now been developed for transition metal-catalysed AH.[69-70]

1.1.2.1 Conventional ferrocenyl phosphine ligands

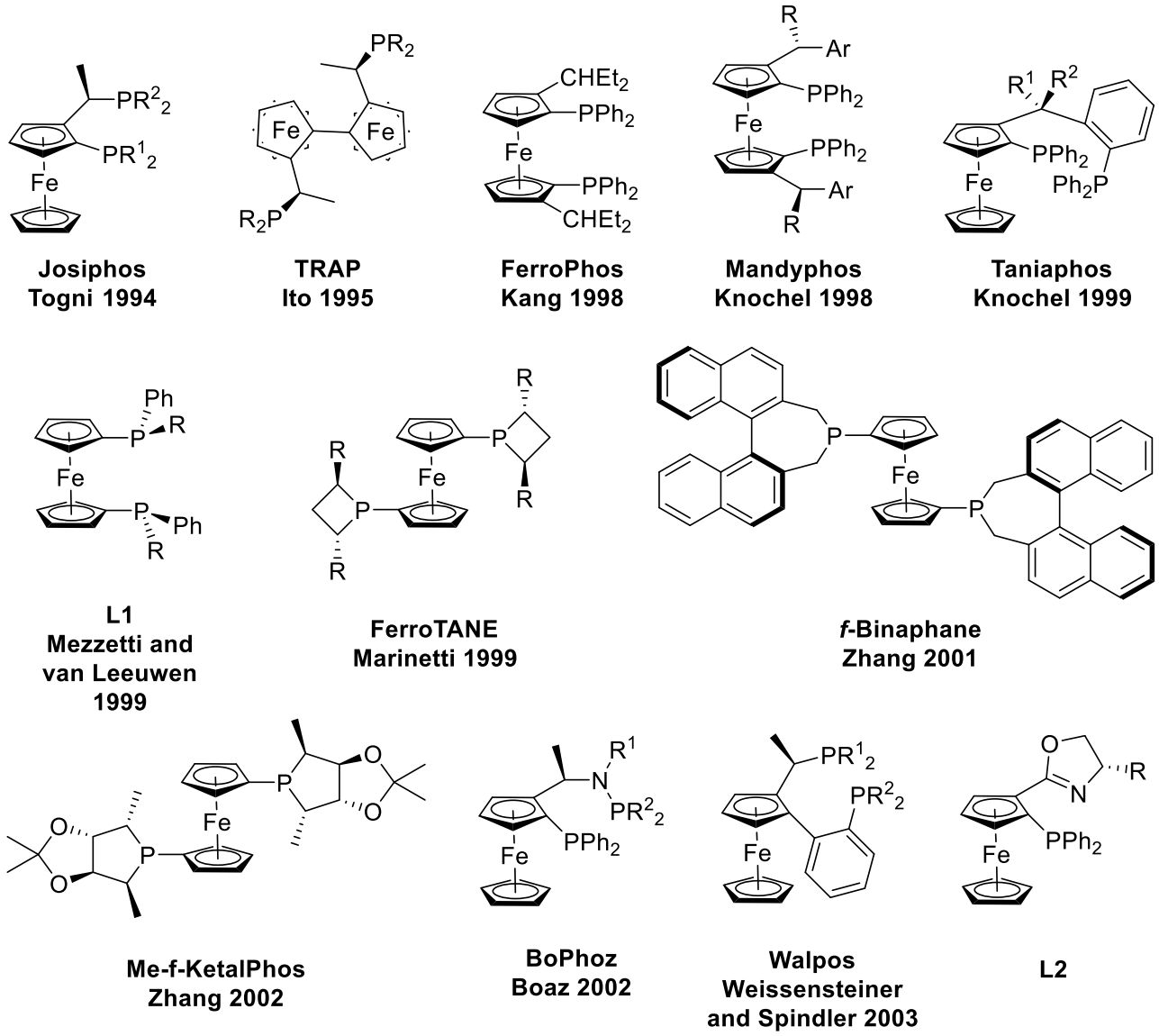

Figure 1.6 Selected conventional ferrocenyl phosphine ligands

In 1994, Togni and Spindler et al. reported a class of famous chiral ferrocenyl phosphine ligands **Josiphos**.[71] These ligands were highly effective for the Rh-catalysed AH of acetamidocinnamate, dimethyl itaconate and *β*-ketoesters (Scheme 1.11). More importantly, **Josiphos**-type ligands have been proven to be highly practical in industrial applications, for example, the commercial synthesis of (+)-biotin and the economical manufacture of the herbicide (*S*)-metolachlor.[72-73] Because of a broad diversity of the substituents at the two phosphorous atoms and their high air-stability, over 150 different Josiphos ligands have now been prepared, with many of them commercially available.

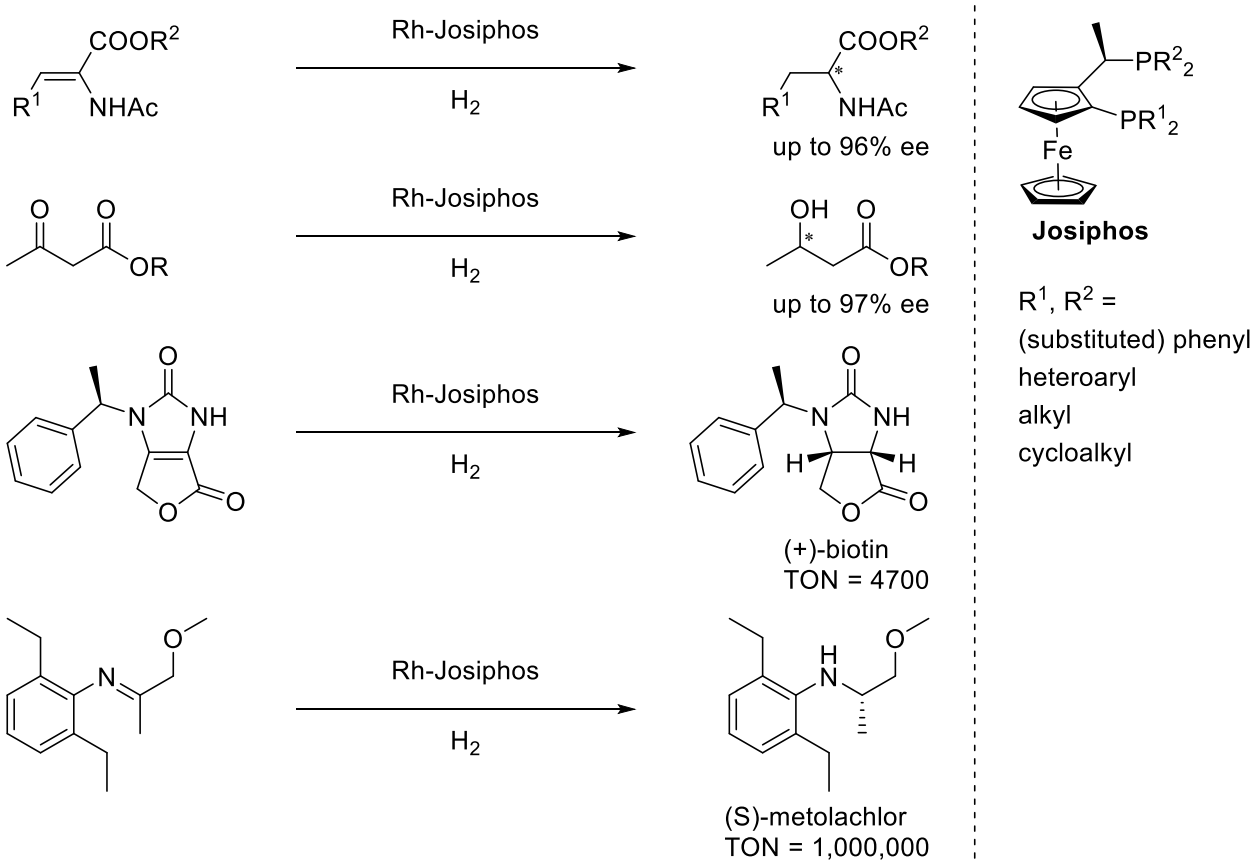

Scheme 1.11 **Josiphos** ligands for Rh-catalyzed AH

In 1995, Ito et al. introduced the synthesis of a series of *trans*-chelating chiral ferrocenyl diphosphine ligands **TRAP**.[74] These ligands were found to have great capabilities for the Rh-catalysed AH of some tetrasubstituted olefins and *N*-acetyl-2-substituted indoline (Scheme 1.12).[75-77]

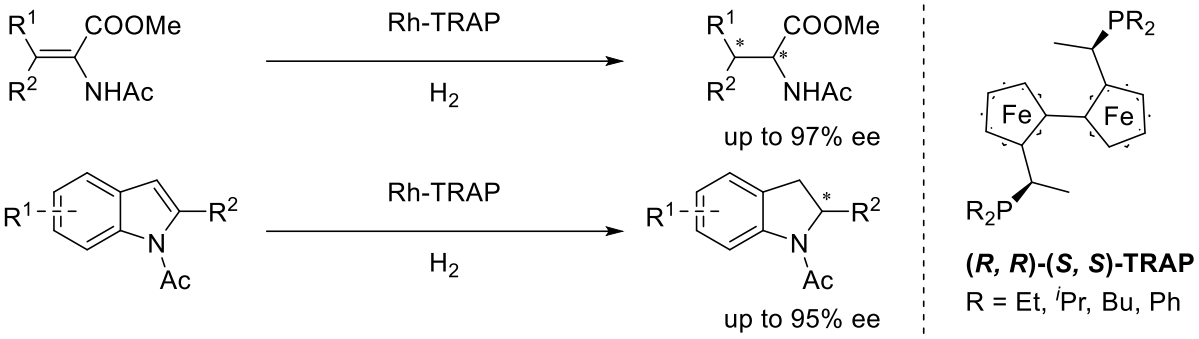

Scheme 1.12 **TRAP** ligands for Rh-catalyzed AH

In 1998, Kang et al. developed a type of C_2-symmetrical ferrocenyl diphosphine ligand, **FerroPhos**,[78] which gave high enantioselectivities in the Rh-catalyzed AH of dehydroamino acid derivatives (Figure 1.6). Meanwhile, Knochel et al. independently reported another set of C_2-symmetrical ferrocenyl diphosphine ligand **Mandyphos**[79-80] via a new synthesis approach based on diastereoselective ortho-lithiation on 1-1'-disubstituted ferrocene. These were found to be good ligands for the Rh-catalysed AH of dehydroamino acids and dehydroaminoesters. The same group also introduced non-C_2-symmetrical ferrocenyl diphosphine ligand **TaniaPhos**,[81] affording good enantioselectivities in the Rh- or Ru-catalyzed AH of a wide range of substrates.

Mezzetti[82] and van Leeuwen[83] et al. independently developed a class of ferrocene ligand **L1** with P-centered chirality (Figure 1.6). Marinetti[84] and Burk[85] et al. independently reported the synthesis of chiral 1,1'-bis(phosphetano)ferrocene **FerroTANE**. The Et-**FerroTANE** ligand was employed successfully in the Rh-catalyzed AH of itaconates and (*E*)-*β*-acylaminoacrylates. In 2001, Zhang et al. developed a 1,1'-bis(dinaphthophosphepinyl)ferrocene ligand ***f*-Binaphane**,[86] which was used it for the Ir-catalyzed AH of acyclic arylimines with high enantioselectivities. Then the same group reported a 1,1'-bis(phospholanyl)ferrocene ligand **Me-*f*-KetalPhos**[87] for the Rh-catalyzed AH of *α*-dehydroamino acid derivatives with excellent enantioselectivities.

In 2002, Boaz et al. prepared a new type of chiral ferrocenyl diphosphine ligand **BoPhoz**,[88] with a phosphine-aminophosphine framework (Figure 1.6). The BoPhoz ligands provided high reactivities and enantioselectivities for the Rh-catalyzed AH of dehydroamino acid derivatives, itaconic acids, and *β*-ketoesters. In 2003, a series of chiral diphosphine ligand **Walphos**[89] with a phenylferrocenylethyl backbone was developed by Weissensteiner and Spindler et al., affording good reactivities and enantioselectivities for the Rh- and Ru-catalyzed AH of olefins and ketones. Furthermore, the Fc-Phox ligands **L2** were a class of highly efficient ligands for the Ru-catalyzed AH of aryl ketones and the Ir-catalyzed AH of quinolines.[90-91]

1.1.2.2 Noncovalent interaction-assisted ferrocenyl phosphine ligands

Noncovalent interactions (such as Van der Waals force, π interactions, electrostatic interactions, and hydrogen bonds) are important considerations in pharmaceutical design,[92] supramolecular chemistry,[93-94] and enzymatic catalysis.[95] In catalysis, noncovalent interactions contribute towards lowering the kinetic barriers of reactions by binding substrates and stabilizing transition states, leading to the rate acceleration and selectivity.[96] Consequently, a new strategy to design ferrocenyl phosphine ligands based on noncovalent interactions has been a growing interest in the field of AH (Figure 1.7).

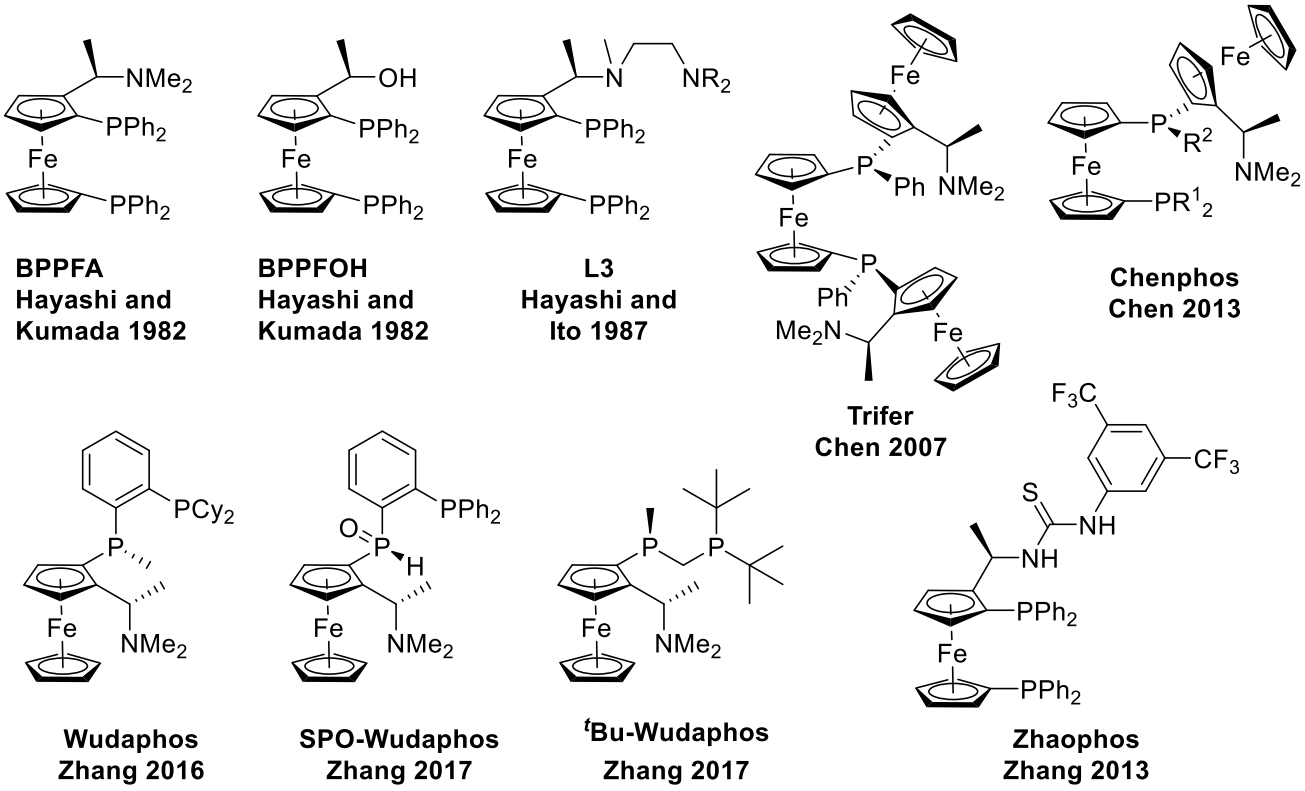

Figure 1.7 Selected ferrocenyl phosphine ligands based on noncovalent interactions

In the 1980s, Hayashi and Kumada[97] reported the synthesis of **BPPFA** and **BPPFOH** ligands, while Hayashi and Ito et al.[98] developed a group of chiral aminoalkyl-ferrocenyl phosphine ligand **L3** (Scheme 1.13). All these ligands were applied successfully in AH. The **BPPFA** ligand with its dimethylamino group was found to give a high enantioselectivity (93% ee) for the Rh-catalyzed AH of (*Z*)-*α*-acetaminocinnamic acid, but its ammonium salt and methyl ester were only hydrogenated with very low enantioselectivities. Hayashi and Kumada proposed that interactions between the dimethylamino group on the **BPPFA** ligand and the carboxyl group on the substrate were responsible for the stereoselectivity. And in the AH of carbonyl compounds catalyzed by the Rh-**BPPFOH** complex, it was postulated that hydrogen bonding between the hydroxyl group on the **BPPFOH** ligand and the carbonyl group on the substrate was the cause of high enantioselectivity. Another set of ferrocenyl phosphine ligand **L3** afforded excellent enantioselectivities for the Rh-catalyzed AH of

trisubstituted acrylic acids. Hayashi and Ito et al. supposed the high enantioselectivities were also probably originated from the attractive interactions between the ligands and substrates.

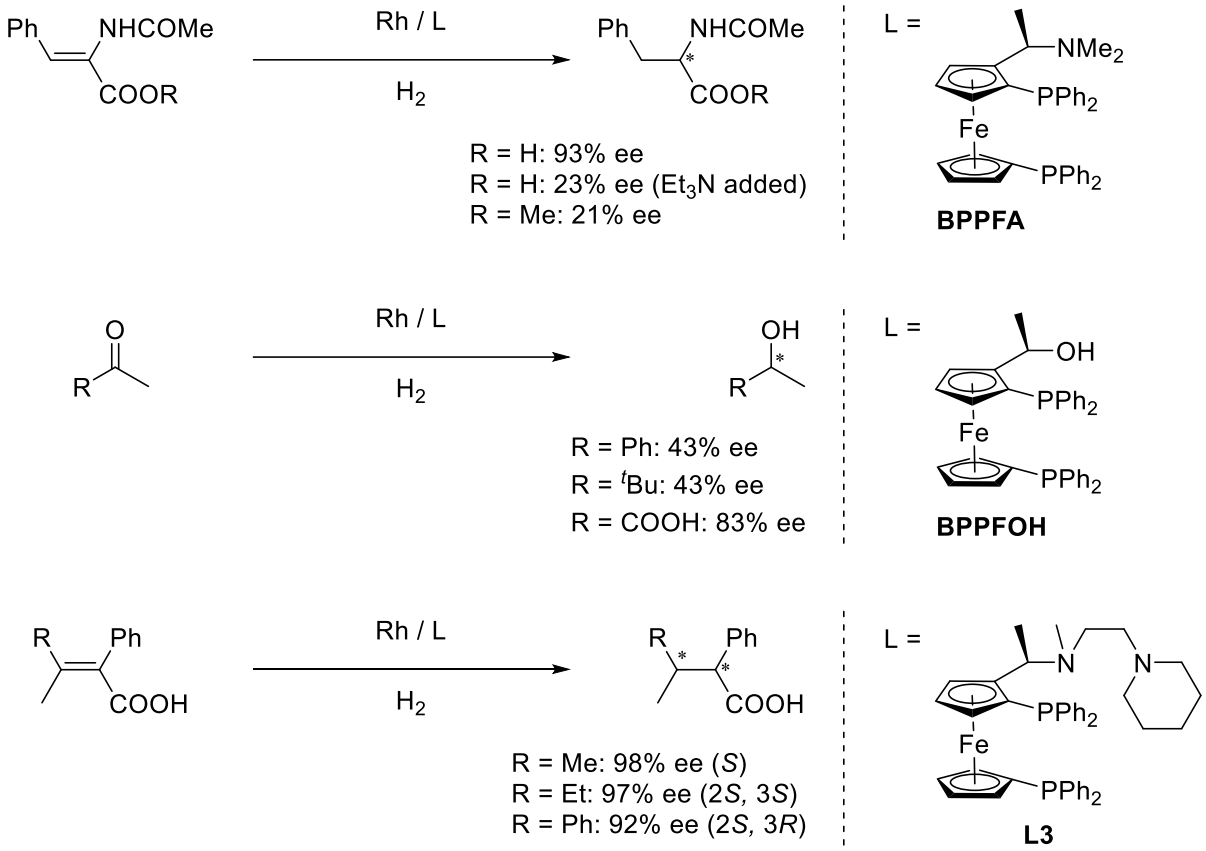

Scheme 1.13 Initial attempts of noncovalent interaction-assisted ferrocenyl phosphine ligands for AH

Subsequently, Chen et al. reported the highly stereoselective synthesis of famous ferrocenyl phosphine ligands **TriFer**[99] and **Chenphos**.[100] These ligands have multiple types of chirality, including C-centered, P-centered and planar chirality, resulting in exceedingly high enantioselectivities in the Rh-catalyzed AH of α-substituted cinnamic acids, with up to 99.6 % ee (Scheme 1.14). The electrostatic interactions between the dimethylamino group on the ligands and the carboxyl groups on the substrates were believed to account for the exceptional stereo-induction. Based on a similar ligand design, the Zhang group recently developed a family of Wudaphos ligands (**Wudaphos**,[101] **SPO-Wudaphos**[102] and **^{t}Bu-Wudaphos**[103]). In addition to ion pairing interactions, the Rh-**Wudaphos** complexes build a

three-blocked quadrant model to achieve the stereo-control. (Scheme 1.15) Three quadrants are blocked by the two large groups of the nonchiral phosphine and the bulky ferrocene backbone, while the last quadrant is kept open by the small substituent on the chiral phosphine. Notably, **SPO-Wudaphos** was proposed to have dual noncovalent interactions, including the ion pairing interactions mentioned above, and hydrogen bonds between the substrates and the hydroxyl group of the trivalent phosphinous acid, which was tautomerized from the pentavalent phosphine oxide of the ligand. The family of **Wudaphos** ligands enabled excellent enantioselectivities and reactivities in the Rh-catalyzed AH of unsaturated carboxylic acids, sulfonates and phosphonic acids.

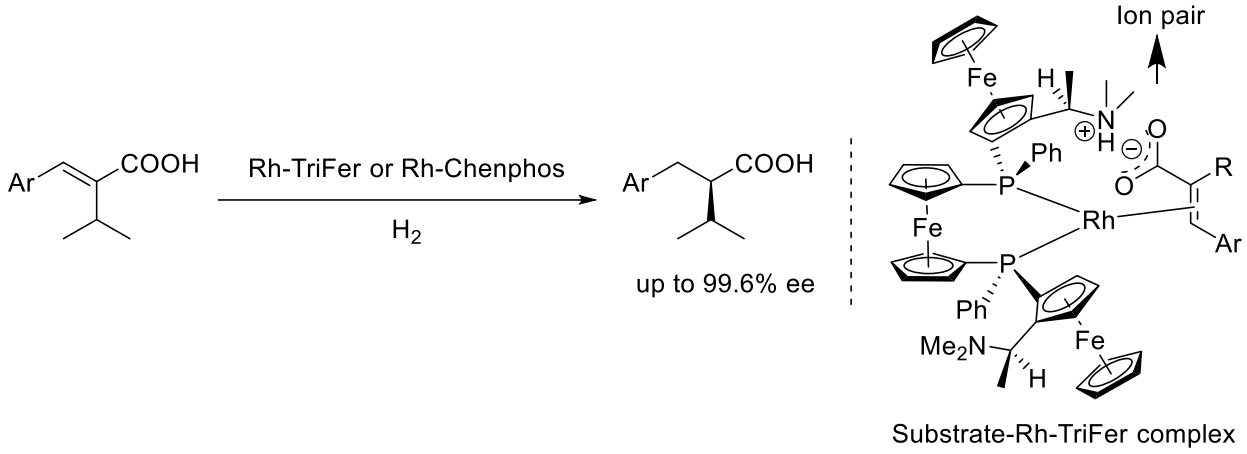

Scheme 1.14 Rh-**TriFer** or Rh-**Chenphos** for the AH of α-substituted cinnamic acids

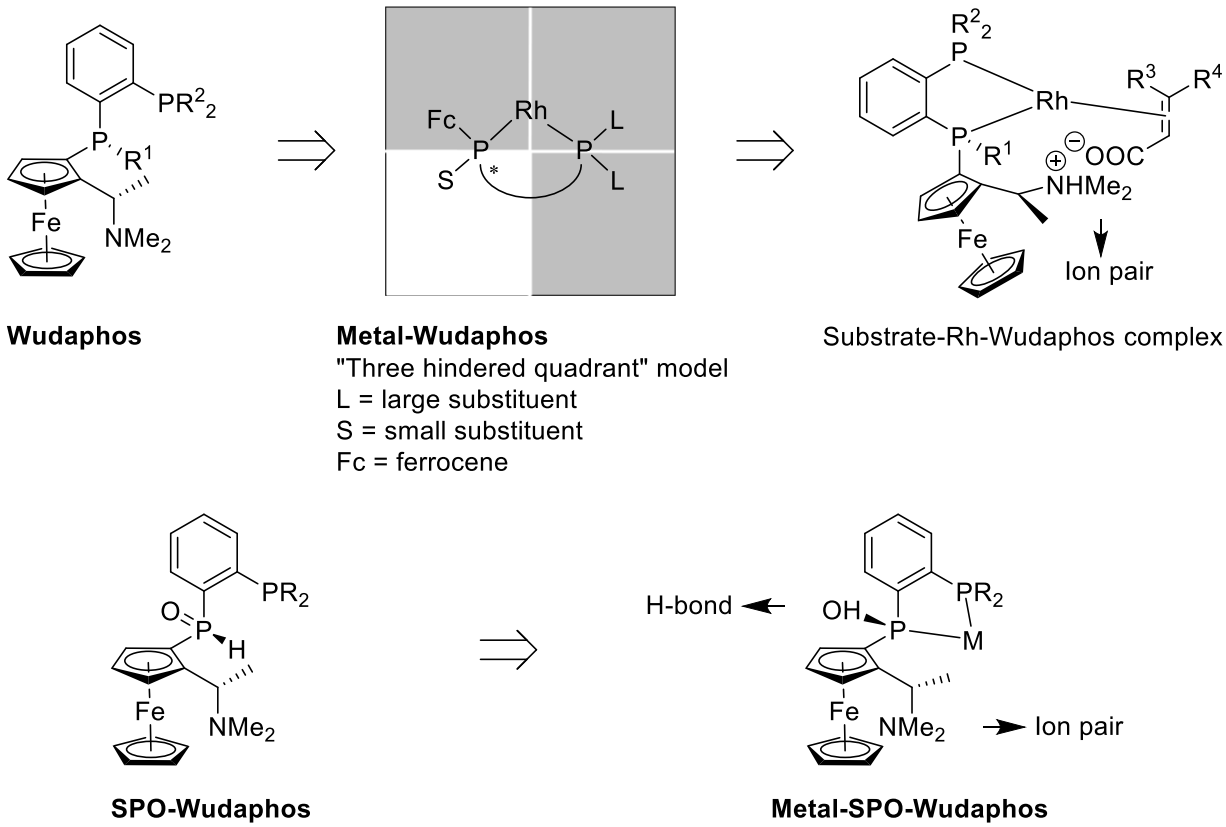

Scheme 1.15 Catalyst designs for metal-(**SPO-**)**Wudaphos** complexes

In 2013, Zhang et al. developed a chiral ferrocenyl bisphosphine-thiourea ligand **Zhaophos**.[104] The H-bond donor properties of the thiourea group improve both the acidity and rigidity of the ligand. This excellent design endowed the **Zhaophos** ligand with high reactivities and excellent enantioselectivities in the Rh- and Ir-catalyzed AH of a broad range of substrates, including C=C bonds of neutral substrates, C=N bonds of ionic substrates and carbocations (Scheme 1.16).[105]

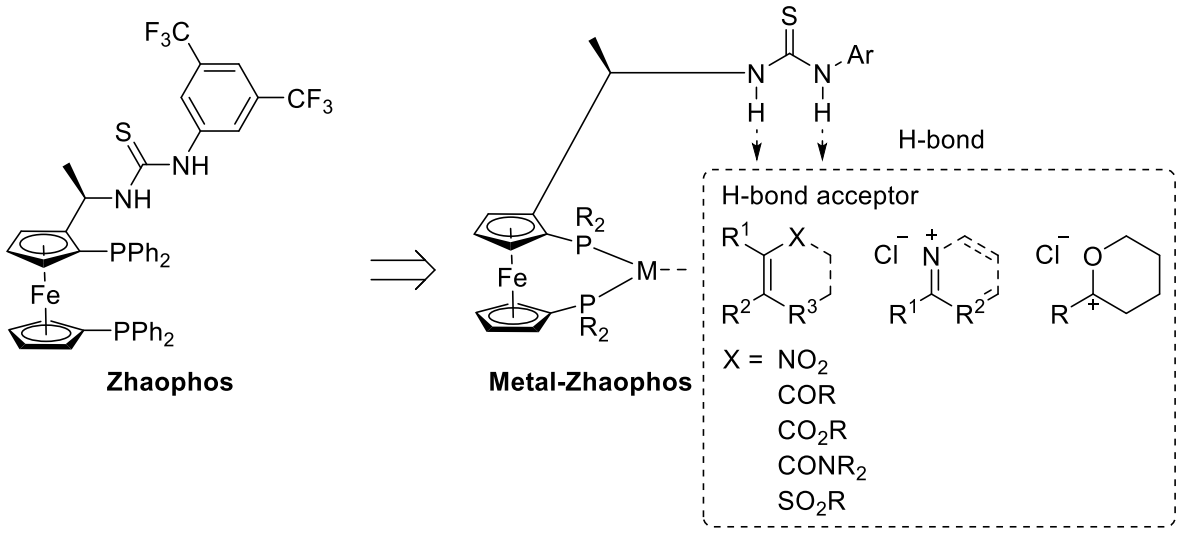

Scheme 1.16 Catalyst design for metal-**Zhaophos** complex

1.1.2.3 Tridentate ferrocenyl phosphine ligands

In general, metal complexes coordinated with multidentate ligands have higher stabilities than those with bidentate ligands due to the chelate effect, avoiding catalyst deactivation caused by ligand dissociation or exchange. Besides, chiral metal-tridentate ligand complexes are endowed with deeper chiral pockets to achieve better stereo-inductions. Based on these considerations, the development of efficient tridentate phosphine ligands for AH has triggered extensive attention over two decades.[106] In the 1990s, Zhang et al. made several initial attempts to use tridentate phosphine ligands for the Ru-catalysed asymmetric transfer hydrogenation (ATH) of ketones,[107-108] and **ambox** ligand was found to afford excellent enantioselectivities (up to 98% ee) (Scheme 1.17).[109]

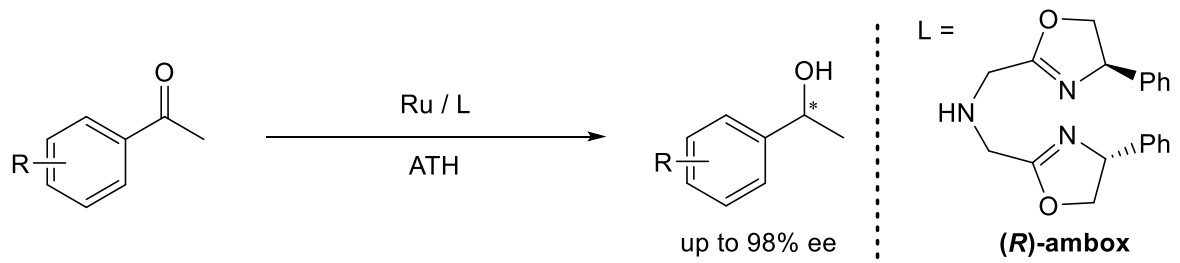

Scheme 1.17 Initial Ru-catalyzed ATH using tridentate phosphine ligands

Tridentate ferrocenyl phosphine ligand **L4** applied for AH was firstly reported by Chen and Zhang S. et al. in 2013 (Figure 1.8).[110] They synthesized a class of ferrocene-based PNN ligands and used the corresponding Ir-PNN complexes to catalyse the AH of aromatic ketones with moderate to good enantioselectivities. In 2016, Hu et al. added extra sterically hindered groups onto the above PNN ligand, providing high *anti*-diastereoselectivities and excellent enantioselectivities for the Ir-catalyzed AH of α-alkyl-substituted β-aryl-β-ketoesters via dynamic kinetic resolution.[111] Recently, Zhong et al developed a new series of ferrocenyl diamine-phosphine-sulfonamide ligands ***f*-diaphos**, affording excellent enantioselectivities and reactivities for the Ir-catalyzed AH of aryl alkyl ketones and diaryl ketones.[112]

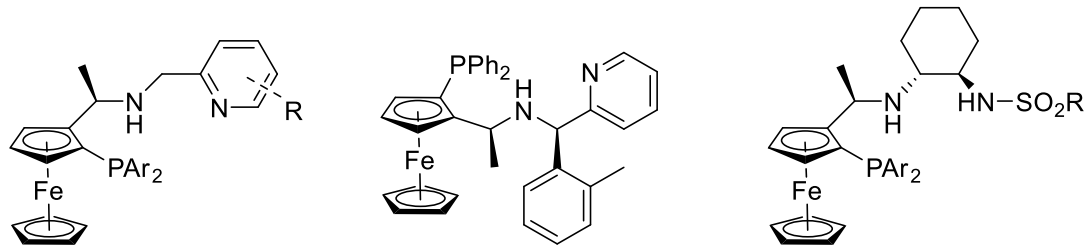

L4
Chen and S. Zhang 2013

L5
Hu 2016

f-diaphos
Zhong 2018

Figure 1.8 Selected tridentate ferrocenyl phosphine ligands

In the last five years, the Zhang group has made significant progress in this area and developed a family of tridentate ferrocenyl phosphine ligands: ***f*-amphox**,[113] ***f*-ampha**,[114] ***f*-amphol**,[115] ***f*-amphamide**[116] and others. Their iridium complexes exhibited excellent efficiencies in the AH of various ketones. More importantly, these catalysts have been successfully applied in the industrial synthesis of several important chiral drugs, including Montelukast, Ezetimibe, Phenylephrine and Crizotinib (Figure 1.9).

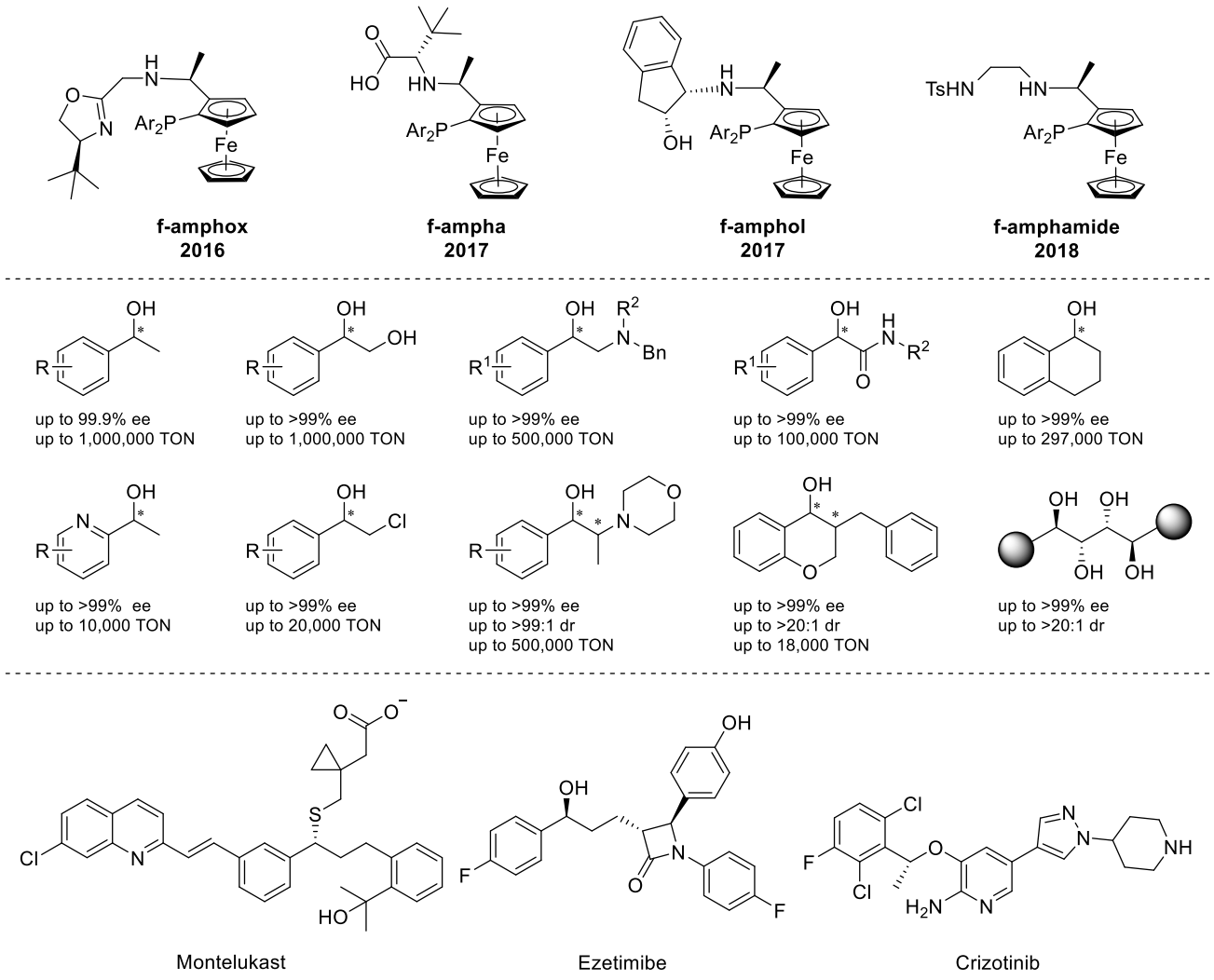

Figure 1.9 Tridentate ferrocenyl phosphine ligands reported by the Zhang group

1.1.3 Earth-abundant metal catalysis

Noble transition metal-catalysed AH has evolved as one of the most efficient catalytic transformations for the production of chiral molecules. However, precious metals such as rhodium, ruthenium, iridium, palladium, and platinum are of low abundance in the Earth's crust and are expensive in the global market, resulting in a big challenge for the sustainability of noble metals. Besides, their high toxicity leads to extra costs in removing scarce metals after catalytic reactions. Consequently, the development of alternative catalysts based on earth-abundant metals such as manganese, iron, cobalt, nickel and copper is becoming an increasingly popular theme.[117-120] However, compared with noble 4d or 5d metals, 3d transition metals possess different chemical natures. Smaller atomic radii and d orbitals

induce lower electronegativities and harder acidities of the 3d metals. Smaller atomic radii also cause the 3d metals to favour forming 5-membered rings instead of 6-membered rings when interacting with ligands or substrates. Furthermore, potential involvement of single-electron processes in catalytic reactions can impair the reactivities of the first-row transition metals. Therefore, new strategies for developing efficient chiral catalyst systems based on 3d transition metals need to be developed.

1.1.3.1 Chiral iron catalysts

In 2004, Gao et al. reported the first iron-catalysed asymmetric transfer hydrogenation (ATH) of ketones with chiral iron catalysts generated *in situ* by mixing carbonyl iron hydride cluster $[Et_3NH][HFe_3(CO)_{11}]$ with diaminodiphosphine ligand **L6**, giving the products with promising reactivities (up to 98% conversion) and enantioselectivities (up to 98% ee) (Scheme 1.18).[121] This pioneering work encouraged other groups to develop more efficient iron-based catalyst systems for ATH, and a lot of (pre-)catalysts have been reported since the past two decades.[122-131]

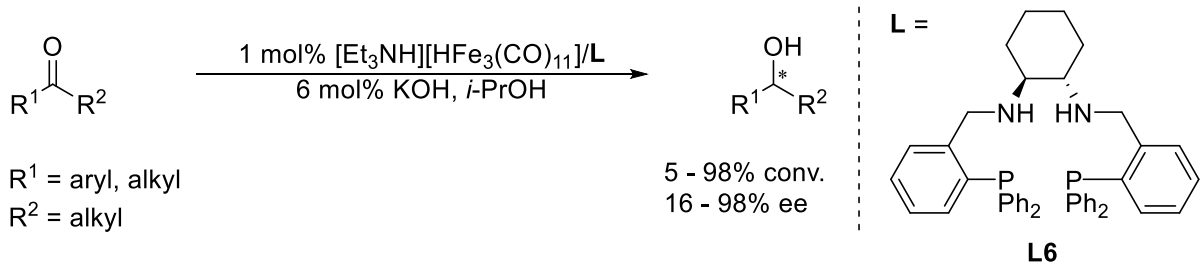

Scheme 1.18 The first Fe-catalyzed ATH of ketones reported by Gao et al.

Compared with ATH, the development of Fe-catalysed AH has been late but also very fast. A large number of chiral iron catalysts have been developed for the AH of ketones (C=O) and imines (C=N), which are comprised of multidentate chelating complexes, macrocyclic ligand-based complexes and Knolker-type complexes.

Chiral iron complexes based on multidentate phosphine ligands have been shown to be as promising catalysts for AH by the groups of Morris,[122] [132-134] Zirakzadeh,[135] Mezzetti[136-137] and Beller[138] (Scheme 1.19). From 2008 to 2017, Morris et al. reported several chiral multidentate phosphine ligands (PNNP and PNP) and their corresponding iron complexes for the AH of ketones. Although the tetradentate complexes **Fe-1**[122] and **Fe-2**[132] only gave poor efficiencies, tridentate complex **Fe-3**[133] exhibited high reactivities (TON up to 5,000) and good enantioselectivities (ee up to 85%), and especially **Fe-5**[134] afforded excellent enantioselectivities (ee up to 96%) for the AH of aryl alkyl ketones. Moreover, Zirakzadeh et al. introduced a class of ferrocene-based iron catalyst **Fe-4**,[135] and Mezzetti et al. reported the C_2-symmetric P-stereogenic iron catalysts **Fe-6**[136] and **Fe-7**[137] for the AH of simple ketones. Recently, Beller et al. developed another chiral iron pincer complex **Fe-8**,[138] providing moderate to good enantioselectivities (99% ee for adamantyl methyl ketone) for the AH of cyclic aliphatic ketones, while offering low enantioselectivities for the AH of aromatic ketones.

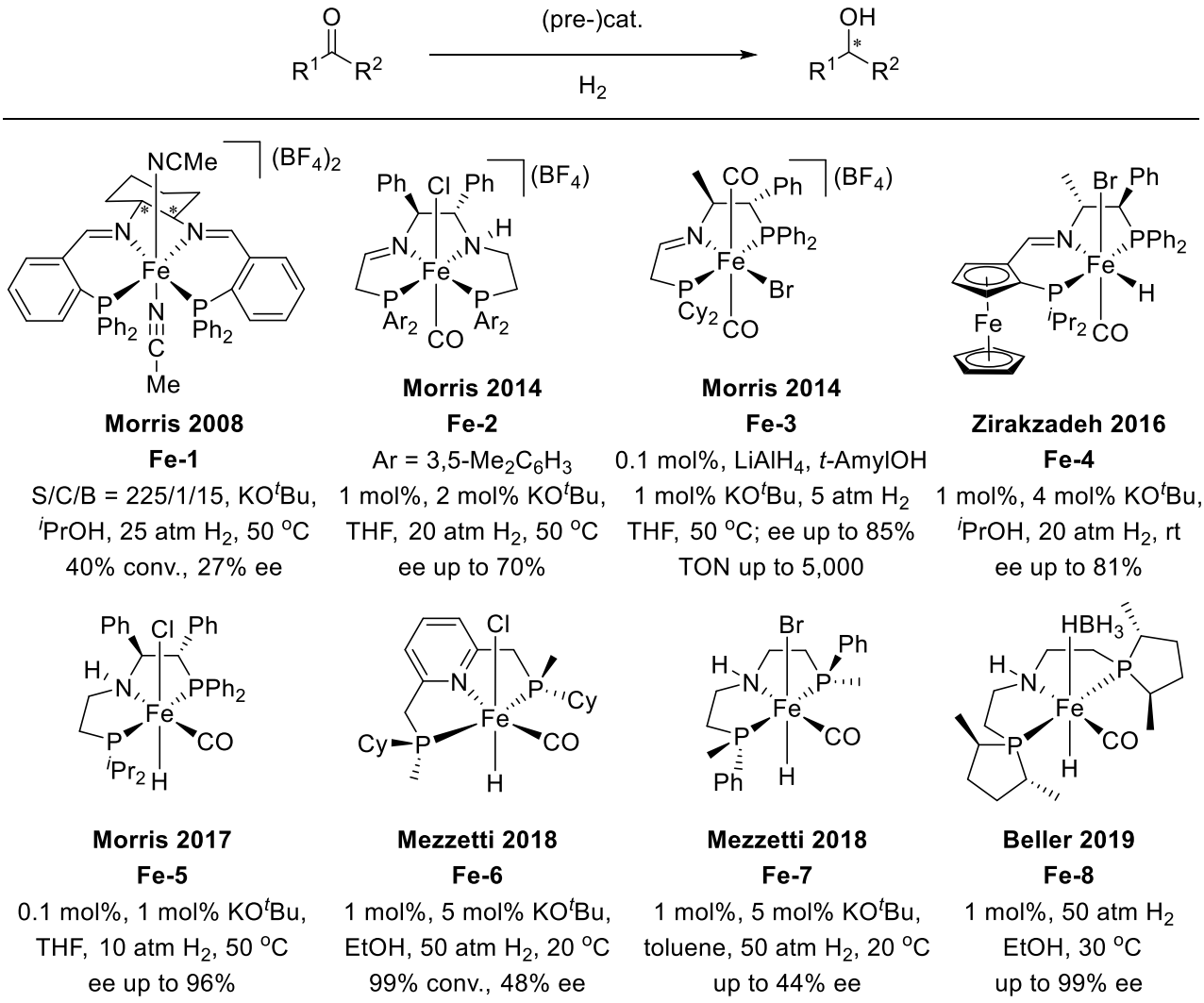

Scheme 1.19 Multidentate Fe complexes for the AH of ketones

In addition, chiral Fe-PNP complexes **Fe-3**[133] and **Fe-5**[139] were also investigated for the AH of imines (Scheme 1.20). In 2014, Morris et al. made initial attempts to use the **Fe-3** for the AH of N-(diphenylphosphonyl)propiophenoneimine with 90% ee. In 2019, the same group reported the **Fe-5**-catalysed AH of imine substrates activated with N-phosphinoyl or N-tosyl groups, affording excellent enantioselectivities for aryl imines.

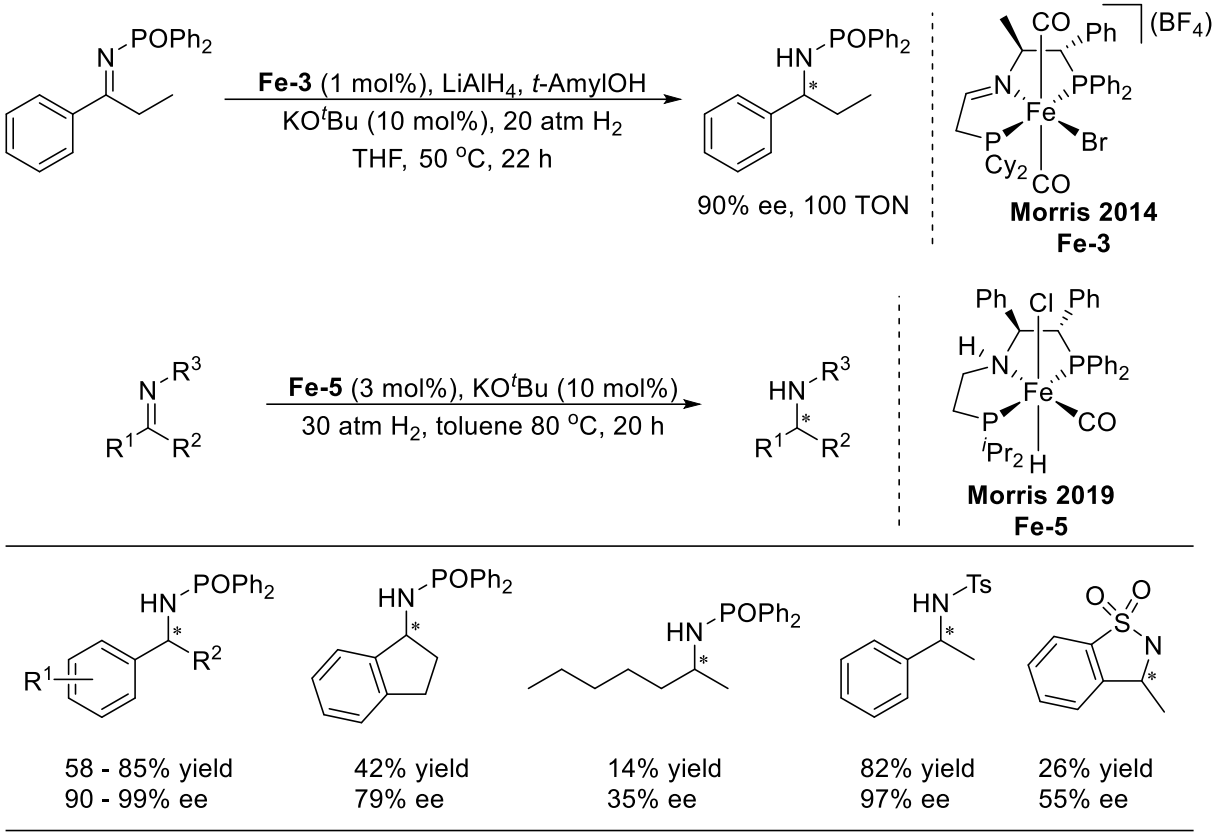

Scheme 1.20 Multidentate Fe complexes for the AH of imines

In 2014, Gao et al. reported a remarkably effective chiral iron catalyst **Fe-9**,[140] providing excellent enantioselectivities and reactivities for the AH of a wide variety of ketones including (hetero-) aryl alkyl ketones and *β*-ketoesters (Scheme 1.21). The catalyst was generated *in situ* by combining the carbonyl iron cluster $Fe_3(CO)_{12}$ with the chiral 22-membered macrocyclic ligand P_2N_4. However, the active iron species were not like the catalysts mentioned above, and instead appeared to be macrocyclic ligand-modified iron nanoparticles.

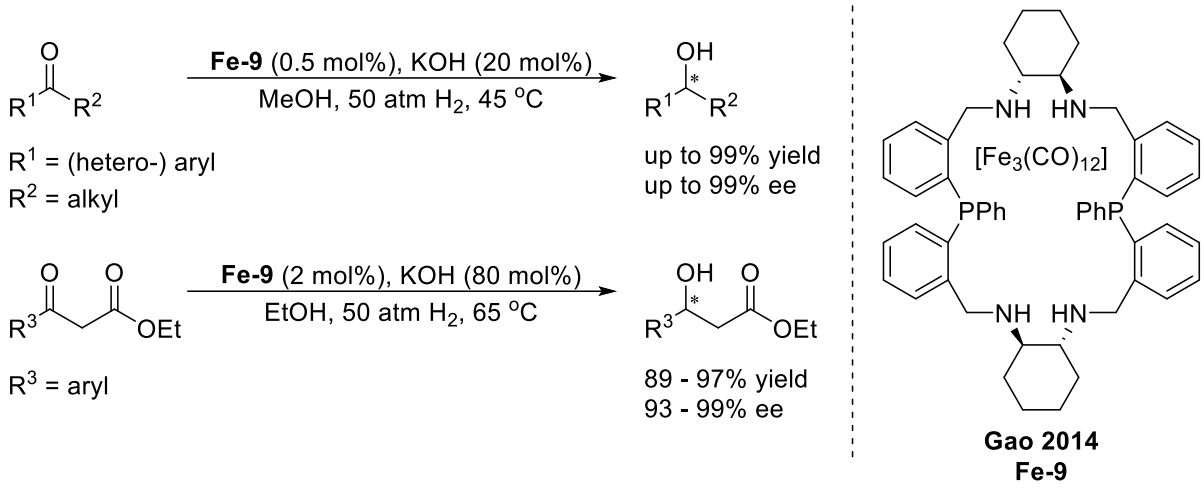

Scheme 1.21 Macrocyclic Fe complex for the AH of ketones

Over the past decade, Knolker-type complexes acting as active catalysts for AH have also attracted extensive interest because of their inherent ligand-metal bifunctional nature, similar to Shvo's catalyst and Fe hydrogenase (Figure 1.10).[141] In 2007, **Fe-10** was successfully used by Casey et al. for the hydrogenation of ketones.[142] This seminal work inspired other groups to develop chiral versions of Knolker-type complex for AH.

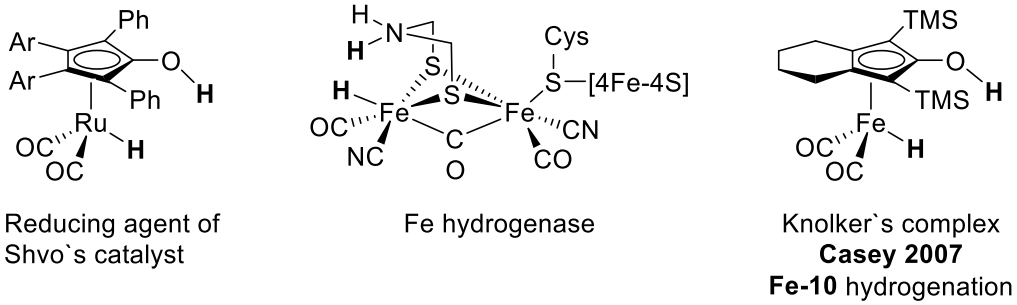

Figure 1.10 Ligand-metal bifunctional complexes

From 2011 to now, there has been a great number of publications concerning the chiral Knolker-type iron complexes for the AH of ketones (Scheme 1.22). In 2011, Berkessel et al. reported the synthesis of a chiral iron(II)-cyclopentadienone-dicarbonyl complex **Fe-11**[124] by replacing one of the three carbonyl groups with a chiral phosphoramidite ligand. The iron complex catalysed the AH of

acetophenone under UV irradiation with high reactivity (90% yield) but low enantioselectivity (31% ee). In 2015, Pignataro/Piarulli/Gennari et al. developed a series of chiral iron(II)-cyclopentadienone-tricarbonyl complexes **Fe-12**[143-144] with a (*R*)-BINOL-derived backbone. The iron complexes catalysed the AH of a range of aromatic ketones and aliphatic ketones with up to 77% ee, which was the highest ee value reported so far in the Knolker-type iron complex-catalysed AH of ketones. Subsequently, the groups of Wills (**Fe-13**),[145] Ward/Renaud (**Fe-14**),[146] Pignataro/Gennari (**Fe-15** and **Fe-16**)[147] and De Wildeman (**Fe-17**)[130] all developed new chiral Knolker-type complexes by introducing carbon-centered chirality or planar chirality onto the cyclopentadienone. However, these iron complexes exhibited poor enantioselectivities for the AH of simple ketones.

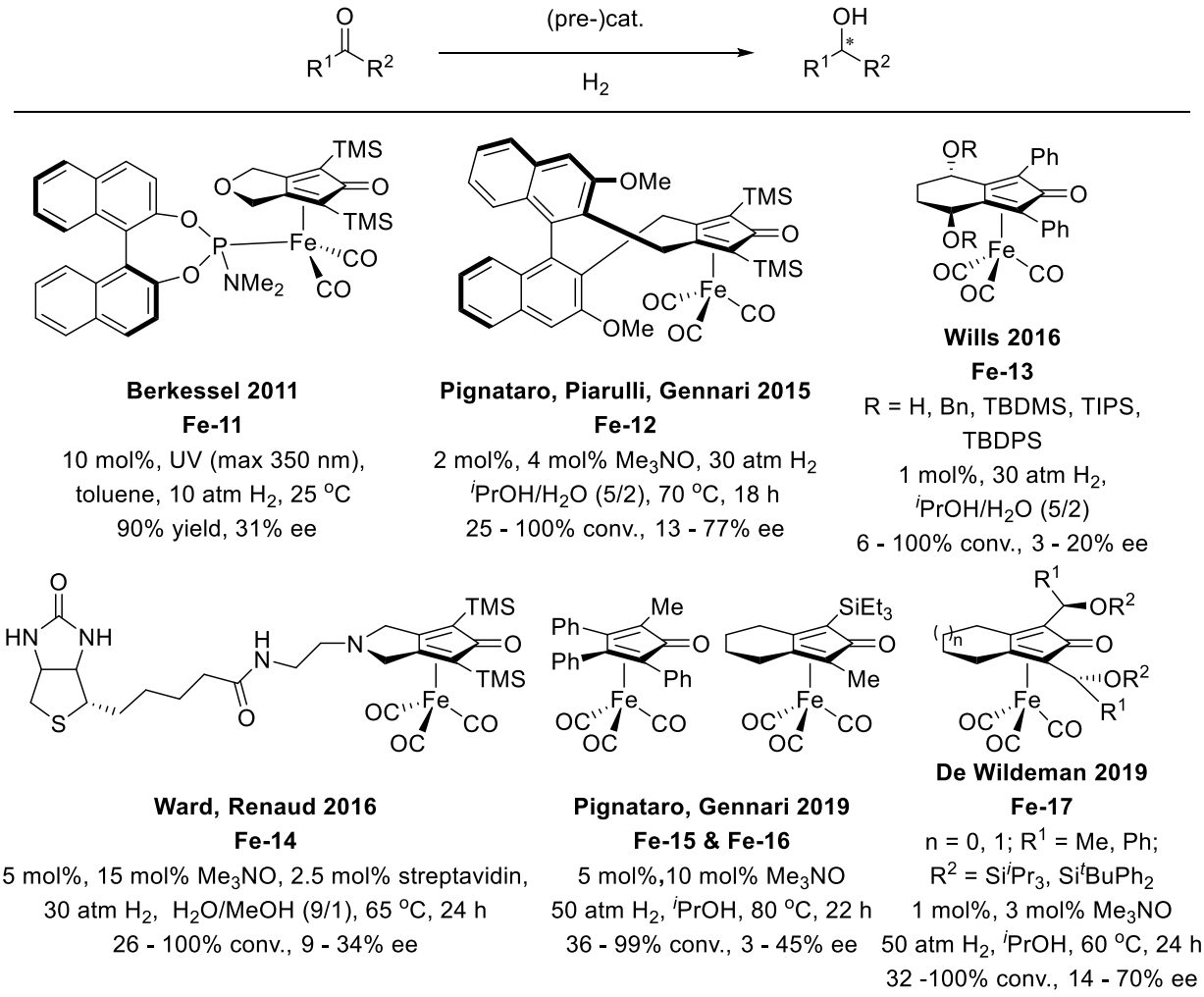

Scheme 1.22 Knolker-type Fe complexes for the AH of ketones

On the other hand, the AH of imines catalysed by chiral Knolker-type iron complexes has made great progress. The Beller group has had several outstanding works in this area (Scheme 1.23).[148-151] In 2011, they reported the first case of the AH of imines catalysed by a complex made by combining Knolker's iron complex **Fe-10** with chiral brønsted acid **(*S*)-TRIP**, providing the secondary amines with great reactivities (up to 94% yield) and enantioselectivities (up to 98% ee).[148] Firstly, the chiral Brønsted acid activated the imine substrate via protonation, and then assisted the achiral Knolker hydride complex to hydrogenate the substrate with enantioinduction. The cooperative iron-Brønsted acid catalyst system was also successfully applied to the AH of quinoxalines and benzoxazines,[149] and the asymmetric reductive amination of ketones.[150] In 2015, Beller et al. developed another iron-Brønsted acid catalyst derived from $Fe_3(CO)_{12}$ and chiral phosphoric acid, giving high yields and enantioselectivities for the AH of benzoxazinones.[151]

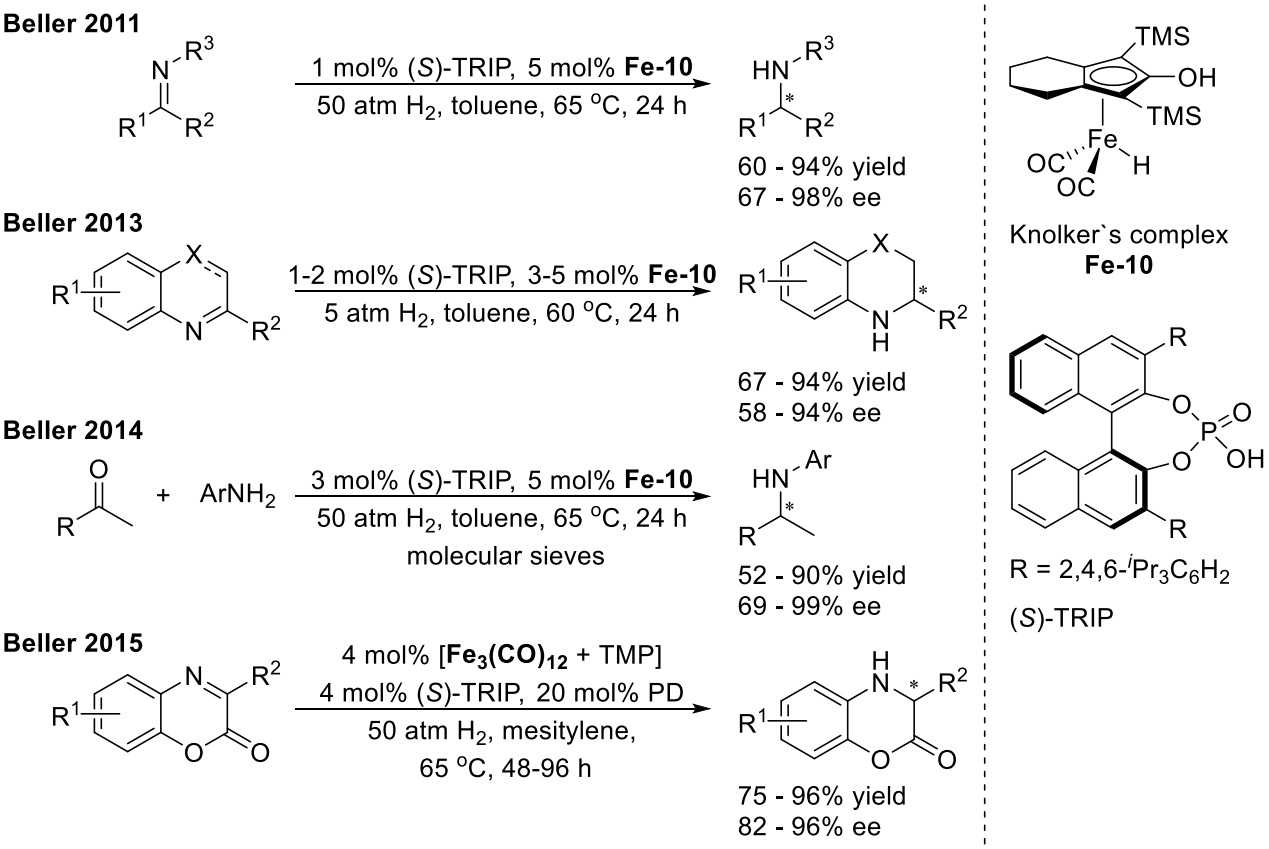

Scheme 1.23 Knolker`s Fe complex with **(*S*)-TRIP** for the AH of C=N bonds

In the last five years, there have not been many important breakthroughs in the AH of C=N bonds catalysed by the chiral Knolker-type iron complexes, despite the efforts of the groups of Ward/Renaud (**Fe-14**),[146] Benaglia (**Fe-18**),[152] and Pignataro/Piarulli/Gennari (**Fe-15**, **Fe-16**, and **Fe-19**)[147, 153] (Scheme 1.24). Notably, **Fe-18** developed by Benaglia et al. in 2017 catalysed the diastereoselective hydrogenation of chiral imines with up to 96% de.

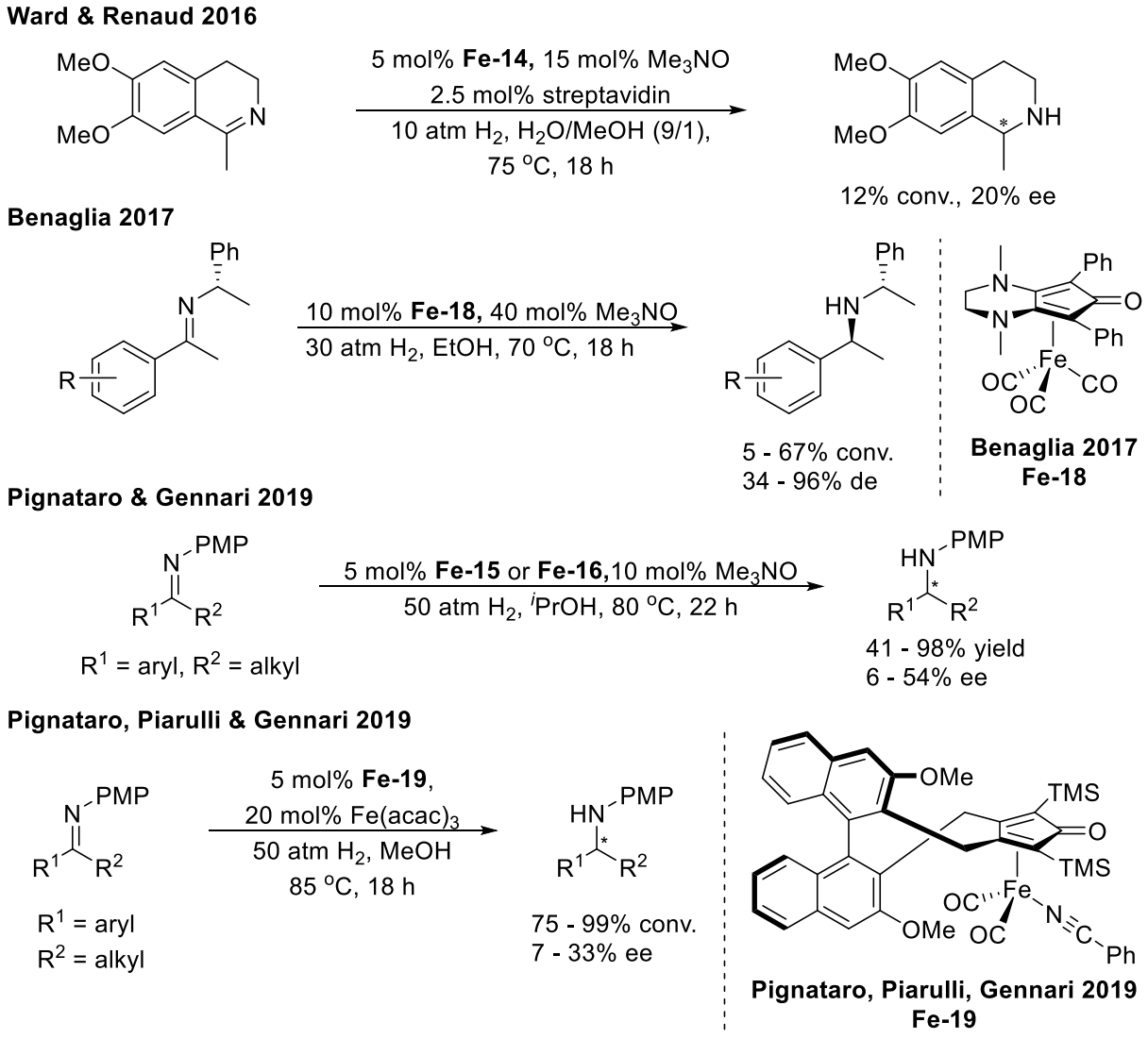

Scheme 1.24 Recent reports of Knolker-type Fe complexes for the AH of C=N bonds

1.1.3.2 Chiral cobalt catalysts

In the 1980s, there were considerable seminal attempts at cobalt-catalysed AH by the groups of Ohgo, Shmidt, Simonneaux, Pfaltz, and Iglesias etc., despite poor enantioselectivities obtained by most of those cobalt catalyst systems.[154-159] Notably, Pfaltz et al. in 1989 reported the cobalt-catalysed AH of *α,β*-unsaturated carboxylates with excellent reactivities (up to 97% yield) and enantioselectivities (up to 94% ee), using a **semicorrin** as chiral ligand in the presence of $NaBH_4$ (Scheme 1.25).[159]

Scheme 1.25 Co-**semicorrin** complexes for the AH of *α,β*-unsaturated carboxylates

Since these early reports, cobalt catalysis in the field of AH was largely neglected until recent decade, when the development of chiral cobalt catalysts for AH became an important topic. Several bidentate and multidentate cobalt complexes have now been published for the AH of C=O, C=C and C=N bonds. The cobalt-catalysed AH of ketones will be elaborated in Chapter 3 of this thesis. Herein, an introduction to chiral cobalt catalysts for the AH of alkenes and imines is described, which includes tridentate and bidentate cobalt complexes.

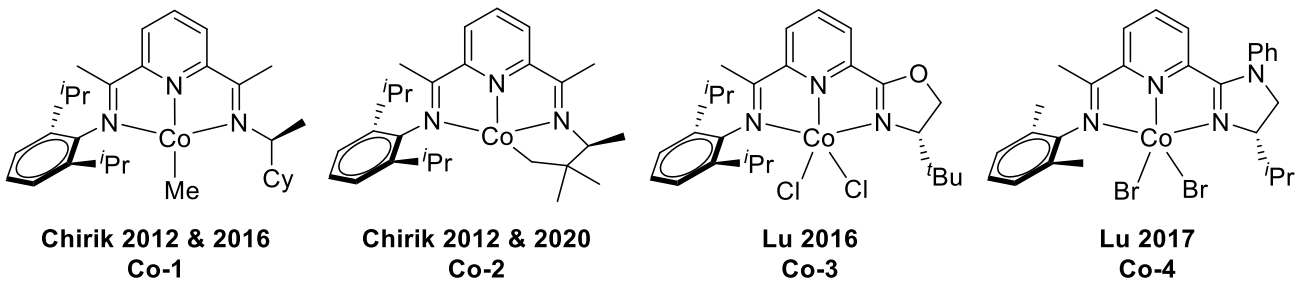

Figure 1.11 Tridentate Co complexes

In 2012, Chirik et al. developed some C_1-symmetric bis(imino)pyridine tridentate cobalt complexes **Co-1** and **Co-2** with the introduction of a chiral alkylamine (Scheme 1.26). Complex **Co-1** afforded high enantioselectivities for the AH of geminal-disubstituted olefins,[160] which subsequently was also found to be very effective for the AH of substituted benzofused five-, six-, and seven-membered alkenes.[161] Recently, Chirik et al. reported the use of complex **Co-2** for the AH of sterically-hindered alkenes.[162] Varieties of 2-substituted 1,1-diboryl alkenes were hydrogenated with high reactivities and enantioselectivities.

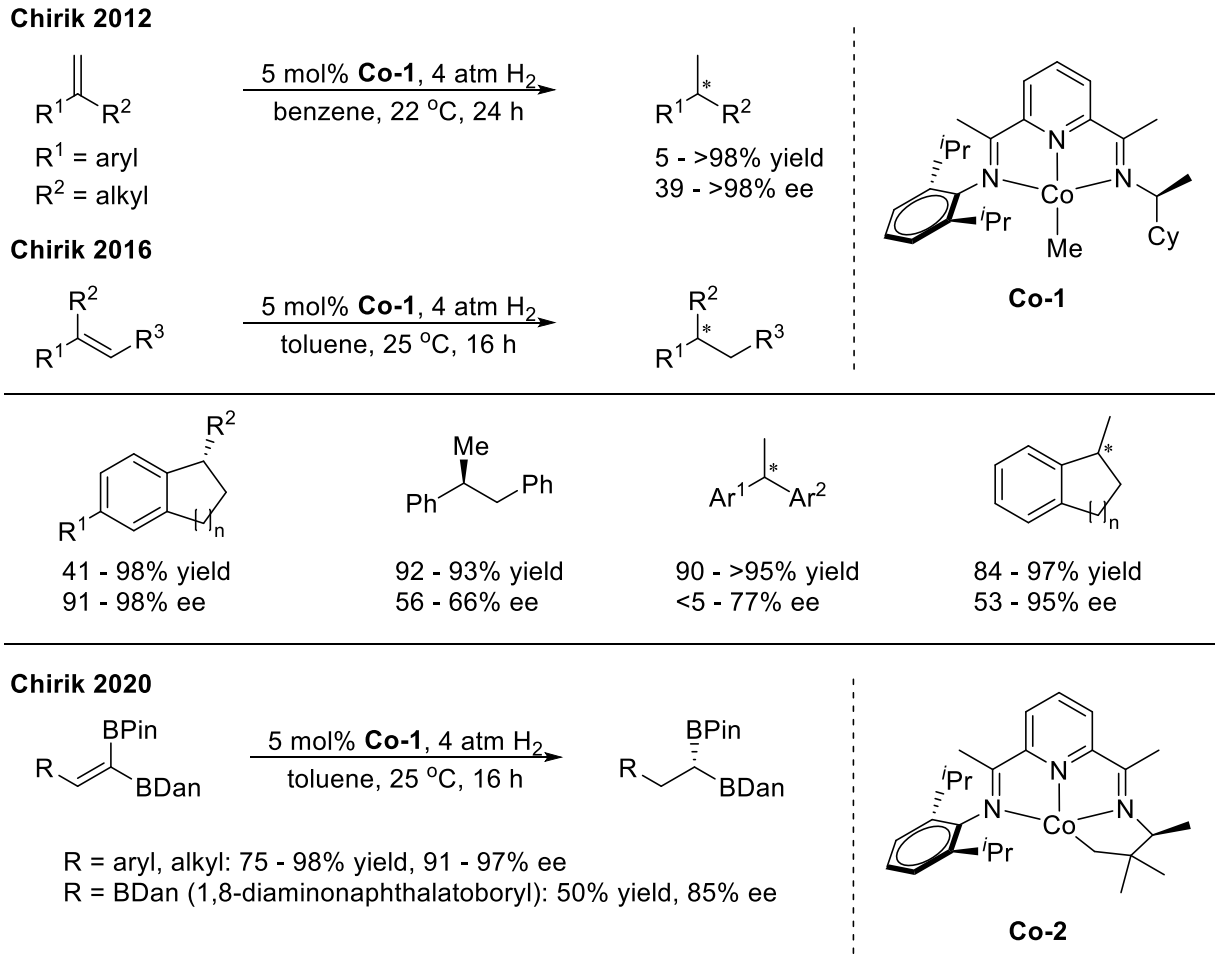

Scheme 1.26 Tridentate Co complexes for the AH of alkenes by the Chirik group

The Lu group has also developed several effective chiral tridentate cobalt complexes **Co-3** and **Co-4** for the AH of alkenes (Scheme 1.27). The chiral oxazoline iminopyridine-cobalt complex **Co-3**

catalysed the AH of 1,1-diarylethenes and α-alkylstyrenes with excellent yields and enantioselectivities.[163] Furthermore, the imidazoline iminopyridine-cobalt complex **Co-4** was highly regio- and enantioselective for the asymmetric sequential hydroboration/hydrogenation of alkynes with HBpin in one pot.[164]

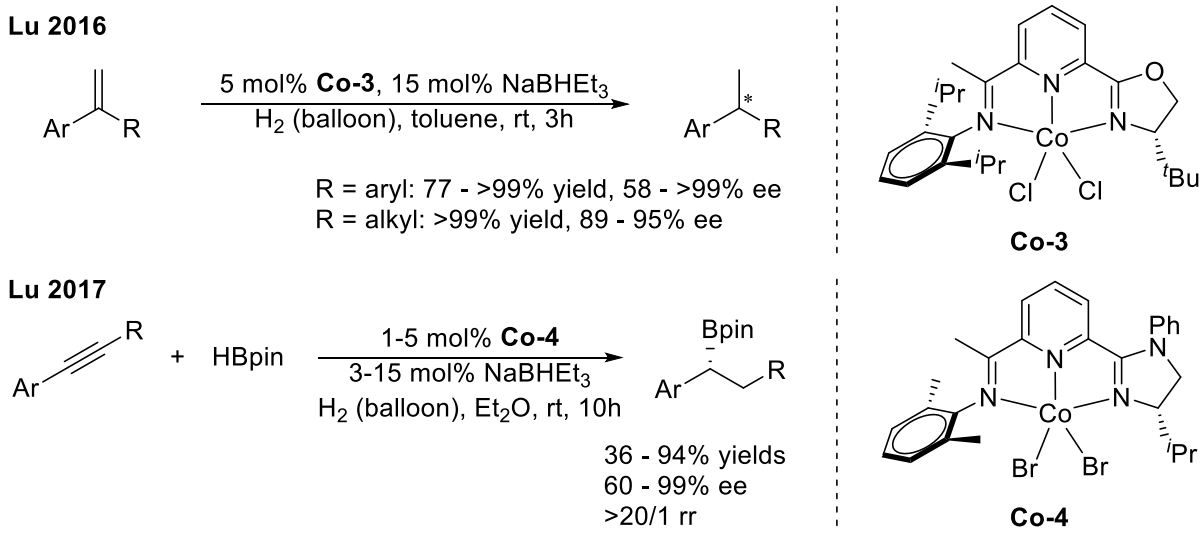

Scheme 1.27 Tridentate Co complexes for the AH of alkenes reported by Lu et al.

In addition to these tridentate cobalt complexes, chiral bidentate cobalt complexes have also been demonstrated as efficient catalysts for the AH of C=C bonds (Scheme 1.28). In 2013, Chirik et al. reported the cobalt-catalysed AH of alkenes via high-throughput screening of 192 commercially available or readily synthesized ligands.[165] They summarized several chiral bidentate phosphine ligands providing excellent enantioselectivities for the cobalt-catalysed AH of functionalized and unfunctionalized olefins. In 2018, the same group developed the cobalt-diphosphine catalyst systems (**Co-5** and **Co-6**) activated by zinc via single-electron reduction for the AH of enamides.[166] This method enabled the rapid asymmetric synthesis of the epilepsy drug levetiracetam on a large scale. Very recently, Chirik et al.[167] and Zhang et al.[168] independently published the AH of *α,β*-unsaturated

carboxylic acids using the Zn-Co(Ⅱ)-diphosphine catalyst system with high reactivities and excellent enantioselectivities.

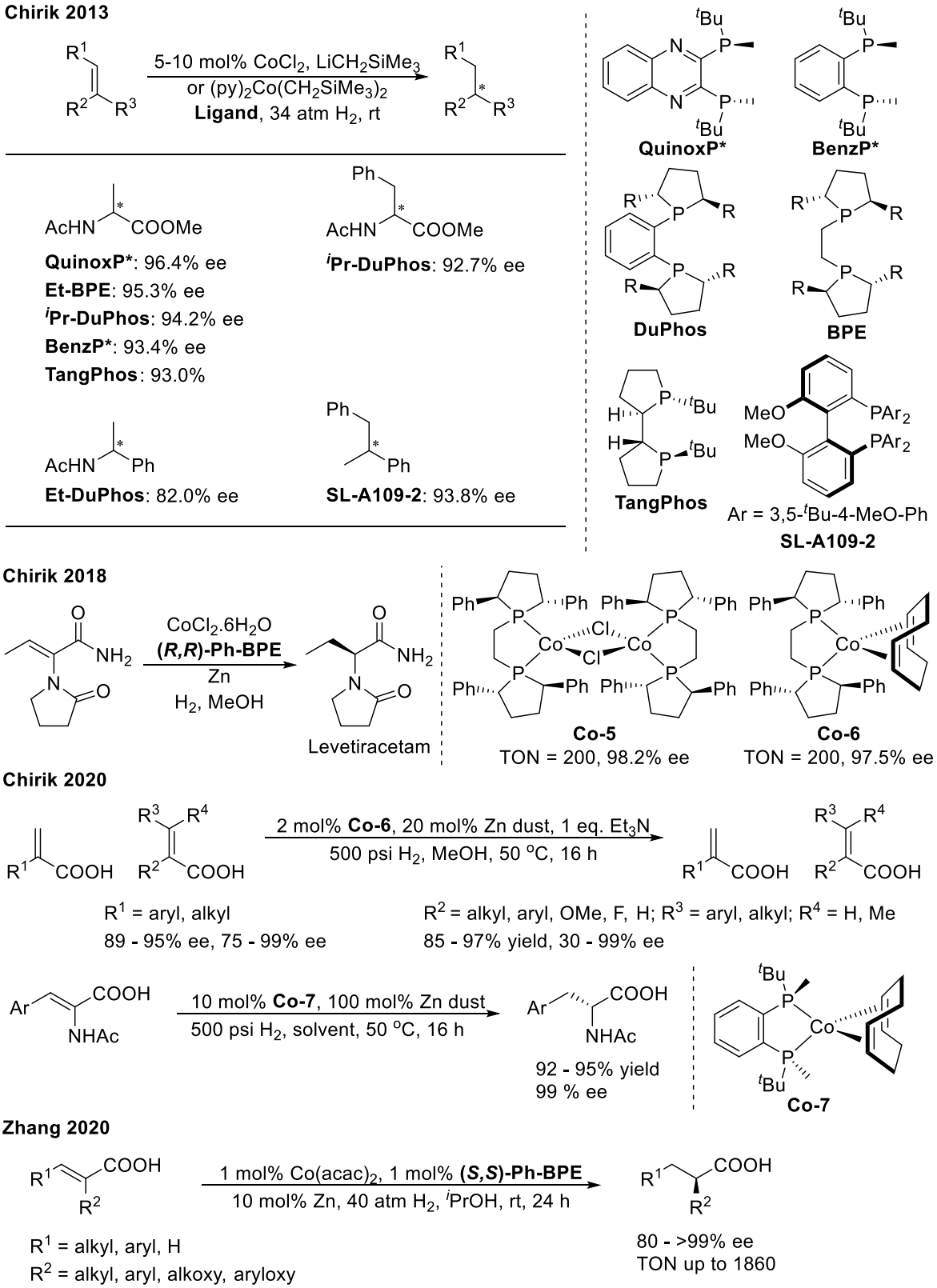

Scheme 1.28 Chiral bidentate phosphines for the Co-catalyzed AH of alkenes

Chiral bidentate cobalt complexes have also been very effective for the AH of C=N bonds (Scheme 1.29). In 2013, Valencia/Cabrera et al. reported the first example of the cobalt-catalysed AH of imines using $Co_2(CO)_8$/**(*R*)-BINAP** as a catalyst precursor, giving products with excellent reactivities and good enantioselectivities.[169] Recently, Zhang W. et al used the Zn-Co(Ⅱ)-diphosphine catalyst system for the AH of hydrazones assisted by the coordination and nonbonding interactions between the catalyst and substrates, providing the chiral hydrazines with high yields and excellent ee values (95 - 98% ee).[170]

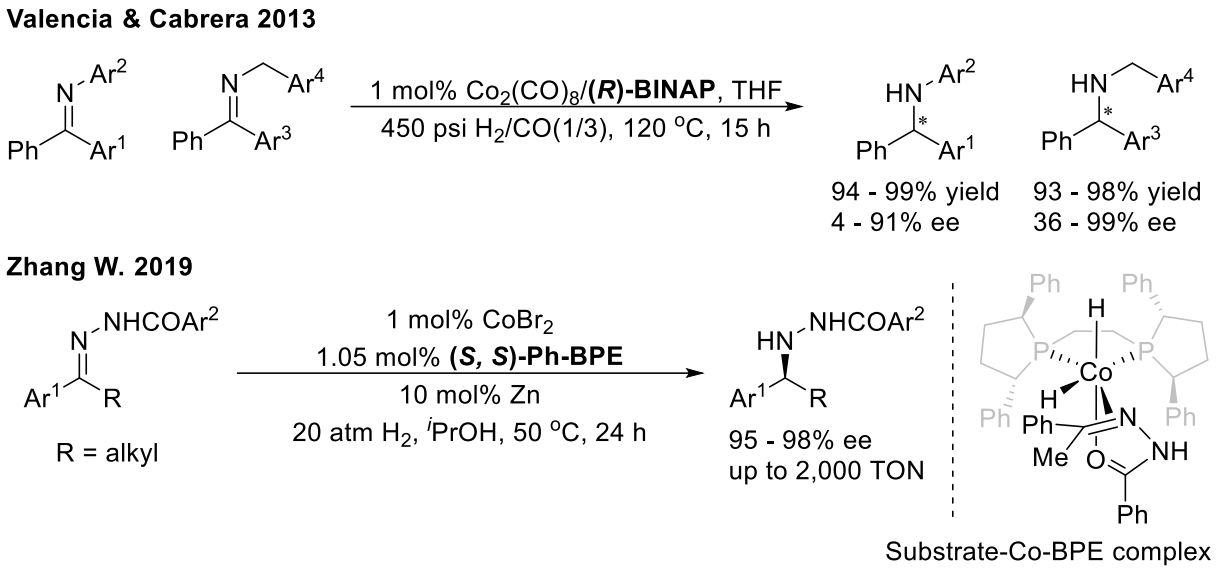

Scheme 1.29 Chiral bidentate phosphines for the Co-catalyzed AH of imines

1.1.3.3 Chiral nickel catalysts

The main strategies for nickel-catalysed AH have focused on the development of chiral bidentate nickel complexes employing bisphosphine ligands, due to the square planar geometry of the stable d^8 nickel (II) complexes. To date, some examples of the AH of C=O, C=C and C=N bonds catalysed by the nickel-bisphosphine complexes have been described.

Firstly, the nickel-catalysed AH of ketones has rarely been reported. In 2008, Hamada et al. used a chiral nickel-**Josiphos** complex for the AH of α-amino-β-keto esters via dynamic kinetic resolution with moderate to good enantioselectivities and excellent diastereoselectivities (Scheme 1.30).[171] Following this work, they also successfully applied the same catalyst system for the AH of aromatic α-aminoketones.[172]

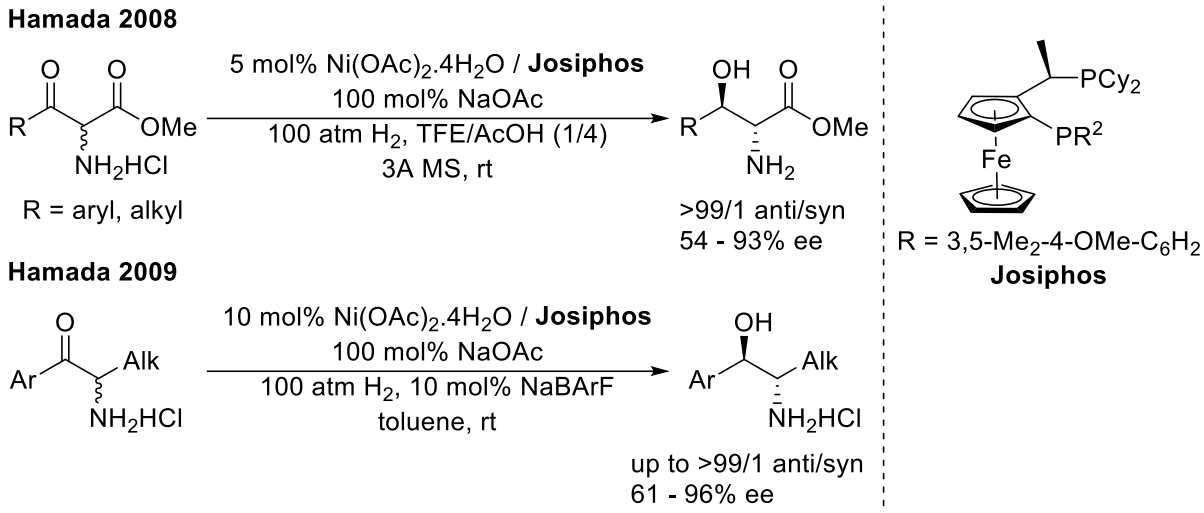

Scheme 1.30 Bidentate phosphines for the Ni-catalyzed AH of ketones via DKR

A few examples of the nickel-catalysed AH of alkenes limited to conjugated olefins have been published by the groups of Chirik, X. Zhang, and W. Zhang over the last five years (Scheme 1.31). In 2016, Shevlin and Chirik et al. discovered the first nickel-catalysed AH of α,β-unsaturated esters with the aid of the high-throughput screening of 192 chiral bidentate phosphine ligands and reaction conditions.[173] They found that the $Ni(OAc)_2$/**(*S*,*S*)-Me-DuPhos** complex with an iodide additive Bu_4NI enabled the AH of α,β-unsaturated esters with high yields and enantioselectivities. Since 2017, the X. Zhang group has developed a $Ni(OAc)_2$/**(*S*)-binapine** complex as an ideal catalyst for the AH of a series of tri- and tetrasubstituted alkene substrates with outstanding efficiencies and enantioselectivities.[174-177] Recently, they employed **(*S*,*S*)-Ph-BPE** as an effective ligand for the nickel-catalysed AH of β-boronic ester substituted α,β-unsaturated carboxylic esters[178] and γ,γ-

disubstituted cyclohexadienones.[179] Notably, the latter work offered a superior method to construct all-carbon quaternary stereocenters. In parallel, W. Zhang et al. established a $Ni(OAc)_2$/**(*S*)-DM-MeO-BIPHEP** catalyst for the AH of 2-amidoacrylates with excellent reactivities and enantioselectivities.[180]

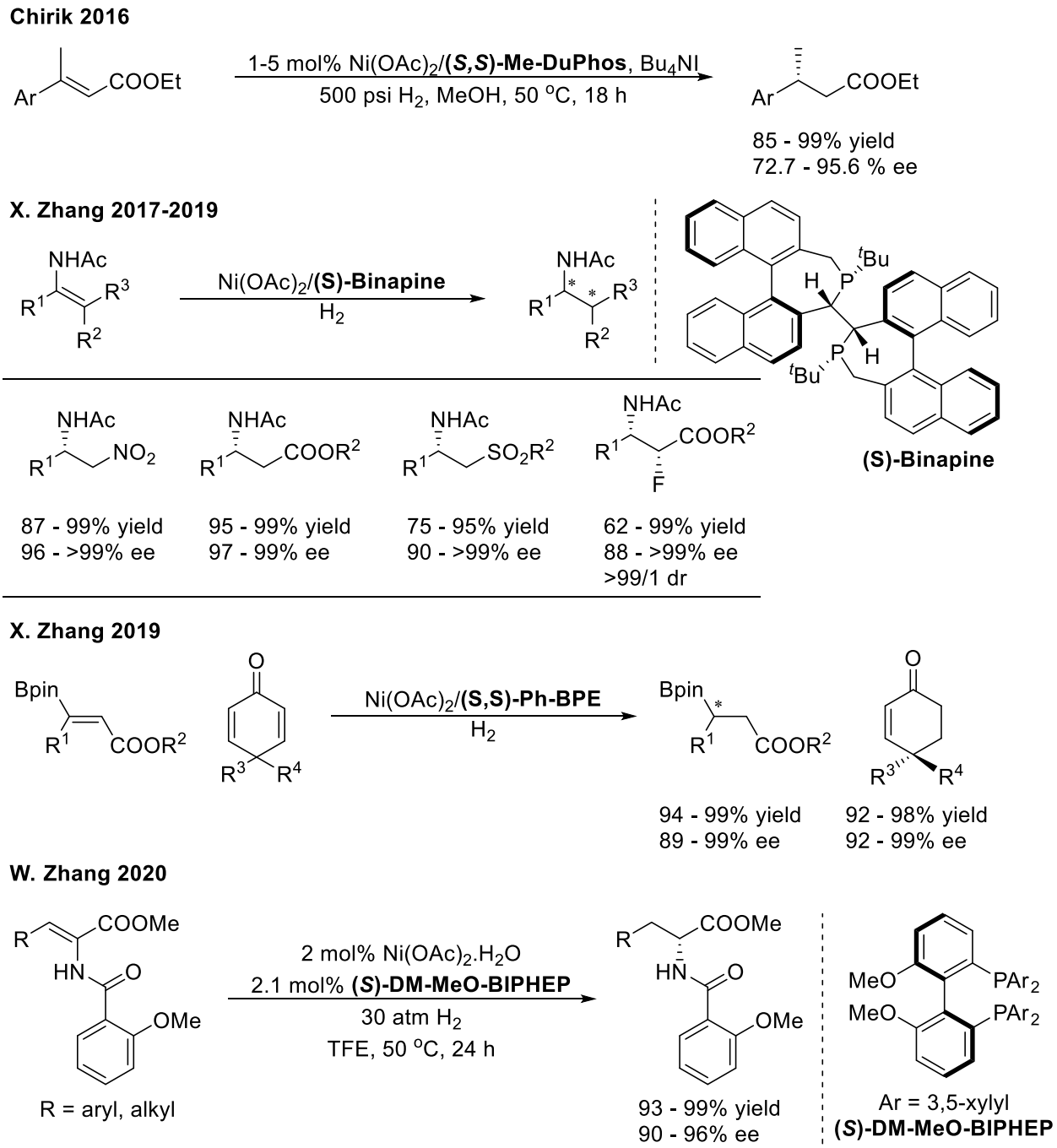

Scheme 1.31 Chiral bidentate phosphines for the Ni-catalyzed AH of C=C bonds

The nickel-catalysed AH of imines has been developed only recently (Scheme 1.32). W. Zhang et al. reported the first nickel-catalysed AH of N-sulfonyl imines using **(*R,R*)-QuinoxP*** as a chiral ligand.[181] This method achieved excellent enantioselectivities (ee up to 99.7%) and extremely high reactivities (TON up to 10,500) for the AH of N-^{t}Bu-sulfonyl imines, representing the highest efficiency so in the field of nickel-catalysed AH. Meanwhile, X. Zhang et al. used the $Ni(OAc)_2$/**(*S,S*)-Ph-BPE** catalyst system for the highly efficient AH of cyclic sulfamidate imines[182] and *α,β*-unsaturated ketoimines.[183]

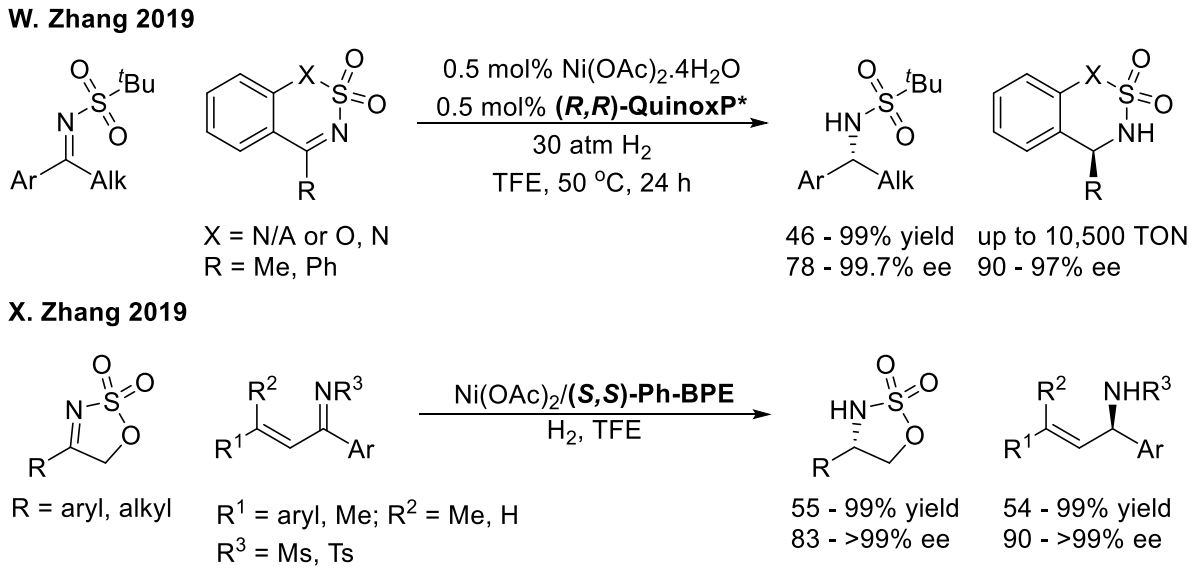

Scheme 1.32 Chiral bidentate phosphines for the Ni-catalyzed AH of C=N bonds

1.1.3.4 Chiral copper catalysts

Copper-catalysed AH has developed very slowly, with only a handful of examples of the AH of C=O and C=C bonds catalysed by Cu(I) or Cu(Ⅱ) precursors with chiral ligands reported to date (Scheme 1.33). Shimizu,[184] Beller,[185] and Hatcher/Johnson[186] et al. respectively described initial attempts at the copper-catalysed AH of simple ketones using bisphosphine or monophosphine ligands. In 2018, Rodriguez/D. Zhang/Kozlowski et al reported the synthesis of a new family of dimeric heterophosphole ligands (**BABIPhos**) and the corresponding copper complexes for the AH of 2-

substituted ketones *via* dynamic kinetic resolution with high diastereoselectivities and enantioselectivities.[187] In an alternative approach, Shimizu/Ohshima/Mashima et al developed a Cu(I)/**DTBM-SEGPHOS** catalyst for the 1,4-selective reduction of enones,[188] and recently Teichert et al. attempted to employ chiral N-heterocyclic carbene ligands for the copper-catalysed AH of enoate.[189]

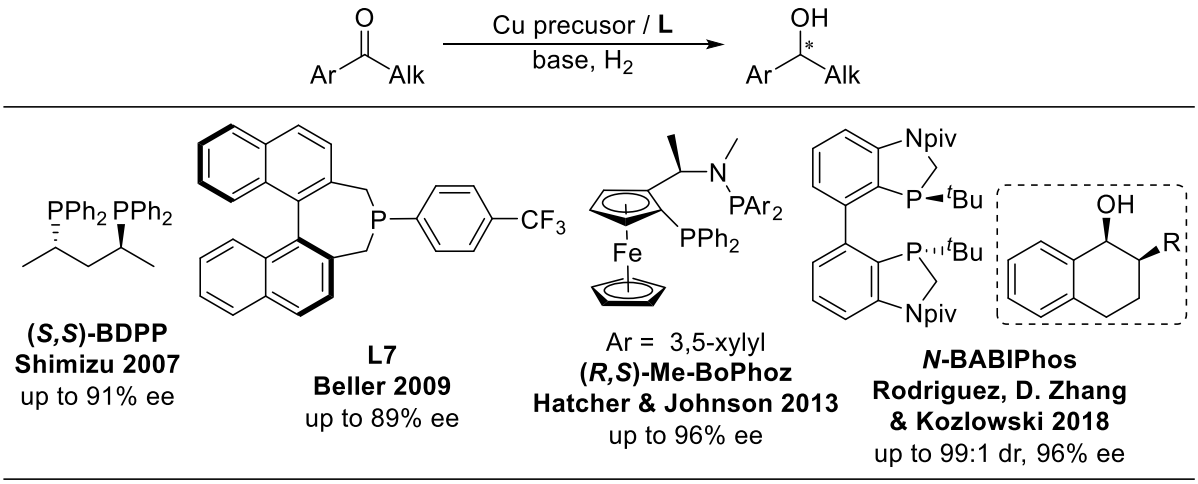

Scheme 1.33 Chiral phosphines for the Cu-catalyzed AH of ketones

1.1.4 Conclusion

Over the past half century, the homogeneous catalysis of AH has experienced a prosperous era. Thousands of chiral phosphine ligands have been developed for a great variety of substrates containing C=C, C=O or C=N bonds, providing products with extremely high reactivities (up to 4,550,000 TON) and ideal enantioselectivities (up to 99.9% ee). Some catalyst systems have been successfully applied for the industrial synthesis of a series of important chiral chemicals. Moreover, all kinds of metals have been used as efficient metal precursors, including noble metals such as rhodium, ruthenium, iridium, palladium and platinum, and non-noble metals such as manganese, iron, cobalt, nickel and copper.

However, there are still some significant challenges in the field of AH. Firstly, a long-standing issue is that challenging substrates such as dialkyl ketones and oxime can not be hydrogenated with excellent enantioselectivities. And secondly, most chiral ligands are not suitable for industrial processes because of low efficiencies, complicated syntheses or poor air stabilities. Finally, earth-abundant metal-catalysed AH is far from satisfactory.

To solve these existing problems in the field of AH, we should still focus on the development of novel efficient chiral ligands. In the Zhang group, ligand design for AH has always been a core topic. Empirically, we summarize four principles for designing chiral ligands: high rigidity, new ligand scaffolds, the opportunity to electronically and sterically fine tune, and ease of synthesis. In this thesis, we aim to develop more efficient chiral ferrocenyl phosphine ligands for AH catalysed in particular by earth-abundant metals.

1.2 References

[1] R. Noyori, *Asymmetric Catalysis In Organic Synthesis*, Wiley, New York, **1994**.

[2] H. Brunner, in *Applied Homogeneous Catalysis with Organometallic Compounds, Second Edition, Vol. 1*, **2008**, pp. 195-212.

[3] J. G. De Vries, C. J. Elsevier, *The Handbook of Homogeneous Hydrogenation*, Wiley-VCH, **2006**.

[4] G. Jannes, V. Dubois, *Chiral Reactions in Heterogeneous Catalysis*, Plenum, New York, **1995**.

[5] E. N. Jacobsen, A. Pfaltz, H. Yamamoto, *Comprehensive Asymmetric Catalysis I–III*, Springer, Berlin Heidelberg, **2003**.

[6] H.-U. Blaser, E. Schmidt, *Asymmetric Catalysis on Industrial Scale: Challenges, Approaches and Solutions*, Wiley, **2007**.

[7] W. S. Knowles, *Angewandte Chemie International Edition* **2002**, *41*, 1998-2007.

[8] R. Noyori, *Angewandte Chemie International Edition* **2002**, *41*, 2008-2022.

[9] W. S. Knowles, M. J. Sabacky, *Chemical Communications (London)* **1968**, 1445-1446.

[10] L. Horner, H. Siegel, H. Büthe, *Angewandte Chemie International Edition in English* **1968**, *7*, 942-942.

[11] J. A. Osborn, J. A. Osborn, F. H. Jardine, J. F. Young, G. Wilkinson, *Journal of the Chemical Society.* **1966**, 1711-1732.

[12] T. P. Dang, H. B. Kagan, *Journal of the Chemical Society D: Chemical Communications* **1971**, 481-481.

[13] H. B. Kagan, T.-P. Dang, *Journal of the American Chemical Society* **1972**, *94*, 6429-6433.

[14] W. S. Knowles, M. J. Sabacky, B. D. Vineyard, D. J. Weinkauff, *Journal of the American Chemical Society* **1975**, *97*, 2567-2568.

[15] B. D. Vineyard, W. S. Knowles, M. J. Sabacky, G. L. Bachman, D. J. Weinkauff, *Journal of the American Chemical Society* **1977**, *99*, 5946-5952.

[16] W. S. Knowles, *Accounts of Chemical Research* **1983**, *16*, 106-112.

[17] W. S. Knowles, *Journal of Chemical Education* **1986**, *63*, 222.

[18] W. S. Knowles, M. J. Sabacky, B. D. Vineyard, *Journal of the Chemical Society, Chemical Communications* **1972**, 10-11.

[19] M. D. Fryzuk, B. Bosnich, *Journal of the American Chemical Society* **1977**, *99*, 6262-6267.

[20] M. D. Fryzuk, B. Bosnich, *Journal of the American Chemical Society* **1979**, *101*, 3043-3049.

[21] M. D. Fryzuk, B. Bosnich, *Journal of the American Chemical Society* **1978**, *100*, 5491-5494.

[22] K. Achiwa, *Journal of the American Chemical Society* **1976**, *98*, 8265-8266.

[23] R. G. Glaser, S.; Twaik,, *Israel journal of chemistry* **1980**, *20*, 102-107.

[24] A. Miyashita, A. Yasuda, H. Takaya, K. Toriumi, T. Ito, T. Souchi, R. Noyori, *Journal of the American Chemical Society* **1980**, *102*, 7932-7934.

[25] R. Noyori, *Chemical Society Reviews* **1989**, *18*, 187-208.

[26] R. Noyori, H. Takaya, *Accounts of Chemical Research* **1990**, *23*, 345-350.

[27] R. Noyori, M. Ohta, Y. Hsiao, M. Kitamura, T. Ohta, H. Takaya, *Journal of the American Chemical Society* **1986**, *108*, 7117-7119.

[28] H. Takaya, T. Ohta, N. Sayo, H. Kumobayashi, S. Akutagawa, S. Inoue, I. Kasahara, R. Noyori, *Journal of the American Chemical Society* **1987**, *109*, 1596-1597.

[29] T. Ohta, H. Takaya, M. Kitamura, K. Nagai, R. Noyori, *The Journal of Organic Chemistry* **1987**, *52*, 3174-3176.

[30] R. Noyori, T. Ohkuma, M. Kitamura, H. Takaya, N. Sayo, H. Kumobayashi, S. Akutagawa, *Journal of the American Chemical Society* **1987**, *109*, 5856-5858.

[31] R. Noyori, T. Ikeda, T. Ohkuma, M. Widhalm, M. Kitamura, H. Takaya, S. Akutagawa, N. Sayo, T. Saito, T. Taketomi, H. Kumobayashi, *Journal of the American Chemical Society* **1989**, *111*, 9134-9135.

[32] T. Ohkuma, H. Ooka, S. Hashiguchi, T. Ikariya, R. Noyori, *Journal of the American Chemical Society* **1995**, *117*, 2675-2676.

[33] T. Chiba, A. Miyashita, H. Nohira, H. Takaya, *Tetrahedron Letters* **1991**, *32*, 4745-4748.

[34] T. Saito, T. Yokozawa, T. Ishizaki, T. Moroi, N. Sayo, T. Miura, H. Kumobayashi, *Advanced Synthesis & Catalysis* **2001**, *343*, 264-267.

[35] Z. Zhang, H. Qian, J. Longmire, X. Zhang, *The Journal of Organic Chemistry* **2000**, *65*, 6223-6226.

[36] G. Michaud, M. Bulliard, L. Ricard, J. P. Gene t, A. Marinetti, *Chem. Eur. J.* **2002**, *8*, 3327-3330.

[37] C.-C. Pai, C.-W. Lin, C.-C. Lin, C.-C. Chen, A. S. C. Chan, W. T. Wong, *Journal of the American Chemical Society* **2000**, *122*, 11513-11514.

[38] W. Tang, X. Zhang, *Chemical Reviews* **2003**, *103*, 3029-3070.

[39] M. J. Burk, J. E. Feaster, R. L. Harlow, *Organometallics* **1990**, *9*, 2653-2655.

[40] M. J. Burk, *Accounts of Chemical Research* **2000**, *33*, 363-372.

[41] T. Imamoto, J. Watanabe, Y. Wada, H. Masuda, H. Yamada, H. Tsuruta, S. Matsukawa, K. Yamaguchi, *Journal of the American Chemical Society* **1998**, *120*, 1635-1636.

[42] I. D. Gridnev, N. Higashi, T. Imamoto, *Journal of the American Chemical Society* **2001**, *123*, 4631-4632.

[43] Ilya D. Gridnev, Y. Yamanoi, N. Higashi, H. Tsuruta, M. Yasutake, T. Imamoto, *Advanced Synthesis & Catalysis* **2001**, *343*, 118-136.

[44] I. D. Gridnev, M. Yasutake, N. Higashi, T. Imamoto, *Journal of the American Chemical Society* **2001**, *123*, 5268-5276.

[45] M. Yasutake, I. D. Gridnev, N. Higashi, T. Imamoto, *Organic Letters* **2001**, *3*, 1701-1704.

[46] W. Tang, X. Zhang, *Angewandte Chemie International Edition* **2002**, *41*, 1612-1614.

[47] W. Tang, X. Zhang, *Organic Letters* **2002**, *4*, 4159-4161.

[48] W. Tang, D. Liu, X. Zhang, *Organic Letters* **2003**, *5*, 205-207.

[49] D. Liu, X. Zhang, *European Journal of Organic Chemistry* **2005**, *2005*, 646-649.

[50] X. Zhang, K. Huang, G. Hou, B. Cao, X. Zhang, *Angewandte Chemie International Edition* **2010**, *49*, 6421-6424.

[51] W. Tang, W. Wang, Y. Chi, X. Zhang, *Angewandte Chemie International Edition* **2003**, *42*, 3509-3511.

[52] W. Tang, B. Qu, A. G. Capacci, S. Rodriguez, X. Wei, N. Haddad, B. Narayanan, S. Ma, N. Grinberg, N. K. Yee, D. Krishnamurthy, C. H. Senanayake, *Organic Letters* **2010**, *12*, 176-179.

[53] A. Pfaltz, *Acta Chemica Scandinavica* **1996**, *50*, 189-194.

[54] G. Helmchen, A. Pfaltz, *Accounts of Chemical Research* **2000**, *33*, 336-345.

[55] A. Lightfoot, P. Schnider, A. Pfaltz, *Angewandte Chemie International Edition* **1998**, *37*, 2897-2899.

[56] D. G. Blackmond, A. Lightfoot, A. Pfaltz, T. Rosner, P. Schnider, N. Zimmermann, *Chirality* **2000**, *12*, 442-449.

[57] S. P. Smidt, N. Zimmermann, M. Studer, A. Pfaltz, *Chemistry* **2004**, *10*, 4685-4693.

[58] A. S. C. Chan, W. Hu, C.-C. Pai, C.-P. Lau, Y. Jiang, A. Mi, M. Yan, J. Sun, R. Lou, J. Deng, *Journal of the American Chemical Society* **1997**, *119*, 9570-9571.

[59] J.-H. Xie, L.-X. Wang, Y. Fu, S.-F. Zhu, B.-M. Fan, H.-F. Duan, Q.-L. Zhou, *Journal of the American Chemical Society* **2003**, *125*, 4404-4405.

[60] S. Liu, J. H. Xie, L. X. Wang, Q. L. Zhou, *Angew Chem Int Ed Engl* **2007**, *46*, 7506-7508.

[61] Z.-T. Zhou, J.-H. Xie, Q.-L. Zhou, *Advanced Synthesis & Catalysis* **2009**, *351*, 363-366.

[62] J. H. Xie, X. Y. Liu, J. B. Xie, L. X. Wang, Q. L. Zhou, *Angew Chem Int Ed Engl* **2011**, *50*, 7329-7332.

[63] J. H. Xie, X. Y. Liu, X. H. Yang, J. B. Xie, L. X. Wang, Q. L. Zhou, *Angew Chem Int Ed Engl* **2012**, *51*, 201-203.

[64] F.-H. Zhang, F.-J. Zhang, M.-L. Li, J.-H. Xie, Q.-L. Zhou, *Nature Catalysis* **2020**, *3*, 621-627.

[65] T. J. Kealy, P. L. Pauson, *Nature* **1951**, *168*, 1039-1040.

[66] G. Wilkinson, *Journal of Organometallic Chemistry* **1975**, *100*, 273-278.

[67] G. B. Kauffman, *Journal of Chemical Education* **1983**, *60*, 185.

[68] A. Togni, T. Hayashi, *Ferrocenes: homogeneous catalysis, organic synthesis, materials science*, Weinheim Cambridge, **1995**.

[69] T. J. Colacot, *Chemical Reviews* **2003**, *103*, 3101-3118.

[70] R. Gomez Arrayas, J. Adrio, J. C. Carretero, *Angew Chem Int Ed Engl* **2006**, *45*, 7674-7715.

[71] A. Togni, C. Breutel, A. Schnyder, F. Spindler, H. Landert, A. Tijani, *Journal of the American Chemical Society* **1994**, *116*, 4062-4066.

[72] H.-U. Blaser, *Chimia* **1999**, *53*, 275-280.

[73] H.-U. Blaser, *Advanced Synthesis & Catalysis* **2002**, *344*, 17-31.

[74] M. Sawamura, H. Hamashima, M. Sugawara, R. Kuwano, Y. Ito, *Organometallics* **1995**, *14*, 4549-4558.

[75] M. Sawamura, R. Kuwano, Y. Ito, *Journal of the American Chemical Society* **1995**, *117*, 9602-9603.

[76] R. Kuwano, S. Okuda, Y. Ito, *The Journal of Organic Chemistry* **1998**, *63*, 3499-3503.

[77] R. Kuwano, K. Sato, T. Kurokawa, D. Karube, Y. Ito, *Journal of the American Chemical Society* **2000**, *122*, 7614-7615.

[78] J. J. Almena Perea, A. Börner, P. Knochel, *Tetrahedron Letters* **1998**, *39*, 8073-8076.

[79] J. J. Almena Perea, M. Lotz, P. Knochel, *Tetrahedron: Asymmetry* **1999**, *10*, 375-384.

[80] M. Lotz, T. Ireland, J. J. Almena Perea, P. Knochel, *Tetrahedron: Asymmetry* **1999**, *10*, 1839-1842.

[81] T. Ireland, G. Grossheimann, C. Wieser-Jeunesse, P. Knochel, *Angewandte Chemie International Edition* **1999**, *38*, 3212-3215.

[82] F. Maienza, M. Wörle, P. Steffanut, A. Mezzetti, F. Spindler, *Organometallics* **1999**, *18*, 1041-1049.

[83] U. Nettekoven, P. C. J. Kamer, P. W. N. M. van Leeuwen, M. Widhalm, A. L. Spek, M. Lutz, *The Journal of Organic Chemistry* **1999**, *64*, 3996-4004.

[84] A. Marinetti, F. Labrue, J.-P. Genêt, *Synlett* **1999**, *1999*, 1975-1977.

[85] U. Berens, M. J. Burk, A. Gerlach, W. Hems, *Angewandte Chemie International Edition* **2000**, *39*, 1981-1984.

[86] D. Xiao, X. Zhang, *Angewandte Chemie International Edition* **2001**, *40*, 3425-3428.

[87] D. Liu, W. Li, X. Zhang, *Organic Letters* **2002**, *4*, 4471-4474.

[88] N. W. Boaz, S. D. Debenham, E. B. Mackenzie, S. E. Large, *Organic Letters* **2002**, *4*, 2421-2424.

[89] T. Sturm, W. Weissensteiner, F. Spindler, *Advanced Synthesis & Catalysis* **2003**, *345*, 160-164.

[90] O. B. Sutcliffe, M. R. Bryce, *Tetrahedron: Asymmetry* **2003**, *14*, 2297-2325.

[91] S.-M. Lu, X.-W. Han, Y.-G. Zhou, *Advanced Synthesis & Catalysis* **2004**, *346*, 909-912.

[92] C. Bissantz, B. Kuhn, M. Stahl, *Journal of Medicinal Chemistry* **2010**, *53*, 5061-5084.

[93] J.-M. Lehn, *Supramolecular Chemistry: Concepts and Perspectives*, Weinheim Cambridge, **1995**.

[94] H.-J. Schneider, *Angewandte Chemie International Edition* **2009**, *48*, 3924-3977.

[95] A. Warshel, P. K. Sharma, M. Kato, Y. Xiang, H. Liu, M. H. M. Olsson, *Chemical Reviews* **2006**, *106*, 3210-3235.

[96] R. R. Knowles, E. N. Jacobsen, *Proc. Natl. Acad. Sci. U. S. A* **2010**, *107*, 20678-20685.

[97] T. Hayashi, M. Kumada, *Accounts of Chemical Research* **1982**, *15*, 395-401.

[98] T. Hayashi, N. Kawamura, Y. Ito, *Journal of the American Chemical Society* **1987**, *109*, 7876-7878.

[99] W. Chen, P. J. McCormack, K. Mohammed, W. Mbafor, S. M. Roberts, J. Whittall, *Angew Chem Int Ed Engl* **2007**, *46*, 4141-4144.

[100] W. Chen, F. Spindler, B. Pugin, U. Nettekoven, *Angew Chem Int Ed Engl* **2013**, *52*, 8652-8656.

[101] C. Chen, H. Wang, Z. Zhang, S. Jin, S. Wen, J. Ji, L. W. Chung, X.-Q. Dong, X. Zhang, *Chem Sci* **2016**, *7*, 6669-6673.

[102] C. Chen, Z. Zhang, S. Jin, X. Fan, M. Geng, Y. Zhou, S. Wen, X. Wang, L. W. Chung, X.-Q. Dong, X. Zhang, *Angewandte Chemie International Edition* **2017**, *56*, 6808-6812.

[103] C. Chen, S. Wen, M. Geng, S. Jin, Z. Zhang, X.-Q. Dong, X. Zhang, *Chemical communications* **2017**, *53*, 9785-

9788.

[104] Q. Zhao, S. Li, K. Huang, R. Wang, X. Zhang, *Organic Letters* **2013**, *15*, 4014-4017.

[105] Q. Zhao, C. Chen, J. Wen, X. Q. Dong, X. Zhang, *Acc Chem Res* **2020**, *53*, 1905-1921.

[106] H. Wang, J. Wen, X. Zhang, *Chemical Reviews* **2021**, *121*, 7530-7567.

[107] Y. Jiang, Q. Jiang, G. Zhu, X. Zhang, *Tetrahedron Letters* **1997**, *38*, 215-218.

[108] J. Yutong, J. Qiongzhong, Z. Guoxin, Z. Xumu, *Tetrahedron Letters* **1997**, *38*, 6565-6568.

[109] Y. Jiang, Q. Jiang, X. Zhang, *Journal of the American Chemical Society* **1998**, *120*, 3817-3818.

[110] H. Nie, G. Zhou, Q. Wang, W. Chen, S. Zhang, *Tetrahedron: Asymmetry* **2013**, *24*, 1567-1571.

[111] C. J. Hou, X. P. Hu, *Org Lett* **2016**, *18*, 5592-5595.

[112] F. Ling, S. Nian, J. Chen, W. Luo, Z. Wang, Y. Lv, W. Zhong, *J Org Chem* **2018**, *83*, 10749-10761.

[113] W. Wu, S. Liu, M. Duan, X. Tan, C. Chen, Y. Xie, Y. Lan, X. Q. Dong, X. Zhang, *Org Lett* **2016**, *18*, 2938-2941.

[114] J. Yu, J. Long, Y. Yang, W. Wu, P. Xue, L. W. Chung, X. Q. Dong, X. Zhang, *Org Lett* **2017**, *19*, 690-693.

[115] J. Yu, M. Duan, W. Wu, X. Qi, P. Xue, Y. Lan, X. Q. Dong, X. Zhang, *Chemistry* **2017**, *23*, 970-975.

[116] Z. Liang, T. Yang, G. Gu, L. Dang, X. Zhang, *Chinese Journal of Chemistry* **2018**, *36*, 851-856.

[117] F. Kallmeier, R. Kempe, *Angew Chem Int Ed Engl* **2018**, *57*, 46-60.

[118] T. Zell, R. Langer, *ChemCatChem* **2018**, *10*, 1930-1940.

[119] Z. Zhang, N. A. Butt, M. Zhou, D. Liu, W. Zhang, *Chinese Journal of Chemistry* **2018**, *36*, 443-454.

[120] J. Wen, F. Wang, X. Zhang, *Chemical Society Reviews* **2021**, *50*, 3211-3237.

[121] J. S. Chen, L. L. Chen, Y. Xing, G. Chen, W. Y. Shen, Z. R. Dong, Y.-Y. Li, J. X. Gao, *Acta Chim. Sinica* **2004**, *62*.

[122] C. Sui-Seng, F. Freutel, A. J. Lough, R. H. Morris, *Angewandte Chemie International Edition* **2008**, *47*, 940-943.

[123] A. Mikhailine, A. J. Lough, R. H. Morris, *Journal of the American Chemical Society* **2009**, *131*, 1394-1395.

[124] A. Berkessel, S. Reichau, A. von der Höh, N. Leconte, J. r.-M. Neudörfl, *Organometallics* **2011**, *30*, 3880-3887.

[125] P. O. Lagaditis, A. J. Lough, R. H. Morris, *Journal of the American Chemical Society* **2011**, *133*, 9662-9665.

[126] W. Zuo, J. Lough Alan, F. Li Young, H. Morris Robert, *Science* **2013**, *342*, 1080-1083.

[127] R. Bigler, E. Otth, A. Mezzetti, *Organometallics* **2014**, *33*, 4086-4099.

[128] R. Bigler, R. Huber, A. Mezzetti, *Angewandte Chemie International Edition* **2015**, *54*, 5171-5174.

[129] L. De Luca, A. Mezzetti, *Angewandte Chemie International Edition* **2017**, *56*, 11949-11953.

[130] C. A. M. R. van Slagmaat, K. C. Chou, L. Morick, D. Hadavi, B. Blom, S. M. A. De Wildeman, *Catalysts* **2019**, *9*.

[131] S. Yu, W. Shen, Y. Li, Z. Dong, Y. Xu, Q. Li, J. Zhang, J. Gao, *Advanced Synthesis & Catalysis* **2012**, *354*, 818-

822.

[132] W. Zuo, S. Tauer, D. E. Prokopchuk, R. H. Morris, *Organometallics* **2014**, *33*, 5791-5801.

[133] P. O. Lagaditis, P. E. Sues, J. F. Sonnenberg, K. Y. Wan, A. J. Lough, R. H. Morris, *J Am Chem Soc* **2014**, *136*, 1367-1380.

[134] S. A. M. Smith, P. O. Lagaditis, A. Lupke, A. J. Lough, R. H. Morris, *Chemistry* **2017**, *23*, 7212-7216.

[135] A. Zirakzadeh, K. Kirchner, A. Roller, B. Stöger, M. Widhalm, R. H. Morris, *Organometallics* **2016**, *35*, 3781-3787.

[136] R. Huber, A. Passera, A. Mezzetti, *Organometallics* **2018**, *37*, 396-405.

[137] R. Huber, A. Passera, E. Gubler, A. Mezzetti, *Advanced Synthesis & Catalysis* **2018**, *360*, 2900-2913.

[138] M. Garbe, Z. Wei, B. Tannert, A. Spannenberg, H. Jiao, S. Bachmann, M. Scalone, K. Junge, M. Beller, *Advanced Synthesis & Catalysis* **2019**, *361*, 1913-1920.

[139] C. S. G. Seo, T. Tannoux, S. A. M. Smith, A. J. Lough, R. H. Morris, *J Org Chem* **2019**, *84*, 12040-12049.

[140] Y. Li, S. Yu, X. Wu, J. Xiao, W. Shen, Z. Dong, J. Gao, *Journal of the American Chemical Society* **2014**, *136*, 4031-4039.

[141] R. Ferraccioli, *Letters in Organic Chemistry* **2017**, *14*.

[142] C. P. Casey, H. Guan, *Journal of the American Chemical Society* **2007**, *129*, 5816-5817.

[143] P. Gajewski, M. Renom-Carrasco, S. V. Facchini, L. Pignataro, L. Lefort, J. G. de Vries, R. Ferraccioli, U. Piarulli, C. Gennari, *European Journal of Organic Chemistry* **2015**, *2015*, 5526-5536.

[144] P. Gajewski, M. Renom-Carrasco, S. V. Facchini, L. Pignataro, L. Lefort, J. G. de Vries, R. Ferraccioli, A. Forni, U. Piarulli, C. Gennari, *European Journal of Organic Chemistry* **2015**, *2015*, 1887-1893.

[145] R. Hodgkinson, A. Del Grosso, G. Clarkson, M. Wills, *Dalton Trans* **2016**, *45*, 3992-4005.

[146] D. S. Mérel, S. Gaillard, T. R. Ward, J.-L. Renaud, *Catalysis Letters* **2016**, *146*, 564-569.

[147] X. Bai, M. Cettolin, G. Mazzoccanti, M. Pierini, U. Piarulli, V. Colombo, A. Dal Corso, L. Pignataro, C. Gennari, *Tetrahedron* **2019**, *75*, 1415-1424.

[148] S. Zhou, S. Fleischer, K. Junge, M. Beller, *Angew Chem Int Ed Engl* **2011**, *50*, 5120-5124.

[149] S. Fleischer, S. Zhou, S. Werkmeister, K. Junge, M. Beller, *Chemistry* **2013**, *19*, 4997-5003.

[150] S. Zhou, S. Fleischer, H. Jiao, K. Junge, M. Beller, *Advanced Synthesis & Catalysis* **2014**, *356*, 3451-3455.

[151] L. Q. Lu, Y. Li, K. Junge, M. Beller, *J Am Chem Soc* **2015**, *137*, 2763-2768.

[152] D. Brenna, S. Rossi, F. Cozzi, M. Benaglia, *Org Biomol Chem* **2017**, *15*, 5685-5688.

[153] M. Cettolin, X. Bai, D. Lübken, M. Gatti, S. V. Facchini, U. Piarulli, L. Pignataro, C. Gennari, *European Journal of Organic Chemistry* **2019**, *2019*, 647-654.

[154] L. Nindakova, F. Shmidt, E. Klabunovskii, V. Sheveleva, V. Pavlov, *Bulletin of the Academy of Sciences of the USSR Division of Chemical Science* **1981**, *30*, 2177-2178.

[155] Y. Ohgo, S. Takeuchi, Y. Natori, J. Yoshimura, *Bulletin of the Chemical Society of Japan* **1981**, *54*, 2124-2135.

[156] K. Yoshinaga, T. Kito, H. Oka, S. Sakaki, K. Ohkubo, *Journal of Catalysis* **1984**, *87*, 517-519.

[157] P. Le Maux, V. Massonneau, G. Simonneaux, *Journal of Organometallic Chemistry* **1985**, *284*, 101-108.

[158] V. Massonneau, P. Le Maux, G. Simonneaux, *Journal of Organometallic Chemistry* **1985**, *288*, c59-c60.

[159] U. Leutenegger, A. Madin, A. Pfaltz, *Angewandte Chemie International Edition in English* **1989**, *28*, 60-61.

[160] S. Monfette, Z. R. Turner, S. P. Semproni, P. J. Chirik, *J Am Chem Soc* **2012**, *134*, 4561-4564.

[161] M. R. Friedfeld, M. Shevlin, G. W. Margulieux, L. C. Campeau, P. J. Chirik, *J Am Chem Soc* **2016**, *138*, 3314-3324.

[162] P. Viereck, S. Krautwald, T. P. Pabst, P. J. Chirik, *J Am Chem Soc* **2020**, *142*, 3923-3930.

[163] J. Chen, C. Chen, C. Ji, Z. Lu, *Org Lett* **2016**, *18*, 1594-1597.

[164] J. Guo, B. Cheng, X. Shen, Z. Lu, *J Am Chem Soc* **2017**, *139*, 15316-15319.

[165] M. R. Friedfeld, M. Shevlin, J. M. Hoyt, S. W. Krska, M. T. Tudge, P. J. Chirik, *Science* **2013**, *342*, 1076.

[166] M. R. Friedfeld, H. Zhong, R. T. Ruck, M. Shevlin, P. J. Chirik, *Science* **2018**, *360*, 888.

[167] H. Zhong, M. Shevlin, P. J. Chirik, *J Am Chem Soc* **2020**, *142*, 5272-5281.

[168] X. Du, Y. Xiao, J. M. Huang, Y. Zhang, Y. N. Duan, H. Wang, C. Shi, G. Q. Chen, X. Zhang, *Nat Commun* **2020**, *11*, 3239.

[169] M. Amézquita-Valencia, A. Cabrera, *Journal of Molecular Catalysis A: Chemical* **2013**, *366*, 17-21.

[170] Y. Hu, Z. Zhang, J. Zhang, Y. Liu, I. D. Gridnev, W. Zhang, *Angew Chem Int Ed Engl* **2019**, *58*, 15767-15771.

[171] Y. Hamada, Y. Koseki, T. Fujii, T. Maeda, T. Hibino, K. Makino, *Chemical Communications* **2008**, 6206-6208.

[172] T. Hibino, K. Makino, T. Sugiyama, Y. Hamada, *ChemCatChem* **2009**, *1*, 237-240.

[173] M. Shevlin, M. R. Friedfeld, H. Sheng, N. A. Pierson, J. M. Hoyt, L.-C. Campeau, P. J. Chirik, *Journal of the American Chemical Society* **2016**, *138*, 3562-3569.

[174] W. Gao, H. Lv, T. Zhang, Y. Yang, L. W. Chung, Y.-D. Wu, X. Zhang, *Chem Sci* **2017**, *8*, 6419-6422.

[175] X. Li, C. You, S. Li, H. Lv, X. Zhang, *Organic Letters* **2017**, *19*, 5130-5133.

[176] J. Long, W. Gao, Y. Guan, H. Lv, X. Zhang, *Organic Letters* **2018**, *20*, 5914-5917.

[177] Y.-Q. Guan, Z. Han, X. Li, C. You, X. Tan, H. Lv, X. Zhang, *Chem Sci* **2019**, *10*, 252-256.

[178] Z. Han, G. Liu, X. Zhang, A. Li, X.-Q. Dong, X. Zhang, *Organic Letters* **2019**, *21*, 3923-3926.

[179] C. You, X. Li, Q. Gong, J. Wen, X. Zhang, *Journal of the American Chemical Society* **2019**, *141*, 14560-14564.

[180] Y. Hu, J. Chen, B. Li, Z. Zhang, I. D. Gridnev, W. Zhang, *Angew Chem Int Ed Engl* **2020**, *59*, 5371-5375.

[181] B. Li, J. Chen, Z. Zhang, I. D. Gridnev, W. Zhang, *Angew Chem Int Ed Engl* **2019**, *58*, 7329-7334.

[182] Y. Liu, Z. Yi, X. Tan, X.-Q. Dong, X. Zhang, *iScience* **2019**, *19*, 63-73.

[183] X. Zhao, F. Zhang, K. Liu, X. Zhang, H. Lv, *Organic Letters* **2019**, *21*, 8966-8969.

[184] H. Shimizu, D. Igarashi, W. Kuriyama, Y. Yusa, N. Sayo, T. Saito, *Organic Letters* **2007**, *9*, 1655-1657.

[185] K. Junge, B. Wendt, D. Addis, S. Zhou, S. Das, S. Fleischer, M. Beller, *Chemistry* **2011**, *17*, 101-105.

[186] S. W. Krabbe, M. A. Hatcher, R. K. Bowman, M. B. Mitchell, M. S. McClure, J. S. Johnson, *Organic Letters* **2013**, *15*, 4560-4563.

[187] Olga V. Zatolochnaya, S. Rodríguez, Y. Zhang, K. S. Lao, S. Tcyrulnikov, G. Li, X.-J. Wang, B. Qu, S. Biswas, H. P. R. Mangunuru, D. Rivalti, J. D. Sieber, J.-N. Desrosiers, J. C. Leung, N. Grinberg, H. Lee, N. Haddad, N. K. Yee, J. J. Song, M. C. Kozlowski, C. H. Senanayake, *Chem Sci* **2018**, *9*, 4505-4510.

[188] H. Shimizu, T. Nagano, N. Sayo, T. Saito, T. Ohshima, K. Mashima, *Synlett* **2009**, *2009*, 3143-3146.

[189] B. M. Zimmermann, S. C. K. Kobosil, J. F. Teichert, *Chemical Communications* **2019**, *55*, 2293-2296.

Chapter 2 *C_1*-Symmetric PNP Ligands for Manganese-Catalyzed Enantioselective Hydrogenation of Ketones: Reaction Scope and Enantioinduction Model

This chapter (page 50 – 192) is adapted with permission from {*ACS Catalysis* **2020**, 10, 23, 13794 – 13799}. Copyright {2020} American Chemical Society. Liyao Zeng is the first author and performed all the synthesis and catalysis studies. Huaxin Yang and Menglong Zhao are acknowledged for their preparations of compound **2**, **3a**, **4a** and PNP ligand **5a** in large scales (up to 20 g) using my synthesis procedures (Scheme 2.1). Dr Jialin Wen is acknowledged for performing the computational modelling studies.

2.1 Introduction

Transition metal-catalyzed asymmetric hydrogenation (AH) of ketones has evolved as one of the most efficient catalytic transformations for the production of chiral molecules. Since Noyori's landmark Ru/bisphosphine-diamine system,[1] this transformation has embraced a prosperous era. Highly enantioselective catalytic systems with remarkably high turnover numbers (TON) have been successfully established with ruthenium(II) and iridium(III).[2-3] However, because of the low abundance of noble metals in the Earth's crust and corresponding future risks of supply, along with high costs and fluctuating prices in the global market, the sustainability of noble metal catalysis may be in jeopardy in the future. This has resulted in the replacement of noble metals in catalysts with earth-abundant metals becoming increasingly popular in the new millennium. The development of iron-catalyzed asymmetric (transfer) hydrogenation of ketones began earlier compared with other first-row transition metals,[4] with several successful catalytic systems emerging in the past two decades.[5-14]

Manganese, with its extremely large reserve as manganese nodules on the sea bottom, is another potential alternative to noble metals. Its high abundance and readily refining technology have made it the second cheapest transition metal for a long time, just behind iron. Accordingly, the development of manganese-catalyzed synthetic methodologies is now a popular area for chemists. However, the manganese-catalyzed AH of ketones is a relatively new topic, and only a few catalytic systems have been developed so far (Figure 2.1).

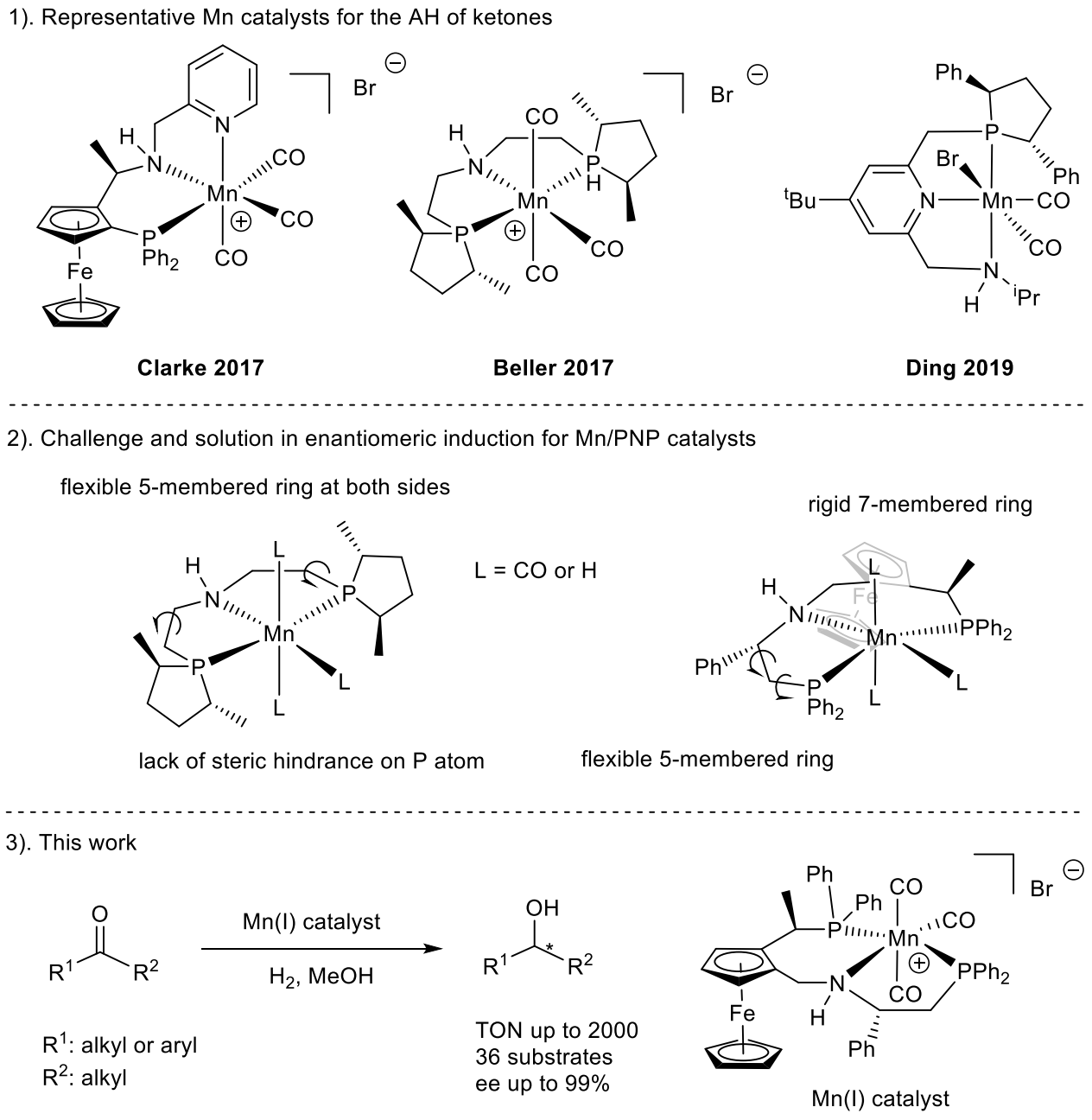

Figure 2.1 Representative Mn catalysts for the AH of ketones: success and limitation.

The first breakthrough was achieved by Clarke and co-workers with a ferrocene-based PNN ligand for the Mn-catalyzed AH. Moderate to high enantioselectivities were obtained with a series of simple ketones.[15] In 2019, the same group developed a more active Mn-PNN catalyst, containing an electron-rich phosphine and an electron-rich pyridine, affording up to 10,000 TON in the AH of ketones.[16] In 2019, Ding and Han reported a lutidine-based chiral PNN ligand for the Mn-catalyzed AH of ketones

with improved ee values.[17] The substrate scope was impressive in this study. In comparison,[18-20] chiral PNP groups have been shown to be a promising category of ligand for controlling stereoselectivity in the Mn(I)-catalyzed hydrogenation of carbonyls.[21] Much of the work in this area has been carried out by Kirchner and Beller. Kirchner and co-workers prepared a Mn/PNP complex via imine coordination and applied this catalyst in the transfer hydrogenation of ketones.[22] Moderate enantioselectivities (20% - 85% ee) were obtained. In the same year, Beller reported the application of a chiral PNP pincer ligand in the Mn-catalyzed direct AH of ketone.[23] Dialkyl ketones were hydrogenated with moderate enantioselectivities (30% - 84% ee). In our analysis, the flexibility of the skeleton and the resulting unchained conformation might be responsible for the insufficient enantiomeric induction. On the basis of our experience in ligand design and homogeneous hydrogenation, we rationalized that increasing the rigidity of the backbone by introducing a 7-membered ring with a planar chiral ferrocene moiety in a fixed conformation would result in the desired enantioinduction.

2.2 Synthesis of PNP ligands

According to the philosophy in ligand design, a series of ferrocene-based chiral **PNP** ligands were readily synthesized (Scheme 2.1). From commercially available Ugi's amine, a four-step synthesis gave the target ligands in good yields. The modular design enables high tunability on both P sides, making a mini library of ligands possible for fast screening.

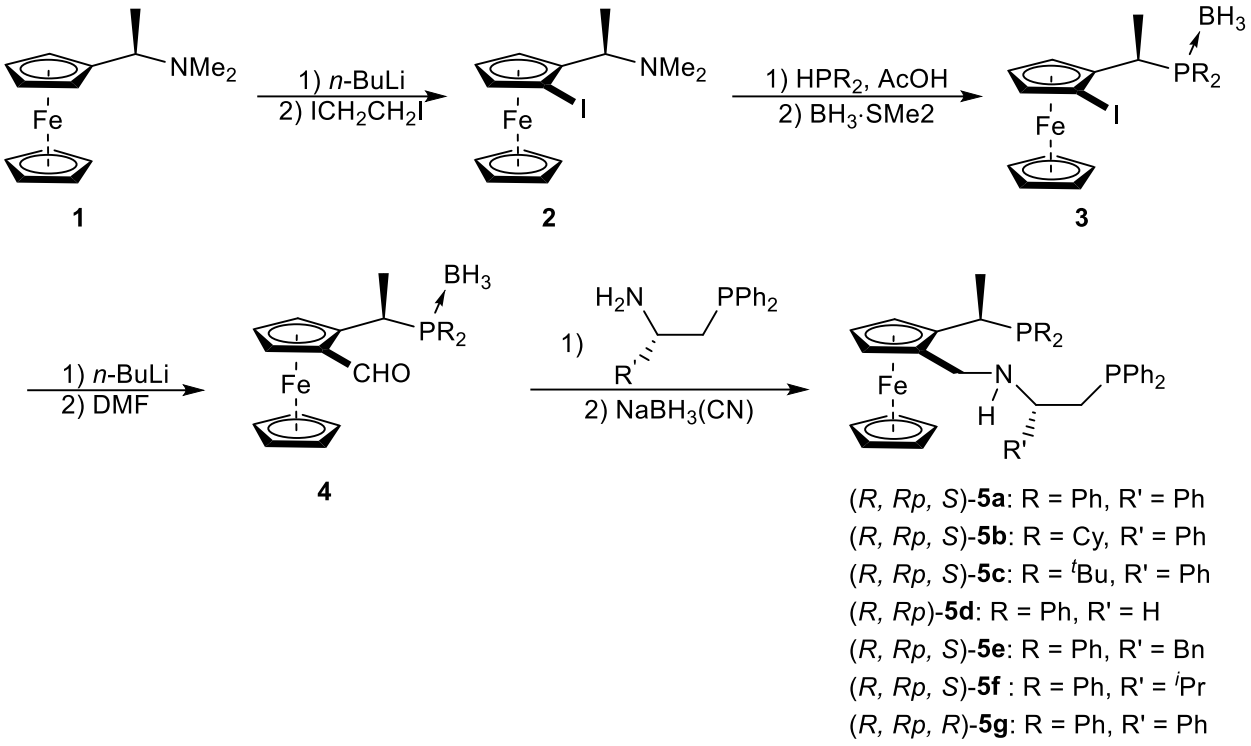

Scheme 2.1 Synthesis of ferrocene-based chiral **PNP** ligands

2.3 Synthesis of Mn/PNP complexes

A suspension of the **PNP** ligand (1 eq.) and $Mn(CO)_5Br$ (1 eq.) in dry toluene was heated at 110 °C and stirred for 18 h under argon (Scheme 2.2). The mixture was cooled to room temperature and concentrated to dryness in vacuo to give an orange solid. In order to obtain pure complexes, the residue was dissolved in DCM and filtered to remove insoluble materials. The product was precipitated by the addition of *n*-hexane, collected by filtration, and washed with *n*-hexane to give an orange powder. A series of Mn complexes was obtained in high yield. However, PNP ligand **5c**, with two tert-butyl groups on one phosphorus atom, failed to form a tridentate complex. This was probably due to steric hindrance in the complexation with the manganese precursor (for details, see experimental).

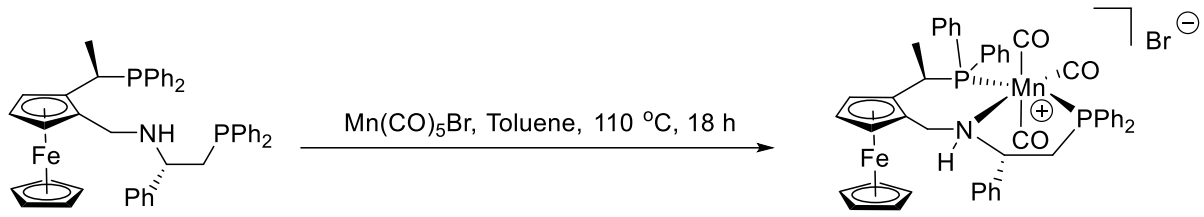

(*R, Rp, S*)-**5a** **6a**

Scheme 2.2 Synthesis of the Mn/PNP complexes

2.4 Asymmetric hydrogenation of ketones

2.4.1 Screening of the reaction conditions

These resulting Mn complexes were applied in the AH of acetophenone in methanol, in the presence of an additional catalytic amount of potassium tert-butoxide (5 mol%). We found that the performance of each complex varied with respect to conversion and enantioselectivity. Complex **6a**, with two phenyl groups on each of its phosphorus atoms, gave the best results (Table 2.1, entry 1). Under slightly modified conditions, the turnover number (TON) of this reaction could reach 2000 (Table 2.1, entry 8), demonstrating a high catalytic efficiency.

Table 2.1 Screening of catalysts (Mn/PNP complexes)

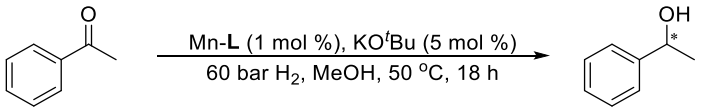

Entry[a]	Ligand	Conversion (%)[b]	Ee (%)[b]
1	(*R, Rp, S*)-**5a**	>99	92 (*R*)
2	(*R, Rp, S*)-**5b**	<5	-
3	(*R, Rp, S*)-**5d**	6	64 (*R*)
4	(*R, Rp*)-**5e**	25	89 (*R*)
5	(*R, Rp, S*)-**5f**	15	86 (*R*)

6		(*R*, *Rp*, *S*)-**5g**	10	83 (*S*)
7	[c]	(*R*, *Rp*, *S*)-**5a**	>99	91 (*R*)
8	[d]	(*R*, *Rp*, *S*)-**5a**	>99	91 (*R*)

[a] Reaction conditions: acetophenone (0.1 mmol), cat.(0.001 mmol), KO^{t}Bu (0.005 mmol), MeOH (1 mL). [b] Conversions and ee values were determined by 1H-NMR and chiral HPLC, respectively. [c] Acetophenone (1 mmol), MeOH (1 mL). [d] Acetophenone (2 mmol), MeOH (1 mL), 48 h.

After screening of different solvents, bases, concentrations, temperatures and reaction times, it was found that using 1 mol% of **6a** and 2 mol% of KOH resulted full conversion and 95% ee for the AH of acetophenone in a concentration of 0.5 M in MeOH under 60 bar of H_2 at RT for 24 h (Table 2.2).

Table 2.2 Further reaction condition optimizations

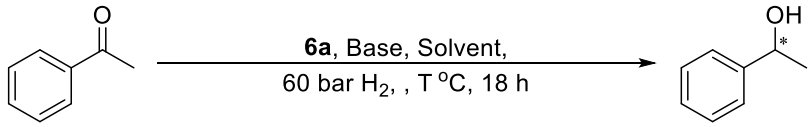

Entry[a]	Solvent[b]	Base	T (°C)	Conv. (%)[c]	Ee (%)[c]
1	MeOH [0.1M]	KO^{t}Bu (5mol%)	50	>99	92
2	THF [0.1M]	KO^{t}Bu (5mol%)	50	15	-
3	Tol [0.1M]	KO^{t}Bu (5mol%)	50	21	-
4	DCE [0.1M]	KO^{t}Bu (5mol%)	50	7	-
5	Hexane [0.1M]	KO^{t}Bu (5mol%)	50	78	95
6	EtOH [0.1M]	KO^{t}Bu (5mol%)	50	96	86
7	PrOH [0.1M]	KO^{t}Bu (5mol%)	50	32	81
8	*i*PrOH [0.1M]	KO^{t}Bu (5mol%)	50	74	89
9	BuOH [0.1M]	KO^{t}Bu (5mol%)	50	35	81
10	*t*BuOH [0.1M]	KO^{t}Bu (5mol%)	50	36	87
11	2-OMe-EtOH [0.1M]	KO^{t}Bu (5mol%)	50	12	83
12	TFE [0.1M]	KO^{t}Bu (5mol%)	50	<5	-

13	[d]	MeOH [0.1M]	KO^{t}Bu (5mol%)	50	83	92
14		Hexane [0.1M]	KO^{t}Bu (5mol%)	rt	<5	-
15		MeOH [0.1M]	NaO^{t}Bu (5mol%)	50	>99	91
16		MeOH [0.1M]	LiO^{t}Bu (5mol%)	50	>99	92
17		MeOH [0.1M]	KOH (5mol%)	50	>99	91
18		MeOH [0.1M]	NaOMe (5mol%)	50	>99	92
19		MeOH [0.1M]	K_2CO_3 (5mol%)	50	84	92
20		MeOH [0.1M]	Cs_2CO_3 (5mol%)	50	78	91
21		MeOH [0.1M]	-	50	29	91
22	[e]	MeOH [1M]	KO^{t}Bu (0.25mol%)	50	52	92
23	[e]	MeOH [1M]	NaO^{t}Bu (0.25mol%)	50	47	92
24	[e]	MeOH [1M]	LiO^{t}Bu (0.25mol%)	50	57	92
25	[e]	MeOH [1M]	KOH (0.25mol%)	50	71	92
26	[e]	MeOH [1M]	NaOMe (0.25mol%)	50	56	92
27		MeOH [0.2M]	KOH (10mol%)	rt	62	94
28		MeOH [0.2M]	KOH (5mol%)	rt	68	95
29		MeOH [0.2M]	KOH (2mol%)	rt	80	95
30		MeOH [0.1M]	KOH (2mol%)	rt	71	95
31		MeOH [0.5M]	KOH (2mol%)	rt	91	95
32	[f]	MeOH [0.5M]	KOH (2mol%)	rt	>99	95

[a] Reaction conditions: 0.2 mmol of acetophenone for entry 1-21 and 27-32, 2 mmol of acetophenone for entry 22-26; 0.002 mmol of **6a** (2 mg) for entry 1-21 and 27-32, 0.001 mmol of **6a** (1 mg) for entry 22-26. [b] Concentration of substrate in solvent. [c] Conversions and ee values were determined by ^{1}H-NMR and chiral HPLC, respectively. [d] 30 bar H_2. [e] S/C = 2000, acetophenone (2 mmol), **6a** (0.001 mmol, 1 mg), base (0.005 mmol), MeOH (2 mL). [f] 24 h.

2.4.2 Substrate scope

The reaction scope was investigated under the optimal conditions (Table 2.3). In general, alkyl aryl ketones are hydrogenated with excellent enantioselectivities, with the ee values for most of the substrates greater than 95%. The substituents on the phenyl group, regardless of their positions, had no significant influence on the enantioselectivity, although steric hindrance at the ortho-position led to a decrease in yield (**8c** and **8d**). Likewise, the electronic properties of the aryl group (i.e., electron-rich or electron-poor), did not create clear differences in enantiomeric discrimination. However, increasing the steric hindrance on the phenyl slightly lowered the ee's (**8p** and **8r**). Heteroaromatic substrates, with their potential to cause inhibition of hydrogenation through transition metal coordination, were compatible in this catalytic system. Substrates with different alkyl groups also gave desired enantioselectivities and reactivities (**8aa** - **8ag**). To our delight, dialkyl ketone **8ah** and **8ai** were hydrogenated smoothly under the reaction conditions with high enantioselectivities. Ketone **8aj** with a lactam functional group, was hydrogenated with a remarkably high diastereoselectivity, suggesting the potential application of this catalyst in late-stage modification of complicated molecules. The broad substrate scope clearly indicated the importance of this catalyst system in the asymmetric synthesis of chiral secondary alcohols.

Table 2.3 Reaction Scope for Mn/PNP-Catalyzed AH of Ketones

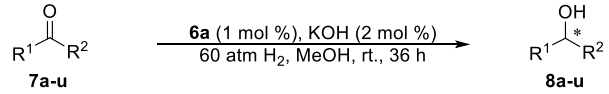

7a-u → **8a-u**

8a	**8b**	**8c**	**8d**	**8e**	**8f**	**8g**	**8h**
>99% (99%) 95% ee	>99% (93%) 96% ee	80% (66%) 98% ee	50% (40%) 98% ee	>99% (92%) 96% ee	>99% (99%) 95% ee	>99% (99%) 95% ee	>99% (99%) 99% ee
8i	**8j**	**8k**	**8l**	**8m**	**8n**	**8o**	**8p**
>99% (99%) 95% ee	>99% (93%) 97% ee	>99% (96%) 96% ee	>99% (97%) 96% ee	>99% (99%) 98% ee	>99% (98%) 97% ee	>99% (98%) 98% ee	>99% (99%) 92% ee
8q	**8r**	**8s**	**8t**	**8u**	**8v**	**8w**[a]	**8x**
>99% (85%) 99% ee	>99% (99%) 93% ee	33% (n.d) 96% ee	>99% (99%) 98% ee	>99% (99%) 97% ee	>99% (99%) 96% ee	91% (75%) 98% ee	>99% (99%) 98% ee
8y	**8z**	**8aa**	**8ab**	**8ac**[a]	**8ad**[a]	**8ae**[a]	**8af**
>99% (92%) 98% ee	>99% (94%) 97% ee	>99% (98%) 97% ee	>99% (83%) 98% ee	86% (67%) 97% ee	95% (86%) 99% ee	40% (n.d) 96% ee	>99% (99%) 96% ee
8ag	**8ah**[a]	**8ai**[a]	**8aj**[a]				
>99% (99%) 98% ee	>99% (94%) 83% ee	>99% (99%) 94% ee	>99% (92%) 98% de				

Typical reaction conditions: substrate (0.2 mmol, 0.5 M), catalyst **6a** (0.002 mmol), KOH (0.004 mmol), 0.4 mL of MeOH, 60 atm of H_2. Conversions were determined by ^1H NMR. Isolated yields were recorded in brackets. The ee values were measured using HPLC or GC on a chiral stationary phase. [a] Reaction carried out at 40 °C.

2.5 Mechanism studies

2.5.1 Investigation of the active species

The success of this catalytic system in the AH of ketones encouraged us to investigate the formation and structure of the Mn complexes in more detail (Scheme 2.3). Complexation of $Mn(CO)_5Br$ with tridentate ligand **5a** gave the precatalyst **9** in a high yield. Unfortunately, attempts to obtain a crystal structure of this complex failed after many trials. However, high-resolution mass spectroscopy confirmed the cationic tricarbonyl structure of this complex. In addition, IR spectra showed three carbonyl peaks, which was also in agreement with the tricarbonyl structure. The size of the coupling constant between the two P atoms J_{P-P} = 102 Hz indicated a meridional geometry.[22] This *mer* preference was in accordance with previously reported manganese and iron PNP complexes. After treatment with potassium tert-butoxide, **9** was converted to a dark red species **10** with a sharper ^{31}P NMR spectrum. This species was assigned to an amido Mn(I) complex[24-25] resulting from removal of the NH proton by the base. Upon pressurizing the solution of **10** with hydrogen gas under an inert atmosphere, this amido complex was consumed instantly and a yellow mixture of Mn hydride complexes was detected. Three major isomers were identified from the ^{31}P and ^{1}H NMR spectra. These Mn(I) hydrides were proposed as probable catalytic species.

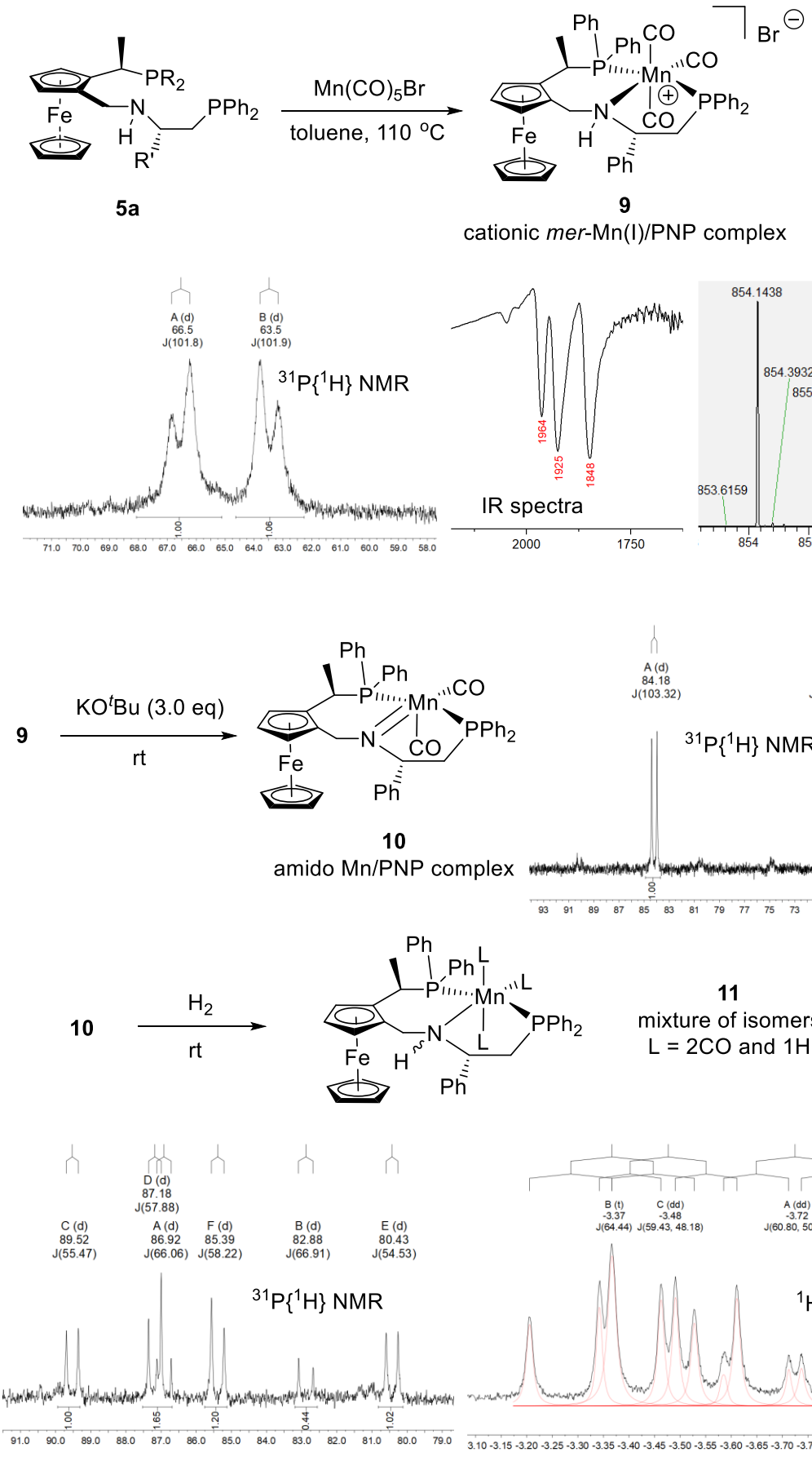

Scheme 2.3 Transformation of the Mn/PNP Complexes

2.5.2 DFT computational studies

Since the isolation of each Mn hydride complex seemed impossible at this stage, we carried out DFT calculations to help with their structural analysis (Figure 2.2). The orientation of the NH group might vary, and therefore two groups of isomeric Mn(PNP)$(CO)_2$H species were proposed. The calculated relative energies of these six species are summarized in Figure 2.2. The three structures with the NH proton *syn* to the phenyl in the 5-membered ring (**D**-**F**) were found to be thermodynamically more stable that those with their NH proton *anti* to the Ph group (**A**-**C**). In addition, the two structures with the metal-bound hydride located *trans* to NH (**B** and **E**) had much higher energies. Gratefully, we found that two isomers (**D** and **F**) with their NH proton *syn* to the phenyl had similar energies, which was accurately reflected in the NMR spectra of the reaction mixture. These two structures had opposite hydride orientations. It should be noted that only those complexes with their metal hydride *cis* to the NH proton (i.e., **A** and **D**) are thought to have catalytic activity according to the HM-NH reaction model.[26-27] This suggests that the more thermodynamically stable **D** is the best candidate as the catalytically active species.

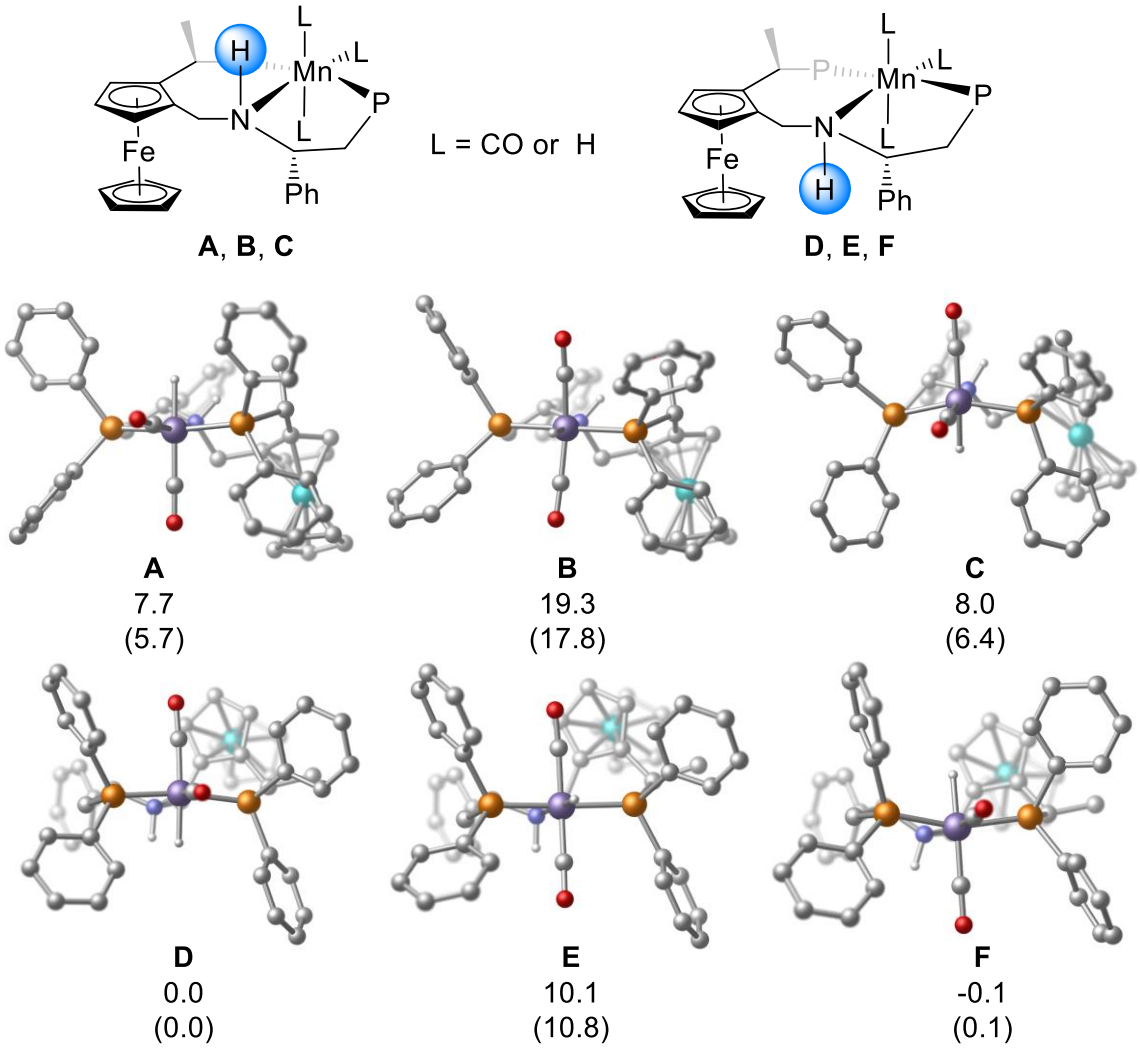

Figure 2.2 Optimized considered structures of $Mn(PNP)(CO)_2H$. Gibbs free energies and electronic energies (in parentheses) are given in kcal/mol relative to D.

In order to gain insight into how the enantioinduction was achieved, we conducted further DFT studies to simulate the hydride transfer step (Figure 2.3). We tentatively compared the two pairs of diastereomeric catalyst–substrate **7a** complexes in the transition states for the hydride transfer steps involving **A** and **D**. We found that the calculated energy barriers for hydride transfer to **7a** with Mn hydride **A** (**TS-A-R** and **TS-A-S**) were much higher than those with **D** (**TS-D-R** and **TS-D-S** in Figure 3). In the transition state which leads to the formation of the favoured (*R*) product (**TS-D-R**), the smaller methyl group on the substrate **7a** points towards the 7-membered-ring side (on the right). On the other hand, the conformation of the phenyl group on the 7-membered-ring side is conformationally

restrained. The formation of the (S) product is unfavored because of inevitable steric repulsion from two phenyl groups in close proximity. The rigid ferrocene moiety is also thought to enhance the ring strain (**TS-D-S**).

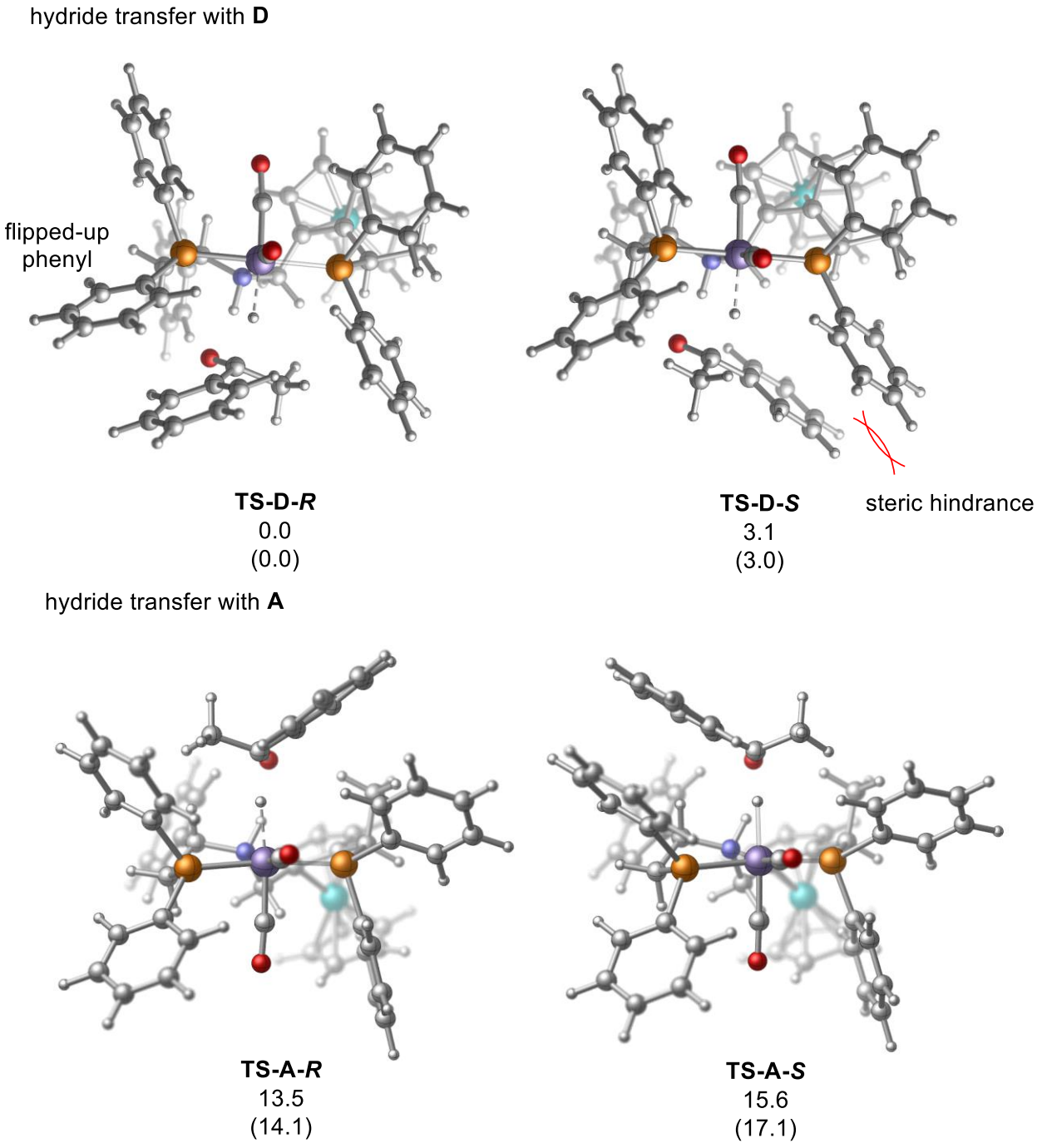

Figure 2.3 Analysis of enantioinduction model. Optimized structures of transition states in the hydride transfer step for complexes A and D. Gibbs free energies and electronic energies are given in kcal/mol relative to TS-D-R. Energies calculated in methanol are given in parentheses.

The steric maps[28] of the best candidate, Mn hydride complex **D**, in its free state and in the transition state for hydride transfer to substrate **7a**, are depicted in Figure 2.4. The parameter of buried volume is introduced to give a quantitative analysis of the chiral environment. While the steric hindrance from the phenylphosphinyl group in the 7-membered ring does not change significantly (buried volume 63.3% vs 63.1% in the southwest quadrant), the phenylphosphinyl group in the 5-membered ring is pushed sideways (59.6% vs 56.3% in the southeast quadrant). From the steric map, we can clearly observe the recession of the phenyl group. An intuitive comparison of this image with the structure of the Mn hydride **D** complex leads us to the conclusion that the diphenylphosphinyl group on the 5-membered ring (left) is flexible, with the benzene ring able to flip up to create room for the larger phenyl group on the substrate.

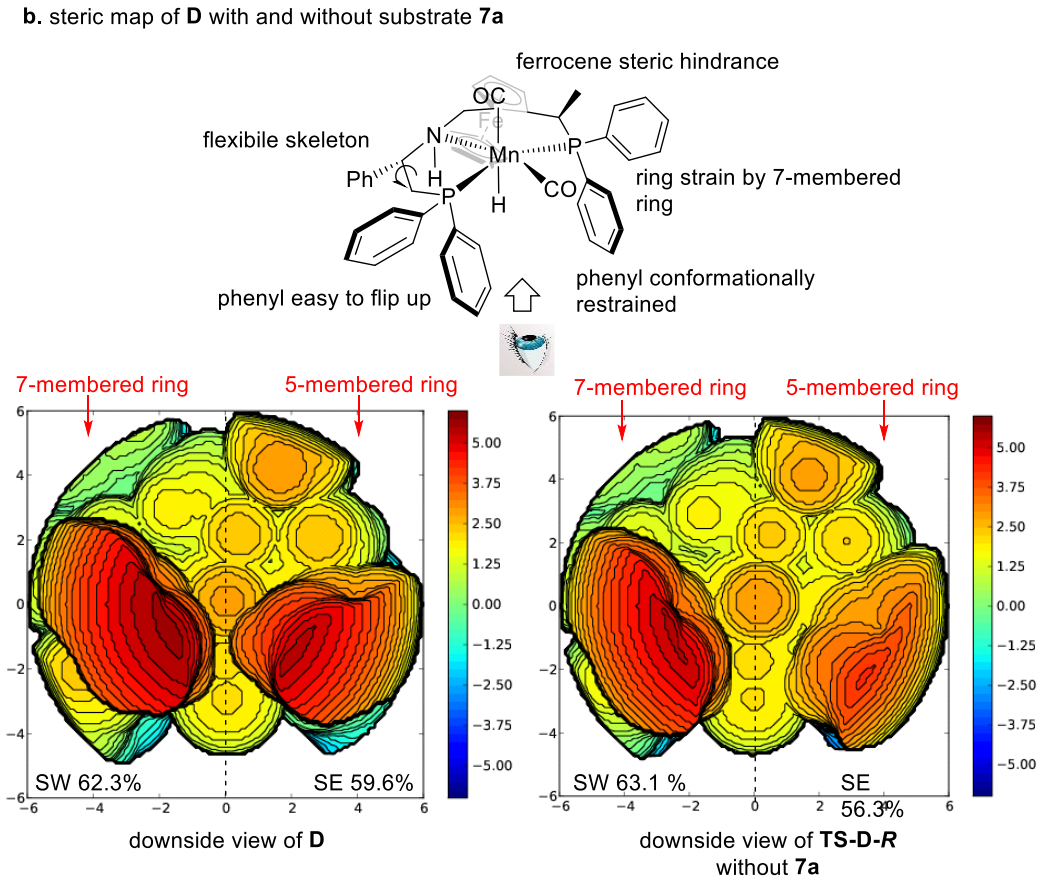

Figure 2.4 Steric maps of the reactive site of the catalyst D in the absence and in the presence of substrate 7a.

2.6 Conclusion

In summary, we report a series of novel C_1-symmetrical PNP ligands and their successful application in the AH of ketones. Remarkably high enantioselectivities were obtained for a broad substrate scope. The potential catalytically active *in-situ* species were identified, with DFT computational studies rendering a plausible model for enantiomeric induction in ketone hydrogenation. Compared to C_2-chiral pincer PNP ligands, the 5,7-fused ring structure enables both a rigid area and a relatively flexible area in the chiral pocket, which leads to effective enantiomeric discrimination in the hydride transfer step.

2.7 Experimental

2.7.1 General experimental details

All the reactions dealing with air- or moisture-sensitive compounds were carried out in a dry reaction vessel under an argon atmosphere or in an argon-filled glove box. Unless otherwise noted, all reagents and solvents were purchased from commercial suppliers without further purification. Toluene was dried with sodium chips and indicated by benzophenone. Other anhydrous solvents were purchased from J&K Chemical and degassed by bubbling argon over a period of 30 min. Purification of products was carried out by flash chromatography using silica gel (200-300 mesh).

^{1}H, ^{13}C, ^{19}F and ^{31}P NMR spectra were recorded on a Bruker Avance 400 MHz or on a Bruker Avance 600 MHz spectrometer with tetramethylsilane as the internal standard. Chemical shifts are reported in parts per million (ppm, δ scale) downfield from TMS at 0.00 ppm and referenced to the $CDCl_3$ at 7.27 ppm for ^{1}H NMR or 77.0 ppm for ^{13}C NMR. Data are reported as: multiplicity (s = singlet, d = doublet, t = triplet, q = quartet, m = multiplet), coupling constant in hertz (Hz) and signal area integration in natural numbers. ^{13}C NMR and ^{31}P NMR analyses were recorded with ^{1}H decoupling. Enantiomeric excess values were determined Agilent 1290 Series HPLC or on an Agilent 7890B GC instrument on a chiral stationary phase. Optical rotations were measured using a 1 mL cell with a 1 dm path length on a Rudolph Autopol I polarimeter at 589 nm. HRMS (ESI) was recorded on Thermo-Fischer Orbitrap Fusion instrument.

2.7.2 Synthesis of the PNP ligands

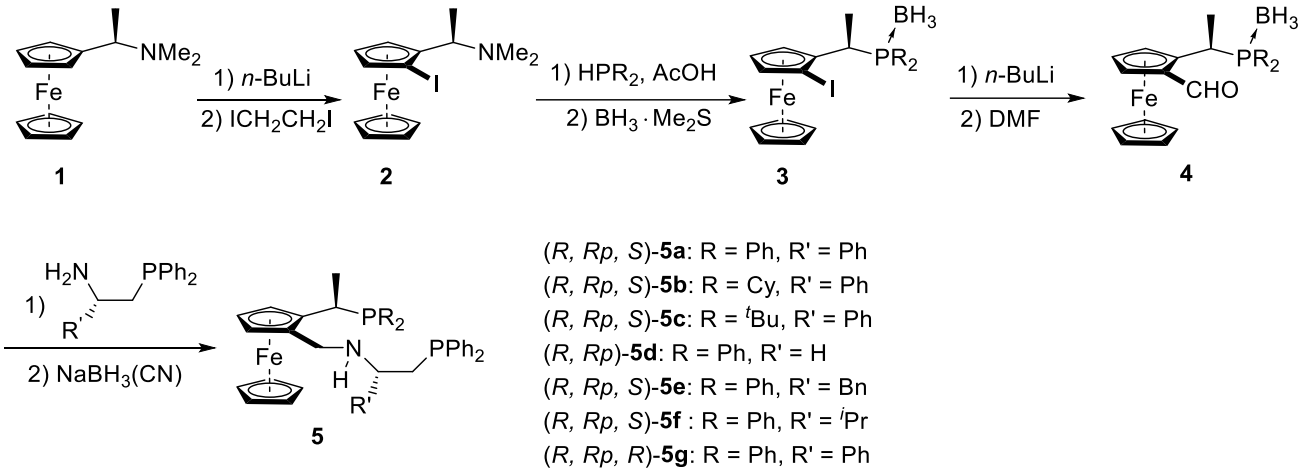

Scheme 2.4 Synthesis of PNP ligands 5a-g

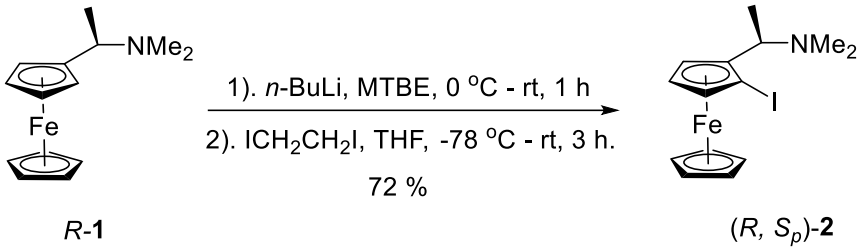

Scheme 2.5 Synthesis of compound (*R, Sp*)-**2**

(*R, Sp*)-**2.** Known compound.[29] To a solution of the starting material *R*-**1** (100 mmol, 21 mL) dissolved in dry MTBE (100 mL), *n*-BuLi (110 mmol, 45.8 mL, 2.4 M in hexane) was added dropwise at 0 °C under argon. Warmed to room temperature, the reaction mixture was stirred for 1 h. Before 1,2-Diiodoethane (120 mmol, 33.8 g) dissolved in dry THF (50 mL) was added, the red solution was cooled to -78 °C. After the addition of 1,2-Diiodoethane, the reaction mixture was allowed to warm to room temperature and stirred for further 3 h. Then the reaction was quenched by the addition of aqueous saturated $Na_2S_2O_3$ solution (50 mL), extracted with ethyl acetate (3*50 mL) and the combined organic layers were dried over anhydrous Na_2SO_4 and concentrated under vacuum. The residue was purified by column chromatography on silica gel (PE/EtOAc/Et_3N, 80/20/1~50/50/1) to yield 27.5 g (72 %) of (*R, Sp*)-**2** as an orange solid. ^{1}H NMR (400 MHz, Chloroform-*d*) δ 4.46 (dd, *J* = 2.5, 1.4 Hz, 1H), 4.24

(td, *J* = 2.6, 0.6 Hz, 1H), 4.14 (dd, *J* = 2.8, 1.3 Hz, 1H), 4.12 (s, 5H), 3.61 (q, *J* = 6.8 Hz, 1H), 2.14 (s, 6H), 1.50 (d, *J* = 6.8 Hz, 3H). ^{13}C NMR (101 MHz, Chloroform-*d*) δ 90.2, 74.3, 71.7, 68.2, 65.6, 57.6, 45.5, 41.2, 16.0. [α]D^{25} = -8.50 (*c* 1.0, $CHCl_3$).

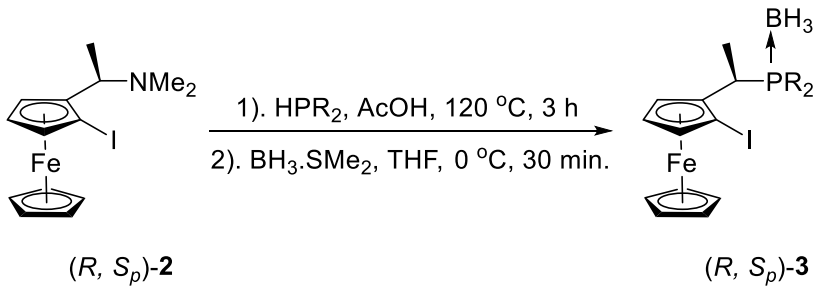

(*R, S$_p$*)-**2** (*R, S$_p$*)-**3**

Scheme 2.6 Synthesis of compound (*R, Sp*)-3

Typical procedure: a solution of (*R, Sp*)-**2** (30 mmol, 11.5 g), $HPPh_2$ (45 mmol, 7.8 mL) in degassed AcOH (10 mL) was heated at 120 °C for 3 h under argon. After cooled to room temperature, the reaction was quenched by the addition of aqueous saturated $NaHCO_3$ solution (20 mL), extracted with ethyl acetate (3*20 mL) and the combined organic layers were dried over anhydrous Na_2SO_4 and concentrated under vacuum. The residue was redissolved in dry THF (50 mL) under argon. After the solution was cooled to 0 °C, $BH_3.SMe_2$ (33 mmol, 16.5 mL, 2.0 M in THF) was added and the reaction mixture was stirred for 30 min at 0 °C. After warmed to room temperature, the reaction was quenched by the addition of water (20 mL), extracted with ethyl acetate (3*20 mL) and the combined organic layers were dried over anhydrous Na_2SO_4 and concentrated under vacuum. The residue was washed by PE to yield 15.5 g (95 %) of (*R, Sp*)-**3a** as an orange solid.

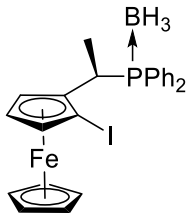

(*R, Sp*)-**3a**. Novel compound. Purified by washing with PE. Orange solid. 15.5 g (95 % yield). ^{1}H NMR (400 MHz, Chloroform-*d*) δ 8.01 (t, *J* = 8.2 Hz, 2H), 7.59 (m, 3H), 7.30 (t, *J* = 7.5 Hz, 1H), 7.12 (dt, *J* = 7.6, 4.0 Hz, 2H), 7.05 – 6.96 (m, 2H), 4.60 – 4.55 (m, 1H), 4.34 (m, 1H), 4.31 (s, 1H), 4.15 (s, 5H), 3.58 (dq, *J* = 14.6, 7.2 Hz, 1H), 1.65 (dd, *J* = 16.5, 7.2 Hz, 3H), 1.25 - 0.45 (br, 3H, BH_3). ^{13}C NMR (101 MHz, Chloroform-*d*) δ 133.7 (d, *J* = 8.3 Hz), 133.3 (d, *J* = 8.6 Hz), 131.7 (d, *J* = 2.5 Hz), 130.7 (d, *J* = 2.6 Hz), 129.0 (d, *J* = 9.5 Hz), 128.4, 127.8 (d, *J* = 9.8 Hz), 126.8 (d, *J* = 51.8 Hz), 89.3 (d, *J* = 4.4 Hz), 73.4, 71.5, 68.9, 67.0, 47.4, 30.9 (d, J = 30.8 Hz), 17.7 (d, J = 5.9 Hz). ^{31}P {^{1}H} NMR (162 MHz, Chloroform-d) δ 26.8 (d, br., J = 72.9 Hz). **HRMS** (ESI) m/z: $[M]^+$ Calcd for $C_{24}H_{25}BFeIP$ = 538.0176; Found: 538.0174. $[\alpha]D^{25}$ = -39.00 (*c* 1.0, $CHCl_3$).

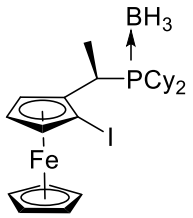

(*R, Sp*)-**3b**. Novel compound. Purified by washing with EtOH. Orange solid. 465 mg. (84 % yield). ^{1}H NMR (400 MHz, Chloroform-*d*) δ 4.48 (dd, *J* = 2.5, 1.4 Hz, 1H), 4.41 – 4.35 (m, 1H), 4.28 (t, *J* = 2.6 Hz, 1H), 4.17 (s, 5H), 3.01 (dq, *J* = 12.6, 7.2 Hz, 1H), 2.12 – 1.98 (m, 2H), 1.85 (dd, *J* = 8.2, 4.6 Hz, 2H), 1.71 (dd, *J* = 14.4, 7.2 Hz, 8H), 1.60 – 1.37 (m, 5H), 1.35 – 1.27 (m, 2H), 1.25 – 1.17 (m, 1H), 1.16 – 1.00 (m, 4H), 0.95 (ddd, *J* = 12.4, 8.6, 3.6 Hz, 1H), 0.70 – -0.20 (br, 3H, BH_3). ^{13}C NMR (101 MHz, Chloroform-*d*) δ 92.8, 73.8, 71.7, 68.8, 67.2 (d, *J* = 1.5 Hz), 44.7 (d, *J* = 1.9 Hz), 33.2 (d, *J* = 27.9 Hz), 31.6 (d, *J* = 29.3 Hz), 28.0, 27.9 (d, *J* = 2.3 Hz), 27.8 (d, *J* = 2.9 Hz), 27.6 (d, *J* = 10.2 Hz), 27.4, 27.2 (d, *J* = 3.4 Hz), 27.1, 26.9 (d, *J* = 11.6 Hz), 26.3, 25.9, 25.7, 19.5 (d, *J* = 4.0 Hz). ^{31}P {^{1}H} NMR (162 MHz, Chloroform-*d*) δ 38.7 (d, br., *J* = 82.1 Hz). **HRMS** (ESI) m/z: $[M]^+$ Calcd for $C_{24}H_{37}BFeIP$ = 550.1115; Found: 550.1112. $[\alpha]D^{25}$ = -13.50 (*c* 1.0, $CHCl_3$).

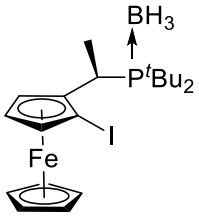

(*R, Sp*)- **3c.** Novel compound. Purified by washing with EtOH. Orange solid. 490 mg. (98 % yield). ^{1}H NMR (400 MHz, Chloroform-*d*) δ 4.48 (dd, *J* = 2.5, 1.3 Hz, 1H), 4.42 (t, *J* = 1.9 Hz, 1H), 4.29 (t, *J* = 2.6 Hz, 1H), 4.18 (s, 5H), 3.06 (dq, *J* = 11.2, 7.3 Hz, 1H), 1.98 (dd, *J* = 12.1, 7.3 Hz, 3H), 1.37 (d, *J* = 12.0 Hz, 9H), 1.22 (d, *J* = 12.3 Hz, 9H), 0.74 – -0.15 (br, 3H, BH_3). ^{13}C NMR (101 MHz, Chloroform-*d*) δ 94.6 (d, *J* = 2.9 Hz), 73.2, 71.8, 68.3, 67.9 (d, *J* = 1.5 Hz), 47.6 (d, *J* = 2.3 Hz), 34.7 (d, *J* = 20.8 Hz), 34.4 (d, *J* = 22.2 Hz), 29.6 (d, *J* = 1.3 Hz), 29.5, 28.4 (d, *J* = 20.1 Hz), 23.5. ^{31}P {^{1}H} NMR (162 MHz, Chloroform-*d*) δ 58.7 (d, br., *J* = 84.3 Hz). **HRMS** (ESI) m/z: $[M]^+$ Calcd for $C_{20}H_{33}BFeIP$ = 498.0802; Found: 498.0792. $[\alpha]D^{25}$ = -4.20 (*c* 1.0, $CHCl_3$).

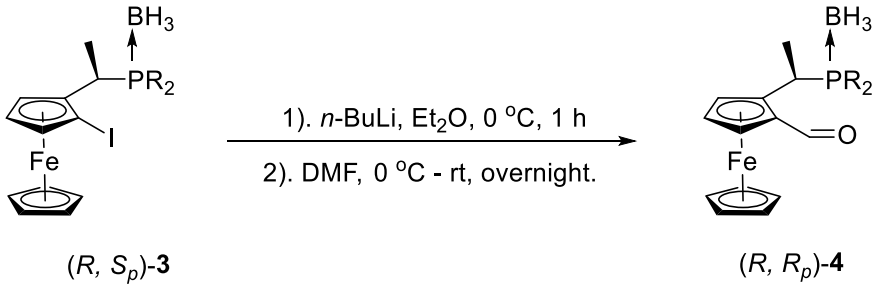

Scheme 2.7 Synthesis of compound (*R, Rp*)-4

Typical procedure: to a solution of the starting material (*R, Sp*)-**3a** (30 mmol, 16.1 g) dissolved in dry Et_2O (60 mL), *n*-BuLi (31.5 mmol, 13.2 mL, 2.4 M in hexane) was added dropwise at 0 °C under argon. The reaction mixture was stirred for 1 h at 0 °C. After the addition of DMF (210 mmol, 16.2 mL), the reaction mixture was allowed to warm to room temperature and stirred overnight. Then the reaction was quenched by the addition of water (20 mL), extracted with ethyl acetate (3*20 mL) and the combined organic layers were dried over anhydrous Na_2SO_4 and concentrated under vacuum. The

residue was purified by column chromatography on silica gel (PE/EtOAc, 20/1~5/1) to yield 9.9 g (75 %) of (*R, Rp*)-**4a** as a red solid.

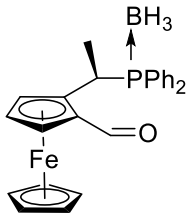

(*R, Rp*)-**4a.** Known compound.[30] Purified by column chromatography on silica gel (PE/EtOAc, 20/1~5/1). Red solid. 9.9 g (75 % yield). ^{1}H NMR (600 MHz, Chloroform-*d*) δ 9.38 (s, 1H), 8.03 (ddd, *J* = 9.9, 7.9, 1.7 Hz, 2H), 7.60 – 7.52 (m, 3H), 7.17 – 7.07 (m, 4H), 4.90 – 4.86 (m, 1H), 4.57 (t, *J* = 2.7 Hz, 1H), 4.46 (dt, *J* = 15.5, 7.3 Hz, 1H), 4.41 (dd, *J* = 2.7, 1.4 Hz, 1H), 4.25 (s, 4H), 1.64 (dd, *J* = 16.5, 7.2 Hz, 3H), 1.11 – 0.63 (br, 3H, BH_3). ^{13}C NMR (101 MHz, Chloroform-*d*) δ 192.6, 133.4 (d, *J* = 8.4 Hz), 133.2 (d, *J* = 8.6 Hz), 131.6 (d, *J* = 2.5 Hz), 130.7 (d, *J* = 2.6 Hz), 128.9 (d, *J* = 9.5 Hz), 128.1 (d, *J* = 54.0 Hz), 127.5 (d, *J* = 9.9 Hz), 127.0 (d, *J* = 51.9 Hz), 90.0 (d, *J* = 3.7 Hz), 76.6 (d, *J* = 1.5 Hz), 73.9 (d, *J* = 2.1 Hz), 71.7, 71.0, 70.1, 28.6 (d, *J* = 30.9 Hz), 16.4 (d, *J* = 5.4 Hz). ^{31}P {^{1}H} NMR (162 MHz, Chloroform-*d*) δ 26.9 (d, br., *J* = 74.8 Hz). **HRMS** (ESI) m/z: $[M+Na]^+$ Calcd for $C_{25}H_{26}BFeNaOP$ = 463.1056; Found: 463.1051. $[\alpha]D^{25}$ = 235.50 (*c* 1.0, $CHCl_3$).

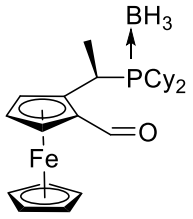

(*R, Rp*)-**4b.** Novel compound. Purified by column chromatography on silica gel (PE/EtOAc, 10/1~4/1). Red solid. 2.17 g (80 % yield). Ethyl formate was applied instead of DMF during the synthesis. ^{1}H NMR (400 MHz, Chloroform-*d*) δ 10.01 (s, 1H), 4.81 – 4.76 (m, 1H), 4.72 (dd, *J* = 2.7, 1.4 Hz, 1H), 4.62 (t, *J* = 2.7 Hz, 1H), 4.29 (s, 5H), 3.73 (dq, *J* = 14.3, 7.2 Hz, 1H), 2.06 – 1.92 (m, 2H), 1.88 – 1.79 (m, 2H), 1.69 (dd, *J* = 13.9, 7.3 Hz, 8H), 1.59 – 1.51 (m, 2H), 1.49 – 1.34 (m, 3H), 1.21 (dd, *J* = 16.5,

5.6 Hz, 4H), 1.14 – 0.98 (m, 3H), 0.91 (tt, *J* = 13.7, 3.6 Hz, 1H), 0.60 – -0.20 (br, 3H, BH_3). ^{13}C NMR (101 MHz, Chloroform-*d*) δ 192.8, 93.0, 74.3, 72.1, 71.0, 70.3, 32.6 (d, *J* = 27.7 Hz), 31.8 (d, *J* = 29.3 Hz), 28.0, 27.9 (d, *J* = 2.1 Hz), 27.8 (d, *J* = 2.4 Hz), 27.5 (d, *J* = 2.8 Hz), 27.5 (d, *J* = 4.3 Hz), 27.3, 27.2, 27.1 (d, *J* = 2.3 Hz), 27.0 (d, *J* = 4.3 Hz), 26.2, 25.9 (d, *J* = 1.5 Hz), 23.7 (d, *J* = 25.8 Hz), 18.1 (d, *J* = 2.5 Hz). ^{31}P {^1H} NMR (162 MHz, Chloroform-*d*) δ 37.2 (d, br., *J* = 80.0 Hz). **HRMS** (ESI) m/z: $[M+Na]^+$ Calcd for $C_{25}H_{38}BFeNaOP$ = 475.1995; Found: 475.1991. $[\alpha]D^{25}$ = 219.80 (*c* 1.0, $CHCl_3$).

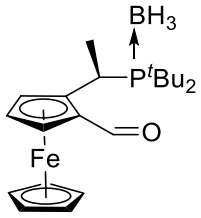

(*R, Rp*)-**4c**. Novel compound. Purified by column chromatography on silica gel (PE/EtOAc, 10/1~4/1). Red solid. 260 mg (65 % yield). Ethyl formate was applied instead of DMF during the synthesis. ^1H NMR (400 MHz, Chloroform-*d*) δ 10.04 (s, 1H), 4.79 (dd, *J* = 2.7, 1.4 Hz, 1H), 4.64 (t, *J* = 1.9 Hz, 1H), 4.57 (t, *J* = 2.7 Hz, 1H), 4.25 (s, 5H), 3.77 (dq, *J* = 10.0, 7.4 Hz, 1H), 2.00 (dd, *J* = 10.5, 7.4 Hz, 3H), 1.30 (dd, *J* = 15.3, 12.3 Hz, 18H), 0.18 (q, *J* = 87.6, 84.0 Hz, 3H, BH_3). ^{13}C NMR (101 MHz, Chloroform-*d*) δ 192.4, 94.0, 78.4, 73.9, 71.0, 70.4, 69.7, 35.0 (d, *J* = 20.0 Hz), 34.1 (d, *J* = 22.2 Hz), 29.6, 29.2, 27.2 (d, *J* = 19.2 Hz), 20.0 (d, *J* = 3.3 Hz). ^{31}P {^1H} NMR (162 MHz, Chloroform-*d*) δ 55.4 (d, br., *J* = 87.4 Hz). **HRMS** (ESI) m/z: $[M+Na]^+$ Calcd for $C_{21}H_{34}BFeNaOP$ = 423.1682; Found: 423.1670. $[\alpha]D^{25}$ = 10.50 (*c* 1.0, $CHCl_3$).

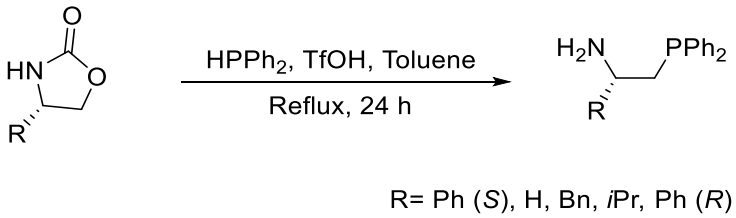

R= Ph (*S*), H, Bn, *i*Pr, Ph (*R*)

Scheme 2.8 Synthesis of the amino-phosphines

The synthesis of the amino-phosphines was according to the procedures in the literature.[31]

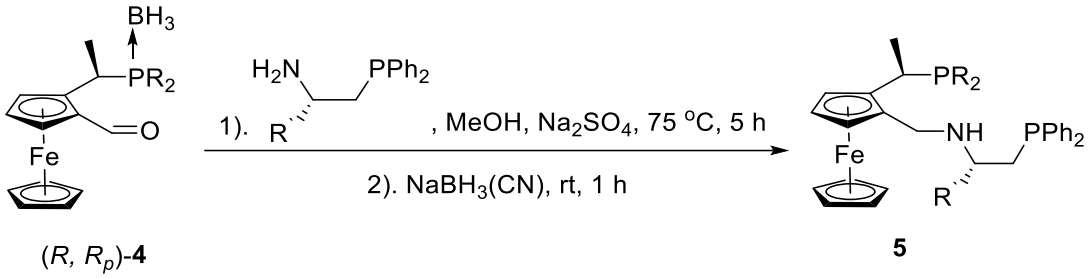

Scheme 2.9 Synthesis of compound 5

Typical procedure **1**: a suspension of (*R, Rp*)-**4a** (1 mmol, 440 mg), (*S*)-2-(diphenylphosphino)-1-phenylethanamine (2.1 mmol, 641 mg) and Na_2SO_4 (284 mg) in degassed MeOH (3 mL) was heated at 75 °C and stirred for 5 h under argon. After cooled to room temperature, $NaBH_3(CN)$ (3 mmol, 241 mg) was added and the reaction mixture was stirred for 1 h. Then the reaction was quenched by the addition of water (10 mL), extracted with DCM (3*5 mL) and the combined organic layers were dried over anhydrous Na_2SO_4 and concentrated under vacuum. The residue was purified by flash chromatography on silica gel (PE/EtOAc, 20/1~10/1) to yield 306 mg (44 %) of (*R, Rp, S*)-**5a** as a yellow solid.

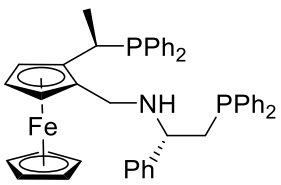

(*R, Rp, S*)-**5a.** Novel compound. Purified by flash chromatography on silica gel (PE/EtOAc, 20/1~5/1). Yellow solid. 306 mg (44 % yield). ^{1}H NMR (400 MHz, Chloroform-*d*) δ 7.49 – 7.23 (m, 18H), 7.19 (dd, *J* = 7.4, 2.2 Hz, 2H), 6.98 – 6.88 (m, 5H), 4.19 (dd, *J* = 2.5, 1.4 Hz, 1H), 4.09 (s, 5H), 4.05 (t, *J* = 2.5 Hz, 1H), 3.91 (dd, *J* = 2.5, 1.4 Hz, 1H), 3.59 (q, *J* = 7.0 Hz, 1H), 3.25 (qd, *J* = 6.9, 3.5 Hz, 1H),

2.73 (d, *J* = 12.9 Hz, 1H), 2.39 (d, *J* = 7.2 Hz, 2H), 2.30 (d, *J* = 13.0 Hz, 1H), 1.42 (dd, *J* = 12.5, 7.0 Hz, 3H). ^{13}C NMR (101 MHz, Chloroform-*d*) δ 144.8 (d, *J* = 5.6 Hz), 138.9 (d, *J* = 12.7 Hz), 138.6 (d, *J* = 13.1 Hz), 137.1 (d, *J* = 17.1 Hz), 135.2 (d, *J* = 16.7 Hz), 134.6 (d, *J* = 19.7 Hz), 133.1, 132.8 (d, *J* = 5.2 Hz), 132.7, 132.6, 132.6, 129.1, 128.6, 128.4 (t, *J* = 3.5 Hz), 128.4, 128.2 (d, *J* = 7.2 Hz), 127.9, 127.6 (d, *J* = 5.8 Hz), 127.0, 126.9, 90.8 (d, *J* = 17.9 Hz), 86.4, 68.7 (d, *J* = 1.4 Hz), 67.5, 66.6 (d, *J* = 4.8 Hz), 65.8, 61.0 (d, *J* = 16.3 Hz), 44.8, 39.1 (d, *J* = 13.9 Hz), 29.5 (d, *J* = 14.5 Hz), 18.2 (d, *J* = 15.0 Hz). ^{31}P {^{1}H} NMR (162 MHz, Chloroform-*d*) δ 7.3, -22.9. **HRMS** (ESI) m/z: $[M+H]^+$ Calcd for $C_{45}H_{44}FeNP_2$ = 716.2293; Found: 716.2281. $[\alpha]D^{25}$ = -6.60 (*c* 1.0, $CHCl_3$).

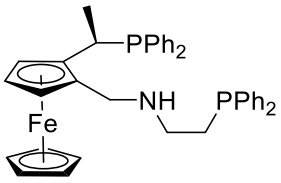

(*R, Rp*)-**5d.** Novel compound. Purified by flash chromatography on silica gel (PE/EtOAc, 5/1~1/1). Yellow solid. 90 mg (20 % yield). ^{1}H NMR (400 MHz, Chloroform-*d*) δ 7.48 – 7.34 (m, 9H), 7.32 (ddt, *J* = 5.9, 4.0, 1.7 Hz, 6H), 7.20 – 7.10 (m, 3H), 7.05 (ddd, *J* = 8.2, 6.4, 1.9 Hz, 2H), 4.14 (t, *J* = 1.9 Hz, 1H), 4.06 (s, 5H), 4.04 (t, *J* = 2.5 Hz, 1H), 3.87 (s, 1H), 3.43 – 3.33 (m, 1H), 3.13 (d, *J* = 13.1 Hz, 1H), 2.98 (d, *J* = 13.1 Hz, 1H), 2.65 (tt, *J* = 14.6, 6.0 Hz, 2H), 2.19 (td, *J* = 7.5, 7.1, 3.9 Hz, 2H), 1.44 (dd, *J* = 11.8, 6.9 Hz, 3H). ^{13}C NMR (101 MHz, Chloroform-*d*) δ 138.6, 138.5, 137.4 (d, *J* = 17.4 Hz), 134.7 (d, *J* = 19.9 Hz), 132.8 (d, *J* = 6.2 Hz), 132.7, 132.7, 132.6, 132.6, 129.3, 128.6 (d, *J* = 4.3 Hz), 128.5 (d, *J* = 1.4 Hz), 128.4 (d, *J* = 1.3 Hz), 128.2 (d, *J* = 7.2 Hz), 128.0, 127.9, 90.9 (d, *J* = 17.9 Hz), 85.0, 68.8, 68.1, 66.8 (d, *J* = 4.5 Hz), 66.0, 47.0, 46.7 (d, *J* = 22.0 Hz), 29.8 (d, *J* = 15.1 Hz), 28.8 (d, *J* = 11.9 Hz), 17.9 (d, *J* = 13.3 Hz). ^{31}P {^{1}H} NMR (162 MHz, Chloroform-*d*) δ 7.7, -20.5. **HRMS** (ESI) m/z: $[M+H]^+$ Calcd for $C_{39}H_{40}FeNP_2$ = 640.1980; Found: 640.1976. $[\alpha]D^{25}$ = -25.00 (*c* 1.0, $CHCl_3$).

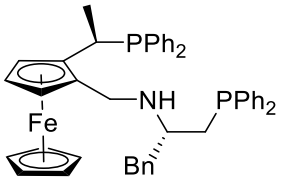

(*R, Rp, S*)-**5e.** Novel compound. Purified by flash chromatography on silica gel (PE/EtOAc, 20/1~5/1). Yellow solid. 120 mg (30 % yield). ^{1}H NMR (400 MHz, Chloroform-*d*) δ 7.51 (t, *J* = 7.0 Hz, 2H), 7.42 – 7.33 (m, 5H), 7.32 – 7.24 (m, 10H), 7.19 (d, *J* = 7.1 Hz, 1H), 7.15 – 7.09 (m, 3H), 7.05 (t, *J* = 7.5 Hz, 2H), 6.94 (t, *J* = 7.0 Hz, 2H), 4.05 – 4.02 (m, 1H), 4.00 (s, 7H), 3.53 – 3.45 (m, 1H), 2.83-2.66 (m, 4H), 2.34 (d, *J* = 12.9 Hz, 1H), 2.20 (d, *J* = 14.2 Hz, 1H), 2.13 – 2.03 (m, 1H), 1.44 (dd, *J* = 13.4, 7.0 Hz, 3H). ^{13}C NMR (101 MHz, Chloroform-*d*) δ 139.2, 137.6 (d, *J* = 17.7 Hz), 135.5, 134.6, 134.4, 133.2, 133.0, 132.9, 132.9, 132.7, 132.7, 129.6, 129.2, 128.5, 128.5, 128.4 (d, *J* = 2.2 Hz), 128.3 (d, *J* = 7.1 Hz), 128.0, 127.7 (d, *J* = 5.8 Hz), 126.3, 90.5 (d, *J* = 17.2 Hz), 86.9, 68.6, 66.9, 66.6, 65.7, 57.9 (d, *J* = 15.7 Hz), 44.3, 41.7, 33.8, 29.7 (d, *J* = 13.6 Hz), 18.4 (d, *J* = 17.4 Hz). ^{31}P {^{1}H} NMR (243 MHz, Chloroform-*d*) δ 6.9, -23.5. **HRMS** (ESI) m/z: $[M+H]^+$ Calcd for $C_{46}H_{46}FeNP_2$ = 730.2449; Found: 730.2441. $[\alpha]D^{25}$ = 6.40 (*c* 1.0, $CHCl_3$).

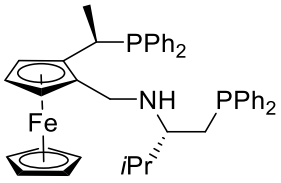

(*R, Rp, S*)-**5f.** Novel compound. Purified by flash chromatography on silica gel (PE/EtOAc, 20/1~5/1). Yellow solid. 150 mg (37 % yield). ^{1}H NMR (400 MHz, Chloroform-*d*) δ 7.51 (ddt, *J* = 9.8, 7.3, 3.9 Hz, 4H), 7.43 – 7.35 (m, 8H), 7.32 (dt, *J* = 7.2, 1.4 Hz, 3H), 7.15 (t, *J* = 7.3 Hz, 1H), 7.09 (t, *J* = 7.2 Hz, 2H), 6.98 (t, *J* = 6.7 Hz, 2H), 4.19 – 4.17 (m, 1H), 4.14 (s, 5H), 4.05 (t, *J* = 2.5 Hz, 1H), 4.01 – 3.98 (m, 1H), 3.40 (qd, *J* = 7.0, 4.2 Hz, 1H), 2.83 (d, *J* = 12.8 Hz, 1H), 2.36 (dq, *J* = 8.7, 4.3, 3.8 Hz, 1H), 2.30 (d, *J* = 12.8 Hz, 1H), 2.27 – 2.21 (m, 1H), 1.94 (ddd, *J* = 13.9, 9.3, 2.7 Hz, 1H), 1.80 – 1.74 (m, 1H), 1.47 (dd, *J* = 13.1, 7.0 Hz, 3H), 0.83 (dd, *J* = 9.6, 6.8 Hz, 6H). ^{13}C NMR (101 MHz, Chloroform-*d*) δ 139.8 (d, *J* = 12.6 Hz), 138.7 (d, *J* = 13.8 Hz), 137.5 (d, *J* = 17.3 Hz), 135.5 (d, *J* =

17.2 Hz), 134.6 (d, *J* = 19.7 Hz), 133.3 (d, *J* = 19.3 Hz), 133.0 (d, *J* = 16.8 Hz), 132.5 (d, *J* = 18.2 Hz), 128.9 (d, *J* = 34.7 Hz), 128.5, 128.4 (d, *J* = 3.3 Hz), 128.3, 128.3 (d, *J* = 3.0 Hz), 128.2, 127.9, 127.7 (d, *J* = 5.8 Hz), 90.5 (d, *J* = 17.5 Hz), 87.3, 68.7 (d, *J* = 1.5 Hz), 66.9, 66.6 (d, *J* = 4.9 Hz), 65.6, 60.8 (d, *J* = 13.6 Hz), 44.9, 30.3 (d, *J* = 12.2 Hz), 30.1 (d, *J* = 7.3 Hz), 29.7 (d, *J* = 14.5 Hz), 18.5, 18.4 (d, *J* = 16.4 Hz), 16.9. ^{31}P {^{1}H} NMR (162 MHz, Chloroform-*d*) δ 6.8, -22.2. **HRMS** (ESI) m/z: $[M+H]^+$ Calcd for $C_{42}H_{46}FeNP_2$ = 682.2449; Found: 682.2442. $[\alpha]D^{25}$ = 3.80 (*c* 1.0, $CHCl_3$).

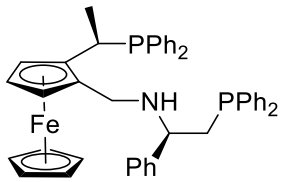

(*R, Rp, R*)-**5g**. Novel compound. Purified by flash chromatography on silica gel (PE/EtOAc, 20/1~5/1). Yellow solid. 130 mg (33 % yield). ^{1}H NMR (600 MHz, Chloroform-*d*) δ 7.44 (t, *J* = 7.2 Hz, 2H), 7.41 – 7.33 (m, 8H), 7.32 – 7.25 (m, 10H), 7.05 (t, *J* = 7.3 Hz, 1H), 6.98 (t, *J* = 7.5 Hz, 2H), 6.91 (t, *J* = 7.0 Hz, 2H), 4.08 (s, 5H), 4.01 (d, *J* = 2.8 Hz, 2H), 3.90 (s, 1H), 3.52 (q, *J* = 7.1 Hz, 1H), 3.48 (dq, *J* = 7.4, 3.7 Hz, 1H), 2.63 (d, *J* = 12.8 Hz, 1H), 2.50 (d, *J* = 12.8 Hz, 1H), 2.46 – 2.41 (m, 2H), 1.43 (dd, *J* = 12.4, 7.0 Hz, 3H). ^{13}C NMR (151 MHz, Chloroform-*d*) δ 144.8 (d, *J* = 5.6 Hz), 138.9 (d, *J* = 12.4 Hz), 138.6 (d, *J* = 13.5 Hz), 137.3 (d, *J* = 17.1 Hz), 135.4 (d, *J* = 17.4 Hz), 134.6 (d, *J* = 19.6 Hz), 133.0, 132.9, 132.8, 132.8, 132.7, 129.1, 128.6 (d, *J* = 14.7 Hz), 128.5, 128.4, 128.2 (d, *J* = 7.0 Hz), 127.8, 127.7 (d, *J* = 5.7 Hz), 127.2, 127.2, 90.7 (d, *J* = 17.9 Hz), 86.8, 68.7, 67.9, 66.7 (d, *J* = 5.2 Hz), 65.7, 61.7 (d, *J* = 16.3 Hz), 45.4, 38.9 (d, *J* = 14.1 Hz), 29.4 (d, *J* = 14.5 Hz), 18.1 (d, *J* = 14.7 Hz). ^{31}P {^{1}H} NMR (243 MHz, Chloroform-*d*) δ 7.0, -23.5. **HRMS** (ESI) m/z: $[M+H]^+$ Calcd for $C_{45}H_{44}FeNP_2$ = 716.2293; Found: 716.2286. $[\alpha]D^{25}$ = -55.30 (*c* 1.0, $CHCl_3$).

Typical procedure **2**: a suspension of (*R, Rp*)-**4b** (0.18 mmol, 80 mg), (*S*)-2-(diphenylphosphino)-1-phenylethanamine (0.9 mmol, 275 mg) and Na_2SO_4 (57 mg) in degassed MeOH (1 mL) was heated at 75 ^{o}C and stirred for 5 h under argon. After cooled to room temperature, $NaBH_3(CN)$ (0.6 mmol, 38

mg) was added and the reaction mixture was stirred for 1 h. The reaction was quenched by the addition of water (10 mL), extracted with DCM (3*5 mL) and the combined organic layers were dried over anhydrous Na_2SO_4 and concentrated under vacuum. Then the residue was redissolved in degassed toluene (3 mL) and triethylenediamine (DABCO, 1 mmol, 112 mg) was added under argon. The reaction mixture was heated at 80 °C and stirred for 6 h. After cooled to room temperature, the reaction mixture was concentrated under vacuum. The residue was purified by flash chromatography on silica gel (PE/EtOAc, 10/1~5/1) to yield 101 mg (77 %) of (*R*, *Rp*, *S*)-**5b** as a yellow solid.

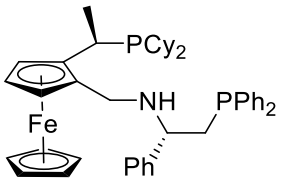

(*R*, *Rp*, *S*)-**5b.** Novel compound. Purified by flash chromatography on silica gel (PE/EtOAc, 10/1~4/1). Yellow solid. 101 mg (77 % yield). ^{1}H NMR (400 MHz, Chloroform-*d*) δ 7.43 – 7.18 (m, 15H), 4.17 (dd, *J* = 2.4, 1.4 Hz, 1H), 4.02 (t, *J* = 1.9 Hz, 1H), 4.00 (s, 5H), 3.81 (q, *J* = 7.1 Hz, 1H), 3.43 (d, *J* = 13.3 Hz, 1H), 3.16 (d, *J* = 13.4 Hz, 1H), 2.81 (q, *J* = 7.1 Hz, 1H), 2.55 (dd, *J* = 13.7, 7.1 Hz, 1H), 2.45 (dd, *J* = 13.7, 7.3 Hz, 1H), 1.81 – 1.53 (m, 11H), 1.48 (t, *J* = 6.6 Hz, 3H), 1.32 – 1.01 (m, 11H). ^{13}C NMR (101 MHz, Chloroform-*d*) δ 144.1, 139.0 (d, *J* = 3.0 Hz), 138.8 (d, *J* = 3.1 Hz), 133.0 (d, *J* = 10.9 Hz), 132.8 (d, *J* = 10.6 Hz), 128.4, 128.4, 128.3, 128.3 (d, *J* = 1.6 Hz), 128.2, 127.6, 127.1, 92.6 (d, *J* = 16.7 Hz), 84.6, 68.9, 66.6, 65.4, 60.4 (d, *J* = 17.8 Hz), 45.4, 38.9 (d, *J* = 13.8 Hz), 32.9 (d, *J* = 18.7 Hz), 32.0 (d, *J* = 17.7 Hz), 31.3, 31.2 (d, *J* = 3.0 Hz), 31.0, 30.4 (d, *J* = 6.3 Hz), 29.8 (d, *J* = 10.5 Hz), 27.8 (d, *J* = 2.4 Hz), 27.7 (d, *J* = 7.9 Hz), 27.3 (d, *J* = 8.2 Hz), 27.1 (d, *J* = 11.0 Hz), 26.5, 26.4, 26.2, 16.0 (d, *J* = 1.9 Hz). ^{31}P {^{1}H} NMR (162 MHz, Chloroform-*d*) δ 15.7, -22.8. **HRMS** (ESI) m/z: $[M+H]^+$ Calcd for $C_{45}H_{56}FeNP_2$ = 728.3232; Found: 728.3220. $[\alpha]D^{25}$ = -24.90 (*c* 1.0, $CHCl_3$).

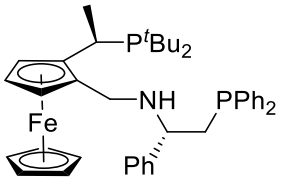

(*R, Rp, S*)-**5c.** Novel compound. Purified by flash chromatography on silica gel (PE/EtOAc, 10/1~4/1). Yellow solid. 45 mg (80 % yield). ^{1}H NMR (400 MHz, Chloroform-*d*) δ 7.44 – 7.35 (m, 4H), 7.34 – 7.20 (m, 11H), 4.15 (dd, *J* = 2.4, 1.4 Hz, 1H), 4.07 (t, *J* = 1.8 Hz, 1H), 3.97 (s, 5H), 3.83 (q, *J* = 7.1 Hz, 1H), 3.56 (d, *J* = 13.6 Hz, 1H), 3.21 (d, *J* = 13.6 Hz, 1H), 3.08 (q, *J* = 7.2 Hz, 1H), 2.54 (dd, *J* = 13.6, 6.6 Hz, 1H), 2.45 (dd, *J* = 13.8, 7.6 Hz, 1H), 1.79 (dd, *J* = 7.3, 3.8 Hz, 3H), 1.24 (d, *J* = 10.6 Hz, 9H), 1.05 (d, *J* = 11.0 Hz, 9H). ^{13}C NMR (101 MHz, Chloroform-*d*) δ 139.1, 139.0 (d, *J* = 2.9 Hz), 133.0 (d, *J* = 2.5 Hz), 132.8 (d, *J* = 2.8 Hz), 128.4, 128.3, 128.3, 128.3, 128.2, 128.2, 127.8, 127.1, 94.2 (d, *J* = 22.7 Hz), 69.6, 69.0, 67.6, 65.1, 59.8 (d, *J* = 18.2 Hz), 45.6, 39.0 (d, *J* = 14.3 Hz), 34.1 (d, *J* = 30.1 Hz), 33.2 (d, *J* = 26.7 Hz), 31.5 (d, *J* = 13.1 Hz), 31.0 (d, *J* = 13.0 Hz), 30.1, 29.8, 16.7 (d, *J* = 2.8 Hz). ^{31}P {^{1}H} NMR (162 MHz, Chloroform-*d*) δ 47.5 (d, *J* = 3.9 Hz), -23.0 (d, *J* = 4.7 Hz). **HRMS** (ESI) m/z: $[M+H]^+$ Calcd for $C_{41}H_{52}FeNP_2$ = 676.2919; Found: 676.2912. $[\alpha]D^{25}$ = -38.90 (*c* 1.0, $CHCl_3$).

2.7.3 Synthesis of the Mn-PNP complexes

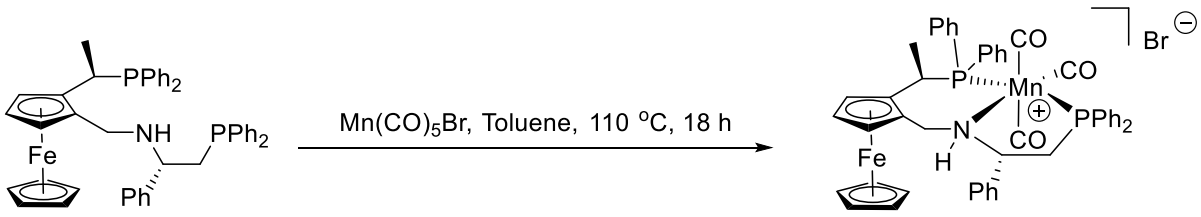

(*R, Rp, S*)-**5a** **9**

Scheme 2.10 Synthesis of Mn-5a complex

Typical procedure **1** (*in situ* synthesis for catalytic reaction): a suspension of the PNP ligand (*R*, *Rp*, *S*)-**5a** (0.05 mmol, 36 mg) and $Mn(CO)_5Br$ (0.05 mmol, 14 mg) in dry toluene (1 mL) was heated at

110 °C and stirred for 18 h under argon. The mixture was cooled to room temperature and concentrated to dryness in vacuo to give an orange solid. The resulting Mn complex was applied in the hydrogenation of ketones without further purification.

Typical procedure **2**[15]: a suspension of the PNP ligand (*R, Rp, S*)-**5a** (0.14 mmol, 100 mg) and $Mn(CO)_5Br$ (0.14 mmol, 39 mg) in dry toluene (2 mL) was heated at 110 °C and stirred for 18 h under argon. The mixture was cooled to room temperature and concentrated to dryness. The residue was dissolved in DCM and filtered to remove insoluble materials. The product was precipitated by the addition of *n*-hexane, collected by filtration, and washed with *n*-hexane to give an orange powder.

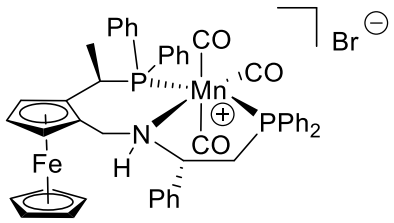

Compound **9**. Novel compound. The Mn complex was made via the procedure **2**. Orange powder. 113 mg (86 % yield). ^{1}H NMR (400 MHz, DMSO-d_6) δ 7.81 – 7.72 (m, 4H), 7.55 (d, *J* = 19.3 Hz, 8H), 7.50 – 7.40 (m, 7H), 7.42 – 7.32 (m, 6H), 4.46 (s, 1H), 4.18 (d, *J* = 18.2 Hz, 2H), 4.10 (d, *J* = 4.6 Hz, 2H), 3.93 (s, 5H), 3.86 (s, 1H), 3.83 – 3.71 (m, 2H), 2.93 (d, *J* = 7.2 Hz, 1H), 1.24 (s, 3H). ^{13}C NMR (151 MHz, Acetone-d_6) δ 133.9 – 133.7 (m), 133.4 – 133.2 (m), 133.1, 132.9 – 132.7 (m), 132.3, 132.1 – 131.9 (m), 130.9, 130.3 – 130.0 (m), 129.5, 129.4, 129.2 – 129.0 (m), 128.7, 128.7 – 128.6 (m), 128.5, 128.5 – 128.3 (m), 128.3, 128.0 – 127.8 (m), 127.7, 127.3 (d, *J* = 8.0 Hz), 81.8 – 81.5 (m), 70.6, 69.0, 68.8 (d, *J* = 2.7 Hz), 67.5 – 67.2 (m), 66.8, 54.3, 51.3 (d, *J* = 36.1 Hz), 46.5, 35.3, 15.1, 13.5. ^{31}P {^{1}H} NMR (162 MHz, Chloroform-*d*) δ 66.6 (d, *J* = 100.8 Hz), 63.5 (d, *J* = 101.4 Hz). IR absorptions: 509, 611, 638, 694, 739, 806, 895, 951, 999, 1028, 1049, 1094, 1433, 1848, 1925, 1964 cm^{-1}. **HRMS** (ESI) m/z: $[M\text{-}Br]^+$ Calcd for $C_{48}H_{43}FeMnNO_3P_2$ = 854.1443; Found: 854.1438. $[\alpha]_D^{23}$ = -250.90 (*c* 1.0, $CHCl_3$).

9

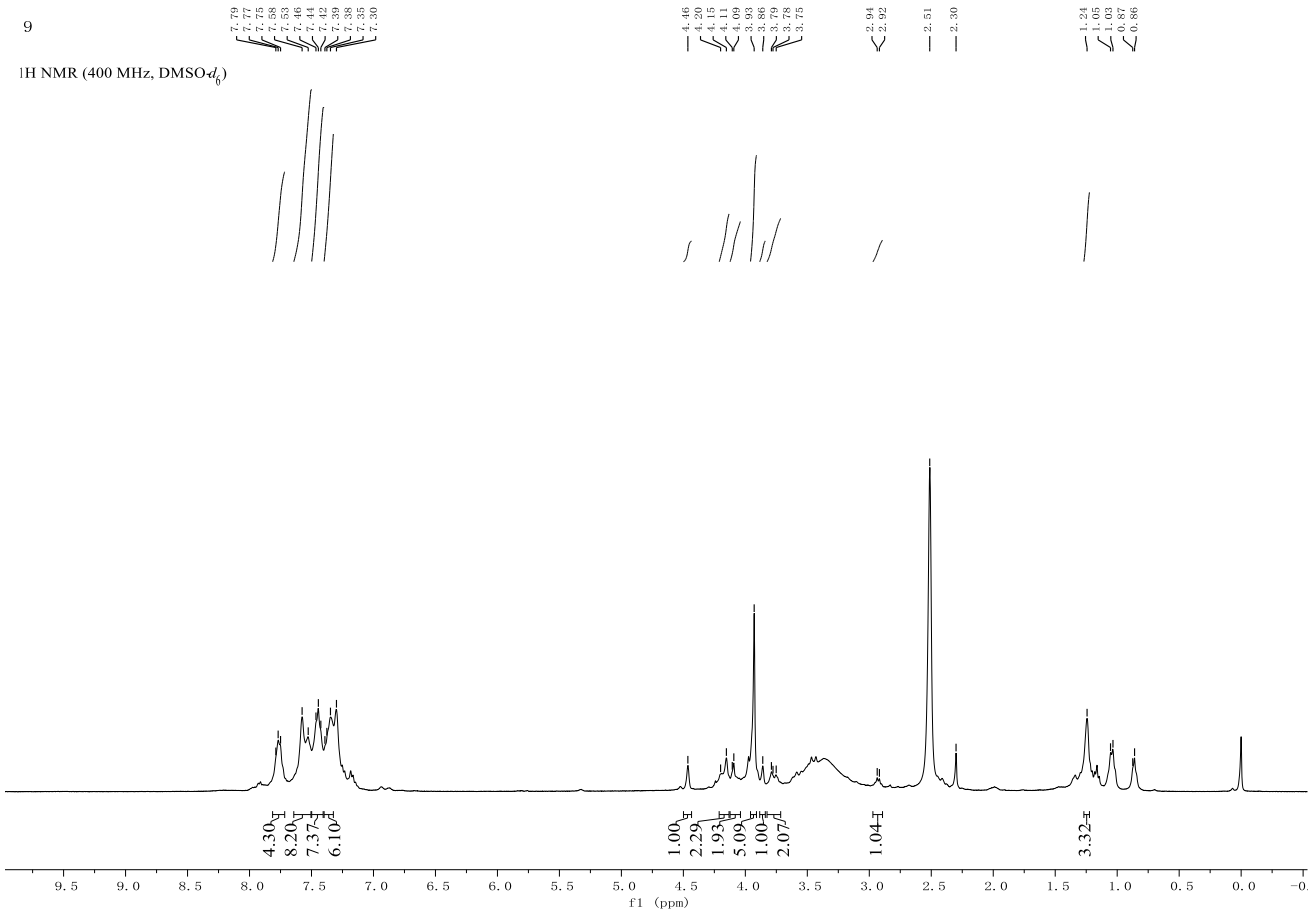

^{1}H NMR (400 MHz, DMSO-d_6)

9

13C NMR (151 MHz, Acetone-d_6)

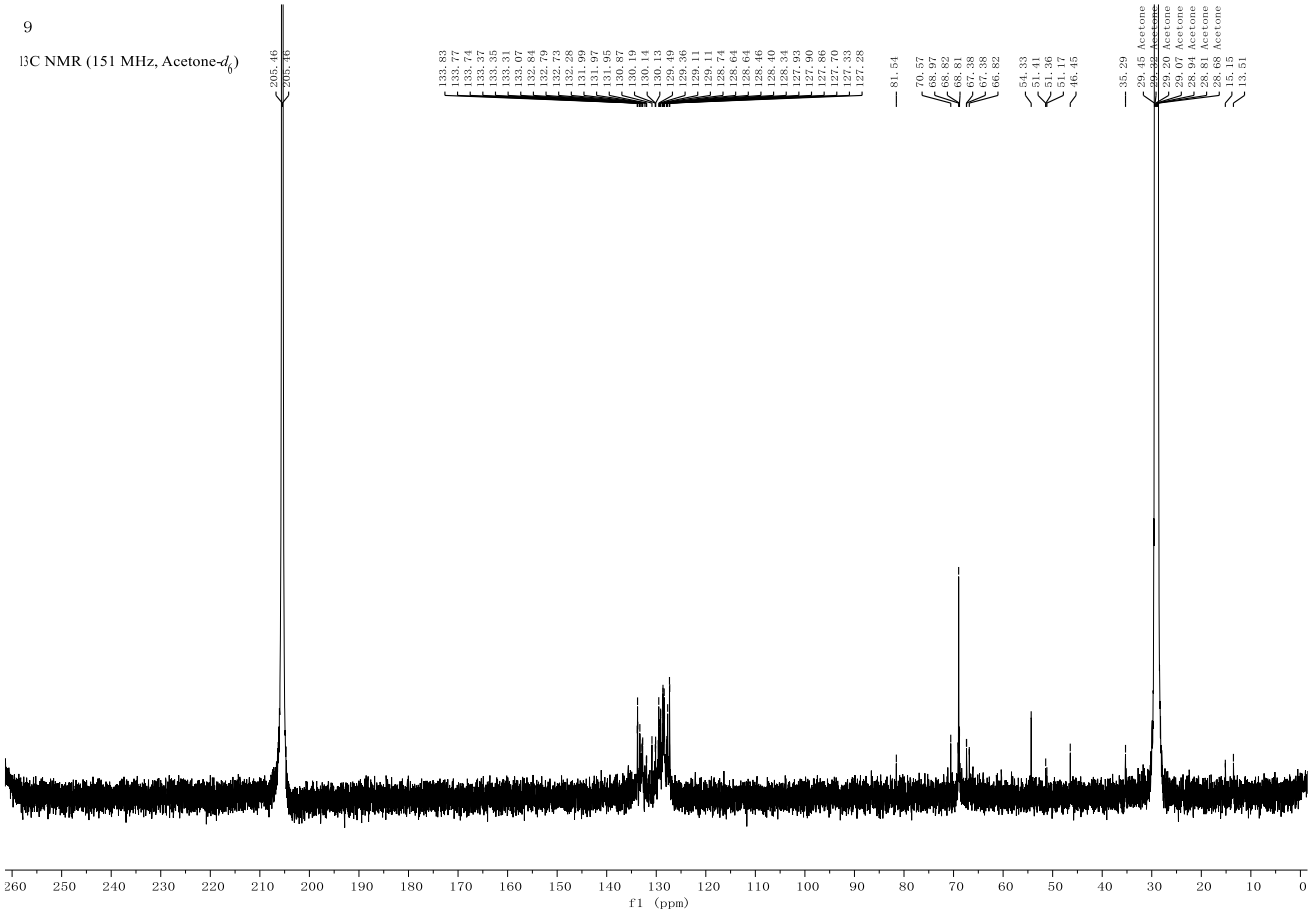

9

31P NMR (162 MHz, Chloroform-d)

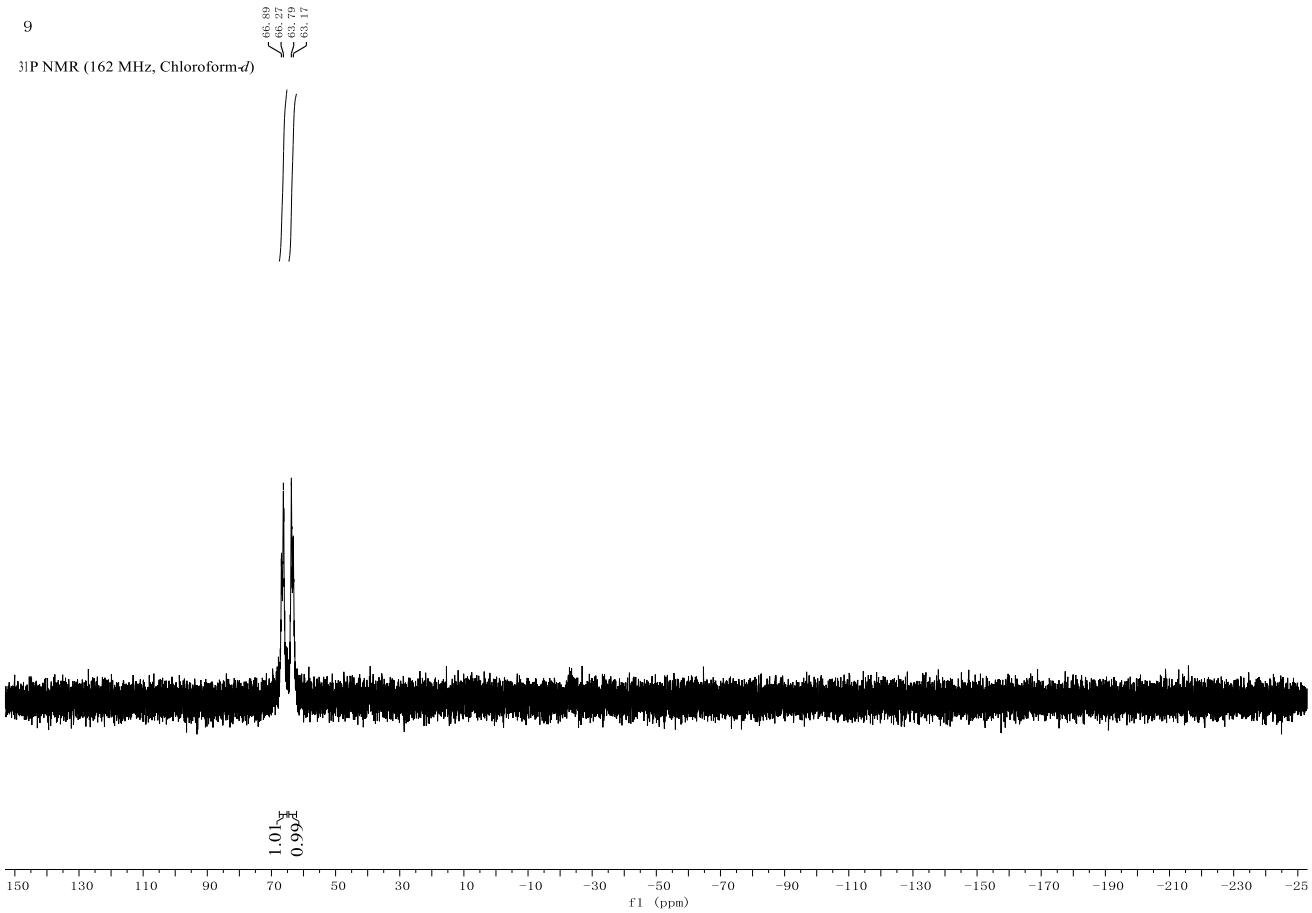

HRMS (ESI) for $[C_{48}H_{43}FeMnNO_3P_2]^+$ ($[M\text{-}Br]^+$)

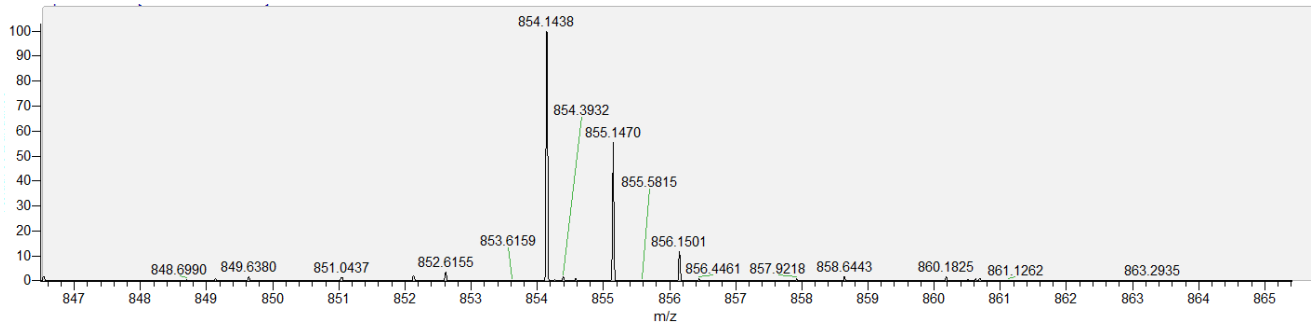

IR spectrum for complex **9**

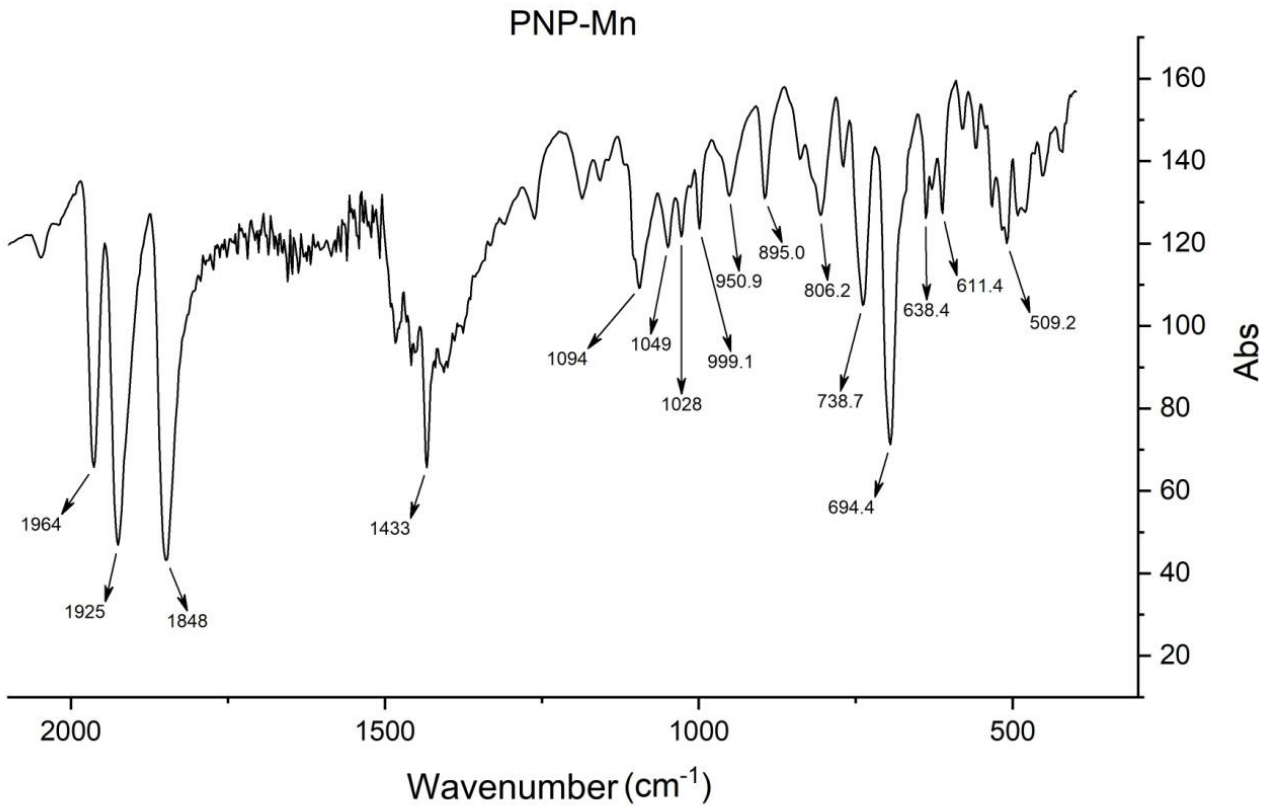

Mn-5b. The Mn complex was made via the procedure **1**. **^{31}P {^{1}H} NMR** (243 MHz, Chloroform-*d*) δ 67.3 (d, *J* = 30.9 Hz) , 62.4 (d, *J* = 30.4 Hz) (major, 1:1); 65.2, 52.2 (minor, 1:1).

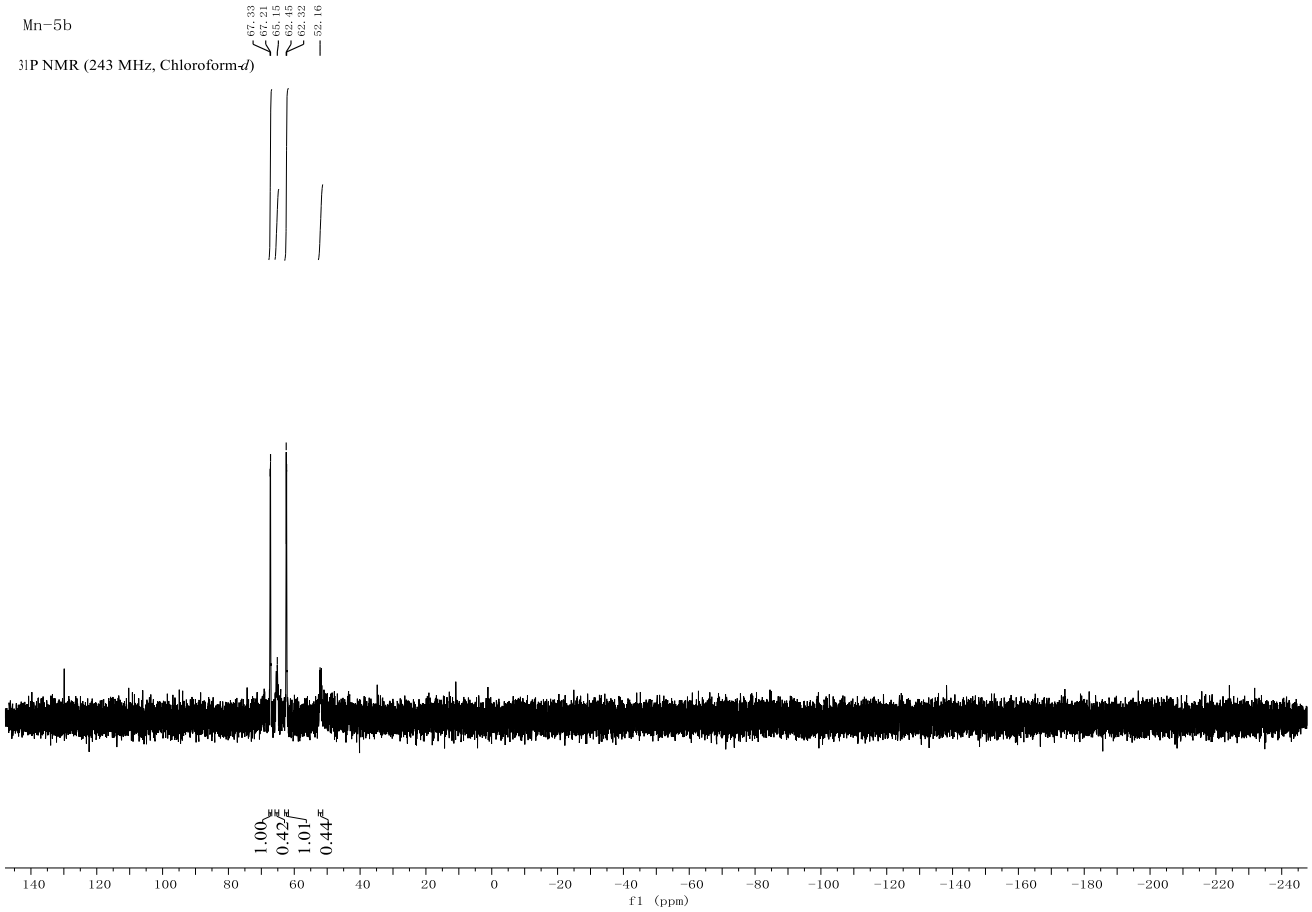

Mn-5c. The Mn complex was made via the procedure **1**. However, the complex could not be obtained probably because of the steric effect of bulky ^{t}Bu group.

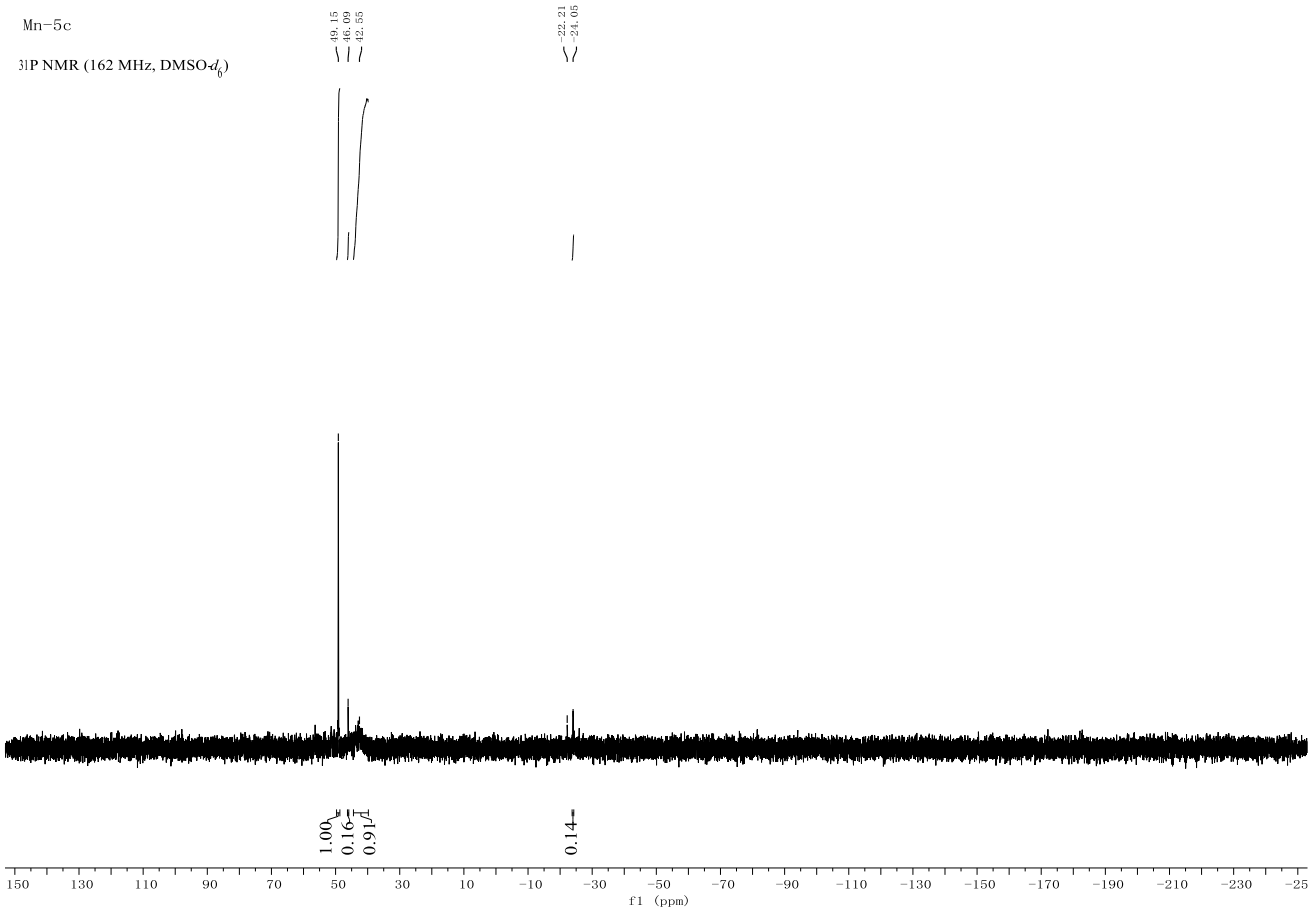

Mn-5d. The Mn complex was made via the procedure **1**. **^{31}P {^{1}H} NMR** (162 MHz, DMSO-d_6) δ 75.1 (d, J = 27.2 Hz), 66.2 (d, J = 24.1 Hz) (major, 1:1); 76.3, 56.3 (minor, 1:1).

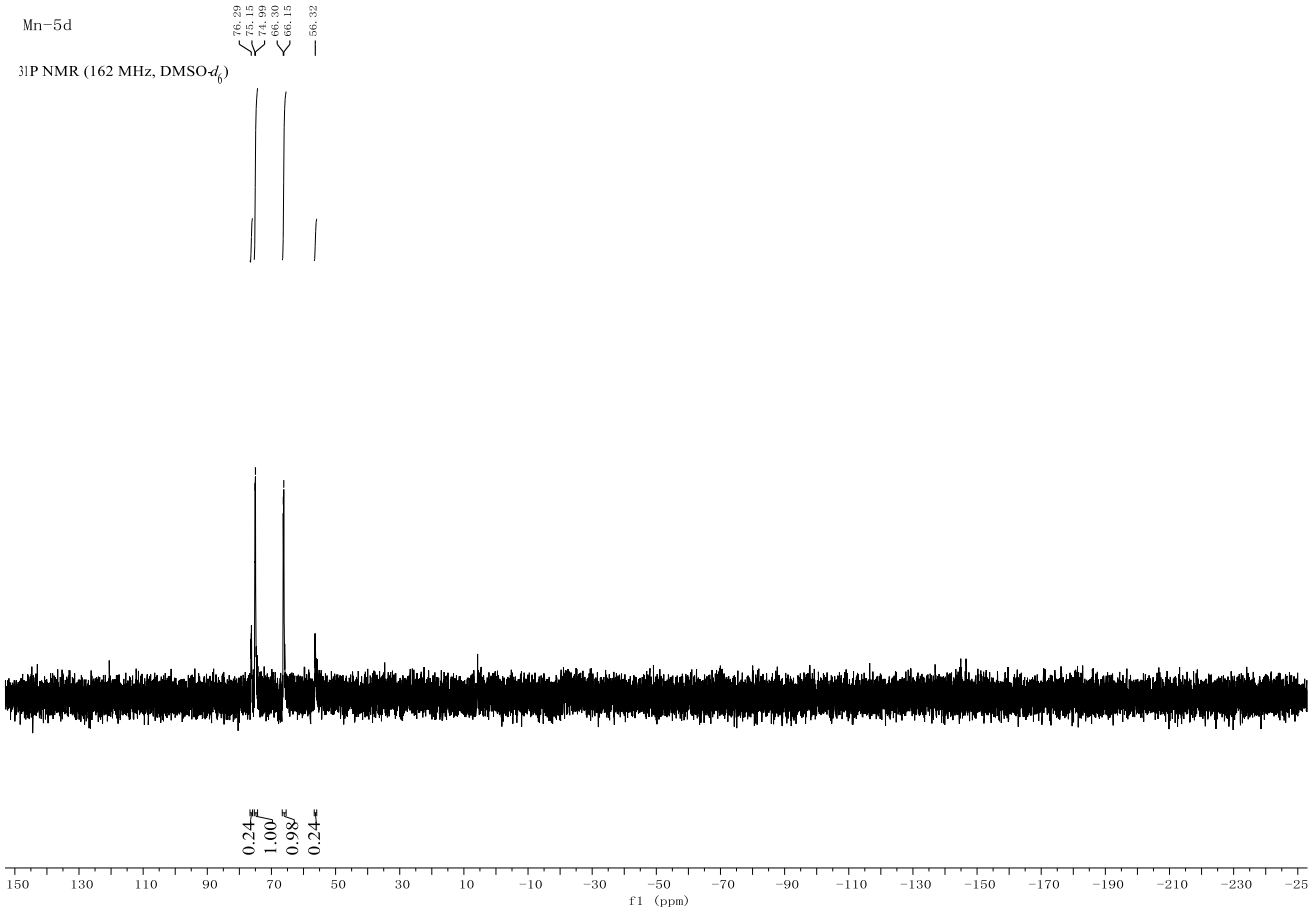

Mn-5e. The Mn complex was made via the procedure **1**. **^{31}P {^{1}H} NMR** (243 MHz, DMSO-d_6) δ 65.0 (d, J = 24.4 Hz), 64.2 (d, J = 24.9 Hz).

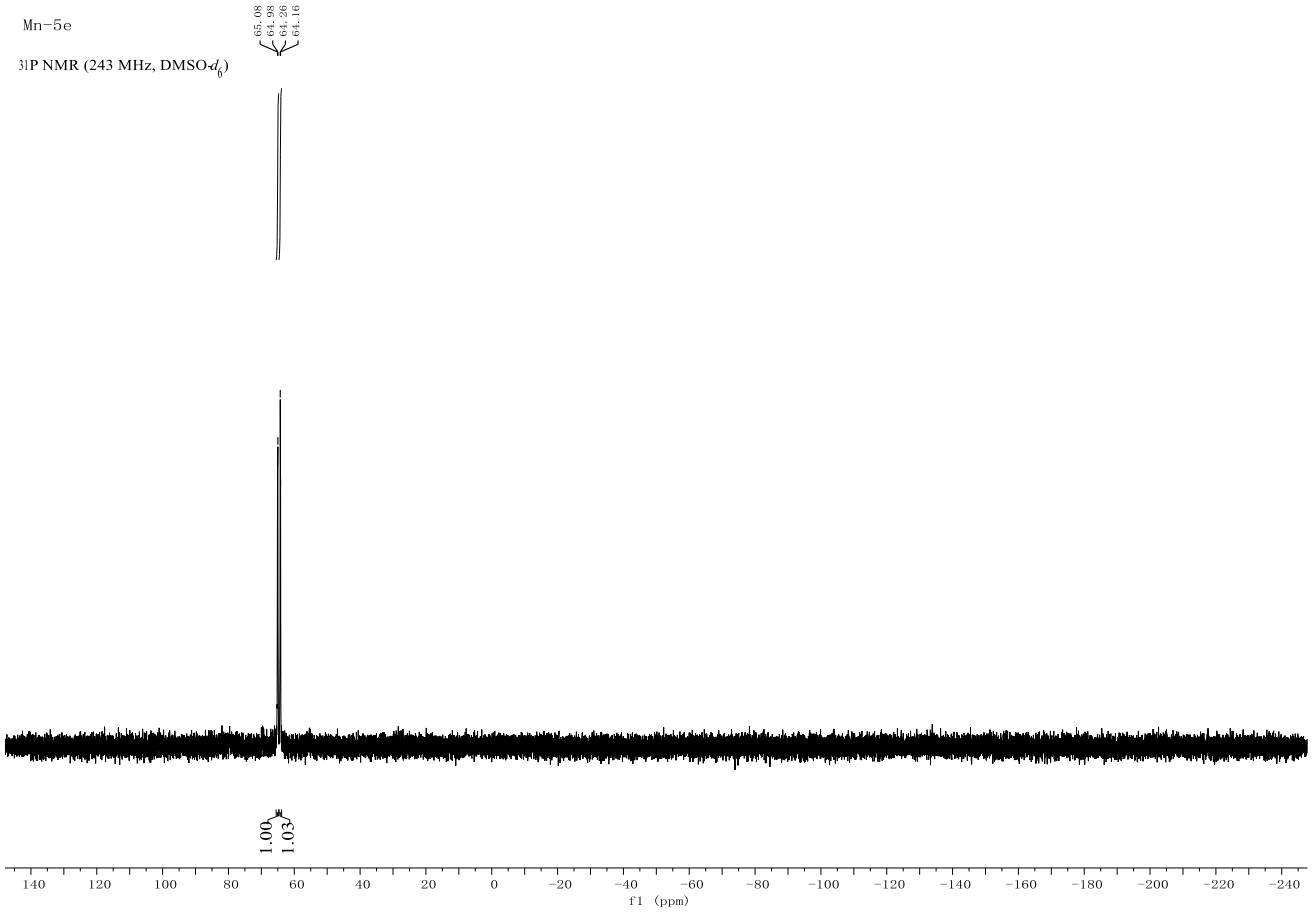

Mn-5f. The Mn complex was made via the procedure **1**. **^{31}P {^{1}H} NMR** (162 MHz, Chloroform-*d*) δ 65.8 (d, *J* = 99.5 Hz), 62.0 (d, *J* = 98.0 Hz). (Major, 1:1)

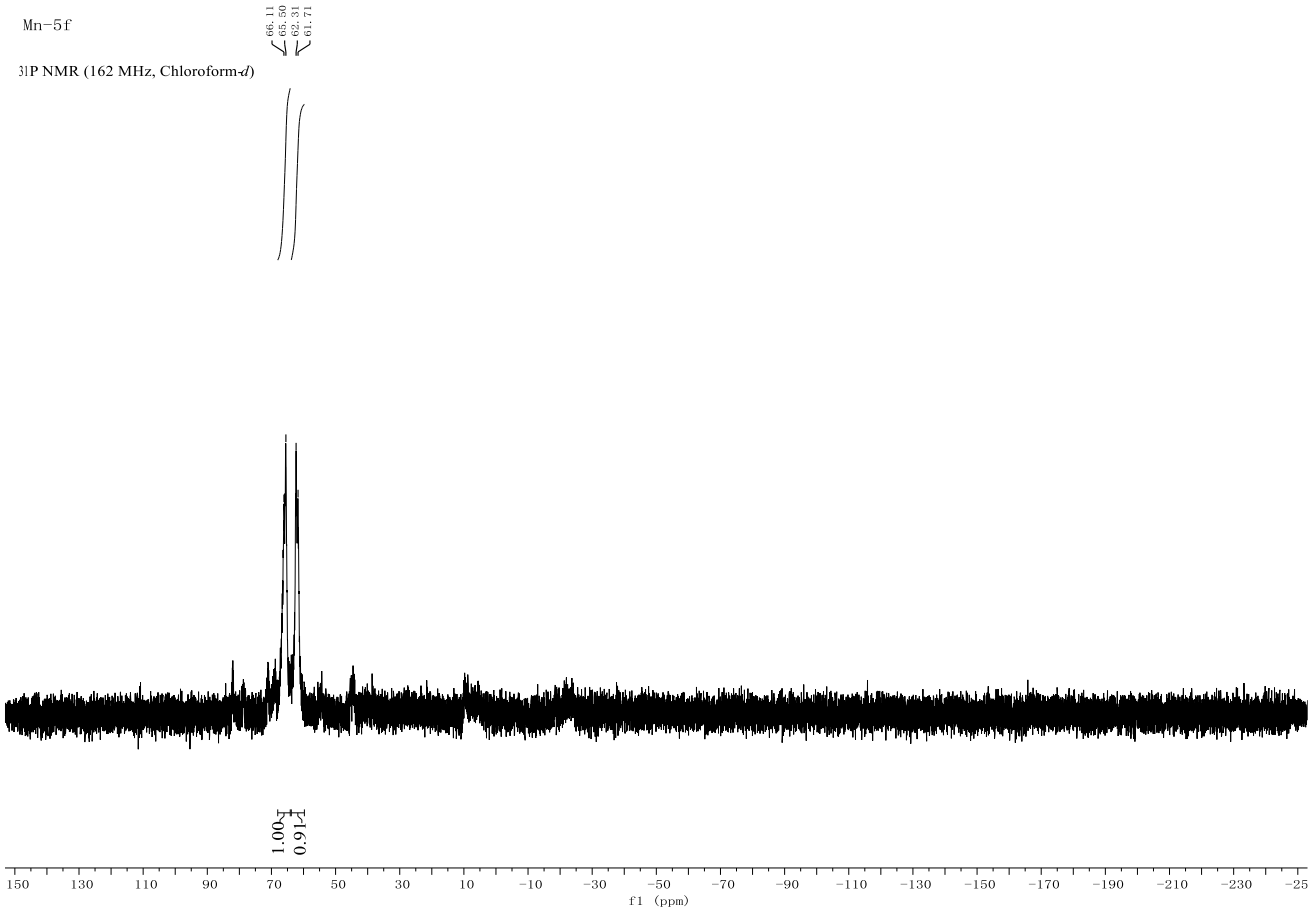

Mn-5g. The Mn complex was made via the procedure **1**. **^{31}P {^{1}H} NMR** (243 MHz, Acetone-d_6) δ 67.5, 54.5 (d, J = 98.4 Hz), 48.1 (d, J = 107.7 Hz) (1: 0.4: 0.6); 6.6, -23.4 (ligand peaks, 1:1).

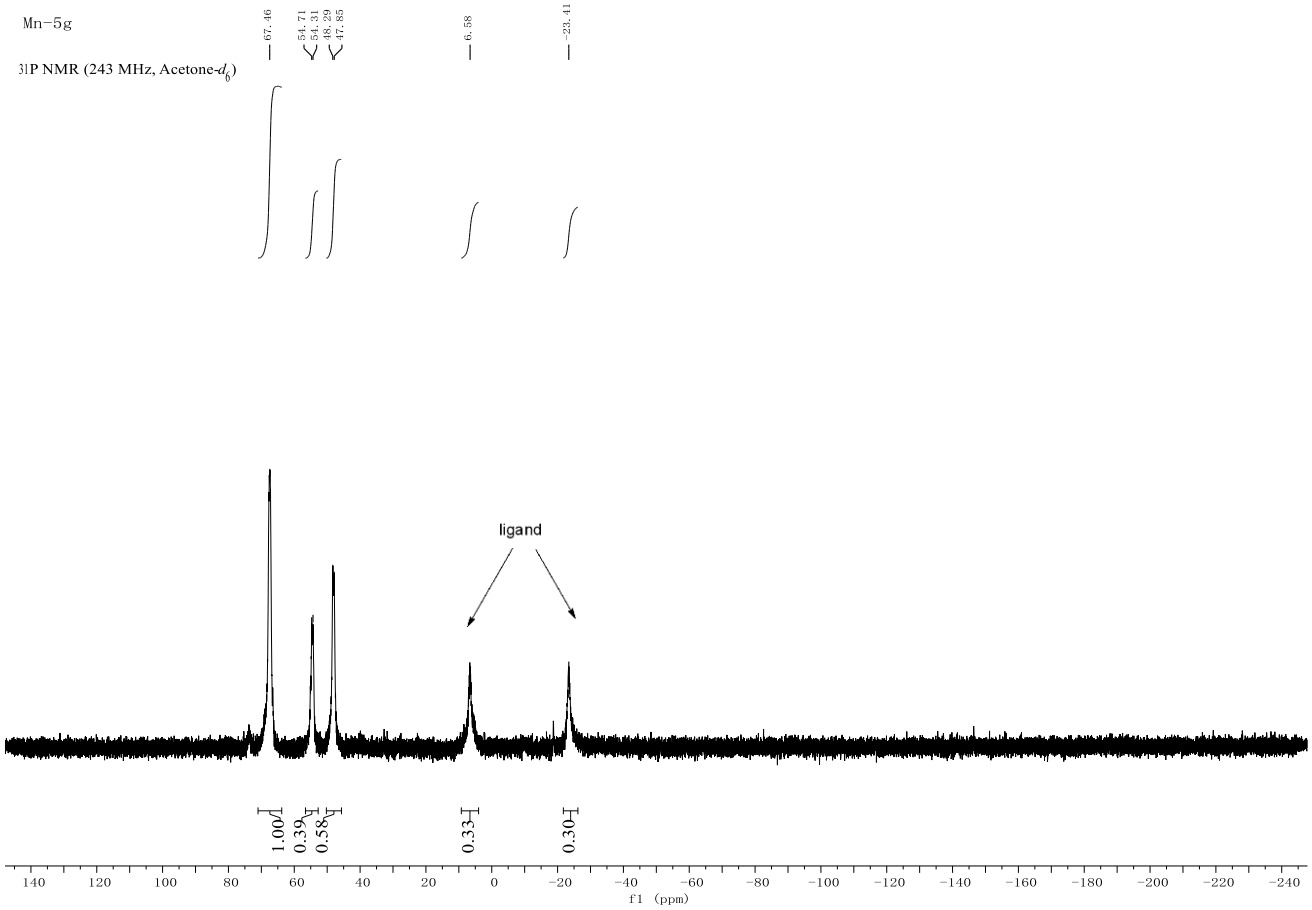

2.7.4 Investigation of the active species

Amido complex

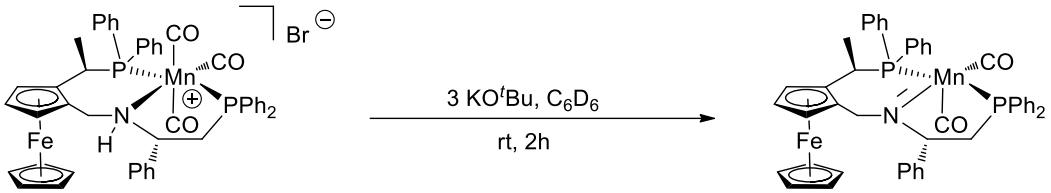

Mn-5a **Amido complex**

Scheme 2.11 Synthesis of the manganese amido complex

In a glove box, the complex **Mn-5a** (10 mg) was placed with 3 equivalents of KO^{t}Bu (3.4 mg) in a vial, and 1 ml of C_6D_6 was added. The yellow solution was turned to red solution immediately. The red solution was transferred to a Youngtube for NMR analysis. **^{31}P {^{1}H} NMR** (243 MHz, Benzene-d^6) δ 84.2 (d, J = 103.3 Hz), 70.1 (d, J = 102.2 Hz) (major, 1:1); 7.0, -22.7 (ligand peaks, 1:1)

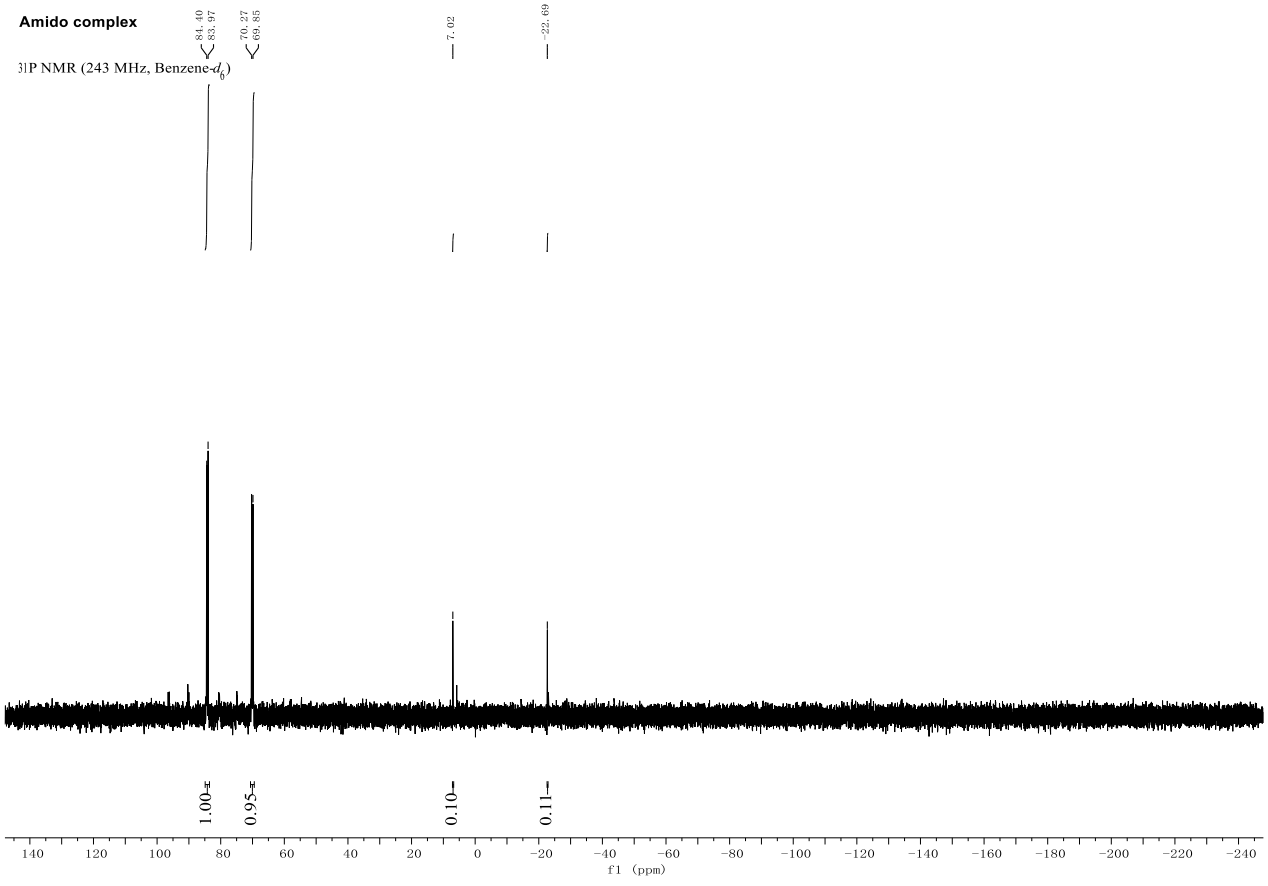

Hydride complex

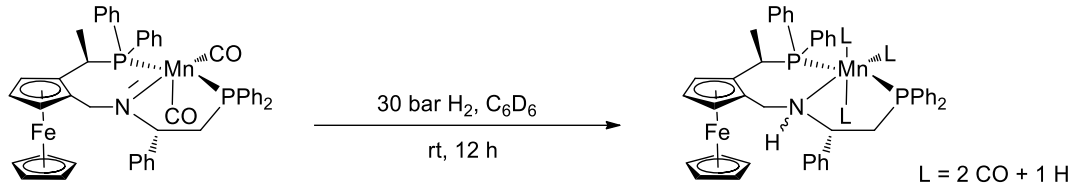

Amido complex **Hydride complex**

Scheme 2.12 Synthesis of the manganese hydride complex

In a glovebox, the amido complex dissolved in 1 mL of C_6D_6 was placed into a vial in the autoclave. The autoclave was purged 3 times with hydrogen gas, then pressurized to 30 bar and stirred for 12 hours at room temperature. The red solution was turned to yellow solution. The yellow solution was transferred to a Youngtube for NMR analysis. **^{1}H NMR** (400 MHz, Benzene-d_6) δ -3.37 (t, J = 64.5 Hz, 2H), -3.48 (dd, J = 58.9, 48.6 Hz, 3H), -3.72 (dd, J = 60.6, 51.2 Hz, 1H).

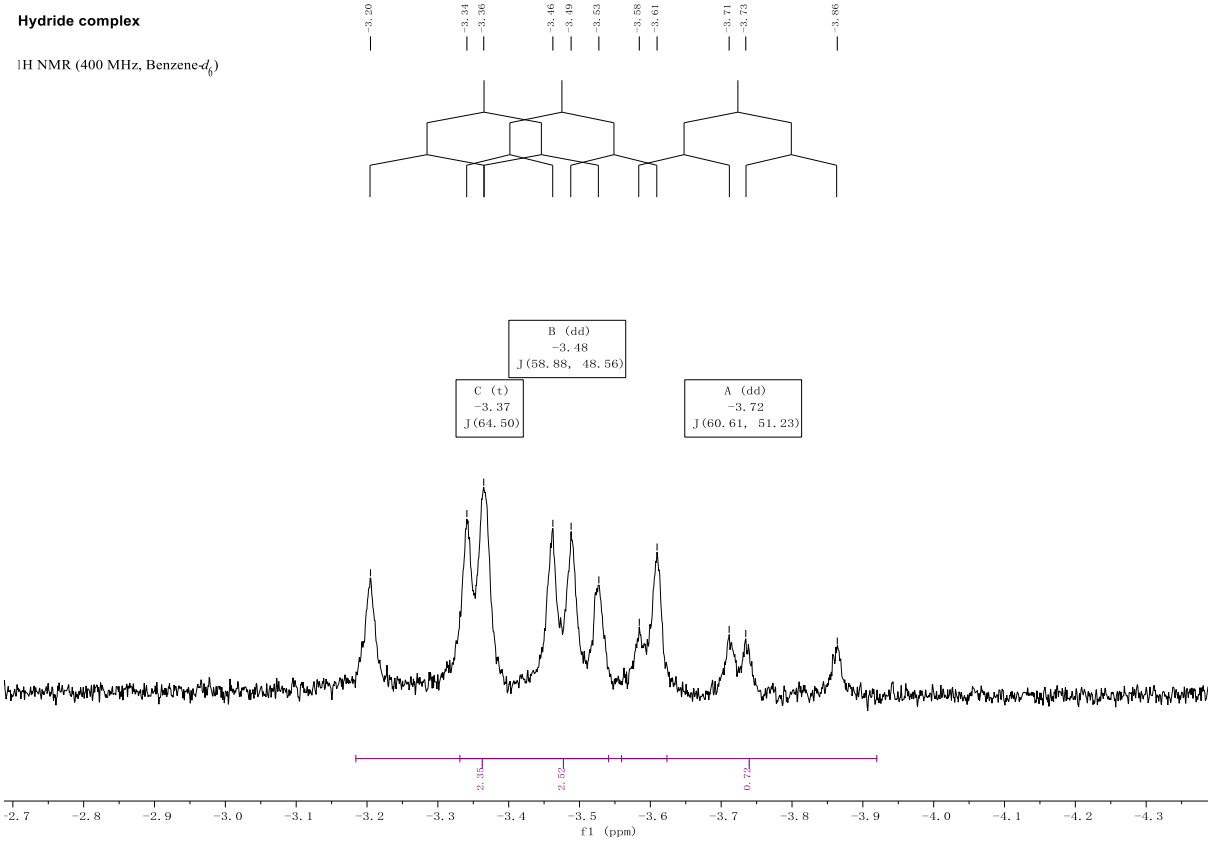

^{31}P {^{1}H} NMR (162 MHz, Benzene-d_6) δ 89.5 (d, J = 54.9 Hz), 80.4 (d, J = 54.5 Hz) (1:1); 87.2 (d, J = 58.2 Hz), 85.4 (d, J = 58.2 Hz) (1:1); 86.9 (d, J = 65.9 Hz), 82.9 (d, J = 66.7 Hz) (1:1); 7.0, -22.7 (ligand peaks, 1:1).

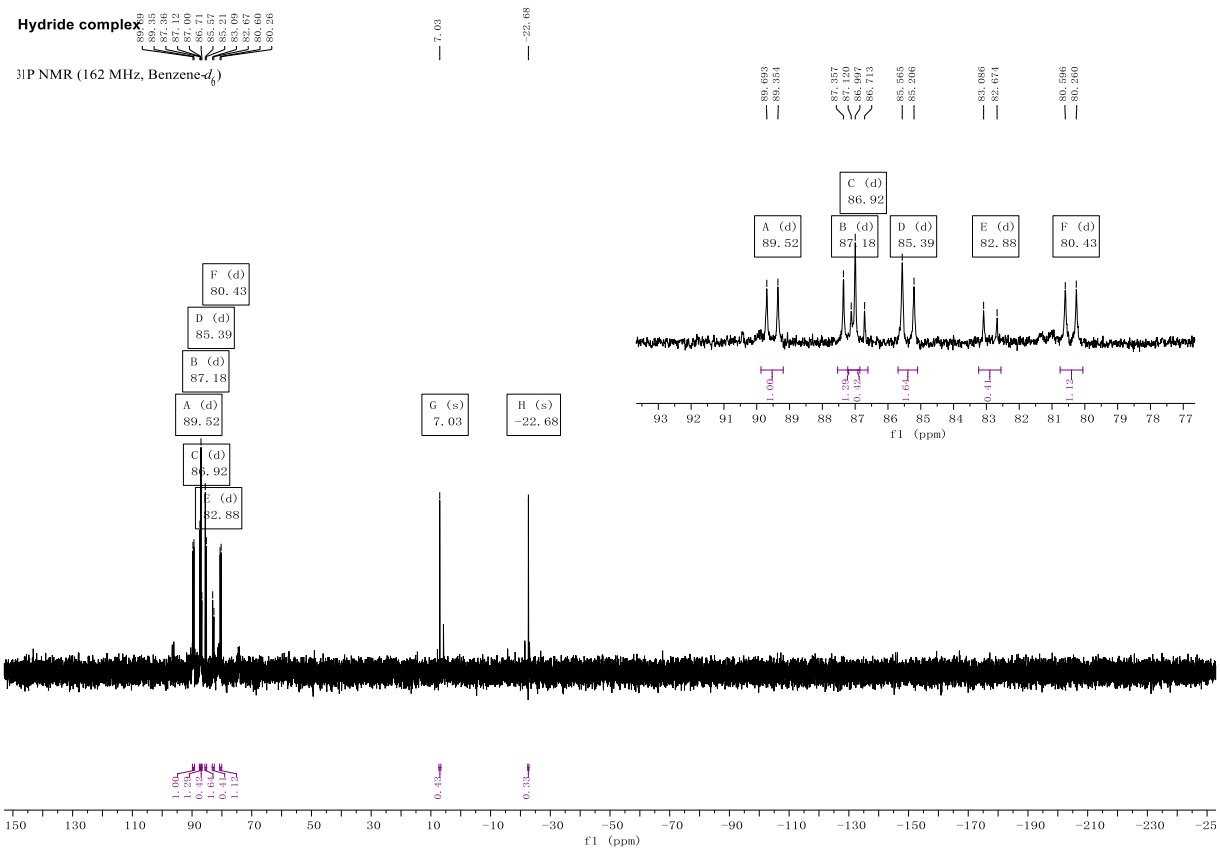

Figure 2.5 Color change of the active species

2.7.5 General procedure for the hydrogenation of ketones

In a glove box, to a vial (3 mL) was charged with catalyst **9** (1 mol %, 1.9 mg), KOH (2 mol %, 40 ul, 0.1 M in MeOH), substrate (0.2 mmol) and MeOH (0.4 mL). The vial was placed into the autoclave. The autoclave was sealed and purged three times with hydrogen gas, then pressurized to 60 bar and stirred at room temperature or specific temperatures for 36 h. Afterwards, the vessel was vented carefully in a hood and the reaction mixture was concentrated *in vacuo*. The residue was purified by flash chromatography on silica (PE/EtOAc, 10/1) to afford the chiral alcohol. The enantiomeric excess (ee) was determined by HPLC or GC on a chiral stationary phase.

2.7.6 Analytical data of the isolated products

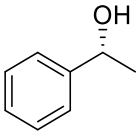

(*R*)-1-Phenylethanol (8a). Colorless oil, 99% isolated yield (99% NMR conversion); 95% *ee*, determined by HPLC analysis on Chiralpak OD-3 column (Hexane/*i*-PrOH = 90/10, flow rate = 1 mL/min, λ= 210 nm), t_R =5.8 min (*major*), t_R = 6.4 min (*minor*). [α]D^{20}= +46.60 (*c* 0.5, $CHCl_3$). (lit.[17] [α]D^{25} = +43.43 (*c* 1.0, $CHCl_3$), *R*). ^{1}H NMR (600 MHz, Chloroform-*d*) δ 7.40 – 7.32 (m, 4H), 7.30 – 7.24 (m, 1H), 4.90 (q, *J* = 6.5 Hz, 1H), 1.85 (s, 1H), 1.50 (d, *J* = 6.2 Hz, 3H). ^{13}C NMR (151 MHz, Chloroform-*d*) δ 145.8, 128.5, 127.5, 125.4, 70.5, 25.2.

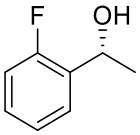

(*R*)-1-(2-Fluorophenyl)ethanol (8b). Colorless oil, 93% isolated yield (99% NMR conversion); 96% *ee*, determined by HPLC analysis on Chiralpak OD-3 column (Hexane/i-PrOH = 95/5, flow rate = 1 mL/min, λ= 220 nm), t_R = 6.6 min (*major*), t_R = 6.9 min (*minor*). [α]D^{25}= +39.60 (*c* 1.0, $CHCl_3$). (lit.[17]

[α]D^{25} = +32.97 (*c* 1.0, $CHCl_3$), *R*). ^{1}H NMR (400 MHz, Chloroform-*d*) δ 7.49 (t, *J* = 7.7 Hz, 1H), 7.24 (q, *J* = 6.9, 5.7 Hz, 1H), 7.15 (t, *J* = 7.5 Hz, 1H), 7.02 (t, *J* = 9.4 Hz, 1H), 5.20 (p, *J* = 5.7 Hz, 1H), 2.01 (s, 1H), 1.52 (d, *J* = 6.5 Hz, 3H). ^{13}C NMR (101 MHz, Chloroform-*d*) δ 159.7 (d, *J* = 245.2 Hz), 132.6 (d, *J* = 13.2 Hz), 128.8 (d, *J* = 8.2 Hz), 126.6 (d, *J* = 4.7 Hz), 124.3 (d, *J* = 3.5 Hz), 115.3 (d, *J* = 21.7 Hz), 64.6 (d, *J* = 3.1 Hz), 24.0. ^{19}F NMR (565 MHz, Chloroform-*d*) δ -120.1.

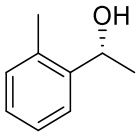

(*R*)-1-(*o*-Tolyl)ethanol (8c). Colorless oil, 66% isolated yield (80% NMR conversion); 98% *ee*, determined by HPLC analysis on Chiralpak AD-3 column (Hexane/i-PrOH = 99/1, flow rate = 0.5 mL/min, λ= 210 nm), t_R = 5.9 min (*major*), t_R = 6.7 min (*minor*). [α]D^{22}= +68.80 (*c* 1.0, $CHCl_3$). (lit.[17] [α]D^{25} = +72.57 (*c* 1.0, $CHCl_3$), *R*). ^{1}H NMR (400 MHz, Chloroform-*d*) δ 7.47 (dd, *J* = 7.6, 1.5 Hz, 1H), 7.25 – 7.18 (m, 1H), 7.18 – 7.06 (m, 2H), 5.06 (q, *J* = 6.4 Hz, 1H), 2.31 (s, 3H), 2.13 (s, 1H), 1.42 (d, *J* = 6.4 Hz, 3H). ^{13}C NMR (101 MHz, Chloroform-*d*) δ 143.9, 134.2, 130.4, 127.2, 126.4, 124.5, 66.8, 24.0, 19.0.

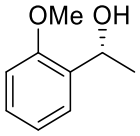

(*R*)-1-(2-Methoxyphenyl)ethanol (8d). Colorless oil, 40% isolated yield (50% NMR conversion); 98% *ee*, determined by HPLC analysis on Chiralpak OD-3 column (Hexane/i-PrOH = 95/5, flow rate = 1 mL/min, λ= 220 nm), t_R = 10.1 min (*minor*), t_R = 10.9 min (*major*). [α]D^{22}= +26.40 (*c* 1.0, $CHCl_3$). (lit.[17] [α]D^{25} = +22.10 (*c* 1.0, $CHCl_3$), *R*). ^{1}H NMR (400 MHz, Chloroform-*d*) δ 7.33 (dd, *J* = 7.5, 1.7 Hz, 1H), 7.24 (dd, *J* = 15.6, 1.7 Hz, 1H), 6.95 (t, *J* = 7.4 Hz, 1H), 6.87 (d, *J* = 8.2 Hz, 1H), 5.08 (q, *J* = 6.5 Hz, 1H), 3.84 (s, 3H), 2.78 (s, 1H), 1.49 (d, *J* = 6.5 Hz, 3H). ^{13}C NMR (101 MHz, Chloroform-*d*) δ 156.5, 133.5, 128.3, 126.1, 120.8, 110.4, 66.4, 55.3, 22.9.

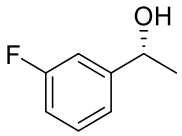

(*R*)-1-(3-Fluorophenyl)ethanol (8e). Colorless oil, 92% isolated yield (99% NMR conversion); 96% *ee*, determined by HPLC analysis on Chiralpak OJ-H column (Hexane/i-PrOH = 95/5, flow rate = 1 mL/min, λ= 210 nm), t_R = 9.3 min (*minor*), t_R = 9.8 min (*major*). [α]D^{20}= +29.50 (*c* 1.0, $CHCl_3$). (lit.[32] [α]D^{20} = +39.7 (*c* 1.18, $CHCl_3$), *R*). ^{1}H NMR (400 MHz, Chloroform-*d*) δ 7.29 (td, *J* = 7.9, 5.8 Hz, 1H), 7.14 – 7.03 (m, 2H), 6.94 (tdd, *J* = 8.4, 2.7, 1.0 Hz, 1H), 4.86 (q, *J* = 6.5 Hz, 1H), 2.30 (s, 1H), 1.46 (d, *J* = 6.5 Hz, 3H). ^{13}C NMR (101 MHz, Chloroform-*d*) δ 163.0 (d, *J* = 245.8 Hz), 148.5 (d, *J* = 6.6 Hz), 130.0 (d, *J* = 8.1 Hz), 120.9 (d, *J* = 2.7 Hz), 114.2 (d, *J* = 21.2 Hz), 112.3 (d, *J* = 21.8 Hz), 69.8 (d, *J* = 1.8 Hz), 25.2. ^{19}F NMR (376 MHz, Chloroform-*d*) δ -113.0.

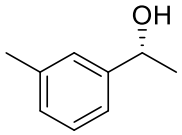

(*R*)-1-(*m*-Tolyl)ethanol (8f). Colorless oil, 99% isolated yield (99% NMR conversion); 95% *ee*, determined by HPLC analysis on Chiralpak OD-3 column (Hexane/i-PrOH = 90/10, flow rate = 1 mL/min, λ= 220 nm), t_R = 5.3 min (*major*), t_R = 5.9 min (*minor*). [α]D^{25}= +40.60 (*c* 1.0, $CHCl_3$). (lit.[17] [α]D^{25} = +38.70 (*c* 1.0, $CHCl_3$), *R*). ^{1}H NMR (400 MHz, Chloroform-*d*) δ 7.29 – 7.14 (m, 3H), 7.10 (d, *J* = 7.2 Hz, 1H), 4.87 (q, *J* = 6.4 Hz, 1H), 2.37 (s, 3H), 1.90 (s, 1H), 1.50 (d, *J* = 6.4 Hz, 3H). ^{13}C NMR (101 MHz, Chloroform-*d*) δ 145.8, 138.2, 128.4, 128.2, 126.1, 122.4, 70.5, 25.1, 21.5.

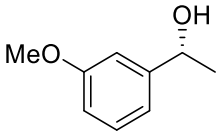

(*R*)-1-(3-Methoxyphenyl)ethanol (8g). Colorless oil, 99% isolated yield (99% NMR conversion); 95% *ee*, determined by HPLC analysis on Chiralpak OD-3 column (Hexane/i-PrOH = 90/10, flow rate = 1 mL/min, λ= 220 nm), t_R = 7.7 min (*major*), t_R = 8.6 min (*minor*). [α]D^{20}= +36.19 (*c* 1.0, $CHCl_3$).

(lit.[17] [α]D^{25} = +36.93 (*c* 1.0, $CHCl_3$), *R*). ^{1}H NMR (400 MHz, Chloroform-*d*) δ 7.26 (t, *J* = 8.1 Hz, 1H), 6.97 – 6.90 (m, 2H), 6.81 (ddd, *J* = 8.3, 2.6, 1.1 Hz, 1H), 4.86 (q, *J* = 6.4 Hz, 1H), 3.81 (s, 3H), 2.03 (s, 1H), 1.48 (d, *J* = 6.4 Hz, 3H). ^{13}C NMR (101 MHz, Chloroform-*d*) δ 159.8, 147.6, 129.5, 117.7, 112.9, 110.9, 70.3, 55.2, 25.2.

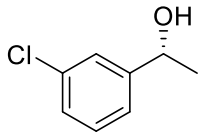

(*R*)-1-(3-Chlorophenyl)ethanol (8h). Colorless oil, 99% isolated yield (99% NMR conversion); 99% *ee*, determined by HPLC analysis on Chiralpak OD-3 column (Hexane/i-PrOH = 98/2, flow rate = 0.4 mL/min, λ= 220 nm), t_R = 22.2 min (*major*), t_R = 23.5 min (*minor*). [α]D^{25}= +59.20 (*c* 1.0, $CHCl_3$). (lit.[17] [α]D^{25} = +27.73 (*c* 0.25, $CHCl_3$), *R*). ^{1}H NMR (600 MHz, Chloroform-*d*) δ 7.59 (dd, *J* = 7.8, 1.7 Hz, 1H), 7.35 – 7.27 (m, 2H), 7.20 (td, *J* = 7.7, 1.7 Hz, 1H), 5.29 (q, *J* = 6.4 Hz, 1H), 2.15 (s, 1H), 1.49 (d, *J* = 6.4 Hz, 3H). ^{13}C NMR (151 MHz, Chloroform-*d*) δ 143.1, 131.6, 129.4, 128.4, 127.2, 126.4, 67.0, 23.5.

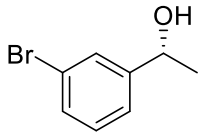

(*R*)-1-(3-Bromophenyl)ethanol (8i). [1] Colorless oil, 99% isolated yield (99% NMR conversion); 95% *ee*, determined by HPLC analysis on Chiralpak OD-3 column (Hexane/i-PrOH = 90/10, flow rate = 1 mL/min, λ= 220 nm), t_R = 5.7 min (*minor*), t_R = 6.1 min (*major*). [α]D^{20}= +30.37 (*c* 1.3, $CHCl_3$). (lit.[17] [α]D^{25} = +25.23 (*c* 1.0, $CHCl_3$), *R*). ^{1}H NMR (400 MHz, Chloroform-*d*) δ 7.53 (t, *J* = 1.9 Hz, 1H), 7.39 (dt, *J* = 7.9, 1.5 Hz, 1H), 7.30 – 7.25 (m, 1H), 7.21 (t, *J* = 7.7 Hz, 1H), 4.86 (q, *J* = 6.5 Hz, 1H), 2.01 (s, 1H), 1.47 (d, *J* = 6.5 Hz, 3H). ^{13}C NMR (101 MHz, Chloroform-*d*) δ 148.1, 130.5, 130.1, 128.6, 124.0, 122.6, 69.7, 25.3.

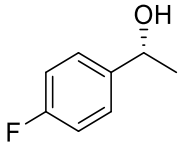

(*R*)-1-(4-Fluorophenyl)ethanol (8j). Colorless oil, 93% isolated yield (99% NMR conversion); 97% *ee*, determined by HPLC analysis on Chiralpak OD-3 column (Hexane/i-PrOH = 98/2, flow rate = 1 mL/min, λ= 210 nm), t_R = 9.9 min (*minor*), t_R = 10.4 min (*major*). $[\alpha]D^{20}$= +45.36 (*c* 1.1, $CHCl_3$). (lit.[17] $[\alpha]D^{25}$ = +39.97 (*c* 1.0, $CHCl_3$), *R*). ^{1}H NMR (600 MHz, Chloroform-*d*) δ 7.34 – 7.29 (m, 2H), 7.01 (t, *J* = 8.2 Hz, 2H), 4.85 (q, *J* = 6.6 Hz, 1H), 2.23 (s, 1H), 1.45 (d, *J* = 6.4 Hz, 3H). ^{13}C NMR (151 MHz, Chloroform-*d*) δ 162.1 (d, *J* = 245.2 Hz), 141.5 (d, *J* = 3.2 Hz), 127.0 (d, *J* = 8.0 Hz), 115.2 (d, *J* = 21.3 Hz), 69.7, 25.3. ^{19}F NMR (565 MHz, Chloroform-*d*) δ -115.4.

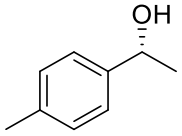

(*R*)-1-(*p*-Tolyl)ethanol (8k). Colorless oil, 96% isolated yield (99% NMR conversion); 96% *ee*, determined by HPLC analysis on Chiralpak OJ-H column (Hexane/i-PrOH = 90/10, flow rate = 1 mL/min, λ= 220 nm), t_R = 7.2 min (*minor*), t_R = 8.0 min (*major*). $[\alpha]D^{25}$= +44.30 (*c* 1.0, $CHCl_3$). (lit.[17] $[\alpha]D^{25}$ = +41.00 (*c* 1.0, $CHCl_3$), *R*). ^{1}H NMR (400 MHz, Chloroform-*d*) δ 7.26 (d, *J* = 8.2 Hz, 2H), 7.16 (d, *J* = 7.8 Hz, 2H), 4.86 (q, *J* = 6.4 Hz, 1H), 2.34 (s, 3H), 1.83 (s, 1H), 1.48 (d, *J* = 6.4 Hz, 3H). ^{13}C NMR (101 MHz, Chloroform-*d*) δ 142.9, 137.2, 129.2, 125.4, 70.3, 25.1, 21.1.

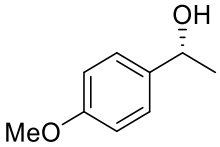

(*R*)-1-(4-Methoxyphenyl)ethanol (8l). Colorless oil, 97% isolated yield (99% NMR conversion); 96% *ee*, determined by HPLC analysis on Chiralpak OD-3 column (Hexane/i-PrOH = 95/5, flow rate = 1 mL/min, λ= 220 nm), t_R = 11.8 min (*major*), t_R = 13.3 min (*minor*). $[\alpha]D^{25}$= +49.10 (*c* 1.0, $CHCl_3$). (lit.[17] $[\alpha]D^{25}$ = +40.00 (*c* 1.0, $CHCl_3$), *R*). ^{1}H NMR (400 MHz, Chloroform-*d*) δ 7.33 – 7.27 (m, 2H),

6.93 – 6.84 (m, 2H), 4.86 (q, *J* = 6.5 Hz, 1H), 3.80 (s, 3H), 1.81 (s, 1H), 1.48 (d, *J* = 6.5 Hz, 3H). ^{13}C NMR (101 MHz, Chloroform-*d*) δ 159.0, 138.0, 126.7, 113.9, 70.0, 55.3, 25.0.

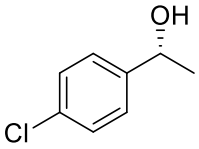

(*R*)-1-(4-Chlorophenyl)ethanol (8m). Colorless oil, 99% isolated yield (99% NMR conversion); 98% *ee*, determined by HPLC analysis on Chiralpak OD-3 column (Hexane/i-PrOH = 95/5, flow rate = 1 mL/min, λ= 220 nm), t_R = 8.0 min (*minor*), t_R = 8.9 min (*major*). [α]D^{25}= +45.70 (*c* 1.0, $CHCl_3$). (lit.[33] [α]D^{20} = -36.24 (*c* 2.2, $CHCl_3$), *S*). ^{1}H NMR (600 MHz, Chloroform-*d*) δ 7.28 (td, *J* = 9.1, 4.5 Hz, 4H), 4.84 (q, *J* = 6.5 Hz, 1H), 2.23 (s, 1H), 1.47 – 1.42 (m, 3H). ^{13}C NMR (151 MHz, Chloroform-*d*) δ 144.3, 133.0, 128.6, 126.8, 69.7, 25.3.

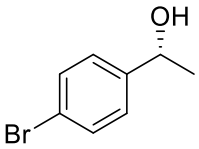

(*R*)-1-(4-Bromophenyl)ethanol (8n). Colorless oil, 98% isolated yield (99% NMR conversion); 97% *ee*, determined by HPLC analysis on Chiralpak OD-3 column (Hexane/i-PrOH = 90/10, flow rate = 1 mL/min, λ= 220 nm), t_R = 5.5 min (*minor*), t_R = 6.0 min (*major*). [α]D^{20}= +38.73 (*c* 1.1, $CHCl_3$). (lit.[33] [α]D^{20} = -28.14 (*c* 2.0, $CHCl_3$), *S*). ^{1}H NMR (400 MHz, Chloroform-*d*) δ 7.50 – 7.42 (m, 2H), 7.26 – 7.21 (m, 2H), 4.85 (q, *J* = 6.5 Hz, 1H), 2.03 (s, 1H), 1.46 (d, *J* = 6.5 Hz, 3H). ^{13}C NMR (101 MHz, Chloroform-*d*) δ 144.8, 131.6, 127.2, 121.2, 69.8, 25.3.

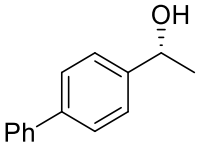

(*R*)-1-([1,1'-Biphenyl]-4-yl)ethanol (8o). White solid, 98% isolated yield (99% NMR conversion); 98% *ee*, determined by HPLC analysis on Chiralpak AD-3 column (Hexane/i-PrOH = 99/1, flow rate = 0.5 mL/min, λ= 210 nm), t_R = 9.3 min (*minor*), t_R = 10.4 min (*major*). [α]D^{20}= +48.42 (*c* 1.2, $CHCl_3$). (lit.[17] [α]D^{25} = +35.20 (*c* 1.07, $CHCl_3$), *R*). ^{1}H NMR (400 MHz, Chloroform-*d*) δ 7.64 – 7.56 (m, 4H), 7.46 (ddd, *J* = 7.8, 4.5, 2.2 Hz, 4H), 7.41 – 7.32 (m, 1H), 4.96 (q, *J* = 6.5 Hz, 1H), 2.05 (s, 1H), 1.55 (d, *J* = 6.5 Hz, 3H). ^{13}C NMR (101 MHz, Chloroform-*d*) δ 144.9, 140.9, 140.5, 128.8, 127.3, 127.3, 127.1, 125.9, 70.2, 25.2.

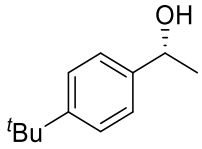

(*R*)-1-(4-(*tert*-Butyl)phenyl)ethanol (8p). Colorless oil, 99% isolated yield (99% NMR conversion); 92% *ee*, determined by HPLC analysis on Chiralpak OD-3 column (Hexane/i-PrOH = 99/1, flow rate = 0.8 mL/min, λ= 220 nm), t_R = 32.6 min (*major*), t_R = 37.1 min (*minor*). [α]D^{25}= +35.90 (*c* 1.0, $CHCl_3$). (lit.[33] [α]D^{20} = -48.23 (*c* 2.0, $CHCl_3$), *S*).^{1}H NMR (600 MHz, Chloroform-*d*) δ 7.42 – 7.37 (m, 2H), 7.34 – 7.30 (m, 2H), 4.88 (q, *J* = 6.5 Hz, 1H), 1.94 (s, 1H), 1.50 (d, *J* = 6.5 Hz, 3H), 1.34 (s, 9H). ^{13}C NMR (151 MHz, Chloroform-*d*) δ 150.5, 142.8, 125.4, 125.2, 70.2, 34.5, 31.4, 24.9.

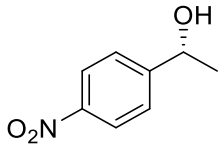

(*R*)-1-(4-Nitrophenyl)ethanol (8q). Colorless oil, 85% isolated yield (99% NMR conversion); 99% *ee*, determined by HPLC analysis on Chiralpak OJ-H column (Hexane/i-PrOH = 90/10, flow rate = 1 mL/min, λ= 220 nm), t_R = 15.6 min (*minor*), t_R = 16.9 min (*major*). [α]D^{25}= +39.20 (*c* 1.0, $CHCl_3$).

(lit.[33] $[\alpha]D^{20}$ = -15.16 (*c* 2.0, $CHCl_3$), *S*). ^{1}H NMR (600 MHz, Chloroform-*d*) δ 8.22 – 8.16 (m, 2H), 7.57 – 7.51 (m, 2H), 5.02 (q, *J* = 6.5 Hz, 1H), 2.11 (s, 1H), 1.51 (d, *J* = 6.5 Hz, 3H). ^{13}C NMR (151 MHz, Chloroform-*d*) δ 153.1, 147.2, 126.1, 123.8, 69.5, 25.5.

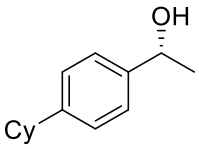

(*R*)-1-(4-Cyclohexylphenyl)ethanol (8r). White solid, 99% isolated yield (99% NMR conversion); 93% *ee*, determined by HPLC analysis on Chiralpak OD-3 column (Hexane/i-PrOH = 95/5, flow rate = 1 mL/min, λ= 220 nm), t_R = 6.1 min (*major*), t_R = 6.7 min (*minor*). $[\alpha]D^{20}$= +36.00 (*c* 1.9, $CHCl_3$). (lit.[34] $[\alpha]D^{20}$ = +38.2 (*c* 1.0, $CHCl_3$), *R*). ^{1}H NMR (600 MHz, Chloroform-*d*) δ 7.33 – 7.28 (m, 2H), 7.23 – 7.18 (m, 2H), 4.86 (q, *J* = 6.5 Hz, 1H), 2.51 (ddt, *J* = 11.5, 7.0, 3.5 Hz, 1H), 1.97 (s, 1H), 1.91 – 1.83 (m, 4H), 1.77 (ddd, *J* = 12.9, 3.2, 1.6 Hz, 1H), 1.50 (d, *J* = 6.5 Hz, 3H), 1.46 – 1.37 (m, 4H), 1.28 (ddq, *J* = 16.3, 10.4, 3.6 Hz, 1H). ^{13}C NMR (151 MHz, Chloroform-*d*) δ 147.4, 143.2, 126.9, 125.4, 70.3, 44.3, 34.5, 26.9, 26.2, 25.0.

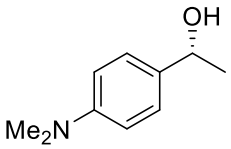

(*R*)-1-(4-(Dimethylamino)phenyl)ethanol (8s). White solid, 33% NMR conversion; 96% *ee*, determined by HPLC analysis on Chiralpak OD-3 column (Hexane/i-PrOH = 90/10, flow rate = 1 mL/min, λ= 220 nm), t_R = 7.3 min (*major*), t_R = 8.1 min (*minor*). $[\alpha]D^{22}$= +64.40 (*c* 0.5, $CHCl_3$). (lit.[32] $[\alpha]D^{20}$ = +55.8 (*c* 0.90, $CHCl_3$), *R*). ^{1}H NMR (400 MHz, Chloroform-*d*) δ 7.28 – 7.20 (m, 2H), 6.76 – 6.67 (m, 2H), 4.80 (q, *J* = 6.4 Hz, 1H), 2.93 (s, 6H), 1.85 (s, 1H), 1.47 (d, *J* = 6.5 Hz, 3H). ^{13}C NMR (101 MHz, Chloroform-*d*) δ 150.2, 133.8, 126.5, 112.7, 70.1, 40.8, 24.7.

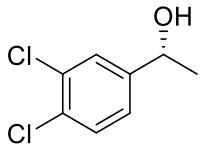

(*R*)-1-(3,4-Dichlorophenyl)ethanol (8t). Colorless oil, 99% isolated yield (99% NMR conversion); 98% *ee*, determined by HPLC analysis on Chiralpak OD-3 column (Hexane/i-PrOH = 95/5, flow rate = 1 mL/min, λ= 220 nm), t_R = 8.2 min (*minor*), t_R = 9.1 min (*major*). [α]D^{20}= +32.71 (*c* 1.4, $CHCl_3$). (lit.[9] [α]D^{20} =-33.7 (*c* 1.44, $CHCl_3$), *S*). ^{1}H NMR (600 MHz, Chloroform-*d*) δ 7.46 (s, 1H), 7.40 (d, *J* = 8.2 Hz, 1H), 7.18 (d, *J* = 7.8 Hz, 1H), 4.84 (q, *J* = 6.8 Hz, 1H), 2.11 (s, 1H), 1.46 (d, *J* = 6.3 Hz, 3H). ^{13}C NMR (151 MHz, Chloroform-*d*) δ 146.0, 132.5, 131.2, 130.4, 127.5, 124.8, 69.2, 25.3.

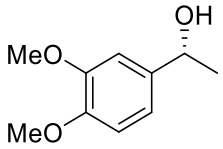

(*R*)-1-(3,4-Dimethoxyphenyl)ethanol (8u). Colorless oil, 99% isolated yield (99% NMR conversion); 97% *ee*, determined by HPLC analysis on Chiralpak OD-3 column (Hexane/i-PrOH = 90/10, flow rate = 1 mL/min, λ= 220 nm), t_R = 12.6 min (*minor*), t_R = 13.6 min (*major*). [α]D^{20}= +40.60 (*c* 1.0, $CHCl_3$). (lit.[9] [α]D^{20} =-37.2 (*c* 1.09, $CHCl_3$), *S*). ^{1}H NMR (400 MHz, Chloroform-*d*) δ 6.98 – 6.80 (m, 3H), 4.86 (q, *J* = 6.6, 6.1 Hz, 1H), 3.89 (d, *J* = 10.3 Hz, 6H), 1.79 (s, 1H), 1.49 (d, *J* = 6.6 Hz, 3H). ^{13}C NMR (151 MHz, Chloroform-*d*) δ 149.0, 148.3, 138.6, 117.5, 111.0, 108.7, 70.2, 56.0, 55.8, 25.1.

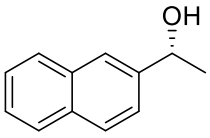

(*R*)-1-(Naphthalen-2-yl)ethanol (8v). White solid, 99% isolated yield (99% NMR conversion); 96% ee, determined by HPLC analysis on Chiralpak OJ-H column (Hexane/i-PrOH = 90/10, flow rate = 1 mL/min, λ= 220 nm), t_R = 15.3 min (*minor*), t_R = 19.8 min (*major*). [α]D^{20}= +43.25 (*c* 1.2, $CHCl_3$). (lit.[17] [α]D^{25} = +38.00 (*c* 1.0, $CHCl_3$), *R*). ^{1}H NMR (400 MHz, Chloroform-*d*) δ 7.91 – 7.75 (m, 4H),

7.57 – 7.42 (m, 3H), 5.06 (q, *J* = 6.6 Hz, 1H), 2.09 (s, 1H), 1.58 (d, *J* = 6.4 Hz, 3H). ^{13}C NMR (151 MHz, Chloroform-*d*) δ 143.2, 133.3, 132.9, 128.3, 128.0, 127.7, 126.2, 125.8, 123.9, 123.8, 70.5, 25.2.

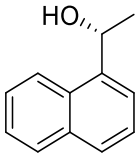

(*R*)-1-(Naphthalen-1-yl)ethanol (8w). Colorless oil, 75% isolated yield (91% NMR conversion); 98% *ee*, determined by HPLC analysis on Chiralpak OD-3 column (Hexane/i-PrOH = 90/10, flow rate = 1 mL/min, λ= 220 nm), t_R = 8.9 min (*minor*), t_R = 14.3 min (*major*). [α]D^{22}= +79.50 (*c* 1.0, $CHCl_3$). (lit.[17] [α]D^{25} = +58.63 (*c* 1.0, $CHCl_3$), *R*). ^{1}H NMR (600 MHz, Chloroform-*d*) δ 8.11 (d, *J* = 8.2 Hz, 1H), 7.89 (d, *J* = 7.8 Hz, 1H), 7.79 (d, *J* = 8.1 Hz, 1H), 7.67 (d, *J* = 7.0 Hz, 1H), 7.51 (dq, *J* = 16.9, 7.8, 7.4 Hz, 3H), 5.66 (q, *J* = 5.9 Hz, 1H), 2.15 (s, 1H), 1.67 (d, *J* = 6.3 Hz, 3H). ^{13}C NMR (101 MHz, Chloroform-*d*) δ 141.4, 133.8, 130.3, 128.9, 127.9, 126.1, 125.6, 123.2, 122.0, 67.1, 24.4.

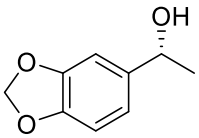

(*R*)-1-(Benzo[*d*][1,3]dioxol-5-yl)ethanol (8x). Colorless oil, 99% isolated yield (99% NMR conversion); 98% *ee*, determined by HPLC analysis on Chiralpak OD-3 column (Hexane/i-PrOH = 95/5, flow rate = 1 mL/min, λ= 220 nm), t_R = 13.8 min (*major*), t_R = 15.1 min (*minor*). [α]D^{20}= +36.67 (*c* 1.5, $CHCl_3$). (lit.[17] [α]D^{25} = +38.70 (*c* 1.0, $CHCl_3$), *R*).^{1}H NMR (400 MHz, Chloroform-*d*) δ 6.89 (d, *J* = 1.7 Hz, 1H), 6.85 – 6.73 (m, 2H), 5.94 (s, 2H), 4.81 (q, *J* = 6.0 Hz, 1H), 1.84 (s, 1H), 1.46 (d, *J* = 6.4 Hz, 3H). ^{13}C NMR (151 MHz, Chloroform-*d*) δ 147.8, 146.8, 140.0, 118.7, 108.1, 106.1, 101.0, 70.2, 25.2.

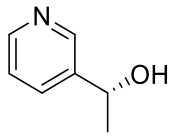

(*R*)-1-(Pyridin-3-yl)ethanol (8y). Colorless oil, 92% isolated yield (99% NMR conversion); 98% *ee*, determined by HPLC analysis on Chiralpak OJ-H column (Hexane/i-PrOH = 90/10, flow rate = 1 mL/min, λ= 254 nm), t_R = 6.7 min (*minor*), t_R = 8.6 min (*major*). $[\alpha]D^{20}$= +56.10 (*c* 1.0, $CHCl_3$). (lit.[33] $[\alpha]D^{20}$ = -44.62 (*c* 2.2, $CHCl_3$), *S*). ^{1}H NMR (400 MHz, Chloroform-*d*) δ 8.48 (d, *J* = 33.8 Hz, 2H), 7.71 (d, *J* = 7.6 Hz, 1H), 7.27 (d, *J* = 5.6 Hz, 1H), 4.91 (q, *J* = 6.4 Hz, 1H), 3.68 (s, 1H), 1.49 (d, *J* = 6.0 Hz, 3H). ^{13}C NMR (101 MHz, Chloroform-*d*) δ 147.9, 147.0, 141.9, 133.6, 123.6, 67.4, 25.2.

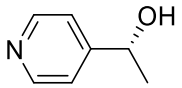

(*R*)-1-(Pyridin-4-yl)ethanol (8z). Colorless oil, 94% isolated yield (99% NMR conversion); 97% *ee*, determined by HPLC analysis on Chiralpak OJ-H column (Hexane/i-PrOH = 90/10, flow rate = 1 mL/min, λ= 254 nm), t_R = 9.1 min (*major*), t_R = 10.0 min (*minor*). $[\alpha]D^{22}$= +46.40 (*c* 1.0, $CHCl_3$). (lit.[33] $[\alpha]D^{20}$ = -36.92 (*c* 2.0, $CHCl_3$), *S*). ^{1}H NMR (400 MHz, Chloroform-d) δ 8.43 – 8.36 (m, 2H), 7.33 – 7.27 (m, 2H), 4.88 (q, J = 6.5 Hz, 1H), 4.55 (s, 1H), 1.47 (d, J = 6.6 Hz, 3H). ^{13}C NMR (101 MHz, Chloroform-*d*) δ 156.0, 149.1, 120.7, 68.3, 25.0.

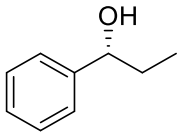

(*R*)-1-Phenylpropan-1-ol (8aa). Colorless oil, 98% isolated yield (99% NMR conversion); 97% *ee*, determined by HPLC analysis on Chiralpak OD-3 column (Hexane/i-PrOH = 95/5, flow rate = 1 mL/min, λ= 220 nm), t_R = 8.4 min (*major*), t_R = 9.0 min (*minor*). $[\alpha]D^{20}$= +39.50 (*c* 1.0, $CHCl_3$). (lit.[15] $[\alpha]D^{25}$ = +38.07 (*c* 0.5, $CHCl_3$), *R*). ^{1}H NMR (400 MHz, Chloroform-*d*) δ 7.34 (d, *J* = 5.4 Hz, 4H),

7.32 – 7.23 (m, 1H), 4.58 (t, *J* = 6.6 Hz, 1H), 1.92 (s, 1H), 1.88 – 1.68 (m, 2H), 0.91 (t, *J* = 7.4 Hz, 3H). ^{13}C NMR (101 MHz, Chloroform-*d*) δ 144.6, 128.4, 127.5, 126.0, 76.0, 31.9, 10.2.

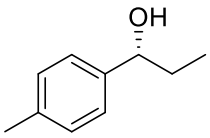

(*R*)-1-(*p*-Tolyl)propan-1-ol (8ab). Colorless oil, 83% isolated yield (99% NMR conversion); 98% *ee*, determined by HPLC analysis on Chiralpak AD-3 column (Hexane/i-PrOH = 99/1, flow rate = 0.5 mL/min, λ= 210 nm), t_R = 6.4 min (*major*), t_R = 7.4 min (*minor*). [α]D^{20}= +44.91 (*c* 1.1, $CHCl_3$). (lit.[9] [α]D^{20} = -43.4 (*c* 1.2, $CHCl_3$), *S*). ^{1}H NMR (400 MHz, Chloroform-*d*) δ 7.23 (d, *J* = 8.1 Hz, 2H), 7.16 (d, *J* = 7.9 Hz, 2H), 4.55 (t, *J* = 6.7 Hz, 1H), 2.36 (s, 3H), 2.02 (s, 1H), 1.78 (ddt, *J* = 28.4, 13.6, 7.3 Hz, 2H), 0.91 (t, *J* = 7.4 Hz, 3H). ^{13}C NMR (101 MHz, Chloroform-*d*) δ 141.7, 137.1, 129.1, 126.0, 75.9, 31.8, 21.1, 10.2.

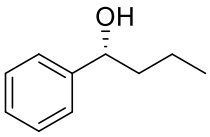

(*R*)-1-Phenylbutan-1-ol (8ac). White solid, 67% isolated yield (86% NMR conversion); 97% *ee*, determined by HPLC analysis on Chiralpak OJ-H column (Hexane/i-PrOH = 97/3, flow rate = 1 mL/min, λ= 220 nm), t_R = 9.9 min (*minor*), t_R = 10.7 min (*major*). [α]D^{22}= +45.90 (*c* 1.0, $CHCl_3$). (lit.[15] [α]D^{25} = +52.57 (*c* 1.0, $CHCl_3$), *R*). ^{1}H NMR (400 MHz, Chloroform-*d*) δ 7.37 – 7.20 (m, 5H), 4.62 (dd, *J* = 7.5, 5.9 Hz, 1H), 2.23 – 2.05 (m, 1H), 1.82 – 1.70 (m, 1H), 1.65 (ddt, *J* = 13.5, 9.9, 5.8 Hz, 1H), 1.40 (dddd, *J* = 15.0, 7.5, 6.1, 3.8 Hz, 1H), 1.29 (dddd, *J* = 18.9, 10.1, 7.6, 6.1 Hz, 1H), 0.91 (t, *J* = 7.4 Hz, 3H). ^{13}C NMR (101 MHz, Chloroform-*d*) δ 145.0, 128.4, 127.5, 125.9, 74.4, 41.3, 19.1, 14.0.

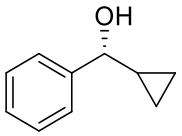

(*R*)-Cyclopropyl(phenyl)methanol (8ad). Colorless oil, 86% isolated yield (95% NMR conversion); 99% *ee*, determined by HPLC analysis on Chiralpak OD-3 column (Hexane/i-PrOH = 98/2, flow rate = 0.5 mL/min, λ= 210 nm), t_R = 22.1 min (*major*), t_R = 23.5 min (*minor*). [α]D^{22}= -33.20 (*c* 1.0, $CHCl_3$). (lit.[15] [α]D^{25} = -23.67 (*c* 1.0, $CHCl_3$), *R*). ^{1}H NMR (600 MHz, Chloroform-*d*) δ 7.43 (d, *J* = 7.6 Hz, 2H), 7.36 (t, *J* = 7.5 Hz, 2H), 7.32 – 7.27 (m, 1H), 4.00 (d, *J* = 8.2 Hz, 1H), 2.16 (s, 1H), 1.22 (tq, *J* = 8.2, 4.9, 4.2 Hz, 1H), 0.64 (tt, *J* = 8.7, 5.1 Hz, 1H), 0.56 (tt, *J* = 8.8, 5.1 Hz, 1H), 0.48 (dq, *J* = 10.2, 5.1 Hz, 1H), 0.38 (dq, *J* = 9.9, 5.1 Hz, 1H). ^{13}C NMR (151 MHz, Chloroform-*d*) δ 143.7, 128.4, 127.5, 126.1, 78.6, 19.2, 3.6, 2.9.

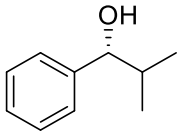

(*R*)-2-Methyl-1-phenylpropan-1-ol (8ae). Colorless oil, 40% NMR conversion; 96% *ee*, determined by HPLC analysis on Chiralpak OD-3 column (Hexane/i-PrOH = 95/5, flow rate = 1 mL/min, λ= 210 nm), t_R = 6.9 min (*minor*), t_R = 8.2 min (*major*). [α]D^{22}= +16.00 (*c* 0.5, $CHCl_3$). (lit.[15] [α]D^{25} = +25.60 (*c* 0.25, $CHCl_3$), *R*). ^{1}H NMR (400 MHz, Chloroform-*d*) δ 7.40 – 7.24 (m, 5H), 4.36 (d, *J* = 6.9 Hz, 1H), 2.08 (s, 1H), 1.97 (dq, *J* = 13.5, 6.7 Hz, 1H), 1.02 (d, *J* = 6.6 Hz, 3H), 0.81 (d, *J* = 6.8 Hz, 3H). ^{13}C NMR (101 MHz, Chloroform-*d*) δ 143.7, 128.2, 127.4, 126.6, 80.0, 35.3, 19.0, 18.3.

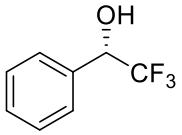

(*S*)-2,2,2-Trifluoro-1-phenylethanol (8af). Colorless oil, 99% isolated yield (99% NMR conversion); 96% *ee*, determined by HPLC analysis on Chiralpak OD-3 column (Hexane/i-PrOH = 90/10, flow rate = 0.6 mL/min, λ= 210 nm), t_R = 12.2 min (*minor*), t_R = 12.8 min (*major*). [α]D^{25}= +27.40 (*c* 1.0,

$CHCl_3$). (lit.[35] $[\alpha]D^{25}$ =-20.41 (*c* 0.48, $CHCl_3$), *R*). ^1H NMR (600 MHz, Chloroform-*d*) δ 7.50 – 7.45 (m, 2H), 7.43 (s, 3H), 5.00 (q, *J* = 6.8 Hz, 1H), 2.78 (s, 1H). ^{13}C NMR (151 MHz, Chloroform-*d*) δ 134.0, 129.6, 128.7, 127.5, 124.3 (q, *J* = 282.0 Hz), 72.8 (q, *J* = 32.0 Hz). ^{19}F NMR (565 MHz, Chloroform-*d*) δ -78.3.

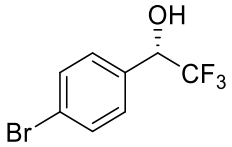

(*S*)-1-(4-Bromophenyl)-2,2,2-trifluoroethanol (8ag). Colorless oil, 99% isolated yield (99% NMR conversion); 98% *ee*, determined by HPLC analysis on Chiralpak OD-3 column (Hexane/i-PrOH = 95/5, flow rate = 1 mL/min, λ= 220 nm), t_R = 9.4 min (*minor*), t_R = 14.0 min (*major*). $[\alpha]D^{20}$= +18.25 (*c* 1.6, $CHCl_3$). ^1H NMR (400 MHz, Chloroform-*d*) δ 7.55 (d, *J* = 8.5 Hz, 2H), 7.35 (d, *J* = 8.2 Hz, 2H), 4.98 (q, *J* = 6.6 Hz, 1H), 2.80 (s, 1H). ^{13}C NMR (101 MHz, Chloroform-*d*) δ 132.8, 131.8, 129.1, 123.9 (q, *J* = 282.2 Hz), 123.8, 72.2 (q, *J* = 32.2 Hz). ^{19}F NMR (376 MHz, Chloroform-*d*) δ -78.5.

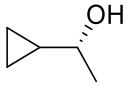

(*R*)-1-Cyclopropylethanol (8ah). Colorless oil, 94% isolated yield (99% NMR conversion); 83% *ee*, determined by GC (Supelco β-DEX^{TM} 225, carrier gas, N_2 (flow rate 1 mL/min); injection temp, 250 ^oC; oven temperature, initial column temperature, 70 ^oC for 11 minutes; progress rate, 0.5 ^oC /min; final column temperature, 100 ^oC; detector temperature, 300 ^oC); *t*R = 13.6 min (*major*); *t*R = 14.4 min (*minor*). $[\alpha]D^{24}$=+4.20 (*c* 0.5, CH_3OH). ^1H NMR (600 MHz, Chloroform-*d*) δ 3.04 (dq, *J* = 8.3, 6.2 Hz, 1H), 1.93 (s, 1H), 1.24 (d, *J* = 6.3 Hz, 3H), 0.87 (qt, *J* = 8.2, 4.9 Hz, 1H), 0.50 – 0.41 (m, 2H), 0.24 (dtd, *J* = 7.6, 4.4, 3.9, 2.0 Hz, 1H), 0.14 (ddt, *J* = 11.0, 5.1, 2.1 Hz, 1H). ^{13}C NMR (151 MHz, Chloroform-*d*) δ 70.7, 20.2, 17.0, 0.8.

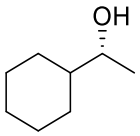

(*R*)-1-Cyclohexylethanol (8ai). Colorless oil, 99% isolated yield (99% NMR conversion); 94% *ee*, determined by GC (Supelco β-DEX^{TM} 225, carrier gas, N_2 (flow rate 1 mL/min); injection temp, 250 ^{o}C; oven temperature, initial column temperature, 70 ^{o}C for 11 minutes; progress rate, 0.5 ^{o}C /min; final column temperature, 100 ^{o}C; detector temperature, 300 ^{o}C); *t*R = 41.9 min (*minor*); *t*R = 43.1 min (*major*). $[\alpha]D^{26}$= -3.50 (*c* 1.0, $CHCl_3$). (lit.[15] $[\alpha]D^{25}$ = -8.1 (*c* 1.0, $CHCl_3$), *R*). ^{1}H NMR (400 MHz, Chloroform-*d*) δ 3.54 (p, *J* = 6.2 Hz, 1H), 1.88 – 1.81 (m, 1H), 1.79 – 1.71 (m, 2H), 1.66 (dt, *J* = 13.7, 3.2 Hz, 2H), 1.31 – 1.17 (m, 4H), 1.15 (d, *J* = 6.3 Hz, 3H), 0.97 (dqd, *J* = 16.0, 12.3, 3.5 Hz, 2H). ^{13}C NMR (151 MHz, Chloroform-*d*) δ 72.1, 45.1, 28.7, 28.4, 26.5, 26.2, 26.1, 20.3.

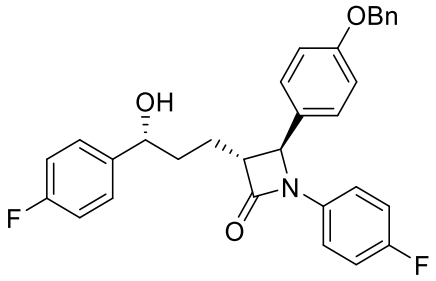

(3*R*,4*S*)-4-(4-(benzyloxy)phenyl)-1-(4-fluorophenyl)-3-((*R*)-3-(4-fluorophenyl)-3-hydroxypropyl)azetidin-2-one (8aj). White solid, 92% isolated yield (99% NMR conversion); 98% *de*, determined by HPLC analysis on Chiralpak ICU column (Hexane/i-PrOH = 80/20, flow rate = 0.5 mL/min, λ= 254 nm), t_R = 3.5 min (*minor*), t_R = 4.1 min (*major*). $[\alpha]D^{26}$= +17.50 (*c* 1.0, $CHCl_3$). (lit.[15] $[\alpha]D^{25}$ = -34.83 (*c* 2.0, $CHCl_3$), 3*R*,4*S*,3'*S*). ^{1}H NMR (600 MHz, Chloroform-*d*) δ 7.39 (dt, *J* = 15.1, 7.4 Hz, 4H), 7.33 (t, *J* = 7.2 Hz, 1H), 7.31 – 7.27 (m, 2H), 7.26 – 7.20 (m, 4H), 7.05 – 6.97 (m, 2H), 6.97 – 6.94 (m, 2H), 6.94 – 6.87 (m, 2H), 5.04 (s, 2H), 4.69 (dd, *J* = 7.5, 4.7 Hz, 1H), 4.55 (d, *J* = 2.4 Hz, 1H), 3.10 (td, *J* = 7.2, 2.4 Hz, 1H), 2.49 (s, 1H), 2.05 – 1.93 (m, 2H), 1.85 (ddd, *J* = 15.8, 9.6, 5.4 Hz, 2H). ^{13}C NMR (151 MHz, Chloroform-*d*) δ 167.7, 162.2 (d, *J* = 245.6 Hz), 159.1, 159.0 (d, *J* = 243.5 Hz), 140.0 (d, *J* = 3.1 Hz), 136.7, 133.9 (d, *J* = 2.7 Hz), 129.6, 128.7, 128.1, 127.5, 127.5 (d, *J*

= 8.1 Hz), 127.2, 118.4 (d, *J* = 7.9 Hz), 115.8 (d, *J* = 22.6 Hz), 115.6, 115.4 (d, *J* = 21.3 Hz), 73.3, 70.1, 61.1, 60.4, 36.5, 25.0. ^{19}F NMR (565 MHz, Chloroform-*d*) δ -114.9, -118.0.

2.8 Appendix

2.8.1 DFT computational studies

DFT calculations were performed using the Gaussian 16 package.[36] All the structures are optimized using the M06 functional with the basis set SDD for Mn and Fe[37] and 6-31G* for other main group atoms[38-39]. Geometric structures of all species were optimized at T = 298.15 K. Vibrational analyses were performed to ensure intermediates to have no imaginary frequencies and the transition state structures to have only one imaginary frequency. Transition state structures were confirmed to connect appropriate reactants or products by intrinsic reaction coordinate (IRC) calculations.[40] Solvent effects were considered using the SMD mode[41] at the M06/6-311++G** level with SDD for Ir and Fe.

The outcome structures were analyzed by a web tool, SambVca 2.1 (https://www.molnac.unisa.it/OMtools/sambvca2.1/index.html). The iridium atom was selected for the center of the sphereIr-H bond *trans* to a phosphorus atom was selected as the z-axil and another Ir-P bond as the x-axil in the Cartesian coordinate system. Bondi atomic model (scaled by 1.17) was selected for atomic radii. Defined radius of the semi-sphere was set at 6.0 Å.

Coordinate of optimized structures:

A

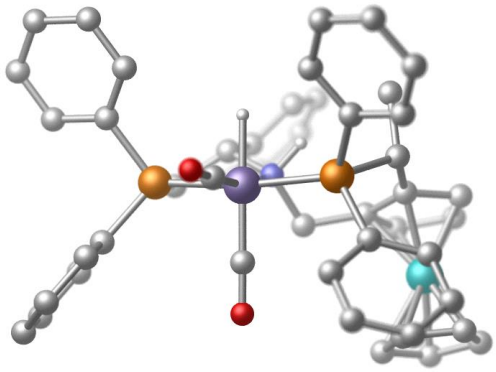

C -2.38180200 -2.24557300 0.50098000

C -3.77257500 -2.10383200 0.44978600

C -4.59327300 -2.75348400 1.36744500

C -4.03838900 -3.55361300 2.35989400

C -3.87204300 2.78651500 2.48864200

C -2.57983400 3.31087700 -0.36969800

Mn 0.79390900 -0.79394700 0.06350300

C -3.87782600 3.03004000 -0.87342300

C -3.40753500 0.53599100 2.31518100

C -2.86818100 1.79617600 2.69061700

H -2.87327700 -0.40834600 2.34139900

C -4.74629400 0.74607100 1.87369600

H -5.42021200 -0.01597200 1.49593000

N 0.50337900 1.22096600 -0.71559200

C 1.80178800 1.86082900 -1.10453100

C 2.73342100 1.79097000 0.09105700

Fe -3.45864300 1.85207100 0.72782800

H -1.85478800 1.96502600 3.04239100

H -3.75579400 3.85532300 2.64140000

C -0.38013100 2.09751100 0.08847900

H -2.24024800 4.25530200 0.04899300

H -5.96085900 2.62282700 1.69092400

H -4.73546700 1.12263800 -1.68076400

H 0.02271400 1.04118800 -1.59328000

H 3.71994800 2.22002800 -0.13193600

H 2.20190500 1.19356500 -1.88690400

P -1.20784300 -1.49314400 -0.71700400

C -2.60633000 1.07768500 -1.00469500

C -1.79119300 2.11869500 -0.42459700

C -3.89165100 1.66309500 -1.25697700

C -5.03590600 2.13615400 1.98519500

H -4.71611800 3.71862400 -0.91133500

C -2.65742600 -3.70715400 2.42128200

C -1.83960000 -3.06270100 1.49950500

C -1.20453500 -2.85976800 -1.97977800

C -0.03812300 -3.17545900 -2.67967900

C -0.04225900 -4.15941000 -3.66424200

C -1.21424900 -4.84280800 -3.96617600

C -2.38299100 -4.54228600 -3.27226200

C -2.37598100 -3.56362900 -2.28520700

H -4.23852300 -1.46121600 -0.29661000

H -4.67993000 -4.05502800 3.08259700

H -0.76128000 -3.20025400 1.56067400

H 0.87636300 -2.63149300 -2.44624000

H -1.21758900 -5.61375900 -4.73538300

H -3.29592500 -3.35987600 -1.73724800

H -0.33513300 1.76890700 1.13222700

H 0.87973600 -4.39393700 -4.19448200

H -3.30490200 -5.07812200 -3.49424200

H -5.67400900 -2.62530400 1.30850800

H -2.20871700 -4.33189000 3.19165700

H -0.01057600 3.13493700 0.06349300

C 1.60464700 3.23019100 -1.72078400

C 2.09731800 4.40392400 -1.15122900

C 0.86607300 3.32514400 -2.90519300

C 1.85615800 5.64057400 -1.74574200

H 2.67741300 4.35941700 -0.23007400

C 0.61787600 4.55557900 -3.49833300

H 0.48094100 2.41588700 -3.37298000

C 1.11388100 5.72067000 -2.91750200

H 2.25050600 6.54529500 -1.28572700

H 0.04033700 4.60621800 -4.41978800

H 0.92398600 6.68698600 -3.38142000

H 2.29902500 2.33519500 0.94457900

P 2.82379900 -0.01119600 0.52706900

C 3.43911400 -0.03450900 2.25467600

C 3.45387000 -1.27154900 2.90959700

C 3.87901000 1.09874100 2.94227600

C 3.89929100 -1.37033000 4.22141500

H 3.10879400 -2.16442600 2.38570900

C 4.31941000 0.99976200 4.26008400

H 3.88870100 2.07270900 2.45260400

C 4.32985400 -0.23352000 4.90092100

H 3.90356800 -2.33900700 4.71828100

H 4.65660900 1.89218200 4.78541500

H 4.67191400 -0.30997200 5.93176000

C 4.32593500 -0.56880400 -0.38719900

C 5.59393500 -0.09707600 -0.02670700

C 4.21332200 -1.46023200 -1.45472900

C 6.72268000 -0.49740200 -0.72958600

H 5.70067900 0.58066600 0.82198100

C 5.34619400 -1.86735000 -2.15516500

H 3.22475900 -1.82496800 -1.73388400

C 6.59939500 -1.38528800 -1.79641300

H 7.70332200 -0.12214600 -0.44056400

H 5.24631400 -2.56731300 -2.98334800

H 7.48493100 -1.70449700 -2.34412600

C -2.28162200 -0.25603000 -1.64535100

H -3.24841000 -0.75762800 -1.80497400

C -1.70095500 -0.03687900 -3.05564600

H -0.61060500 0.11690500 -3.05953900

H -1.88023200 -0.91244800 -3.69091300

H -2.17327200 0.83619400 -3.52607200

C 1.30050600 -2.44542600 0.36808800

O 1.69238400 -3.53741300 0.53232100

C 0.18493900 -0.49635300 1.71924200

O -0.20388900 -0.30996000 2.80717800

H 1.33196800 -0.98465200 -1.45090600

B

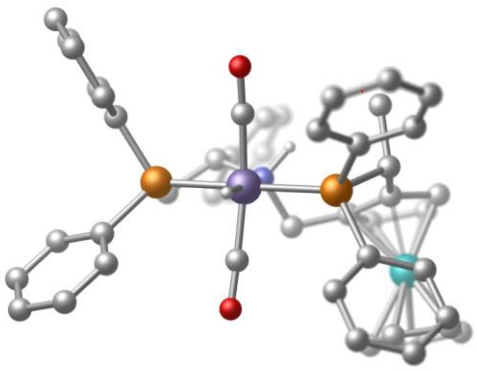

C -2.41704800 -2.19111300 0.56112700

C -3.80740300 -2.12040000 0.43539800

C -4.63861500 -2.74188700 1.36185100

C -4.09357600 -3.44864700 2.42898700

C -3.95853900 2.87263400 2.32391000

C -2.55283600 3.30966400 -0.50859500

Mn 0.78519000 -0.77550800 -0.02740700

C -3.83828200 3.03128400 -1.04309000

C -3.47536100 0.62091400 2.22540800

C -2.95541300 1.89457400 2.58329200

H -2.93879300 -0.32033000 2.28915500

C -4.80117300 0.81039600 1.73775600

H -5.45642400 0.03281700 1.35863300

N 0.55804300 1.28940700 -0.71712400

C 1.89076600 1.94778200 -0.91277300

C 2.72275800 1.74773500 0.34500900

Fe -3.48371300 1.89259400 0.60363500

H -1.95456900 2.08431600 2.96020000

H -3.85343000 3.94578100 2.45201200

C -0.39607500 2.09186000 0.08449900

H -2.21193300 4.26147100 -0.10771700

H -6.02054500 2.67322000 1.46736900

H -4.69616600 1.11261100 -1.82100500

H 0.15307800 1.21481100 -1.64809600

H 3.70458100 2.23247600 0.25847900

H 2.35762000 1.36382700 -1.72530200

P -1.23126300 -1.50960700 -0.68874000

C -2.59096300 1.05762000 -1.07646900

C -1.77877400 2.10559900 -0.50095100

C -3.85826800 1.65422600 -1.38695800

C -5.10227500 2.20087200 1.80286200

H -4.66554100 3.72895500 -1.12731200

C -2.71148300 -3.54133700 2.55510800

C -1.88162200 -2.92308700 1.62576700

C -1.27645600 -3.00992700 -1.79391400

C -0.24038200 -3.94125600 -1.69137300

C -0.27081100 -5.12724700 -2.41907800

C -1.33933800 -5.40349800 -3.26314000

C -2.38678300 -4.49242900 -3.36356900

C -2.35912600 -3.31340700 -2.62762300

H -4.26402200 -1.56021700 -0.38028700

H -4.74498600 -3.92928900 3.15710600

H -0.79837800 -3.00372400 1.72276900

H 0.59750900 -3.72989000 -1.02736200

H -1.36130100 -6.32802200 -3.83815900

H -3.20520000 -2.63039800 -2.70931200

H -0.39707700 1.70519300 1.10830900

H 0.55105100 -5.83565300 -2.32616600

H -3.23525400 -4.70259400 -4.01350200

H -5.72029900 -2.66893300 1.24978300

H -2.27340800 -4.09807500 3.38202900

H -0.06303200 3.14067300 0.13977300

C 1.76106300 3.37347000 -1.40754800

C 2.13450700 4.48494900 -0.65229100

C 1.19592900 3.58478100 -2.66962600

C 1.94397000 5.77483700 -1.14252300

H 2.57612300 4.34841600 0.33445800

C 0.99945200 4.86863600 -3.16056200

H 0.90901800 2.72483900 -3.28017500

C 1.37376200 5.97046200 -2.39474100

H 2.24179700 6.63018400 -0.53812600

H 0.55840900 5.01089200 -4.14563700

H 1.22430100 6.97864300 -2.77721600

H 2.21713300 2.18095100 1.22299900

P 2.78854000 -0.08672900 0.62779700

C 3.40304400 -0.23314500 2.35183200

C 2.90699800 -1.24077000 3.18068900

C 4.40486500 0.61550600 2.83428700

C 3.39381900 -1.38730400 4.47664900

H 2.13219400 -1.90870700 2.80296800

C 4.88431700 0.47479600 4.13054000

H 4.82549800 1.38656500 2.18688500

C 4.37711000 -0.52771300 4.95389100

H 2.99801300 -2.17409700 5.11679100

H 5.66051500 1.14420600 4.49854500

H 4.75350000 -0.63982400 5.96959200

C 4.28016900 -0.63845400 -0.29717800

C 5.05453400 0.18816800 -1.11177600

C 4.60576100 -1.99686600 -0.20915800

C 6.13674000 -0.33024000 -1.81990700

H 4.82261200 1.24879400 -1.21102100

C 5.68853000 -2.51189200 -0.90811000

H 3.99147500 -2.65480200 0.40879500

C 6.45710000 -1.67820700 -1.71758600

H 6.73006700 0.32666700 -2.45434100

H 5.93032800 -3.57053700 -0.82808300

H 7.30255300 -2.08242200 -2.27189400

C -2.27053600 -0.29567400 -1.67828300

H -3.24743700 -0.76789800 -1.86386600

C -1.63225600 -0.09015000 -3.06257700

H -0.58210500 0.23005600 -3.00594600

H -1.63367700 -1.01612000 -3.64943300

H -2.18651200 0.67613600 -3.62105600

C 0.14597000 -0.52607300 1.63980900

C 1.51399300 -1.34757200 -1.58711300

O 2.00930800 -1.74233300 -2.56463700

O -0.25816000 -0.40224000 2.72894800

H 1.09428100 -2.23978200 0.50161100

C

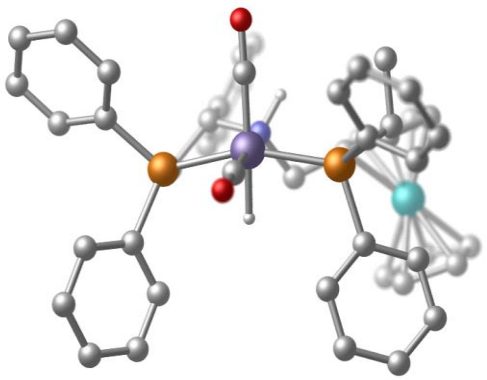

C 1.71180200 2.23606800 0.93886600

C 3.08998500 2.43773300 1.07380400

C 3.63305100 2.93198800 2.25634400

C 2.80527400 3.22928300 3.33368500

C 4.99091300 -2.48640600 1.71612300

C 2.85412800 -2.80839300 -0.71896500

Mn -1.13600700 0.72654700 -0.48770200

C 4.04253900 -2.47424400 -1.42203700

C 3.84779500 -0.53470500 2.16463600

C 3.80775700 -1.95047400 2.30340500

H 3.07701200 0.16191200 2.48117700

C 5.05824800 -0.19591600 1.49141200

H 5.37630100 0.80298000 1.21204700

N -0.34752700 -1.30290200 -0.64134500

C -1.43920300 -2.32473100 -0.52931400

C -2.24375800 -2.02523500 0.72385300

Fe 3.92224400 -1.44642900 0.32921000

H 2.99375300 -2.52540300 2.73562700

H 5.23412100 -3.54011300 1.61887000

C 0.82032800 -1.56189300 0.24986400

H 2.58268000 -3.78491800 -0.32309100

H 6.70471800 -1.48138000 0.67964200

H 4.77221500 -0.49775900 -2.19137100

H 0.00117500 -1.37137600 -1.59844500

H -3.06375400 -2.74357500 0.85127300

H -2.09016600 -2.12495100 -1.39853400

P 0.91523900 1.70189200 -0.64829600

C 2.79127900 -0.52658900 -1.15575700

C 2.09169200 -1.61248900 -0.52558400

C 4.00744300 -1.07534000 -1.67689200

C 5.76480400 -1.40020800 1.21648600

H 4.85624700 -3.15030500 -1.66569600

C 1.43314500 3.03236500 3.21625900

C 0.89257800 2.54257100 2.03124000

C 0.95193600 3.32320500 -1.57082700

C -0.04951000 3.60977600 -2.50456600

C -0.02389100 4.78621800 -3.24632600

C 1.00272700 5.70576700 -3.06493600

C 2.00253700 5.43925900 -2.13595100

C 1.97590300 4.26091900 -1.39747900

H 3.76304000 2.19603300 0.25160200

H 3.22912700 3.61182400 4.26086000

H -0.18209500 2.38375000 1.95313000

H -0.86007000 2.90113800 -2.65862400

H 1.02081400 6.62977000 -3.64093100

H 2.76042200 4.08863300 -0.66293900

H 0.84198400 -0.78068000 1.01832300

H -0.81725700 4.98351600 -3.96546700

H 2.80823000 6.15481300 -1.97727200

H 4.71044800 3.07428100 2.33800500

H 0.77232300 3.26332500 4.05061300

H 0.70206800 -2.52765200 0.76466300

C -0.92190600 -3.73950600 -0.67663800

C -0.81713900 -4.63366900 0.38956400

C -0.49501600 -4.15705400 -1.94103000

C -0.28842100 -5.90827900 0.19953600

H -1.15541400 -4.33733800 1.38252700

C 0.03445600 -5.42617100 -2.13566800

H -0.58725700 -3.47377400 -2.78824900

C 0.14124700 -6.30669400 -1.06150600

H -0.21653100 -6.59332200 1.04287800

H 0.35820500 -5.73225400 -3.12896500

H 0.55096500 -7.30427400 -1.21030500

H -1.61142900 -2.06541100 1.62248600

P -2.83503600 -0.27799300 0.49428500

C -3.34029000 0.28540800 2.16984700

C -4.56348000 0.92709600 2.37724800

C -2.45016300 0.17013800 3.24340600

C -4.89563800 1.42866300 3.63298400

H -5.26454300 1.04234600 1.55103900

C -2.78861300 0.65563000 4.50003500

H -1.46965000 -0.28247700 3.08868300

C -4.01403800 1.28772500 4.69782600

H -5.84999700 1.93311400 3.77539100

H -2.08789400 0.54910000 5.32703200

H -4.27602900 1.67665000 5.68057300

C -4.47013700 -0.53496300 -0.31868100

C -5.39923800 -1.46593700 0.16259700

C -4.80667100 0.23986100 -1.42948800

C -6.62599800 -1.63255900 -0.46675400

H -5.17154500 -2.05284300 1.05401600

C -6.03905300 0.07831000 -2.05878700

H -4.09419500 0.97298100 -1.80570700

C -6.94586200 -0.86080500 -1.58236800

H -7.33808200 -2.36246900 -0.08441500

H -6.28636500 0.68829500 -2.92587200

H -7.90736200 -0.99136000 -2.07667000

C 2.32682800 0.84703000 -1.58341200

H 3.19190700 1.53009300 -1.54881800

C 1.90211400 0.73853800 -3.05713700

H 1.02664400 0.08508500 -3.17673300

H 1.64404700 1.71529100 -3.48259700

H 2.71780800 0.31055400 -3.65361900

C -1.87776100 2.29219100 -0.17256800

O -2.40159000 3.30587900 0.08267100

C -1.58810500 0.64717200 -2.21343200

O -1.89249400 0.52502900 -3.33994700

H -0.74216700 0.58228300 1.05724200

D

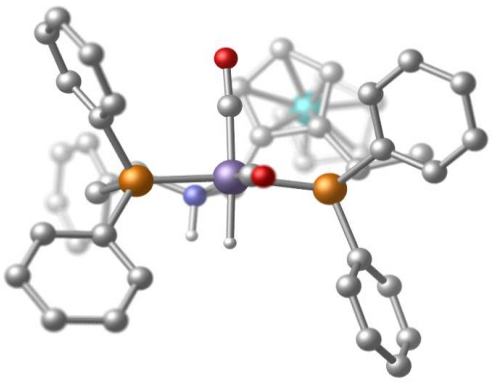

C 0.78393500 2.93978400 1.91498000

C 1.80335300 2.94163500 2.86859400

C 1.66629600 3.65274200 4.06081100

C 0.51374700 4.38567900 4.30841500

C 5.76466700 -2.33521100 -0.94446400

C 2.20834200 -2.07216700 -1.32106100

Mn -0.95924400 0.63451700 -0.04756800

C 2.94940700 -1.39106700 -2.32662500

C 4.75547500 -2.25272000 1.12756000

C 5.01199300 -3.08921300 0.00209100

H 4.18043700 -2.52586400 2.00761200

C 5.35022300 -0.98199300 0.87655200

H 5.30847600 -0.11835900 1.53433600

N -0.17656100 -1.21273100 0.97046600

C -0.93791700 -2.41525200 0.54147300

C -2.42086900 -2.12947700 0.75747900

Fe 3.97748900 -1.42468400 -0.56655800

H 4.65941400 -4.10745500 -0.12834400

H 6.08490200 -2.67865300 -1.92295100

C 1.28814300 -1.43697500 1.03959100

H 1.90051100 -3.11484100 -1.34175300

H 6.48147700 -0.21085100 -0.90054900

H 3.76689700 0.69273200 -2.40105700

H -3.04600100 -2.97460700 0.43859100

H -0.73955200 -2.52396900 -0.53879900

P 0.82651600 1.99979500 0.32553200

C 2.60473400 0.08684000 -0.58162100

C 1.99144900 -1.16307000 -0.24206800

C 3.19127600 -0.06219900 -1.87323000

C 5.97320800 -1.03260100 -0.40517600

H 3.30197200 -1.81756700 -3.25991700

C -0.50767700 4.40078400 3.35992000

C -0.37810700 3.67803500 2.18277300

C 1.02601100 3.36891500 -0.90059200

C 0.94620800 3.05832700 -2.26307600

C 1.18641700 4.03149500 -3.22720000

C 1.49543900 5.33354800 -2.84612900

C 1.56746000 5.65530500 -1.49521800

C 1.34021000 4.67953400 -0.52955700

H 2.72777400 2.39149300 2.69711500

H 0.40861500 4.94539500 5.23651900

H -1.18896400 3.68849300 1.45338100

H 0.69224200 2.04759000 -2.57849300

H 1.67493500 6.09737400 -3.60128800

H 1.41365400 4.94573400 0.52448300

H 1.67097000 -0.76710000 1.82318500

H 1.12083500 3.76974600 -4.28216900

H 1.80439300 6.67266800 -1.18679900

H 2.47274400 3.63538900 4.79270100

H -1.41506000 4.97460600 3.54235500

H 1.50333200 -2.46483000 1.37353000

C -0.55266000 -3.70872100 1.22501300

C -0.53781400 -3.82285500 2.61771300

C -0.25002600 -4.83293200 0.45762200

C -0.21952300 -5.03057800 3.22611600

H -0.77149000 -2.95479400 3.23762700

C 0.06076300 -6.04774300 1.06316700

H -0.26323400 -4.75288600 -0.63131500

C 0.07960300 -6.14809600 2.44968000

H -0.20715600 -5.10220300 4.31253800

H 0.29257300 -6.91598300 0.44836900

H 0.32667200 -7.09470400 2.92703700

H -2.61451900 -1.97928700 1.83200600

P -2.83300100 -0.53247500 -0.07918200

C -4.35985100 -0.00653700 0.79581500

C -4.33718400 1.08943000 1.65991300

C -5.54955800 -0.72583500 0.63324100

C -5.48732900 1.45927900 2.35214600

H -3.40626300 1.64268500 1.78878800

C -6.69437900 -0.35908800 1.32947000

H -5.58089900 -1.57430200 -0.05242200

C -6.66401800 0.73688000 2.18909800

H -5.46248600 2.31956600 3.01933000

H -7.61484700 -0.92599400 1.19770000

H -7.56311800 1.02895300 2.72995600

C -3.49875300 -1.02615000 -1.71627900

C -3.35030500 -2.30540600 -2.25407800

C -4.08374000 -0.02580000 -2.50208000

C -3.78693600 -2.58437100 -3.54706300

H -2.88298900 -3.10188900 -1.67308800

C -4.52251600 -0.30557000 -3.78934600

H -4.19290100 0.98278200 -2.09902300

C -4.37501300 -1.58709300 -4.31529700

H -3.66435500 -3.58728900 -3.95345800

H -4.97772300 0.48214300 -4.38744700

H -4.71466500 -1.80521900 -5.32648500

C 2.59260000 1.28906700 0.30671200

H 2.73692600 0.92793500 1.33824600

C 3.69285000 2.29099400 -0.01268900

H 3.58581100 2.70075600 -1.02526800

H 3.68104600 3.14197500 0.67982100

H 4.67672800 1.80417700 0.05307200

C -1.84286700 2.04683500 -0.58252200

O -2.47827900 2.98264600 -0.88756900

C -0.50686500 0.09606200 -1.70087200

O -0.30327500 -0.26152800 -2.79491600

H -0.49309000 -0.95422000 1.90566700

H -1.40140100 0.99521000 1.46951300

E

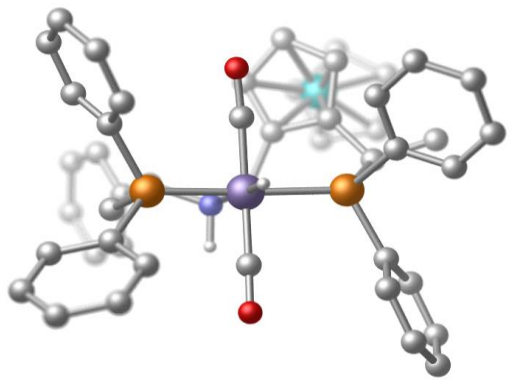

C -0.85717000 3.16473700 -1.69834200

C -1.58698000 2.93183300 -2.86552100

C -1.39067300 3.71804400 -3.99923000

C -0.46222900 4.75101300 -3.98188200

C -5.65540500 -2.52218800 0.82752100

C -2.10091600 -2.15380000 1.23983200

Mn 0.91822600 0.70238200 -0.10168000

C -2.88006700 -1.49896300 2.23366000

C -4.59603200 -2.48927400 -1.22041400

C -4.85994500 -3.29030200 -0.07129400

H -3.99167000 -2.77930200 -2.07498000

C -5.22917000 -1.22630700 -1.03213100

H -5.19299400 -0.38723000 -1.72130400

N 0.26801700 -1.21966900 -1.06206000

C 1.08404900 -2.35012300 -0.54369600

C 2.56148400 -1.97826100 -0.67518100

Fe -3.88244800 -1.57923900 0.46026900

H -4.48482900 -4.29335600 0.10581700

H -5.99186800 -2.83768200 1.80998400

C -1.18579200 -1.51848600 -1.11505700

H -1.75753200 -3.18530700 1.26605300

H -6.42518000 -0.42105200 0.68685800

H -3.77217600 0.55400300 2.29143900

H 3.19930200 -2.80526900 -0.33401400

H 0.82508700 -2.43660400 0.52536200

P -0.88936100 2.04518400 -0.23316700

C -2.57006000 -0.01257800 0.48670000

C -1.90332500 -1.24102800 0.15906600

C -3.16469700 -0.18187700 1.77242900

C -5.88331500 -1.24637100 0.23492400

H -3.22894400 -1.93591700 3.16353500

C 0.27227300 4.99446300 -2.82386400

C 0.08051300 4.20619600 -1.69759900

C -1.25293400 3.25848100 1.12288900

C -1.01799500 2.91307300 2.45720800

C -1.37870900 3.77165300 3.49228500

C -1.97058200 4.99795600 3.21368400

C -2.20444800 5.35902000 1.89056000

C -1.85378600 4.49641500 0.85814800

H -2.32212700 2.12829900 -2.91047500

H -0.30726200 5.36356100 -4.86857100

H 0.67653900 4.38753100 -0.80175100

H -0.54599900 1.96741500 2.70506500

H -2.24582500 5.67232300 4.02338100

H -2.05192100 4.79630600 -0.16989400

H -1.60100100 -0.89061000 -1.91668700

H -1.18517600 3.47730400 4.52275900

H -2.66504200 6.31808600 1.65703500

H -1.97123600 3.51895100 -4.89902800

H 1.00772100 5.79722500 -2.80162100

H -1.35198100 -2.56719000 -1.41494200

C 0.82028100 -3.68606500 -1.20335100

C 0.88995800 -3.84139700 -2.59031600

C 0.54242100 -4.80475200 -0.41812600

C 0.67727100 -5.08315500 -3.17634800

H 1.11164400 -2.98172300 -3.22620900

C 0.33713100 -6.05273100 -1.00053400

H 0.49164800 -4.69353800 0.66698600

C 0.40059200 -6.19376800 -2.38225900

H 0.73076100 -5.18635500 -4.25897000

H 0.12277400 -6.91536400 -0.37163500

H 0.23585900 -7.16669300 -2.84185000

H 2.80470100 -1.80868900 -1.73789300

P 2.83061400 -0.36221700 0.19474300

C 4.43001200 0.23206400 -0.48345100

C 4.60929100 1.59325900 -0.73465200

C 5.49218600 -0.65015600 -0.70669200

C 5.82791800 2.06317800 -1.21627900

H 3.78343500 2.28113100 -0.54966600

C 6.70510500 -0.18196900 -1.19656200

H 5.37579000 -1.71215100 -0.48430500

C 6.87293800 1.17699500 -1.45290600

H 5.95798300 3.12636600 -1.41189600

H 7.52462000 -0.87714200 -1.37316400

H 7.82401900 1.54477200 -1.83526700

C 3.35142600 -0.84901700 1.88935900

C 3.27644700 -2.15212400 2.38179100

C 3.77021300 0.17460100 2.74629500

C 3.62183300 -2.42960600 3.70242500

H 2.93788000 -2.97010400 1.74442000

C 4.11967000 -0.10252300 4.06086300

H 3.81143200 1.20050600 2.37576400

C 4.04570800 -1.40744700 4.54265500

H 3.55701000 -3.45140400 4.07376500

H 4.44550800 0.70424900 4.71554200

H 4.31452500 -1.62489800 5.57513200

C -2.59122400 1.20243500 -0.38375200

H -2.60462100 0.84870900 -1.42778800

C -3.80130100 2.09627400 -0.16238500

H -3.82721600 2.50044200 0.85758300

H -3.79883600 2.95011700 -0.85202900

H -4.72827400 1.52739400 -0.32230900

C 0.48557600 0.17091200 1.57706000

O 0.29395300 -0.18209800 2.67210000

H 0.56444200 -1.05856700 -2.02566500

H 1.56502400 1.98509500 0.56651300

C 1.52071600 1.33614900 -1.69117900

O 1.92949500 1.72501200 -2.71127300

F

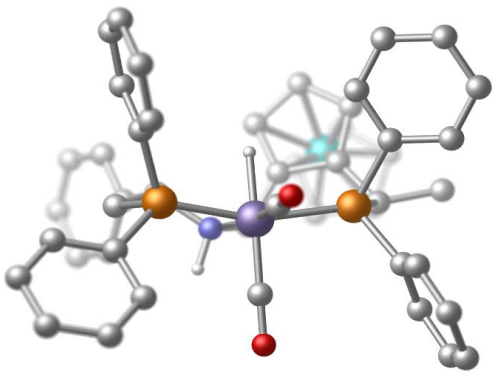

C -0.48952300 3.41127400 -1.46741900

C -1.13723200 3.35001300 -2.70496000

C -0.88704100 4.29882400 -3.69147200

C 0.02461700 5.32251900 -3.46053000

C -6.03303600 -1.79129800 0.59172200

C -2.49204400 -1.89218600 1.14818200

Mn 1.07930000 0.58641100 -0.43854700

C -3.20987600 -1.13417200 2.11608800

C -4.91136100 -1.84117800 -1.42218100

C -5.31229300 -2.63154700 -0.30585300

H -4.32113100 -2.18333200 -2.26732400

C -5.38497400 -0.51307000 -1.21507500

H -5.21999600 0.33178700 -1.87772800

N 0.07590600 -1.35982800 -1.01899200

C 0.58305600 -2.49546100 -0.20614300

C 2.10666500 -2.49028400 -0.26246800

Fe -4.14365800 -1.07393800 0.30526700

H -5.07326500 -3.67854600 -0.14811600

H -6.43961500 -2.08639700 1.55379800

C -1.40001700 -1.38409500 -1.16638000

H -2.30587700 -2.96316400 1.17612500

H -6.52364200 0.39461300 0.49104800

H -3.80962000 1.02361400 2.14891000

H 2.52535200 -3.26554000 0.39451900

H 0.25553100 -2.28082200 0.82252800

P -0.63969400 2.04028600 -0.24469100

C -2.62890400 0.29045500 0.39011400

C -2.12696300 -1.01504300 0.08022100

C -3.29150800 0.20948700 1.65055600

C -6.07732000 -0.48183400 0.03100300

H -3.65926000 -1.52039600 3.02537000

C 0.68829700 5.38681800 -2.23907000

C 0.43732500 4.43920800 -1.25330300

C -0.77314100 2.93144000 1.36976700

C -0.43957400 2.26356000 2.55162300

C -0.61241600 2.87818600 3.78840800

C -1.11074500 4.17406800 3.86330300

C -1.43974500 4.85352800 2.69398900

C -1.27596900 4.23620300 1.45892100

H -1.83980700 2.54408200 -2.92028700

H 0.22363600 6.06365700 -4.23289500

H 0.97814100 4.49564500 -0.30889100

H -0.02787600 1.25585300 2.48914700

H -1.23724400 4.65812900 4.83078100

H -1.53697500 4.78266200 0.55304500

H -1.64393300 -0.67678300 -1.97141600

H -0.34391400 2.34104200 4.69690900

H -1.82508200 5.87114900 2.74122500

H -1.40457400 4.23139700 -4.64727500

H 1.41296000 6.17753600 -2.05078300

H -1.73071100 -2.38146800 -1.50181500

C 0.07609900 -3.86644400 -0.60209300

C 0.08202900 -4.30102400 -1.92969600

C -0.33454900 -4.75776000 0.38957400

C -0.33143900 -5.58672500 -2.25821700

H 0.41033200 -3.62678300 -2.72370200

C -0.74073500 -6.04946500 0.06696000

H -0.32655200 -4.43222000 1.43225700

C -0.74531400 -6.46535700 -1.26008000

H -0.32716200 -5.90628000 -3.29906200

H -1.05651600 -6.73093400 0.85528200

H -1.06751200 -7.47269700 -1.51759800

H 2.43645700 -2.72951100 -1.28701700

P 2.72544300 -0.78477200 0.10582400

C 4.36607100 -0.78550000 -0.72675600

C 4.66798900 0.19496600 -1.67182400

C 5.32197100 -1.76468800 -0.43023200

C 5.90125300 0.19253500 -2.32002600

H 3.93116000 0.96332600 -1.90324500

C 6.54811700 -1.77227300 -1.08224800

H 5.10738000 -2.52062800 0.32738300

C 6.83844200 -0.79136400 -2.02932700

H 6.12639800 0.96425200 -3.05420100

H 7.28344100 -2.54084200 -0.84836100

H 7.80155700 -0.79484700 -2.53768300

C 3.24233100 -0.84323300 1.86606200

C 2.68759200 -1.74774100 2.77384900

C 4.16093400 0.10319700 2.33010800

C 3.05110200 -1.71611800 4.11640100

H 1.95548200 -2.48483600 2.44016400

C 4.51941000 0.13859700 3.67273900

H 4.59812500 0.82081600 1.63501100

C 3.96790100 -0.77263600 4.56862500

H 2.61495100 -2.43231500 4.81147200

H 5.23449500 0.88274500 4.01972100

H 4.25175500 -0.74663700 5.61954400

C -2.43997900 1.49485800 -0.47084000

H -2.48417500 1.16455900 -1.52224400

C -3.49199900 2.57192800 -0.25882800

H -3.46800800 2.96626200 0.76460500

H -3.34250500 3.41651400 -0.94310700

H -4.49550400 2.15895600 -0.43503500

H 0.46084200 -1.46370300 -1.96036300

C 1.37887600 0.93375600 -2.17398000

O 1.53667500 1.14716100 -3.31313400

C 2.07668400 1.90007300 0.14849200

O 2.77992900 2.74205700 0.56062800

H 0.65027600 0.13459700 1.04579900

TS-D-*R*

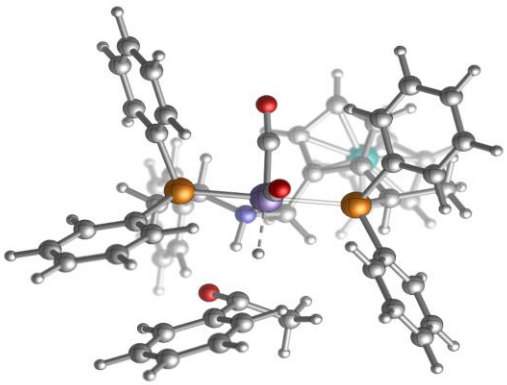

C -0.46119900 3.35755000 -1.14233700

C -1.20500000 3.65491200 -2.28669300

C -0.76102600 4.60798500 -3.20044400

C 0.43141500 5.28677100 -2.98047000

C -6.56568500 -1.49679200 -0.41873100

C -3.21798500 -1.86753000 0.78872600

Mn 0.60775100 0.34940800 0.44717600

C -4.07892600 -1.18010900 1.68933200

C -5.07657500 -1.34639900 -2.17334700

C -5.70783800 -2.25121300 -1.27084700

H -4.34160300 -1.60813700 -2.92886100

C -5.54508900 -0.03303800 -1.87922400

H -5.23214100 0.88029100 -2.37738200

N -0.25021500 -1.26499500 -0.75703300

C 0.08922200 -2.62146600 -0.23362100

C 1.60729300 -2.69703000 -0.07984600

Fe -4.63821100 -0.85037000 -0.24352100

H -5.53113000 -3.32068000 -1.21470200

H -7.15821300 -1.89173100 0.40034600

C -1.66326900 -1.16445600 -1.18751300

H -3.07791700 -2.94380600 0.72534900

H -6.96888200 0.70660500 -0.31102600

H -4.59291000 0.99178700 1.87232800

H 1.91164100 -3.66474400 0.33927500

H -0.39520500 -2.71589200 0.75295900

P -0.93742200 2.07534000 0.09591300

C -3.11415000 0.39091300 0.29338400

C -2.61563400 -0.90215600 -0.07374800

C -4.01596700 0.21041700 1.38612200

C -6.46485500 -0.12542900 -0.79346200

H -4.70781200 -1.63682700 2.44656200

C 1.18033900 5.00539200 -1.84050400

C 0.74214500 4.04625900 -0.93527300

C -1.26412300 3.13714700 1.58281300

C -1.63599200 2.52372600 2.78561900

C -1.99389600 3.28384200 3.89431000

C -1.98085600 4.67277600 3.82756200

C -1.61867800 5.29460300 2.63847600

C -1.27127000 4.53517800 1.52559300

H -2.14071100 3.13690600 -2.49150500

H 0.77790200 6.03222800 -3.69406000

H 1.34207900 3.83698000 -0.04843300

H -1.66585400 1.44112900 2.86836100

H -2.25400500 5.26763700 4.69771300

H -1.01241500 5.04846400 0.60170000

H -1.71195900 -0.34919700 -1.92367000

H -2.27938400 2.78064600 4.81674400

H -1.60936800 6.38140400 2.56895200

H -1.35465400 4.81786800 -4.08876500

H 2.11788100 5.52881300 -1.65710200

H -1.96191600 -2.08023500 -1.72203800

C -0.37446100 -3.77078000 -1.10228900

C -0.05897400 -3.81881900 -2.46478800

C -1.08141700 -4.82876900 -0.53238500

C -0.46060500 -4.90327600 -3.23522700

H 0.49995700 -2.99708500 -2.91878000

C -1.47538800 -5.91997500 -1.30330400

H -1.31852200 -4.79946500 0.53365300

C -1.16884200 -5.95628100 -2.65878200

H -0.21520800 -4.92930200 -4.29593900

H -2.02435800 -6.74010500 -0.84285600

H -1.47851000 -6.80465500 -3.26701000

H 2.06687400 -2.58117800 -1.07300500

P 2.17108700 -1.24537300 0.89059100

C 3.96813300 -1.12316800 0.55901100

C 4.61984300 0.10737200 0.65747000

C 4.71903700 -2.27724100 0.31421300

C 6.00249900 0.17961600 0.52367700

H 4.04895500 1.01765900 0.83392500

C 6.09884800 -2.20014000 0.16604100

H 4.22770600 -3.24827100 0.24851900

C 6.74286400 -0.97119000 0.27735800

H 6.49872500 1.14592500 0.59715000

H 6.67355800 -3.10466600 -0.02775500

H 7.82471600 -0.91083000 0.16688000

C 2.20717700 -1.81675300 2.63735600

C 1.68802900 -3.04415600 3.04992500

C 2.71298200 -0.93724500 3.60086600

C 1.67873000 -3.38913400 4.39898500

H 1.26955500 -3.74273100 2.32485300

C 2.70619000 -1.28278700 4.94551500

H 3.11250300 0.03141800 3.29613900

C 2.18714000 -2.51099700 5.34813200

H 1.26787500 -4.34951900 4.70674700

H 3.10393700 -0.58800600 5.68339000

H 2.17709400 -2.78067200 6.40294200

C -2.72514100 1.66581100 -0.38610600

H -2.65917000 1.45394900 -1.46698700

C -3.72405100 2.79313400 -0.16246000

H -3.82600100 3.03460400 0.90289900

H -3.42408600 3.71589600 -0.67379600

H -4.71396500 2.49494400 -0.53609100

C 1.55546500 1.56622300 1.29025900

O 2.20469200 2.36946300 1.84284700

C -0.24164400 -0.21500100 1.89960700

O -0.75476900 -0.66559600 2.84614500

H 0.33604400 -1.15826700 -1.61096300

H 1.46433300 0.66116900 -1.07364300

C 3.68570800 2.06869500 -2.04796400

C 3.34697200 0.75546100 -2.38099200

C 4.35611500 -0.12573000 -2.76753000

C 5.67819000 0.30065700 -2.83621200

C 6.00661600 1.61412400 -2.51603900

C 5.00627100 2.49634600 -2.11310900

H 2.90530000 2.75963100 -1.72762800

H 4.07530400 -1.14678900 -3.01987700

H 6.45738400 -0.39850100 -3.13864700

H 7.04154700 1.95008800 -2.57362800

H 5.25650000 3.52431800 -1.85177100

C 1.91275200 0.27481500 -2.45171600

C 1.00229400 1.20299100 -3.24404200

H -0.04579900 0.89975200 -3.11717900

O 1.71750300 -0.97151000 -2.62168400

H 1.10457200 2.25983300 -2.98180600

H 1.26418800 1.07841700 -4.30518100

TS-D-*S*

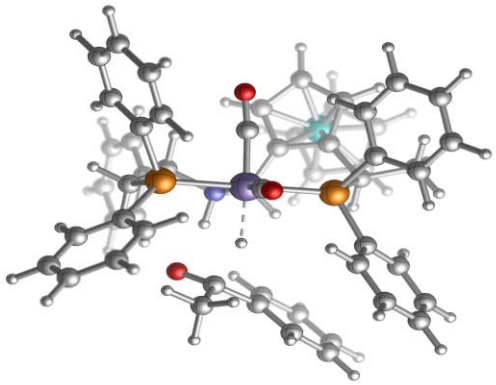

C -0.99013400 3.26656200 -0.56637500

C -2.12067000 3.62406400 -1.30336400

C -2.16266400 4.82553500 -2.00585700

C -1.07080100 5.68443600 -1.99388600

C -5.65261500 -2.91175800 0.80309900

C -2.15698300 -2.55479700 1.35469300

Mn 0.97720000 0.45783300 0.38757200

C -2.93892300 -2.12552500 2.46313700

C -4.65655800 -2.21012000 -1.15503300

C -4.85012100 -3.33229800 -0.29745100

H -4.06340800 -2.19662900 -2.06485300

C -5.33914300 -1.09712500 -0.58454300

H -5.35892800 -0.08890600 -0.98858800

N 0.22406800 -1.25176100 -0.70605500

C 0.93685100 -2.52747800 -0.39359600

C 2.43127800 -2.27928700 -0.59812300

Fe -3.93489700 -1.81475600 0.71187600

H -4.42238200 -4.32033700 -0.43671400

H -5.94614100 -3.52510600 1.64906800

C -1.24295000 -1.42130200 -0.81261600

H -1.81996700 -3.56939400 1.15783800

H -6.51830600 -0.90675300 1.31414200

H -3.83379400 -0.13433800 2.95446200

H 3.02427000 -3.16782500 -0.34692700

H 0.72908400 -2.76940000 0.66231900

P -0.91641200 1.81606600 0.56984700

C -2.61901900 -0.30294400 1.07225100

C -1.95419600 -1.43440300 0.49361000

C -3.22186400 -0.73988300 2.29249200

C -5.95416300 -1.52989700 0.62677000

H -3.29455000 -2.75102700 3.27540800

C 0.08063800 5.31850500 -1.30165800

C 0.12218900 4.11939400 -0.60029800

C -1.06139600 2.68128100 2.20679200

C -1.07171200 1.91243600 3.37790500

C -1.27210600 2.50500600 4.62000800

C -1.45943100 3.87964700 4.71969900

C -1.45678800 4.65323800 3.56534600

C -1.26712300 4.06045000 2.32040800

H -2.98744800 2.96730200 -1.34710800

H -1.11012500 6.62964200 -2.53337500

H 1.02039500 3.86712600 -0.03789500

H -0.93903100 0.83491000 3.33273300

H -1.60926600 4.34491100 5.69270600

H -1.29061900 4.68949000 1.43242300

H -1.60834700 -0.58544500 -1.42336600

H -1.27627200 1.88337700 5.51400300

H -1.60819700 5.72995600 3.62715700

H -3.05711600 5.08296600 -2.57187500

H 0.95045900 5.97378400 -1.29727600

H -1.47700400 -2.34200600 -1.37185400

C 0.50882400 -3.70027400 -1.24885200

C 0.52432300 -3.61321200 -2.64603600

C 0.12655500 -4.89863500 -0.64828500

C 0.14798400 -4.70694100 -3.41617400

H 0.82953800 -2.67953800 -3.12654400

C -0.24230500 -5.99728000 -1.42138700

H 0.12616100 -4.97344300 0.44137000

C -0.23658200 -5.90085800 -2.80812900

H 0.15821100 -4.62829800 -4.50228000

H -0.53565200 -6.92771400 -0.93740400

H -0.52837400 -6.75509200 -3.41697300

H 2.59015400 -2.03216500 -1.65762300

P 2.90789500 -0.76383600 0.31693300

C 4.47409600 -0.20467600 -0.45618000

C 4.96270700 1.07549100 -0.17262000

C 5.19571700 -1.02972500 -1.32222400

C 6.14829600 1.51917900 -0.74649200

H 4.40118300 1.74681700 0.47619100

C 6.37602600 -0.57898300 -1.90425500

H 4.83518800 -2.02907400 -1.56050800

C 6.85407000 0.69542300 -1.61823400

H 6.51345700 2.51998500 -0.52200800

H 6.92210300 -1.22803100 -2.58687000

H 7.77596100 1.04828400 -2.07762600

C 3.50284200 -1.34099700 1.95887900

C 3.44404800 -2.67704200 2.35792900

C 3.96139200 -0.38464100 2.87230800

C 3.84540400 -3.05201400 3.63737500

H 3.07123700 -3.44400000 1.67975800

C 4.36716500 -0.75989200 4.14589400

H 3.98975100 0.66925500 2.59388200

C 4.30982300 -2.09640800 4.53244900

H 3.79045900 -4.09846200 3.93347200

H 4.72194700 -0.00263900 4.84301000

H 4.62169600 -2.39015800 5.53333900

C -2.65723700 1.06795600 0.46652800

H -2.82471700 0.95534000 -0.61974200

C -3.76447300 1.92925300 1.06428800

H -3.63185100 2.05580500 2.14599700

H -3.79389300 2.93416500 0.62902000

H -4.73992700 1.44966200 0.89834400

C 1.84733800 1.79861100 1.11830900

O 2.46130000 2.66468100 1.61510500

C 0.65329400 -0.33981200 1.93364400

O 0.47811800 -0.94088000 2.91808700

H 0.57981800 -0.99136800 -1.65232600

H 1.22735900 1.02464700 -1.32779900

C 0.13466700 2.72735100 -3.73244800

C 0.23409900 1.39242900 -3.33870000

C -0.80835700 0.52603400 -3.68173200

C -1.93782800 0.98420800 -4.34947700

C -2.02253600 2.31881000 -4.73934200

C -0.97418000 3.18175900 -4.44104000

H 0.93470500 3.42757300 -3.49820000

H -0.69320500 -0.53509000 -3.46504600

H -2.73661400 0.28774400 -4.60507600

H -2.89206400 2.67806000 -5.28860900

H -1.01886500 4.22434800 -4.75451800

C 1.48473800 0.80570200 -2.68667600

C 2.72366000 1.68463300 -2.82303200

H 3.58822000 1.14010200 -2.43412100

O 1.64827600 -0.45387000 -2.88931300

H 2.89951300 1.88705300 -3.88973400

H 2.63927500 2.64207400 -2.29043500

TS-A-*R*

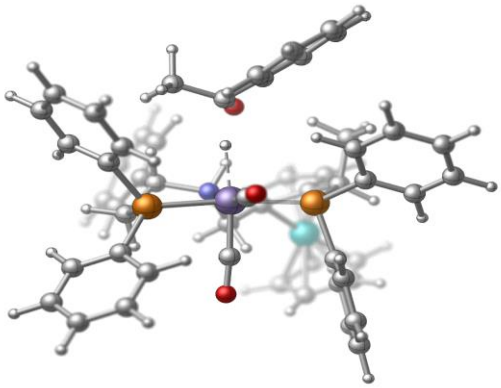

C 1.54462400 1.78627500 2.20537900

C 2.71023200 1.10120000 2.53400500

C 3.16438600 1.06256400 3.85176500

C 2.45216600 1.71111800 4.85255800

C 6.30571800 -1.93237300 -0.00507500

C 3.29624000 -1.96984800 -1.56186900

Mn -1.03898100 0.27662100 0.54854400

C 4.24764200 -1.19931300 -2.27989700

C 4.85627200 -1.37932200 1.69872700

C 5.32498500 -2.45188900 0.88848800

H 4.08529500 -1.45115800 2.46117300

C 5.55240400 -0.19523600 1.30649500

H 5.41562600 0.79983900 1.71966600

N 0.08923600 -1.20863500 -0.46521500

C -0.72294200 -2.41287600 -0.83147500

C -1.55038700 -2.84535500 0.36932100

Fe 4.52481300 -0.98598800 -0.28491000

H 4.96521300 -3.47571400 0.91507800

H 6.81758300 -2.49010000 -0.78331800

C 1.41500500 -1.52221000 0.14664400

H 3.18589400 -3.05118600 -1.58390400

H 7.09029600 0.14896100 -0.28455300

H 4.66628200 0.99770700 -2.25140500

H 0.24698900 -0.72369100 -1.36952300

H -2.13210100 -3.75142400 0.15291200

H -1.42292900 -2.02361700 -1.58058900

P 0.84149900 1.75256200 0.50493000

C 2.98417700 0.25513000 -0.96860300

C 2.52983900 -1.08608000 -0.74020200

C 4.07176500 0.15929900 -1.89838500

C 6.44528000 -0.53838100 0.25337200

H 5.01452500 -1.58274500 -2.94588100

C 1.28439000 2.40087800 4.53170100

C 0.83200500 2.43741800 3.22012900

C 0.55668700 3.56793200 0.32614100

C -0.60359300 4.05213400 -0.27141400

C -0.79567800 5.42172800 -0.43914200

C 0.17465000 6.31921800 -0.01301400

C 1.34036400 5.84535000 0.58676000

C 1.52862800 4.48074600 0.75819100

H 3.26231100 0.58442400 1.75089100

H 2.80377200 1.68101100 5.88256600

H -0.08722200 2.97455600 2.98058800

H -1.36179700 3.35586000 -0.62275600

H 0.02568100 7.39010000 -0.14401100

H 2.43646300 4.12270300 1.24484000

H 1.48791900 -1.05150800 1.13335500

H -1.71011600 5.77649100 -0.91234700

H 2.10376400 6.54359900 0.92713700

H 4.08127500 0.52439900 4.09328000

H 0.72023200 2.91135400 5.31071100

H 1.50169700 -2.60534600 0.31748100

C 0.07085800 -3.49011200 -1.53334300

C 0.42569800 -4.69819600 -0.93338000

C 0.47320200 -3.24004700 -2.85024600

C 1.17544800 -5.64176400 -1.63282300

H 0.11540200 -4.91107100 0.09053900

C 1.21656900 -4.18267100 -3.54934500

H 0.20649300 -2.28312300 -3.30763800

C 1.57126300 -5.38583200 -2.94175900

H 1.44530200 -6.58161200 -1.15340200

H 1.52256300 -3.97716800 -4.57391500

H 2.15153000 -6.12590800 -3.49081800

H -0.92185500 -3.05331400 1.25050600

P -2.56706400 -1.35765700 0.78350400

C -3.29839300 -1.73473400 2.42455000

C -3.54980300 -0.70698800 3.33618600

C -3.67120900 -3.04161700 2.75246600

C -4.15459800 -0.98437000 4.55778900

H -3.27054600 0.31812000 3.09417300

C -4.26608700 -3.31944100 3.97741400

H -3.50470500 -3.85307400 2.04288100

C -4.50792300 -2.28966800 4.88222300

H -4.34333800 -0.17523000 5.26116800

H -4.54528100 -4.34244000 4.22480300

H -4.97464200 -2.50628500 5.84180000

C -4.07850100 -1.45730100 -0.25344600

C -4.41522700 -2.54055700 -1.06478000

C -4.93647800 -0.35247100 -0.20070800

C -5.58332200 -2.51468000 -1.82309300

H -3.76212900 -3.41120400 -1.12946700

C -6.10612000 -0.33142000 -0.94979600

H -4.67911400 0.50264500 0.42797300

C -6.42838100 -1.41208000 -1.76818000

H -5.83094100 -3.36171300 -2.46093500

H -6.76507600 0.53389200 -0.90032800

H -7.33979100 -1.39341400 -2.36327400

C 2.38339500 1.60812000 -0.62228600

H 3.14980400 2.22314900 -0.11833000

C 2.00800600 2.25954200 -1.96406600

H 1.26385400 1.63224300 -2.47473800

H 1.60306500 3.27040000 -1.84756900

H 2.89146100 2.32912500 -2.60938100

C -2.12372800 1.54998000 1.11353600

O -2.89072500 2.35704900 1.47382100

C -0.54211500 -0.22149800 2.17561400

O -0.24332000 -0.63576600 3.22490400

H -1.59376600 0.58531400 -1.11720100

C -2.90861400 2.65146000 -2.41380600

C -1.75013900 2.03035900 -2.89111000

C -0.90603600 2.74289400 -3.74017700

C -1.19609900 4.05975100 -4.08768200

C -2.34514900 4.67344300 -3.60155700

C -3.20376600 3.96344500 -2.76272500

H -3.57592800 2.10553900 -1.74436300

H -0.02697200 2.23834200 -4.13678800

H -0.52535700 4.60494800 -4.75054900

H -2.57609000 5.70195900 -3.87663500

H -4.10666000 4.43628100 -2.37748000

C -1.46456800 0.56031200 -2.64253800

C -2.67758300 -0.27495600 -3.04981900

H -2.48596100 -1.34747700 -2.93916100

O -0.31932600 0.09237200 -2.92230500

H -2.83472000 -0.08143400 -4.12152800

H -3.60080700 -0.01626100 -2.52130200

TS-A-*S*

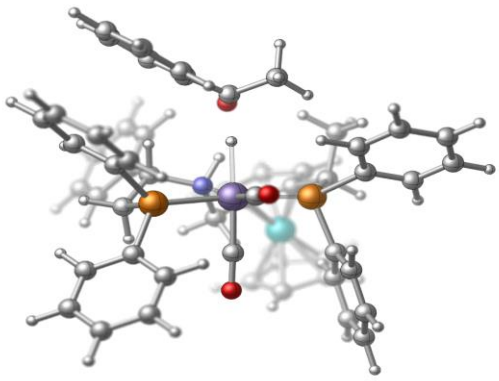

C -2.24697500 -2.59395900 0.62469700

C -3.32324600 -2.00689700 1.28253800

C -3.91240100 -2.63417300 2.37938800

C -3.42591900 -3.85622400 2.82638100

C -5.90437500 2.67920900 1.11573900

C -2.93302500 2.93467500 -0.41807400

Mn 0.70525500 -0.93049500 0.13960500

C -3.96986800 2.84360300 -1.38291800

C -4.75344500 0.94047500 2.09633400

C -4.89526500 2.35628300 2.06862500

H -4.04469300 0.38582100 2.70542100

C -5.68021700 0.38762200 1.16047200

H -5.81375500 -0.66528600 0.92986600

N 0.00400900 1.07029800 0.02812100

C 1.07125500 2.08910200 0.29714500

C 1.81257200 1.69133800 1.56261900

Fe -4.38347100 1.66879000 0.21528700

H -4.30443700 3.06723700 2.63793900

H -6.21188200 3.67977100 0.82743000

C -1.28390700 1.32476100 0.73616700

H -2.62722600 3.82390100 0.12807700

H -7.13801000 1.37289400 -0.22493200

H -4.77790500 1.07719500 -2.49208300

H -0.15791000 1.14845800 -0.99230100

H 2.59213200 2.41826700 1.82582000

H 1.76084700 1.97263000 -0.55421500

P -1.34907700 -1.73432200 -0.73253400

C -3.05910100 0.71618100 -1.09795500

C -2.38340200 1.62998200 -0.22221100

C -4.06268800 1.48160500 -1.78059800

C -6.38889800 1.46242900 0.55528200

H -4.61976800 3.65071100 -1.70669400

C -2.34923900 -4.45139300 2.17160700

C -1.76251400 -3.82610300 1.08018900

C -1.30669000 -3.16424900 -1.90975200

C -0.11525400 -3.57803100 -2.50111000

C -0.09128500 -4.66504400 -3.37269600

C -1.26297600 -5.35207900 -3.66070900

C -2.45995400 -4.95704900 -3.06513000

C -2.47949300 -3.87811100 -2.19237500

H -3.69247300 -1.04138000 0.94101000

H -3.88262100 -4.34648400 3.68459200

H -0.91628200 -4.29869800 0.57916100

H 0.80576600 -3.04573100 -2.27857600

H -1.24679000 -6.20134900 -4.34205200

H -3.41873200 -3.59447000 -1.71591900

H -1.54234200 0.46228400 1.35968000

H 0.85125900 -4.97278400 -3.82261400

H -3.38093400 -5.49826700 -3.27660700

H -4.75433700 -2.16164800 2.88583300

H -1.96276100 -5.40951600 2.51569000

H -1.17318100 2.17654300 1.42363500

C 0.56471800 3.51520600 0.24834000

C 0.46656600 4.32735700 1.37861200

C 0.16181700 4.03091300 -0.98925500

C -0.02291800 5.62833600 1.27964300

H 0.77469900 3.94762500 2.35309500

C -0.32049400 5.32994700 -1.08976800

H 0.21452400 3.38435900 -1.86817500

C -0.41531700 6.13348000 0.04486700

H -0.09204400 6.24863400 2.17209700

H -0.62848100 5.71656700 -2.06012400

H -0.79146400 7.15233600 -0.03474400

H 1.12668100 1.60936900 2.42162700

P 2.45449700 -0.01170000 1.24237900

C 2.87643600 -0.64139400 2.92049600

C 2.74875500 -1.99784500 3.22688100

C 3.39439800 0.22525200 3.88794300

C 3.11955000 -2.47509900 4.47991500

H 2.35294600 -2.69091900 2.48504300

C 3.75492300 -0.24970400 5.14335800

H 3.53051400 1.28274700 3.65829200

C 3.61679600 -1.60231500 5.44129600

H 3.01133700 -3.53455200 4.70572200

H 4.14991200 0.43788300 5.88968700

H 3.89972000 -1.97579400 6.42416600

C 4.17393600 0.20288900 0.62713900

C 4.77873300 1.44017600 0.40938500

C 4.93800400 -0.96284300 0.49147400

C 6.13227200 1.51253600 0.09088900

H 4.20205500 2.36271400 0.47512200

C 6.28966700 -0.88792400 0.18371800

H 4.47167800 -1.93732600 0.64960500

C 6.89249100 0.35347800 -0.00726500

H 6.59151600 2.48492800 -0.08232500

H 6.87606400 -1.80150600 0.09749400

H 7.95389200 0.41507800 -0.24340100

C -2.72418600 -0.69042100 -1.57314800

H -3.63021200 -1.31431900 -1.47905500

C -2.37161800 -0.55011500 -3.06530700

H -1.51943400 0.13343300 -3.18860800

H -2.13637300 -1.51234400 -3.53349000

H -3.22258100 -0.12455700 -3.60969400

C 1.50719600 -2.49746400 0.02313600

O 2.10504800 -3.50285400 -0.03249200

C 0.05738600 -1.23299000 1.76280600

O -0.36042600 -1.37701400 2.84250000

H 1.32558300 -0.52565100 -1.46532100

C 3.86078300 -0.11168600 -2.70510400

C 2.78962100 0.78466400 -2.75780100

C 3.05409200 2.13663700 -2.97935000

C 4.35945100 2.58431400 -3.16478500

C 5.41393900 1.67899300 -3.14454700

C 5.16069600 0.32894100 -2.90948000

H 3.67181500 -1.16652700 -2.49573200

H 2.21214000 2.82438800 -3.04099500

H 4.54873700 3.64147900 -3.34797200

H 6.43619100 2.02203900 -3.30228500

H 5.98494000 -0.38176300 -2.87001900

C 1.34381700 0.32652000 -2.77137400

C 1.13004000 -0.80381300 -3.76885200

H 0.12293200 -1.21904400 -3.69126700

O 0.43697000 1.20572200 -2.67850300

H 1.86211700 -1.61344900 -3.67633000

H 1.24197500 -0.36054100 -4.76978500

2.8.2 NMR spectra

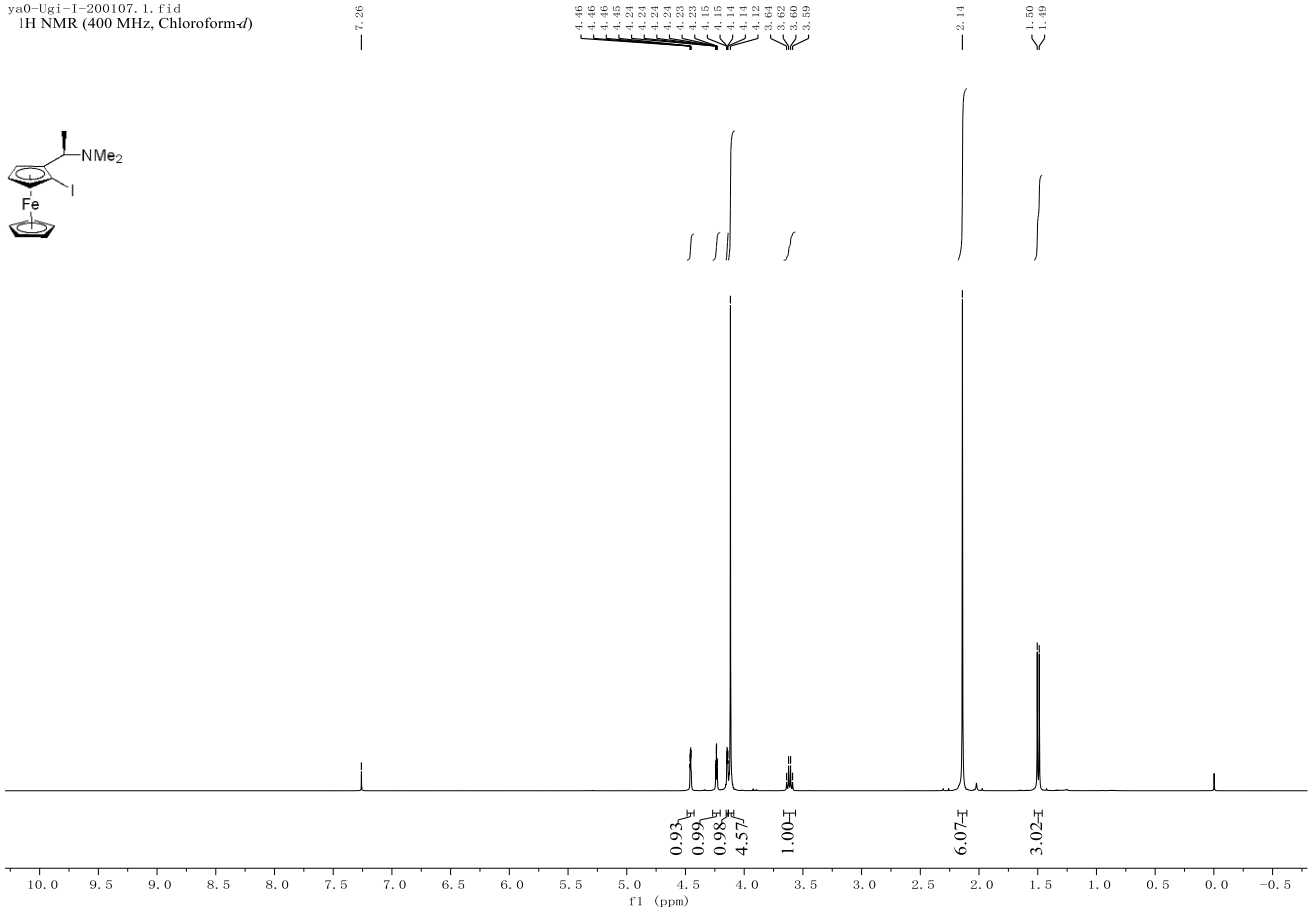

yao-Ugi-I-200107-C.1.fid
13C NMR (101 MHz, Chloroform-*d*)

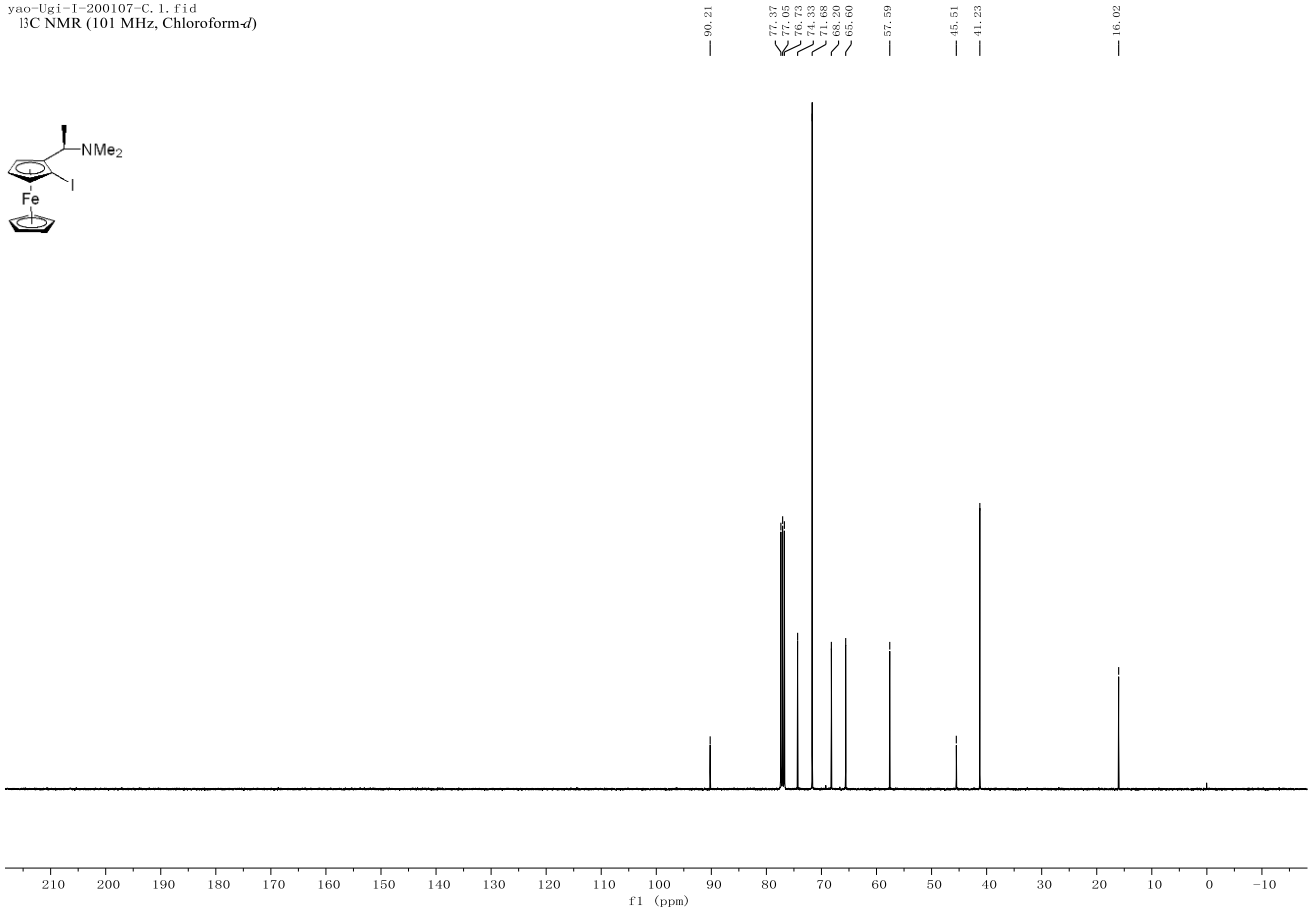

yao-200415-BH3PPh2-I.1.fid
1H NMR (400 MHz, Chloroform-*d*)

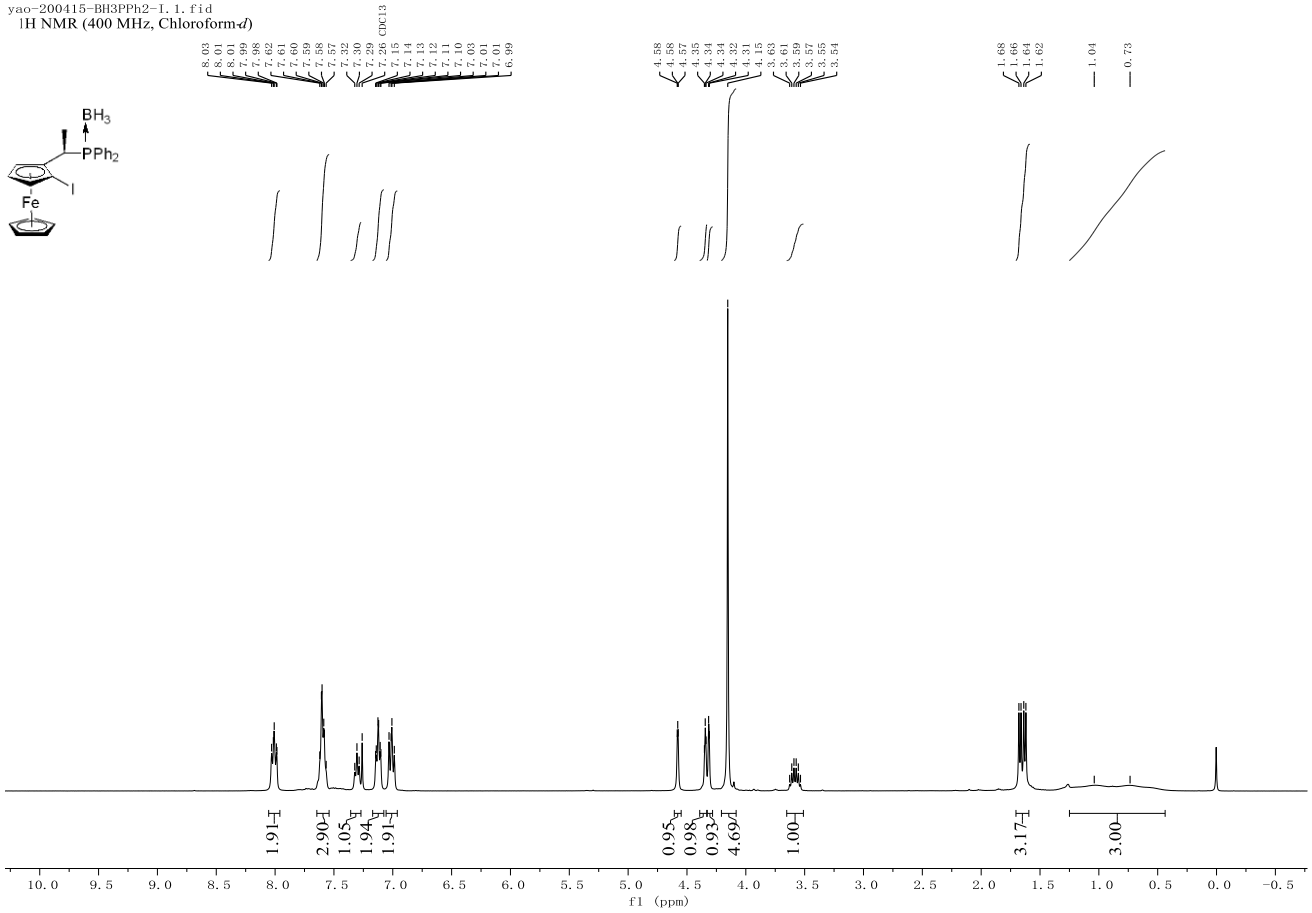

yao-200402-BH3PPh2-I. 3. fid

^{13}C NMR (101 MHz, Chloroform-*d*)

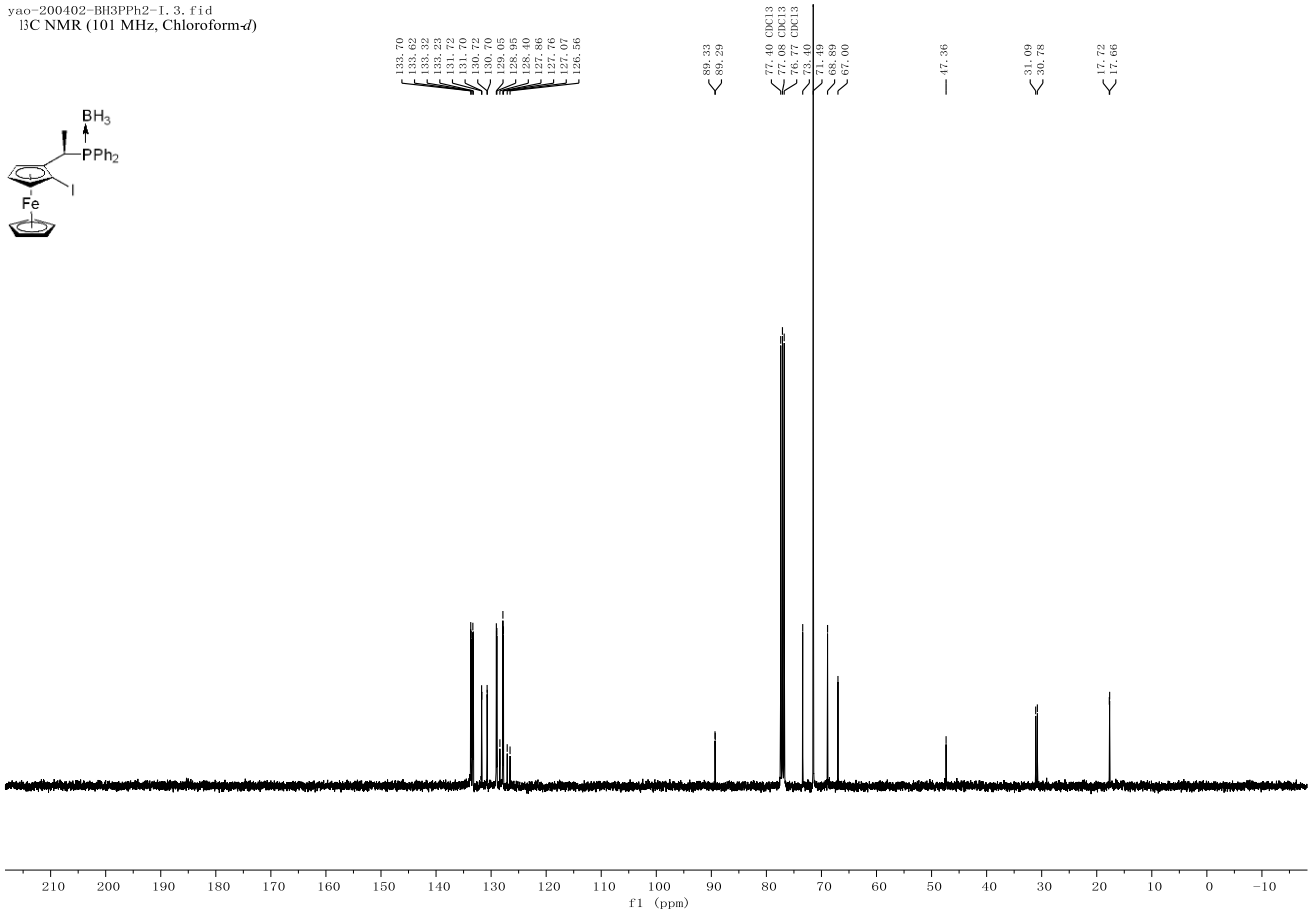

yao-200402-BH3PPh2-I. 2. fid

^{31}P NMR (162 MHz, Chloroform-*d*)

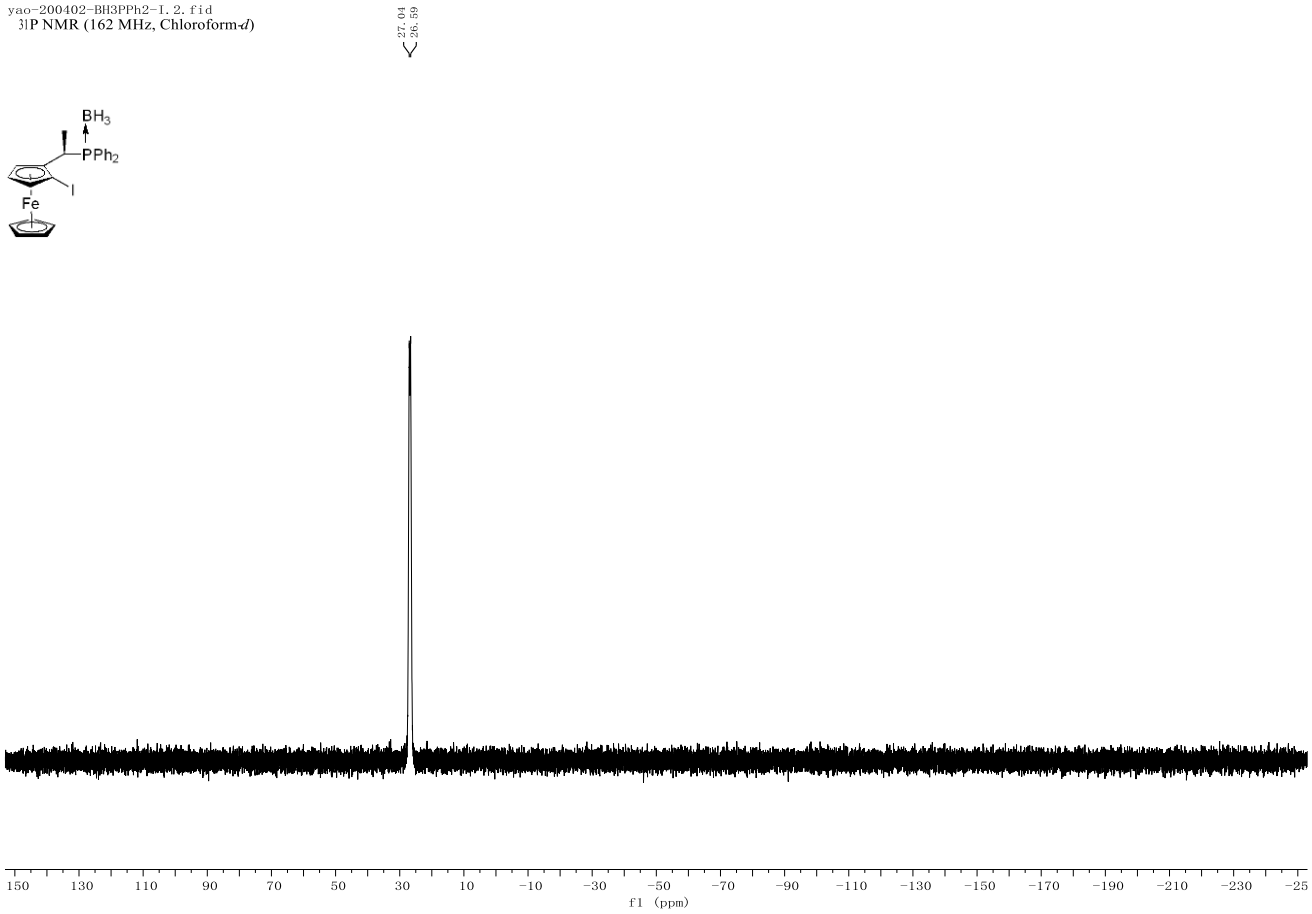

yao-20191127-Cy-I.3.fid

1H NMR (400 MHz, Chloroform-*d*)

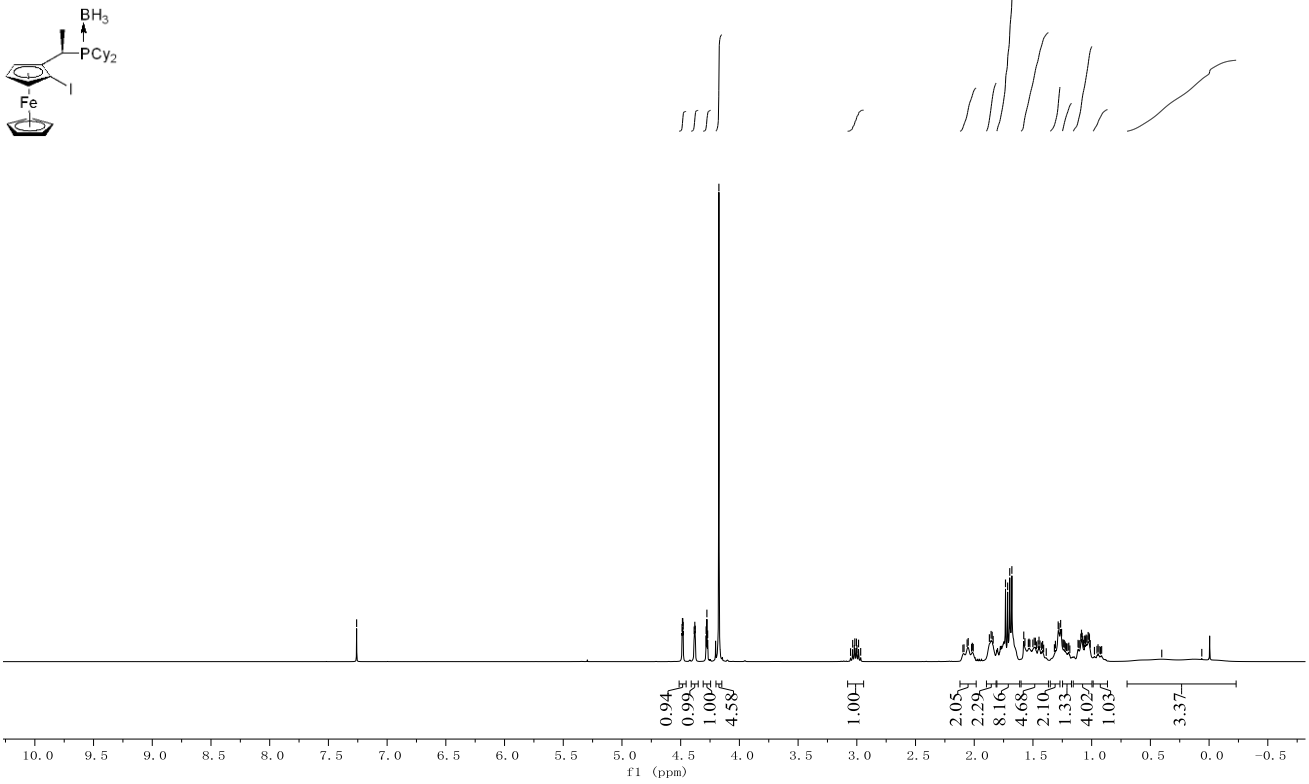

yao-20191127-Cy-I.3.fid

13C NMR (101 MHz, Chloroform-*d*)

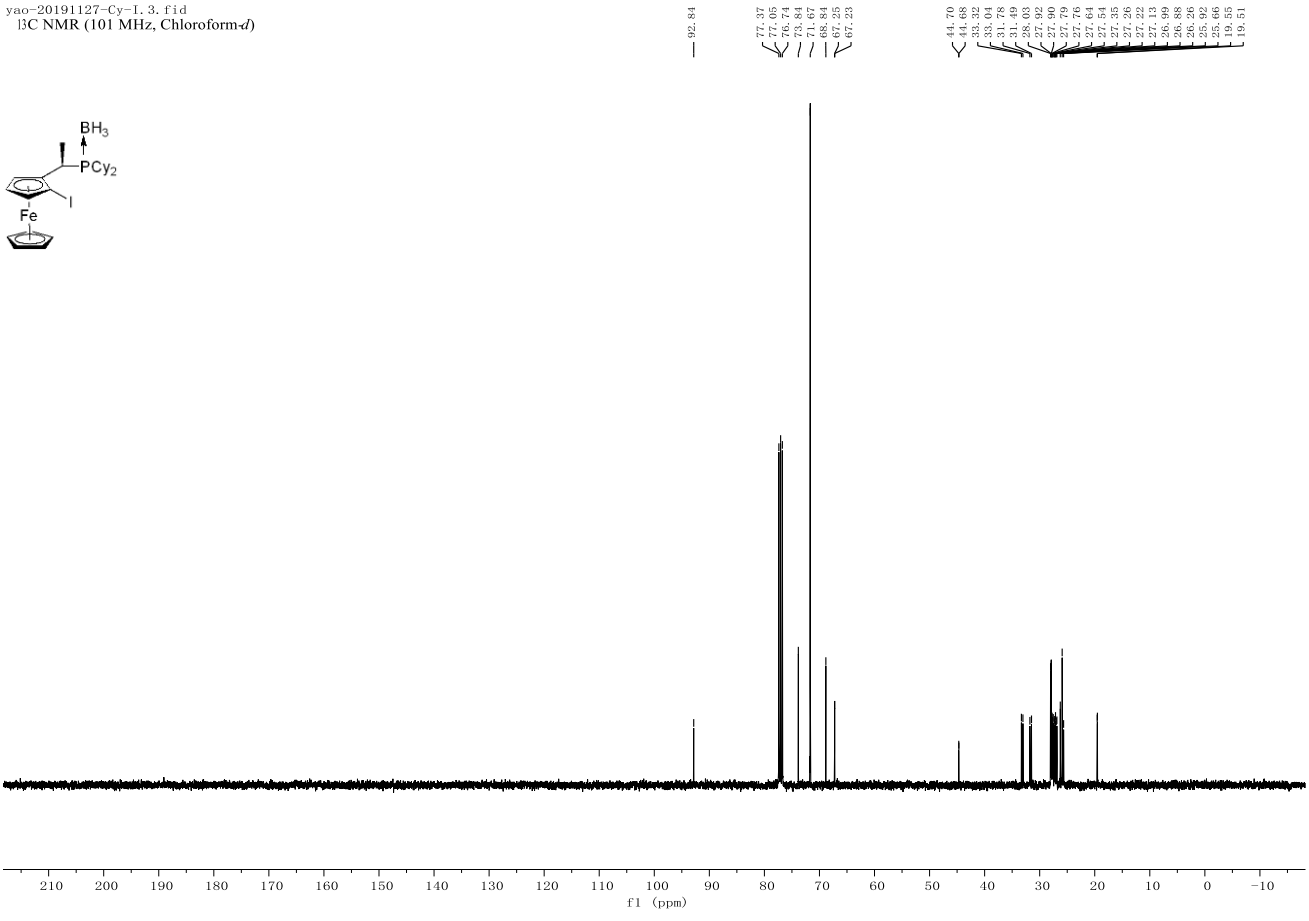

yao-20191127-Cy-I.2.fid
31P NMR (162 MHz, Chloroform-*d*)

39.00
38.49

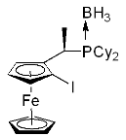

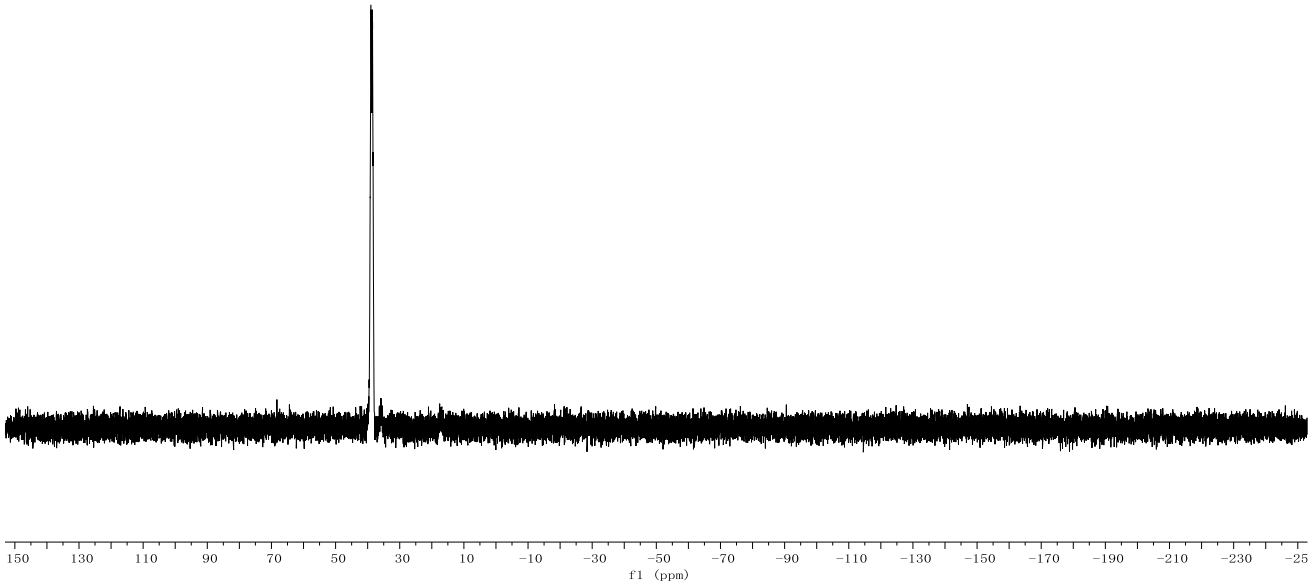

150 130 110 90 70 50 30 10 −10 −30 −50 −70 −90 −110 −130 −150 −170 −190 −210 −230 −25
f1 (ppm)

yao-20191127-tBu-I.1.fid
1H NMR (400 MHz, Chloroform-*d*)

7.26

4.49 4.48 4.48 4.46 4.43 4.42 4.30 4.29 4.28 4.18
3.10 3.08 3.07 3.06 3.05 3.04 3.03 3.02
2.00 1.98 1.97 1.95
HDO
1.57 1.39 1.36 1.23 1.20
0.62 0.41 0.14 0.07 −0.00 −0.06

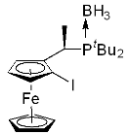

10.0 9.5 9.0 8.5 8.0 7.5 7.0 6.5 6.0 5.5 5.0 4.5 4.0 3.5 3.0 2.5 2.0 1.5 1.0 0.5 0.0 −0.5
f1 (ppm)

yao-20191127-tBu-I.6.fid
13C NMR (101 MHz, Chloroform-*d*)

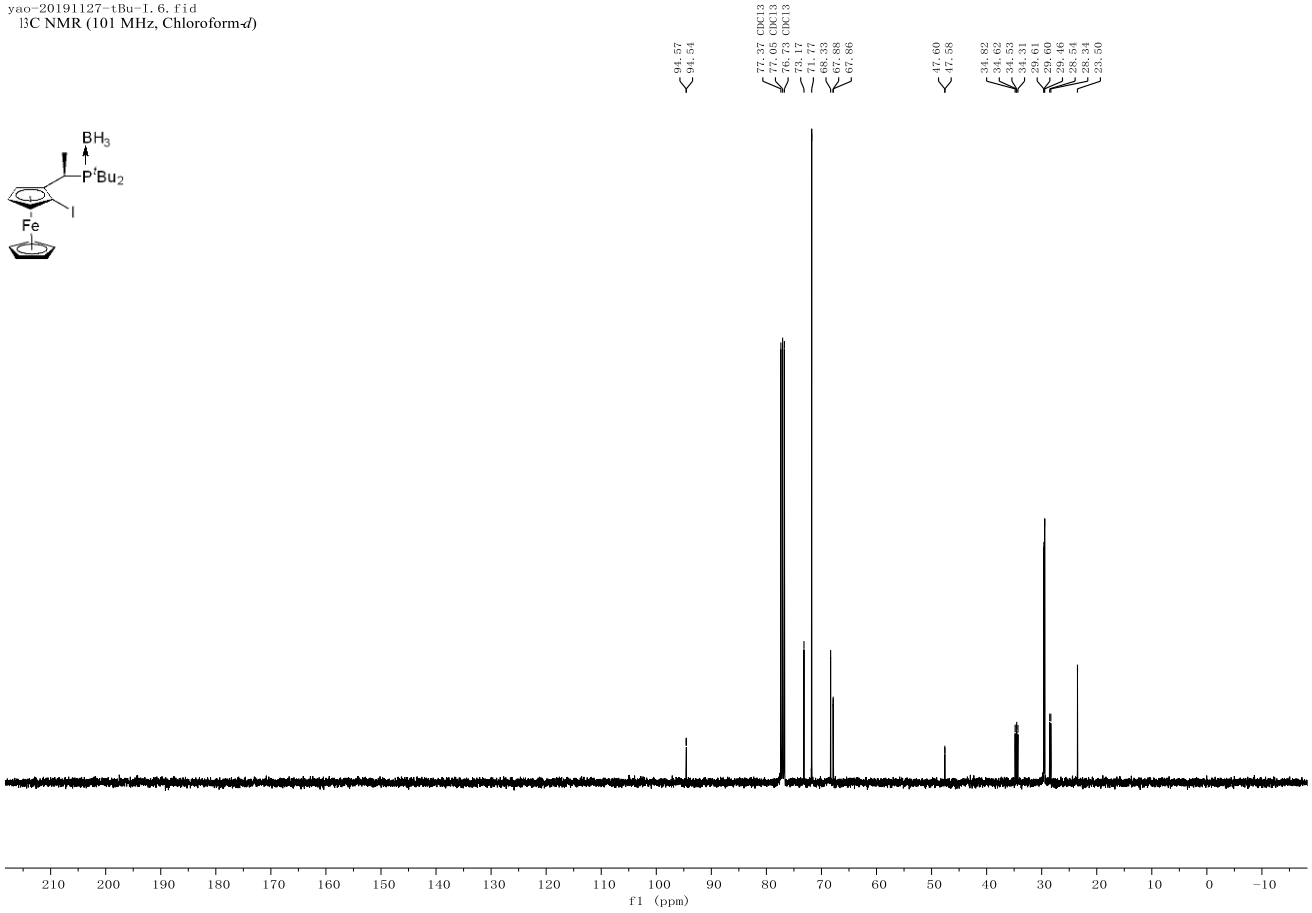

yao-20191127-tBu-I.2.fid
31P NMR (162 MHz, Chloroform-*d*)

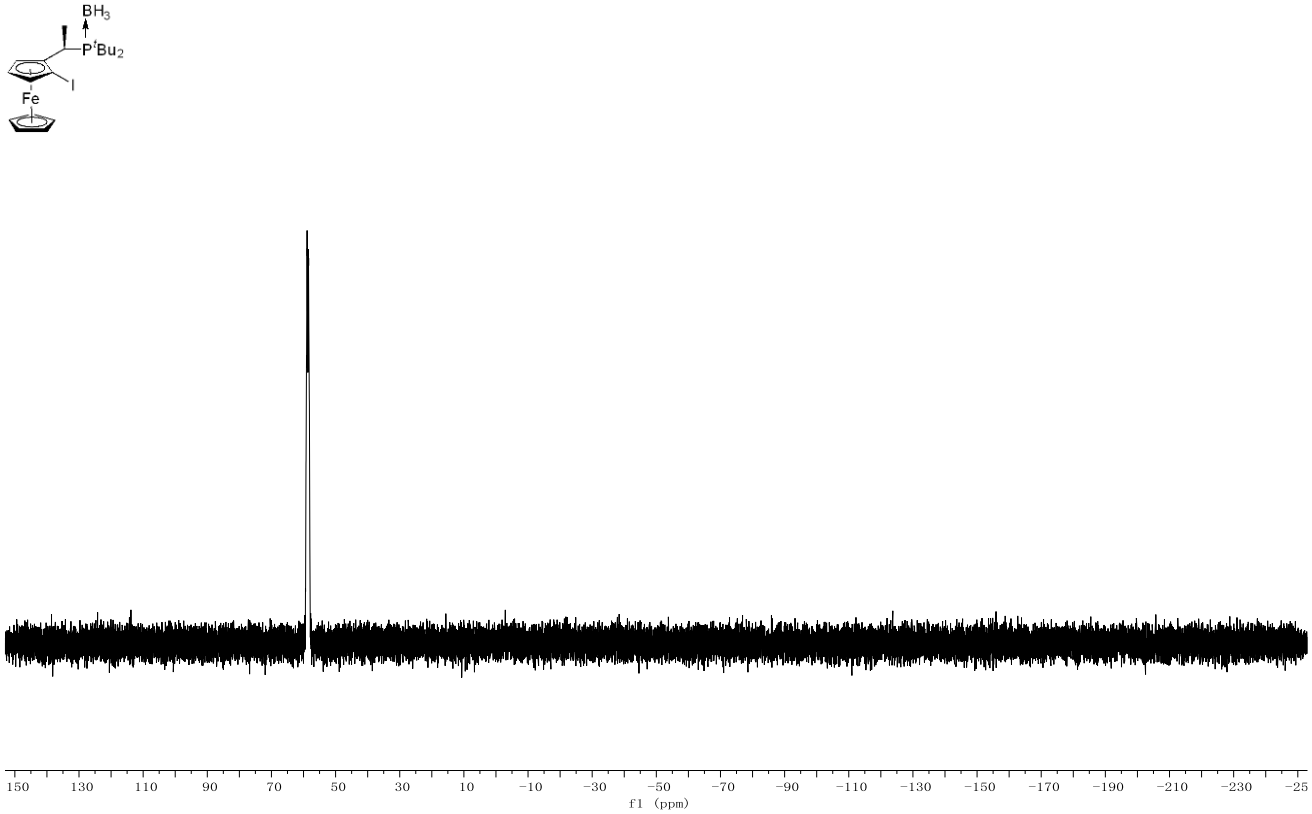

yao-190606-1.10.fid

1H NMR (600 MHz, Chloroform-*d*)

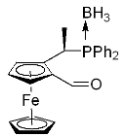

yao-200327-BH3PPh2-CHO.3.fid

13C NMR (101 MHz, Chloroform-*d*)

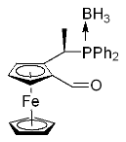

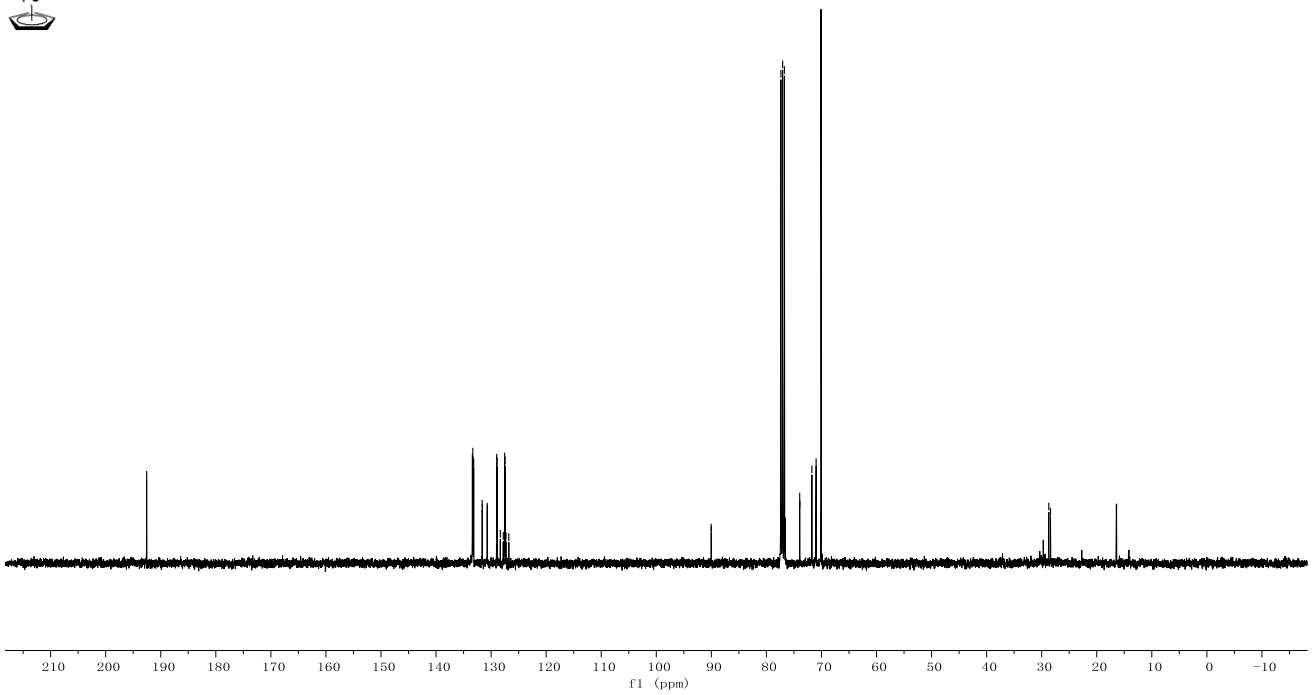

yao-200327-BH3PPh2-CHO. 2. fid

31P NMR (162 MHz, Chloroform-*d*)

27.13
26.66

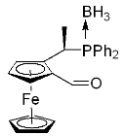

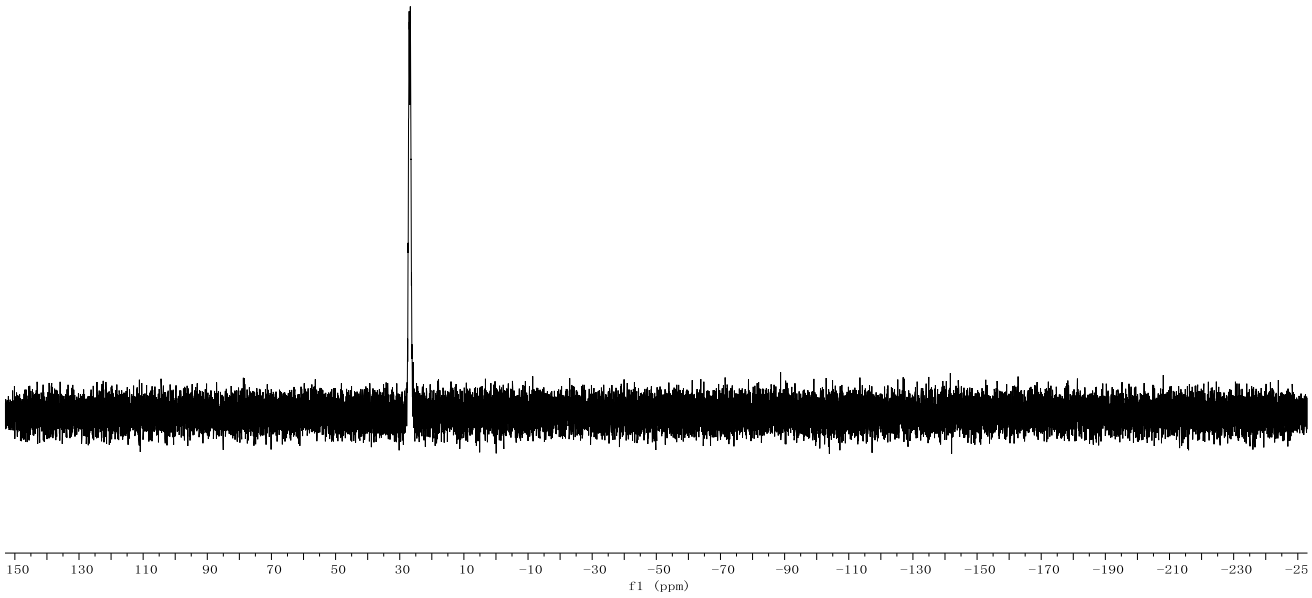

yao-20191127-Cy. 1. fid

1H NMR (400 MHz, Chloroform-*d*)

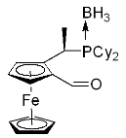

yao-20191127-Cy.3.fid

13C NMR (101 MHz, Chloroform-*d*)

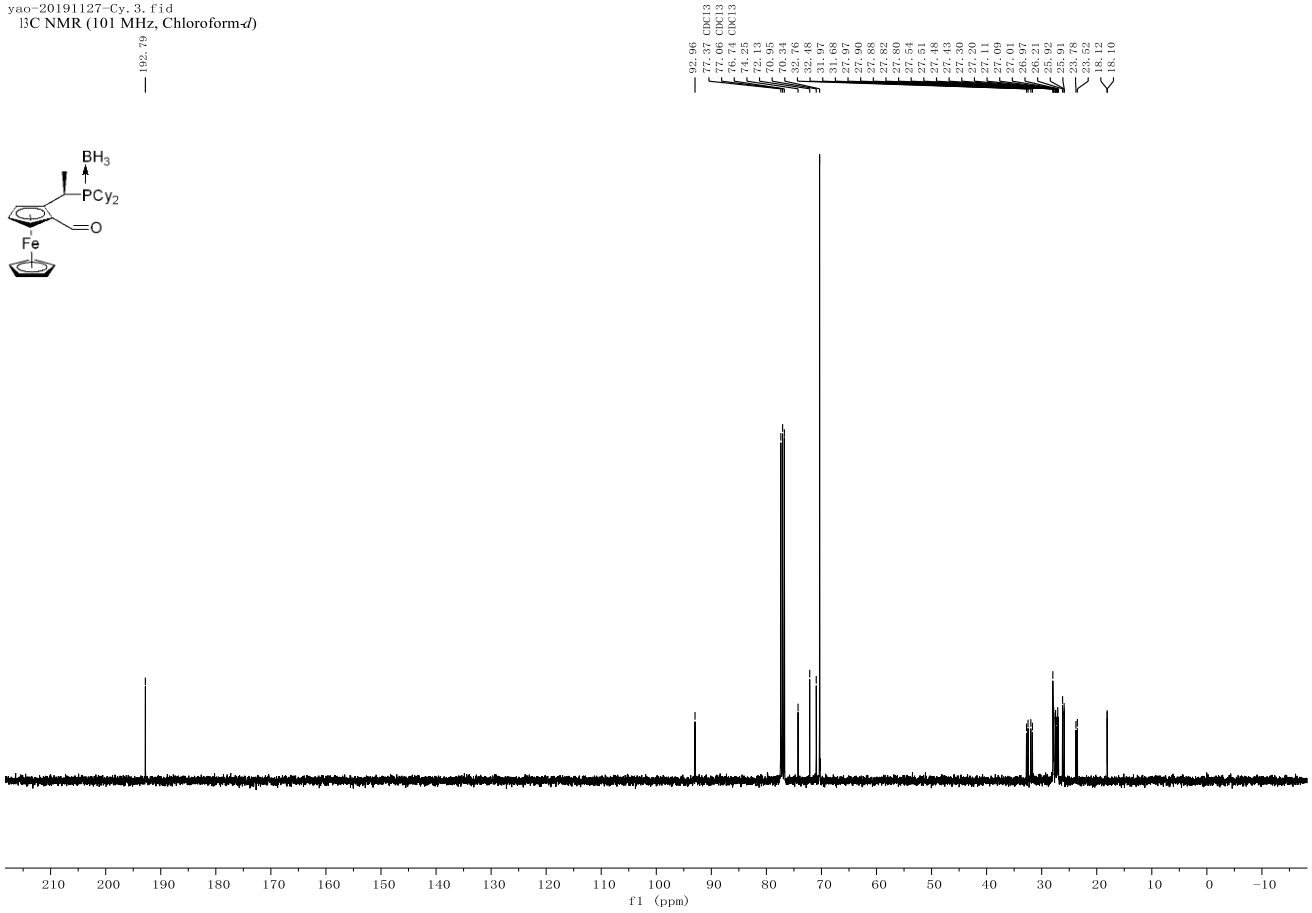

yao-20191127-Cy.2.fid

31P NMR (162 MHz, Chloroform-*d*)

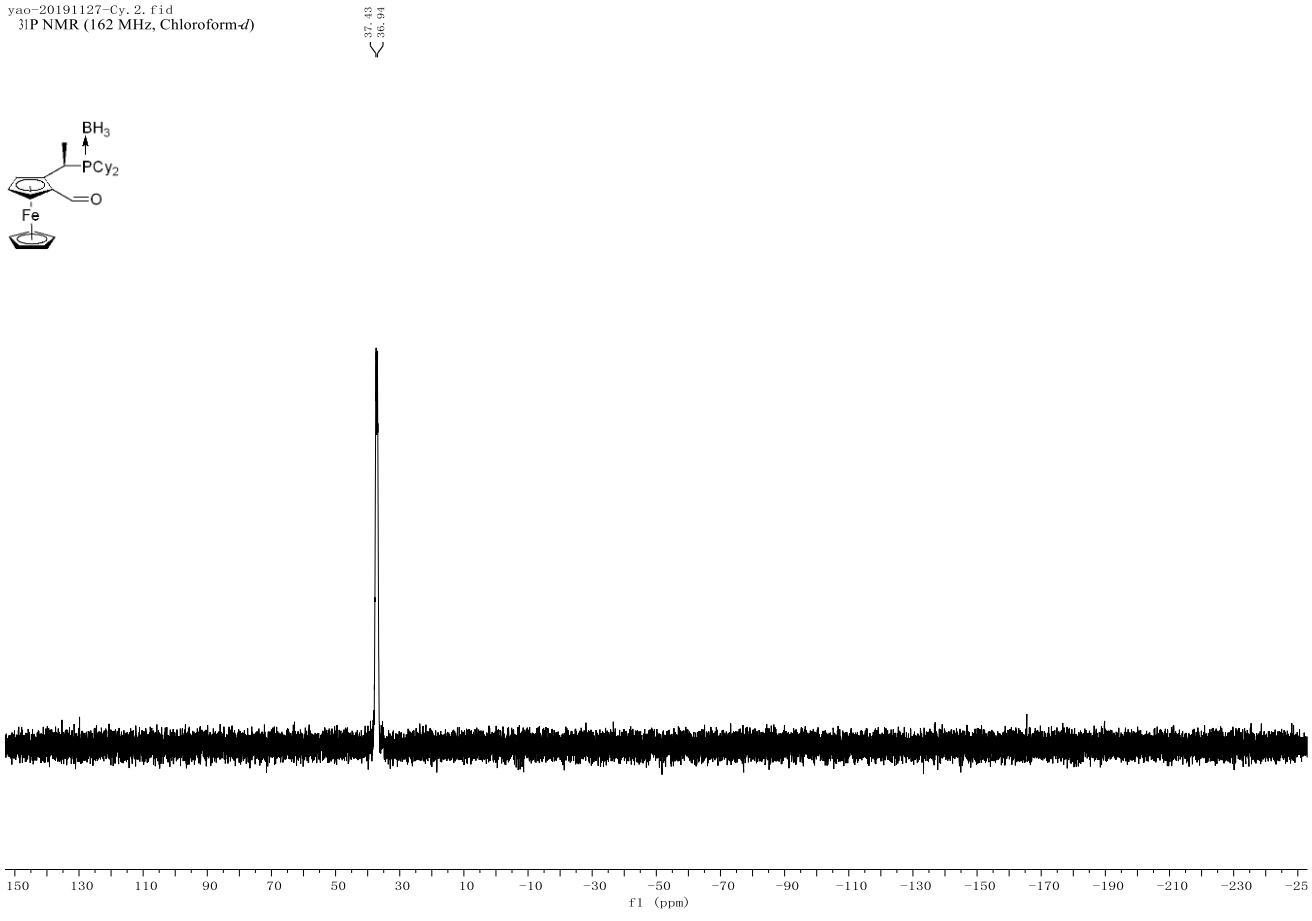

yao-20191127-tBu. 1. fid

1H NMR (400 MHz, Chloroform-*d*)

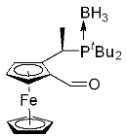

yao-20191127-tBu. 3. fid

13C NMR (101 MHz, Chloroform-*d*)

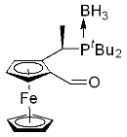

yao-20191127-tBu. 2. fid

31P NMR (162 MHz, Chloroform-*d*)

55.62
55.08

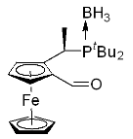

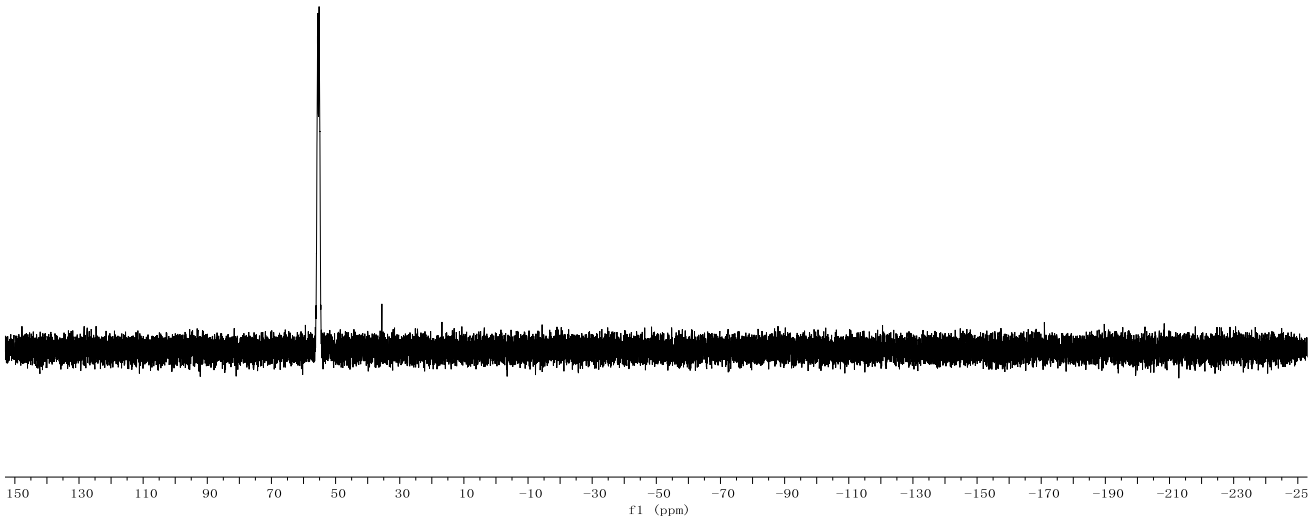

yao-PNP-20191127-21. fid

1H NMR (400 MHz, Chloroform-*d*)

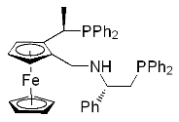

yao-PNP-200107.3.fid
13C NMR (101 MHz, Chloroform-*d*)

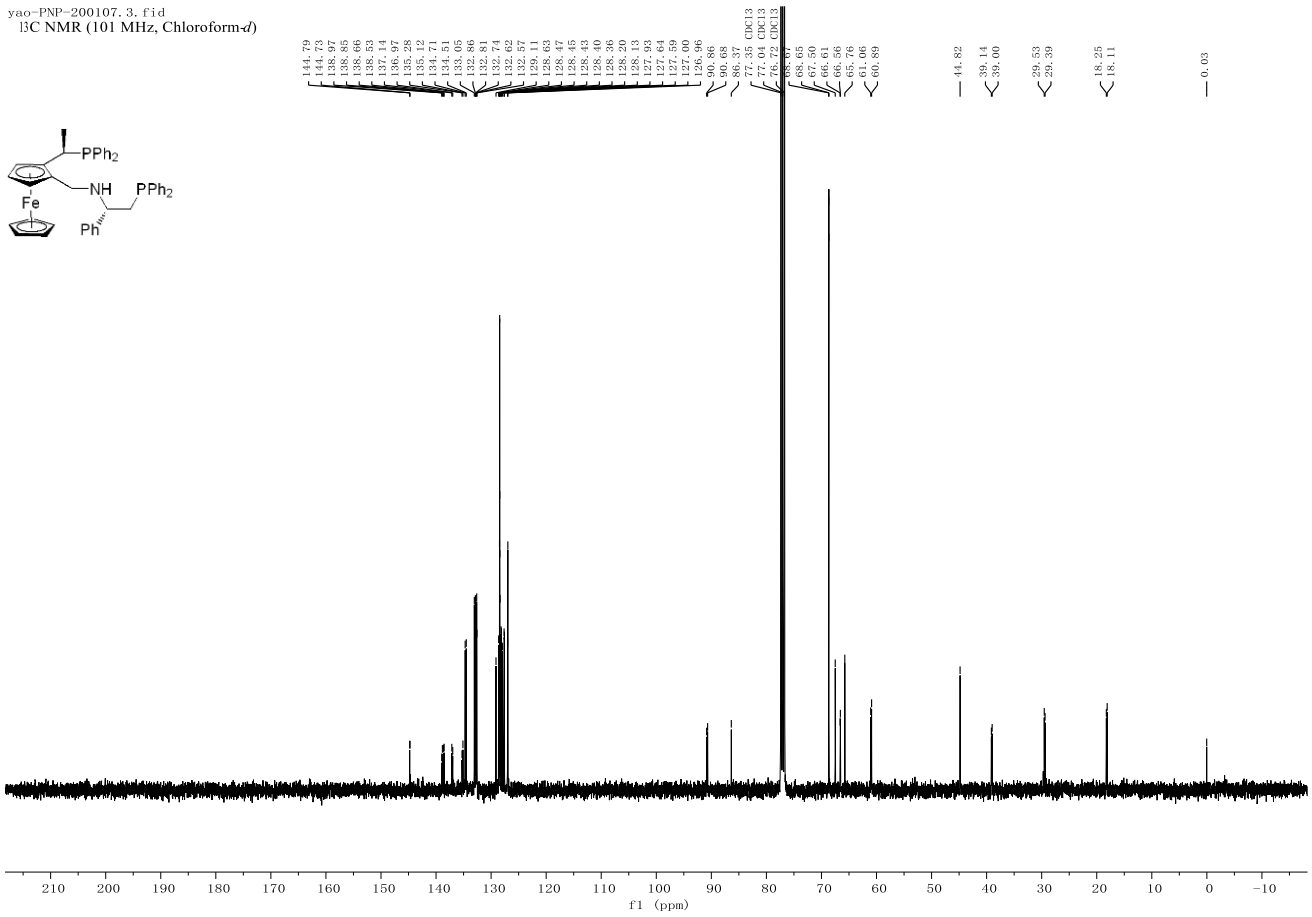

yao-PNP-200107.2.fid
31P NMR (162 MHz, Chloroform-*d*)

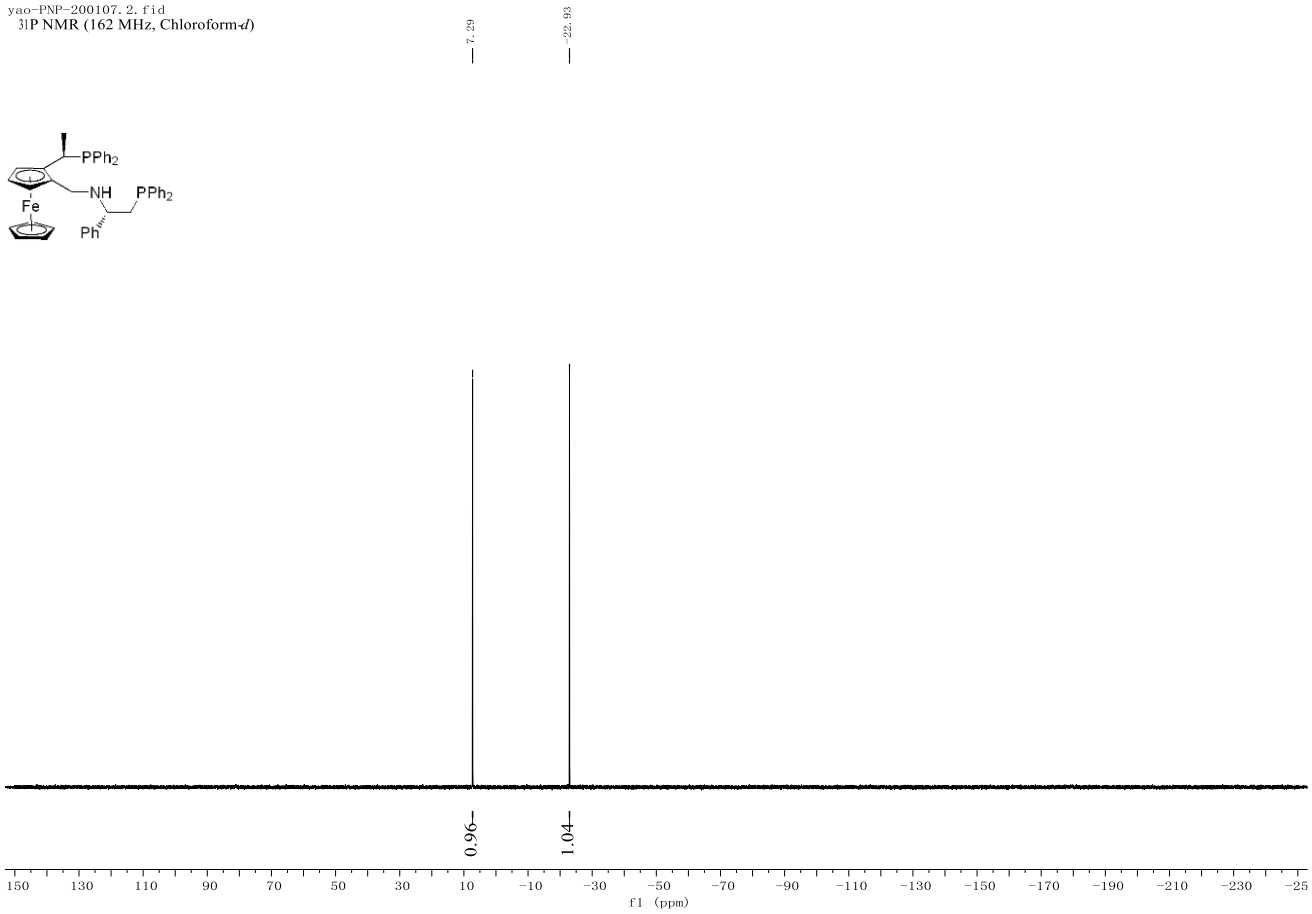

yao-200327-CyPNP. 1. fid

1H NMR (400 MHz, Chloroform-*d*)

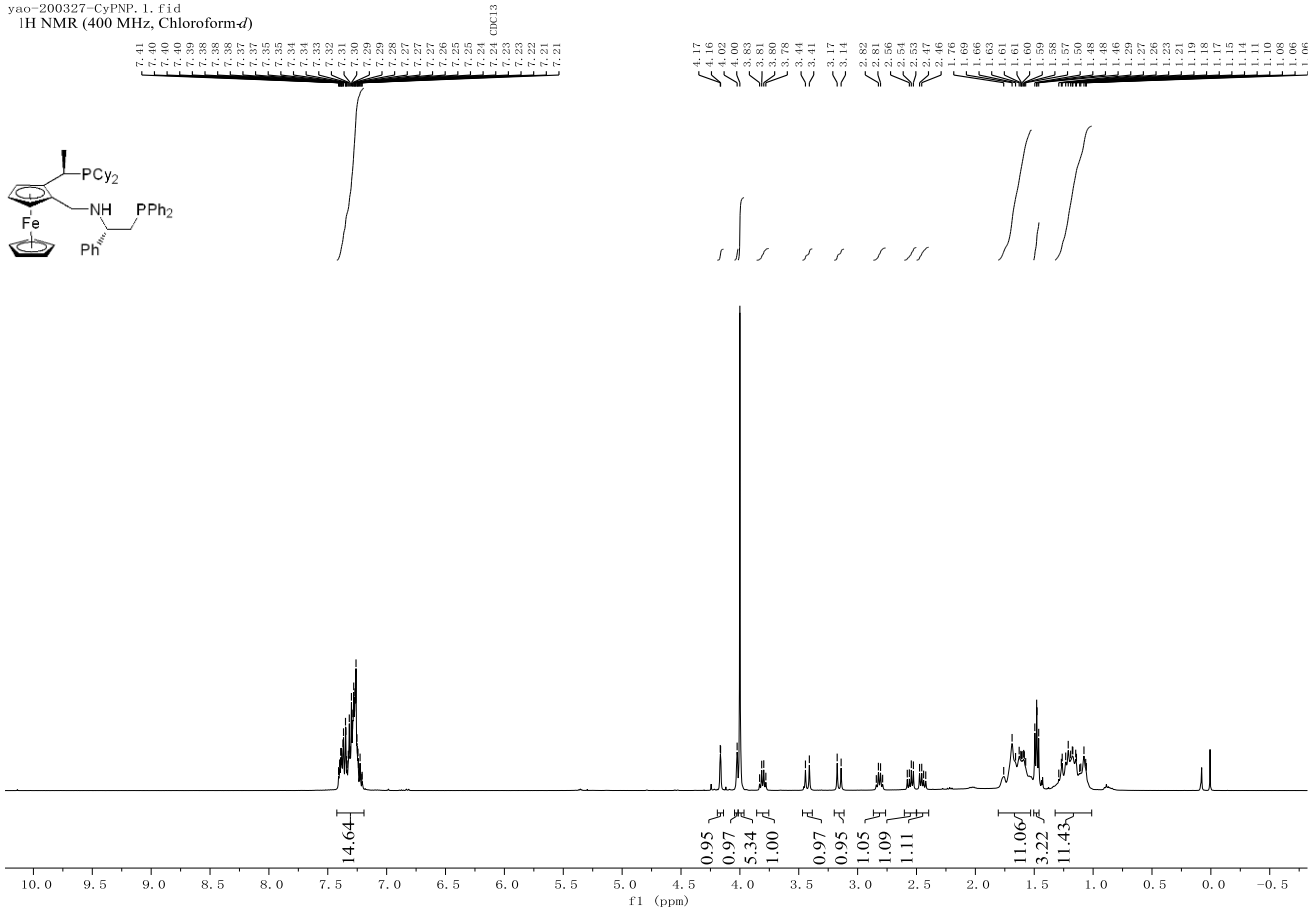

yao-200327-CyPNP. 3. fid

13C NMR (101 MHz, Chloroform-*d*)

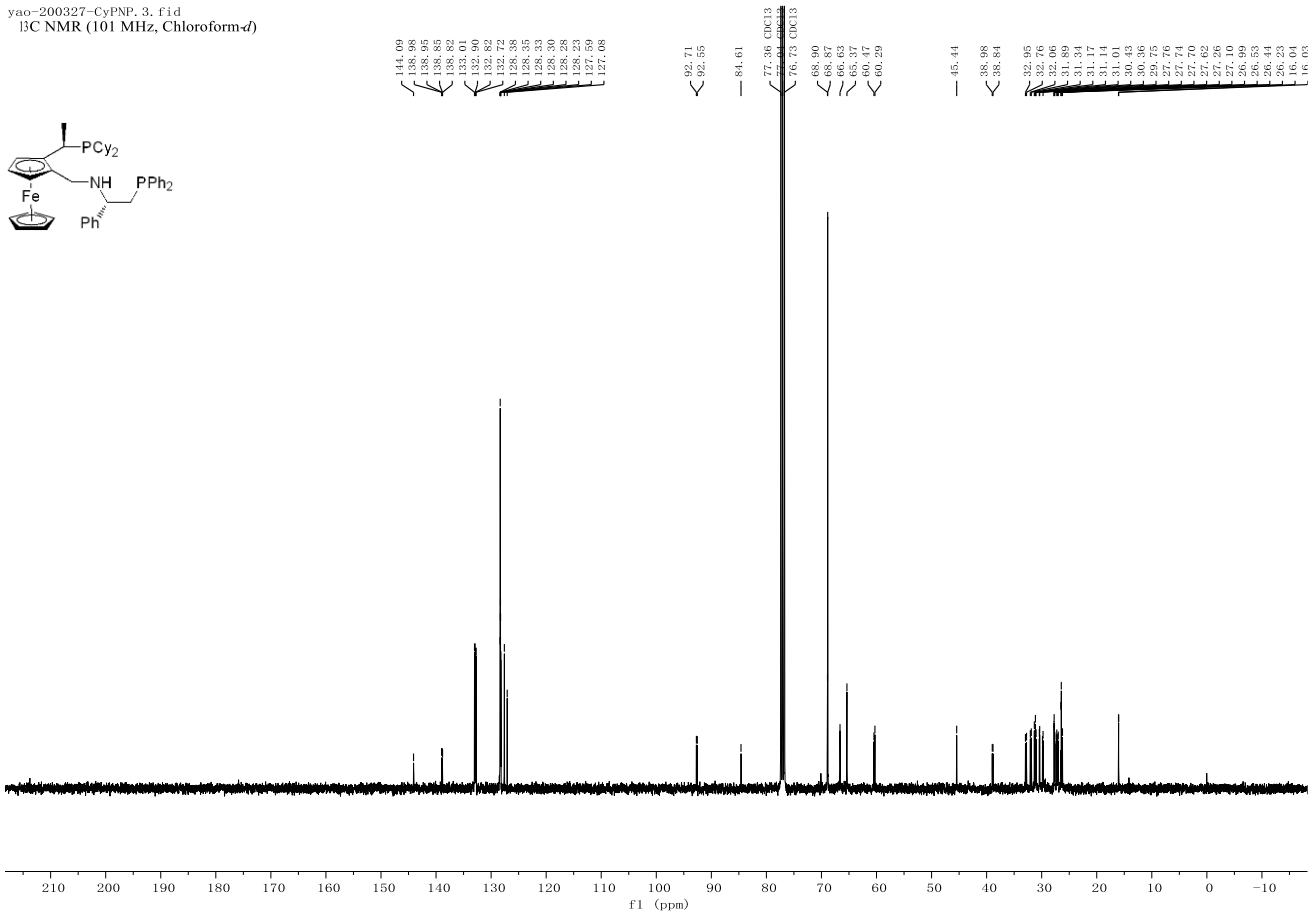

yao-200327-CyPNP.2.fid
31P NMR (162 MHz, Chloroform-*d*)

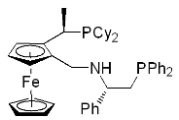

yao-200410-tBuPNP-5.1.fid
1H NMR (400 MHz, Chloroform-*d*)

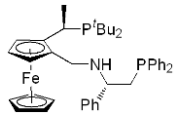

yao-200410-tBuPNP-5.2.fid

^{13}C NMR (101 MHz, Chloroform-*d*)

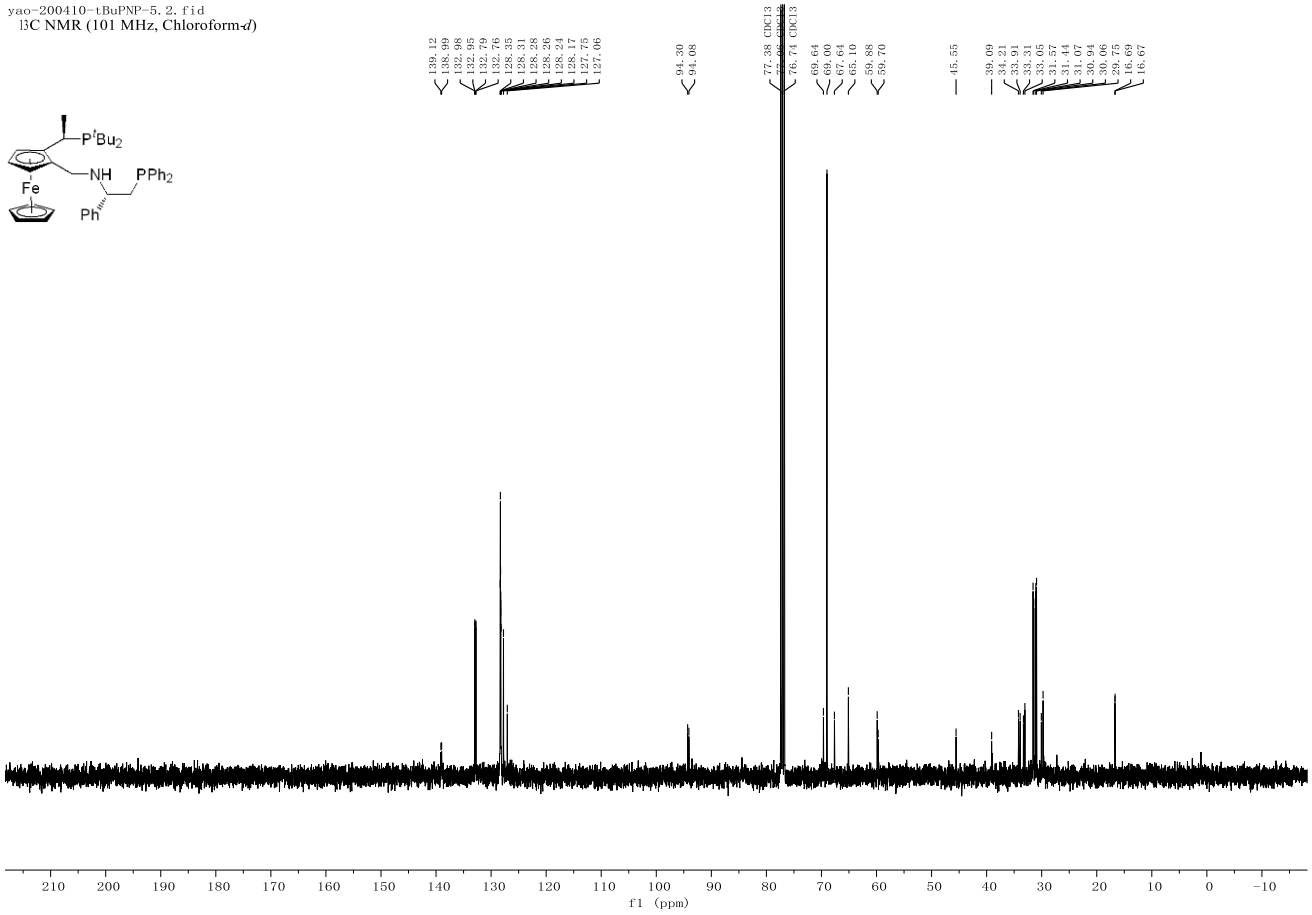

yao-191104-PNPtBu.2.fid

^{31}P NMR (162 MHz, Chloroform-*d*)

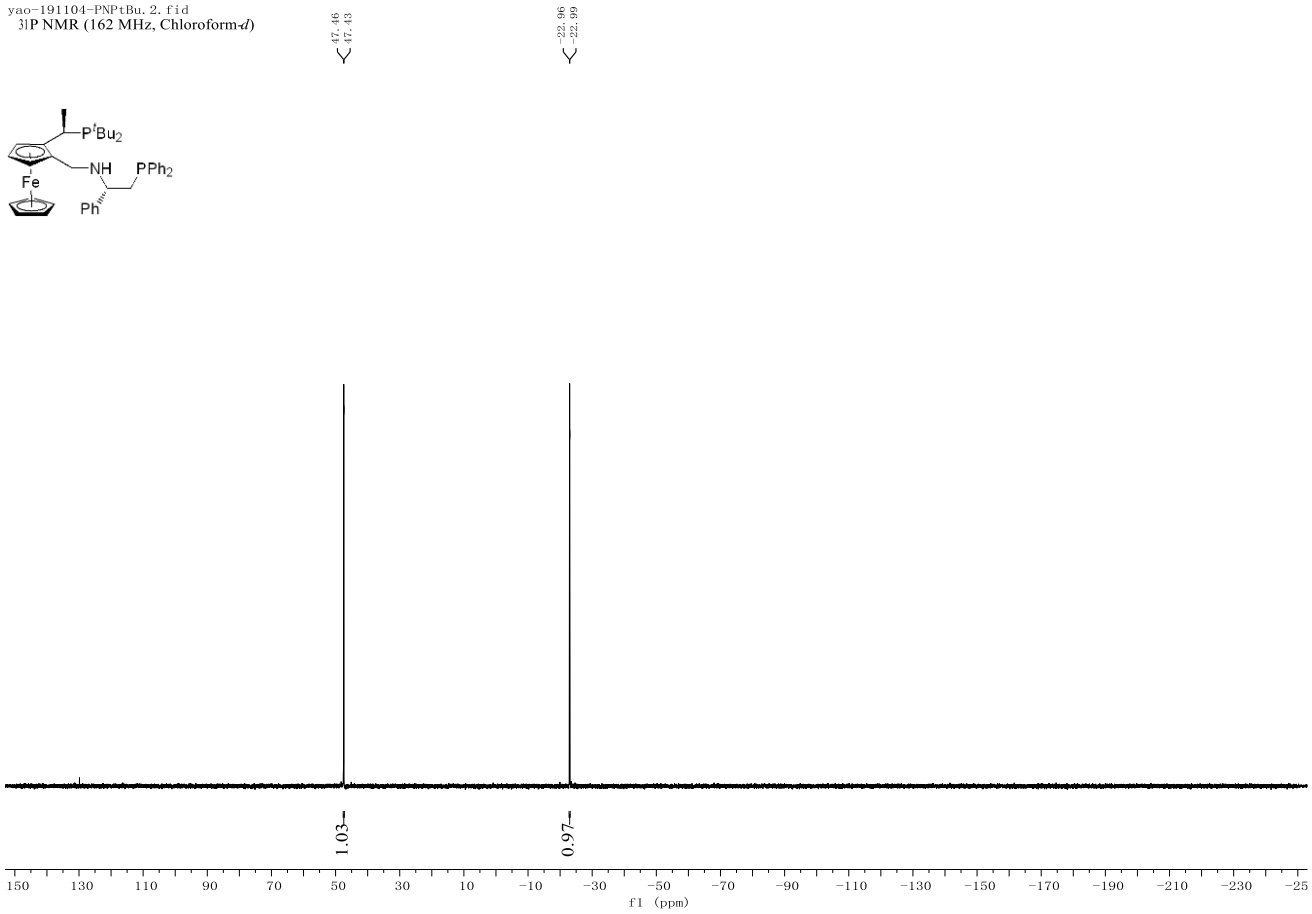

yao-200327-PNPH-3.2.fid

1H NMR (400 MHz, Chloroform-*d*)

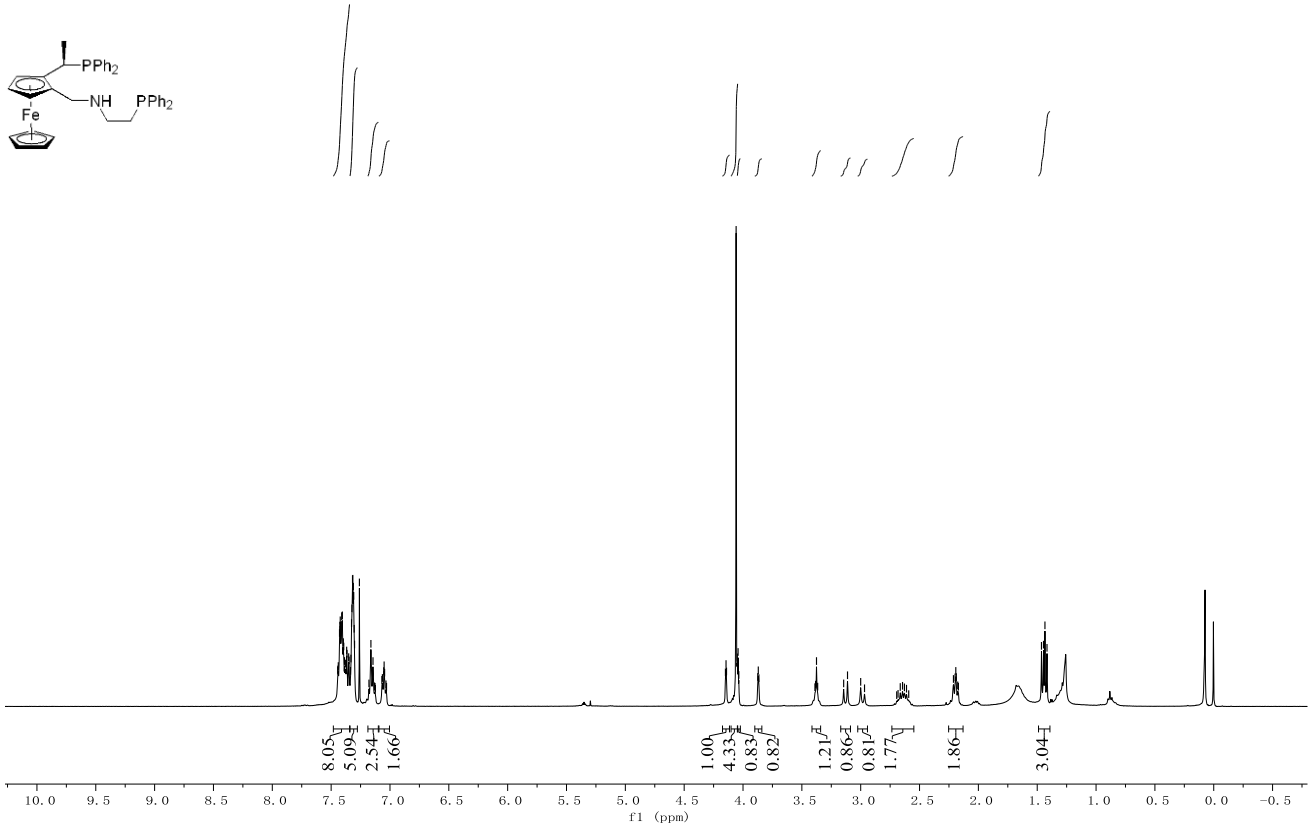

yao-200327-PNPH-3.7.fid

13C NMR (101 MHz, Chloroform-*d*)

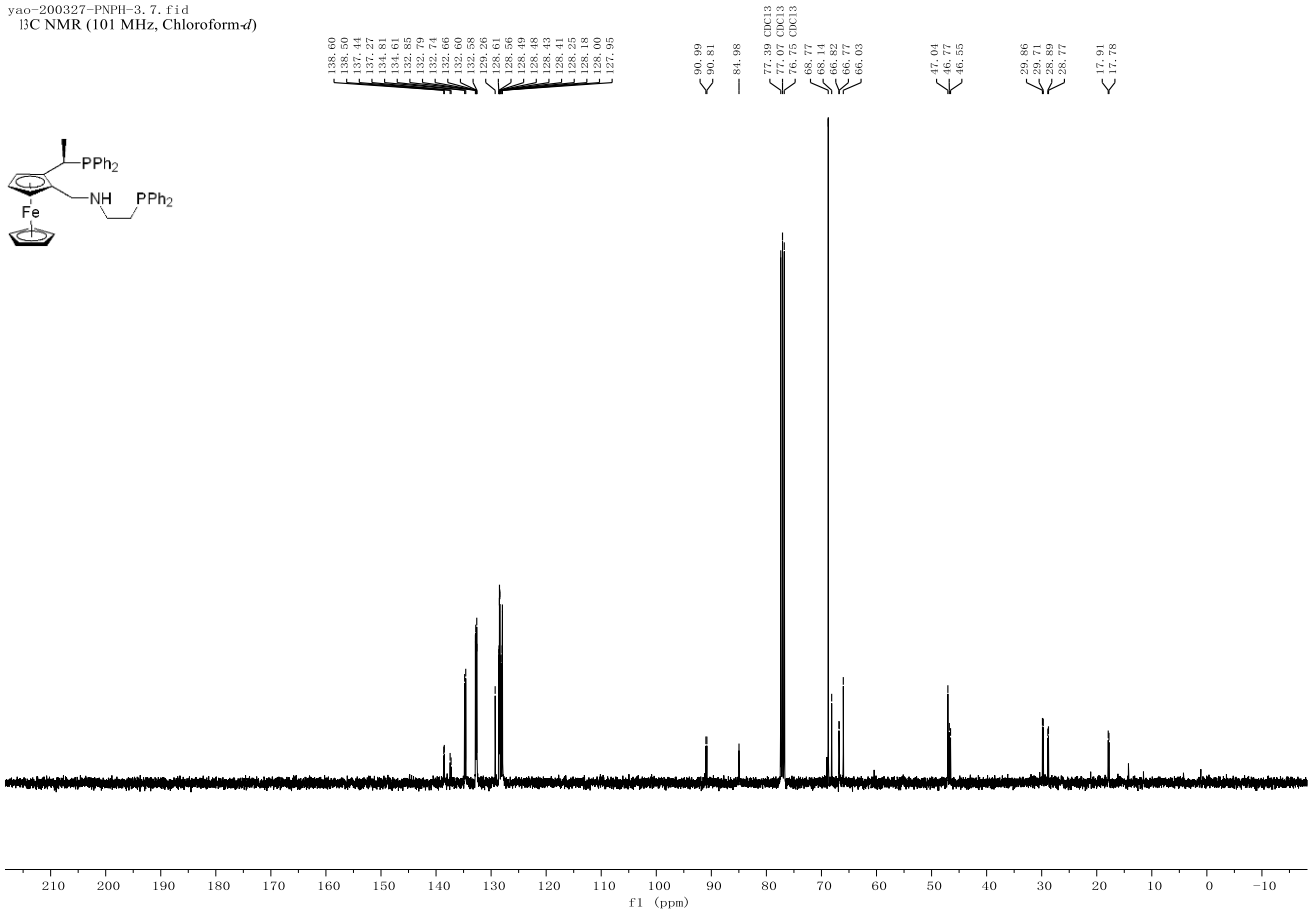

yao-200327-PNPH-2.2.fid

31P NMR (162 MHz, Chloroform-*d*)

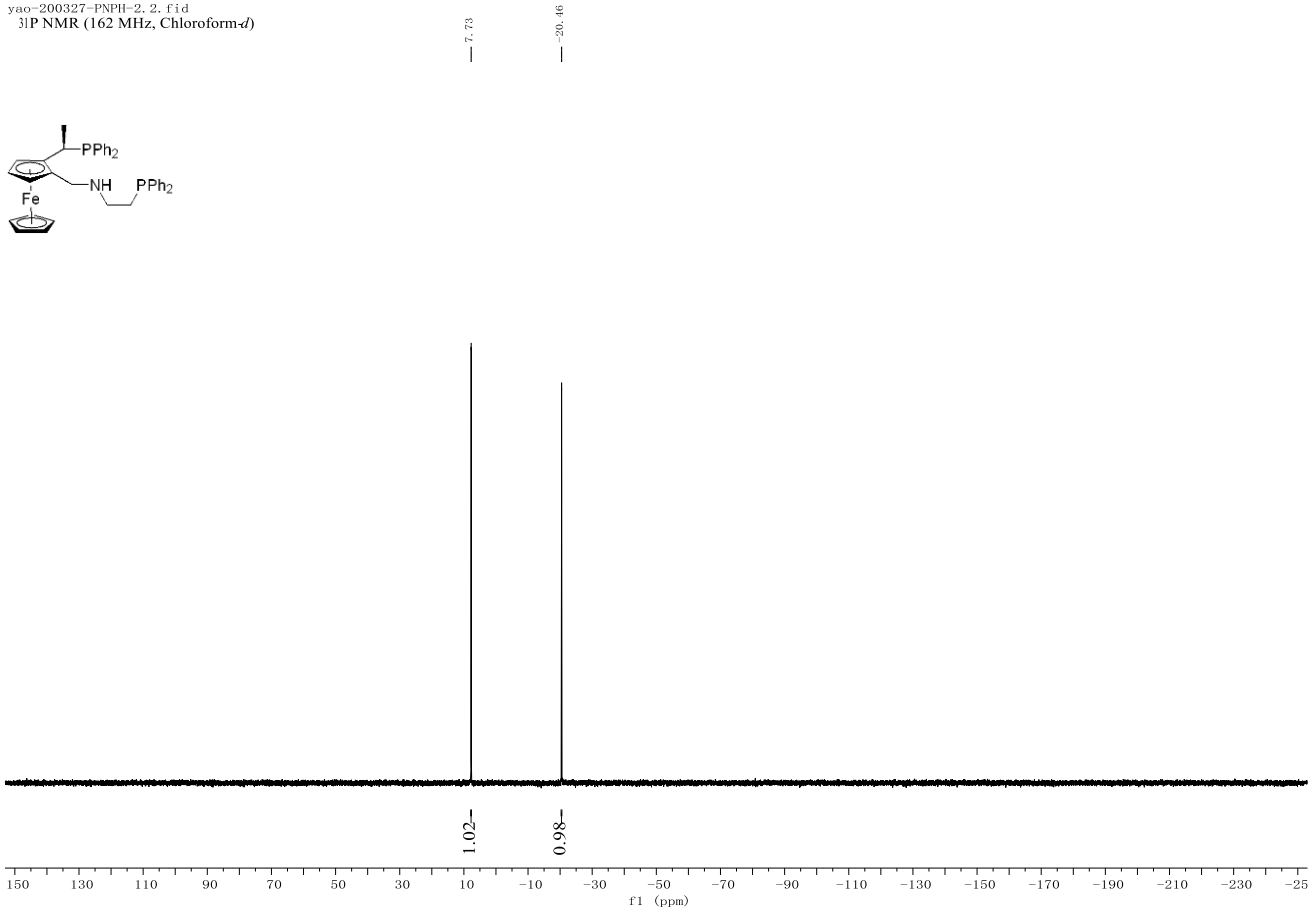

yao-200330-PNPBn.1.fid

1H NMR (400 MHz, Chloroform-*d*)

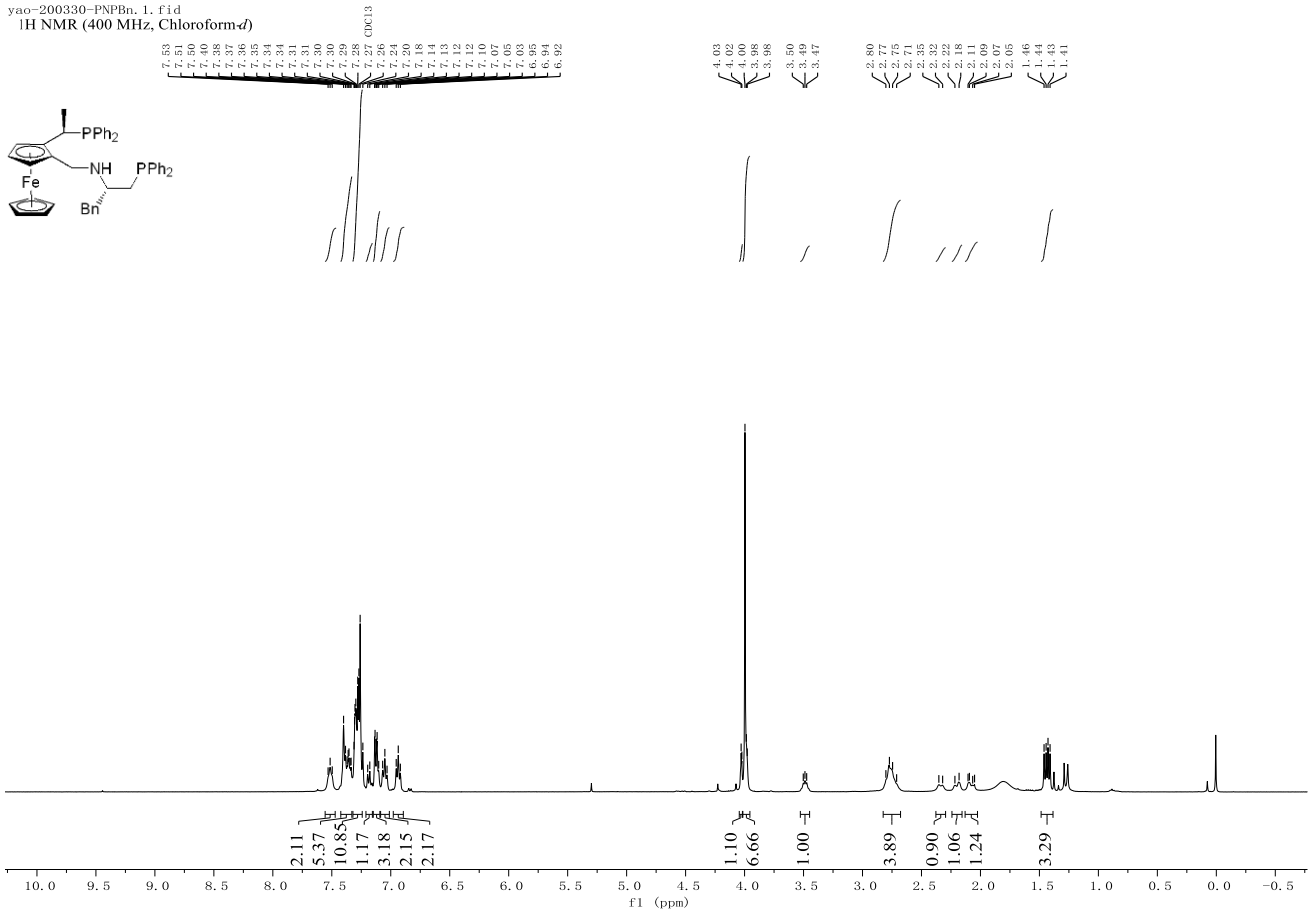

yao-200330-PNPRPh-3.3.fid

^{13}C NMR (101 MHz, Chloroform-*d*)

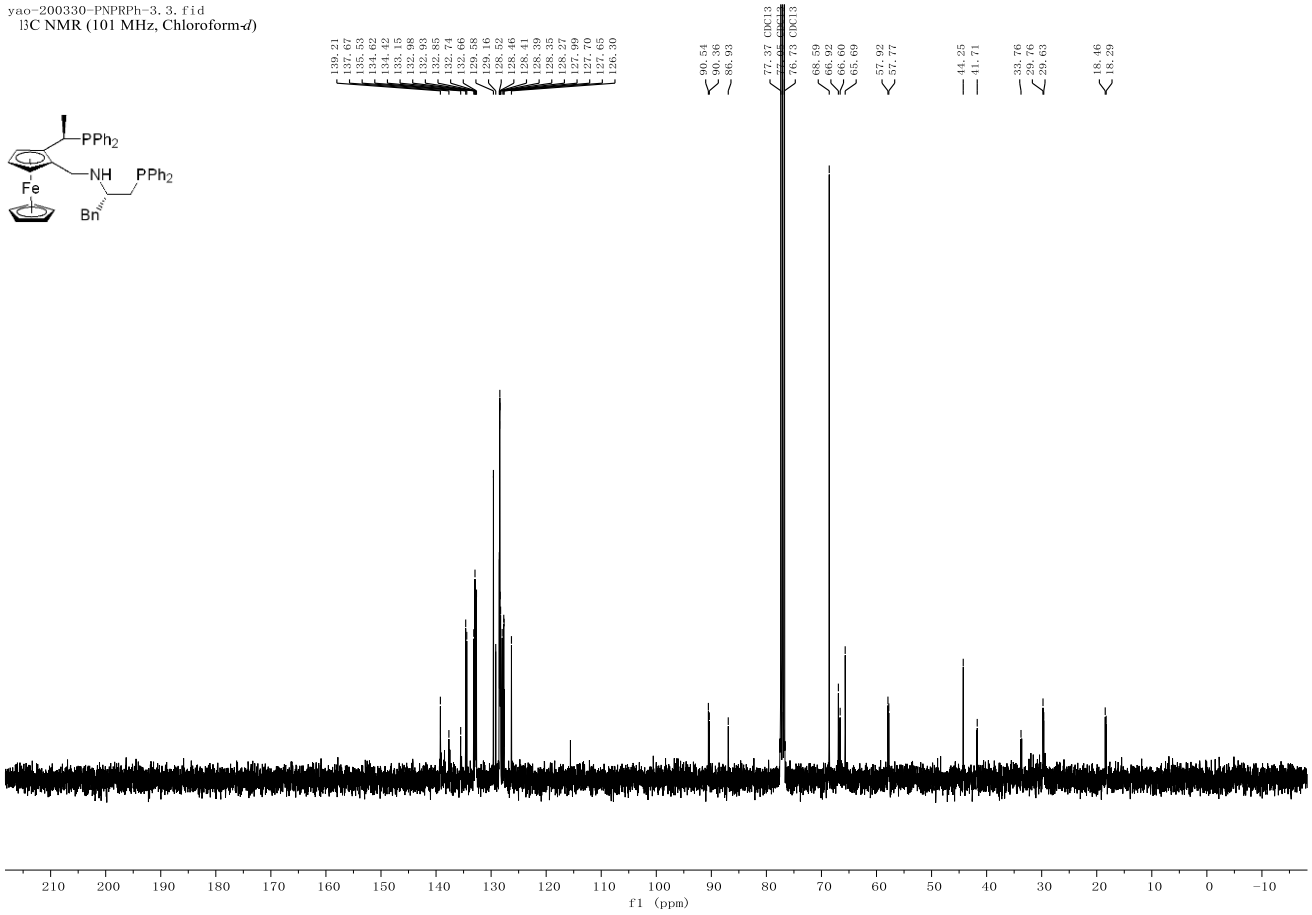

yao-200331-PNPBn.11.fid

^{31}P NMR (243 MHz, Chloroform-*d*)

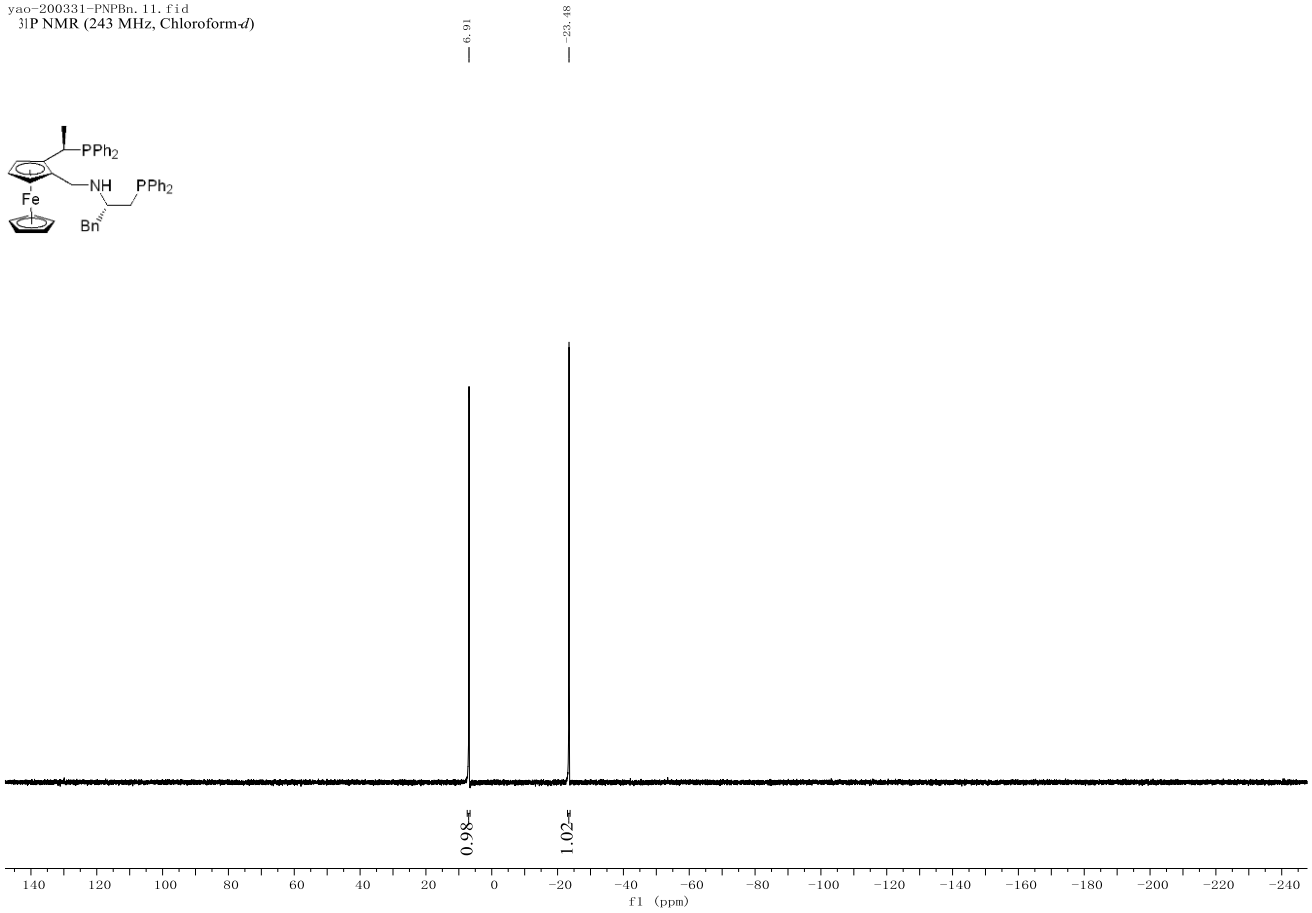

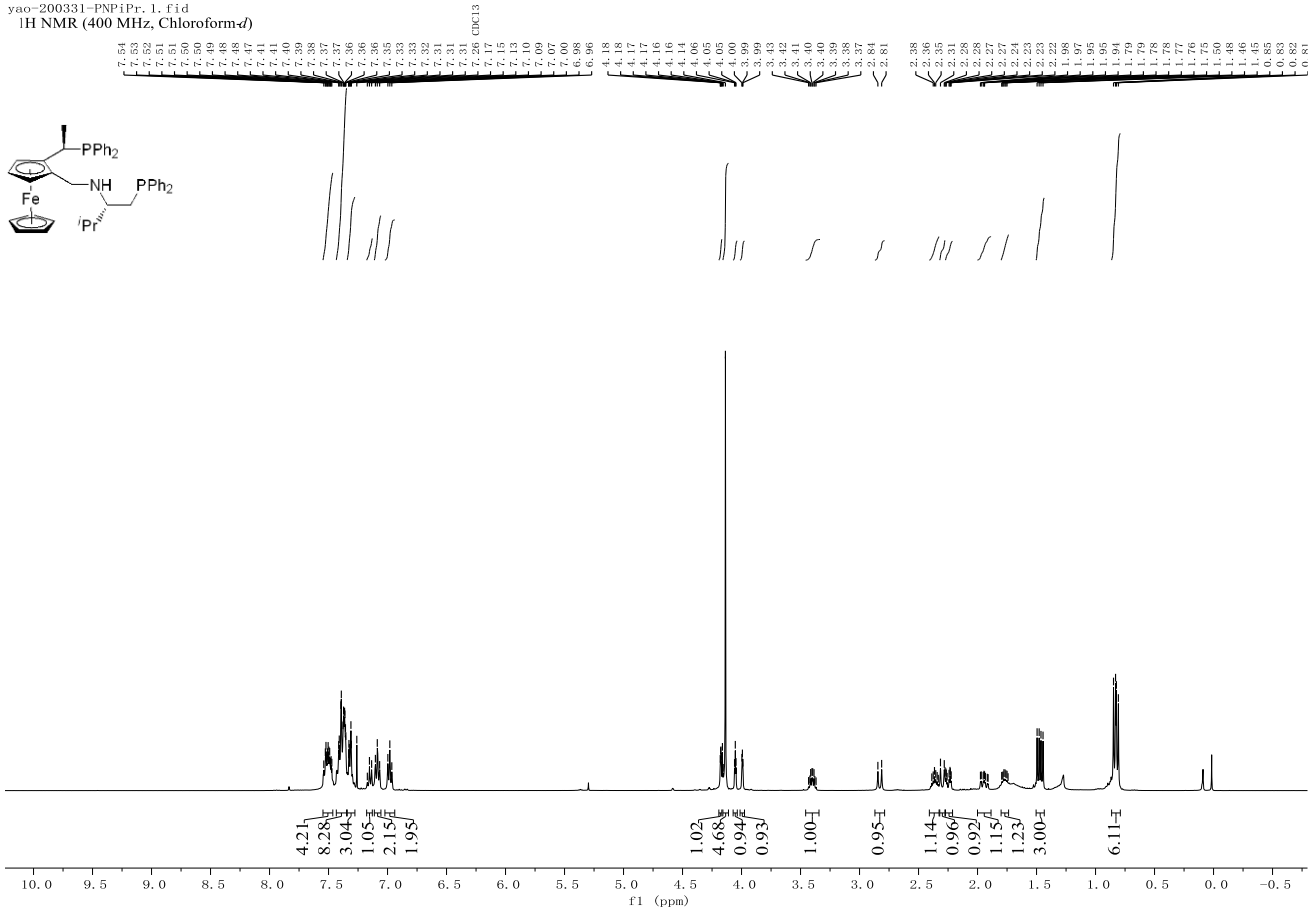
yao-200331-PNPiPr.1.fid
1H NMR (400 MHz, Chloroform-d)
PPh2
NH
PPh2
Fe
iPr
4.21
8.28
3.04
1.05
2.15
1.95
1.02
4.68
0.94
0.93
1.00
0.95
1.14
0.96
0.92
1.15
1.23
3.00
6.11
f1 (ppm)

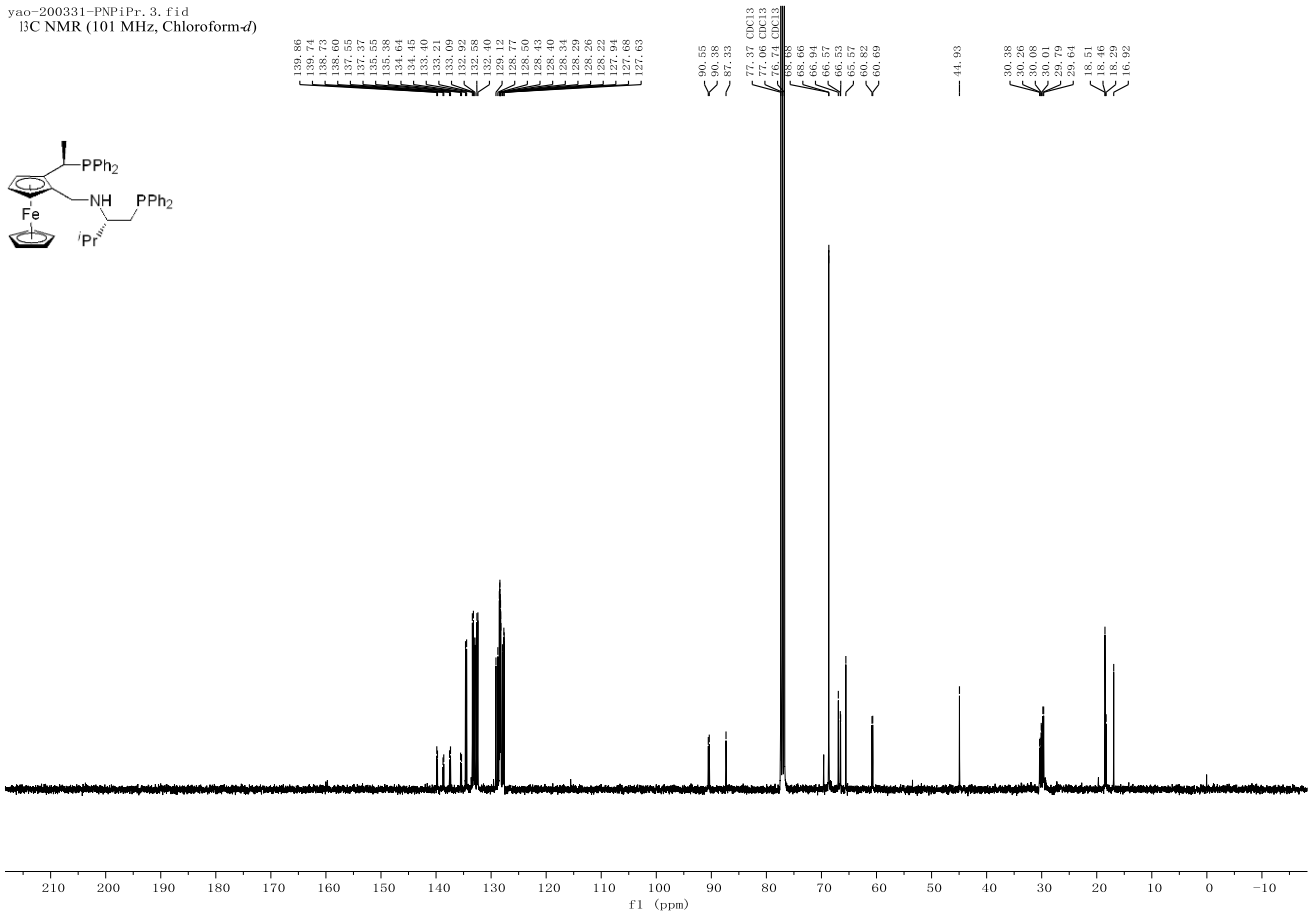
yao-200331-PNPiPr.3.fid
13C NMR (101 MHz, Chloroform-d)
PPh2
NH
PPh2
Fe
iPr
f1 (ppm)

yao-200331-PNPiPr-2.2.fid
31P NMR (162 MHz, Chloroform-*d*)

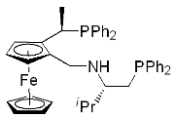

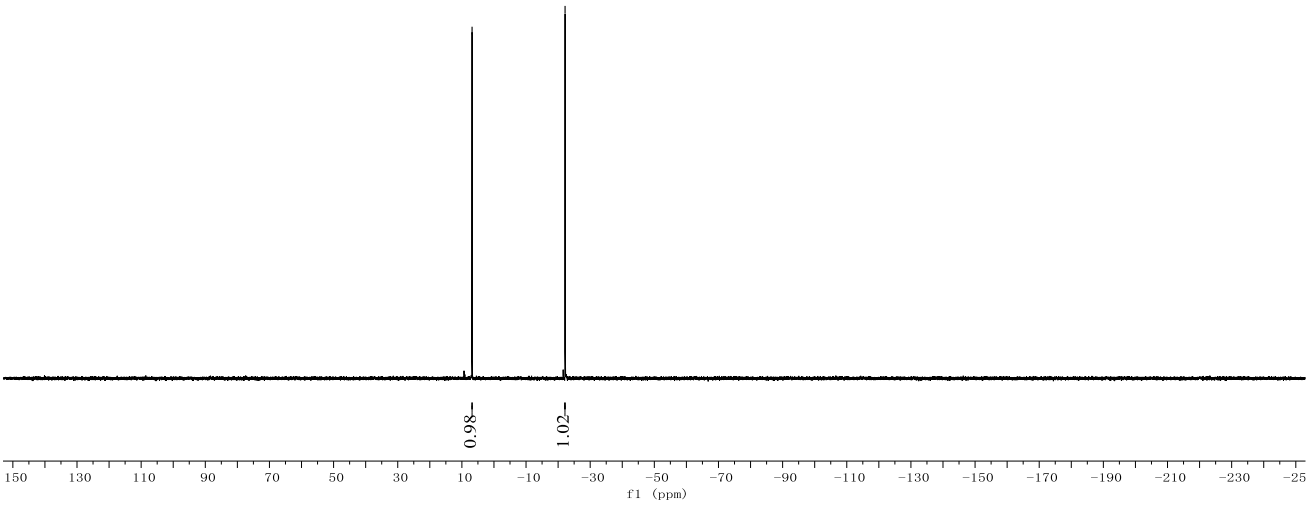

yao-200330-PNPRPh-3.10.fid
1H NMR (600 MHz, Chloroform-*d*)

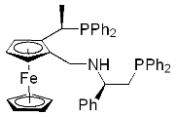

yao-200330-PNPRPh-3.12.fid
13C NMR (151 MHz, Chloroform-*d*)

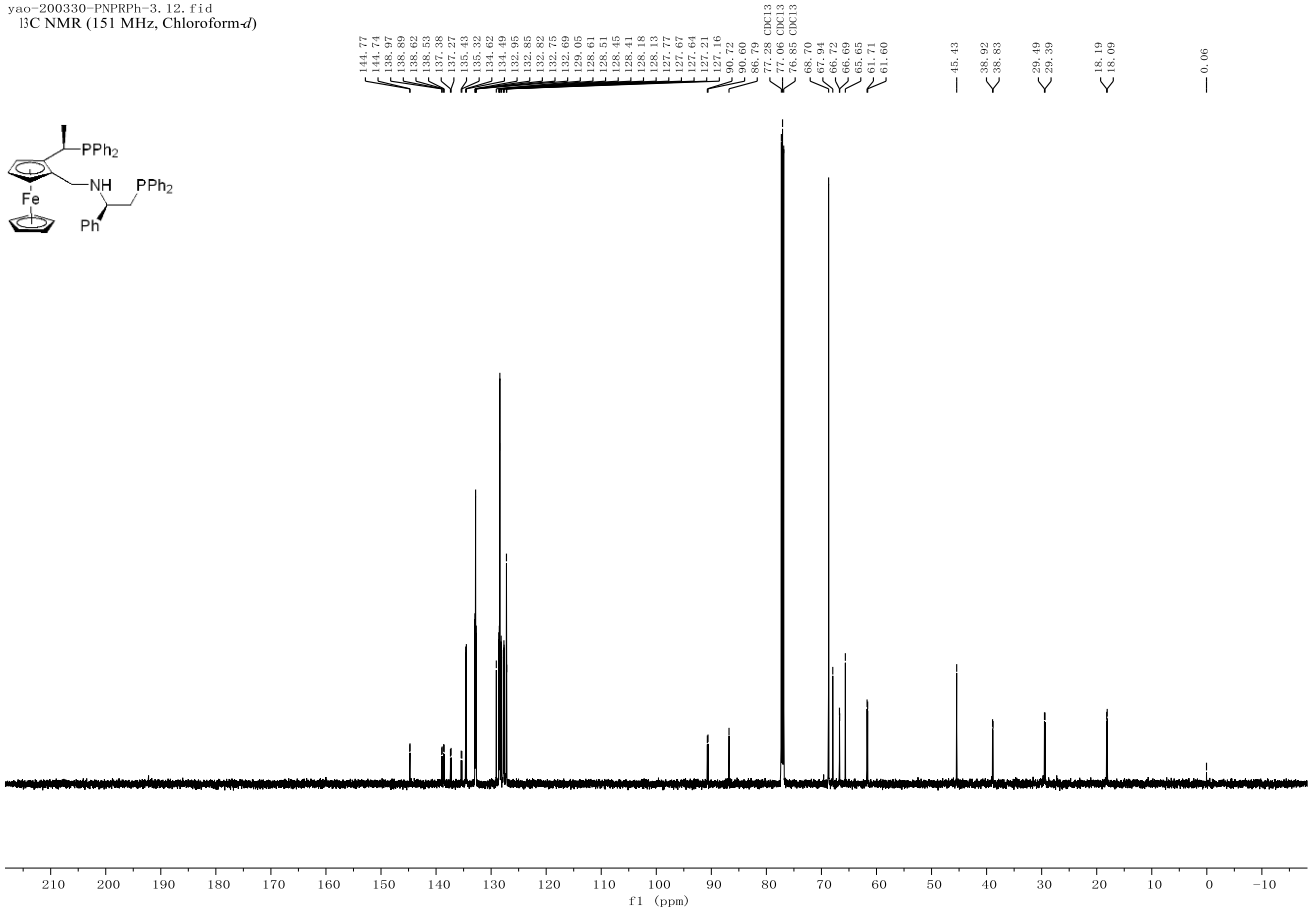

yao-200330-PNPRPh-2.11.fid
31P NMR (243 MHz, Chloroform-*d*)

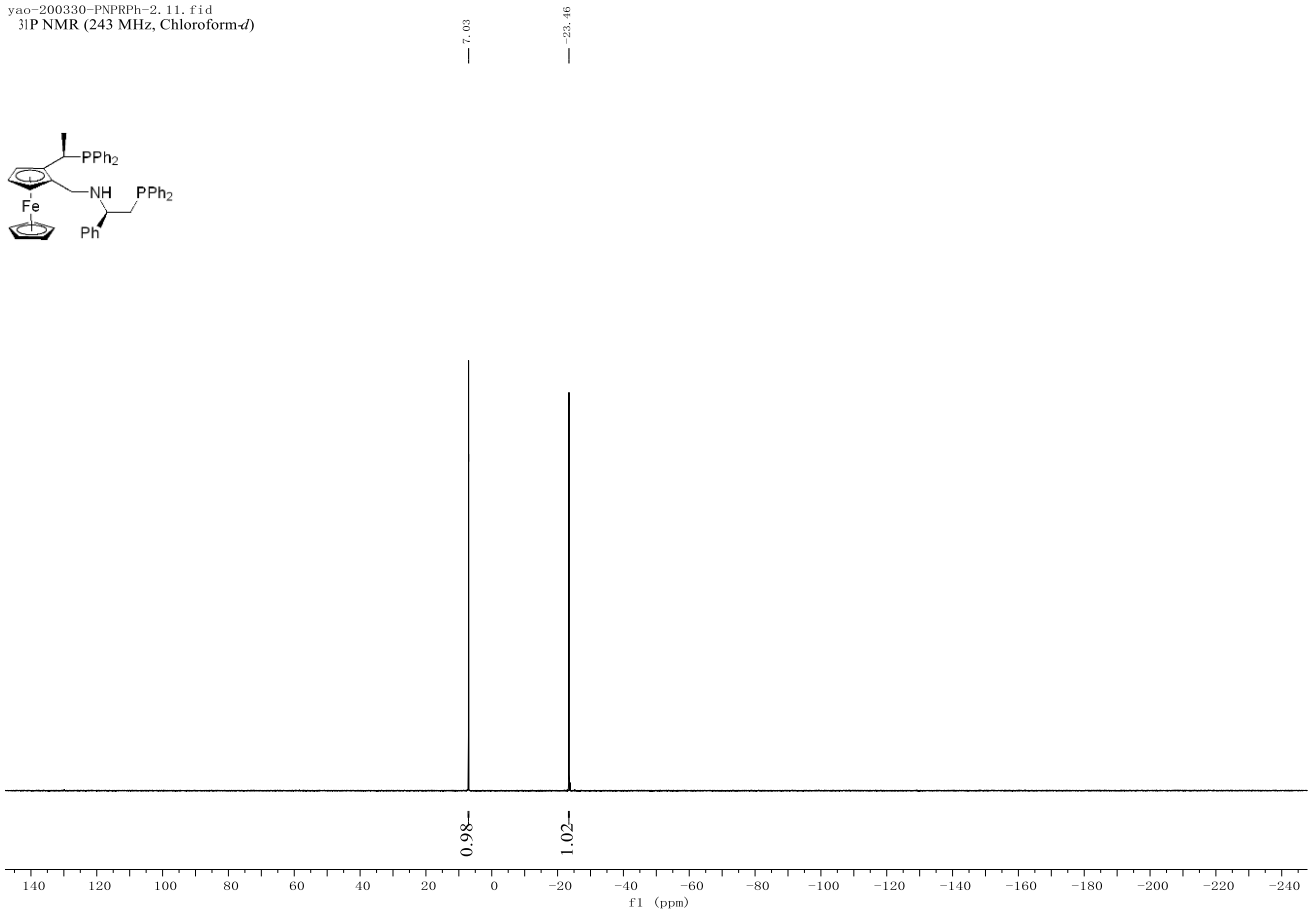

(*R*)-1-Phenylethanol (8a).

^{1}H NMR (600 MHz, Chloroform-*d*)

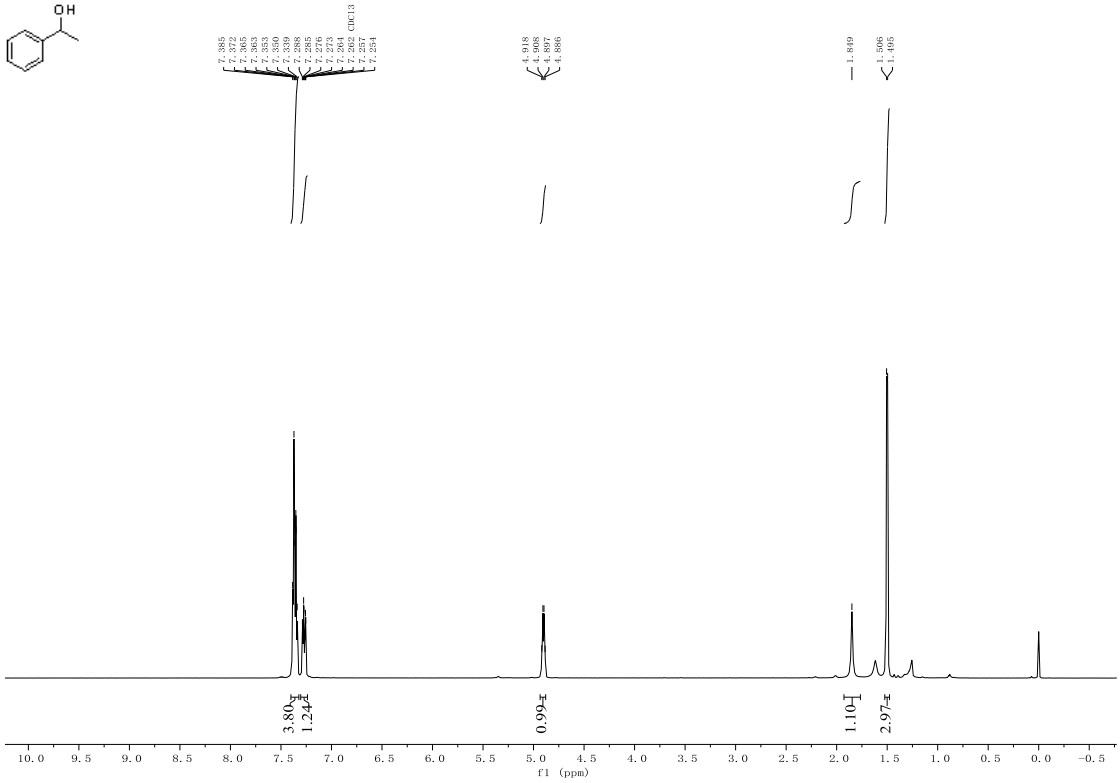

^{13}C NMR (151 MHz, Chloroform-*d*)

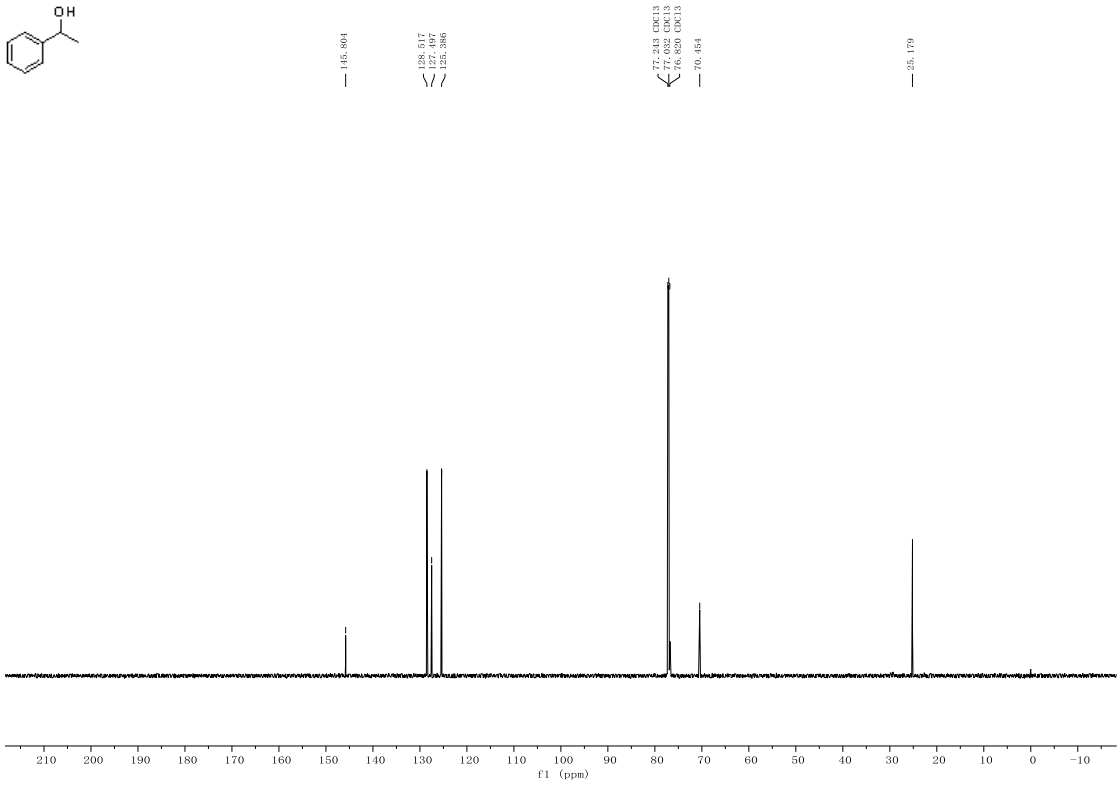

(*R*)-1-(2-Fluorophenyl)ethanol (8b).

^{1}H NMR (400 MHz, Chloroform-*d*)

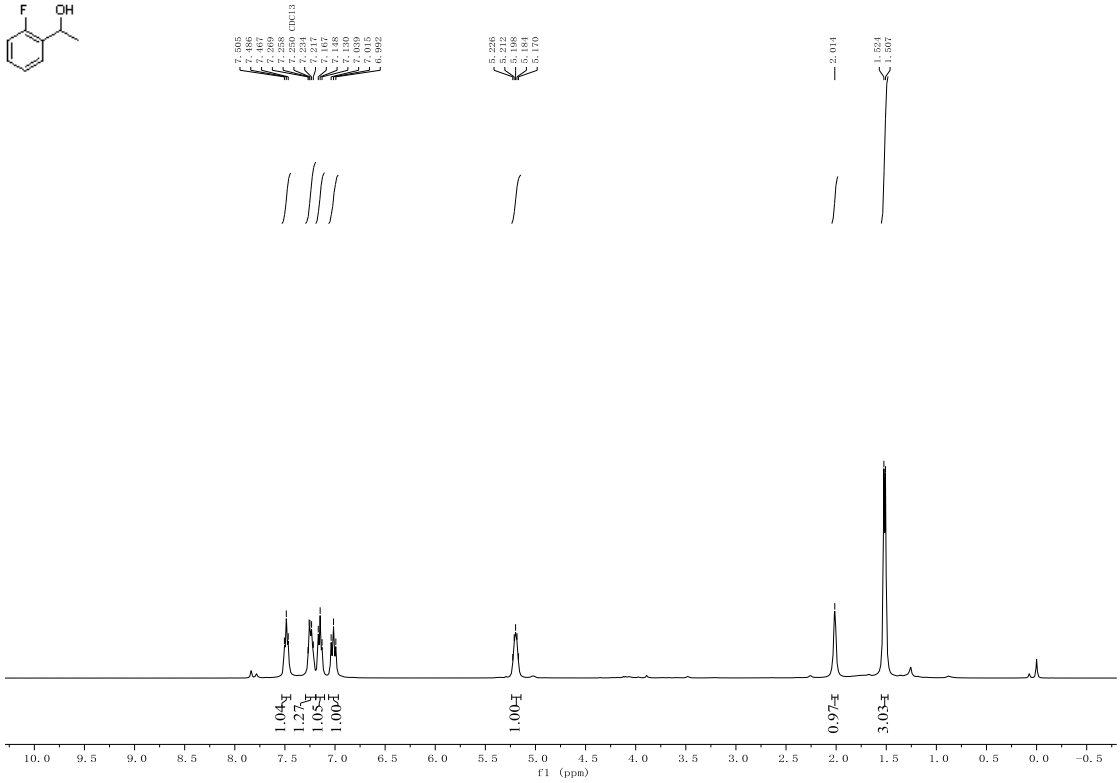

^{13}C NMR (101 MHz, Chloroform-*d*)

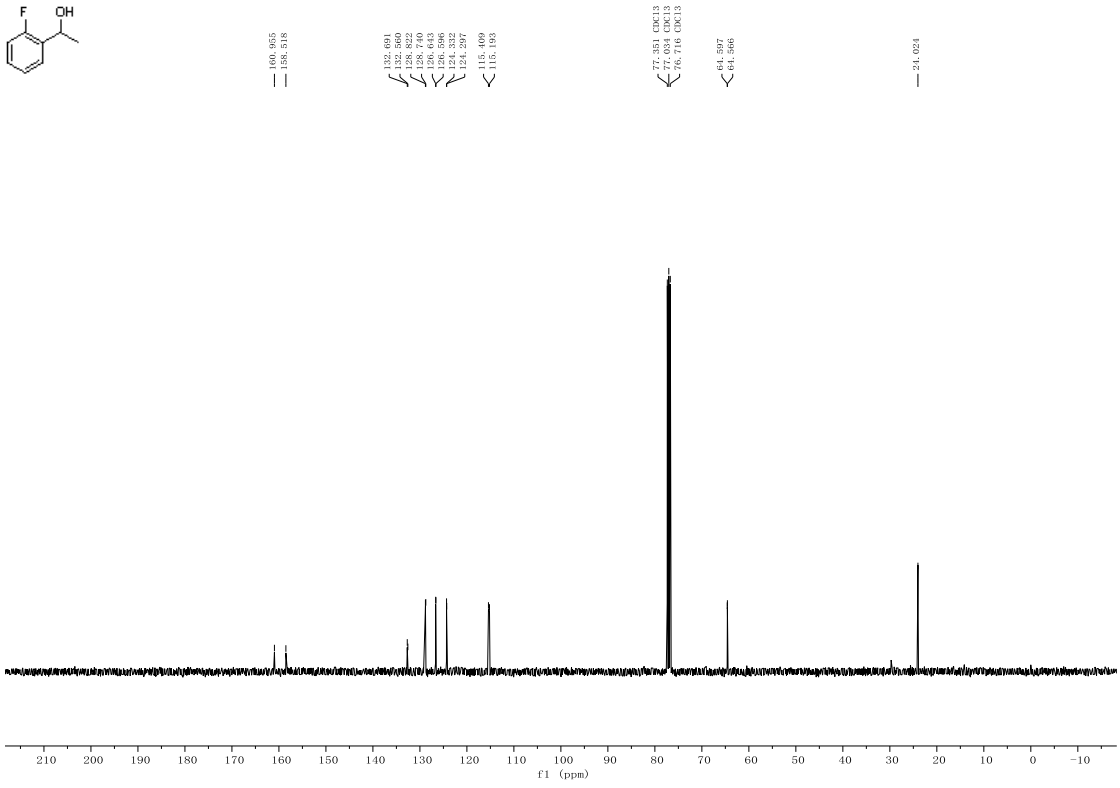

^{19}F NMR (565 MHz, Chloroform-*d*)

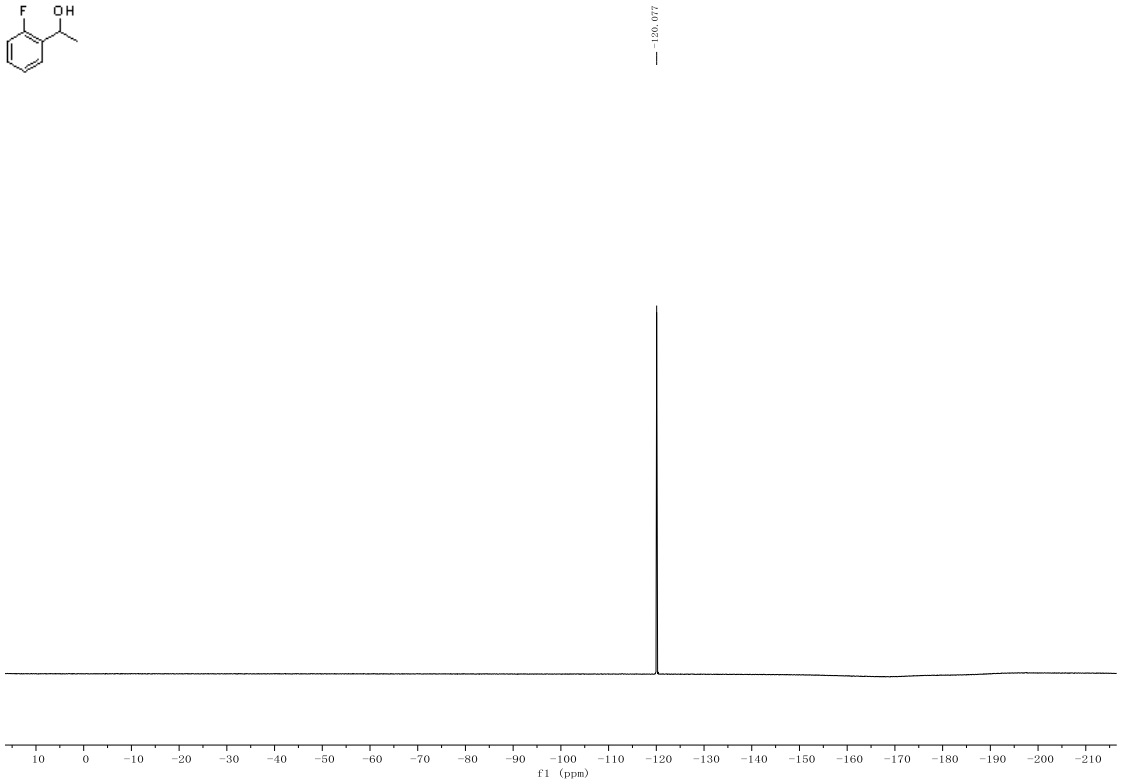

(*R*)-1-(*o*-Tolyl)ethanol (8c).

^{1}H NMR (400 MHz, Chloroform-*d*)

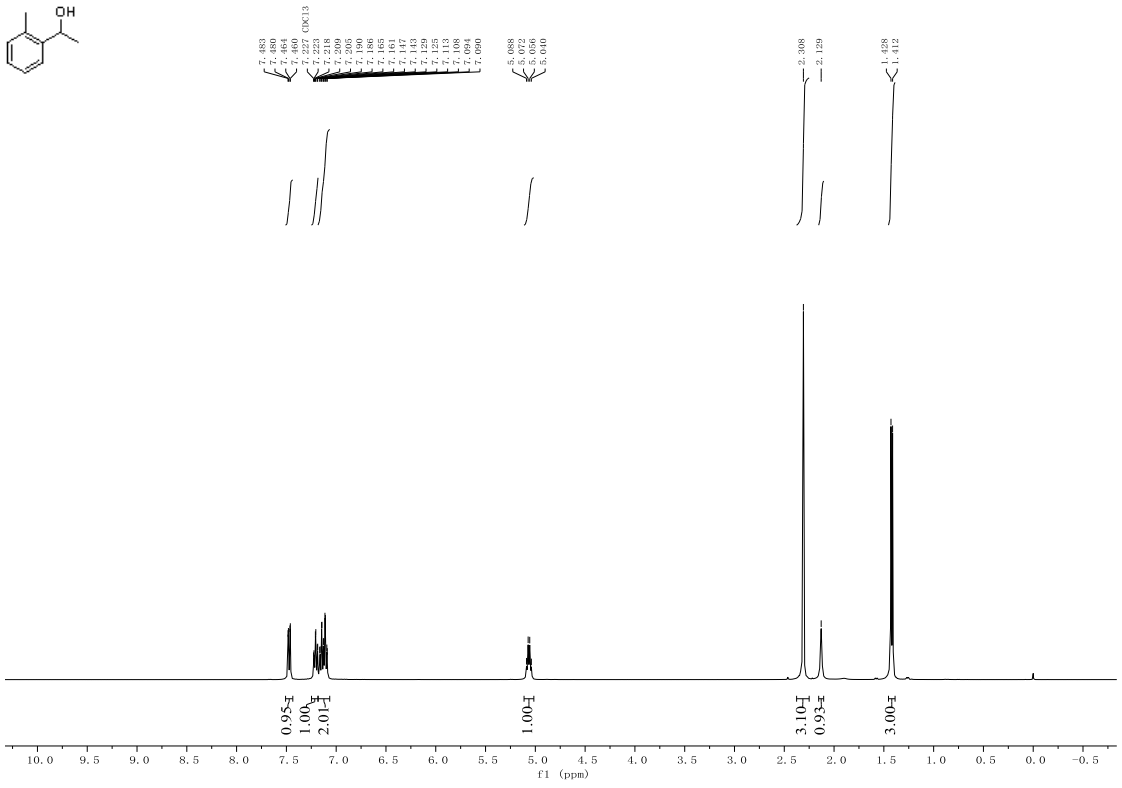

^{13}C NMR (101 MHz, Chloroform-*d*)

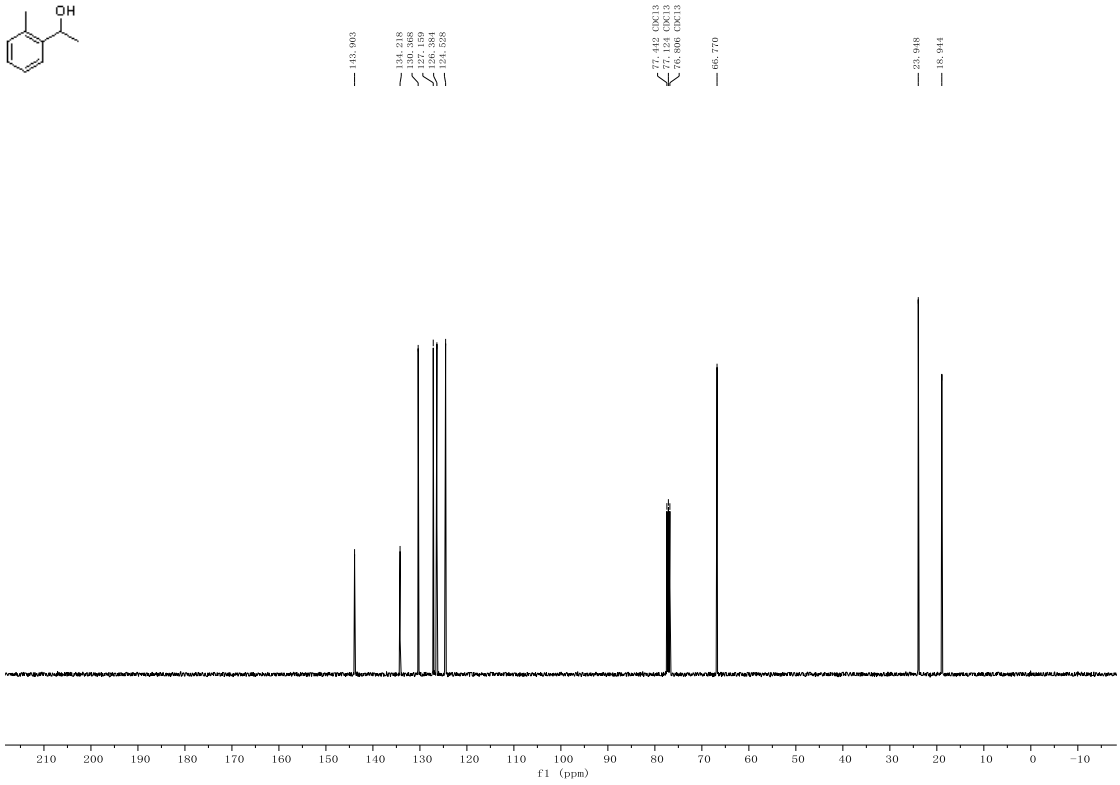

(*R*)-1-(2-Methoxyphenyl)ethanol (8d).

^{1}H NMR (400 MHz, Chloroform-*d*)

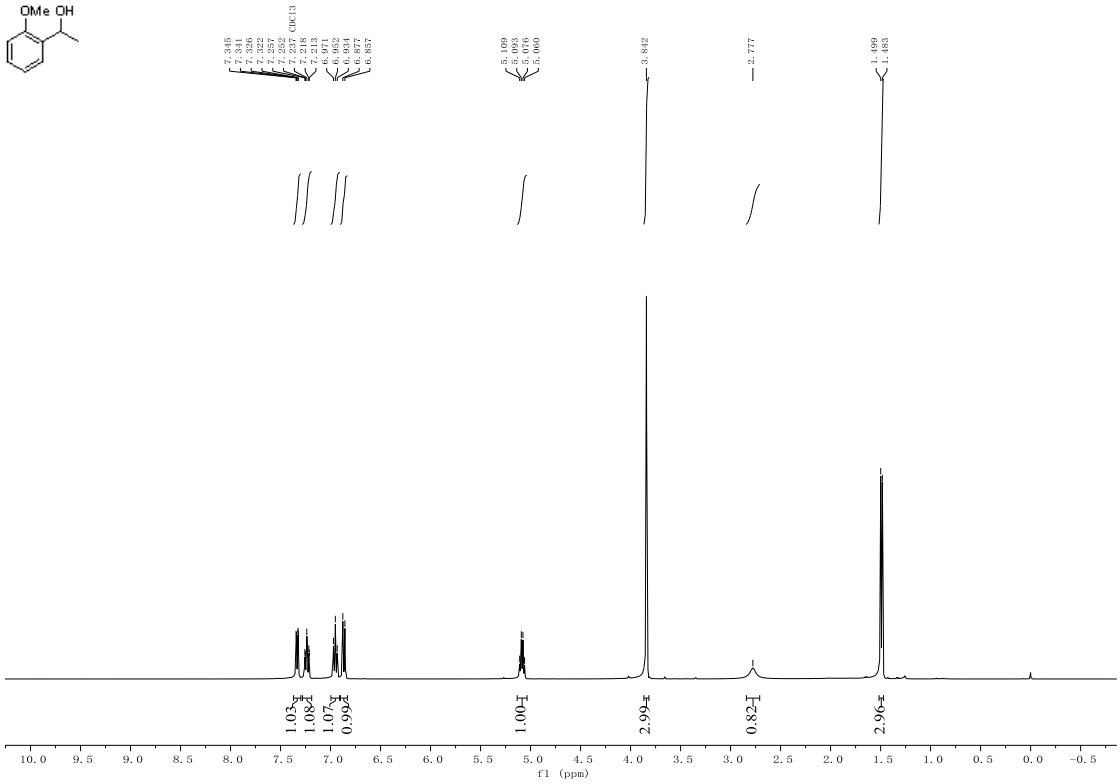

^{13}C NMR (101 MHz, Chloroform-*d*)

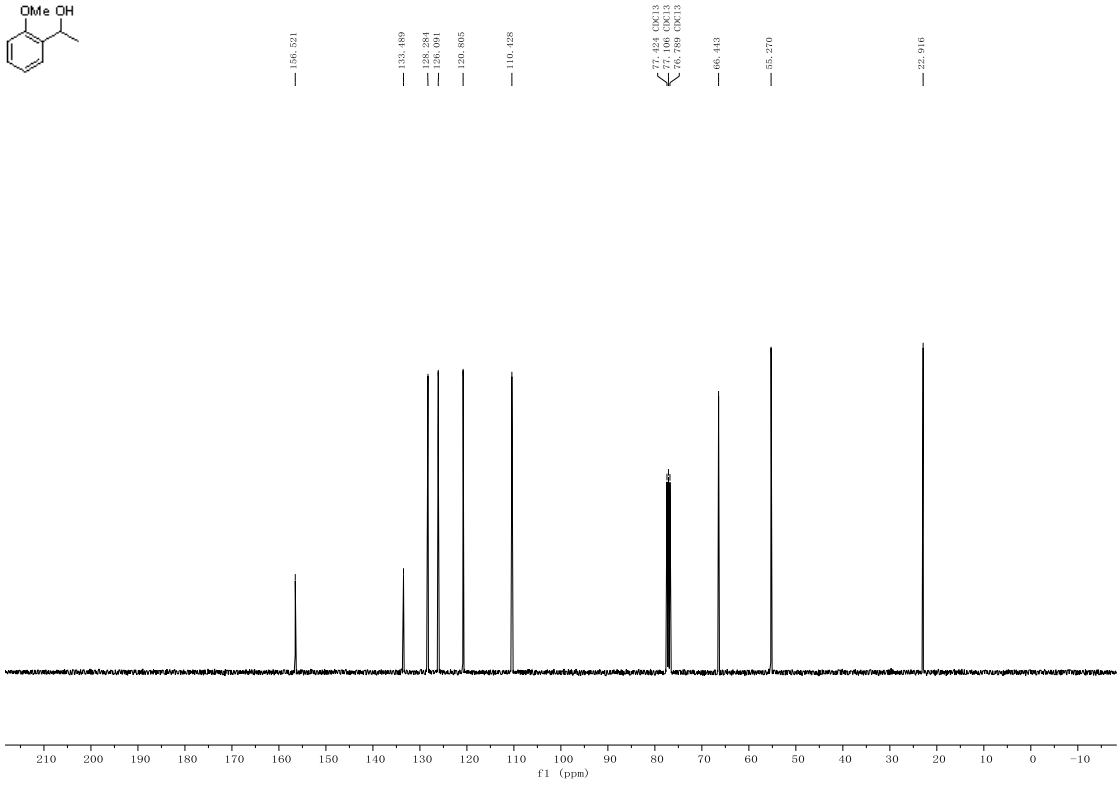

(*R*)-1-(3-Fluorophenyl)ethanol (8e).

^{1}H NMR (400 MHz, Chloroform-*d*)

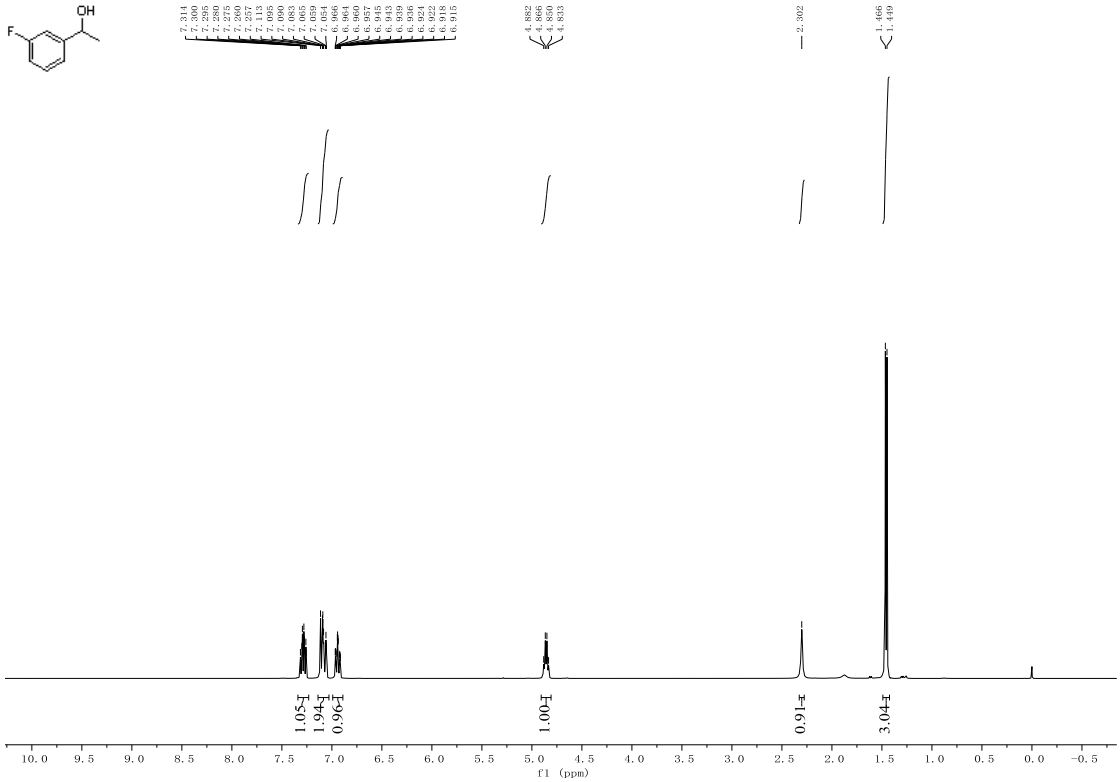

^{13}C NMR (101 MHz, Chloroform-*d*)

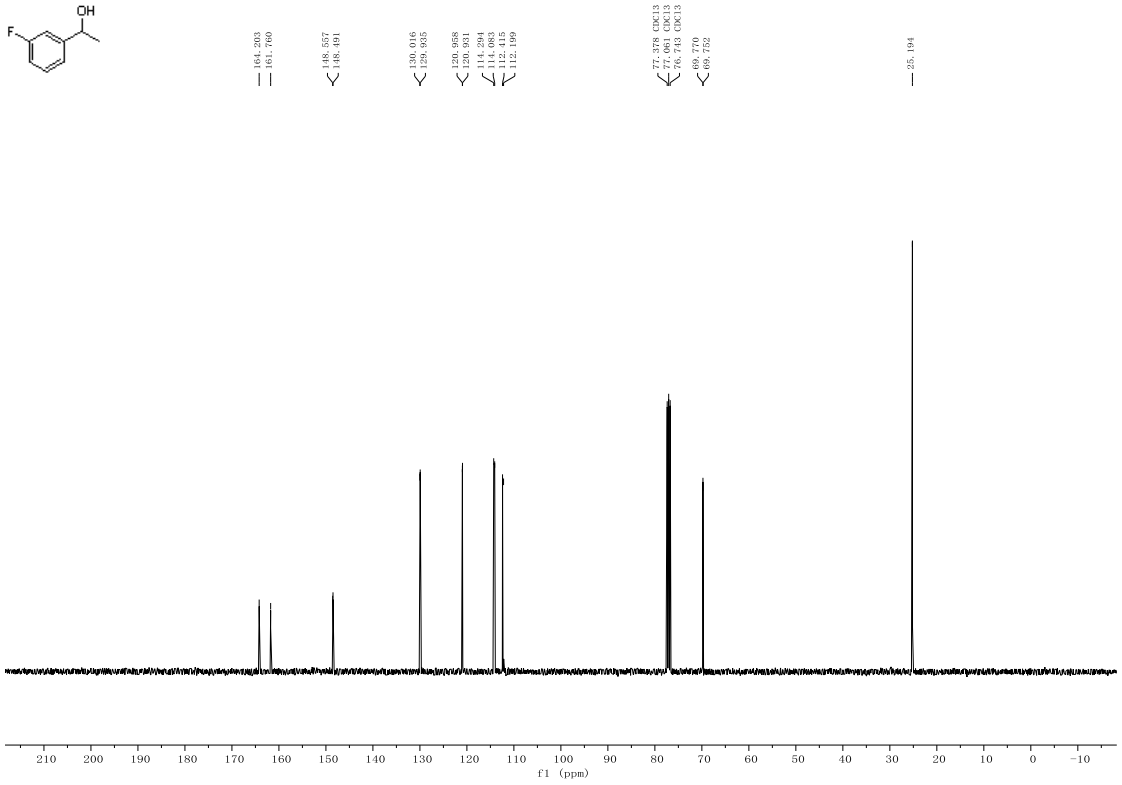

^{19}F NMR (376 MHz, Chloroform-*d*)

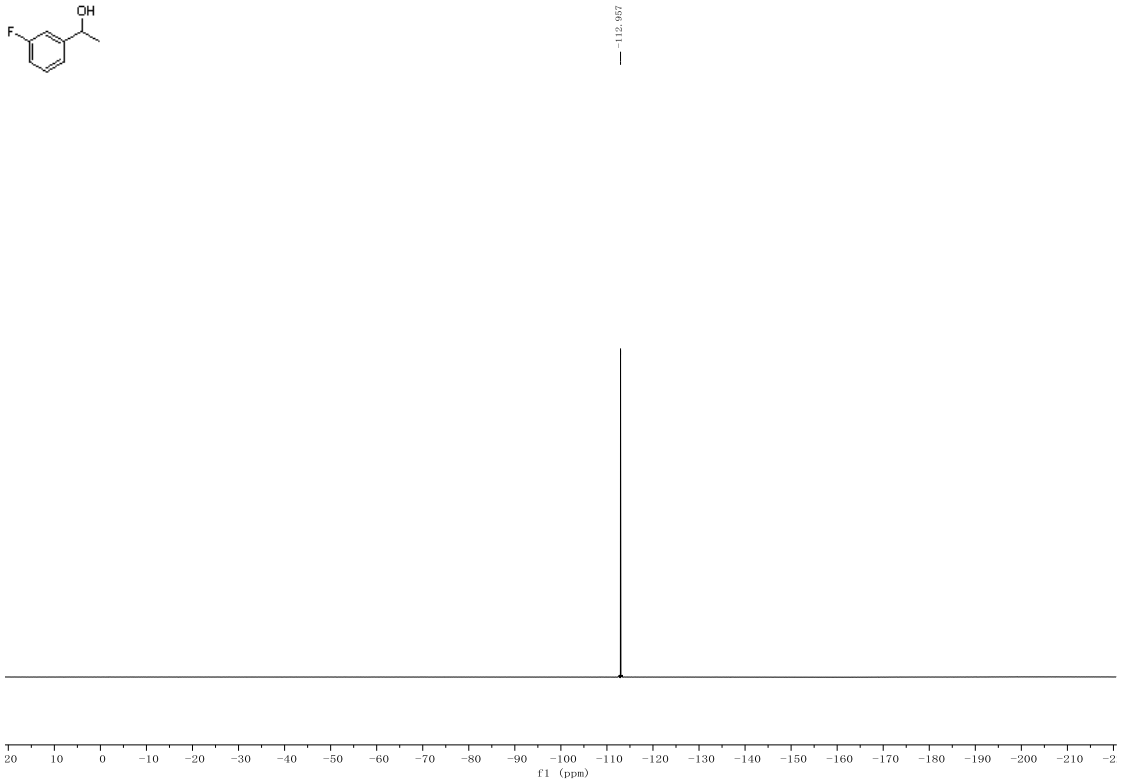

(*R*)-1-(*m*-Tolyl)ethanol (8f).

^{1}H NMR (400 MHz, Chloroform-*d*)

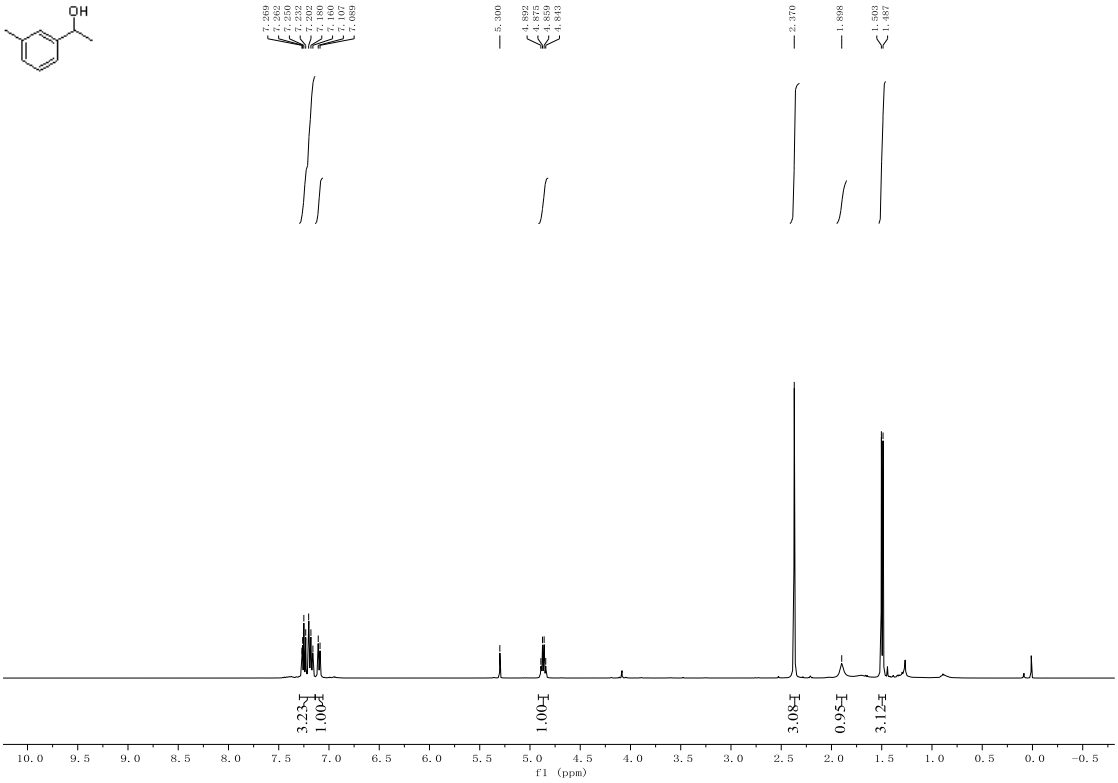

^{13}C NMR (101 MHz, Chloroform-*d*)

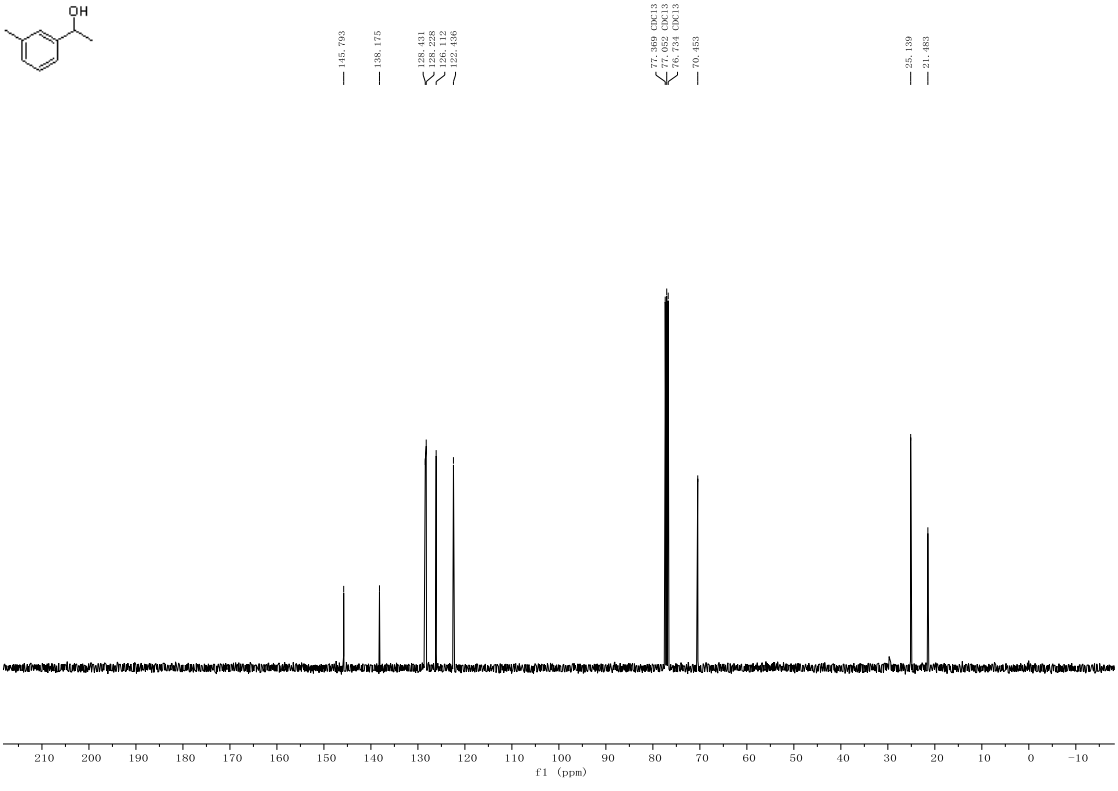

(*R*)-1-(3-Methoxyphenyl)ethanol (8g).

^{1}H NMR (400 MHz, Chloroform-*d*)

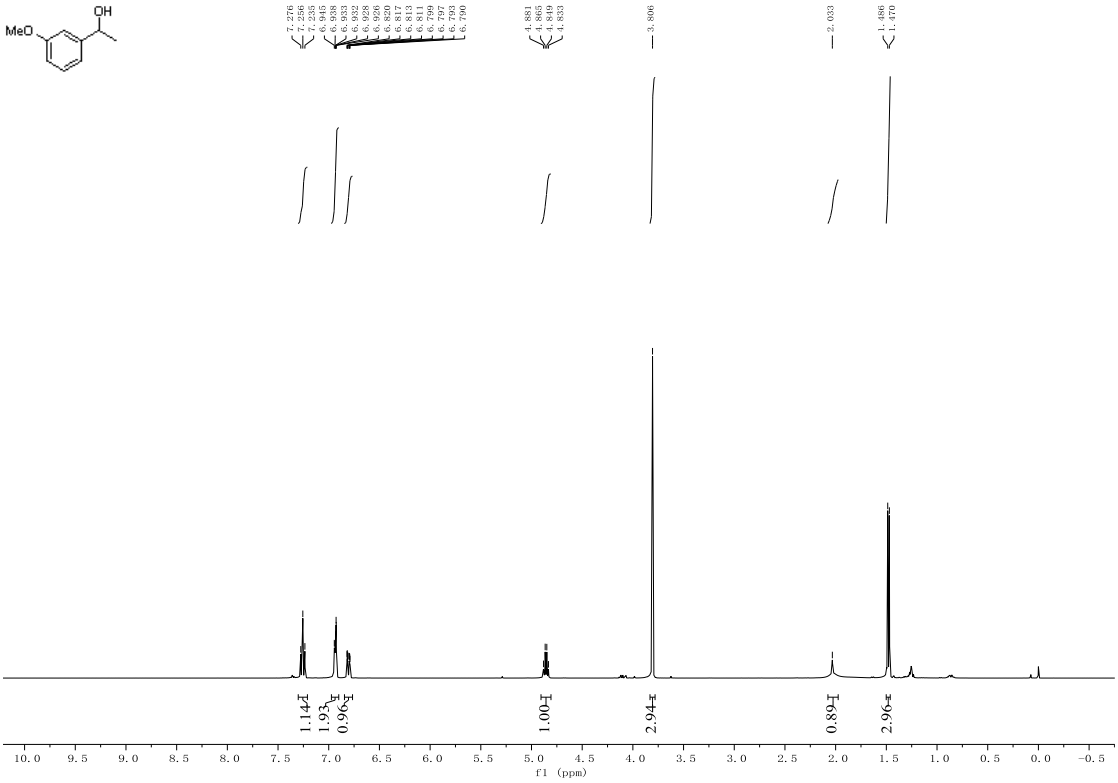

^{13}C NMR (101 MHz, Chloroform-*d*)

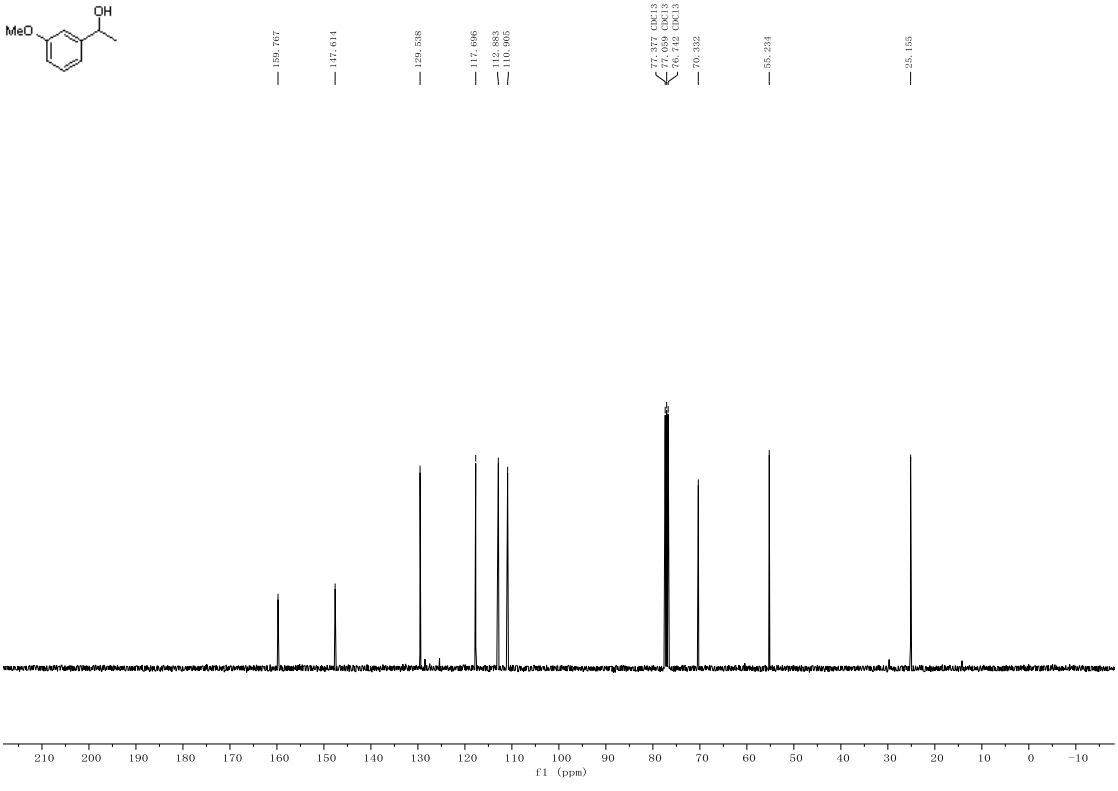

(*R*)-1-(3-Chlorophenyl)ethanol (8h).

^{1}H NMR (600 MHz, Chloroform-d)

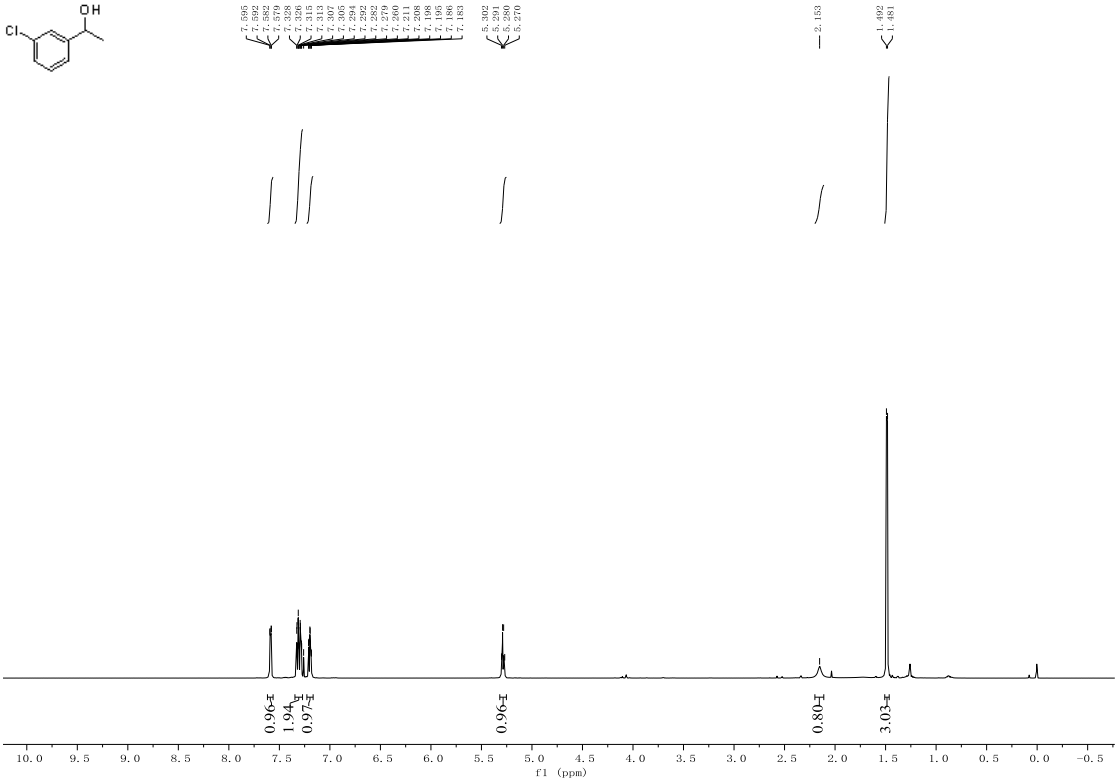

^{13}C NMR (151 MHz, Chloroform-*d*)

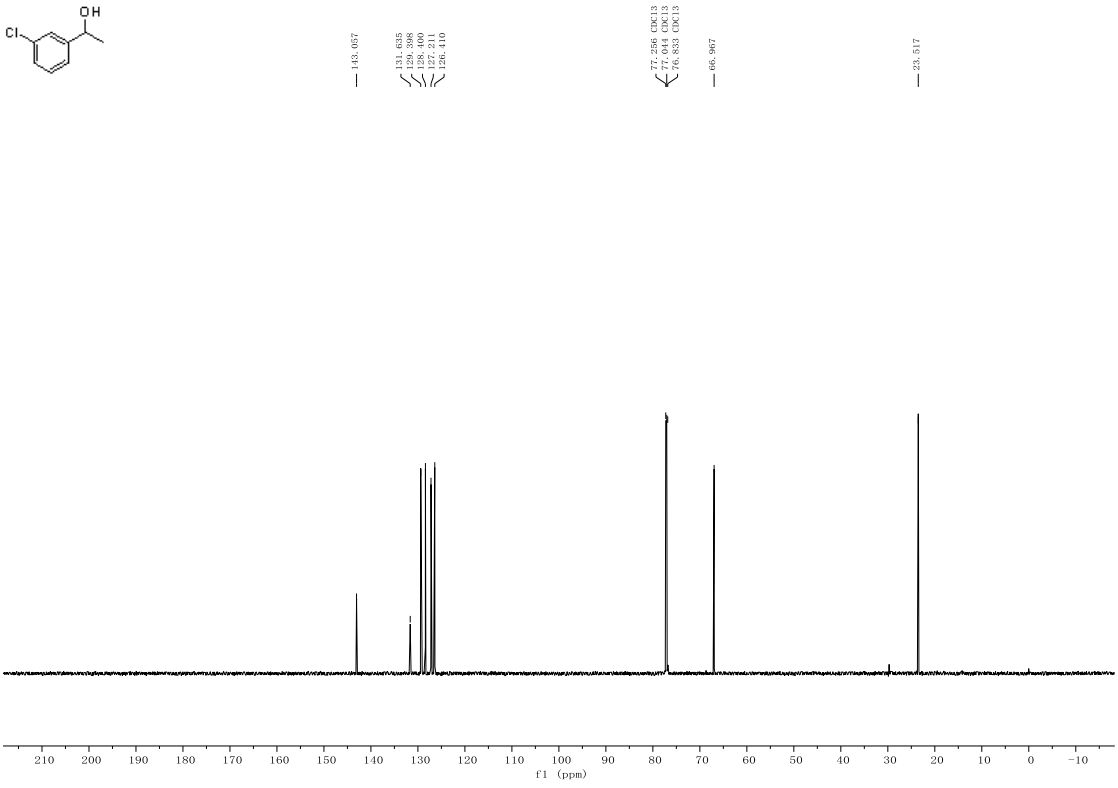

(*R*)-1-(3-Bromophenyl)ethanol (8i).

^{1}H NMR (400 MHz, Chloroform-*d*)

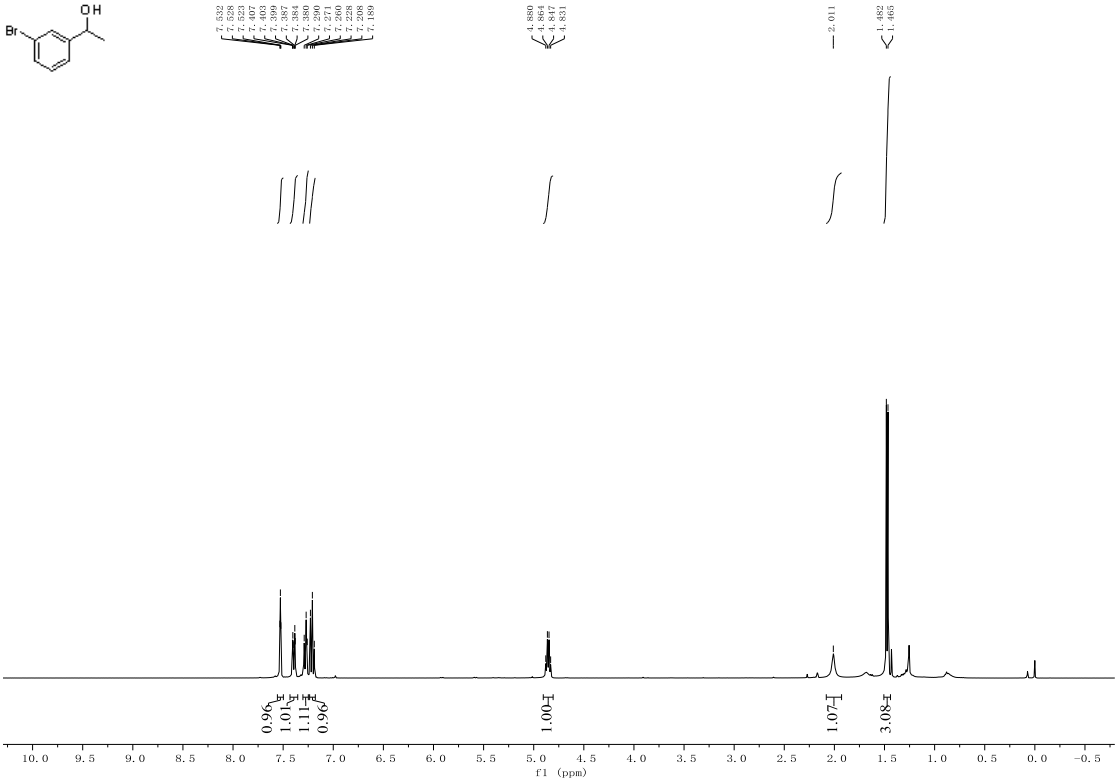

^{13}C NMR (101 MHz, Chloroform-*d*)

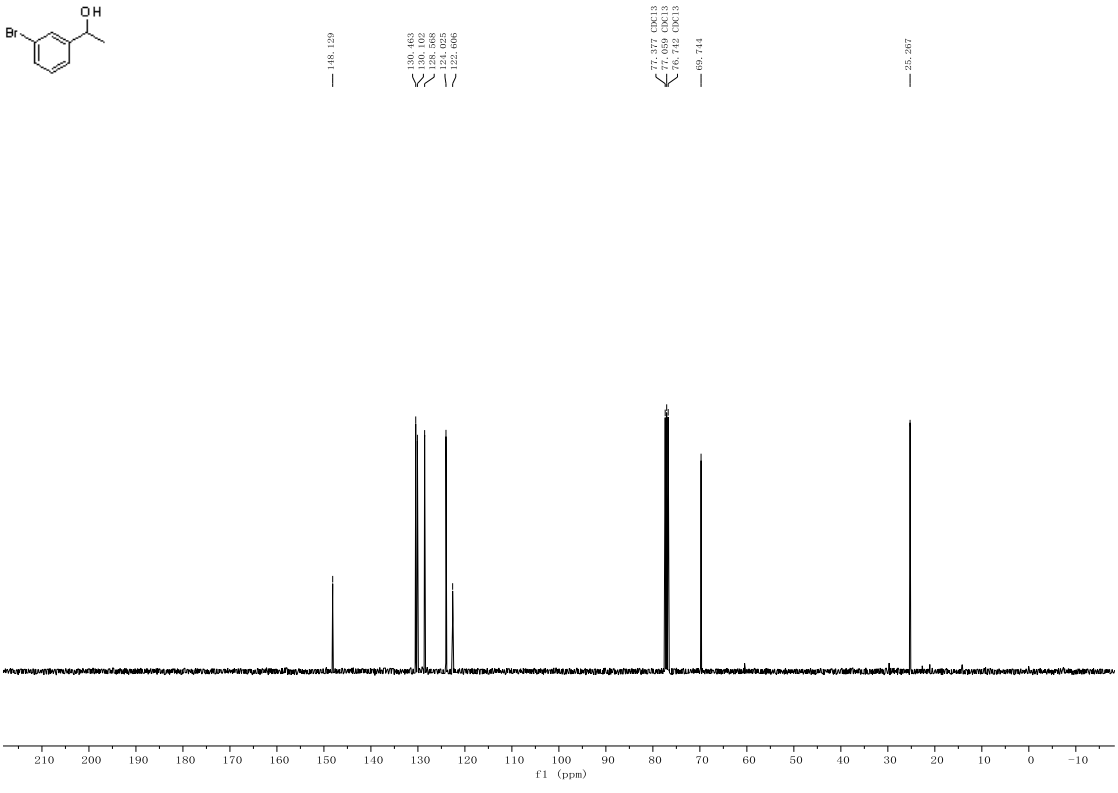

(*R*)-1-(4-Fluorophenyl)ethanol (8j).

^{1}H NMR (600 MHz, Chloroform-d)

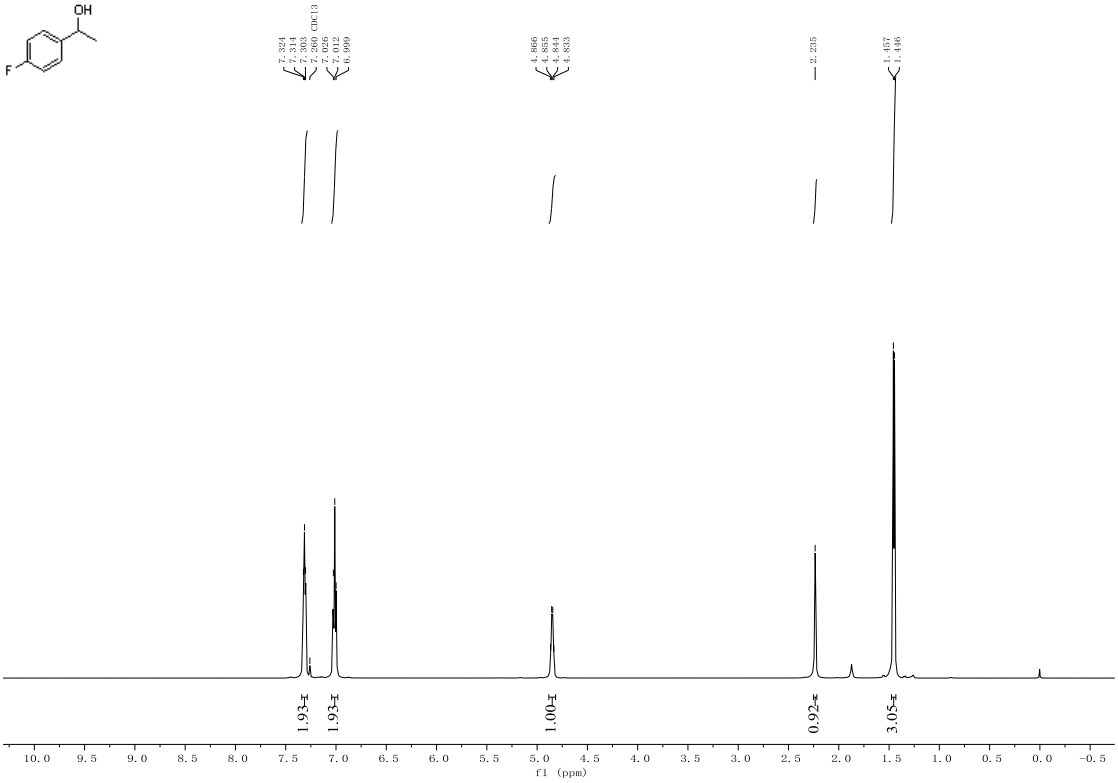

^{13}C NMR (151 MHz, Chloroform-*d*)

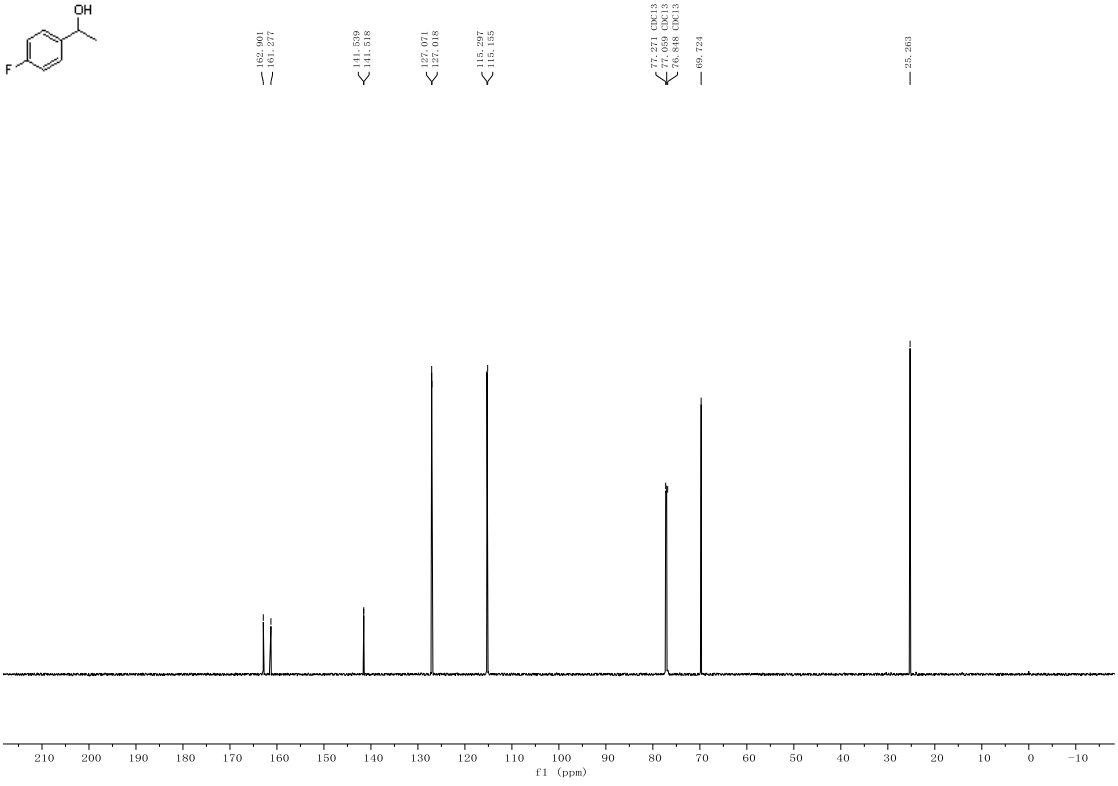

^{19}F NMR (565 MHz, Chloroform-*d*)

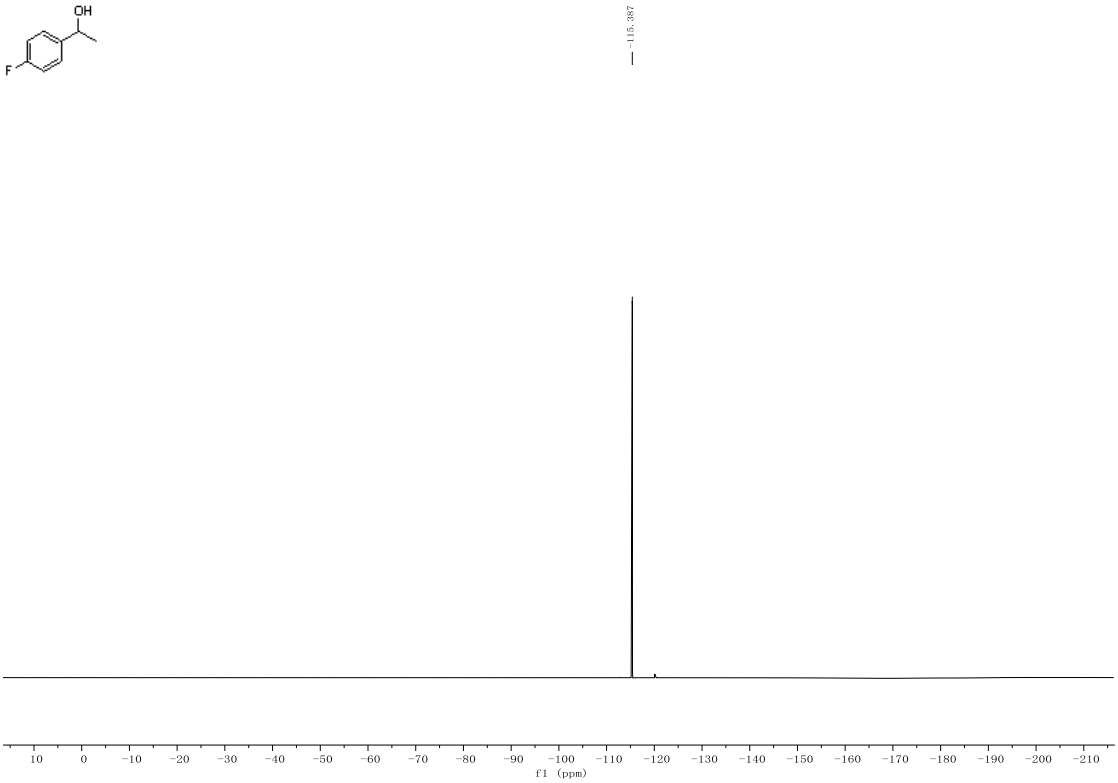

(*R*)-1-(*p*-Tolyl)ethanol (8k).

^{1}H NMR (400 MHz, Chloroform-*d*)

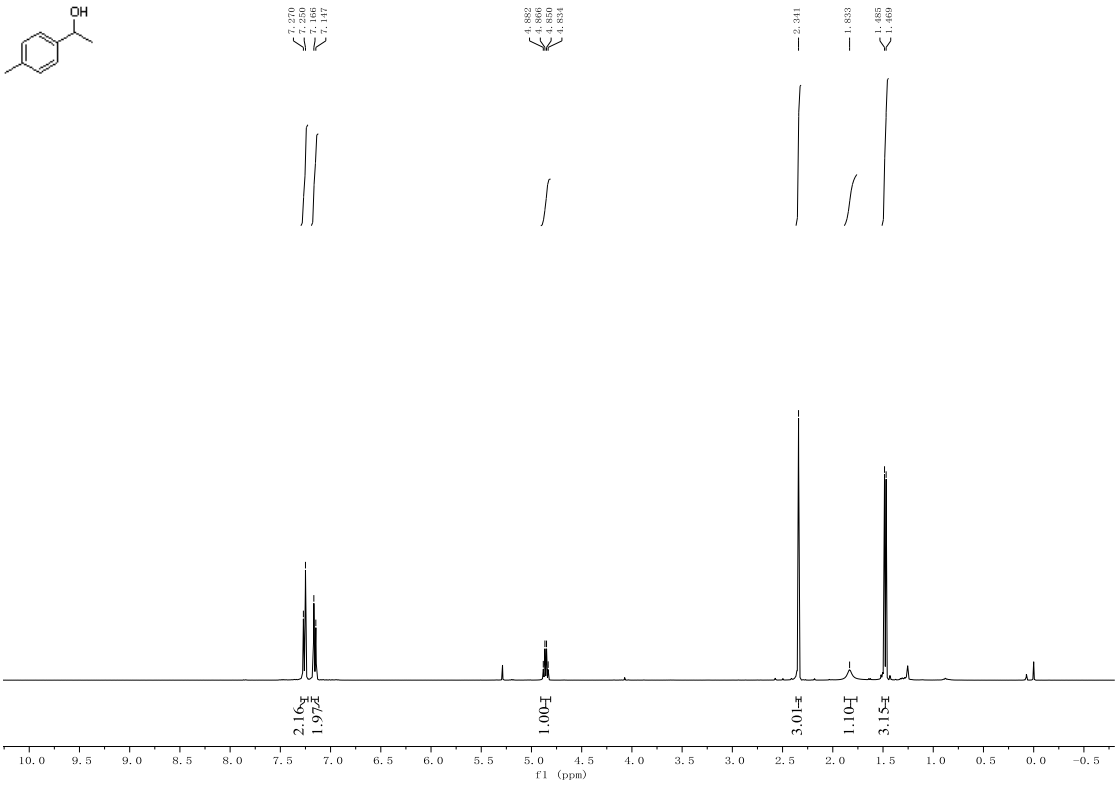

^{13}C NMR (101 MHz, Chloroform-*d*)

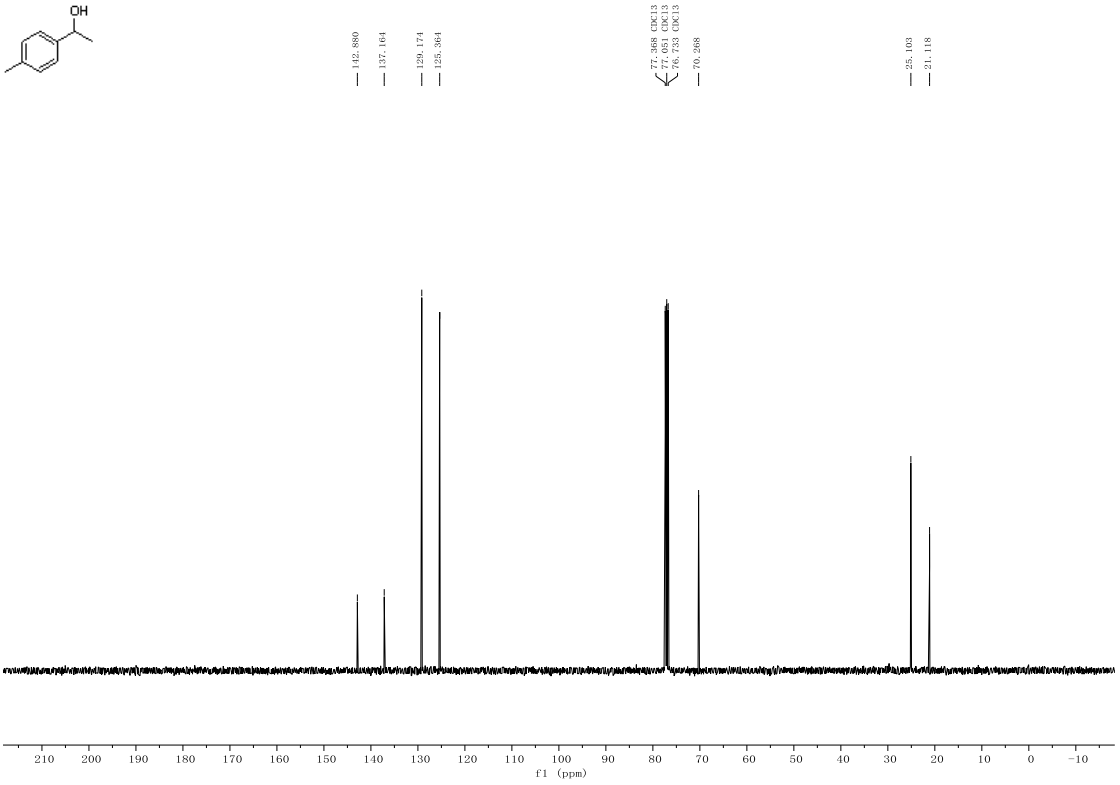

(*R*)-1-(4-Methoxyphenyl)ethanol (8l).

^{1}H NMR (400 MHz, Chloroform-*d*)

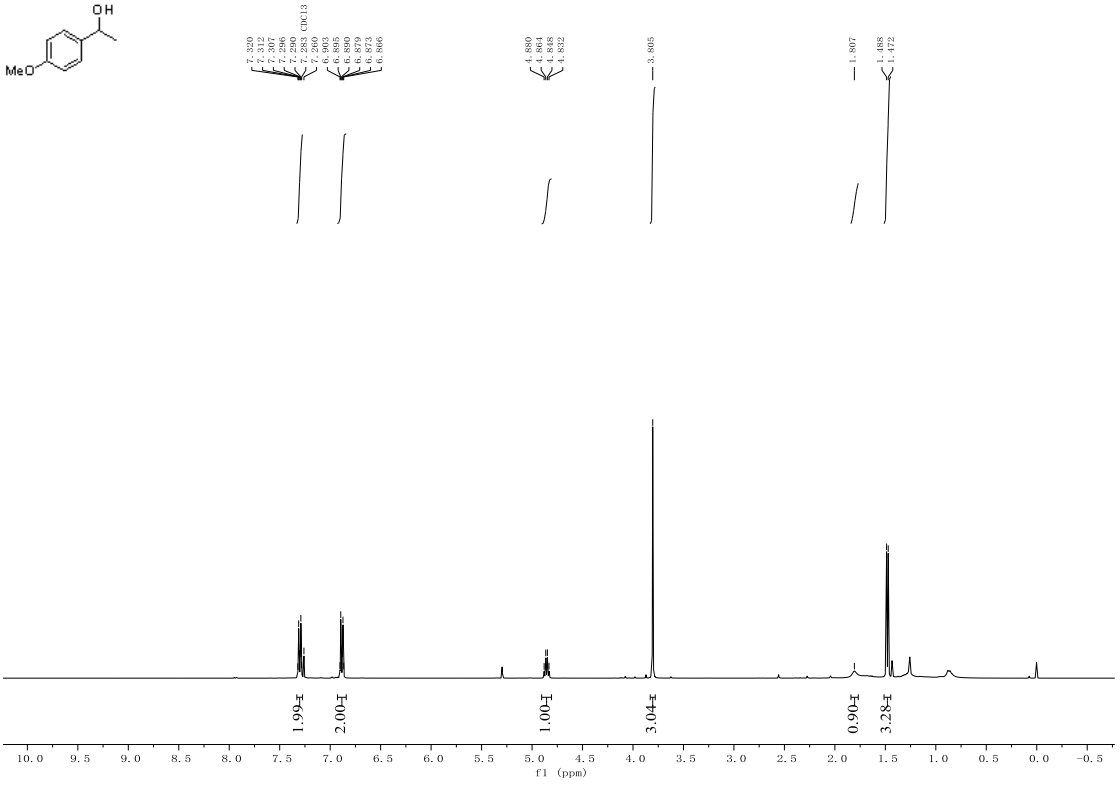

^{13}C NMR (101 MHz, Chloroform-*d*)

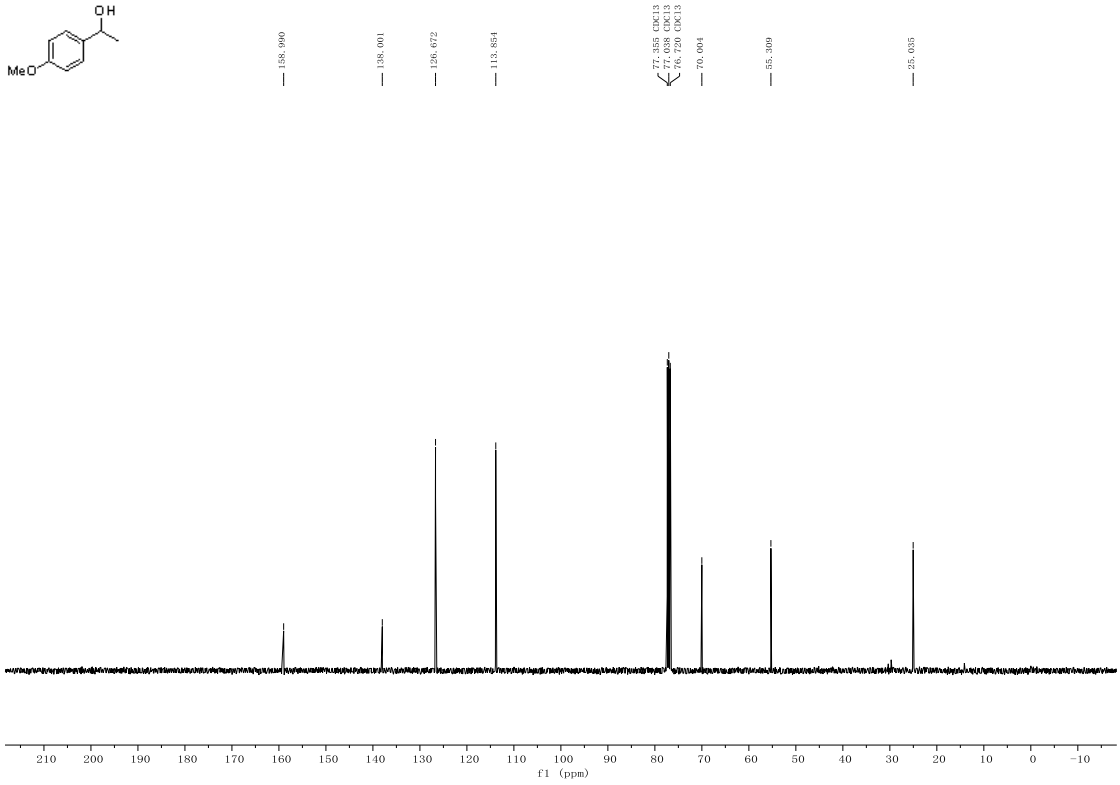

(*R*)-1-(4-Chlorophenyl)ethanol (8m).

^{1}H NMR (600 MHz, Chloroform-d)

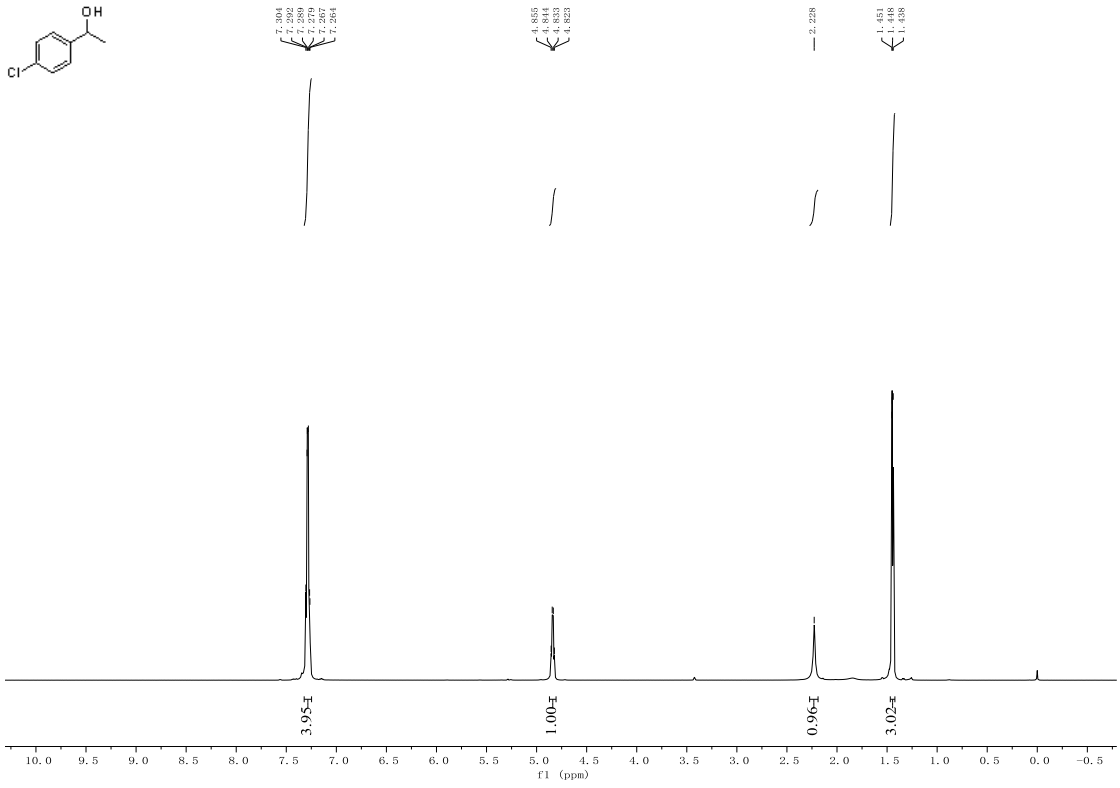

^{13}C NMR (151 MHz, Chloroform-*d*)

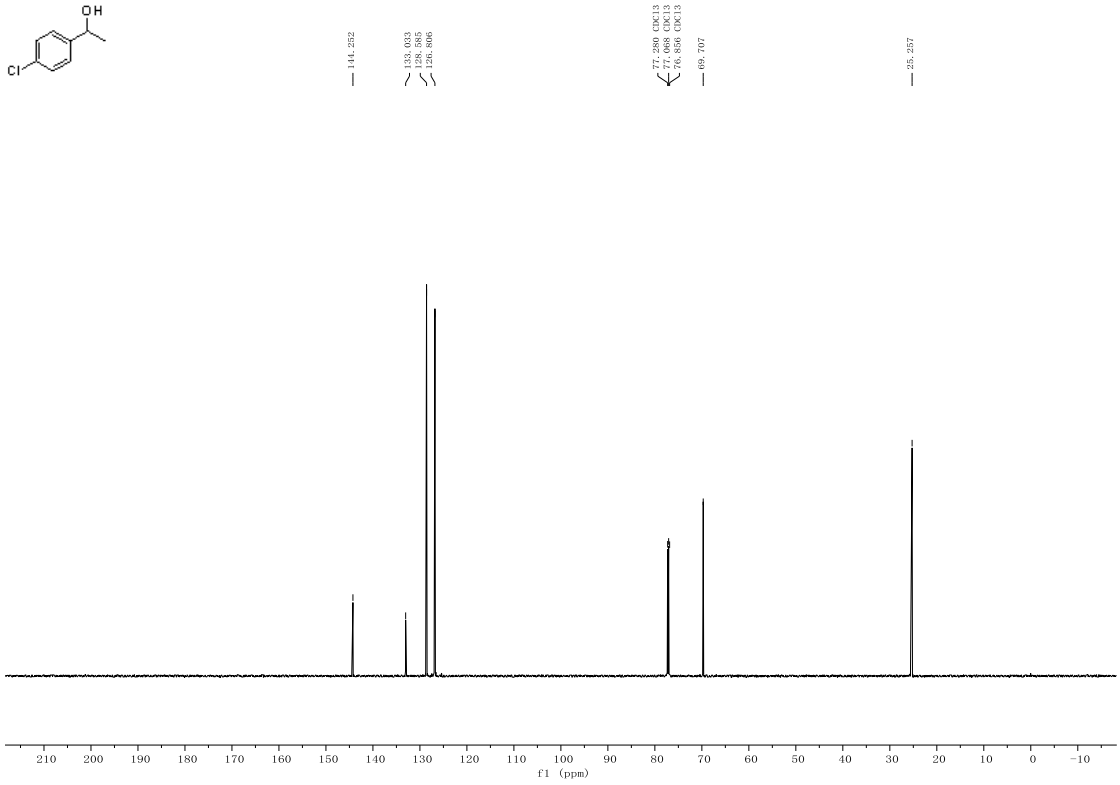

(*R*)-1-(4-Bromophenyl)ethanol (8n).

^{1}H NMR (400 MHz, Chloroform-*d*)

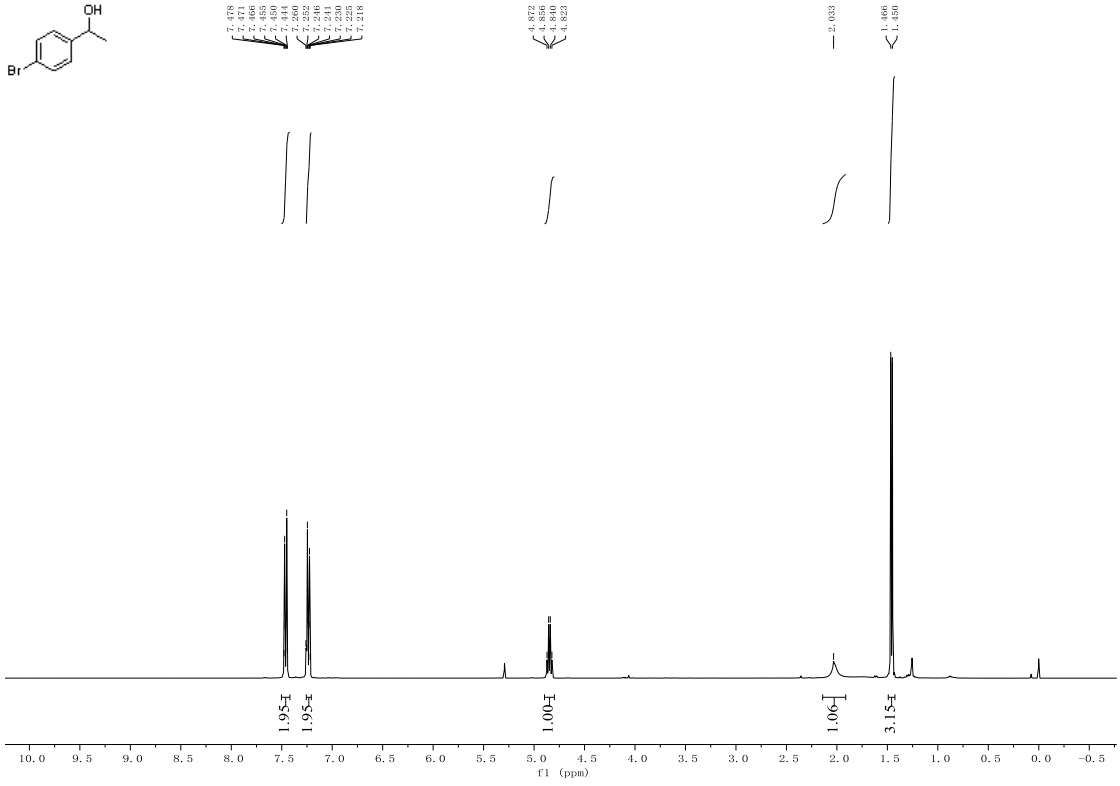

^{13}C NMR (101 MHz, Chloroform-*d*)

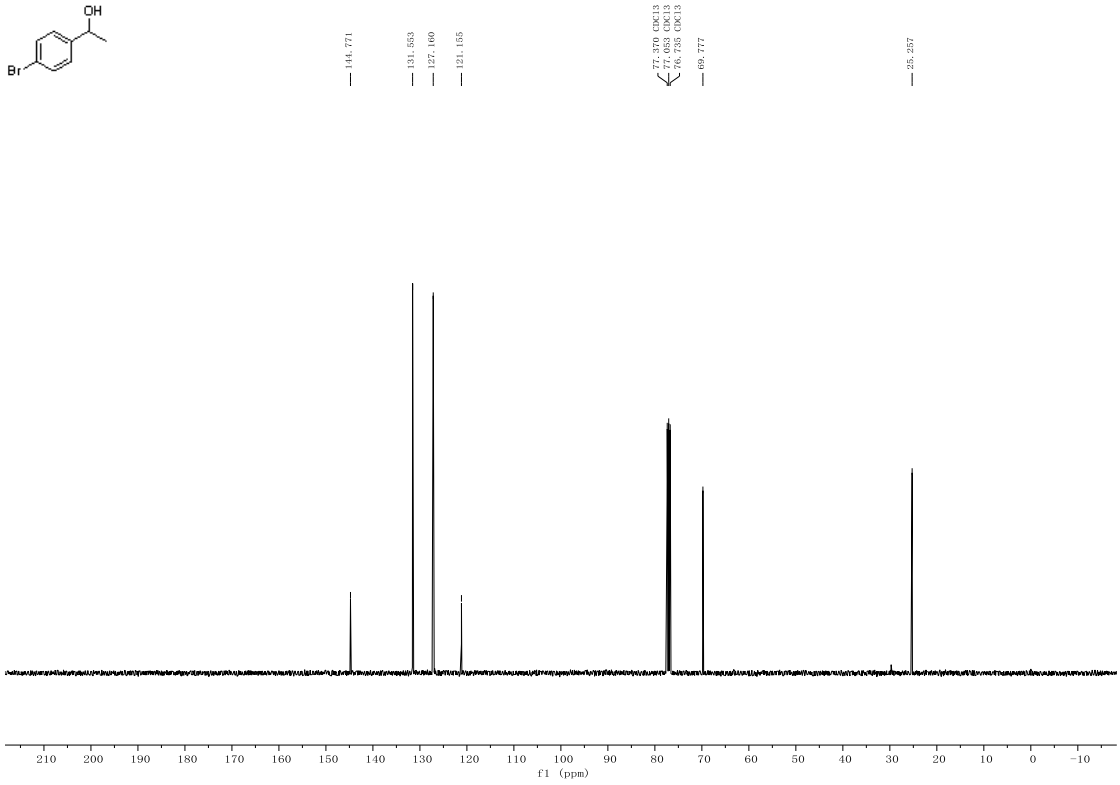

(*R*)-1-([1,1'-Biphenyl]-4-yl)ethanol (8o).

^{1}H NMR (400 MHz, Chloroform-*d*)

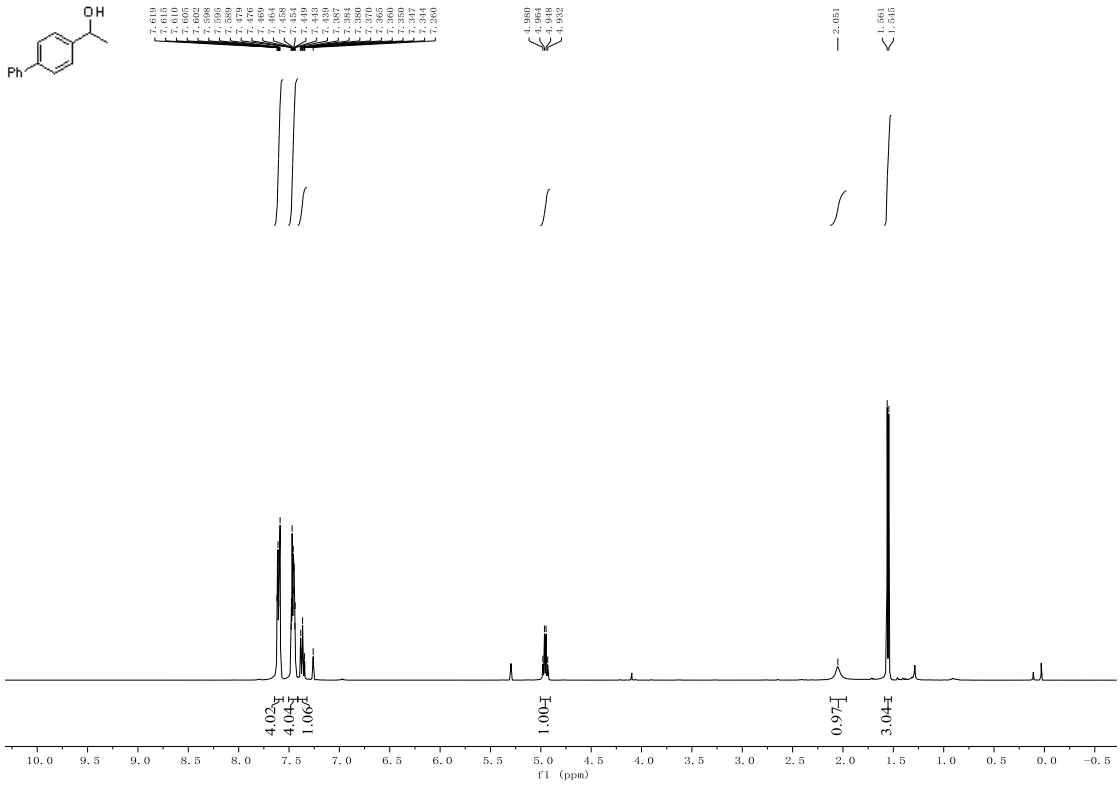

^{13}C NMR (101 MHz, Chloroform-*d*)

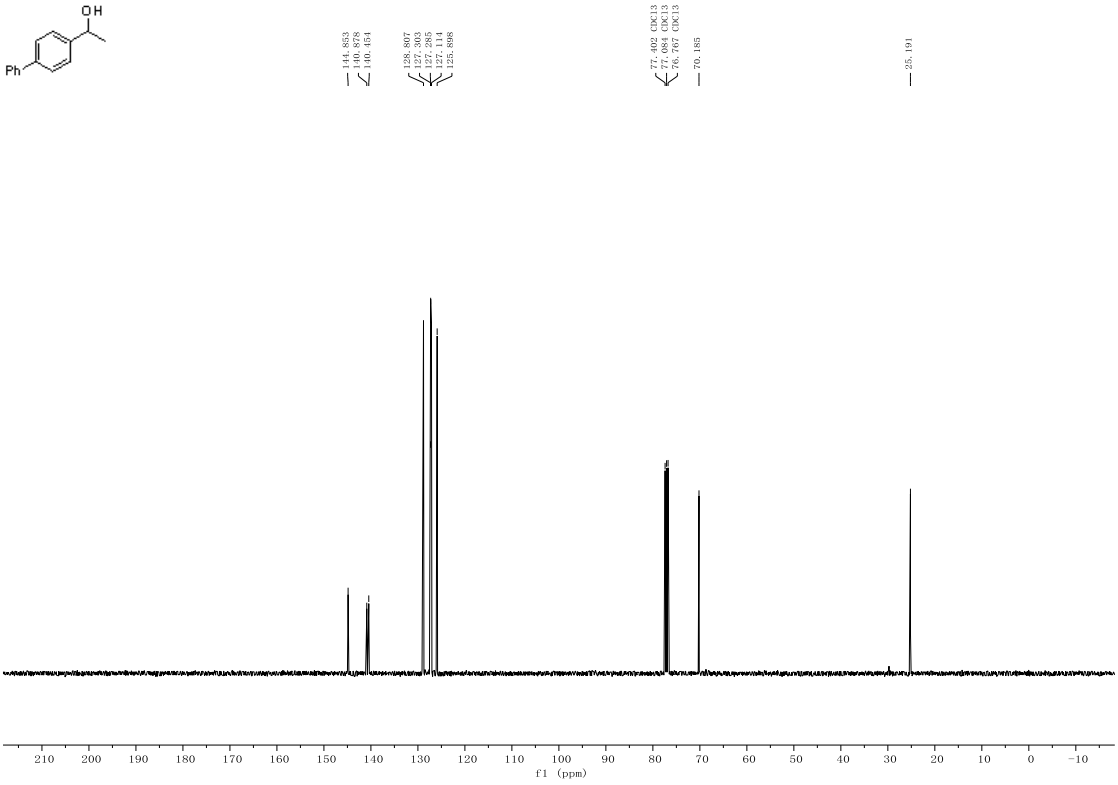

(*R*)-1-(4-(*tert*-Butyl)phenyl)ethanol (8p).

^{1}H NMR (600 MHz, Chloroform-*d*)

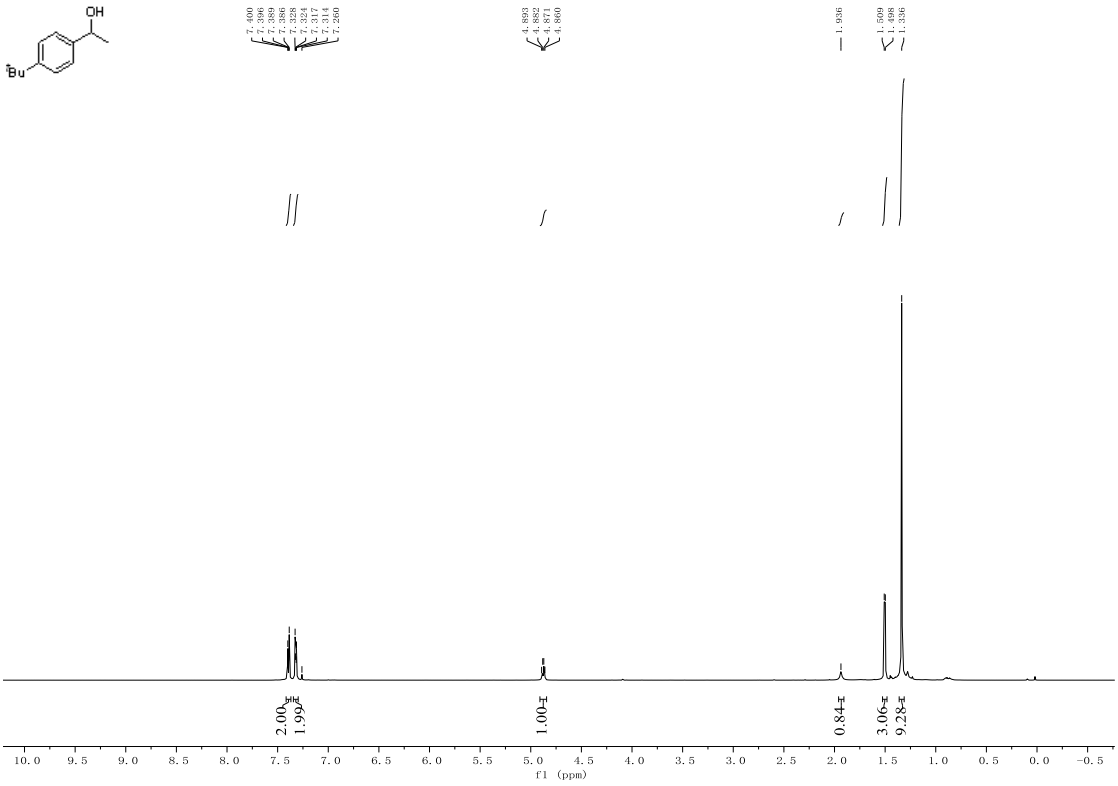

^{13}C NMR (151 MHz, Chloroform-*d*)

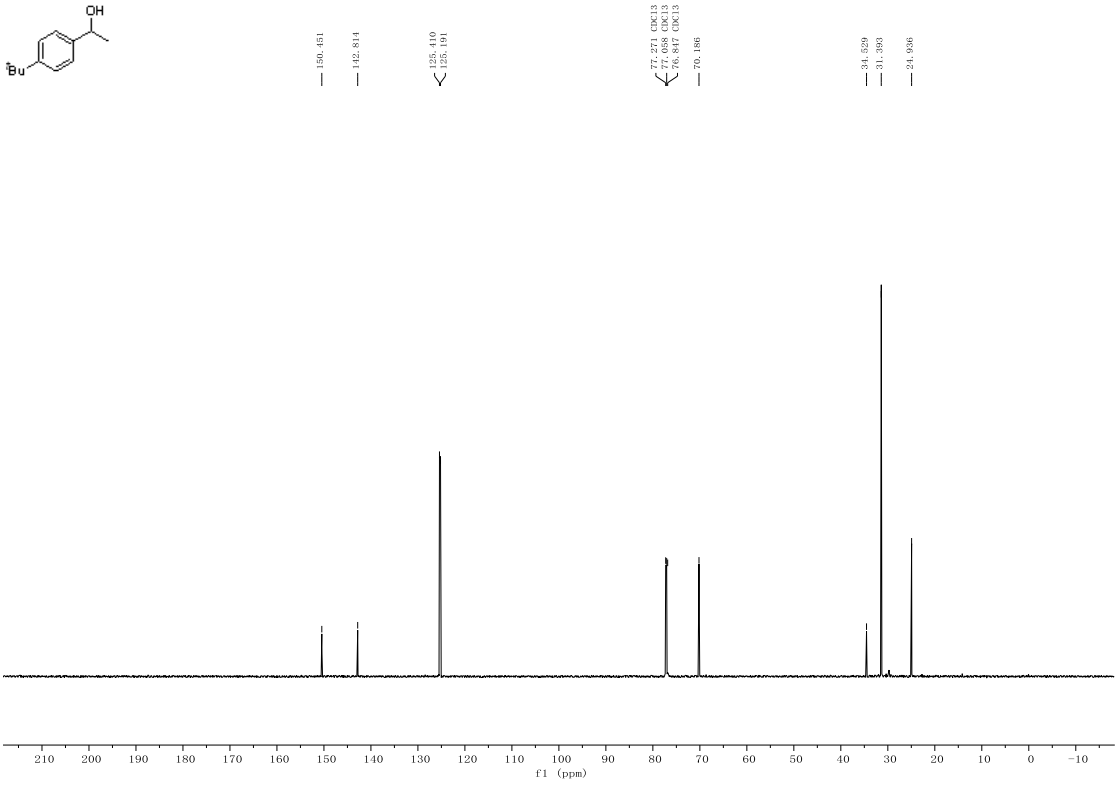

(*R*)-1-(4-Nitrophenyl)ethanol (8q).

^{1}H NMR (600 MHz, Chloroform-*d*)

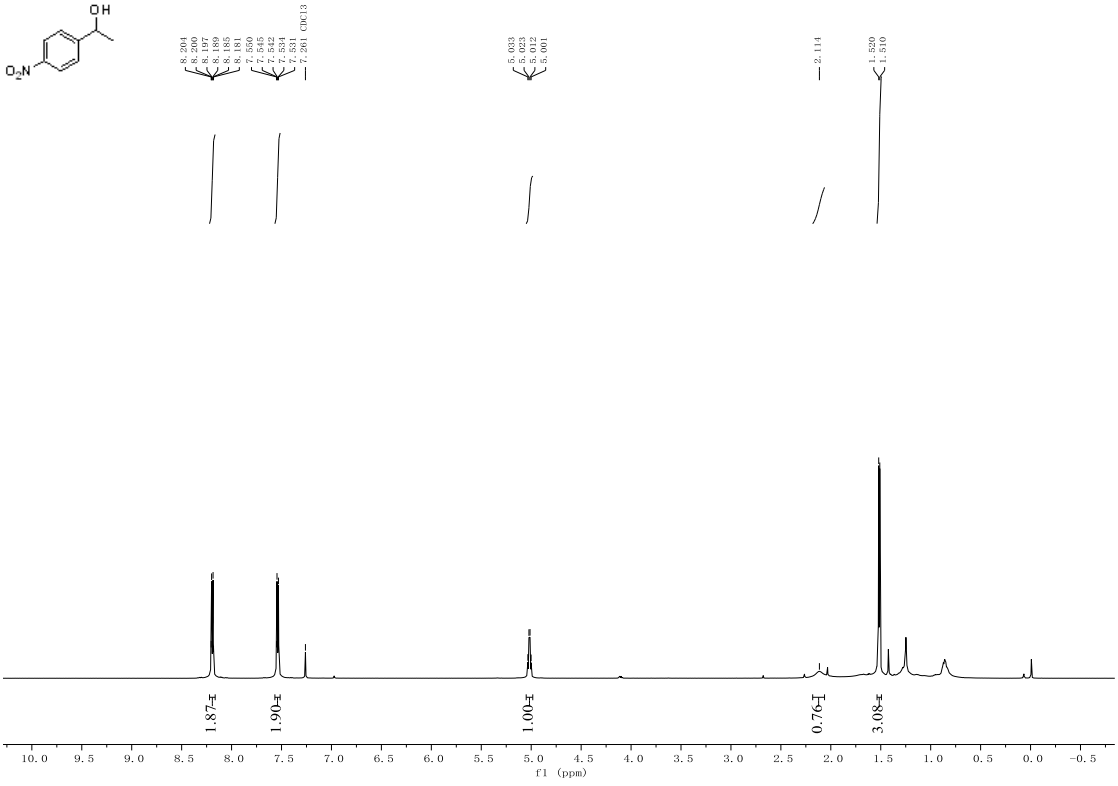

^{13}C NMR (151 MHz, Chloroform-*d*)

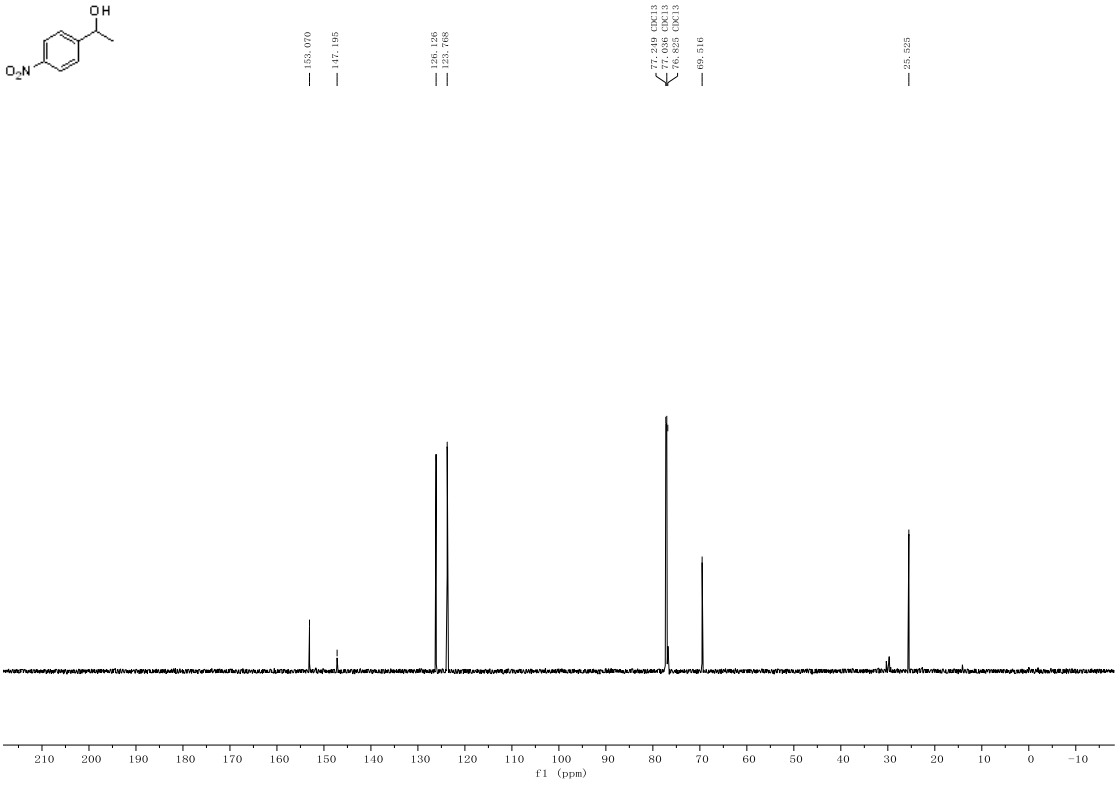

(*R*)-1-(4-Cyclohexylphenyl)ethanol (8r).

^{1}H NMR (600 MHz, Chloroform-*d*)

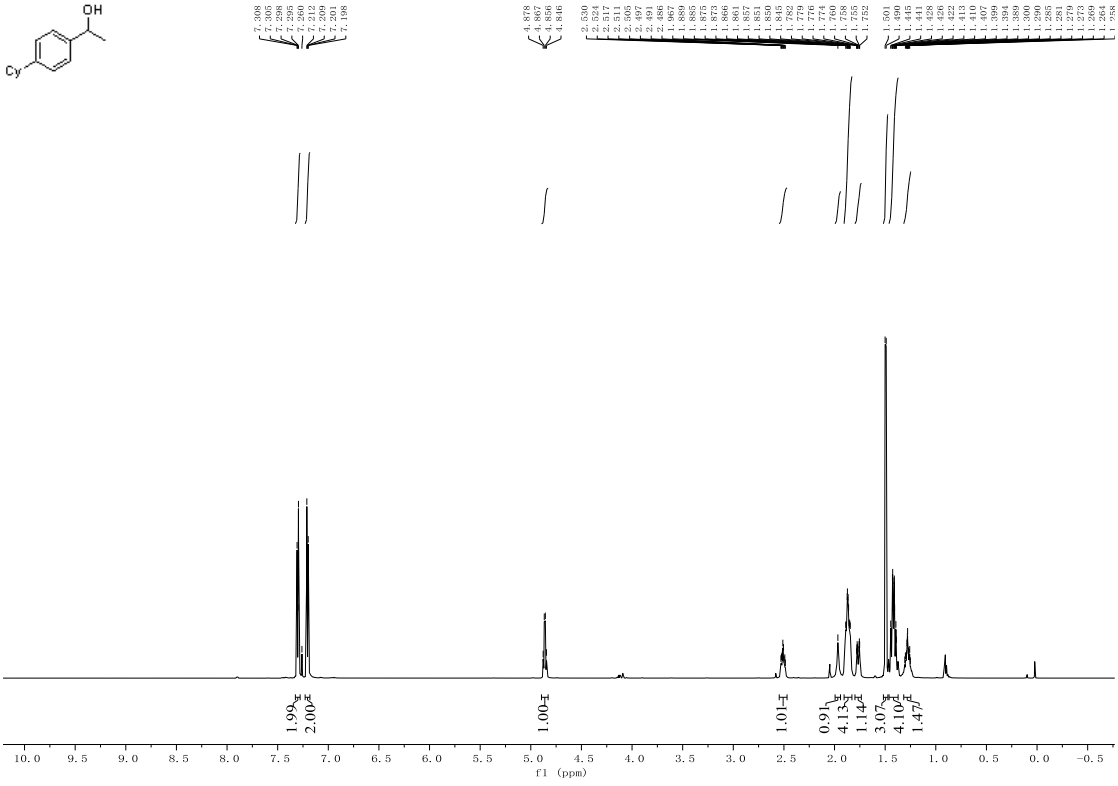

^{13}C NMR (151 MHz, Chloroform-*d*)

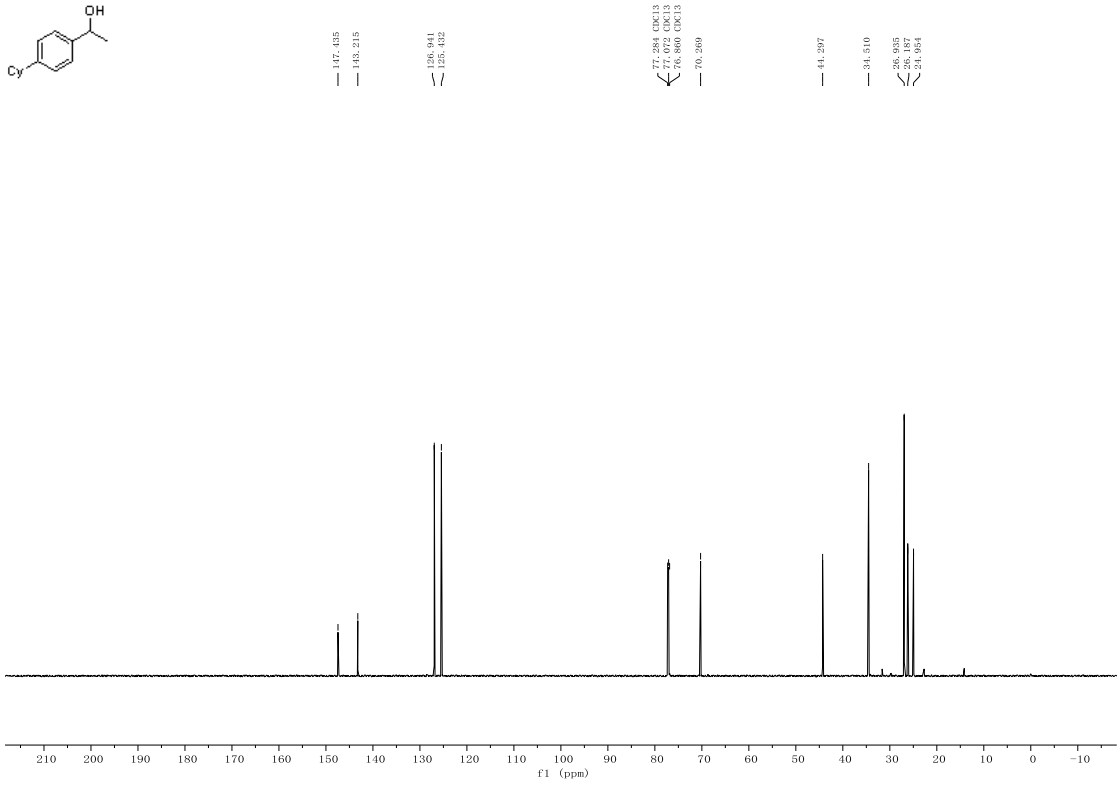

(*R*)-1-(4-(Dimethylamino)phenyl)ethanol (8s).

^{1}H NMR (400 MHz, Chloroform-*d*)

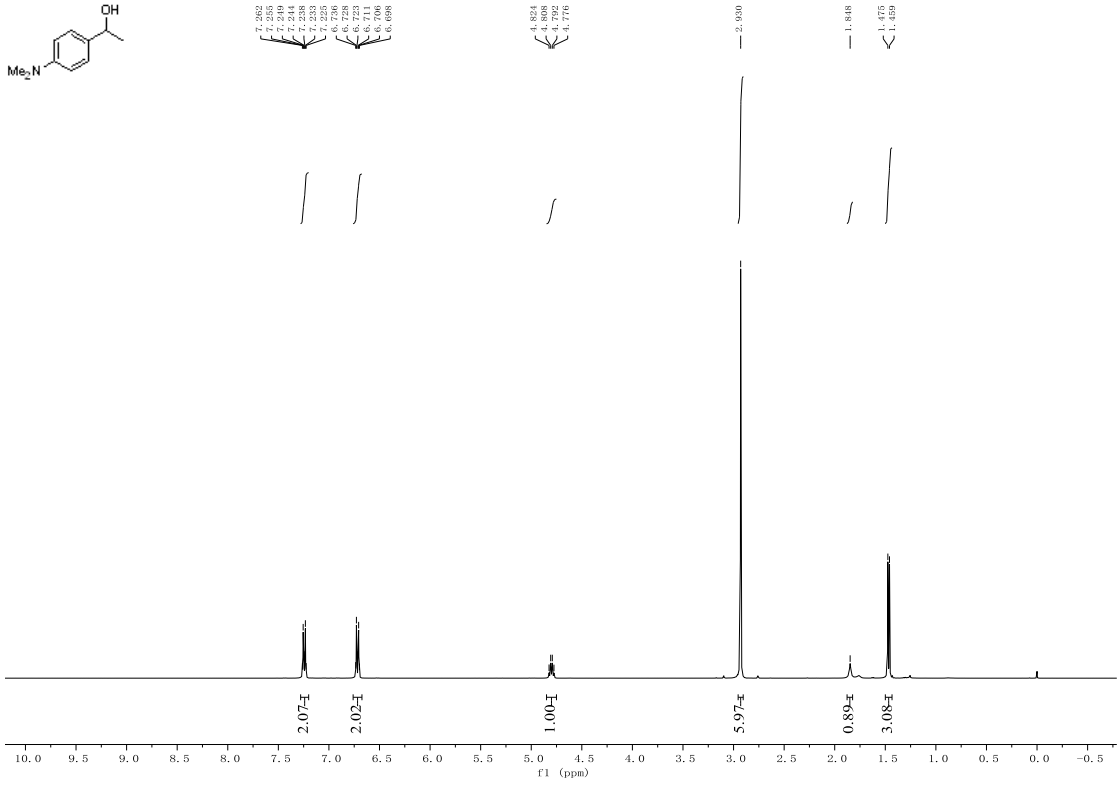

^{13}C NMR (101 MHz, Chloroform-*d*)

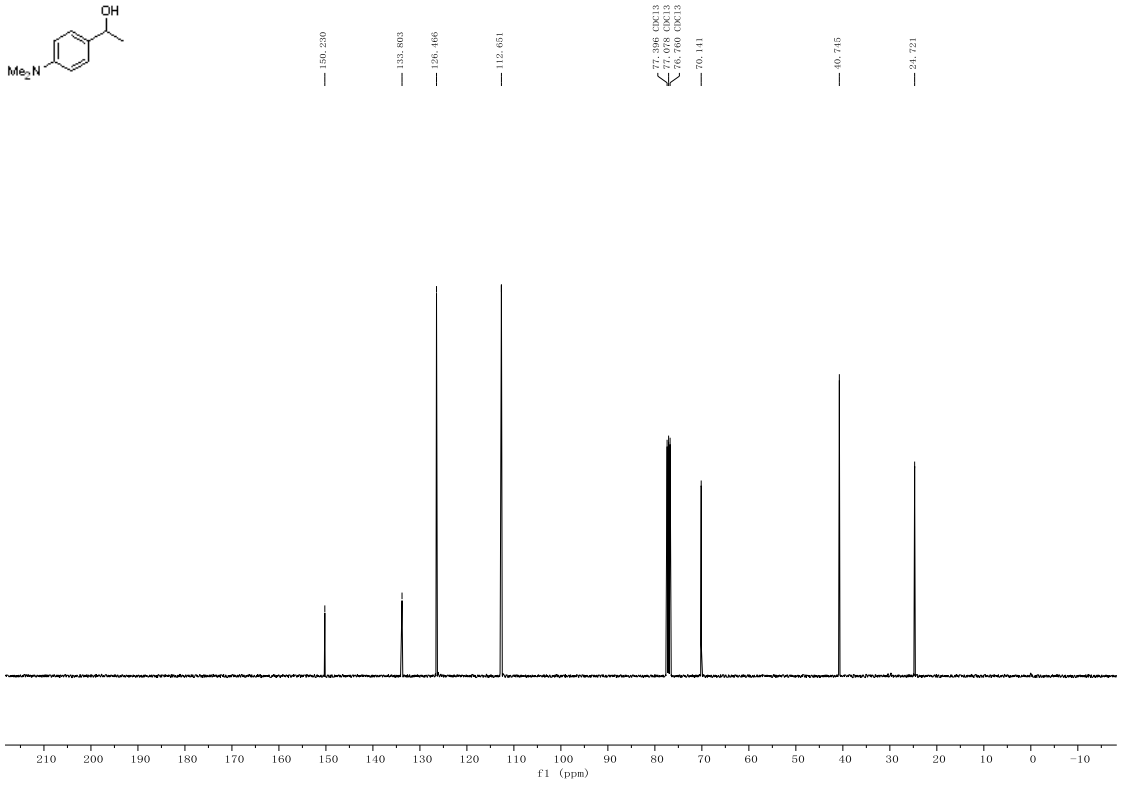

(*R*)-1-(3,4-Dichlorophenyl)ethanol (8t).

^{1}H NMR (600 MHz, Chloroform-*d*)

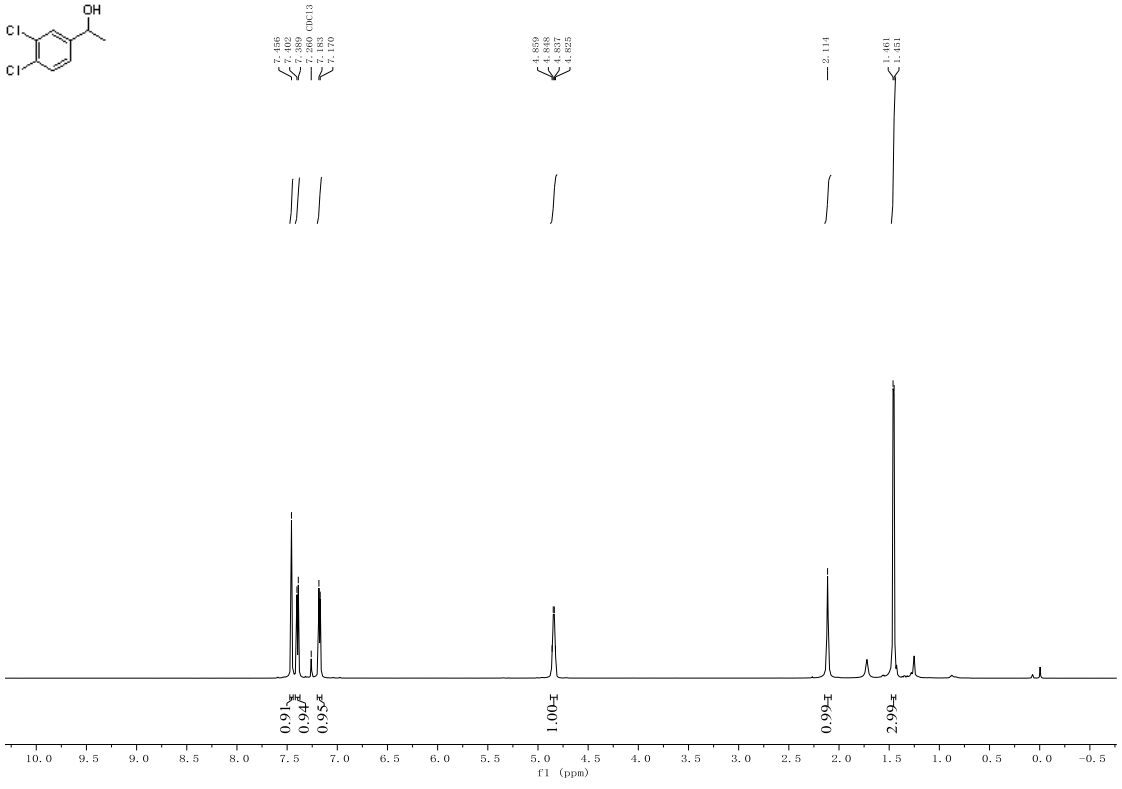

^{13}C NMR (151 MHz, Chloroform-*d*)

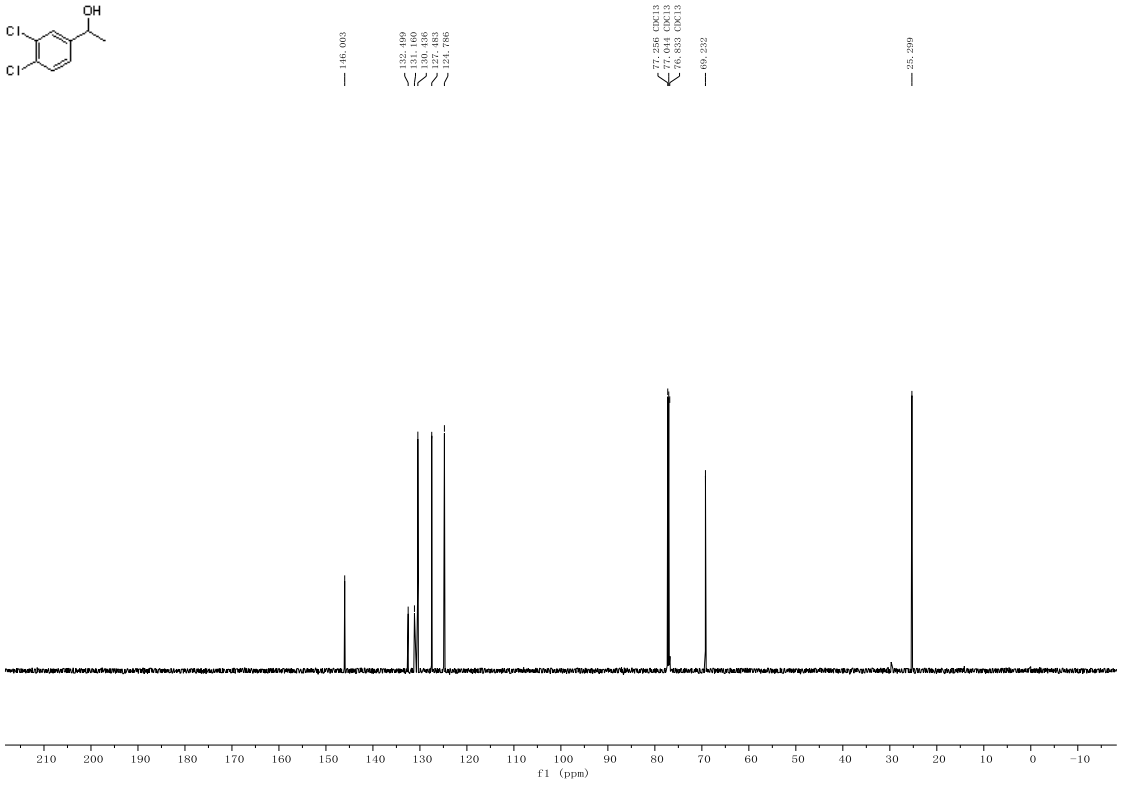

(*R*)-1-(3,4-Dimethoxyphenyl)ethanol (8u).

^{1}H NMR (400 MHz, Chloroform-*d*)

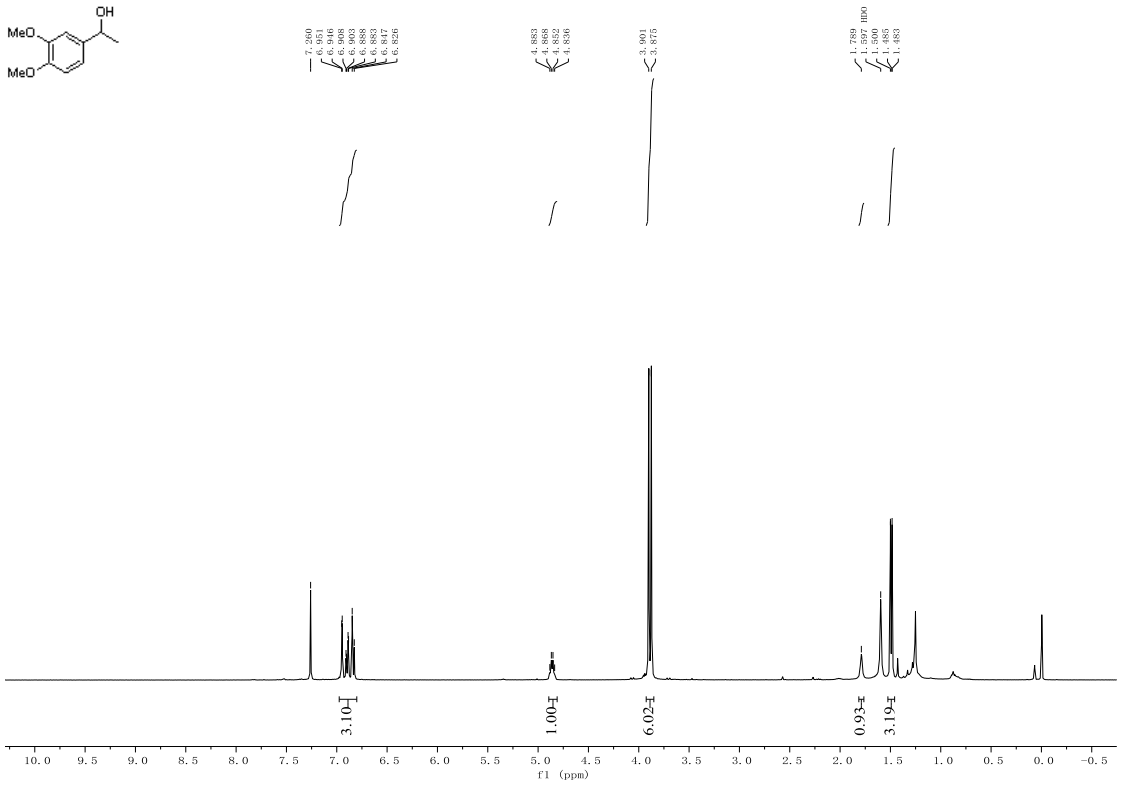

^{13}C NMR (151 MHz, Chloroform-*d*)

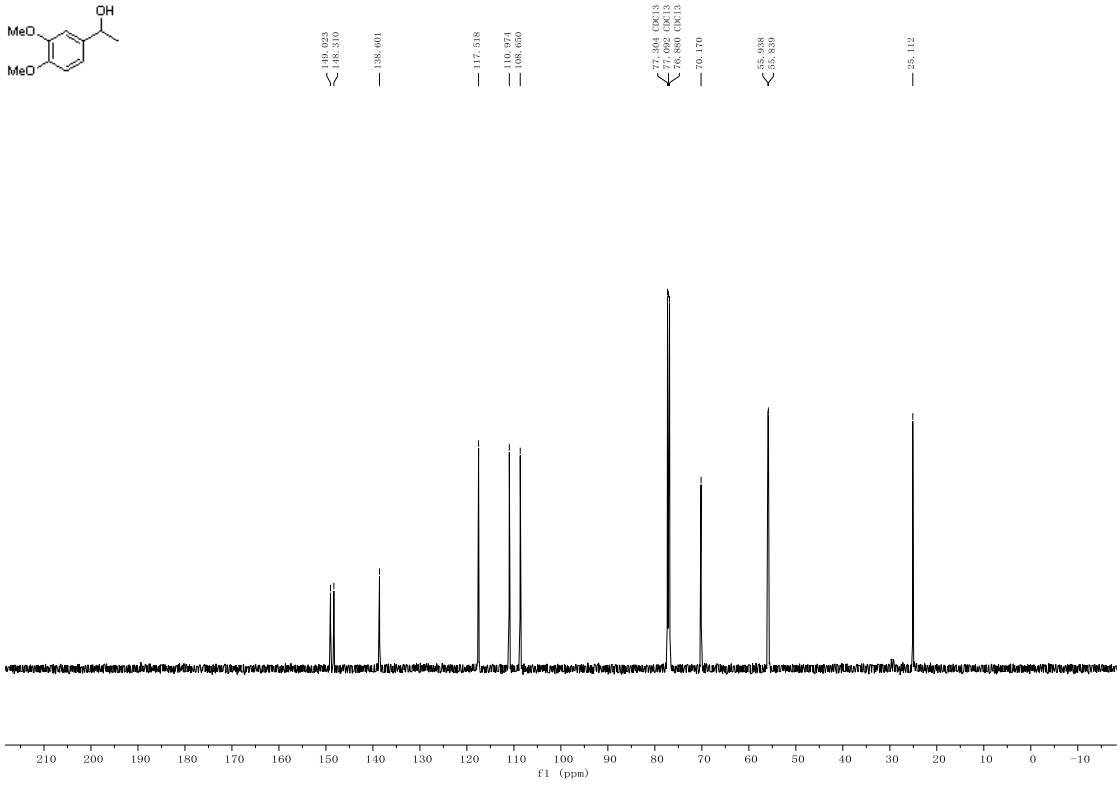

(*R*)-1-(Naphthalen-2-yl)ethanol (8v).

^{1}H NMR (400 MHz, Chloroform-*d*)

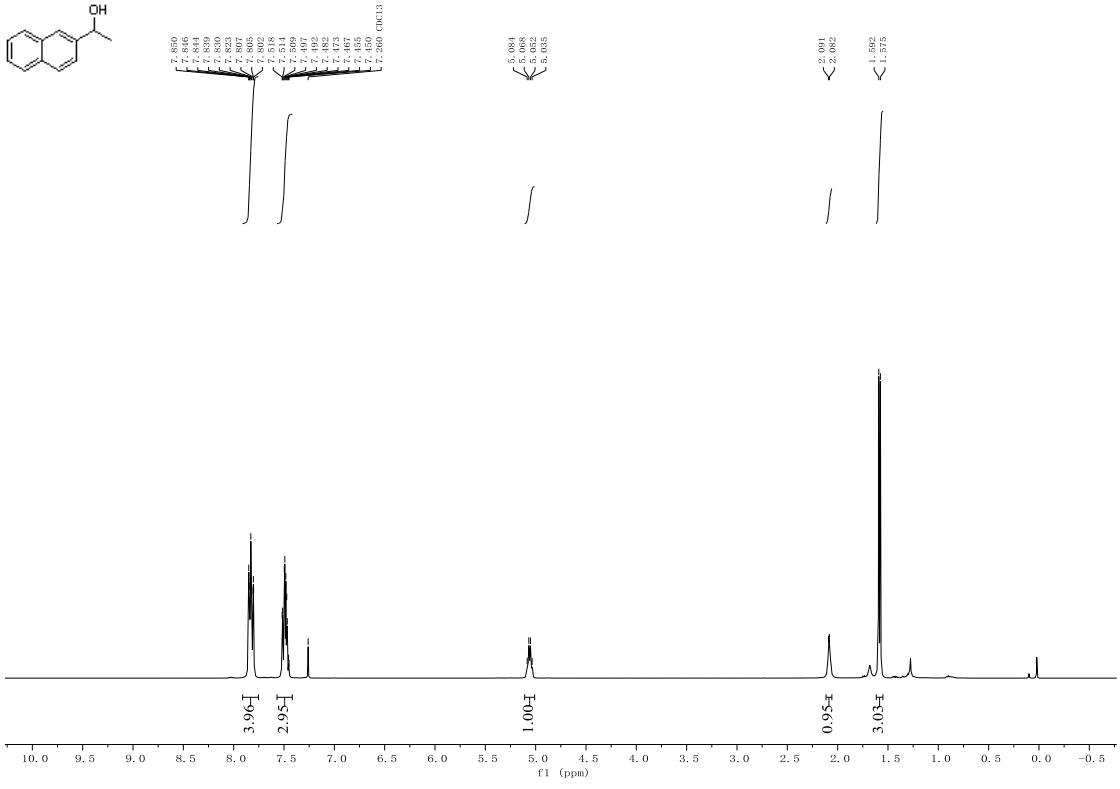

^{13}C NMR (151 MHz, Chloroform-*d*)

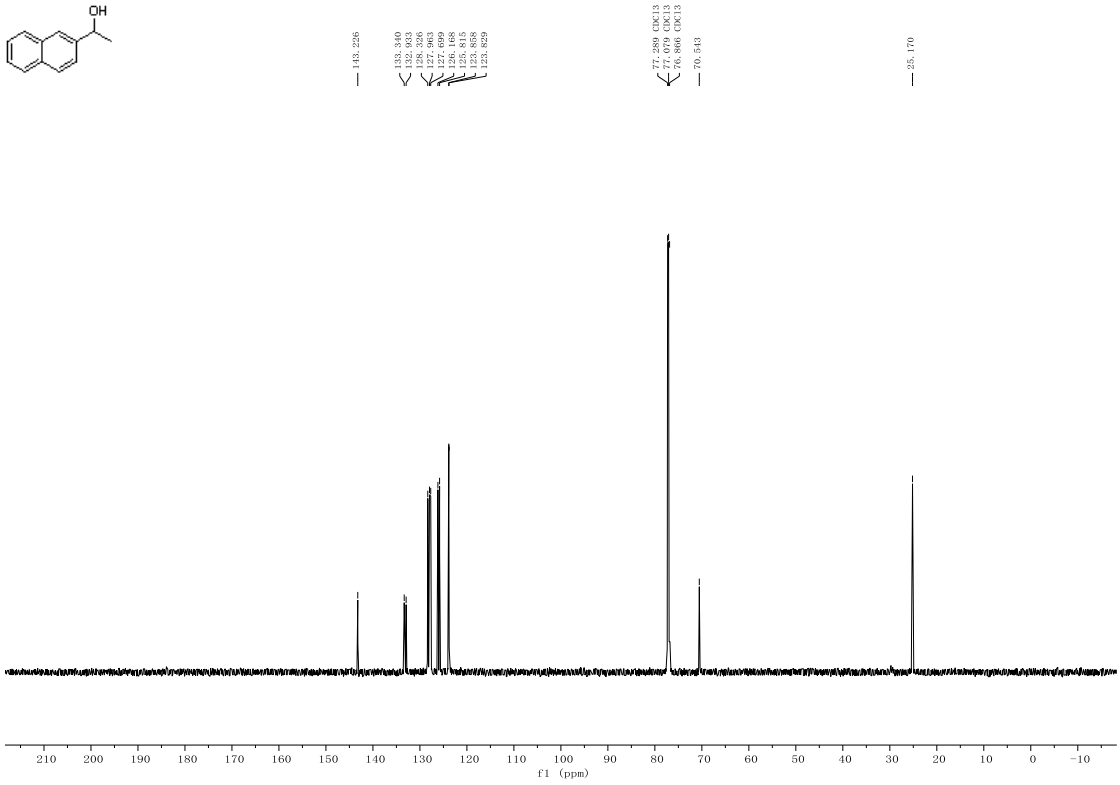

(*R*)-1-(Naphthalen-1-yl)ethanol (8w).

^{1}H NMR (600 MHz, Chloroform-*d*)

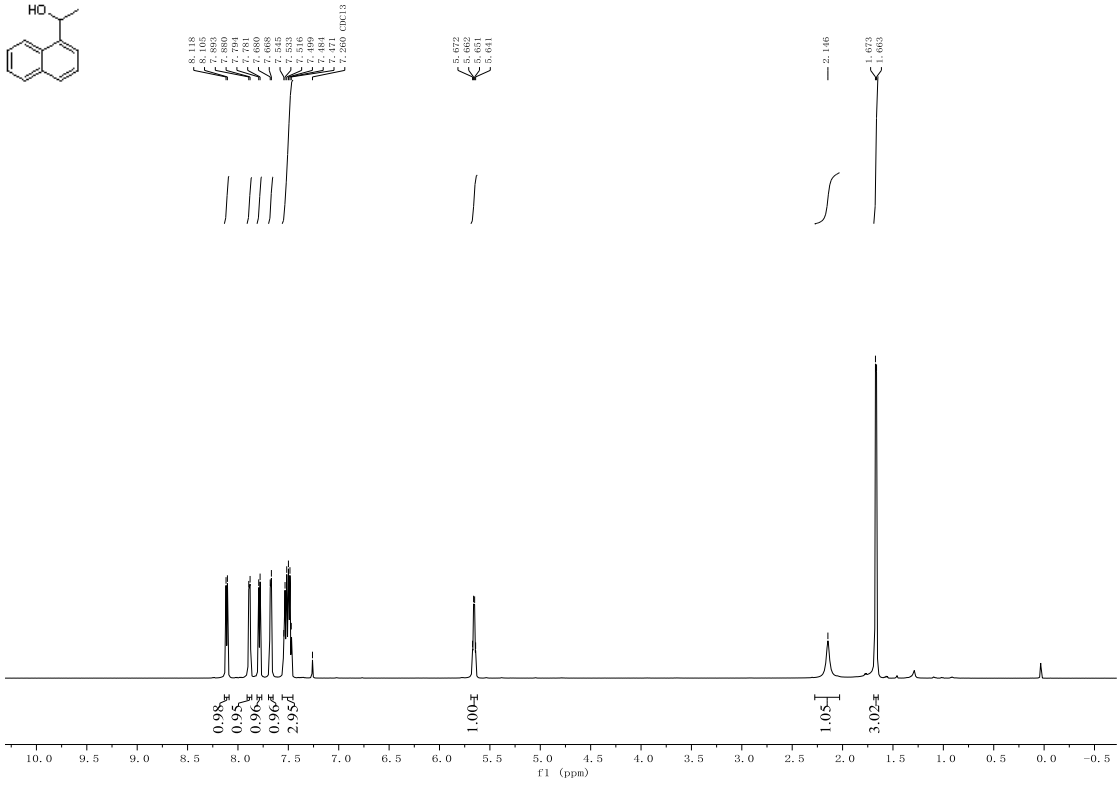

^{13}C NMR (101 MHz, Chloroform-*d*)

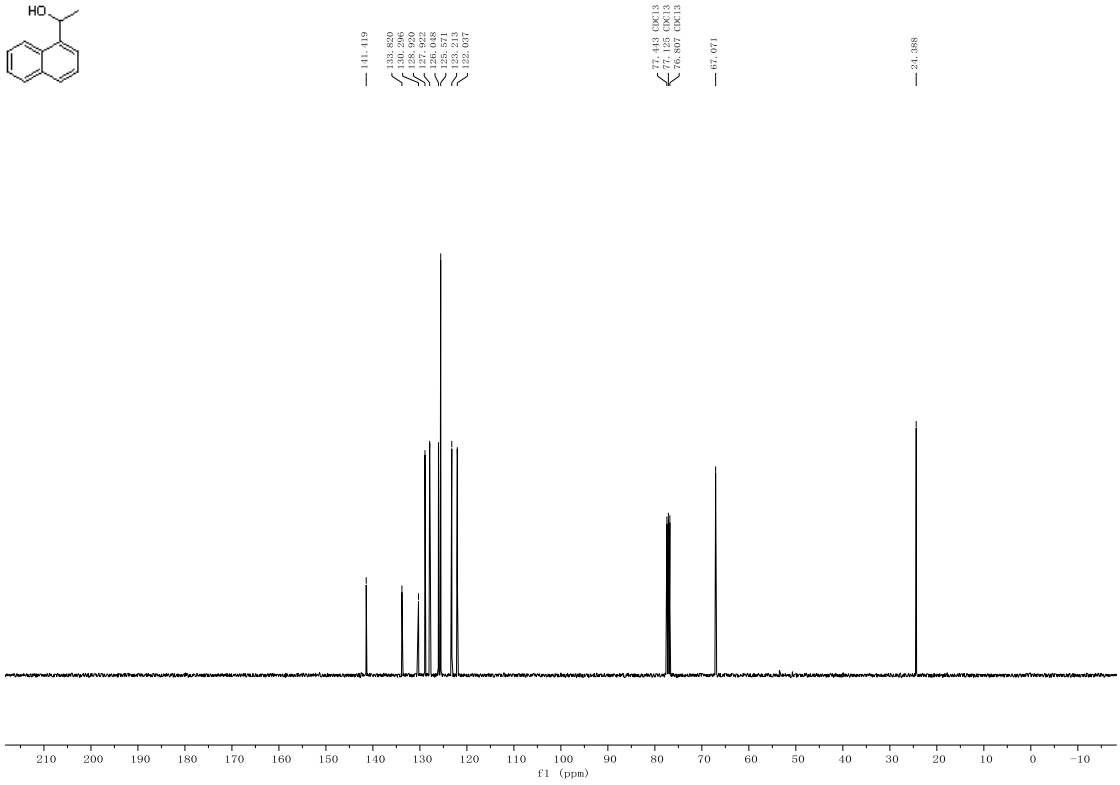

(*R*)-1-(Benzo[*d*][1,3]dioxol-5-yl)ethanol (8x).

^{1}H NMR (400 MHz, Chloroform-*d*)

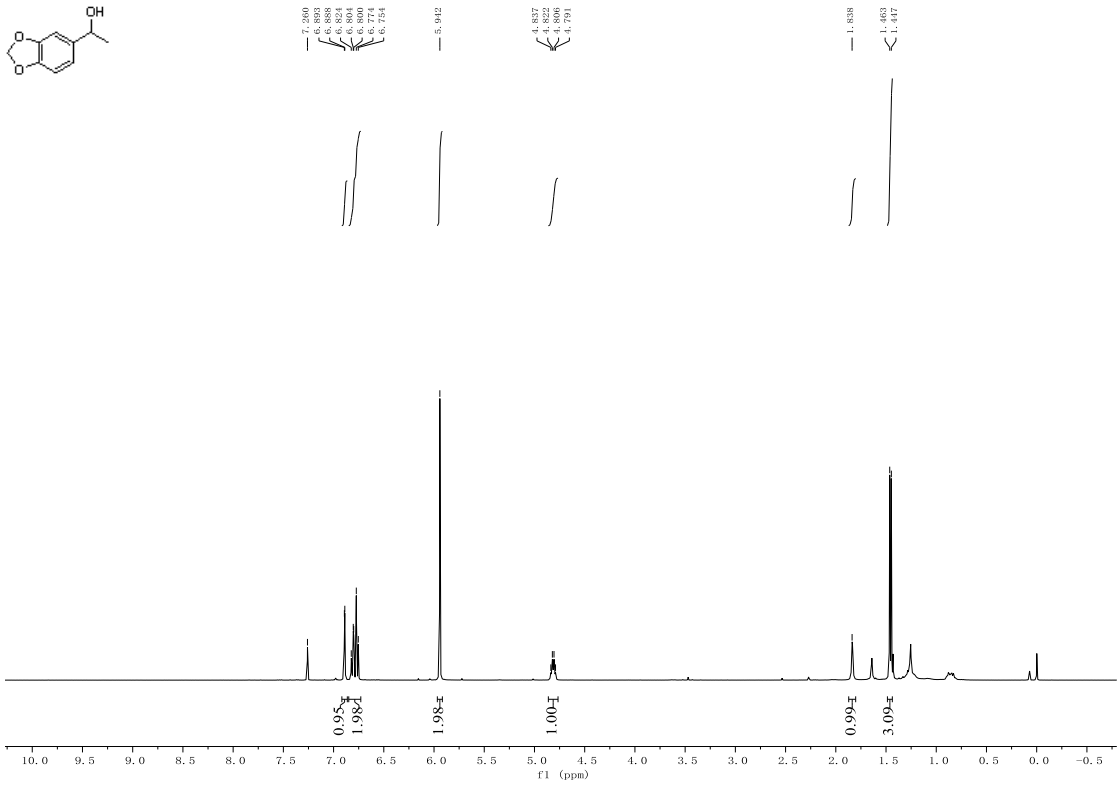

^{13}C NMR (151 MHz, Chloroform-*d*)

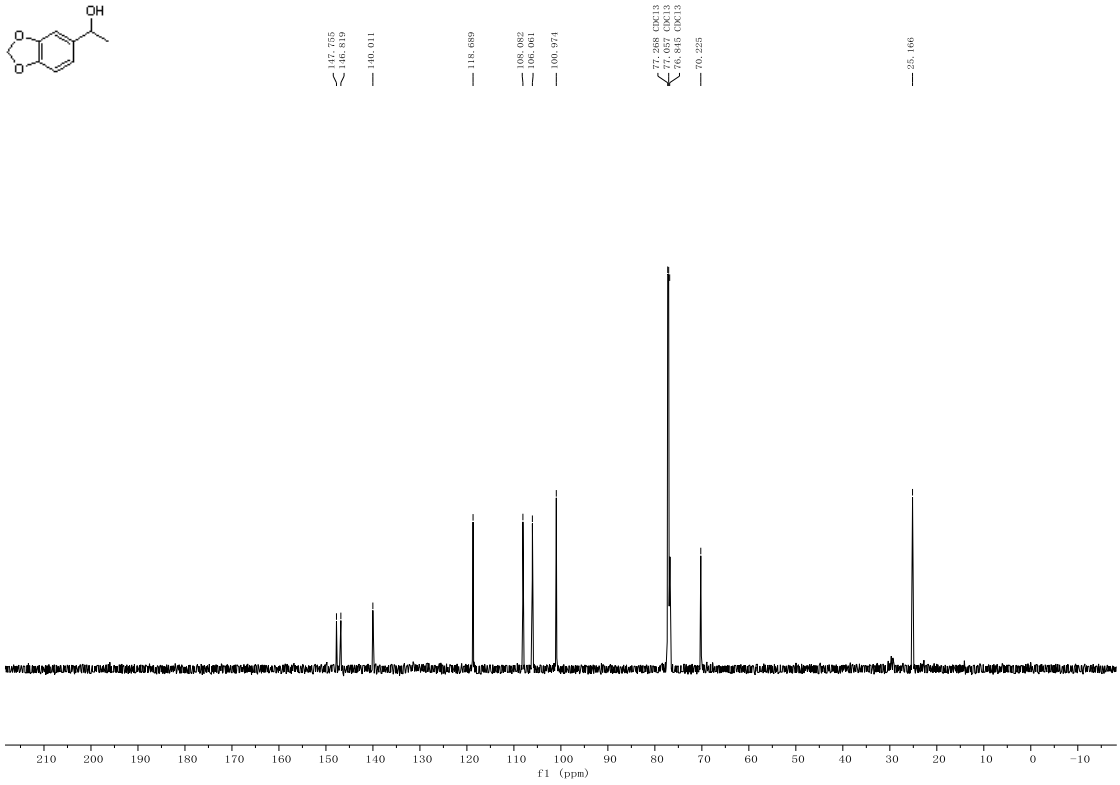

(*R*)-1-(Pyridin-3-yl)ethanol (8y).

^{1}H NMR (400 MHz, Chloroform-*d*)

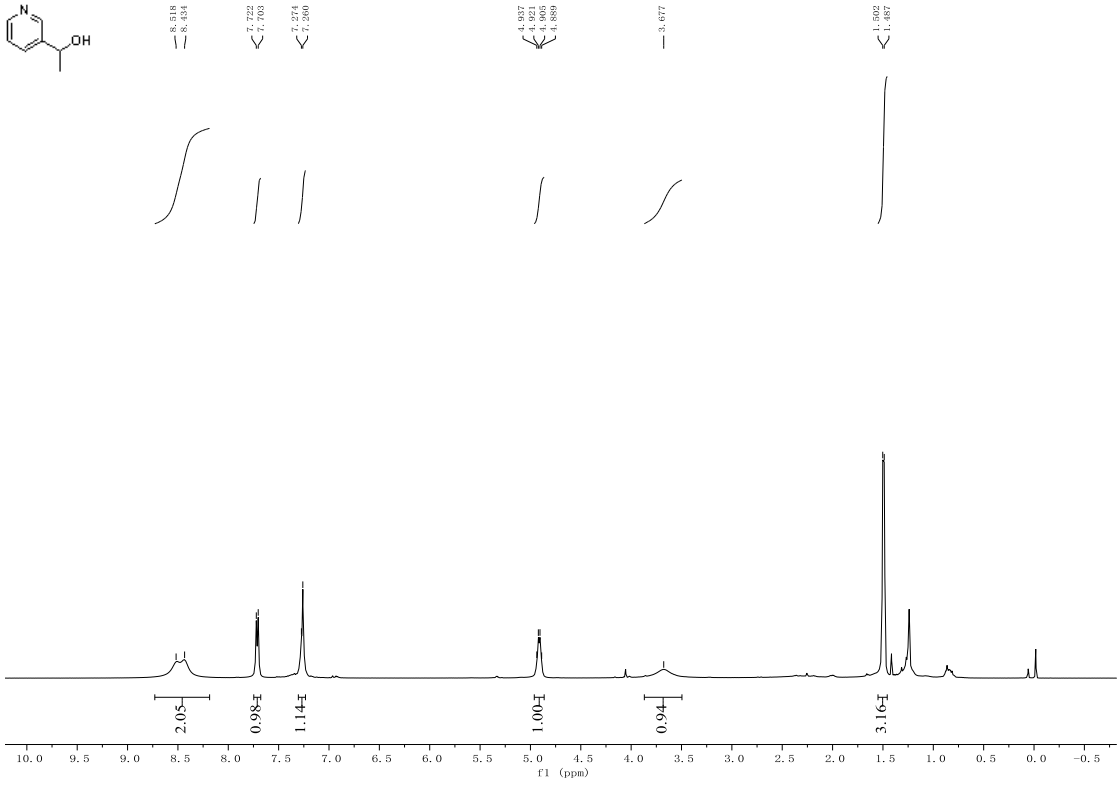

^{13}C NMR (101 MHz, Chloroform-*d*)

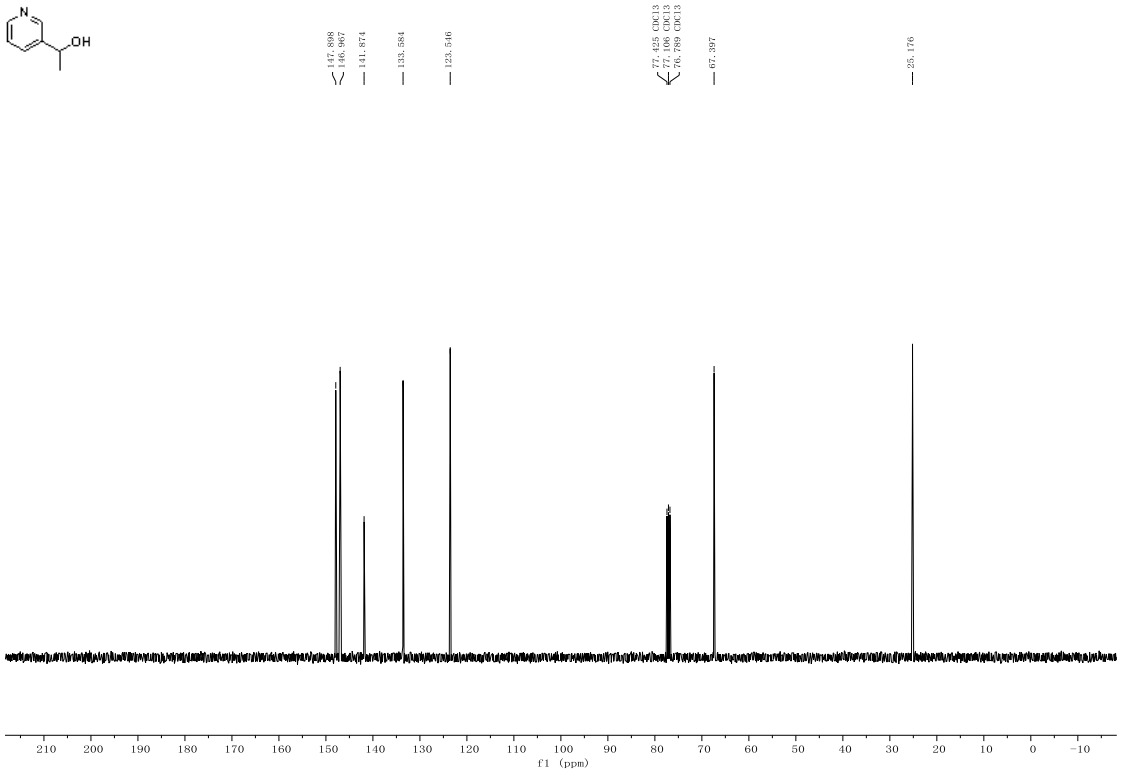

(*R*)-1-(Pyridin-4-yl)ethanol (8z).

^{1}H NMR (400 MHz, Chloroform-*d*)

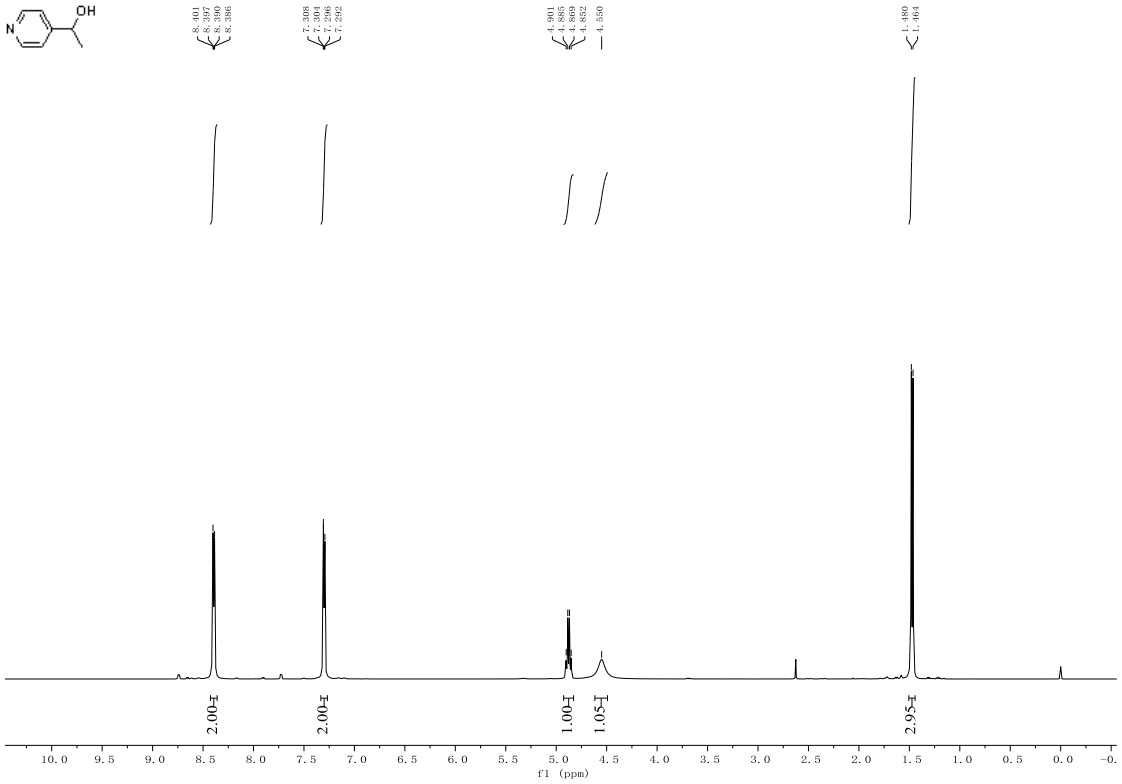

^{13}C NMR (101 MHz, Chloroform-*d*)

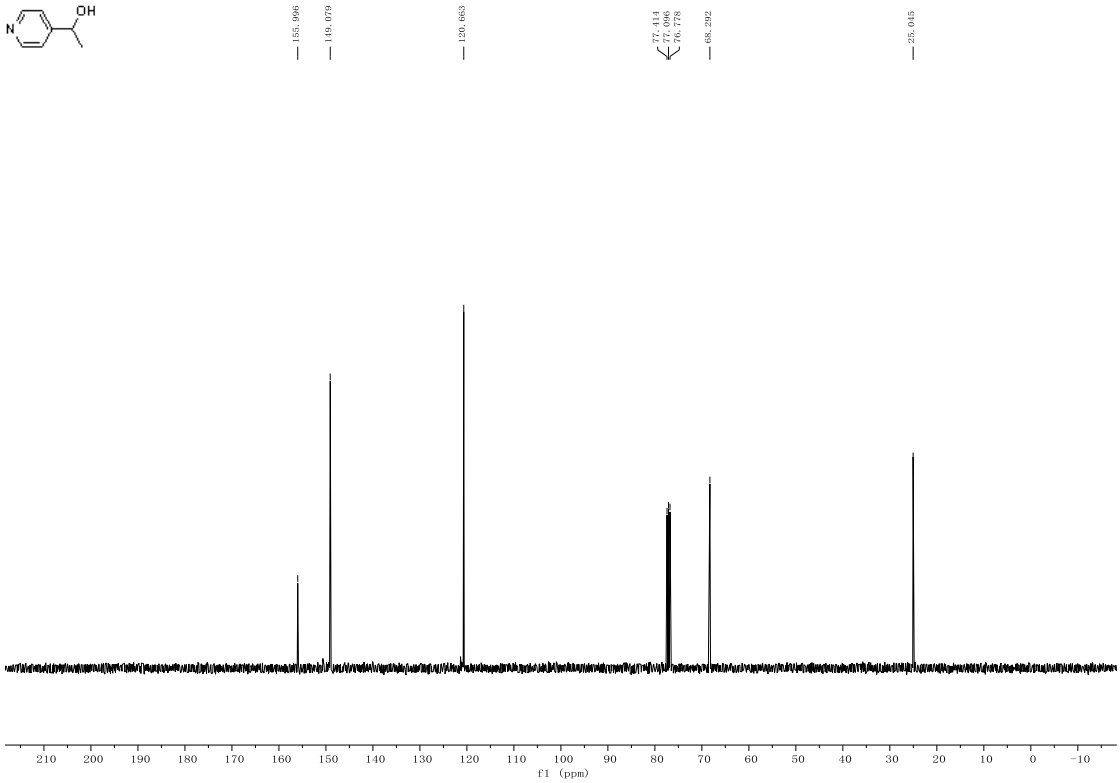

(*R*)-1-Phenylpropan-1-ol (8aa).

^{1}H NMR (400 MHz, Chloroform-*d*)

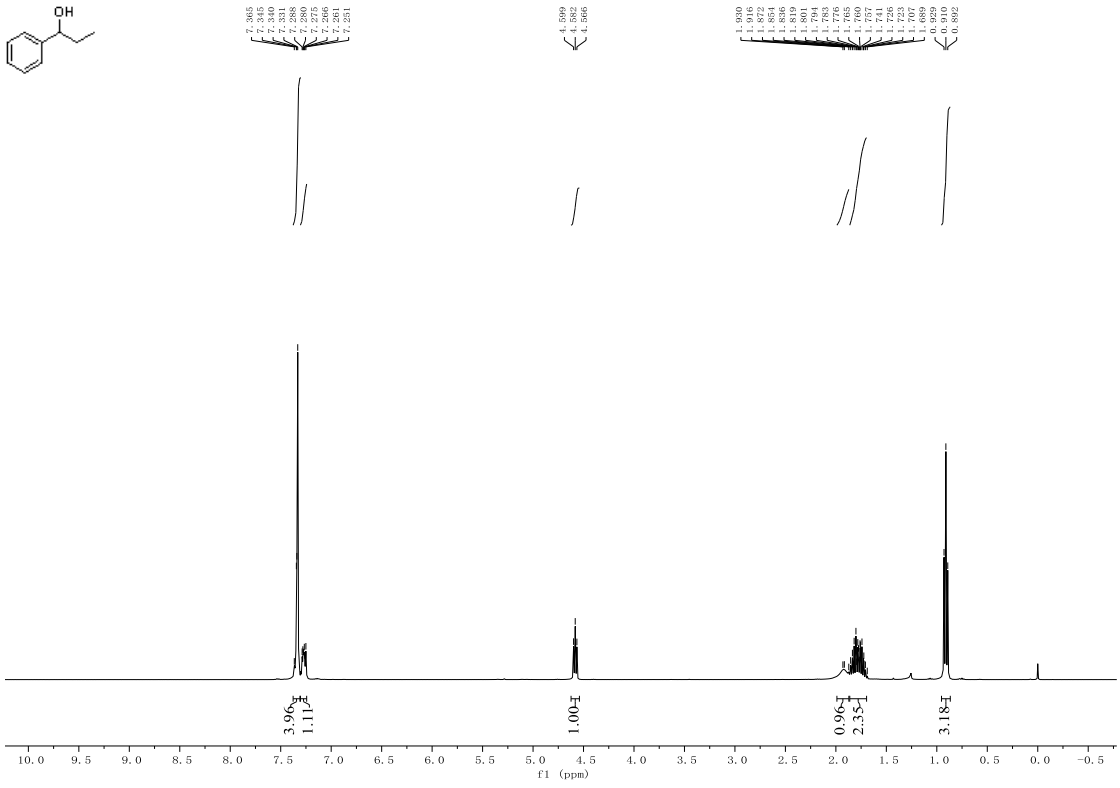

^{13}C NMR (101 MHz, Chloroform-*d*)

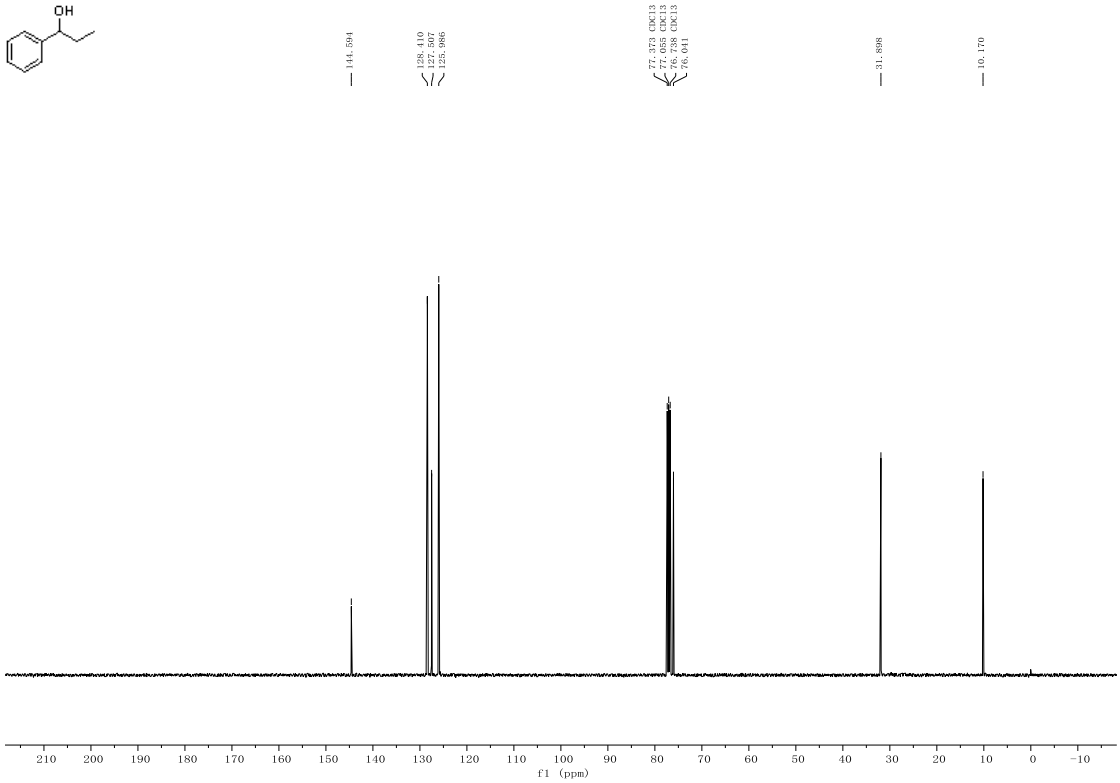

(*R*)-1-(*p*-Tolyl)propan-1-ol (8ab).

^{1}H NMR (400 MHz, Chloroform-*d*)

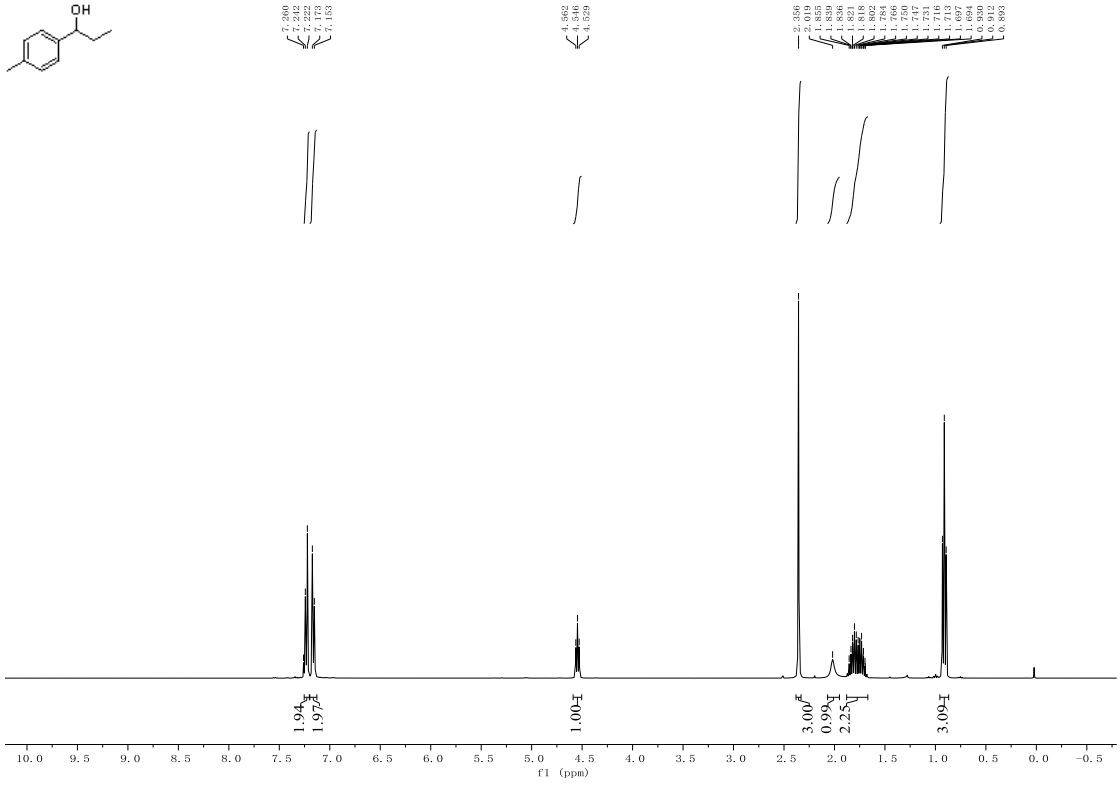

^{13}C NMR (101 MHz, Chloroform-*d*)

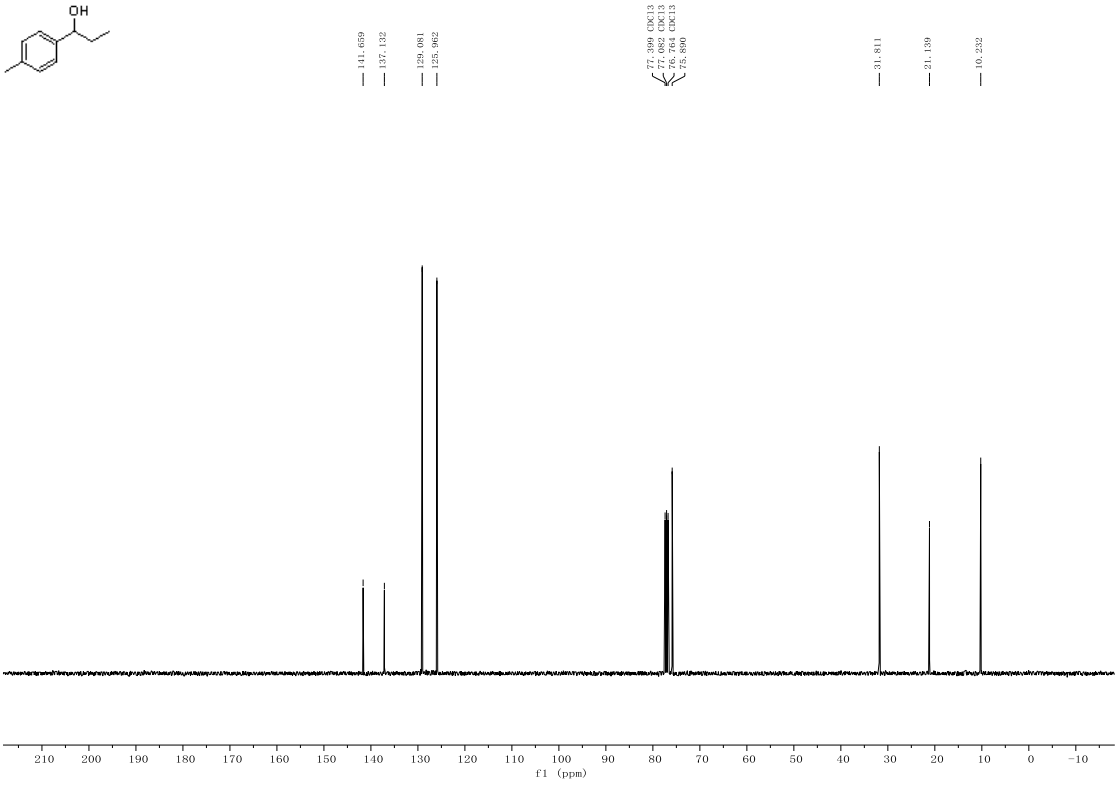

(*R*)-1-Phenylbutan-1-ol (8ac).

^{1}H NMR (400 MHz, Chloroform-*d*)

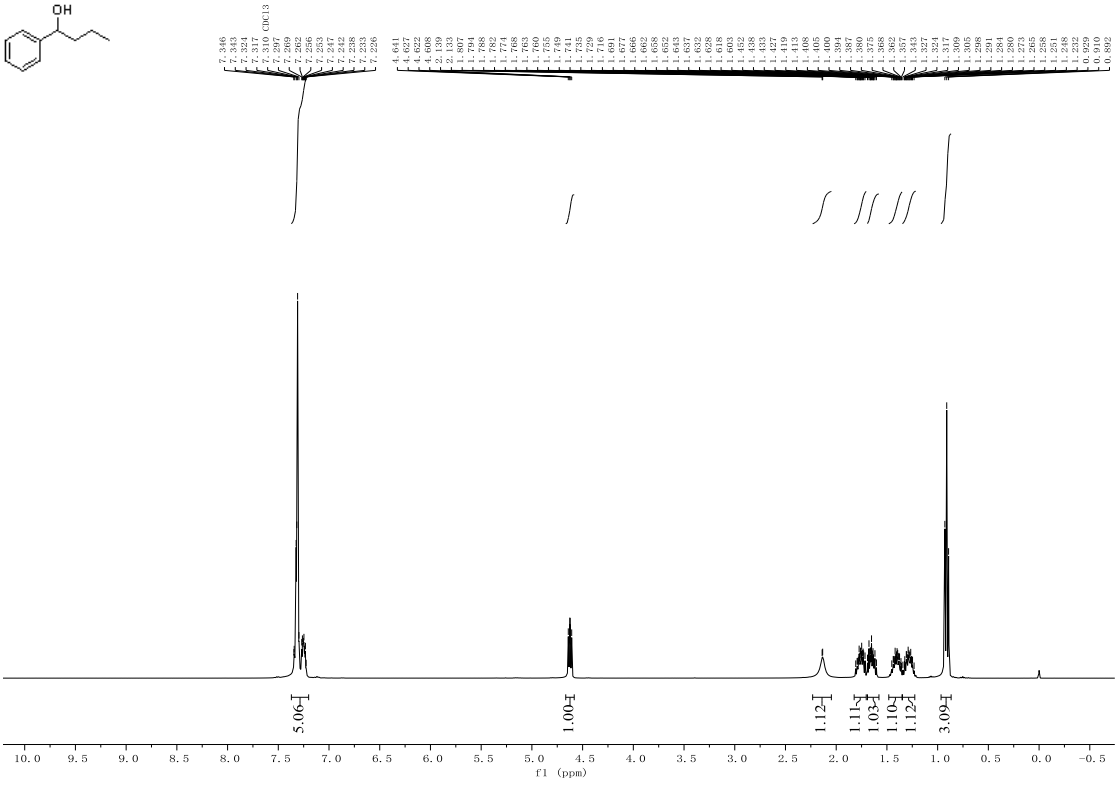

^{13}C NMR (101 MHz, Chloroform-*d*)

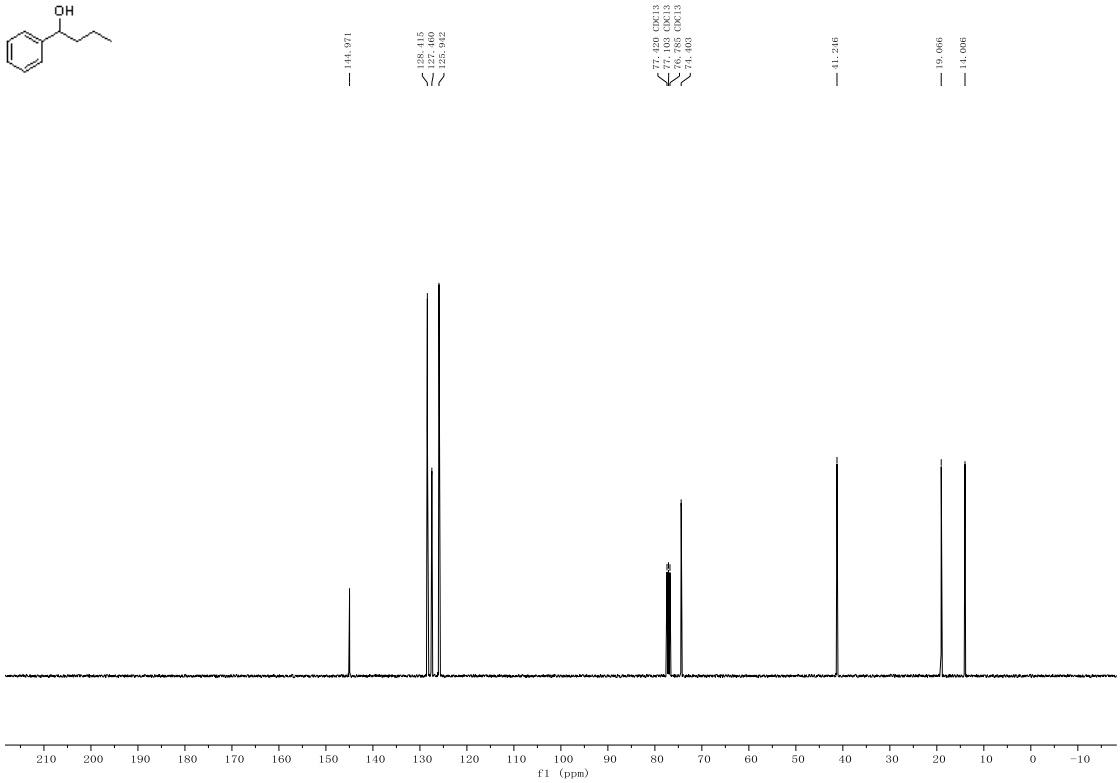

(*R*)-Cyclopropyl(phenyl)methanol (8ad).

^{1}H NMR (600 MHz, Chloroform-*d*)

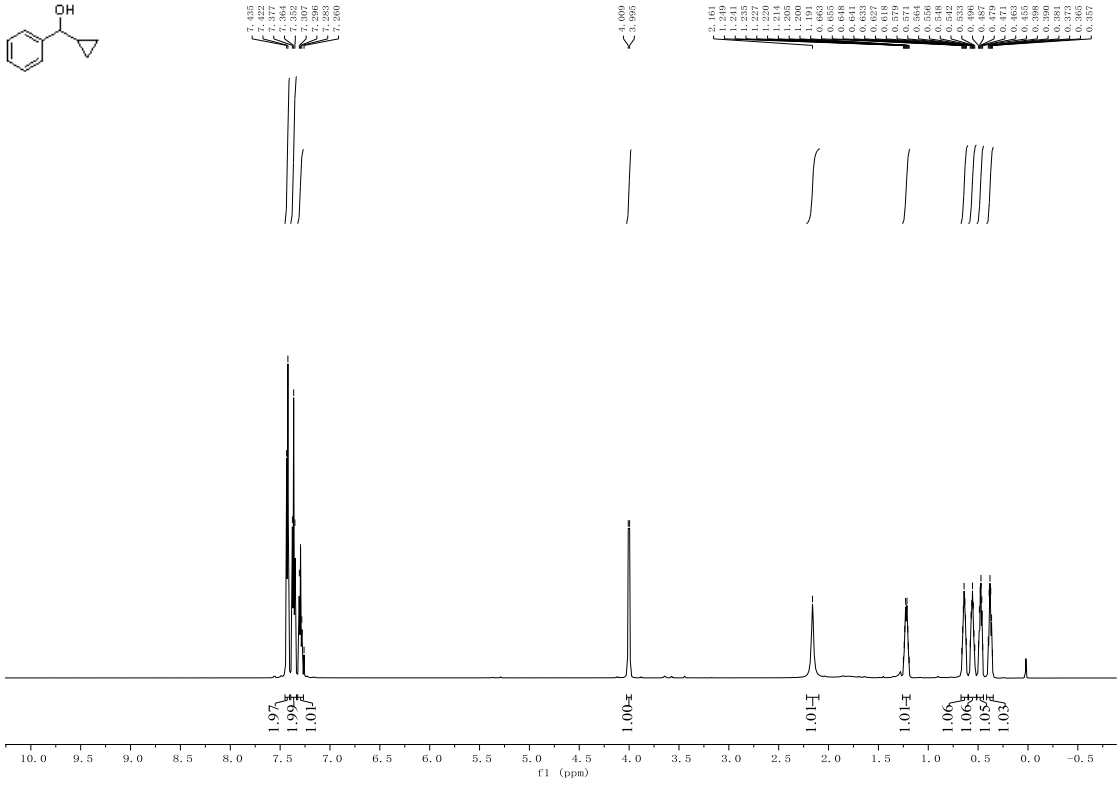

^{13}C NMR (151 MHz, Chloroform-*d*)

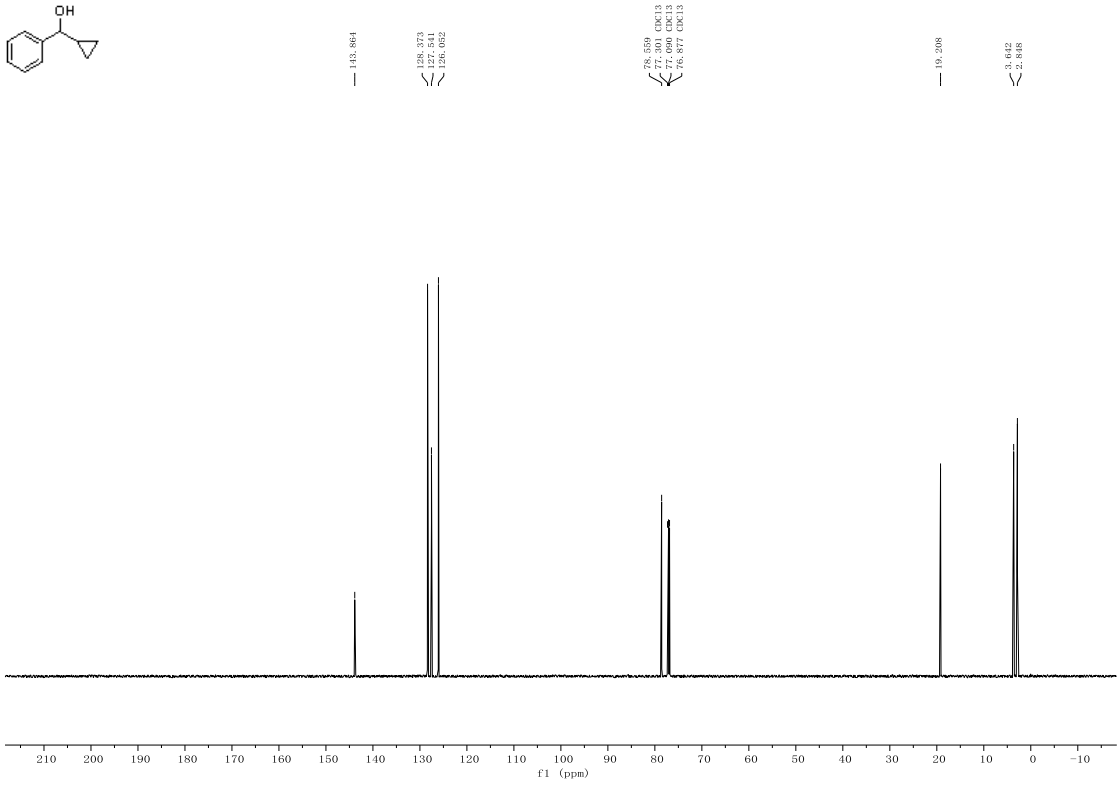

(*R*)-2-Methyl-1-phenylpropan-1-ol (8ae).

^{1}H NMR (400 MHz, Chloroform-*d*)

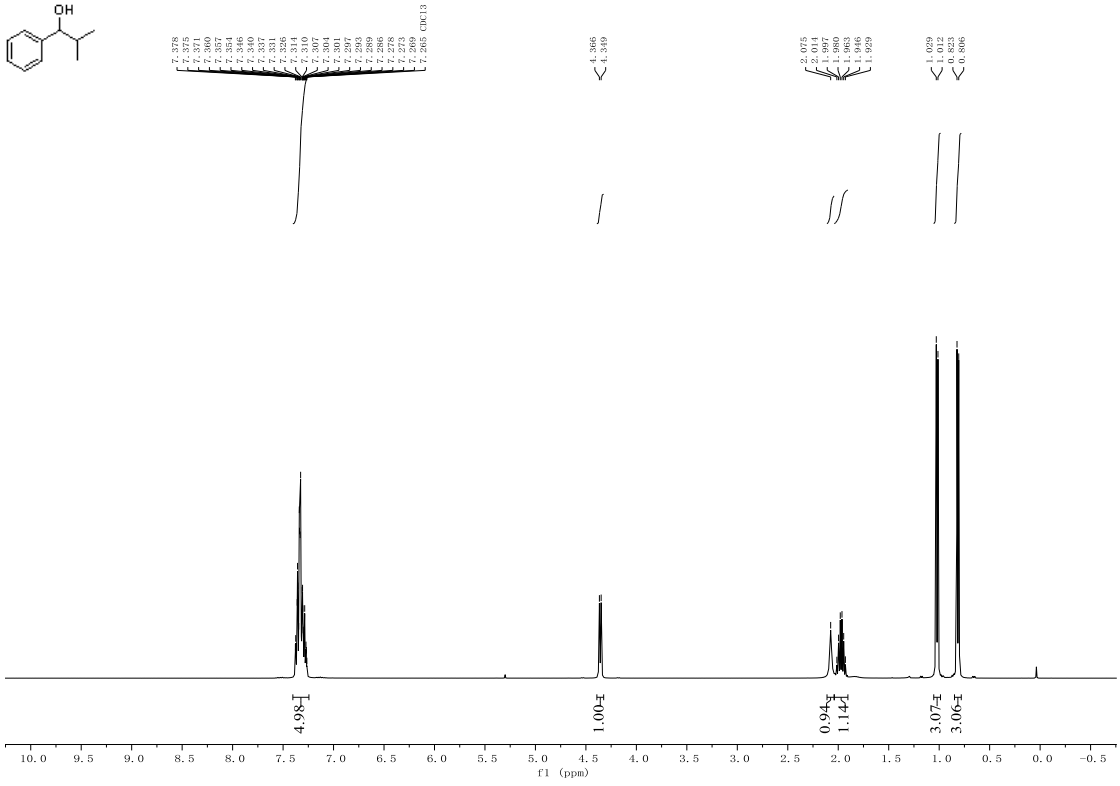

^{13}C NMR (101 MHz, Chloroform-*d*)

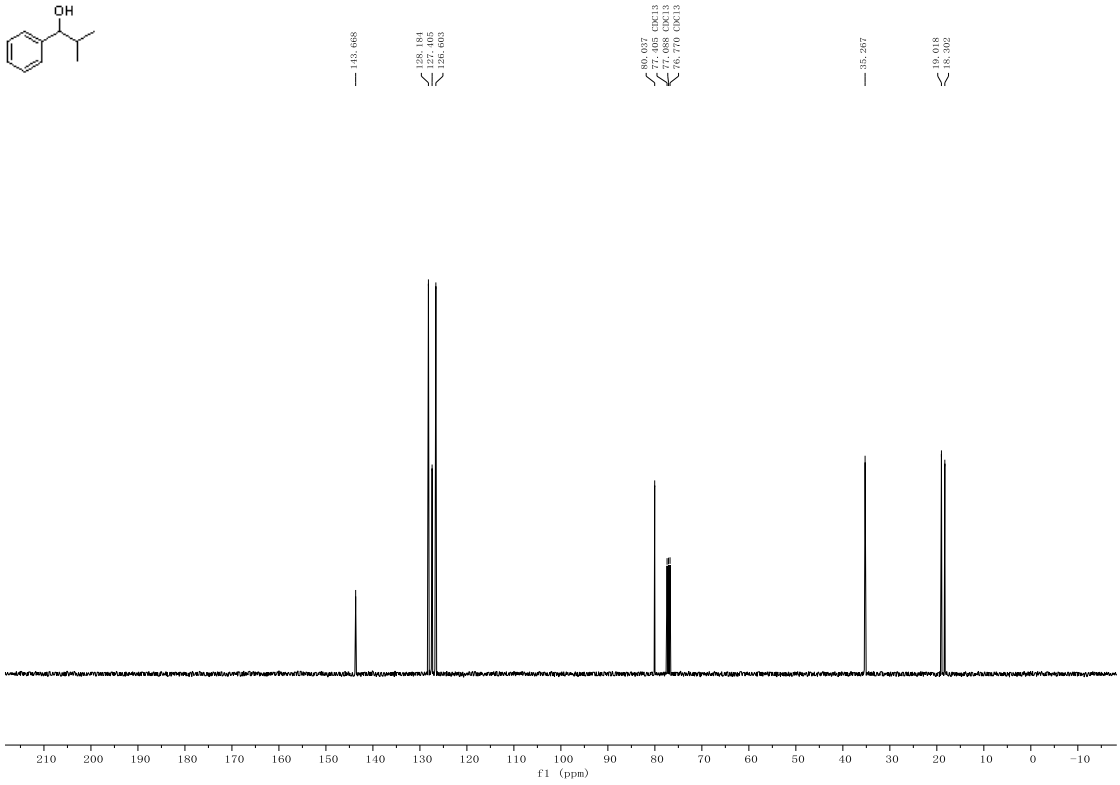

(*S*)-2,2,2-Trifluoro-1-phenylethanol (8af).

^{1}H NMR (600 MHz, Chloroform-*d*)

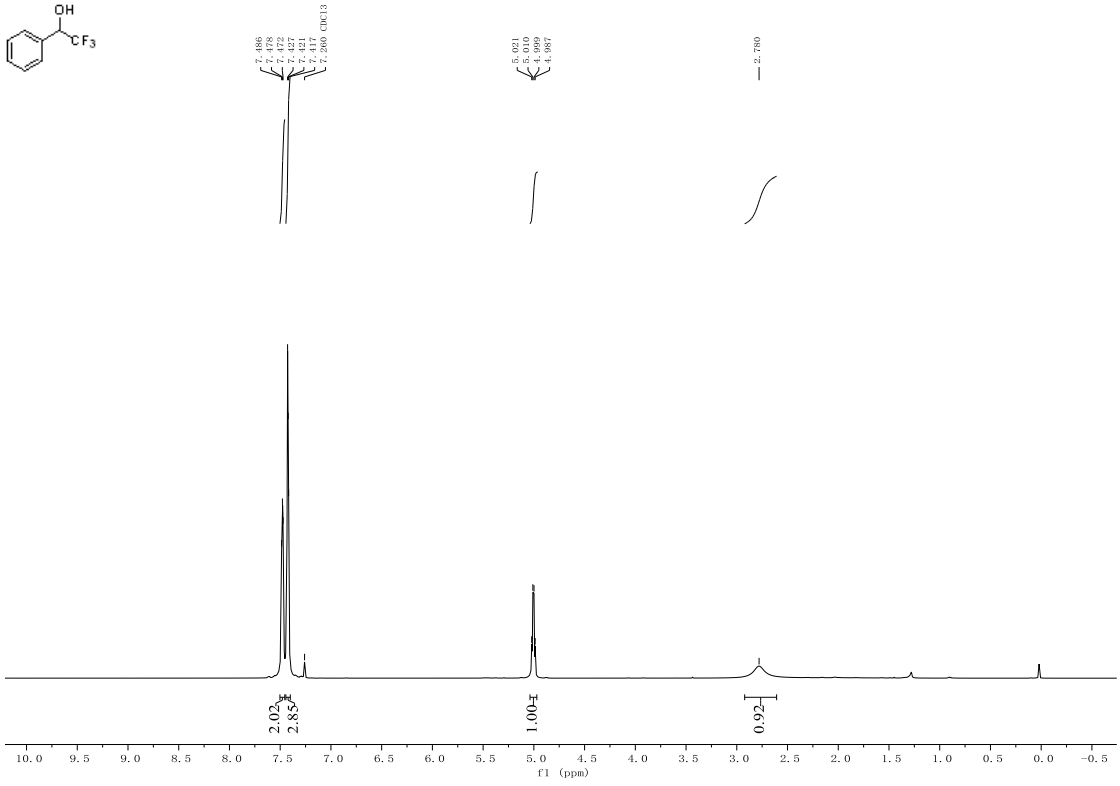

^{13}C NMR (151 MHz, Chloroform-*d*)

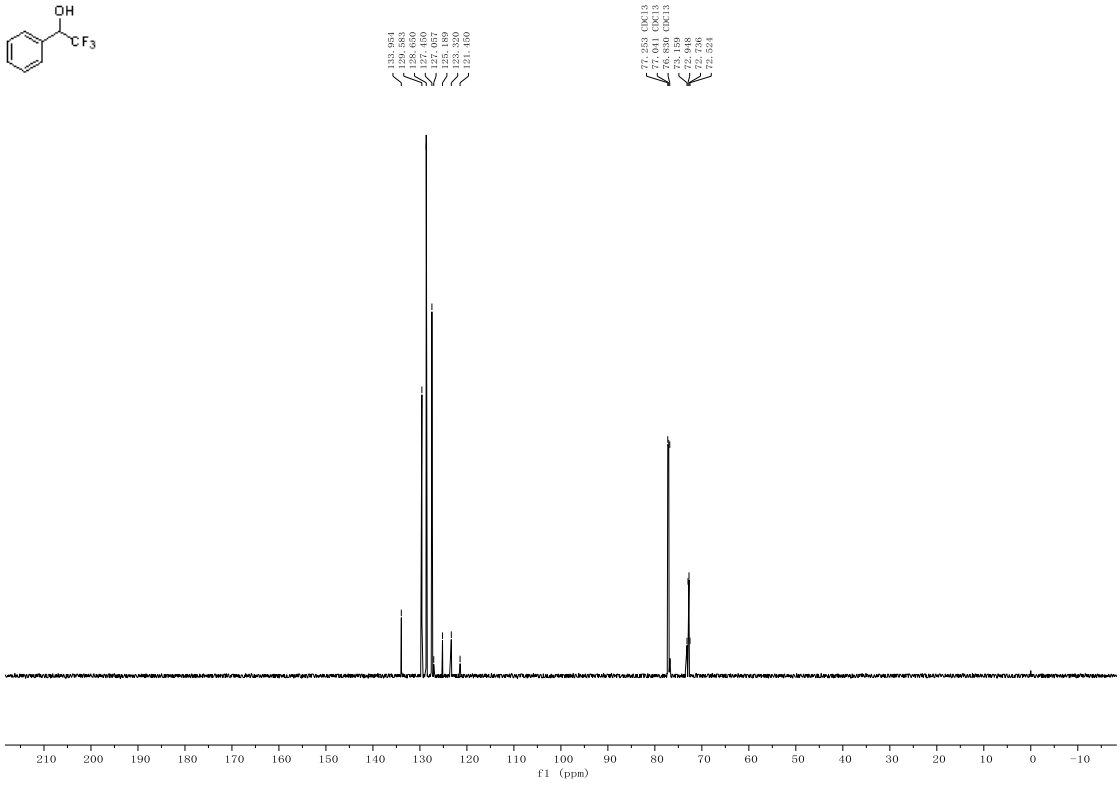

^{19}F NMR (565 MHz, Chloroform-*d*)

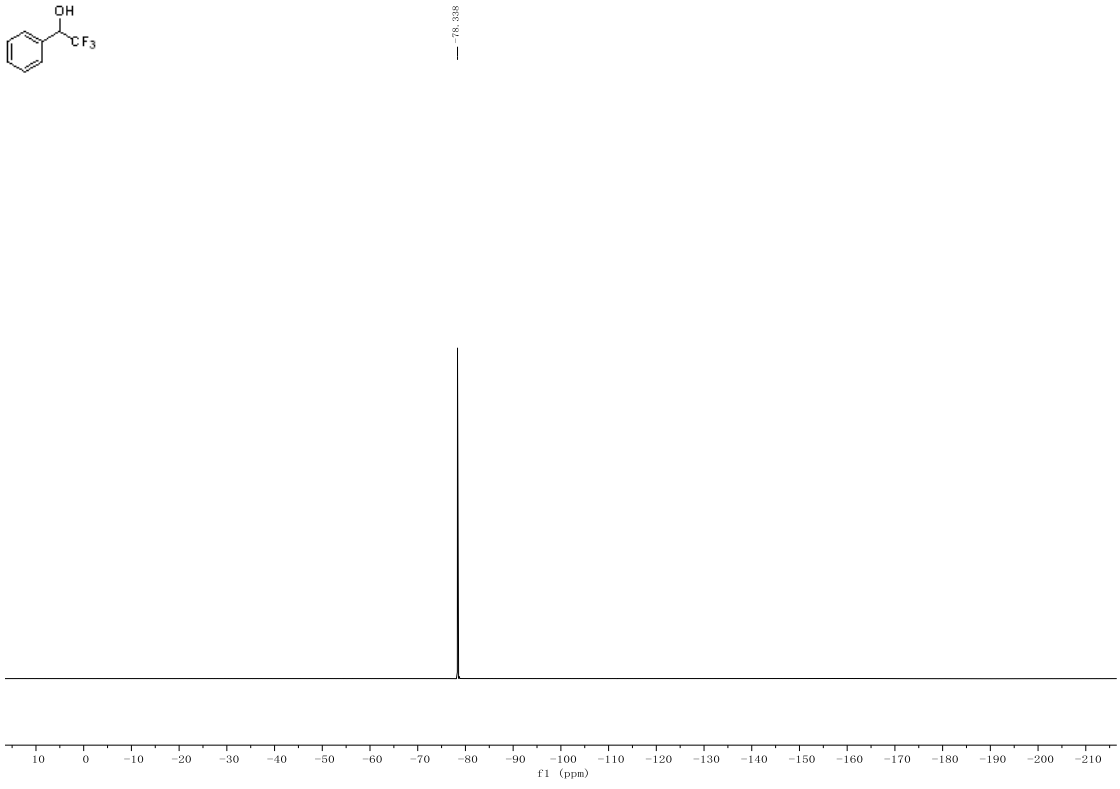

(*S*)-1-(4-Bromophenyl)-2,2,2-trifluoroethanol (8ag).

^{1}H NMR (400 MHz, Chloroform-*d*)

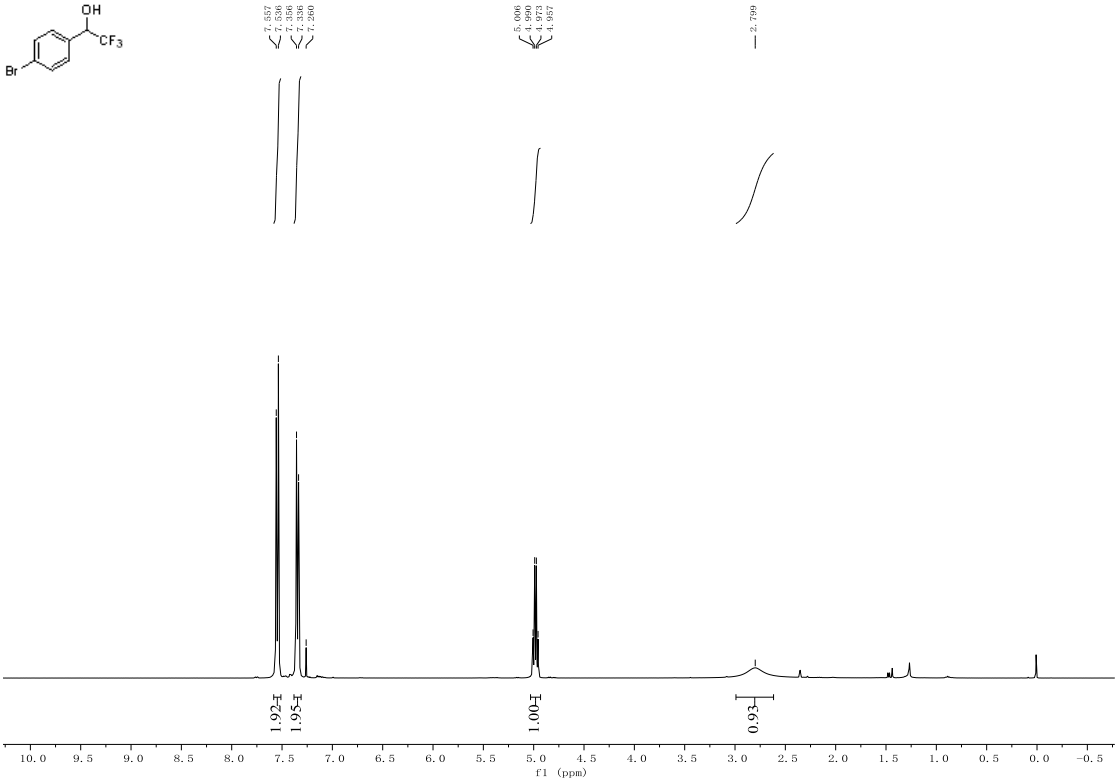

^{13}C NMR (101 MHz, Chloroform-*d*)

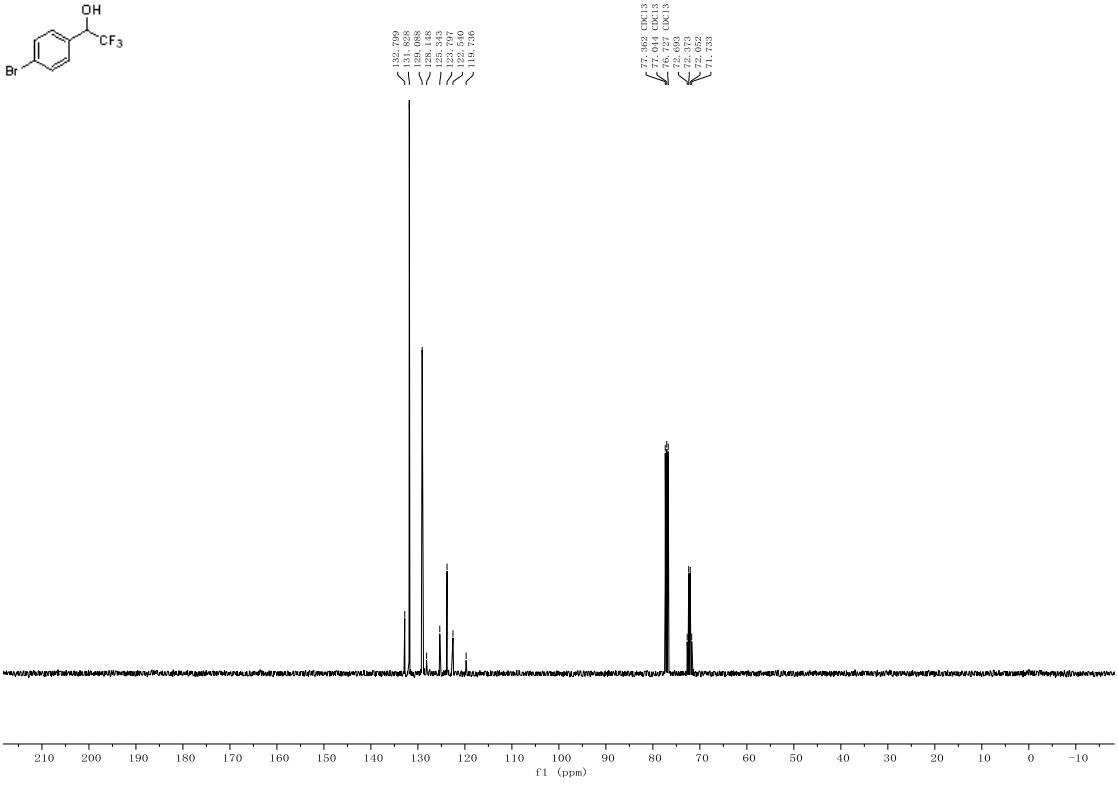

^{19}F NMR (376 MHz, Chloroform-*d*)

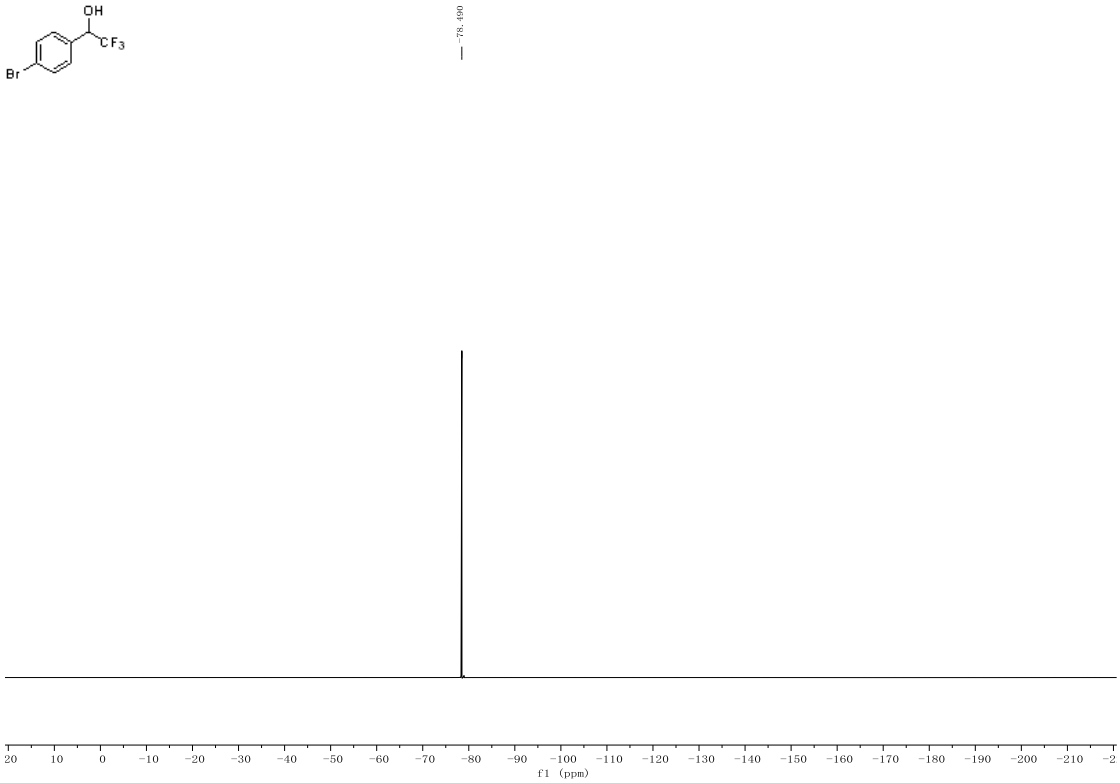

(*R*)-1-Cyclopropylethanol (8ah).

^{1}H NMR (600 MHz, Chloroform-*d*)

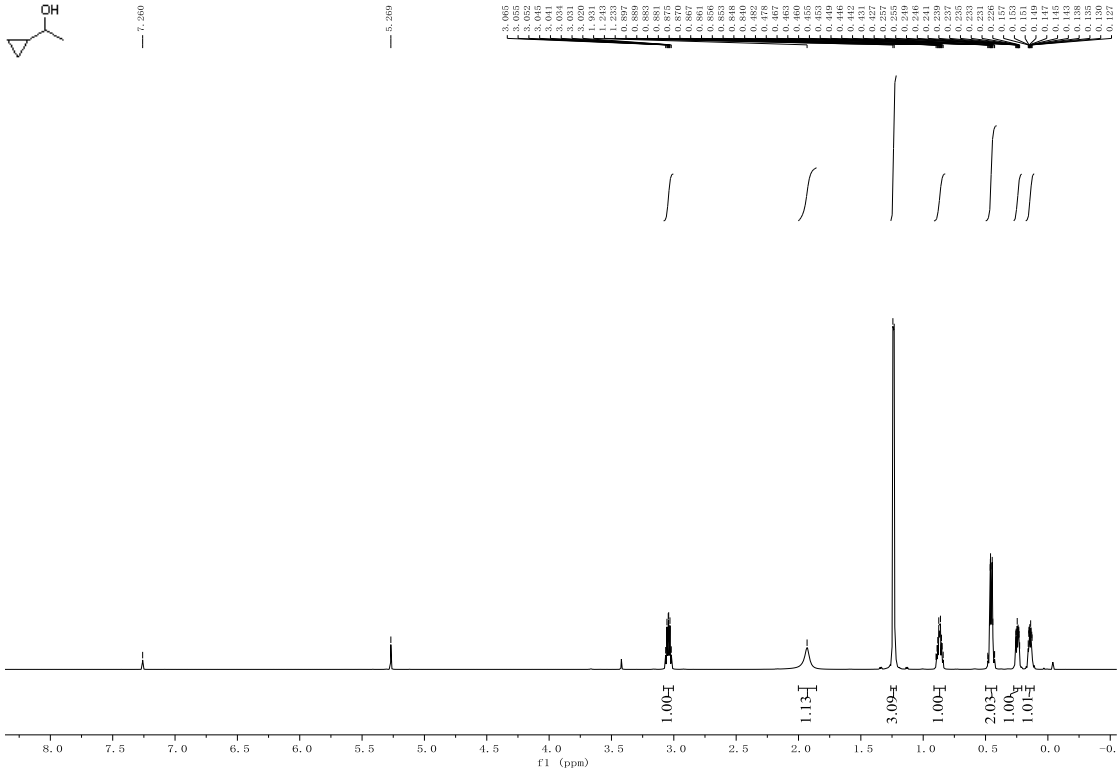

^{13}C NMR (151 MHz, Chloroform-*d*)

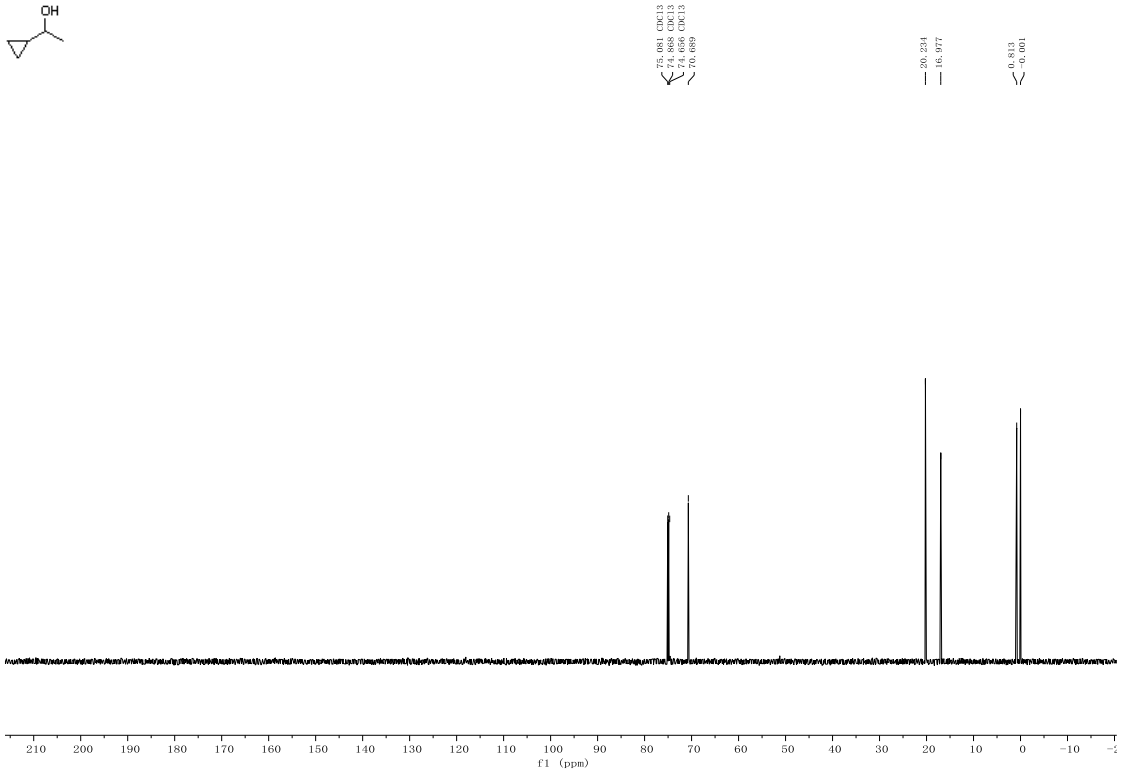

(*R*)-1-Cyclohexylethanol (8ai).

^{1}H NMR (400 MHz, Chloroform-*d*)

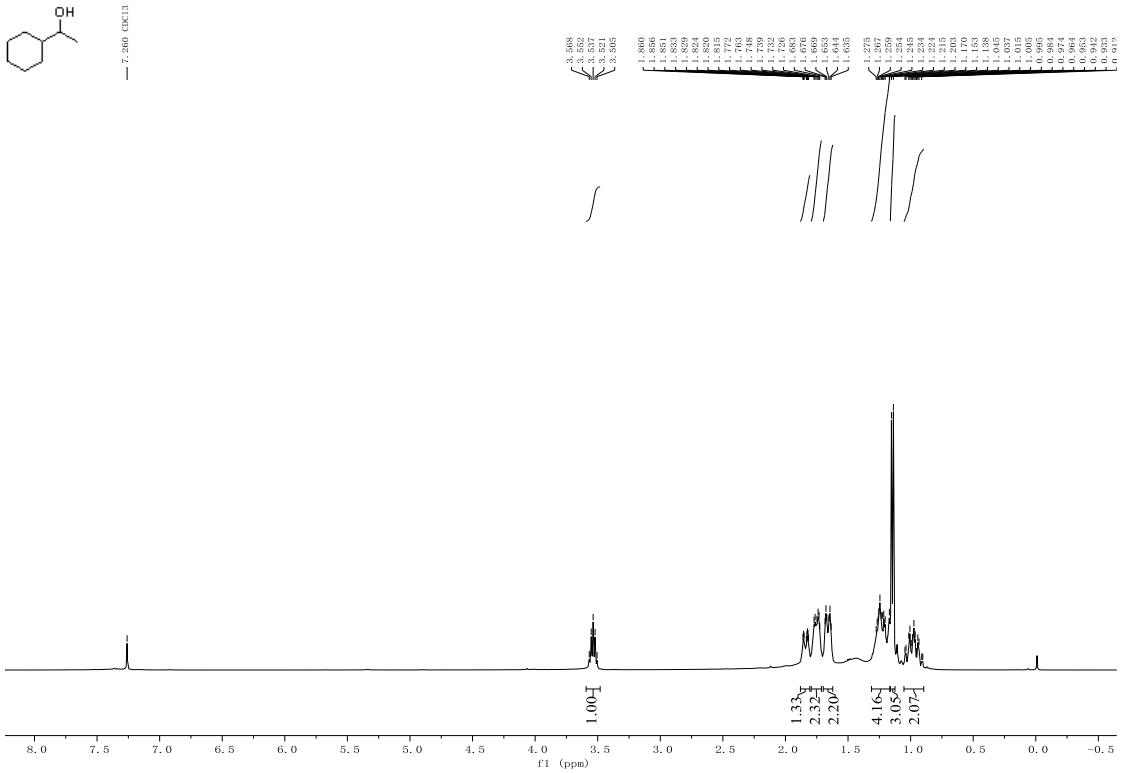

^{13}C NMR (151 MHz, Chloroform-*d*)

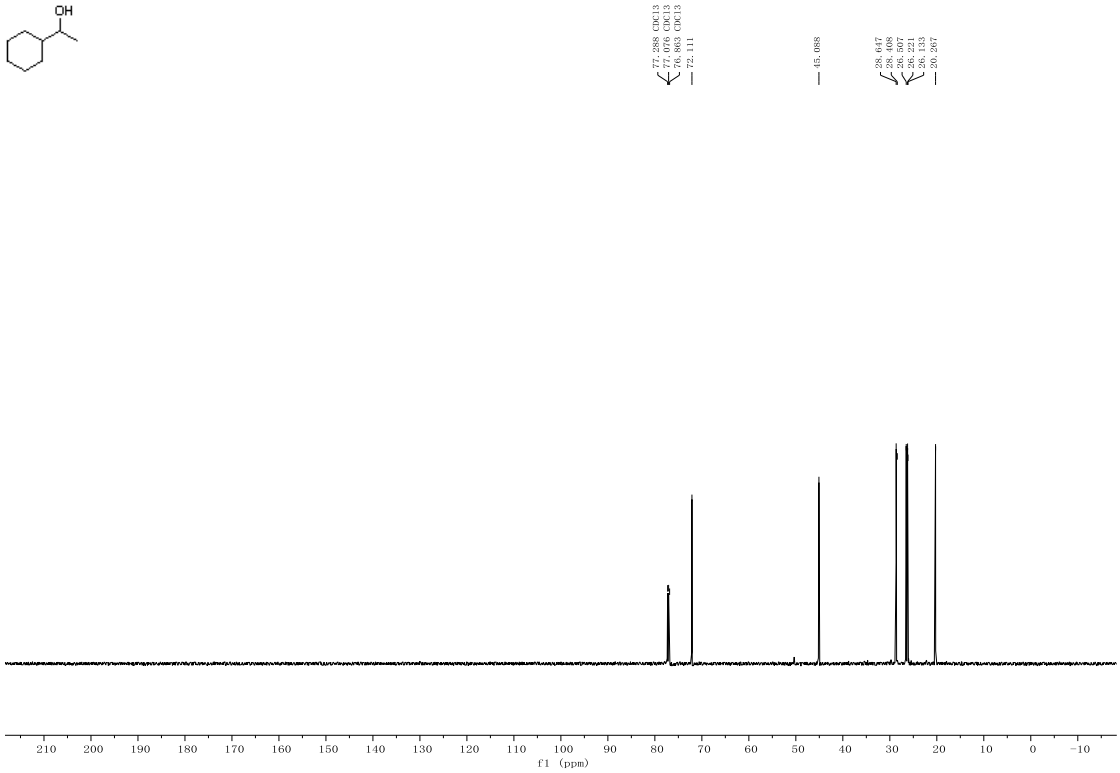

(3*R*,4*S*)-4-(4-(benzyloxy)phenyl)-1-(4-fluorophenyl)-3-((*R*)-3-(4-fluorophenyl)-3-hydroxypropyl)azetidin-2-one (8aj).

^{1}H NMR (600 MHz, Chloroform-*d*)

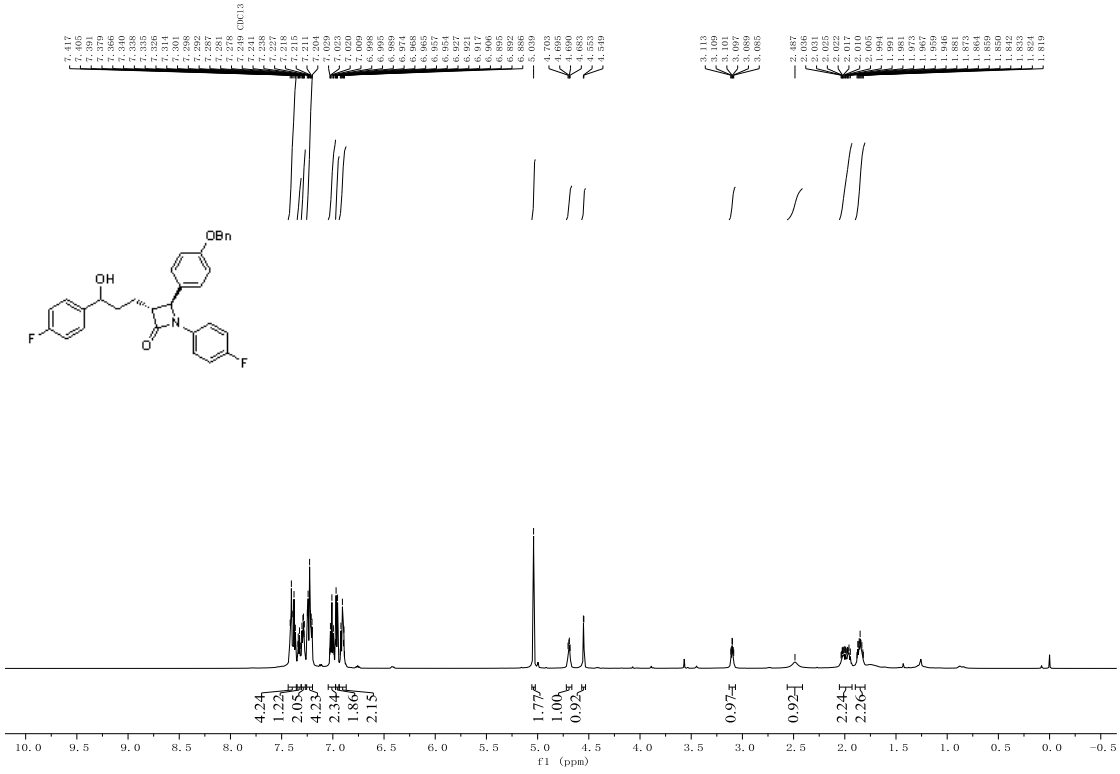

^{13}C NMR (151 MHz, Chloroform-*d*)

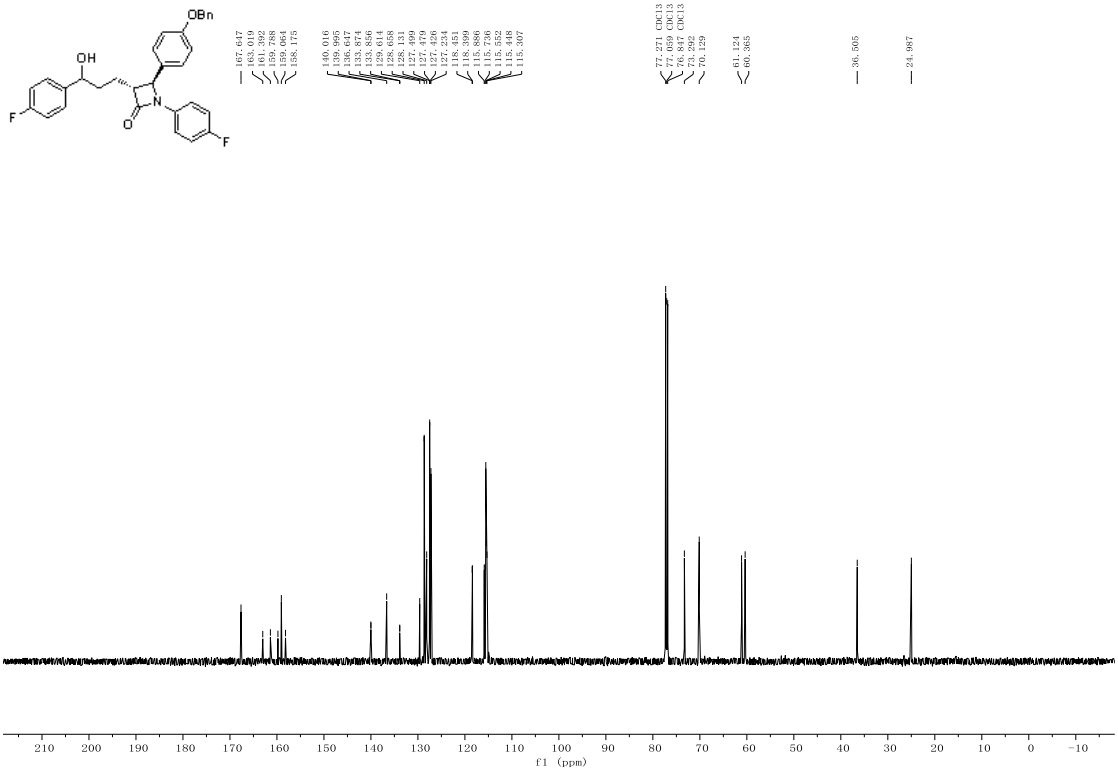

^{19}F NMR (565 MHz, Chloroform-*d*)

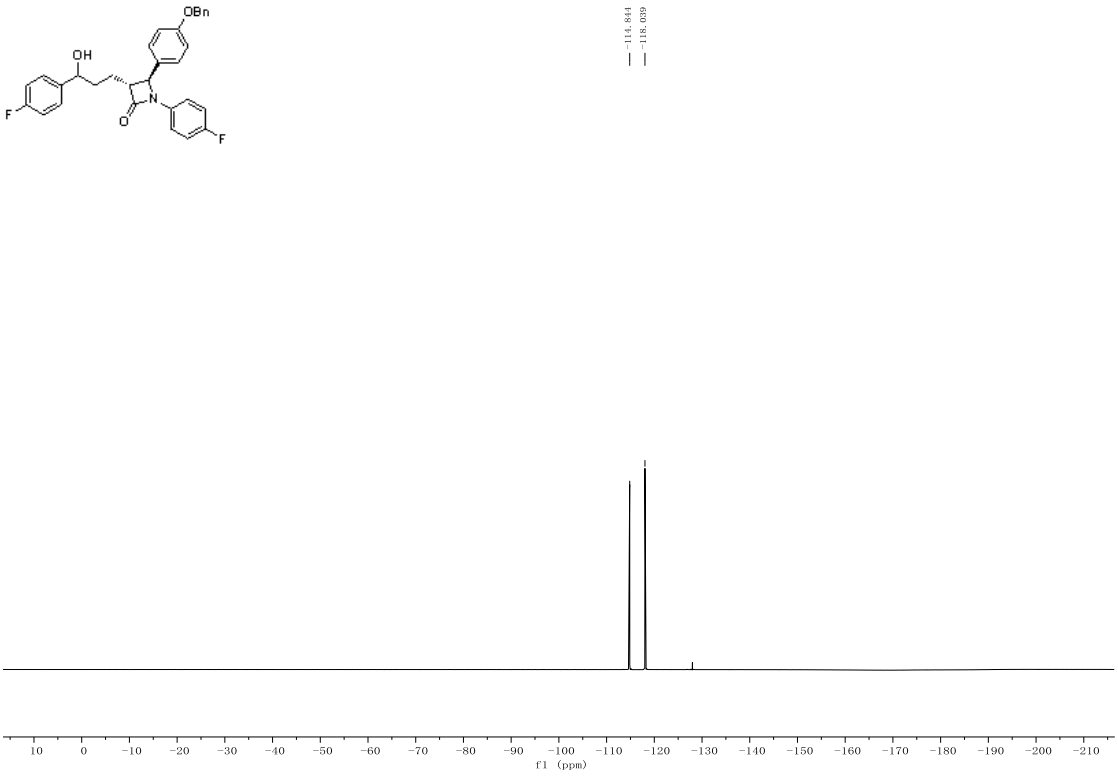

2.9 References

[1] R. Noyori, T. Ohkuma, *Angewandte Chemie International Edition* **2001**, *40*, 40-73.

[2] J.-H. Xie, X.-Y. Liu, J.-B. Xie, L.-X. Wang, Q.-L. Zhou, *Angewandte Chemie International Edition* **2011**, *50*, 7329-7332.

[3] W. Wu, S. Liu, M. Duan, X. Tan, C. Chen, Y. Xie, Y. Lan, X.-Q. Dong, X. Zhang, *Organic Letters* **2016**, *18*, 2938-2941.

[4] Y.-Y. Li, S.-L. Yu, W.-Y. Shen, J.-X. Gao, *Accounts of Chemical Research* **2015**, *48*, 2587-2598.

[5] C. Sui-Seng, F. Freutel, A. J. Lough, R. H. Morris, *Angewandte Chemie International Edition* **2008**, *47*, 940-943.

[6] A. Mikhailine, A. J. Lough, R. H. Morris, *Journal of the American Chemical Society* **2009**, *131*, 1394-1395.

[7] N. Meyer, A. J. Lough, R. H. Morris, *Chemistry – A European Journal* **2009**, *15*, 5605-5610.

[8] W. Zuo, J. Lough Alan, F. Li Young, H. Morris Robert, *Science* **2013**, *342*, 1080-1083.

[9] Y. Li, S. Yu, X. Wu, J. Xiao, W. Shen, Z. Dong, J. Gao, *Journal of the American Chemical Society* **2014**, *136*, 4031-4039.

[10] P. O. Lagaditis, P. E. Sues, J. F. Sonnenberg, K. Y. Wan, A. J. Lough, R. H. Morris, *Journal of the American Chemical Society* **2014**, *136*, 1367-1380.

[11] R. Bigler, R. Huber, A. Mezzetti, *Angewandte Chemie International Edition* **2015**, *54*, 5171-5174.

[12] J. F. Sonnenberg, K. Y. Wan, P. E. Sues, R. H. Morris, *ACS Catalysis* **2017**, *7*, 316-326.

[13] L. De Luca, A. Mezzetti, *Angewandte Chemie International Edition* **2017**, *56*, 11949-11953.

[14] F. Kallmeier, R. Kempe, *Angewandte Chemie International Edition* **2018**, *57*, 46-60.

[15] M. B. Widegren, G. J. Harkness, A. M. Z. Slawin, D. B. Cordes, M. L. Clarke, *Angewandte Chemie International Edition* **2017**, *56*, 5825-5828.

[16] M. B. Widegren, M. L. Clarke, *Catalysis Science & Technology* **2019**, *9*, 6047-6058.

[17] L. Zhang, Y. Tang, Z. Han, K. Ding, *Angewandte Chemie International Edition* **2019**, *58*, 4973-4977.

[18] K. Z. Demmans, M. E. Olson, R. H. Morris, *Organometallics* **2018**, *37*, 4608-4618.

[19] D. Wang, A. Bruneau-Voisine, J.-B. Sortais, *Catalysis Communications* **2018**, *105*, 31-36.

[20] F. Ling, H. Hou, J. Chen, S. Nian, X. Yi, Z. Wang, D. Song, W. Zhong, *Organic Letters* **2019**, *21*, 3937-3941.

[21] L. Alig, M. Fritz, S. Schneider, *Chemical Reviews* **2019**, *119*, 2681-2751.

[22] A. Zirakzadeh, S. R. M. M. de Aguiar, B. Stöger, M. Widhalm, K. Kirchner, *ChemCatChem* **2017**, *9*, 1744-1748.

[23] M. Garbe, K. Junge, S. Walker, Z. Wei, H. Jiao, A. Spannenberg, S. Bachmann, M. Scalone, M. Beller, *Angewandte Chemie International Edition* **2017**, *56*, 11237-11241.

[24] S. Elangovan, C. Topf, S. Fischer, H. Jiao, A. Spannenberg, W. Baumann, R. Ludwig, K. Junge, M. Beller, *Journal of the American Chemical Society* **2016**, *138*, 8809-8814.

[25] S. Elangovan, M. Garbe, H. Jiao, A. Spannenberg, K. Junge, M. Beller, *Angewandte Chemie International Edition*

2016, *55*, 15364-15368.

[26] B. Zhao, Z. Han, K. Ding, *Angewandte Chemie International Edition* **2013**, *52*, 4744-4788.

[27] P. A. Dub, J. C. Gordon, *Nature Reviews Chemistry* **2018**, *2*, 396-408.

[28] L. Falivene, Z. Cao, A. Petta, L. Serra, A. Poater, R. Oliva, V. Scarano, L. Cavallo, *Nature Chemistry* **2019**, *11*, 872-879.

[29] B. Yucel, B. Sanli, H. Soylemez, H. Akbulut, *Journal of Organometallic Chemistry* **2012**, *704*, 49-64.

[30] P. Barbaro, C. Bianchini, G. Giambastiani, A. Togni, *Tetrahedron Letters* **2003**, *44*, 8279-8283.

[31] M. Ito, A. Osaku, C. Kobayashi, A. Shiibashi, T. Ikariya, *Organometallics* **2009**, *28*, 390-393.

[32] J. Guo, J. Chen, Z. Lu, *Chemical Communications* **2015**, *51*, 5725-5727.

[33] C. A. S. P, A. Varenikov, G. d. Ruiter, *Organometallics* **2020**, *39*, 247-257.

[34] J. Yu, M. Duan, W. Wu, X. Qi, P. Xue, Y. Lan, X.-Q. Dong, X. Zhang, *Chemistry – A European Journal* **2017**, *23*, 970-975.

[35] Q. Xu, H. Zhou, X. Geng, P. Chen, *Tetrahedron* **2009**, *65*, 2232-2238.

[36] *Gaussian 16 (Wallingford, CT, 2016)*.

[37] M. Dolg, U. Wedig, H. Stoll, H. Preuss, *The Journal of Chemical Physics* **1987**, *86*, 866-872.

[38] G. A. Petersson, A. Bennett, T. G. Tensfeldt, M. A. Al‐Laham, W. A. Shirley, J. Mantzaris, *The Journal of Chemical Physics* **1988**, *89*, 2193-2218.

[39] G. A. Petersson, M. A. Al‐Laham, *The Journal of Chemical Physics* **1991**, *94*, 6081-6090.

[40] K. Fukui, *Accounts of Chemical Research* **1981**, *14*, 363-368.

[41] A. V. Marenich, C. J. Cramer, D. G. Truhlar, *The Journal of Physical Chemistry B* **2009**, *113*, 6378-6396.

Chapter 3 Ferrocene-based Secondary Phosphine Oxide Ligands for Cobalt-Catalysed Enantioselective Hydrogenation of Ketones

3.1 Introduction

This chapter describes further research on the asymmetric hydrogenation (AH) of ketones catalysed by earth-abundant transition metals. As described in Chapter 2, manganese has proven to be an efficient metal precursor for the AH of ketones. Herein, the focus is on the study of cobalt catalysis. As another inexpensive transition metal, despite less abundant than manganese in the Earth's crust,[1] cobalt is a promising metal for catalysis and has shown supreme catalytic abilities in the asymmetric hydrogenation of alkenes and imines (for details, see 1.1.3.2 in Chapter 1). However, the cobalt-catalysed AH of ketones is underdeveloped and has been rarely reported.[2-3] Initial attempts made by Lemaire[4] and Gao[5] et al in the cobalt(II)-catalysed asymmetric transfer hydrogenation (ATH) of ketones gave low reactivities and enantioselectivities. In 2016, Gao and co-workers reported the first case of the AH of simple ketones using chiral Co(II)/**PNNP** complexes, affording moderate enantioselectivities for most ketone substrates.[6] Recently, Tang and co-workers developed a chiral Co(II)/**PNN** complex combined with an achiral mono-phosphine ligand, which slightly increased the enantioselectivities for the AH of aryl alkyl ketones.[7]

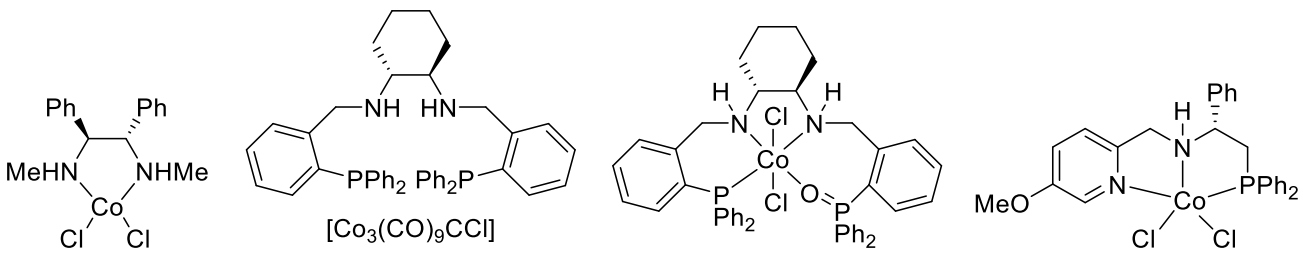

Lemaire 1997 ATH | **Gao 2003 ATH** | **Gao 2016 AH** | **Tang 2020 AH**

Figure 3.1 Representative Co catalysts for the ATH and AH of ketones

Despite these efforts, the development of state-of-the-art chiral cobalt catalysts for the AH of ketones is still a significant challenge. In contrast to octahedral Mn(I) and Fe(II) complexes, many divalent cobalt complexes do not possess a stable 18 e^- structure. Unpaired electrons on the metal centre can

potentially cause one-electron processes, which can bring about different reaction mechanisms.[1] On the other hand, the philosophy of chiral ligand design for octahedral complexes is often not suitable for the trigonal bipyramidal, square pyramidal or tetrahedral geometries often favoured by Co(II) complexes. Based on these considerations, there is always the opportunity to explore novel chiral ligand systems for the cobalt-catalysed AH of ketones.

Secondary phosphine oxides (**SPO**) are a class of special phosphorus ligands,[8-12] existing a tautomeric equilibrium between the pentavalent phosphine oxide and trivalent phosphinous acid. The equilibrium is generally in favour of the phosphine oxide, while it shifts towards the phosphinous acid upon coordination to a transition metal. Some **SPO**-Metal complexes have been developed as effective catalysts for AH over the last two decades.[13-17] Recently, however, it was found that bis-ferrocene-based secondary phosphine oxide ligands (**Fc-SPO**) could bind to $CoCl_2$ in an unusual way, via PO bidentate instead of the expected PPP tridentate coordination to the metal centre. Surprisingly, the resulting cobalt complexes (**Fc-SPO-Co**) showed good catalytical ability in the AH of ketones, especially for aryl-aryl ketones, providing high reactivities (up to 99% yield) and enantioselectivities (up to 92% ee) (Scheme 3.1).

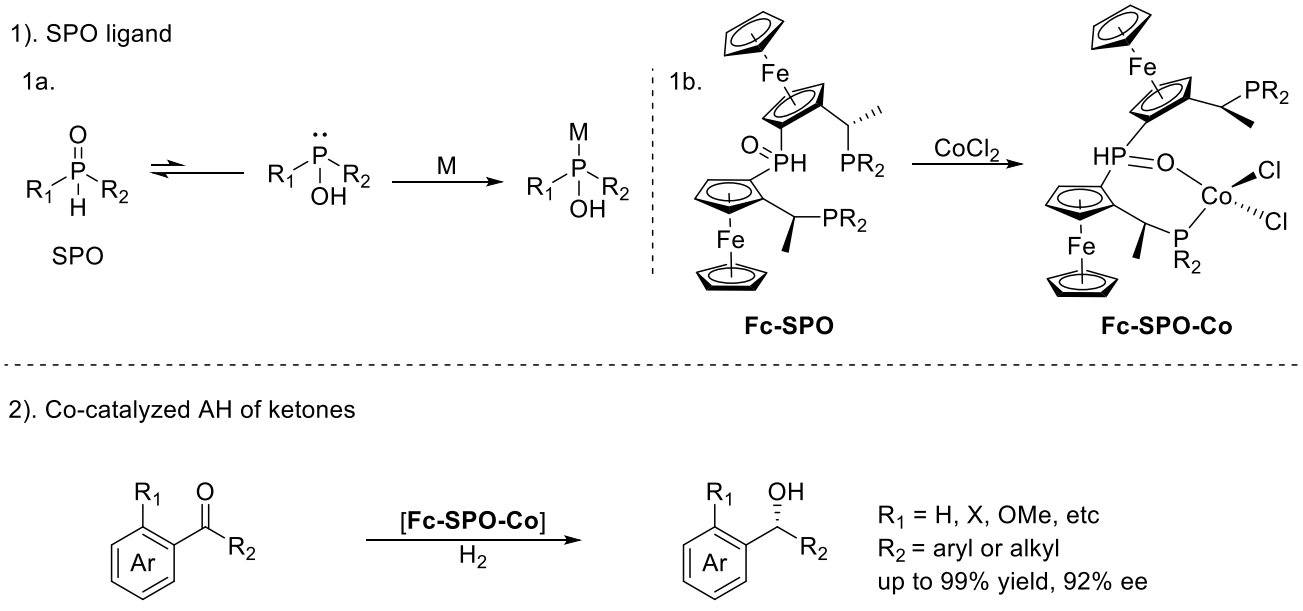

Scheme 3.1 1a). General coordination model of **SPO** ligands with metals. 1b). Unusual coordination of **Fc-SPO** ligands with $CoCl_2$. 2). **Fc-SPO**-Co complexes for the AH of ketones

3.2 Synthesis of Fc-SPO ligands

Fc-SPO ligands **L1** – **L2** were synthesized successfully, albeit in low to moderate yields (Scheme 3.2). Compounds **2** and **3** had been made previously from commercially available Ugi's amine as described in Chapter 2. After the lithium-halogen exchange of compounds **3a** and **3b** with *n*-BuLi, followed by treatment with 0.5 eq. of dichloro(diethylamino)phosphine, the mixture was quenched with diluted hydrochloric acid, giving the products **L1** and **L2** respectively.[17] Unfortunately, when the phenyl group on the phosphorus atom was replaced by cyclohexyl or tert-butyl groups in reactions with compound **2**, the expected ligands were not obtained successfully. This was presumably due to steric hindrance from these bulky groups, which prevented C-P bond formation.

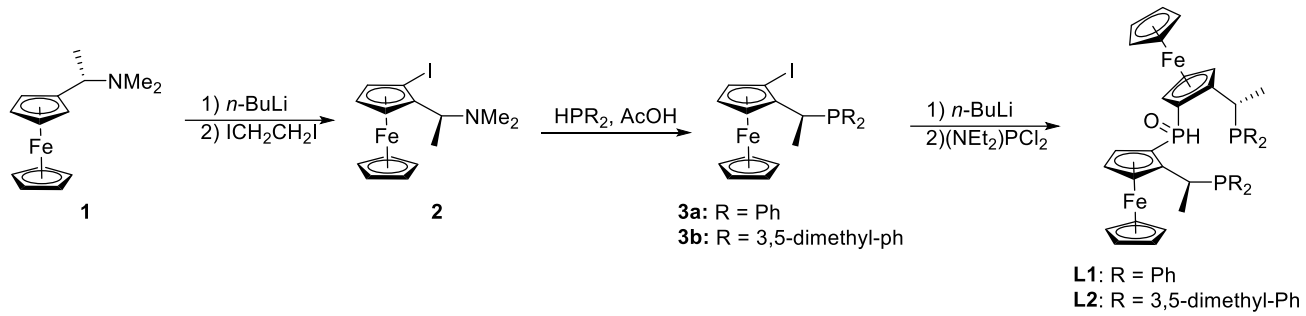

Scheme 3.2 Synthesis of **Fc-SPO** ligands **L1** and **L2**

Ligand **L3** was obtained in a similar way, but using 1 eq. of dichloro(diethylamino)phosphine and an excess of *o*-lithiophenyl diphenylphosphine (Scheme 3.3). Luckily, a single diastereomer of ligand **L3** could be isolated after column chromatography on silica. It was directly used for the AH of acetophenone without the identification of its absolute configuration.

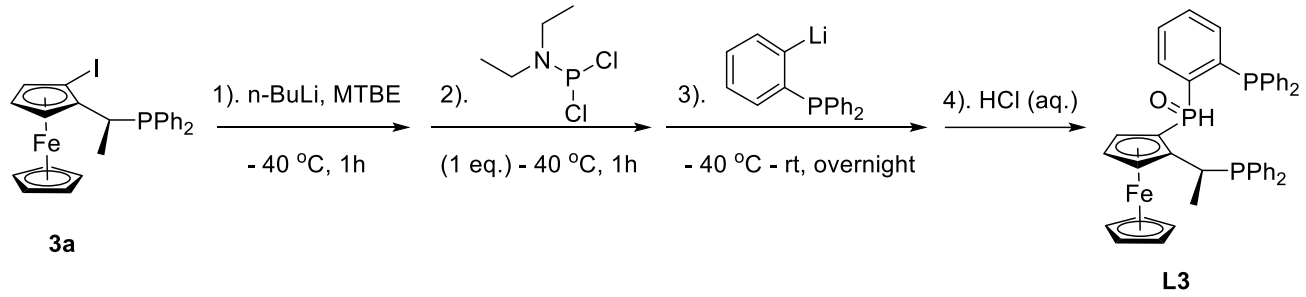

Scheme 3.3 Synthesis of **Fc-SPO** ligand **L3**

3.3 Synthesis of Fc-SPO-Co complexes

Mixing ligands **L1** – **L2** with $CoCl_2$ in THF at RT precipitated the corresponding green cobalt complexes **Co-1** – **Co-2** respectively in highly yields (Scheme 3.4).[18] They were found to be air-sensitive and had to be handled and stored under argon. Luckily, the structure of **Co-1** was confirmed by X-Ray crystallography from green crystals grown from DCM/hexane (Scheme 3.4).

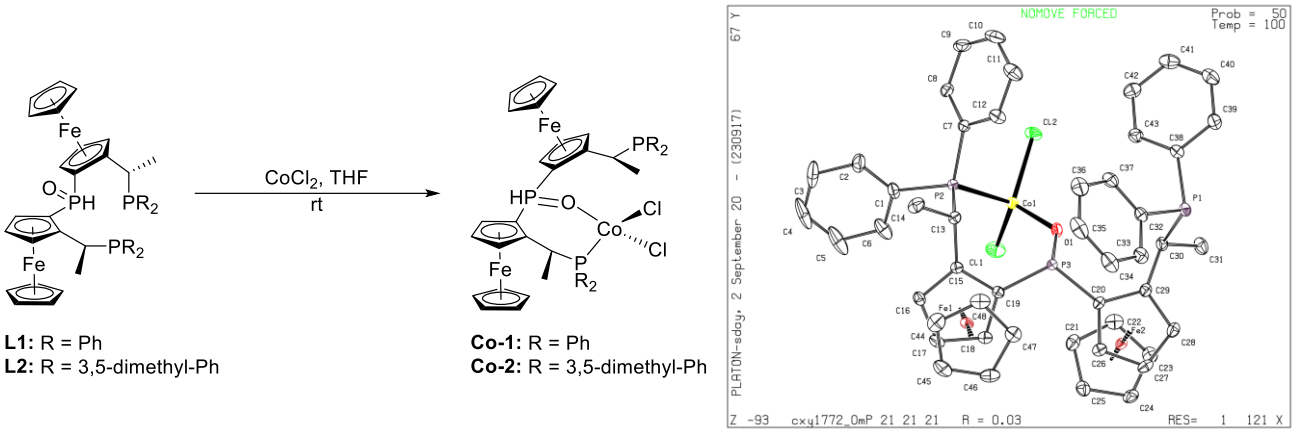

Scheme 3.4 Synthesis of the Fc-SPO-Co complexes, and crystal structure of Co-1 with ellipsoids drawn at the 50% probability level with hydrogen atoms omitted for clarity.

3.4 Asymmetric hydrogenation of ketones

3.4.1 Conditions screening for the AH of acetophenone

With the ligands **L1** – **L3** in hand, first the AH of acetophenone was tried using the corresponding cobalt complexes generated *in situ* (Table 3.1). Different cobalt ligand precursors had a significant effect on the reactions, and it was pleasing to find the combination of $CoCl_2$ and **L1** could catalyse the reaction with moderate reactivity (28% conversion) and good enantioselectivity (80% ee) (Entry 1). Interestingly, the $CoBr_2$/**L1** catalyst was highly reactive (89% conversion), but only gave the product with an ee value of 7% (Entry 2). The combination of $CoCl_2$ and **L2** provided the highest ee value (83%), despite a low reactivity (Entry 6). Therefore, the ligands **L1** and **L2** were potentially promising for the cobalt-catalysed AH of ketones. However, the ligand **L3** was not effective for the cobalt-catalysed AH of acetophenone (Entry 7).

Table 3.1 Screening of ligands and cobalt precursors

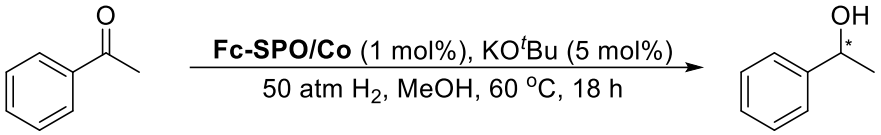

Entry[a]	Co precursors	Ligands	Conversion (%)[b]	ee (%)[b]
1	$CoCl_2$	**L1**	28	80
2	$CoBr_2$	**L1**	89	7
3	$Co(OAc)_2{\cdot}4H_2O$	**L1**	5	74
4	$Co(BF_4)_2{\cdot}6H_2O$	**L1**	6	59
5	$Co(acac)_2$	**L1**	< 5	-
6	$CoCl_2$	**L2**	10	83
7	$CoCl_2$	**L3**	8	17

[a] Reaction conditions: acetophenone (0.1 mmol), cat. (0.001 mmol), KO^{t}Bu (0.005 mmol), MeOH (0.4 mL). [b] Conversions and ee values were determined by ^{1}H-NMR and chiral HPLC, respectively.

Having obtained promising results using the *in-situ* generated complexes, next the AH of ketones was attempted using the isolated **Fc-SPO-Co** complexes to screen the conditions for acetophenone and diaryl ketone reduction. To begin with, the AH of acetophenone was studied in detail for **Co-1** under a range of reaction conditions (Table 3.2). Unfortunately, screening different solvents, bases, and additives did not improve both the catalytic reactivity and the enantioselectivity for any one set of conditions. For example, the use of TFE as a solvent produced an excellent conversion (99%) but at the expense of ee (16%) (Entry 10).

Table 3.2 Further reaction condition optimizations for the AH of acetophenone

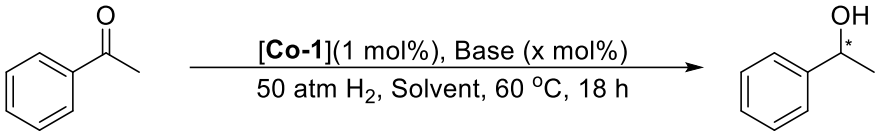

Entry[a]	Solvent	Base	Conversion (%)[b]	Ee (%)[b]
1	THF	KO^{t}Bu (5mol%)	13	28
2	Tol	KO^{t}Bu (5mol%)	20	58
3	DCE	KO^{t}Bu (5mol%)	< 5	-
4	Cyclohexane	KO^{t}Bu (5mol%)	57	59
5	EtOH	KO^{t}Bu (5mol%)	49	71
6	PrOH	KO^{t}Bu (5mol%)	29	74
7	*i*PrOH	KO^{t}Bu (5mol%)	74	65
8	BuOH	KO^{t}Bu (5mol%)	16	76
9	$H_3COCH_2CH_2OH$	KO^{t}Bu (5mol%)	10	58
10	TFE	KO^{t}Bu (5mol%)	99	16
11	EtOAc	KO^{t}Bu (5mol%)	< 5	-
12	MeOH	KO^{t}Bu (5mol%)	46	79
13	MeOH	NaO^{t}Bu (5mol%)	44	79
14	MeOH	LiO^{t}Bu (5mol%)	22	79
15	MeOH	KOH (5mol%)	26	79
16	MeOH	NaOMe (5mol%)	41	79
17	MeOH	K_2CO_3 (5mol%)	28	79
18	MeOH	Cs_2CO_3 (5mol%)	27	79
19	MeOH	-	28	rac.
20	MeOH (10mol% TFE)	KO^{t}Bu (5mol%)	85	-24

21		MeOH (10mol% HFIP)	KO^{t}Bu (5mol%)	71	rac.
22		MeOH (2 eq. *i*-PrOH)	KO^{t}Bu (5mol%)	9	78
23		MeOH (10mol% Zn)	-	5	-
24		MeOH	KO^{t}Bu (1mol%)	38	2
25		MeOH	KO^{t}Bu (2mol%)	80	39
26		MeOH	KO^{t}Bu (10mol%)	37	78
27	[c]	MeOH	KO^{t}Bu (10mol%)	64	78
28	[d]	MeOH	KO^{t}Bu (15mol%)	74	79

[a] Reaction conditions: acetophenone (0.1 mmol), **Co-1** (0.001 mmol), solvent (0.4 mL). [b] Conversions and ee values were determined by ^{1}H-NMR and chiral HPLC, respectively. [c] 2 mol% of cat., 24 h. [d] 3 mol% of cat., 24 h.

3.4.2 Conditions screening for the AH of 2-bromobenzophenone

Better results were obtained upon changing the substrate from acetophenone to 2-bromobenzophenone (Table 3.3). **Co-1** was found to be highly reactive with good enantioselectivity for this substrate using. EtOH as a solvent with a doubling of catalyst loading to 2 mol% of **Co-1** resulted in essentially full conversion into product (Entry 9). Reducing the reaction temperature did not impair the reactivity but enhanced the enantioselectivity slightly to 85% (Entry 10). However, **Co-2** was less reactive under the same conditions, despite giving a higher enantioselectivity (Entry 8). Only when 5 mol% of **Co-2** was applied, 2-bromobenzophenone was hydrogenated with full conversion and excellent enantioselectivity (90% ee) (Entry 12). To the best of our knowledge, this is the first example of cobalt-catalysed AH of an unsymmetrical benzophenone.

Table 3.3 Reaction condition optimizations for the AH of 2-bromobenzophenone

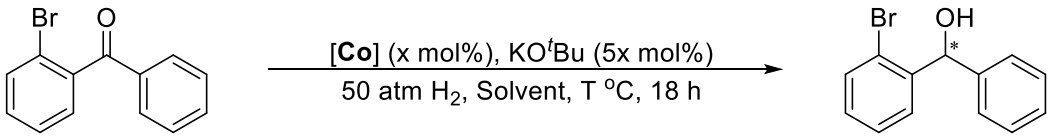

Entry[a]	Solvent	[Co] (x mol%)	T (^{o}C)	Conversion (%)[b]	Ee (%)[b]
1	MeOH	**Co-1** (1 mol%)	60	31	83
2	THF	**Co-1** (1 mol%)	60	13	58
3	DCM	**Co-1** (1 mol%)	60	6	52
4	hexane	**Co-1** (1 mol%)	60	35	77
5	*i*PrOH	**Co-1** (1 mol%)	60	8	85
6	TFE	**Co-1** (1 mol%)	60	34	-34
7	EtOH	**Co-1** (1 mol%)	60	63	84
8	EtOH	**Co-2** (1 mol%)	60	32	91
9 [c]	EtOH	**Co-1** (2 mol%)	60	>99	83
10 [c]	EtOH	**Co-1** (2 mol%)	40	>99	85
11 [c]	EtOH	**Co-2** (2 mol%)	60	60	87
12 [c]	EtOH	**Co-2** (5 mol%)	60	>99	90

[a] Reaction conditions: 2-bromobenzophenone (0.1 mmol), solvent (0.4 mL), 18 h. [b] Conversions and ee values were determined by ^{1}H-NMR and chiral HPLC, respectively. [c] 24 h.

3.4.3 Substrate scope for diaryl ketones

Next the substrate scope for diaryl ketone hydrogenations was investigated under the optimal conditions using the isolated cobalt complexes (Table 3.4). Both **Co-1** and **Co-2** afforded excellent yields and good enantioselectivities for the AH of various *ortho*-substituted benzophenones (**5a** – **5g**). **Co-2** generally gave slightly better enantioselectivities, although the highest ee value (92%) was also obtained for the **Co-1**-catalysed AH of 2-methoxybenzophenone (**5f**).

Considering the difficulty of the synthesis of ligand **L2** and the lower efficiency of **Co-2** (a catalyst loading of 5 mol% was required), it was concluded that **Co-1** was overall the better catalyst for the AH of 2-methoxybenzophenone. Therefore this complex was studied in more detail for the hydrogenation of a series of 2-methoxy-substituted diaryl ketones, which included studying additional substitutions at the 3-, 4-, and 5-position. The dimethoxy substrates (2,3- and 2,4-dimethoxybenzophenone) gave lower enantioselectivities due to increasing steric hindrance (**5i** and **5j**). However compounds with halide substituents at the 4-position (**5k** – **5l**) could be hydrogenated with excellent ee values (90 – 91%). Moreover, substitutions at the 5-position did not adversely affect the enantioselectivities of the products (**5m** – **5o**).

Substituents on the other phenyl ring were also examined (**5p** – **5aa**). In these cases, the electronic properties of the substituents at the *meta*- or *para*-position created clear differences in enantiomeric discrimination. Substrates containing electron-donating groups (**5q and 5v – 5z**) continued to be hydrogenated with excellent enantioselectivities (90 – 92%). In contrast, electron-withdrawing groups (**5p and 5s** – **5u**) resulted in a small but clear decrease in ee values (80 – 89%). Interestingly, increasing the steric hindrance of the substituents at the *para*-position (**5v** – **5z**) had no effect on the enantioselectivity.

Table 3.4 Reaction scope for the cobalt-catalysed AH of ketones

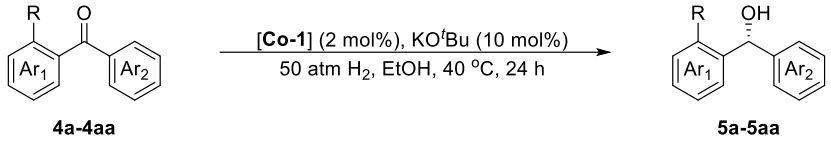

4a-4aa **5a-5aa**

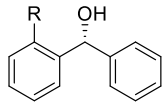

Co-1[a]
5a R = Br 99%, 85% ee
5b R = F 85%, 88% ee
5c R = Cl 99%, 87% ee
5d R = Me 99%, 82% ee
5e R = Et 99%, 86% ee
5f R = OMe 97%, 92% ee
5g R = OEt 99%, 83% ee

Co-2[b]
5a R = Br 99%, 90% ee
5b R = F 90%, 88% ee
5c R = Cl 99%, 91% ee
5d R = Me 94%, 92% ee
5f R = OMe 99%, 91% ee

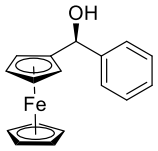

5h 99%, 86% ee

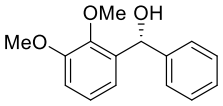

5i 98%, 81% ee

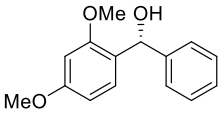

5j 98%, 84% ee

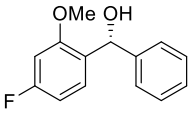

5k 95%, 90% ee

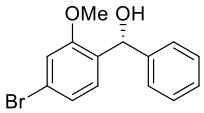

5l 99%, 91% ee

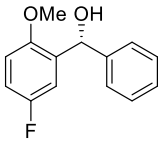

5m 86%, 91% ee

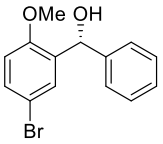

5n 99%, 91% ee

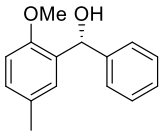

5o 99%, 90% ee

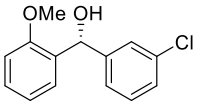

5p 99%, 86% ee

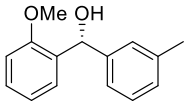

5q 99%, 90% ee

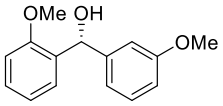

5r 99%, 87% ee

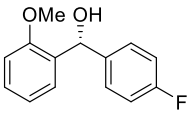

5s 99%, 89% ee

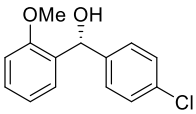

5t 99%, 88% ee

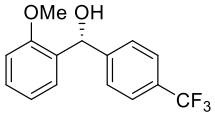

5u 99%, 80% ee

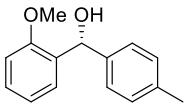

5v 99%, 92% ee

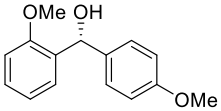

5w 99%, 91% ee

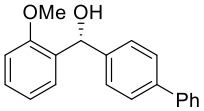

5x 99%, 91% ee

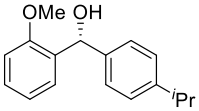

5y 99%, 92% ee

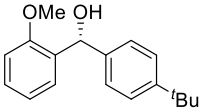

5z 99%, 92% ee

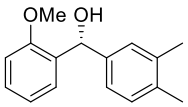

5aa 99%, 90% ee

[a]Reaction conditions: substrate (0.1 mmol), **Co-1** (0.002 mmol), KO^{t}Bu (0.01 mmol), 0.4 mL of EtOH, 50 atm of H_2, 40 °C, 24 h. [b] Reaction conditions: **Co-2** (0.005 mmol), KO^{t}Bu (0.025 mmol), 60 °C. **5h** – **5aa** were hydrogenated by **Co-1**. Isolated yields were recorded. The ee values were measured using HPLC on a chiral stationary phase.

3.5 Conclusion

In summary, we report the synthesis of novel ferrocene-based secondary phosphine oxide ligands **Fc-SPO** and their successful applications in the cobalt-catalysed AH of ketones. Despite low efficiencies for aryl-alkyl ketones, the **Fc-SPO-Co** complexes afforded high reactivities and good to excellent enantioselectivities for the AH of various *ortho*-substituted aryl-aryl ketones, with a series of 2-methoxy-substituted ketones hydrogenated with the highest enantioselectivities (up to 92% ee). Furthermore, it is not applicable to use the *in-situ* NMR technique to study the reaction mechanism because of the paramagnetic properties of the cobalt(II) species, but DFT study is underway.

3.6 Experimental

3.6.1 Synthesis of the Fc-SPO ligands

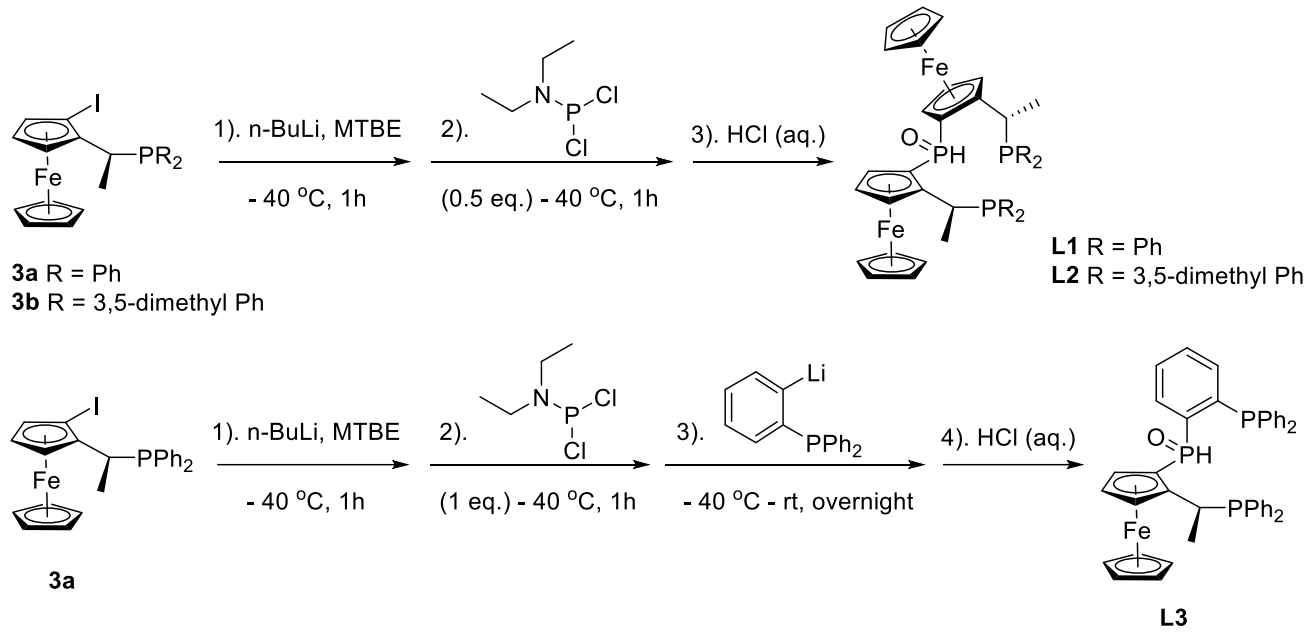

Scheme 3.5 Synthesis of the **Fc-SPO** ligands from compound **3**

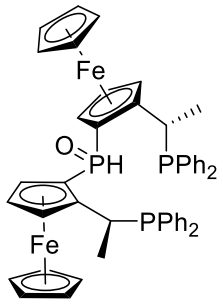

L1

(*S, S, Rp, Rp*)-**L1.** Novel compound. To a solution of the starting material **3a** (4.0 mmol, 2.10 g) dissolved in dry MTBE (20 mL), *n*-BuLi (4.8 mmol, 2.20 mL, 2.17 M in hexane) was added dropwise at -40 °C under argon. The reaction mixture was stirred for 1 h under -40 °C. After 1 h, dry 1,1-dichloro-*N,N*-diethylphosphanamine (2.0 mmol, 0.29 mL) was added dropwise at -40 °C under argon. The reaction mixture was stirred under -40 °C for 1 h. Then it was allowed to warm to room temperature and stirred for further 3 h. Then the reaction was quenched by the addition of aq. 1M HCl solution (5

mL), extracted with ethyl acetate (3*50 mL) and the combined organic layers were dried over anhydrous Na_2SO_4 and concentrated under vacuum. The residue was purified by column chromatography on silica gel (PE/EtOAc, 90/10~80/20) to yield 900 mg (53 %) of (*S, S, Rp, Rp*)-**L1** as an orange solid. ^{1}H NMR (600 MHz, Chloroform-*d*) δ 7.80 (s, 0.5H), 7.47 (t, *J* = 7.2 Hz, 2H), 7.40 (t, *J* = 6.8 Hz, 2H), 7.31 (dt, *J* = 29.5, 7.3 Hz, 6H), 7.25 – 7.18 (m, 7H), 7.15 (t, *J* = 7.4 Hz, 1H), 7.06 (t, *J* = 6.9 Hz, 2H), 6.99 (s, 0.5H), 4.46 (s, 1H), 4.22 (s, 7H), 4.12 (s, 7H), 3.91 (s, 1H), 3.65 (d, *J* = 7.0 Hz, 2H), 1.48 (dd, *J* = 12.3, 6.9 Hz, 3H), 1.30 (t, *J* = 6.6 Hz, 3H). ^{13}C NMR (151 MHz, Chloroform-*d*) δ 138.0 (dd, *J* = 28.0, 18.9 Hz), 136.1 (d, *J* = 21.1 Hz), 135.1, 135.0, 134.8 (d, *J* = 3.3 Hz), 134.7, 132.9 (d, *J* = 16.3 Hz), 131.5 (d, *J* = 14.1 Hz), 129.5, 129.3, 128.4 (d, *J* = 7.5 Hz), 128.3 (d, *J* = 4.0 Hz), 128.1 (d, *J* = 5.4 Hz), 128.0, 127.7 (d, *J* = 7.5 Hz), 127.3, 99.1 (dd, *J* = 22.0, 10.4 Hz), 95.2 (dd, *J* = 17.3, 13.1 Hz), 75.1, 74.4, 72.6 (dd, *J* = 13.5, 9.0 Hz), 70.3, 70.1, 69.9 (d, *J* = 26.8 Hz), 69.7 (d, *J* = 23.4 Hz), 69.2 (d, *J* = 11.5 Hz), 67.4, 66.6, 30.0 (d, *J* = 16.4 Hz), 28.5 (d, *J* = 19.5 Hz), 19.2 (d, *J* = 14.7 Hz), 17.1. ^{31}P NMR (162 MHz, Chloroform-*d*) δ 19.85 (d, *J* = 10.8 Hz), 11.13, 8.86 (d, *J* = 10.6 Hz). **HRMS** (ESI) m/z: $[M+H]^+$ Calcd for $C_{48}H_{46}Fe_2OP_3^+$ = 843.1455; Found: 843.1453. $[\alpha]D^{24}$ = +86.00 (*c* 0.5, $CHCl_3$).

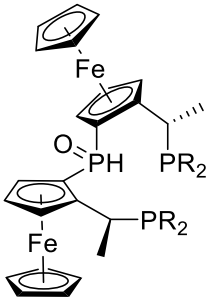

L2 R = 3,5-dimethyl-ph

(*S, S, Rp, Rp*)-**L2.** Novel compound. **L2** was prepared via the similar procedure depicted in the synthesis of **L1**. 180 mg of (*S, S, Rp, Rp*)-**L2** was obtained with 15% yield as an orange solid. ^{1}H NMR (600 MHz, Chloroform-*d*) δ 7.81 (s, 1H), 7.15 (d, *J* = 7.8 Hz, 2H), 7.09 – 7.04 (m, 3H), 7.00 (d, *J* = 7.3 Hz, 3H), 6.94 (s, 1H), 6.85 (s, 1H), 6.75 (d, *J* = 6.7 Hz, 2H), 4.49 (s, 1H), 4.31 (s, 5H), 4.27 (d, *J*

= 2.4 Hz, 1H), 4.22 (s, 5H), 4.19 (q, *J* = 3.5, 2.7 Hz, 3H), 3.97 (d, *J* = 3.1 Hz, 1H), 3.80 (d, *J* = 2.5 Hz, 1H), 3.67 (dq, *J* = 7.0, 4.1 Hz, 1H), 2.34 (s, 6H), 2.27 (s, 12H), 2.25 (s, 6H), 1.56 (dd, *J* = 12.2, 6.9 Hz, 3H), 1.43 (t, *J* = 7.0 Hz, 3H). ^{13}C NMR (151 MHz, Chloroform-*d*) δ 137.9 (d, *J* = 18.5 Hz), 137.6, 137.6, 137.5, 137.4 (d, *J* = 4.4 Hz), 137.2 (d, *J* = 5.8 Hz), 136.9 (d, *J* = 7.8 Hz), 134.7 (d, *J* = 20.1 Hz), 134.4 (d, *J* = 16.7 Hz), 133.7 (d, *J* = 21.1 Hz), 132.6 (d, *J* = 20.4 Hz), 131.0 (d, *J* = 27.2 Hz), 130.6 (d, *J* = 16.5 Hz), 129.7, 129.2, 129.1 (d, *J* = 9.5 Hz), 99.4 (dd, *J* = 21.1, 10.6 Hz), 95.5 (dd, *J* = 17.9, 12.9 Hz), 75.7, 75.0, 72.6 (dd, *J* = 14.2, 9.9 Hz), 70.5 – 70.2 (m), 70.2, 70.0 (d, *J* = 2.0 Hz), 69.6 – 69.3 (m), 68.8 (d, *J* = 11.8 Hz), 67.5 (d, *J* = 3.3 Hz), 66.7 (d, *J* = 3.8 Hz), 30.0 (d, *J* = 16.8 Hz), 28.3 (d, *J* = 19.4 Hz), 21.5, 21.3 (d, *J* = 14.4 Hz), 19.1 (d, *J* = 14.6 Hz), 17.9. ^{31}P NMR (243 MHz, Chloroform-*d*) δ 19.57 (d, *J* = 12.7 Hz), 10.68, 10.04 (d, *J* = 11.9 Hz). **HRMS** (ESI) m/z: $[M+H]^+$ Calcd for $C_{56}H_{62}Fe_2OP_3^+$ = 955.2707; Found: 955.2697. $[\alpha]D^{24}$ = +45.40 (*c* 0.5, $CHCl_3$).

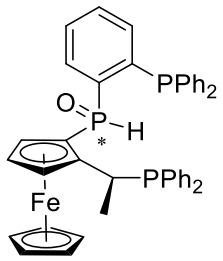

L3

L3. Novel compound. To a solution of the starting material **3a** (1.0 mmol, 524 mg) dissolved in dry ethyl ether (5 mL), *n*-BuLi (1.0 mmol, 0.63 mL, 1.6 M in hexane) was added dropwise at -40 °C under argon. The reaction mixture was stirred for 1 h under -40 °C. After 1 h, dry 1,1-dichloro-*N*,*N*-diethylphosphanamine (1.0 mmol, 0.15 mL) was added dropwise. The reaction mixture was stirred for 1 h under -40 °C. 2-diphenylphosphanyl-phenyl-lithium (1.0 mmol, prepared by treating 2-bromophenyl-diphenyl-phosphane with *n*-BuLi in a 1:1 molar ratio under -40 °C for 1 h in dry ethyl ether) was added dropwise. The reaction mixture was stirred for 1 h under -40 °C. Then it was allowed to warm to room temperature and stirred overnight. The reaction was quenched by the addition of

aqueous 1M HCl solution (1 mL), extracted with ethyl acetate (3*10 mL) and the combined organic layers were dried over anhydrous Na_2SO_4 and concentrated under vacuum. The residue was purified by column chromatography on silica gel (PE/EtOAc, 90/10~80/20) to yield 80 mg (11 %) of **L3** as an orange solid. ^{1}H NMR (400 MHz, Chloroform-*d*) δ 8.27 (ddd, *J* = 10.9, 6.9, 2.5 Hz, 1H), 7.66 – 7.46 (m, 6H), 7.44 – 7.25 (m, 13H), 7.25 – 7.11 (m, 4H), 7.11 – 7.02 (m, 1H), 4.29 (s, 5H), 4.22 (p, *J* = 4.5, 3.8 Hz, 1H), 4.16 (dt, *J* = 9.7, 3.0 Hz, 2H), 3.96 (t, *J* = 2.0 Hz, 1H), 1.51 (dd, *J* = 10.6, 7.0 Hz, 3H). ^{31}P NMR (162 MHz, Chloroform-*d*) δ 11.97 (dd, *J* = 85.1, 16.0 Hz), 8.25 (d, *J* = 15.8 Hz), -18.13 (d, *J* = 85.2 Hz).

3.6.2 Synthesis of the cobalt complexes

A suspension of the ligand (*S, S, Rp, Rp*)-**L1** (0.5 mmol, 421 mg) and cobalt precursor $CoCl_2$ (0.5 mmol, 65 mg) in dry THF (8 mL) was stirred for 12 h under argon at room temperature. The green mixture was concentrated to dryness under high vacuum. The residue was dissolved in DCM and filtered to remove insoluble materials. The product was precipitated by the addition of *n*-hexane, collected by filtration, and washed with *n*-hexane to yield 470 mg (97 %) of **Co-1** as a green solid. The similar procedure also gave 80 mg (96%) of **Co-2** as a green solid.

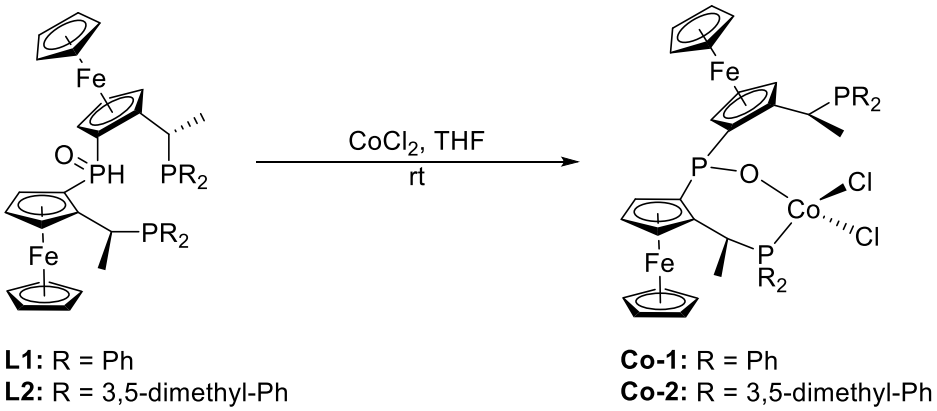

L1: R = Ph
L2: R = 3,5-dimethyl-Ph

Co-1: R = Ph
Co-2: R = 3,5-dimethyl-Ph

Scheme 3.6 Synthesis of the cobalt complexes

3.6.3 Synthesis of diaryl ketone substrates

Substrates **4a**, **4b**, **4c**, **4d**, **4h**, **4i**, **4j**, **4l**, **4m** and **4q** were purchased from commercial suppliers without further purification. And other substrates were synthesized according to the procedures in literature.[27]

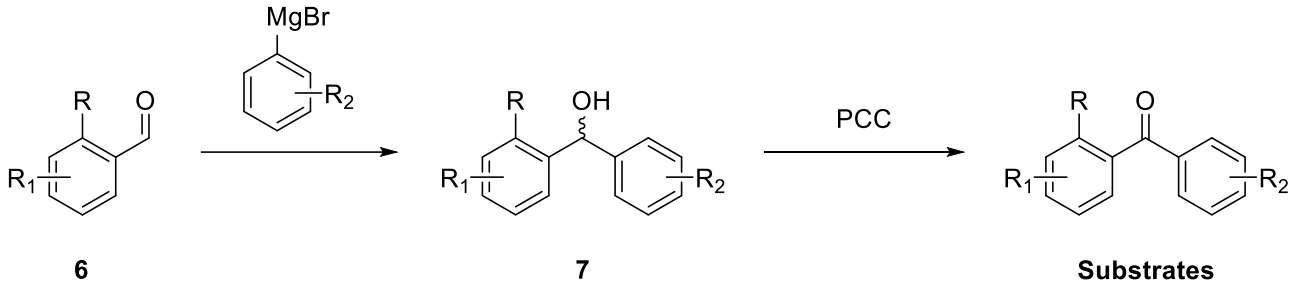

Scheme 3.7 Synthesis of diaryl ketone substrates

To a solution of aryl aldehydes **6** (1.0 eq.) in dry THF, arylmagnesium bromide (1.2 eq.) was added dropwise at -40 ℃ under argon. Warmed to room temperature, the reaction mixture was stirred for 4 h. Then the reaction was quenched by the addition of aqueous saturated ammonium chloride solution, extracted with ethyl acetate and the combined organic layers were dried over anhydrous sodium sulfate and concentrated under vacuum. The crude products **7** were used for next reactions without purification. To a solution of diarylalcohol **7** (1.0 eq.) in DCM, a mixture of PCC (3.0 eq.) and silica gel (1:1 by mass) was added at room temperature. After stirred for 2 h, the reaction mixture was filtered through a pad of silica gel and concentrated under vacuum. The residue was purified by column chromatography on silica gel. (PE:EA=10:1, v/v)

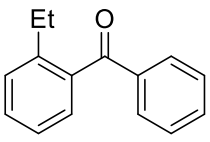

(2-ethylphenyl)(phenyl)methanone (4e). Known compound.[19] Purified by column chromatography (silica gel, PE:EA=10:1, v/v). Colorless oil. ^{1}H NMR (400 MHz, Chloroform-*d*) δ 7.68 – 7.63 (m, 2H), 7.40 – 7.34 (m, 1H), 7.27 (d, *J* = 1.7 Hz, 1H), 7.24 (dt, *J* = 7.3, 2.5 Hz, 2H), 7.16 (d, *J* = 7.6 Hz, 1H),

7.07 (dtd, *J* = 14.7, 7.6, 1.5 Hz, 2H), 2.52 (q, *J* = 7.6 Hz, 2H), 1.00 (t, *J* = 7.6 Hz, 3H). ^{13}C NMR (101 MHz, Chloroform-*d*) δ 197.45, 141.85, 137.27, 136.69, 132.07, 129.16, 129.02, 128.32, 127.31, 127.14, 124.05, 25.32, 14.86. HRMS (ESI) calcd. for $[C_{15}H_{15}O]^+$ ($[M+H]^+$): 211.1117, found: 211.1115.

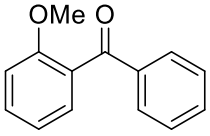

(2-methoxyphenyl)(phenyl)methanone (4f). Known compound.[20] Purified by column chromatography (silica gel, PE:EA=10:1, v/v). Colorless oil. ^{1}H NMR (400 MHz, Chloroform-*d*) δ 7.69 – 7.62 (m, 2H), 7.38 – 7.32 (m, 1H), 7.31 – 7.16 (m, 4H), 6.86 (t, *J* = 7.5 Hz, 1H), 6.81 (d, *J* = 8.4 Hz, 1H), 3.50 (s, 3H). ^{13}C NMR (101 MHz, Chloroform-*d*) δ 196.44, 157.34, 137.83, 132.98, 131.98, 129.78, 129.51, 128.85, 128.28, 120.53, 111.55, 55.56. HRMS (ESI) calcd. for $[C_{14}H_{13}O_2]^+$ ($[M+H]^+$): 211.1117, found: 211.1115.

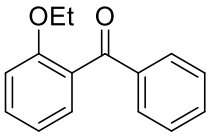

(2-ethoxyphenyl)(phenyl)methanone (4g). Known compound.[21] Purified by column chromatography (silica gel, PE:EA=10:1, v/v). Colorless oil. ^{1}H NMR (400 MHz, Chloroform-*d*) δ 7.69 (dd, *J* = 8.3, 1.4 Hz, 2H), 7.47 – 7.40 (m, 1H), 7.38 – 7.27 (m, 4H), 6.96 – 6.89 (m, 1H), 6.85 (d, *J* = 8.3 Hz, 1H), 3.84 (q, *J* = 7.0 Hz, 2H), 0.95 (t, *J* = 7.0 Hz, 3H). ^{13}C NMR (101 MHz, Chloroform-*d*) δ 195.76, 155.81, 137.27, 131.57, 130.97, 128.65, 128.49, 128.02, 127.01, 119.45, 111.42, 62.95, 13.22. HRMS (ESI) calcd. for $[C_{15}H_{15}O_2]^+$ ($[M+H]^+$): 227.1067, found: 227.1062.

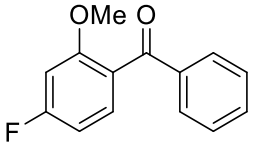

(4-fluoro-2-methoxyphenyl)(phenyl)methanone (4k). Novel compound. Purified by column chromatography (silica gel, PE:EA=10:1, v/v). Colorless oil. ^{1}H NMR (400 MHz, Chloroform-*d*) δ 7.78 (dd, *J* = 8.1, 1.5 Hz, 2H), 7.58 – 7.50 (m, 1H), 7.46 – 7.34 (m, 3H), 6.78 – 6.67 (m, 2H), 3.70 (s, 3H). ^{13}C NMR (101 MHz, Chloroform-*d*) δ 195.26, 165.17 (d, *J* = 250.5 Hz), 159.27 (d, *J* = 10.2 Hz), 137.91, 132.95, 131.48 (d, *J* = 10.6 Hz), 129.72, 128.25, 124.85 (d, *J* = 3.2 Hz), 107.24 (d, *J* = 21.8 Hz), 99.76 (d, *J* = 25.8 Hz), 55.84. ^{19}F NMR (376 MHz, Chloroform-*d*) δ -106.14. HRMS (ESI) calcd. for $[C_{14}H_{12}FO_2]^+$ ($[M+H]^+$): 231.0816, found: 231.0814.

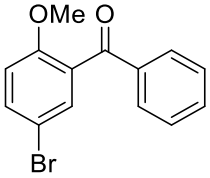

(5-bromo-2-methoxyphenyl)(phenyl)methanone (4n). Known compound.[22] Purified by column chromatography (silica gel, PE:EA=10:1, v/v). Colorless oil. ^{1}H NMR (600 MHz, Chloroform-*d*) δ 7.82 – 7.76 (m, 2H), 7.56 (ddd, *J* = 8.8, 6.4, 2.0 Hz, 2H), 7.47 – 7.41 (m, 3H), 6.88 (d, *J* = 8.8 Hz, 1H), 3.70 (s, 3H). ^{13}C NMR (151 MHz, Chloroform-*d*) δ 194.72, 156.37, 137.16, 134.37, 133.34, 131.93, 130.66, 129.80, 128.39, 113.32, 112.82, 55.92. HRMS (ESI) calcd. for $[C_{14}H_{12}BrO_2]^+$ ($[M+H]^+$): 291.0015, found: 291.0012.

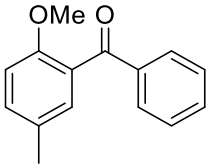

(2-methoxy-5-methylphenyl)(phenyl)methanone (4o). Known compound.[22] Purified by column chromatography (silica gel, PE:EA=10:1, v/v). Colorless oil. ^{1}H NMR (600 MHz, Chloroform-*d*) δ

7.84 – 7.77 (m, 2H), 7.52 (d, *J* = 7.4 Hz, 1H), 7.41 (t, *J* = 7.7 Hz, 2H), 7.24 (dd, *J* = 8.5, 2.2 Hz, 1H), 7.16 (d, *J* = 2.2 Hz, 1H), 6.87 (d, *J* = 8.4 Hz, 1H), 3.66 (s, 3H), 2.31 (s, 3H). ^{13}C NMR (151 MHz, Chloroform-*d*) δ 196.71, 155.33, 137.92, 132.87, 132.32, 129.95, 129.91, 129.82, 128.68, 128.20, 111.54, 55.75, 20.38. HRMS (ESI) calcd. for $[C_{15}H_{15}O_2]^+$ ($[M+H]^+$): 227.1067, found: 227.1063.

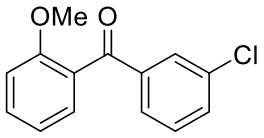

(3-chlorophenyl)(2-methoxyphenyl)methanone (4p). Known compound.[23] Purified by column chromatography (silica gel, PE:EA=10:1, v/v). Colorless oil. ^{1}H NMR (400 MHz, Chloroform-*d*) δ 7.68 (t, *J* = 1.9 Hz, 1H), 7.55 (dt, *J* = 7.8, 1.4 Hz, 1H), 7.43 – 7.33 (m, 2H), 7.30 – 7.24 (m, 2H), 6.94 (td, *J* = 7.5, 0.9 Hz, 1H), 6.91 – 6.87 (m, 1H), 3.60 (s, 3H). ^{13}C NMR (101 MHz, Chloroform-*d*) δ 194.04, 156.36, 138.53, 133.38, 131.66, 131.42, 128.68, 128.50, 128.45, 126.97, 126.82, 119.61, 110.51, 54.50. HRMS (ESI) calcd. for $[C_{14}H_{12}ClO_2]^+$ ($[M+H]^+$): 247.0520, found:247.0517.

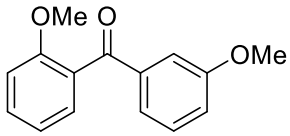

(2-methoxyphenyl)(3-methoxyphenyl)methanone (4r). Known compound.[24] Purified by column chromatography (silica gel, PE:EA=10:1, v/v). Colorless oil. ^{1}H NMR (400 MHz, Chloroform-*d*) δ 7.48 – 7.40 (m, 2H), 7.37 – 7.25 (m, 3H), 7.09 (dt, *J* = 5.7, 3.0 Hz, 1H), 7.05 – 6.95 (m, 2H), 3.82 (s, 3H), 3.71 (s, 3H). ^{13}C NMR (101 MHz, Chloroform-*d*) δ 196.26, 159.62, 157.32, 139.15, 131.86, 129.44, 129.21, 128.89, 123.04, 120.44, 119.58, 113.52, 111.51, 55.64, 55.43. HRMS (ESI) calcd. for $[C_{15}H_{15}O_3]^+$ ($[M+H]^+$): 243.1016, found: 243.1013.

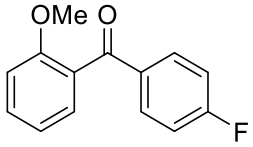

(4-fluorophenyl)(2-methoxyphenyl)methanone (4s). Known compound.[25] Purified by column chromatography (silica gel, PE:EA=10:1, v/v). Colorless oil. ^{1}H NMR (400 MHz, Chloroform-*d*) δ 7.73 – 7.64 (m, 2H), 7.35 – 7.27 (m, 1H), 7.20 (dd, *J* = 7.5, 1.8 Hz, 1H), 6.98 – 6.80 (m, 4H), 3.55 (s, 3H). ^{13}C NMR (101 MHz, Chloroform-*d*) δ 194.83, 165.64 (d, *J* = 254.4 Hz), 157.18, 134.24 (d, *J* = 2.9 Hz), 132.38 (d, *J* = 9.3 Hz), 132.09, 129.45, 128.52, 120.60, 115.32 (d, *J* = 21.8 Hz), 111.48, 55.49. ^{19}F NMR (376 MHz, Chloroform-*d*) δ -105.46. HRMS (ESI) calcd. for $[C_{14}H_{12}FO_2]^+$ ($[M+H]^+$): 231.0816, found: 231.0812.

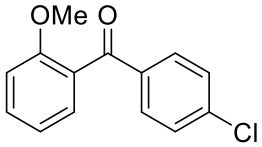

((4-chlorophenyl)(2-methoxyphenyl)methanone (4t). Known compound.[26] Purified by column chromatography (silica gel, PE:EA=10:1, v/v). Colorless oil. ^{1}H NMR (600 MHz, Chloroform-*d*) δ 7.74 (d, *J* = 8.5 Hz, 2H), 7.50 – 7.46 (m, 1H), 7.42 – 7.38 (m, 2H), 7.36 (dd, *J* = 7.4, 1.7 Hz, 1H), 7.09 – 7.03 (m, 1H), 6.99 (d, *J* = 8.4 Hz, 1H), 3.72 (s, 3H). ^{13}C NMR (151 MHz, Chloroform-*d*) δ 195.24, 157.31, 139.27, 136.27, 132.23, 131.15, 129.67, 128.54, 128.35, 120.66, 111.45, 55.57. HRMS (ESI) calcd. for $[C_{14}H_{12}ClO_2]^+$ ($[M+H]^+$): 247.0520, found: 247.0516.

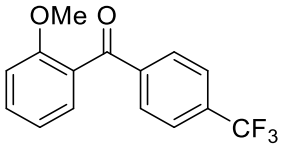

((2-methoxyphenyl)(4-(trifluoromethyl)phenyl)methanone (4u). Known compound.[26] Purified by column chromatography (silica gel, PE:EA=10:1, v/v). Colorless oil. ^{1}H NMR (400 MHz, Chloroform-*d*) δ 7.89 (d, *J* = 8.0 Hz, 2H), 7.69 (d, *J* = 8.1 Hz, 2H), 7.56 – 7.48 (m, 1H), 7.42 (dd, *J* =

7.6, 1.8 Hz, 1H), 7.07 (td, *J* = 7.5, 1.0 Hz, 1H), 7.04 – 6.92 (m, 1H), 3.70 (s, 3H). ^{13}C NMR (101 MHz, Chloroform-*d*) δ 195.44, 157.55, 140.90, 133.91 (d, *J* = 32.4 Hz), 132.77, 130.00, 129.84, 127.89, 125.24, 125.21, 120.77, 111.51, 55.52. ^{19}F NMR (376 MHz, Chloroform-*d*) δ -62.98. HRMS (ESI) calcd. for $[C_{15}H_{12}F_3O_2]^+$ ($[M+H]^+$): 281.0784, found: 281.0779.

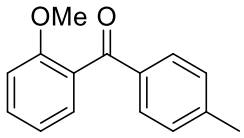

(2-methoxyphenyl)(p-tolyl)methanone (4v). Known compound.[25] Purified by column chromatography (silica gel, PE:EA=10:1, v/v). Colorless oil. ^{1}H NMR (600 MHz, Chloroform-*d*) δ 7.69 – 7.60 (m, 2H), 7.42 – 7.35 (m, 1H), 7.26 (dd, *J* = 7.5, 1.7 Hz, 1H), 7.15 (d, *J* = 7.9 Hz, 2H), 6.96 (td, *J* = 7.4, 0.9 Hz, 1H), 6.92 (d, *J* = 8.4 Hz, 1H), 3.66 (s, 3H), 2.34 (s, 3H). ^{13}C NMR (151 MHz, Chloroform-*d*) δ 195.08, 156.18, 142.77, 134.19, 130.54, 129.02, 128.36, 128.14, 127.92, 119.41, 110.39, 54.61, 20.69. HRMS (ESI) calcd. for $[C_{15}H_{15}O_2]^+$ ($[M+H]^+$): 227.1067, found: 227.1063.

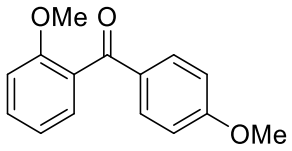

(2-methoxyphenyl)(4-methoxyphenyl)methanone (4w). Known compound.[24] Purified by column chromatography (silica gel, PE:EA=10:1, v/v). Colorless oil. ^{1}H NMR (400 MHz, Chloroform-*d*) δ 7.83 – 7.78 (m, 2H), 7.47 – 7.40 (m, 1H), 7.31 (dd, *J* = 7.5, 1.8 Hz, 1H), 7.06 – 6.96 (m, 2H), 6.93 – 6.87 (m, 2H), 3.86 (s, 3H), 3.74 (s, 3H). ^{13}C NMR (101 MHz, Chloroform-*d*) δ 195.11, 163.56, 157.01, 132.31, 131.42, 130.67, 129.26, 129.21, 120.44, 113.49, 111.38, 55.64, 55.49. HRMS (ESI) calcd. for $[C_{15}H_{15}O_3]^+$ ($[M+H]^+$): 243.1016, found: 243.1012.

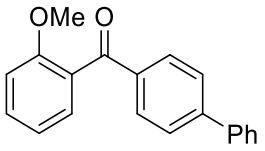

[1,1'-biphenyl]-4-yl(2-methoxyphenyl)methanone (4x). Novel compound. Purified by column chromatography (silica gel, PE:EA=10:1, v/v). Colorless oil. ^{1}H NMR (600 MHz, Chloroform-*d*) δ 7.88 (dt, *J* = 8.4, 2.0 Hz, 2H), 7.67 – 7.58 (m, 4H), 7.48 – 7.41 (m, 3H), 7.40 – 7.33 (m, 2H), 7.07 – 7.01 (m, 1H), 6.98 (d, *J* = 8.4 Hz, 1H), 3.71 (s, 3H). ^{13}C NMR (151 MHz, Chloroform-*d*) δ 196.05, 157.34, 145.62, 140.03, 136.56, 131.93, 131.91, 130.50, 129.56, 128.98, 128.22, 127.32, 126.95, 120.59, 111.54, 55.67. HRMS (ESI) calcd. for $[C_{20}H_{17}O_2]^+$ ($[M+H]^+$): 289.1223, found: 289.1219.

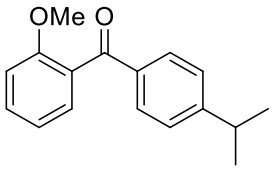

(4-isopropylphenyl)(2-methoxyphenyl)methanone (4y). Novel compound. Purified by column chromatography (silica gel, PE:EA=10:1, v/v). Colorless oil. ^{1}H NMR (400 MHz, Chloroform-*d*) δ 7.81 – 7.70 (m, 2H), 7.44 (ddd, *J* = 8.4, 7.5, 1.8 Hz, 1H), 7.32 (dd, *J* = 7.5, 1.8 Hz, 1H), 7.28 (d, *J* = 2.1 Hz, 1H), 7.23 – 7.05 (m, 1H), 7.05 – 6.96 (m, 2H), 3.73 (s, 3H), 1.26 (d, *J* = 6.9 Hz, 6H), 1.20 (dd, *J* = 7.0, 2.5 Hz, 1H). ^{13}C NMR (101 MHz, Chloroform-*d*) δ 196.11, 157.19, 154.58, 135.49, 131.57, 130.25, 129.34, 129.18, 126.40, 120.41, 111.44, 55.66, 34.32, 23.72. HRMS (ESI) calcd. for $[C_{17}H_{19}O_2]^+$ ($[M+H]^+$): 255.1380, found: 255.1375.

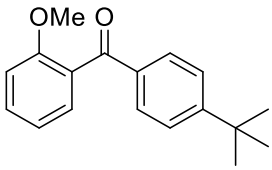

(4-(*tert*-butyl)phenyl)(2-methoxyphenyl)methanone (4z). Novel compound. Purified by column chromatography (silica gel, PE:EA=10:1, v/v). Colorless oil. ^{1}H NMR (400 MHz, Chloroform-*d*) δ

7.80 – 7.73 (m, 2H), 7.48 – 7.39 (m, 3H), 7.31 (dd, *J* = 7.5, 1.8 Hz, 1H), 7.05 – 6.95 (m, 2H), 3.72 (d, *J* = 1.4 Hz, 3H), 1.33 (s, 9H). ^{13}C NMR (101 MHz, Chloroform-*d*) δ 196.07, 157.18, 156.77, 135.03, 131.57, 129.95, 129.30, 129.18, 125.25, 120.40, 111.45, 55.67, 35.15, 31.14. HRMS (ESI) calcd. for $[C_{18}H_{21}O_2]^+$ ($[M+H]^+$): 269.1536, found: 269.1531.

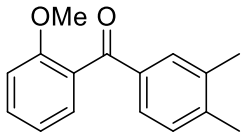

(3,4-dimethylphenyl)(2-methoxyphenyl)methanone (4aa). Novel compound. Purified by column chromatography (silica gel, PE:EA=10:1, v/v). Colorless oil. ^{1}H NMR (400 MHz, Chloroform-*d*) δ 7.64 (d, *J* = 1.9 Hz, 1H), 7.50 (dd, *J* = 7.9, 1.8 Hz, 1H), 7.46 – 7.39 (m, 1H), 7.30 (dd, *J* = 7.4, 1.8 Hz, 1H), 7.16 (d, *J* = 7.8 Hz, 1H), 7.05 – 6.95 (m, 2H), 3.72 (s, 3H), 2.29 (d, *J* = 10.2 Hz, 6H). ^{13}C NMR (101 MHz, Chloroform-*d*) δ 196.35, 157.20, 142.65, 136.65, 135.57, 131.50, 130.74, 129.53, 129.30, 128.01, 120.40, 111.48, 55.66, 20.11, 19.74. HRMS (ESI) calcd. for $[C_{16}H_{17}O_2]^+$ ($[M+H]^+$): 241.1223, found: 241.1220.

3.6.4 General procedures for the AH of ketones

In a glove box, to a vial (3 mL) was charged with the catalyst **Co-1** (2 mol %, 2 mg), K^{t}OBu (10 mol %, 100 uL, 0.1 M in EtOH), substrate (0.1 mmol) and EtOH (0.4 mL). The vial was placed into the autoclave. The autoclave was sealed and purged three times with hydrogen gas, then pressurized to 50 bar and stirred at 40 ^{o}C for 24 h. If the substrates were hydrogenated by **Co-2**, to a vial (3 mL) was charged with the catalyst **Co-2** (5 mol %, 5 mg), K^{t}OBu (25 mol %, 250 uL, 0.1 M in EtOH), substrate (0.1 mmol) and EtOH (0.4 mL), and the autoclave was pressurized to 50 bar and stirred at 60 ^{o}C for 24 h. Afterwards, the vessel was vented carefully in a hood and the reaction mixture was concentrated *in vacuo*. The residue was purified by flash chromatography on silica (PE/EtOAc, 10/1) to afford the chiral alcohol. The enantiomeric excess (ee) was determined by HPLC on a chiral stationary phase.

3.6.5 Analytical data of the isolated products

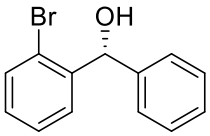

(*R*)-(2-bromophenyl)(phenyl)methanol (5a).[27] Colorless oil, 99% isolated yield (99% NMR conversion); 85% *ee*, determined by HPLC analysis on Chiralpak OD-3 column (Hexane/i-PrOH = 90/10, flow rate = 1 mL/min, λ= 230 nm), t_R = 8.9 min (*major*), t_R = 12.0 min (*minor*). [α]D^{22}= +33.65 (*c* 2.0, $CHCl_3$). ^{1}H NMR (600 MHz, Chloroform-*d*) δ 7.57 (dd, *J* = 7.8, 1.7 Hz, 1H), 7.52 (dd, *J* = 8.0, 1.2 Hz, 1H), 7.39 (d, *J* = 7.3 Hz, 2H), 7.36 – 7.29 (m, 3H), 7.30 – 7.22 (m, 1H), 7.13 (td, *J* = 7.7, 1.7 Hz, 1H), 6.18 (s, 1H), 2.53 (s, 1H). ^{13}C NMR (151 MHz, Chloroform-*d*) δ 142.55, 142.19, 132.85, 129.12, 128.51, 128.49, 127.78, 127.74, 127.06, 122.81, 74.78.

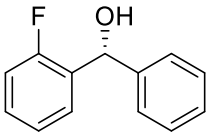

(*R*)-(2-fluorophenyl)(phenyl)methanol (5b).[28] Colorless oil, 85% isolated yield (99% NMR conversion); 88% *ee*, determined by HPLC analysis on Chiralpak OD-3 column (Hexane/i-PrOH = 95/5, flow rate = 1 mL/min, λ= 220 nm), t_R = 10.8 min (*major*), t_R = 11.8 min (*minor*). [α]D^{21}= -3.90 (*c* 2.0, $CHCl_3$). ^{1}H NMR (600 MHz, Chloroform-*d*) δ 7.49 (td, *J* = 7.6, 1.8 Hz, 1H), 7.39 (d, *J* = 7.2 Hz, 2H), 7.32 (t, *J* = 7.7 Hz, 2H), 7.29 – 7.20 (m, 2H), 7.13 (td, *J* = 7.6, 1.2 Hz, 1H), 7.00 (ddd, *J* = 10.5, 8.2, 1.2 Hz, 1H), 6.12 (s, 1H), 2.48 (s, 1H). ^{13}C NMR (151 MHz, Chloroform-*d*) δ 159.92 (d, J = 246.3 Hz), 142.78, 130.99 (d, J = 13.0 Hz), 129.13 (d, J = 8.4 Hz), 128.53, 127.74, 127.69 (d, J = 4.0 Hz), 126.41, 124.34 (d, J = 3.6 Hz), 115.39 (d, J = 21.7 Hz), 70.07 (d, J = 3.3 Hz). ^{19}F NMR (565 MHz, Chloroform-*d*) δ -118.46.

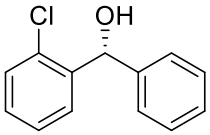

(*R*)-(2-chlorophenyl)(phenyl)methanol (5c).[27] Colorless oil, 99% isolated yield (99% NMR conversion); 87% *ee*, determined by HPLC analysis on Chiralpak OD-H column (Hexane/i-PrOH = 95/5, flow rate = 0.8 mL/min, λ= 220 nm), t_R = 16.4 min (*major*), t_R = 19.7 min (*minor*). $[\alpha]D^{21}$= +18.80 (*c* 2.0, $CHCl_3$). ^{1}H NMR (600 MHz, Chloroform-*d*) δ 7.59 (dd, *J* = 7.8, 1.6 Hz, 1H), 7.37 (d, *J* = 7.2 Hz, 2H), 7.31 (t, *J* = 7.6 Hz, 3H), 7.29 – 7.23 (m, 3H), 7.20 (td, *J* = 7.7, 1.7 Hz, 1H), 6.19 (s, 1H), 2.59 (s, 1H). ^{13}C NMR (151 MHz, Chloroform-*d*) δ 142.29, 141.04, 132.52, 129.56, 128.76, 128.49, 128.06, 127.78, 127.12, 126.95, 72.67.

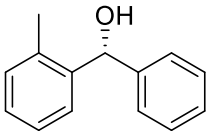

(*R*)-phenyl(o-tolyl)methanol (5d).[27] Colorless oil, 99% isolated yield (99% NMR conversion); 82% *ee*, determined by HPLC analysis on Chiralpak OJ-3 column (Hexane/i-PrOH = 90/10, flow rate = 1 mL/min, λ= 220 nm), t_R = 14.1 min (*major*), t_R = 15.5 min (*minor*). $[\alpha]D^{22}$= -3.30 (*c* 2.0, $CHCl_3$). ^{1}H NMR (600 MHz, Chloroform-*d*) δ 7.49 (dd, *J* = 7.6, 1.5 Hz, 1H), 7.30 (d, *J* = 4.4 Hz, 4H), 7.27 – 7.15 (m, 3H), 7.12 (dd, *J* = 7.5, 1.6 Hz, 1H), 5.96 (s, 1H), 2.22 (s, 3H). ^{13}C NMR (151 MHz, Chloroform-*d*) δ 142.93, 141.51, 135.39, 130.55, 128.48, 127.56, 127.52, 127.15, 126.32, 126.14, 73.35, 19.42.

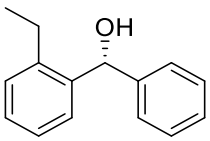

(*R*)-(2-ethylphenyl)(phenyl)methanol (5e).[29] Colorless oil, 99% isolated yield (99% NMR conversion); 86% *ee*, determined by HPLC analysis on Chiralpak OD-3 column (Hexane/i-PrOH =

95/5, flow rate = 1.0 mL/min, λ= 220 nm), t_R = 13.3 min (*major*), t_R = 14.5 min (*minor*). [α]D^{25}= +21.70 (*c* 2.0, $CHCl_3$). ^{1}H NMR (600 MHz, Chloroform-d) δ 7.38 (t, J = 8.2 Hz, 1H), 7.29 – 7.20 (m, 3H), 7.22 – 7.10 (m, 4H), 5.96 (q, J = 4.0 Hz, 1H), 2.66 – 2.47 (m, 2H), 1.11 – 1.03 (m, 3H). ^{13}C NMR (151 MHz, Chloroform-d) δ 143.5, 141.5, 140.9, 128.7, 128.5, 127.9, 127.5, 127.1, 126.9, 126.2, 72.7, 25.3, 15.3.

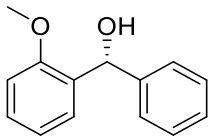

(*R*)-(2-methoxyphenyl)(phenyl)methanol (5f).[30] Colorless oil, 97% isolated yield (99% NMR conversion); 92% *ee*, determined by UPLC analysis on Chiralpak IBU column (Hexane/i-PrOH = 90/10, flow rate = 0.5 mL/min, λ= 230 nm), t_R = 3.6 min (*major*), t_R = 3.3 min (*minor*). [α]D^{24}= +33.15 (*c* 2.0, $CHCl_3$). ^{1}H NMR (400 MHz, Chloroform-*d*) δ 7.41 – 7.35 (m, 2H), 7.31 (t, *J* = 7.4 Hz, 2H), 7.27 – 7.20 (m, 3H), 6.93 (td, *J* = 7.5, 1.1 Hz, 1H), 6.87 (dd, *J* = 8.2, 1.0 Hz, 1H), 6.04 (s, 1H), 3.78 (s, 3H), 2.78 (s, 1H). ^{13}C NMR (101 MHz, Chloroform-*d*) δ 156.76, 143.31, 132.00, 128.75, 128.19, 127.87, 127.18, 126.58, 120.83, 110.79, 72.25, 55.44.

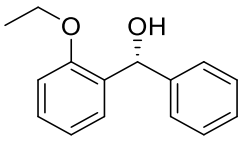

(*R*)-(2-ethoxyphenyl)(phenyl)methanol (5g).[31] Colorless oil, 99% isolated yield (99% NMR conversion); 86% *ee*, determined by HPLC analysis on Chiralpak OD-H column (Hexane/i-PrOH = 90/10, flow rate = 1.0 mL/min, λ= 220 nm), t_R = 7.7 min (*major*), t_R = 8.6 min (*minor*). [α]D^{24}= +27.20 (*c* 2.0, $CHCl_3$). ^{1}H NMR (600 MHz, Chloroform-d) δ 7.38 (t, J = 8.2 Hz, 1H), 7.29 – 7.22 (m, 4H), 7.21 – 7.11 (m, 4H), 5.96 (q, J = 4.0 Hz, 1H), 2.60 (ddd, J = 12.6, 8.7, 6.3 Hz, 1H), 2.53 (dddd, J =

15.3, 12.8, 7.7, 4.1 Hz, 1H), 1.13 – 1.01 (m, 3H). ^{13}C NMR (151 MHz, Chloroform-d) δ 156.08, 143.63, 132.23, 128.66, 128.14, 127.80, 127.10, 126.61, 120.71, 111.67, 72.56, 63.75, 14.84.

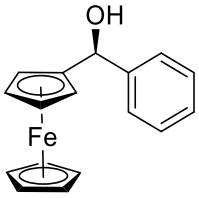

(*S*)-Phenyl-ferrocenyl-methanol (5h).[29] Yellow solid, 99% isolated yield (99% NMR conversion); 86% *ee*, determined by HPLC analysis on Chiralpak OD-3 column (Hexane/i-PrOH = 90/10, flow rate = 1 mL/min, λ= 210 nm), t_R = 15.7 min (*major*), t_R = 10.5 min (*minor*). [α]D^{22}= +79.20 (*c* 2.0, $CHCl_3$). ^{1}H NMR (600 MHz, Chloroform-*d*) δ 7.38 (d, *J* = 7.0 Hz, 2H), 7.31 (t, *J* = 7.5 Hz, 2H), 7.24 (t, *J* = 7.4 Hz, 1H), 5.46 (s, 1H), 4.21 (s, 5H), 4.19 – 4.14 (m, 3H), 2.53 (s, 1H). ^{13}C NMR (151 MHz, Chloroform-*d*) δ 143.29, 128.23, 127.45, 126.26, 94.22, 72.06, 68.52, 68.19, 68.12, 67.45, 66.06.

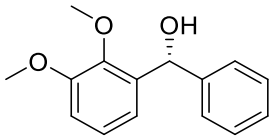

(*R*)-(2,3-dimethoxyphenyl)(phenyl)methanol (5i).[32] Colorless oil, 98% isolated yield (99% NMR conversion); 81% *ee*, determined by HPLC analysis on Chiralpak OD-3 column (Hexane/i-PrOH = 95/5, flow rate = 1.0 mL/min, λ= 220 nm), t_R = 19.7 min (*major*), t_R = 21.9 min (*minor*). [α]D^{25}= +23.10 (*c* 2.0, $CHCl_3$). ^{1}H NMR (600 MHz, Chloroform-d) δ 7.41 – 7.34 (m, 2H), 7.31 (td, J = 7.4, 6.6, 3.4 Hz, 2H), 7.27 – 7.18 (m, 1H), 7.05 (tt, J = 7.0, 2.8 Hz, 1H), 6.98 – 6.91 (m, 1H), 6.91 – 6.79 (m, 1H), 6.01 (t, J = 2.8 Hz, 1H), 3.84 (t, J = 2.9 Hz, 3H), 3.58 (t, J = 2.9 Hz, 3H), 3.05 (s, 1H). ^{13}C NMR (151 MHz, Chloroform-d) δ 152.68, 146.37, 144.00, 137.62, 128.24, 127.19, 126.37, 124.08, 119.77, 111.98, 72.44, 60.48, 55.78.

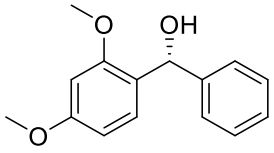

(*R*)-(2,4-dimethoxyphenyl)(phenyl)methanol (5j).[33] Colorless oil, 98% isolated yield (99% NMR conversion); 85% *ee*, determined by UPLC analysis on Chiralpak IBU column (Hexane/i-PrOH = 90/10, flow rate = 0.5 mL/min, λ= 210 nm), t_R = 5.5 min (*major*), t_R = 3.8 min (*minor*). [α]D^{25}= +23.60 (*c* 1.0, $CHCl_3$). ^{1}H NMR (400 MHz, Chloroform-d) δ 7.41 (d, J = 7.2 Hz, 2H), 7.35 (t, J = 7.6 Hz, 2H), 7.33 – 7.20 (m, 1H), 7.10 (d, J = 8.3 Hz, 1H), 6.53 – 6.43 (m, 2H), 6.04 (s, 1H), 3.82 (d, J = 1.5 Hz, 6H), 2.94 (s, 1H). ^{13}C NMR (151 MHz, Chloroform-d) δ 160.40, 157.87, 143.50, 128.66, 128.14, 127.06, 126.49, 124.76, 104.16, 98.85, 71.83, 55.45, 55.40.

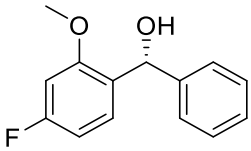

(*R*)-(4-fluoro-2-methoxyphenyl)(phenyl)methanol (5k). Novel compound. Colorless oil, 95% isolated yield (99% NMR conversion); 88% *ee*, determined by UPLC analysis on Chiralpak IBU column (Hexane/i-PrOH = 90/10, flow rate = 0.5 mL/min, λ= 230 nm), t_R = 2.9 min (*major*), t_R = 2.5 min (*minor*). [α]D^{23}= +20.00 (*c* 0.2, $CHCl_3$). ^{1}H NMR (400 MHz, Chloroform-d) δ 7.42 – 7.27 (m, 5H), 7.23 – 7.16 (m, 1H), 6.69 – 6.56 (m, 2H), 6.04 (d, J = 4.3 Hz, 1H), 3.80 (s, 3H), 2.76 (d, J = 5.0 Hz, 1H). ^{13}C NMR (101 MHz, Chloroform-d) δ 163.1 (d, J = 245.4 Hz), 157.8 (d, J = 9.8 Hz), 143.2, 128.6 (d, J = 10.0 Hz), 128.3, 128.0 (d, J = 3.3 Hz), 127.3, 126.5, 106.9 (d, J = 21.0 Hz), 99.1 (d, J = 25.8 Hz), 71.3, 55.7. ^{19}F NMR (376 MHz, Chloroform-d) δ -112.24 (p, J = 8.4 Hz).

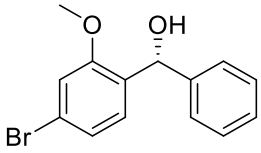

(*R*)-(4-bromo-2-methoxyphenyl)(phenyl)methanol (5l). Novel compound. Colorless oil, 95% isolated yield (99% NMR conversion); 91% *ee*, determined by UPLC analysis on Chiralpak IBU column (Hexane/i-PrOH = 90/10, flow rate = 0.5 mL/min, λ= 210 nm), t_R = 3.0 min (*major*), t_R = 2.5 min (*minor*). [α]D^{25}= +23.45 (*c* 2.0, $CHCl_3$). ^{1}H NMR (600 MHz, Chloroform-d) δ 7.38 – 7.28 (m, 4H), 7.24 (d, J = 6.6 Hz, 1H), 7.15 (d, J = 8.2 Hz, 1H), 7.08 (d, J = 8.1 Hz, 1H), 6.99 (s, 1H), 6.00 (s, 1H), 3.77 (s, 3H), 2.80 (s, 1H). ^{13}C NMR (151 MHz, Chloroform-d) δ 157.19, 142.79, 131.23, 128.85, 128.31, 127.43, 126.52, 123.81, 121.92, 114.32, 71.38, 55.75.

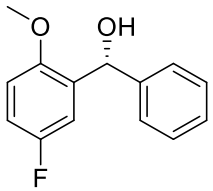

(*R*)-(5-fluoro-2-methoxyphenyl)(phenyl)methanol (5m). Novel compound. Colorless oil, 86% isolated yield (99% NMR conversion); 92% *ee*, determined by UPLC analysis on Chiralpak IBU column (Hexane/i-PrOH = 90/10, flow rate = 0.5 mL/min, λ= 230 nm), t_R = 2.6 min (*major*), t_R = 2.3 min (*minor*). [α]D^{25}= +17.95 (*c* 2.0, $CHCl_3$). ^{1}H NMR (400 MHz, Chloroform-d) δ 7.40 – 7.28 (m, 4H), 7.30 – 7.21 (m, 1H), 7.19 (dd, J = 8.3, 6.7 Hz, 1H), 6.68 – 6.52 (m, 2H), 6.03 (s, 1H), 3.79 (s, 3H), 2.80 (s, 1H). ^{13}C NMR (101 MHz, Chloroform-d) δ 158.38, 156.01, 152.68, 142.65, 133.82 (d, J = 6.6 Hz), 128.34, 127.51, 126.57, 114.48 (t, J = 24.0 Hz), 111.63 (d, J = 8.2 Hz), 71.47, 55.98. ^{19}F NMR (376 MHz, Chloroform-d) δ -123.08 (td, J = 8.5, 4.3 Hz).

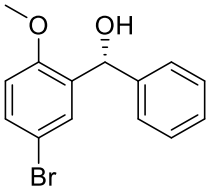

(*R*)-(5-bromo-2-methoxyphenyl)(phenyl)methanol (5n).[34] Colorless oil, 99% isolated yield (99% NMR conversion); 91% *ee*, determined by UPLC analysis on Chiralpak IBU column (Hexane/i-PrOH = 95/5, flow rate = 0.5 mL/min, λ= 230 nm), t_R = 4.5 min (*major*), t_R = 3.9 min (*minor*). [α]D^{25}= -16.10 (*c* 2.0, $CHCl_3$). ^{1}H NMR (400 MHz, Chloroform-d) δ 7.45 (d, J = 2.4 Hz, 1H), 7.44 – 7.21 (m, 6H), 6.74 (d, J = 8.8 Hz, 1H), 6.02 (s, 1H), 3.77 (d, J = 1.5 Hz, 3H), 2.80 (s, 1H). ^{13}C NMR (101 MHz, Chloroform-d) δ 155.65, 142.62, 134.21, 131.26, 130.33, 128.35, 127.53, 126.55, 113.30, 112.48, 71.38, 55.70.

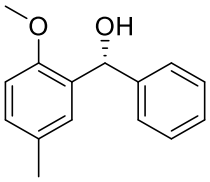

(*R*)-(2-methoxy-5-methylphenyl)(phenyl)methanol (5o). Novel compound. Colorless oil, 99% isolated yield (99% NMR conversion); 90% *ee*, determined by UPLC analysis on Chiralpak IBU column (Hexane/i-PrOH = 95/5, flow rate = 0.5 mL/min, λ= 210 nm), t_R = 3.9 min (*major*), t_R = 3.5 min (*minor*). [α]D^{25}= +16.90 (*c* 2.0, $CHCl_3$). ^{1}H NMR (400 MHz, Chloroform-d) δ 7.43 – 7.29 (m, 4H), 7.34 – 7.14 (m, 1H), 7.04 (d, J = 6.8 Hz, 2H), 6.81 – 6.74 (m, 1H), 6.01 (s, 1H), 3.77 (s, 3H), 3.05 (s, 1H), 2.26 (s, 3H). ^{13}C NMR (101 MHz, Chloroform-d) δ 154.68, 143.44, 131.63, 130.08, 128.94, 128.51, 128.16, 127.10, 126.50, 110.82, 72.39, 55.56, 20.61.

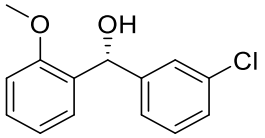

(*R*)-(3-chlorophenyl)(2-methoxyphenyl)methanol (5p). Novel compound. Colorless oil, 99% isolated yield (99% NMR conversion); 86% *ee*, determined by UPLC analysis on Chiralpak IBU column (Hexane/i-PrOH = 95/5, flow rate = 0.5 mL/min, λ= 230 nm), t_R = 2.7 min (*major*), t_R = 3.3 min (*minor*). [α]D^{25}= +46.90 (*c* 1.0, $CHCl_3$). ^{1}H NMR (400 MHz, Chloroform-d) δ 7.42 – 7.35 (m, 1H), 7.33 – 7.17 (m, 5H), 7.00 – 6.86 (m, 2H), 6.00 (s, 1H), 3.81 (d, J = 1.3 Hz, 3H), 3.07 (s, 1H). ^{13}C NMR (101 MHz, Chloroform-d) δ 156.63, 145.48, 134.10, 131.29, 129.42, 129.06, 127.85, 127.26, 126.65, 124.64, 120.94, 110.86, 71.77, 55.43.

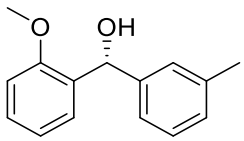

(*R*)-(2-methoxyphenyl)(m-tolyl)methanol (5q). Colorless oil, 99% isolated yield (99% NMR conversion); 86% *ee*, determined by UPLC analysis on Chiralpak ICU column (Hexane/i-PrOH = 90/10, flow rate = 0.5 mL/min, λ= 230 nm), t_R = 3.0 min (*major*), t_R = 3.4 min (*minor*). [α]D^{24}= +21.45 (*c* 2.0, $CHCl_3$). ^{1}H NMR (400 MHz, Chloroform-d) δ 7.26 (d, J = 1.5 Hz, 1H), 7.25 – 7.14 (m, 4H), 7.06 (d, J = 7.3 Hz, 1H), 6.98 – 6.85 (m, 2H), 6.06 – 6.00 (m, 1H), 3.82 (s, 3H), 3.00 (d, J = 4.4 Hz, 1H), 2.33 (s, 3H). ^{13}C NMR (101 MHz, Chloroform-d) δ 156.77, 143.34, 137.79, 132.18, 128.70, 128.12, 127.99, 127.90, 127.33, 123.76, 120.86, 110.80, 72.03, 55.46, 21.60.

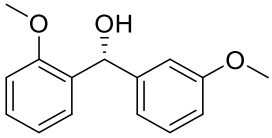

(*R*)-(2-methoxyphenyl)(3-methoxyphenyl)methanol (5r).[35] Colorless oil, 98% isolated yield (99% NMR conversion); 87% *ee*, determined by UPLC analysis on Chiralpak IBU column (Hexane/i-PrOH

= 97/3, flow rate = 0.5 mL/min, λ= 230 nm), t_R = 7.9 min (*major*), t_R = 7.3 min (*minor*). [α]D^{25}= +29.00 (*c* 2.0, $CHCl_3$). ^{1}H NMR (600 MHz, Chloroform-d) δ 7.23 (dd, J = 16.2, 7.9 Hz, 3H), 6.98 (d, J = 2.4 Hz, 1H), 6.93 (dd, J = 10.8, 7.2 Hz, 2H), 6.88 (d, J = 8.2 Hz, 1H), 6.78 (d, J = 8.0 Hz, 1H), 6.02 (s, 1H), 3.82 – 3.75 (m, 6H), 3.08 (s, 1H). ^{13}C NMR (151 MHz, Chloroform-d) δ 159.56, 156.75, 145.00, 131.85, 129.17, 128.78, 127.92, 120.85, 118.95, 112.66, 112.15, 110.78, 72.10, 55.45, 55.20.

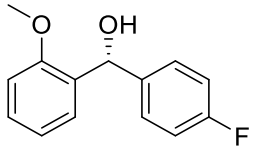

(*R*)-(4-fluorophenyl)(2-methoxyphenyl)methanol (5s).[35] Colorless oil, 99% isolated yield (99% NMR conversion); 89% *ee*, determined by HPLC analysis on Chiralpak OD-3 column (Hexane/i-PrOH = 95/5, flow rate = 1.0 mL/min, λ= 220 nm), t_R = 14.5 min (*major*), t_R = 18.7 min (*minor*). [α]D^{25}= +24.85 (*c* 2.0, $CHCl_3$). ^{1}H NMR (400 MHz, Chloroform-d) δ 7.38 – 7.29 (m, 2H), 7.23 (ddd, J = 17.3, 7.7, 1.7 Hz, 2H), 7.04 – 6.90 (m, 3H), 6.88 (dd, J = 8.2, 1.0 Hz, 1H), 6.01 (s, 1H), 3.79 (s, 3H), 3.06 (s, 1H). ^{13}C NMR (101 MHz, Chloroform-d) δ 162.0 (d, J = 245.0 Hz), 156.6, 139.0 (d, J = 3.2 Hz), 131.8, 128.9, 128.2 (d, J = 8.1 Hz), 127.6, 120.9, 114.9 (d, J = 21.4 Hz), 110.8, 71.7, 55.4. ^{19}F NMR (376 MHz, Chloroform-d) δ -115.81 (ddd, J = 14.2, 8.8, 5.2 Hz).

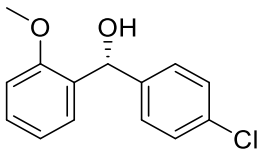

***(R)*-(4-chlorophenyl)(2-methoxyphenyl)methanol (5t).**[36] Colorless oil, 99% isolated yield (99% NMR conversion); 88% *ee*, determined by HPLC analysis on Chiralpak OD-H column (Hexane/i-PrOH = 90/10, flow rate = 1.0 mL/min, λ= 210 nm), t_R = 10.1 min (*major*), t_R = 12.5 min (*minor*). [α]D^{21}= +32.70 (*c* 2.0, $CHCl_3$). ^{1}H NMR (600 MHz, Chloroform-d) δ 7.34 – 7.27 (m, 5H), 7.20 (dd, J = 7.5, 1.7 Hz, 1H), 6.95 (td, J = 7.5, 1.0 Hz, 1H), 6.89 (dd, J = 8.2, 1.0 Hz, 1H), 6.01 (d, J = 5.5 Hz,

1H), 3.81 (s, 3H), 3.00 (d, J = 5.7 Hz, 1H). ^{13}C NMR (151 MHz, Chloroform-d) δ 156.66, 141.82, 132.84, 131.51, 128.99, 128.28, 127.92, 127.75, 120.90, 110.81, 71.79, 55.41.

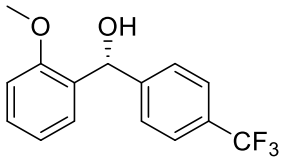

(*R*)-(2-methoxyphenyl)(4-(trifluoromethyl)phenyl)methanol (5u).[35] Colorless oil, 99% isolated yield (99% NMR conversion); 80% *ee*, determined by UPLC analysis on Chiralpak IBU column (Hexane/i-PrOH = 95/5, flow rate = 0.5 mL/min, λ= 230 nm), t_R = 4.1 min (*major*), t_R = 4.9 min (*minor*). [α]D^{29} = +37.35 (*c* 2.0, $CHCl_3$). ^{1}H NMR (400 MHz, Chloroform-d) δ 7.57 – 7.44 (m, 4H), 7.31 – 7.17 (m, 2H), 6.93 (t, J = 7.5 Hz, 1H), 6.87 (d, J = 8.2 Hz, 1H), 6.04 (d, J = 5.4 Hz, 1H), 3.76 (d, J = 1.1 Hz, 3H), 3.32 – 3.25 (m, 1H). ^{13}C NMR (101 MHz, Chloroform-*d*) δ 156.58, 147.45, 131.26, 129.16, 127.75, 126.74, 125.08 (q, *J* = 3.7 Hz), 120.98, 110.87, 71.65, 55.38. ^{19}F NMR (376 MHz, Chloroform-d) δ -62.33.

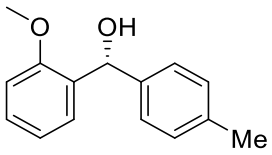

***(R)*-(2-methoxyphenyl)(p-tolyl)methanol (5v).**[35] Colorless oil, 93% isolated yield (99% NMR conversion); 92% *ee*, determined by UPLC analysis on Chiralpak IA-U column (Hexane/i-PrOH = 90/10, flow rate = 0.5 mL/min, λ= 230 nm), t_R = 3.6 min (*major*), t_R = 3.2 min (*minor*). [α]D^{21}= +24.30 (*c* 2.0, $CHCl_3$). ^{1}H NMR (600 MHz, Chloroform-d) δ 7.29 – 7.21 (m, 4H), 7.13 (d, J = 7.8 Hz, 2H), 6.94 (td, J = 7.5, 1.0 Hz, 1H), 6.89 (dd, J = 8.2, 1.0 Hz, 1H), 6.03 (d, J = 5.4 Hz, 1H), 3.81 (s, 3H), 2.96 (d, J = 5.5 Hz, 1H), 2.33 (s, 3H). ^{13}C NMR (151 MHz, Chloroform-d) δ 156.75, 140.30, 136.78, 132.08, 128.88, 128.64, 127.80, 126.51, 120.78, 110.73, 72.18, 55.42, 21.12.

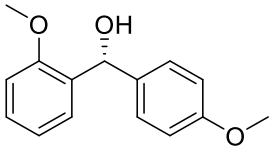

(*R*)-(2-methoxyphenyl)(4-methoxyphenyl)methanol (5w).[35] Colorless oil, 99% isolated yield (99% NMR conversion); 91% *ee*, determined by UPLC analysis on Chiralpak IBU column (Hexane/i-PrOH = 95/5, flow rate = 0.5 mL/min, λ= 230 nm), t_R = 7.5 min (*major*), t_R = 7.1 min (*minor*). $[\alpha]D^{29}$ = +26.60 (*c* 2.0, $CHCl_3$). ^{1}H NMR (400 MHz, Chloroform-*d*) δ 7.25 (dd, *J* = 12.7, 8.1 Hz, 4H), 6.92 (t, *J* = 7.5 Hz, 1H), 6.84 (t, *J* = 8.3 Hz, 3H), 5.98 (d, *J* = 4.4 Hz, 1H), 3.75 (dd, *J* = 4.3, 1.1 Hz, 6H), 3.08 (d, *J* = 4.8 Hz, 1H). ^{13}C NMR (101 MHz, Chloroform-*d*) δ 158.75, 156.68, 135.61, 132.27, 128.61, 127.89, 127.62, 120.80, 113.59, 110.74, 71.71, 55.44, 55.26.

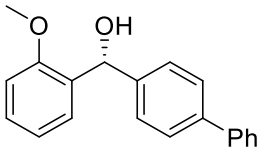

(*R*)-[1,1'-biphenyl]-4-yl(2-methoxyphenyl)methanol (5x). Novel compound. Colorless oil, 99% isolated yield (99% NMR conversion); 91% *ee*, determined by UPLC analysis on Chiralpak IBU column (Hexane/i-PrOH = 95/5, flow rate = 0.5 mL/min, λ= 254 nm), t_R = 7.1 min (*major*), t_R = 8.3 min (*minor*). $[\alpha]D^{28}$ = +47.25 (*c* 2.0, $CHCl_3$). ^{1}H NMR (400 MHz, Chloroform-d) δ 7.54 – 7.43 (m, 4H), 7.39 (d, J = 8.3 Hz, 2H), 7.37 – 7.23 (m, 3H), 7.27 – 7.18 (m, 1H), 7.16 (td, J = 7.8, 1.8 Hz, 1H), 6.88 (td, J = 7.5, 1.1 Hz, 1H), 6.75 (dd, J = 8.3, 1.1 Hz, 1H), 6.03 (s, 1H), 3.62 (s, 3H), 3.43 (s, 1H). ^{13}C NMR (101 MHz, Chloroform-d) δ 156.75, 142.85, 141.11, 140.04, 132.23, 128.96, 128.87, 127.84, 127.38, 127.26, 127.23, 127.06, 121.03, 110.92, 71.69, 55.51.

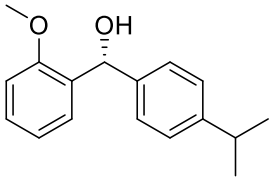

(*R*)-(4-isopropylphenyl)(2-methoxyphenyl)methanol (5y).[35] Colorless oil, 99% isolated yield (99% NMR conversion); 92% *ee*, determined by UPLC analysis on Chiralpak IBU column (Hexane/i-PrOH = 95/5, flow rate = 0.5 mL/min, λ= 230 nm), t_R = 3.5 min (*major*), t_R = 4.0 min (*minor*). $[\alpha]D^{29}$ = +24.60 (*c* 2.0, $CHCl_3$). ^{1}H NMR (400 MHz, Chloroform-d) δ 7.31 – 7.11 (m, 6H), 6.90 (td, J = 7.5, 1.1 Hz, 1H), 6.82 (dd, J = 8.2, 1.1 Hz, 1H), 6.00 (d, J = 4.5 Hz, 1H), 3.72 (s, 3H), 3.13 (d, J = 5.0 Hz, 1H), 2.86 (hept, J = 6.9 Hz, 1H), 1.21 (d, J = 7.0 Hz, 6H). ^{13}C NMR (101 MHz, Chloroform-d) δ 156.74, 147.75, 140.85, 132.23, 128.64, 127.80, 126.66, 126.30, 120.85, 110.76, 71.94, 55.44, 33.88, 24.13.

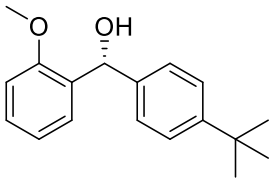

(*R*)-(4-(*tert*-butyl)phenyl)(2-methoxyphenyl)methanol (5z). Novel compound. Colorless oil, 99% isolated yield (99% NMR conversion); 92% *ee*, determined by UPLC analysis on Chiralpak IBU column (Hexane/i-PrOH = 95/5, flow rate = 0.5 mL/min, λ= 230 nm), t_R = 3.2 min (*major*), t_R = 4.1 min (*minor*). $[\alpha]D^{23}$ = +19.40 (*c* 1.0, $CHCl_3$). ^{1}H NMR (400 MHz, Chloroform-d) δ 7.37 – 7.26 (m, 4H), 7.29 – 7.17 (m, 2H), 6.93 (td, J = 7.5, 1.1 Hz, 1H), 6.87 (d, J = 8.3 Hz, 1H), 6.03 (d, J = 5.2 Hz, 1H), 3.79 (s, 3H), 3.04 (d, J = 5.5 Hz, 1H), 1.30 (s, 9H). ^{13}C NMR (101 MHz, Chloroform-d) δ 156.74, 150.00, 140.30, 132.07, 128.62, 127.82, 126.31, 125.13, 120.82, 110.72, 72.02, 55.43, 34.51, 31.43.

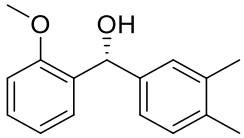

(*R*)-(3,4-dimethylphenyl)(2-methoxyphenyl)methanol (5aa). Novel compound. Colorless oil, 99% isolated yield (99% NMR conversion); 90% *ee*, determined by UPLC analysis on Chiralpak IBU column (Hexane/i-PrOH = 95/5, flow rate = 0.5 mL/min, λ= 230 nm), t_R = 5.5 min (*major*), t_R = 6.2 min (*minor*). [α]D^{25}= +28.05 (*c* 2.0, $CHCl_3$). ^{1}H NMR (600 MHz, Chloroform-d) δ 7.24 (t, J = 7.4 Hz, 2H), 7.16 (s, 1H), 7.08 (d, J = 2.3 Hz, 2H), 6.93 (td, J = 7.5, 1.1 Hz, 1H), 6.90 – 6.85 (m, 1H), 6.00 (s, 1H), 3.81 (s, 3H), 2.97 (s, 1H), 2.23 (d, J = 1.9 Hz, 6H). ^{13}C NMR (151 MHz, Chloroform-d) δ 156.76, 140.71, 136.35, 135.47, 132.14, 129.44, 128.59, 127.89, 127.83, 124.04, 120.78, 110.72, 72.06, 55.44, 19.90, 19.48.

3.7 Appendix

3.7.1 NMR spectra

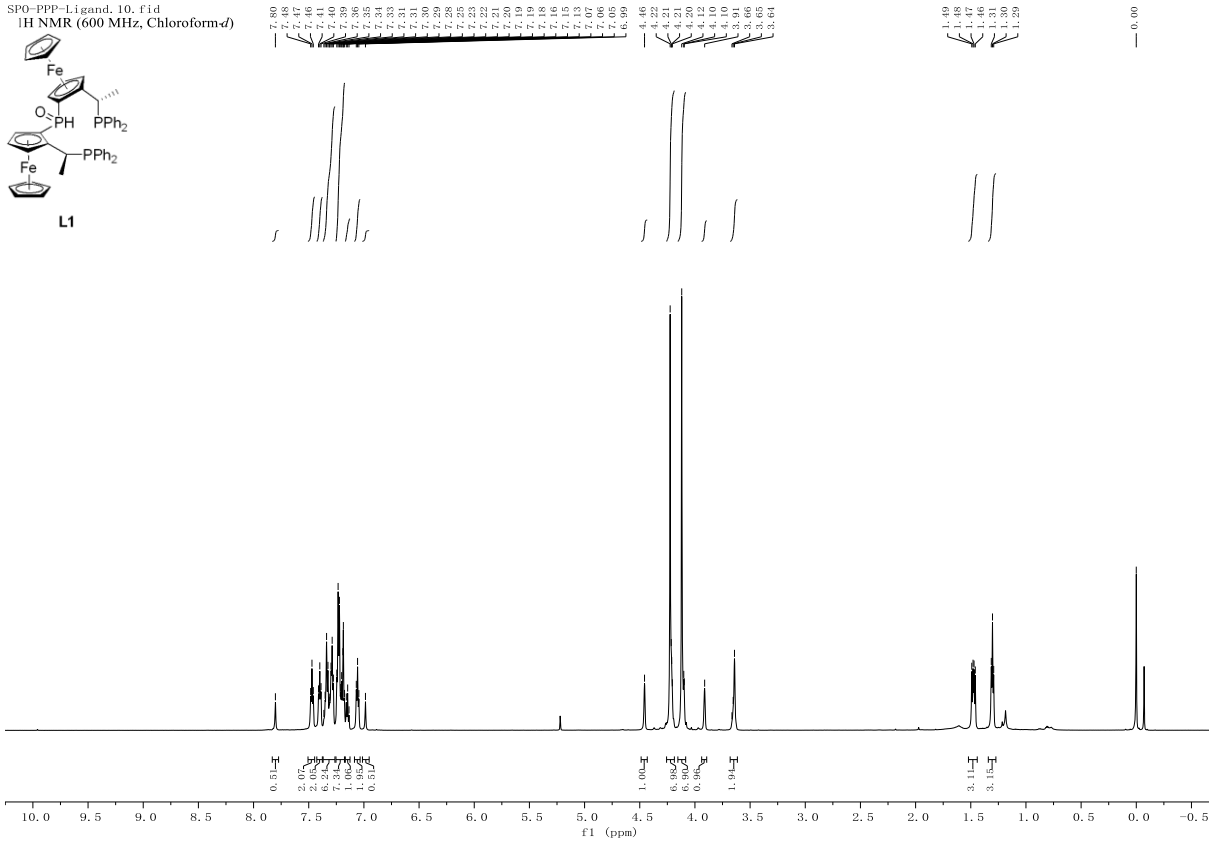

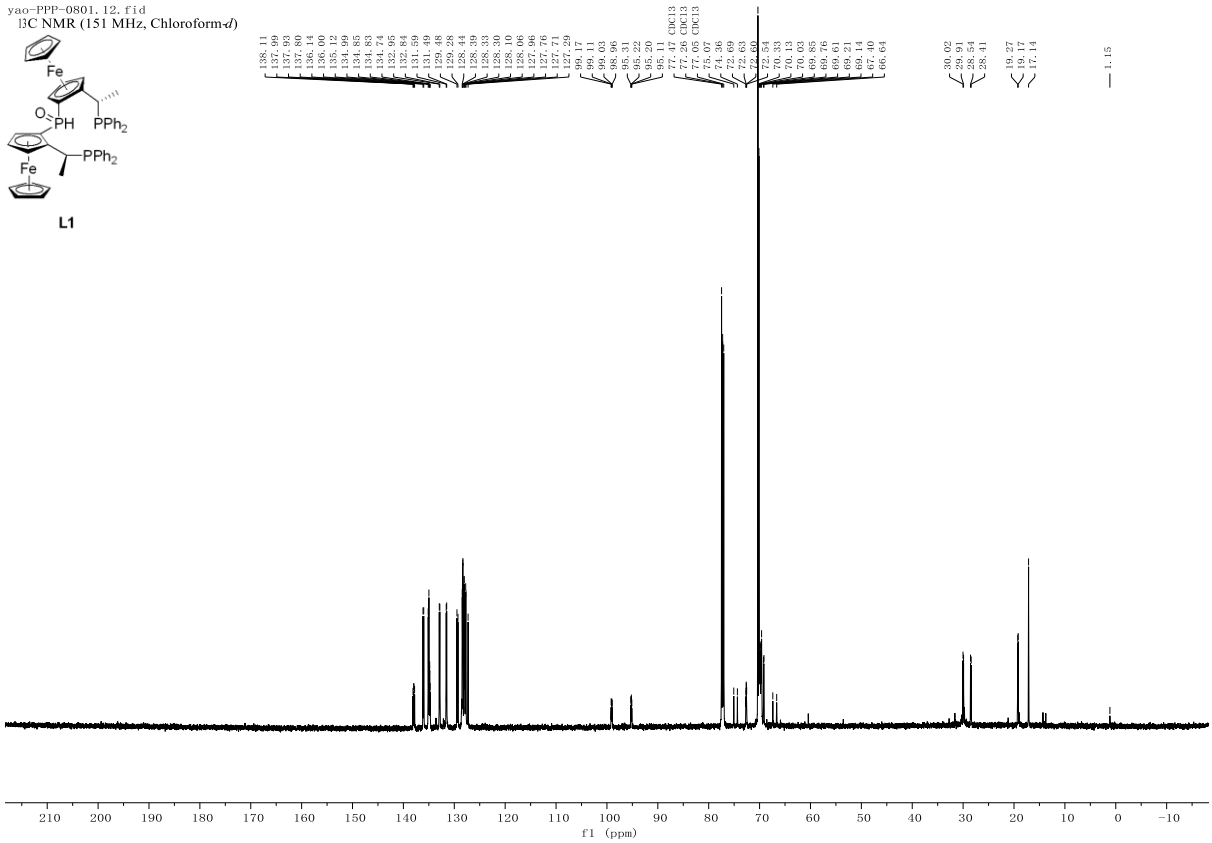
yao-PPP-0801.12.fid
13C NMR (151 MHz, Chloroform-d)
L1
CDCl3
CDCl3
CDCl3
f1 (ppm)

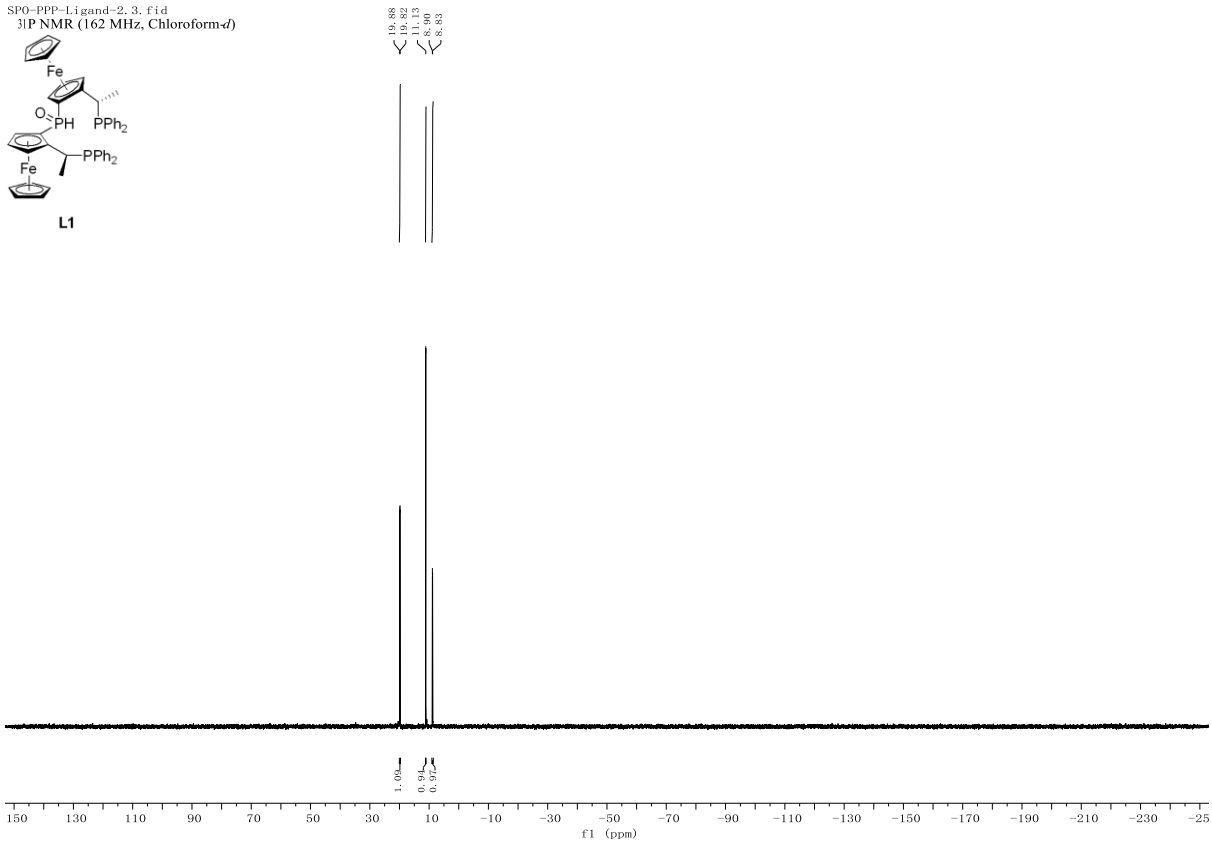
SPO-PPP-Ligand-2.3.fid
31P NMR (162 MHz, Chloroform-d)
L1
f1 (ppm)

Liyao-210517-PPP-1.10.fid
1H NMR (600 MHz, Chloroform-*d*)

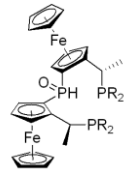

L2 R = 3,5-dimethyl-ph

Liyao-210517-PPP-1.12.fid
13C NMR (151 MHz, Chloroform-*d*)

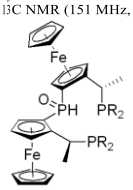

L2 R = 3,5-dimethyl-ph

yao-517-PPP-0801.11.fid

31P NMR (243 MHz, Chloroform-*d*)

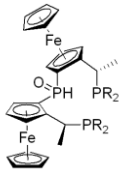

L2 R = 3,5-dimethyl-ph

yao-201026-5.1.fid

1H NMR (400 MHz, Chloroform-*d*)

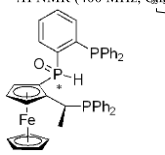

L3

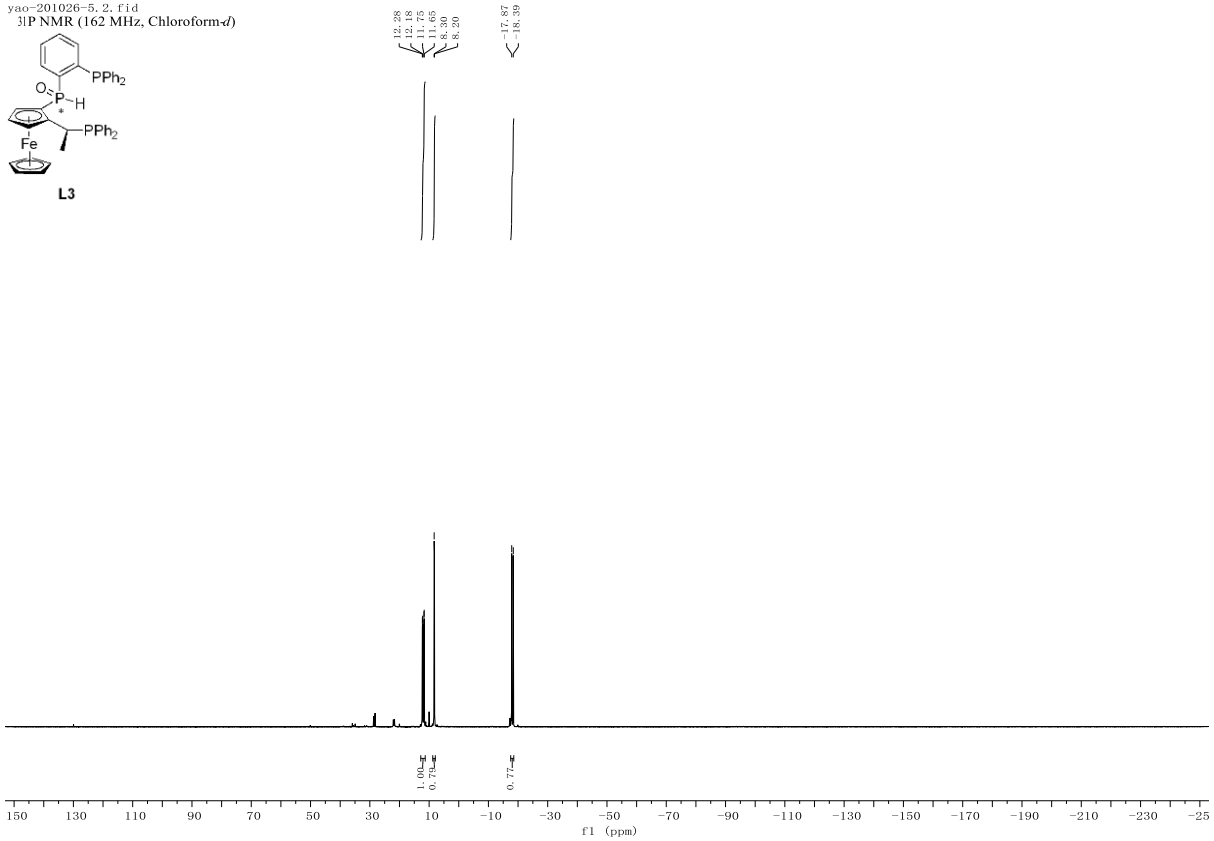
yao-201026-5.2.fid
31P NMR (162 MHz, Chloroform-d)
PPh2
O
P
H
PPh2
Fe
L3
12.28
12.18
11.75
11.65
8.30
8.20
-17.87
-18.39
1.00
0.79
0.77
150 130 110 90 70 50 30 10 -10 -30 -50 -70 -90 -110 -130 -150 -170 -190 -210 -230 -25
f1 (ppm)

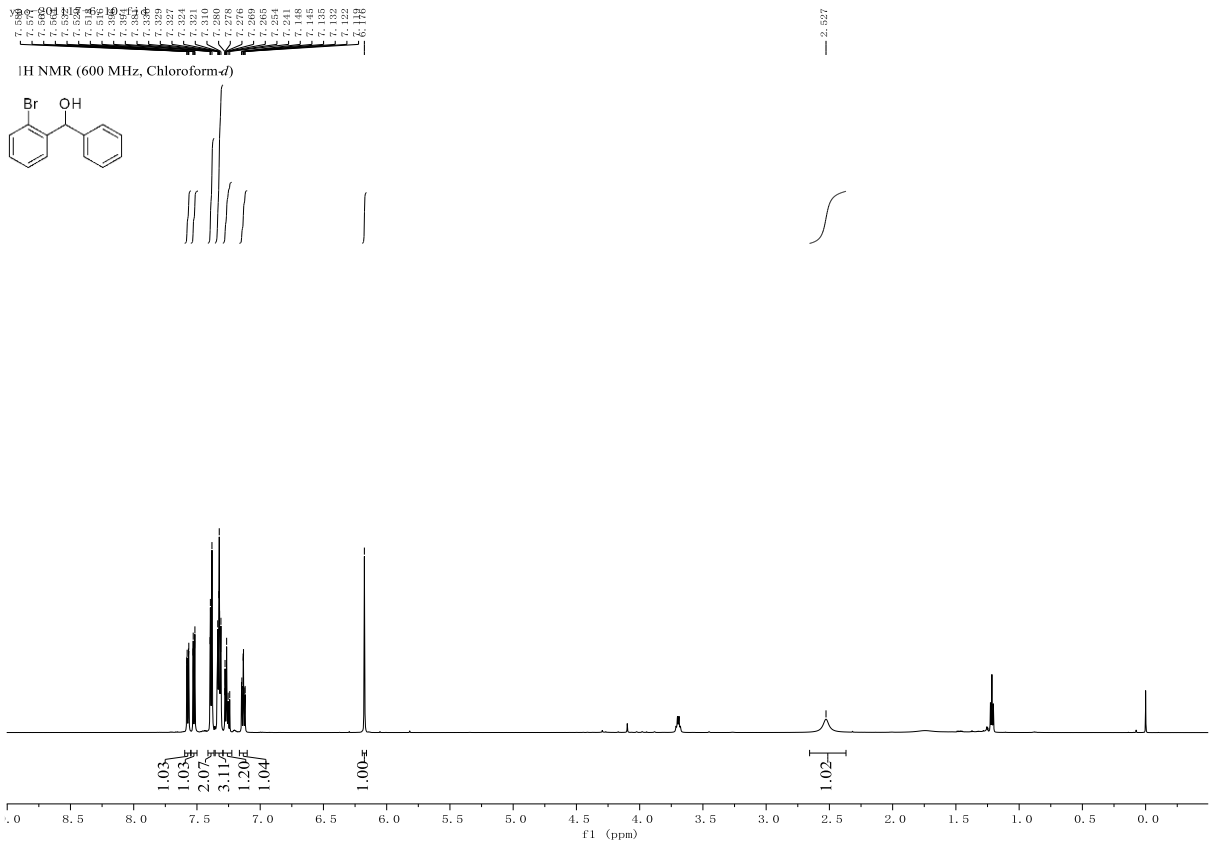
1H NMR (600 MHz, Chloroform-d)
Br
OH
2.527
1.03
1.03
2.07
3.11
1.20
1.04
1.00
1.02
8.5 8.0 7.5 7.0 6.5 6.0 5.5 5.0 4.5 4.0 3.5 3.0 2.5 2.0 1.5 1.0 0.5 0.0
f1 (ppm)

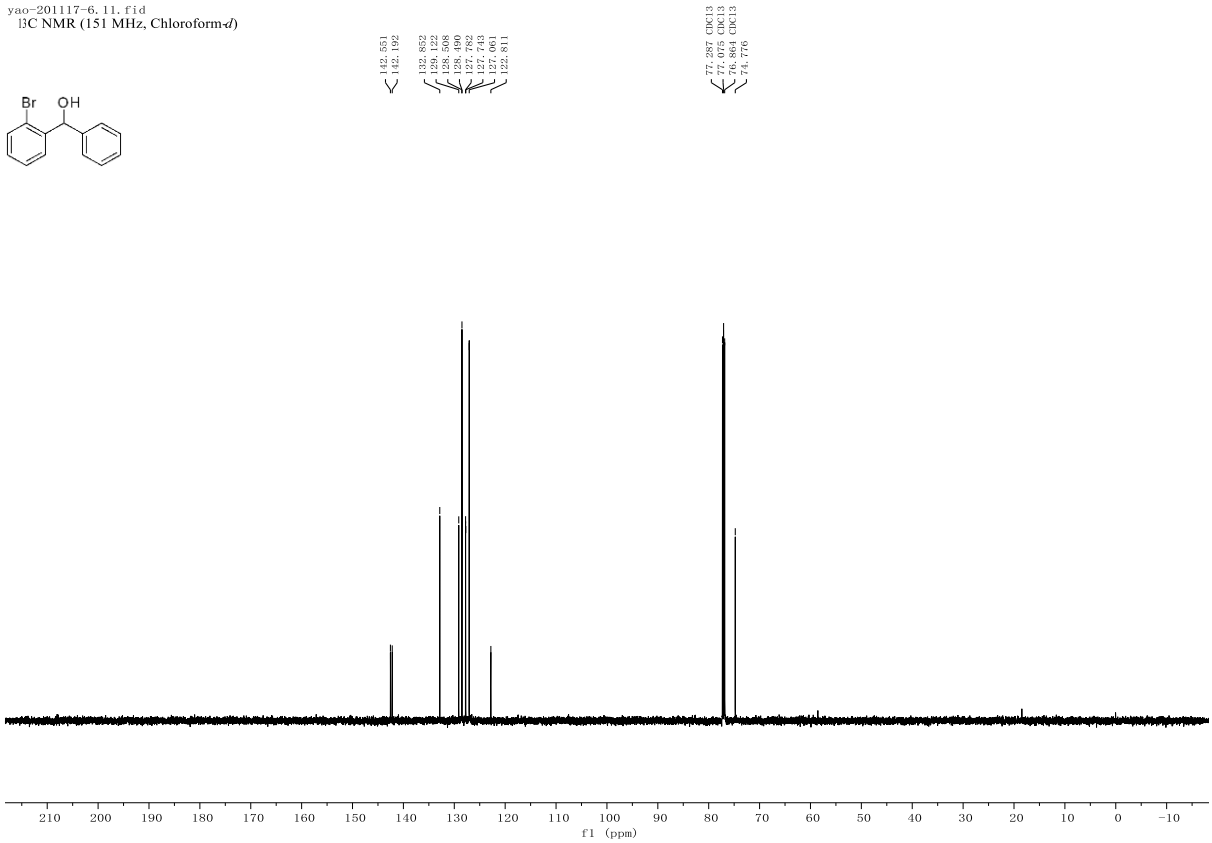
yao-201117-6.11.fid
13C NMR (151 MHz, Chloroform-d)
Br
OH
142.551
142.192
132.852
129.272
128.508
128.490
127.782
127.743
127.001
122.611
77.287 CDCl3
77.075 CDCl3
76.864 CDCl3
74.776
f1 (ppm)

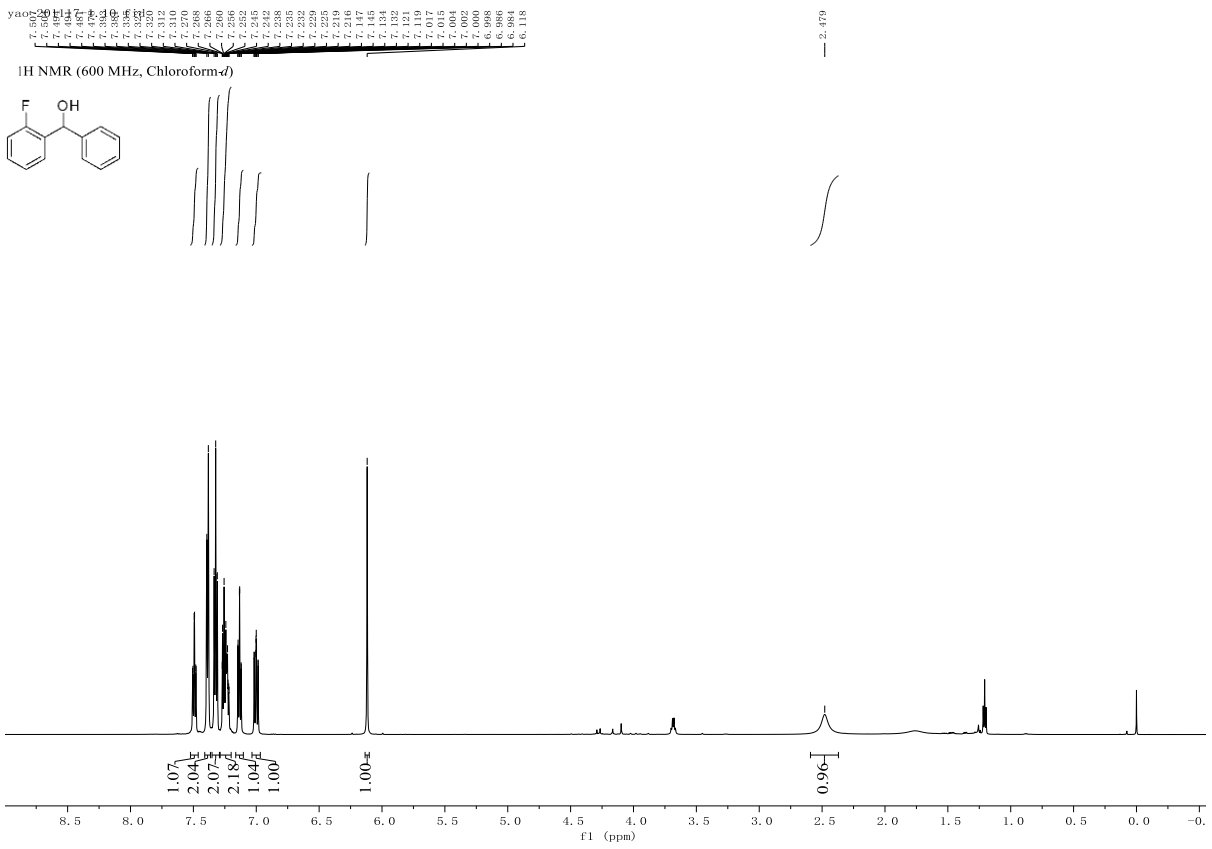
1H NMR (600 MHz, Chloroform-d)
F
OH
2.479
1.07
2.04
2.07
2.18
1.04
1.00
1.00
0.96
f1 (ppm)

yao-201117-1.12.fid
13C NMR (151 MHz, Chloroform-d)

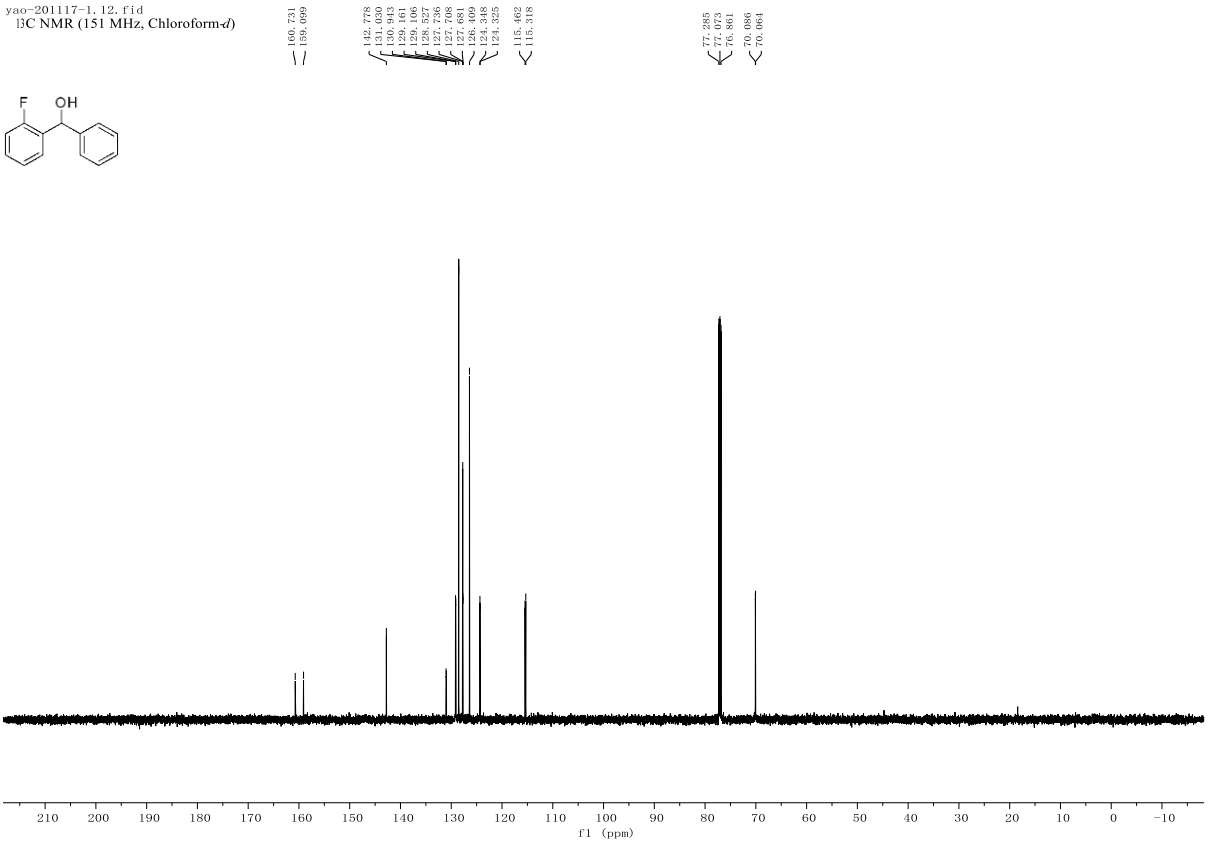

yao-201117-1.11.fid
19F NMR (565 MHz, Chloroform-d)

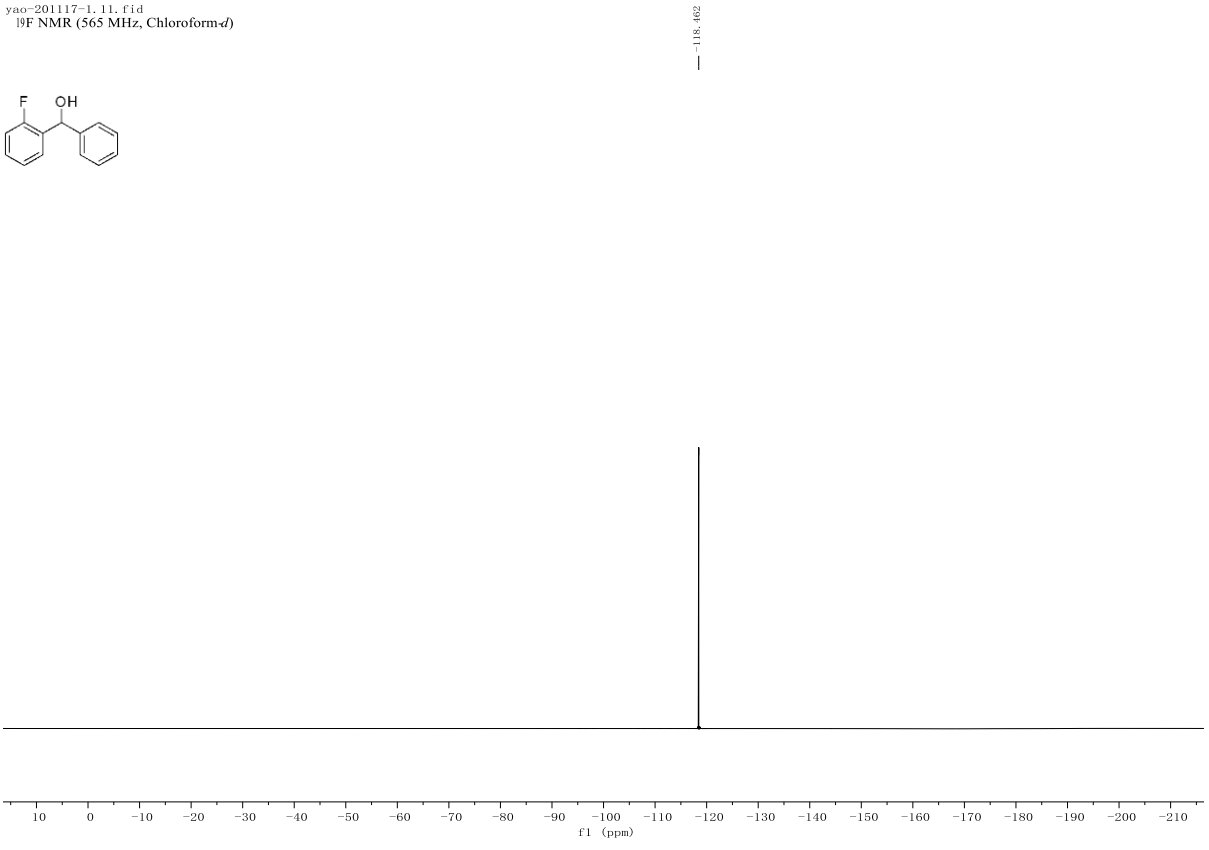

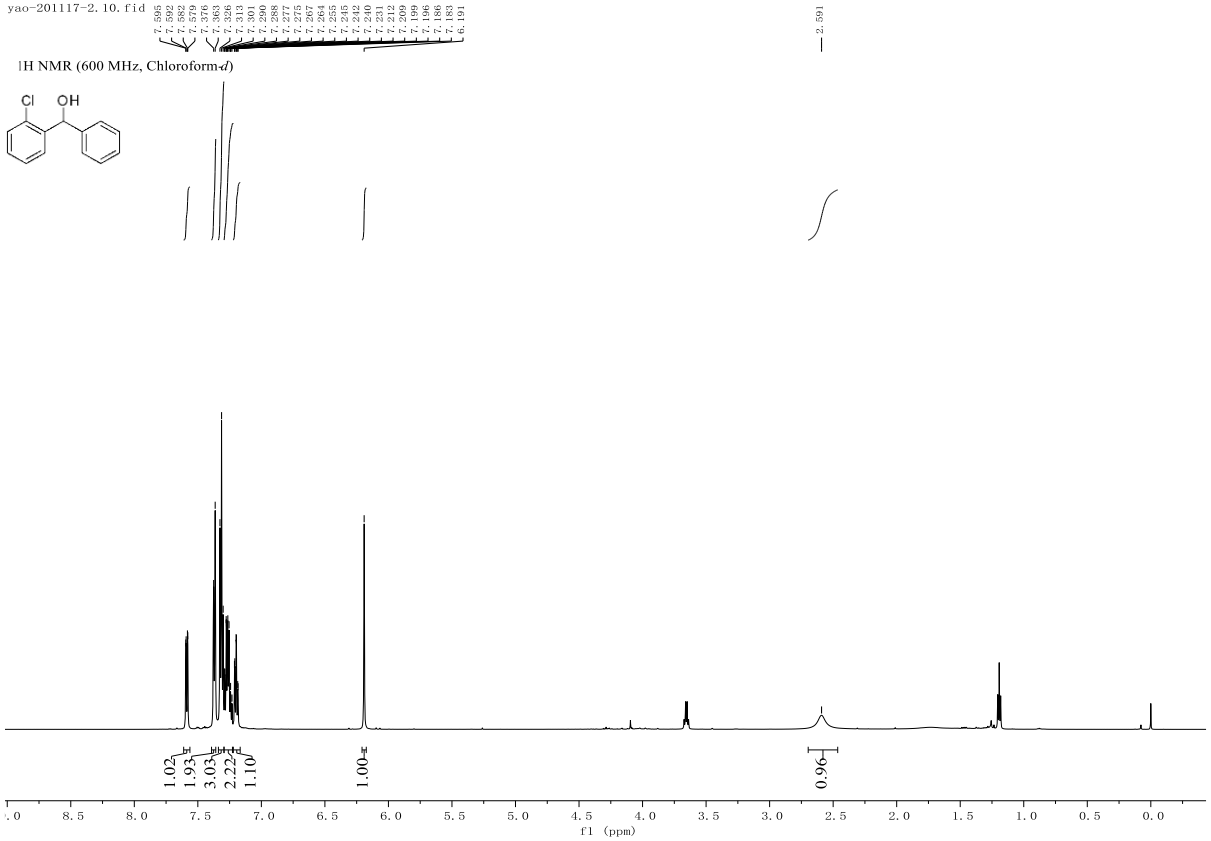
yao-201117-2.10.fid
1H NMR (600 MHz, Chloroform-d)
Cl
OH
1.02
1.93
3.03
2.22
1.10
1.00
0.96
f1 (ppm)

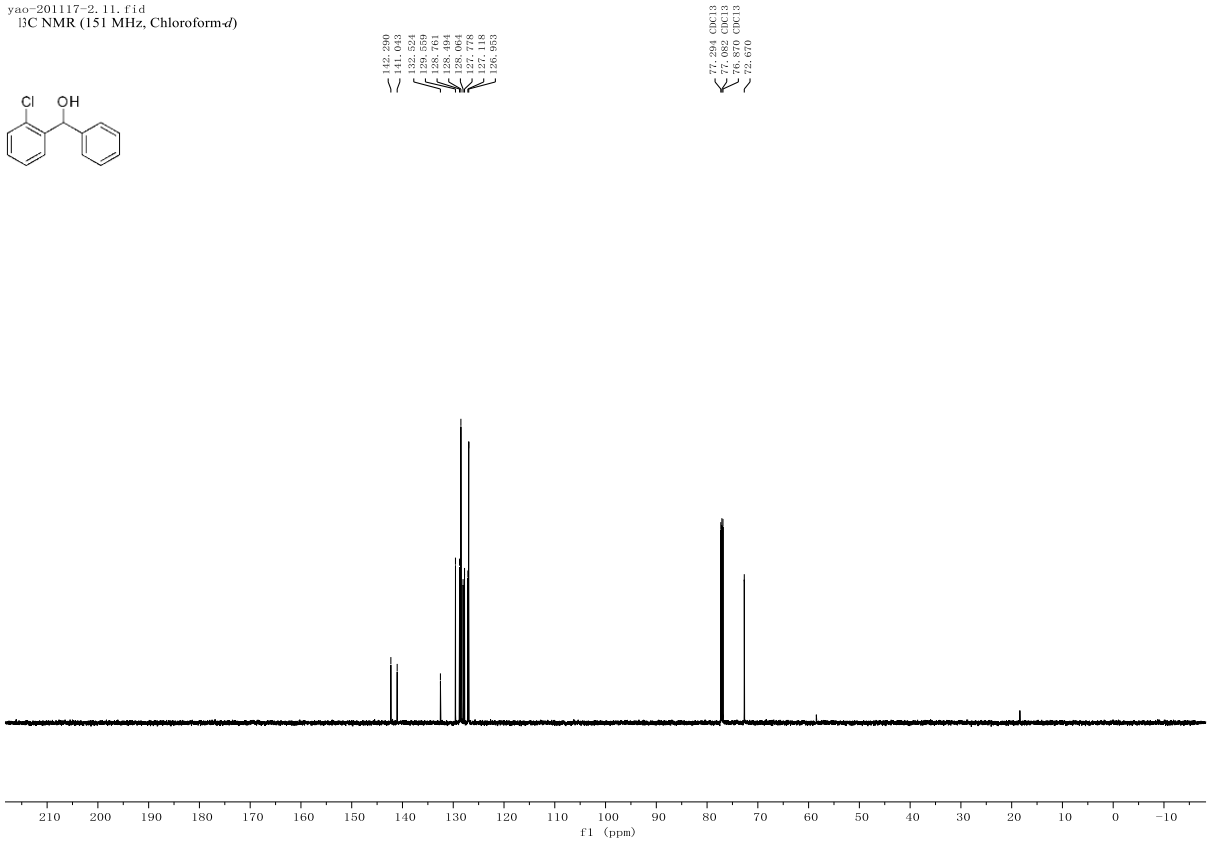
yao-201117-2.11.fid
13C NMR (151 MHz, Chloroform-d)
Cl
OH
f1 (ppm)

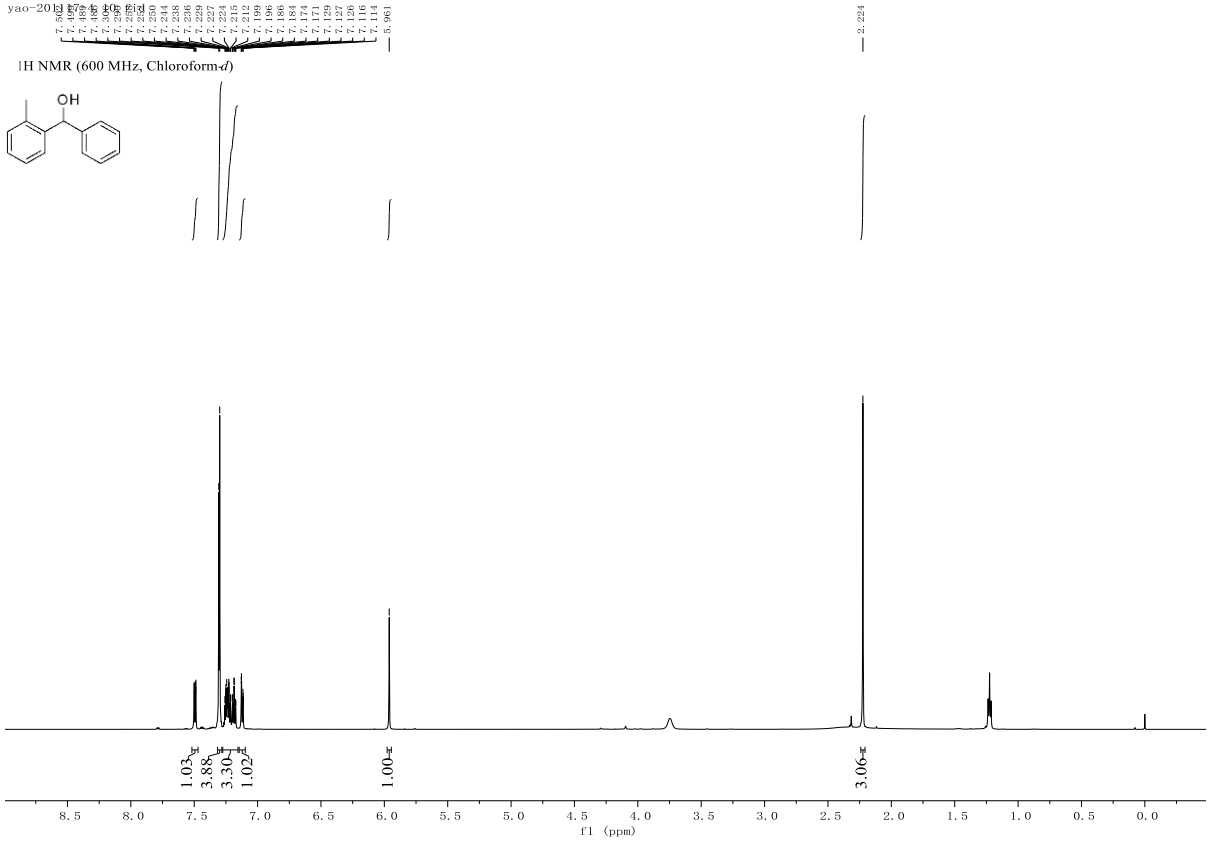
1H NMR (600 MHz, Chloroform-d)
OH
1.03
3.88
3.30
1.02
1.00
3.06
f1 (ppm)

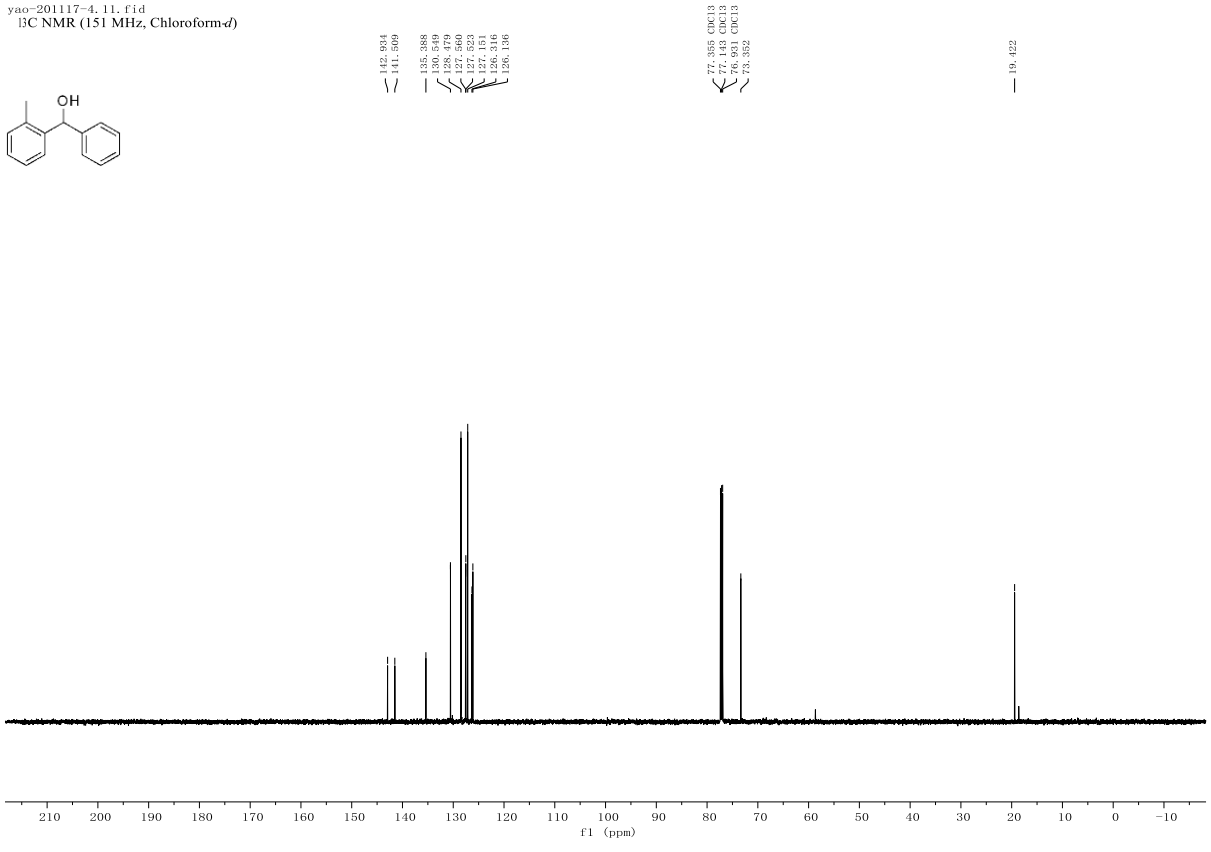
yao-201117-4.11.fid
13C NMR (151 MHz, Chloroform-d)
OH
f1 (ppm)

zml-210728-1.10.fid
1H NMR (600 MHz, Chloroform-*d*)

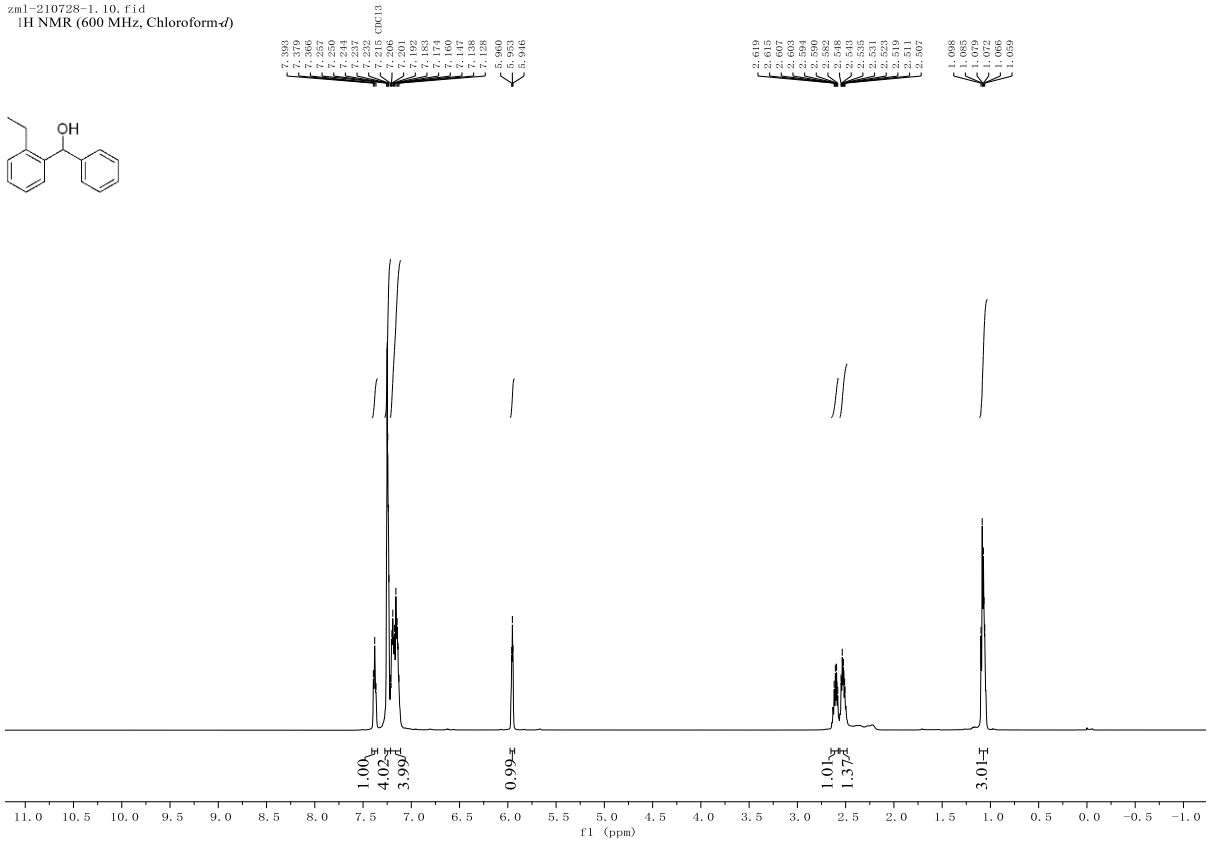

zml-210728-1.11.fid
13C NMR (151 MHz, Chloroform-*d*)

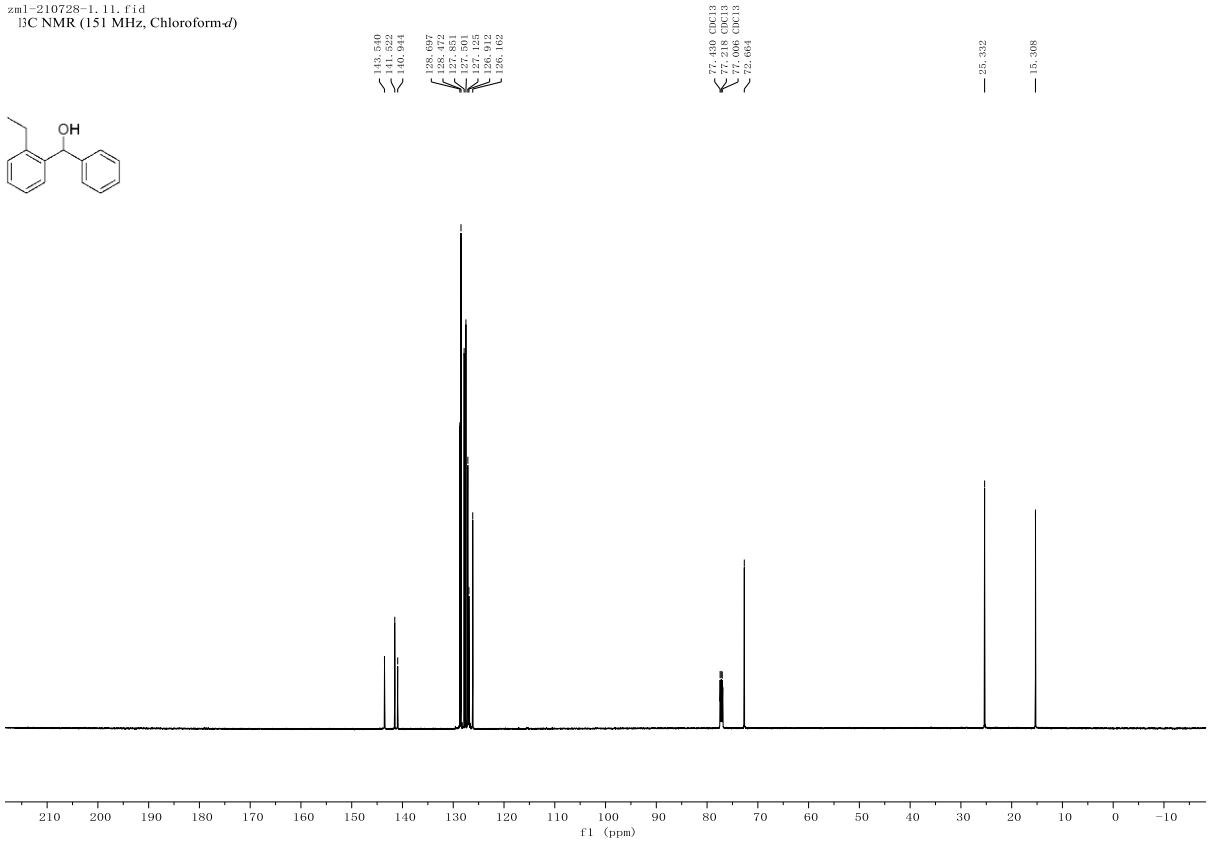

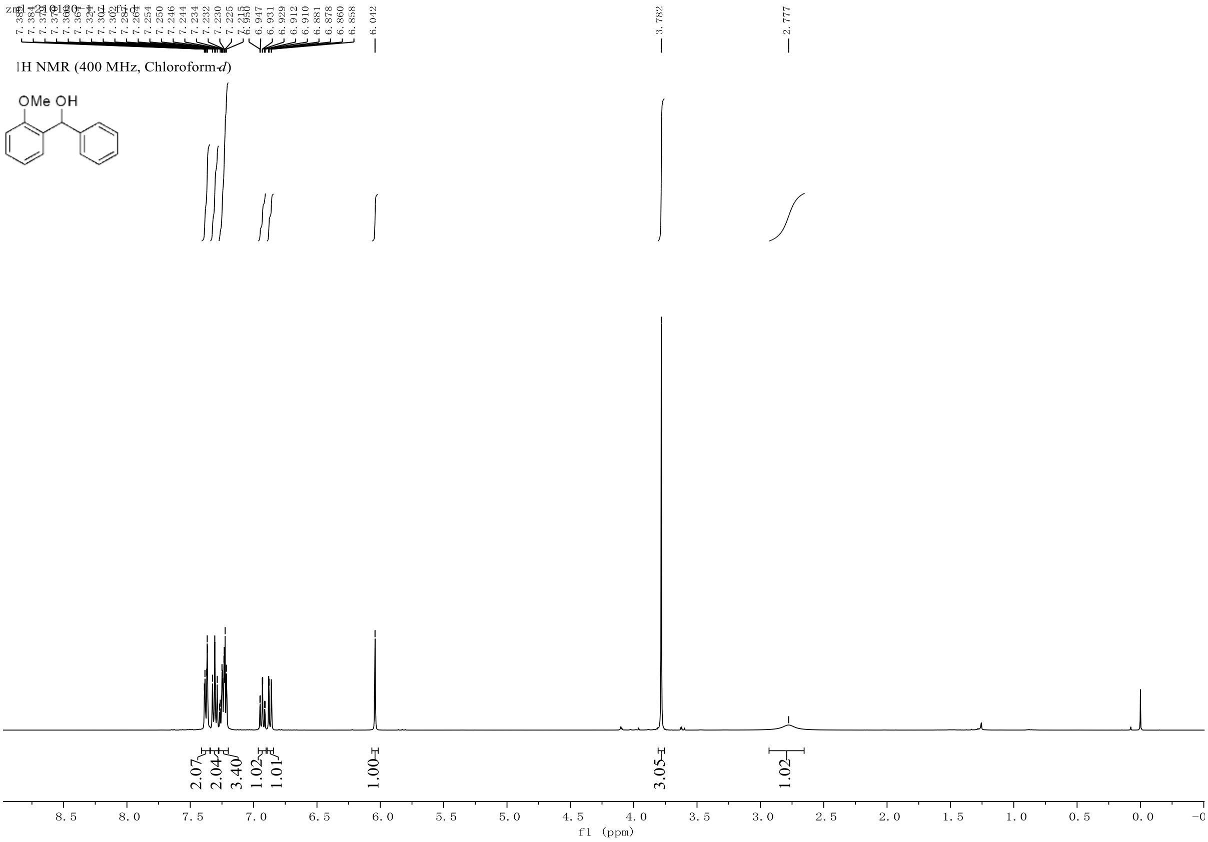
1H NMR (400 MHz, Chloroform-d)
OMe OH
7.230
7.225
6.947
6.931
6.929
6.912
6.910
6.881
6.878
6.860
6.858
6.042
3.782
2.777
2.07
2.04
3.40
1.02
1.01
1.00
3.05
1.02
f1 (ppm)

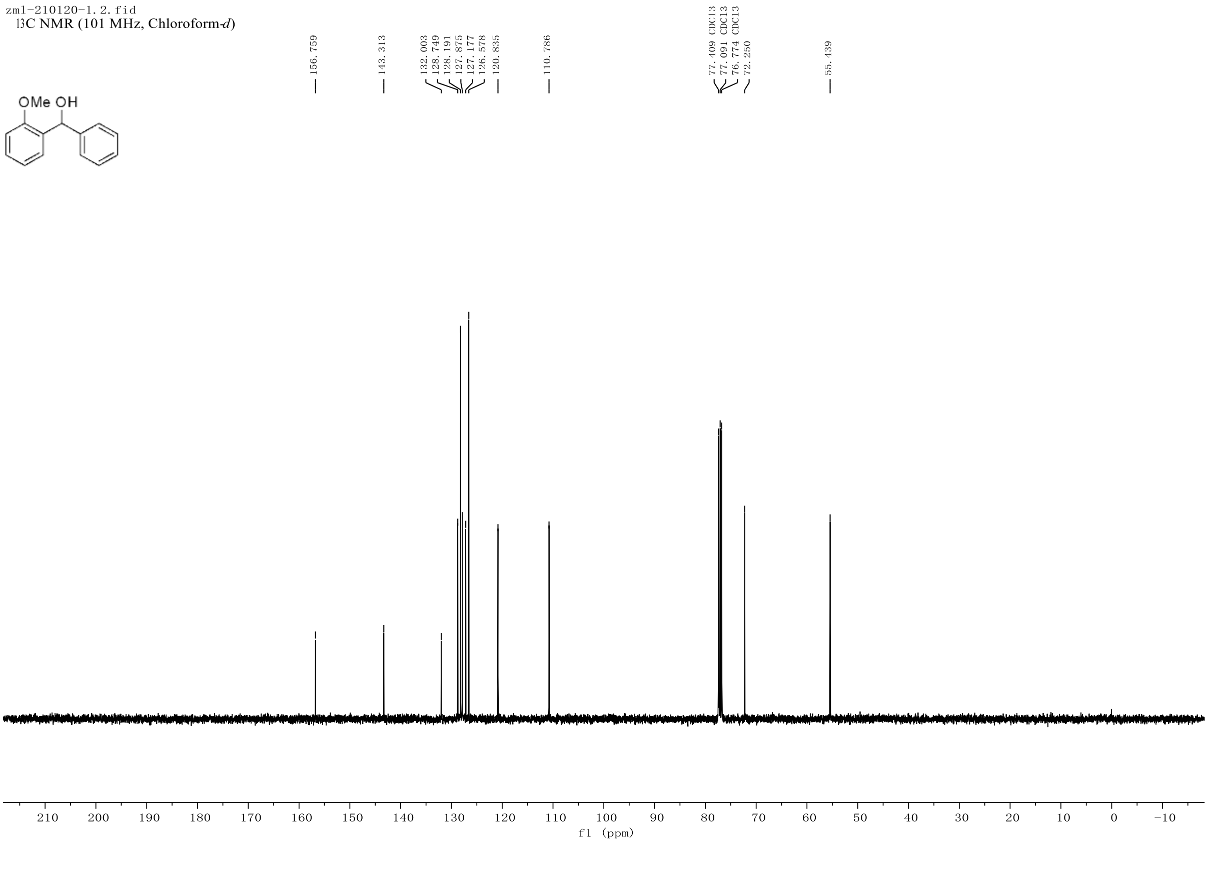
zml-210120-1.2.fid
13C NMR (101 MHz, Chloroform-d)
OMe OH
156.759
143.313
132.003
128.749
128.191
127.875
127.177
126.578
120.835
110.786
77.409 CDCl3
77.091 CDCl3
76.774 CDCl3
72.250
55.439
f1 (ppm)

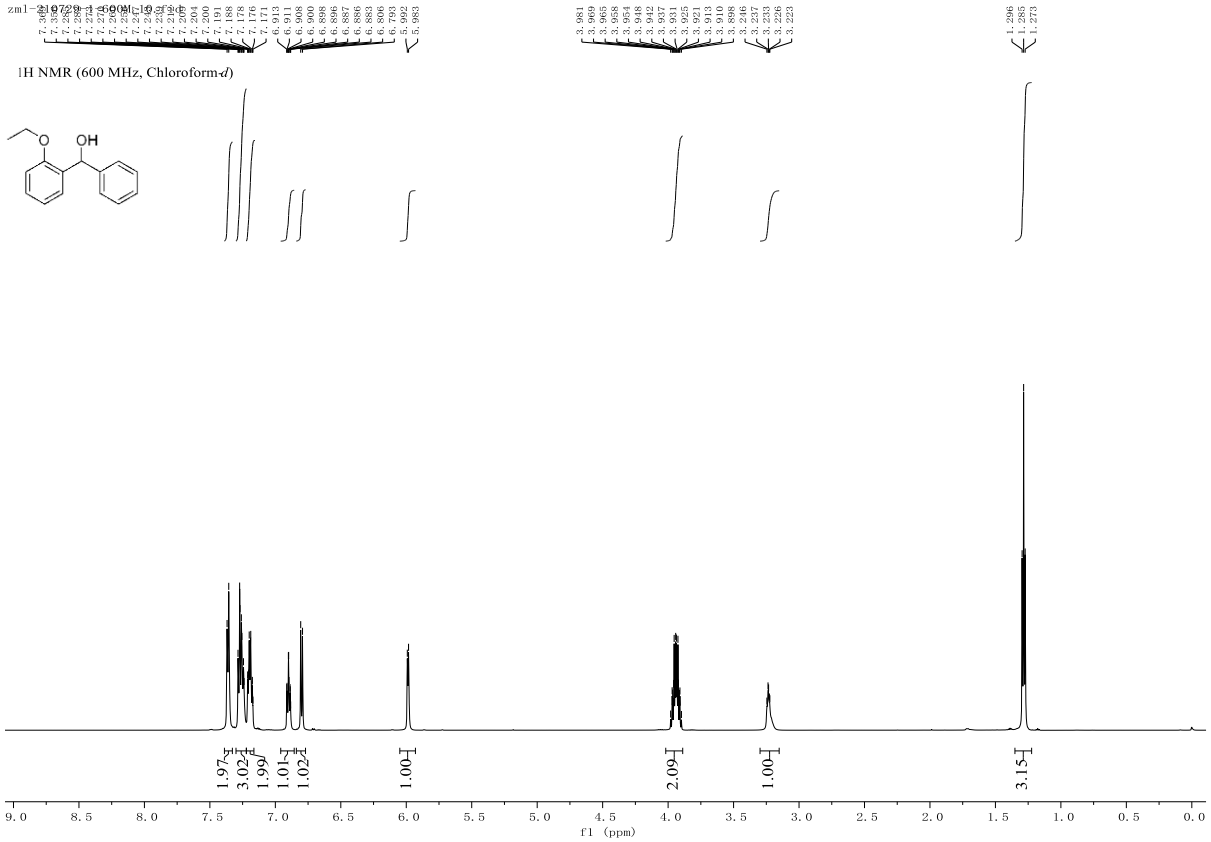
zm1-210729-1-600M.10.fid
1H NMR (600 MHz, Chloroform-d)
1.97
3.02
1.99
1.01
1.02
1.00
2.09
1.00
3.15
f1 (ppm)

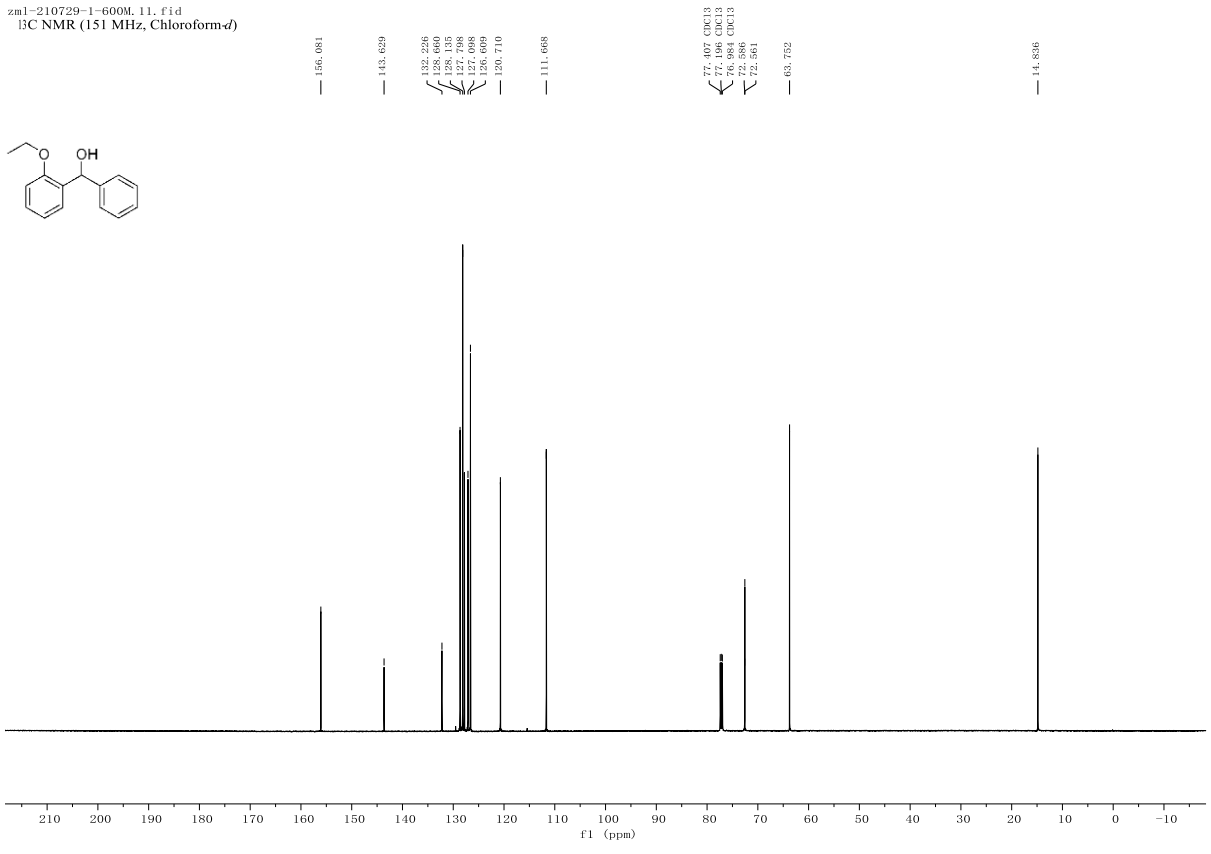
zm1-210729-1-600M.11.fid
13C NMR (151 MHz, Chloroform-d)
156.081
143.629
132.226
128.660
128.115
127.798
127.098
126.609
120.710
111.668
77.407 CDCl3
77.196 CDCl3
76.984 CDCl3
72.980
72.561
63.752
14.836
f1 (ppm)

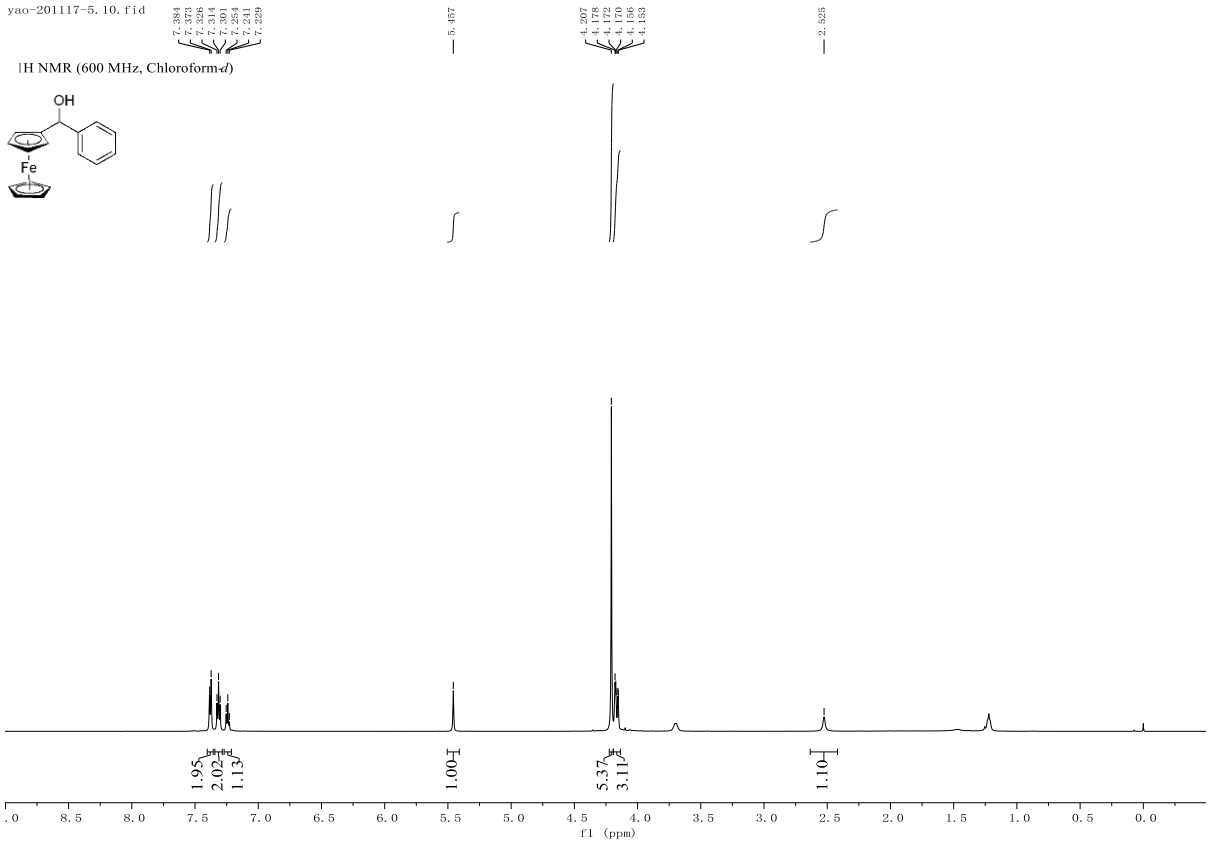
yao-201117-5.10.fid
1H NMR (600 MHz, Chloroform-d)
7.384
7.373
7.326
7.314
7.300
7.254
7.241
7.229
5.457
4.207
4.178
4.172
4.170
4.156
4.153
2.525
OH
Fe
1.95
2.02
1.13
1.00
5.37
3.11
1.10
f1 (ppm)

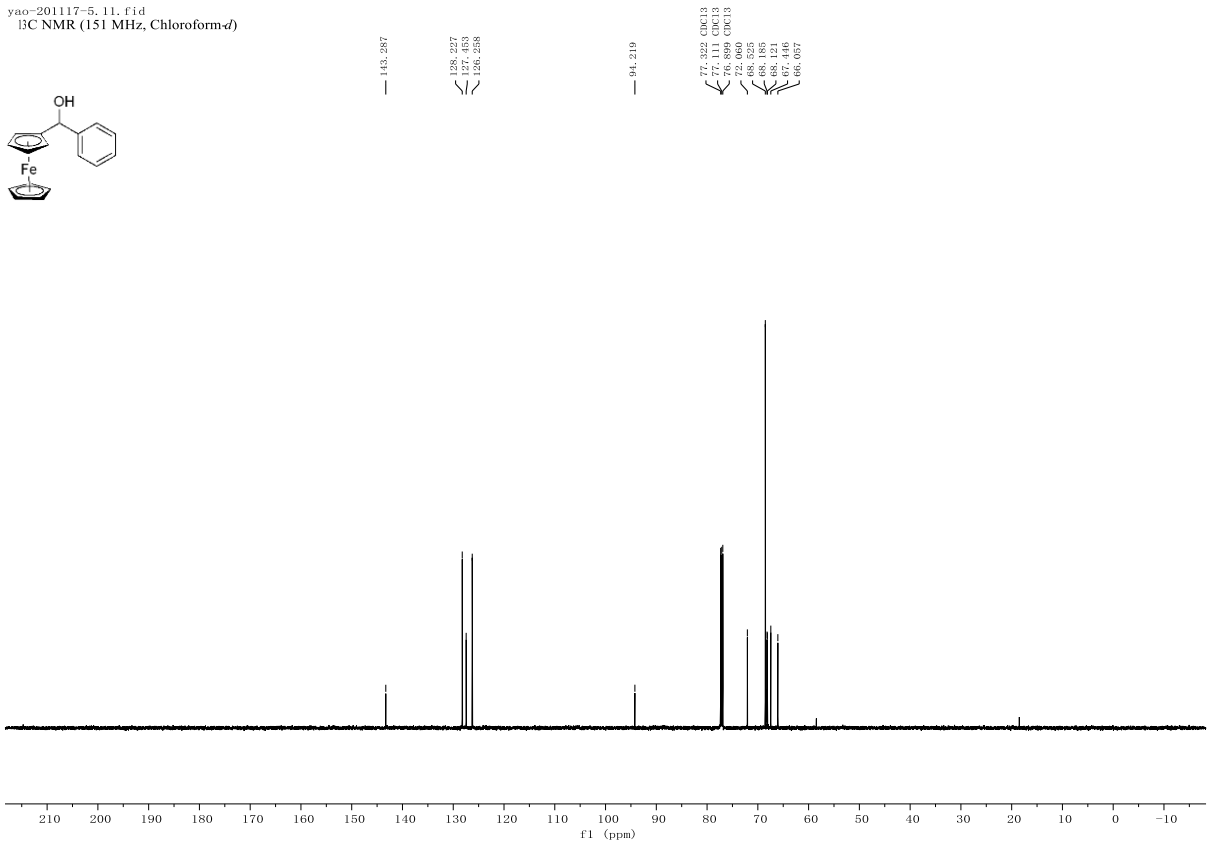
yao-201117-5.11.fid
13C NMR (151 MHz, Chloroform-d)
143.287
128.227
127.453
126.258
94.219
77.322 CDCl3
77.111 CDCl3
76.899 CDCl3
72.060
68.525
68.185
68.121
67.446
66.607
OH
Fe
f1 (ppm)

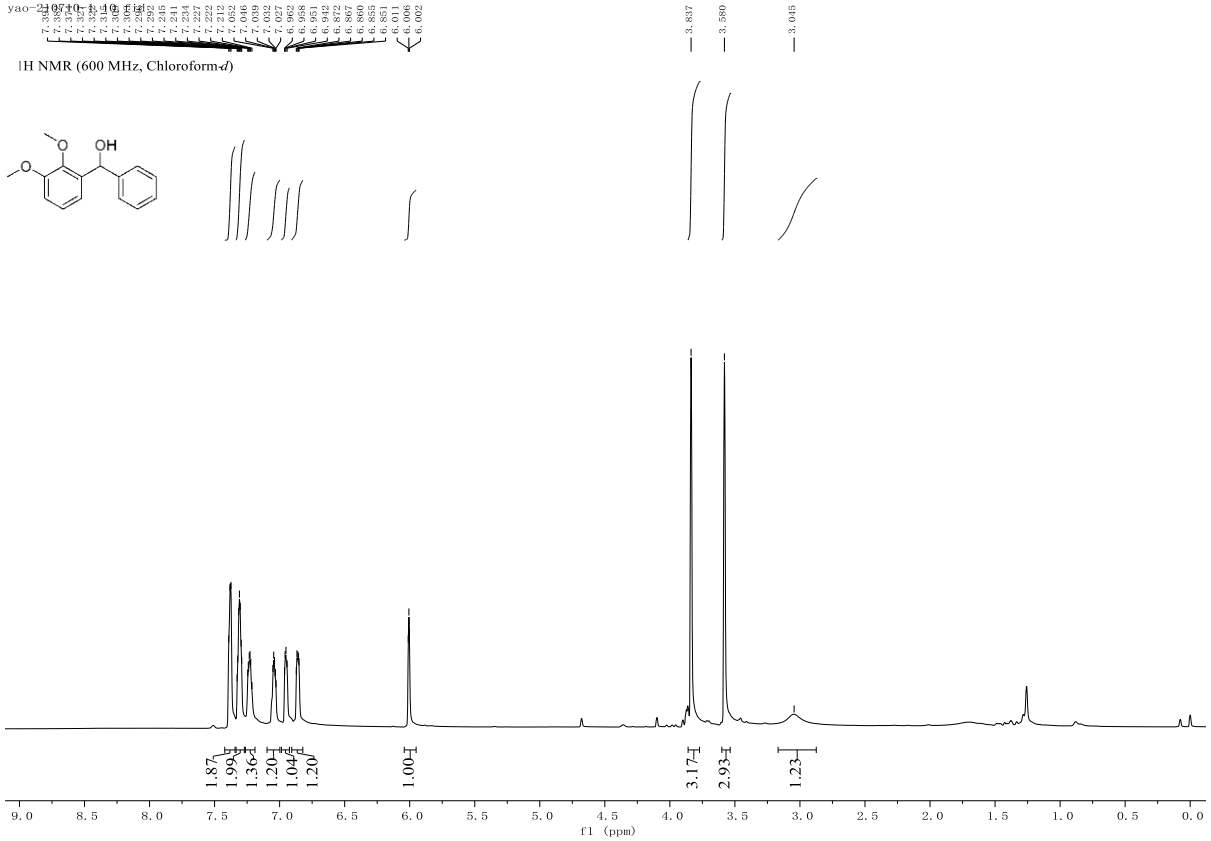
1H NMR (600 MHz, Chloroform-d)
3.837
3.580
3.045
1.87
1.99
1.36
1.20
1.04
1.20
1.00
3.17
2.93
1.23
f1 (ppm)

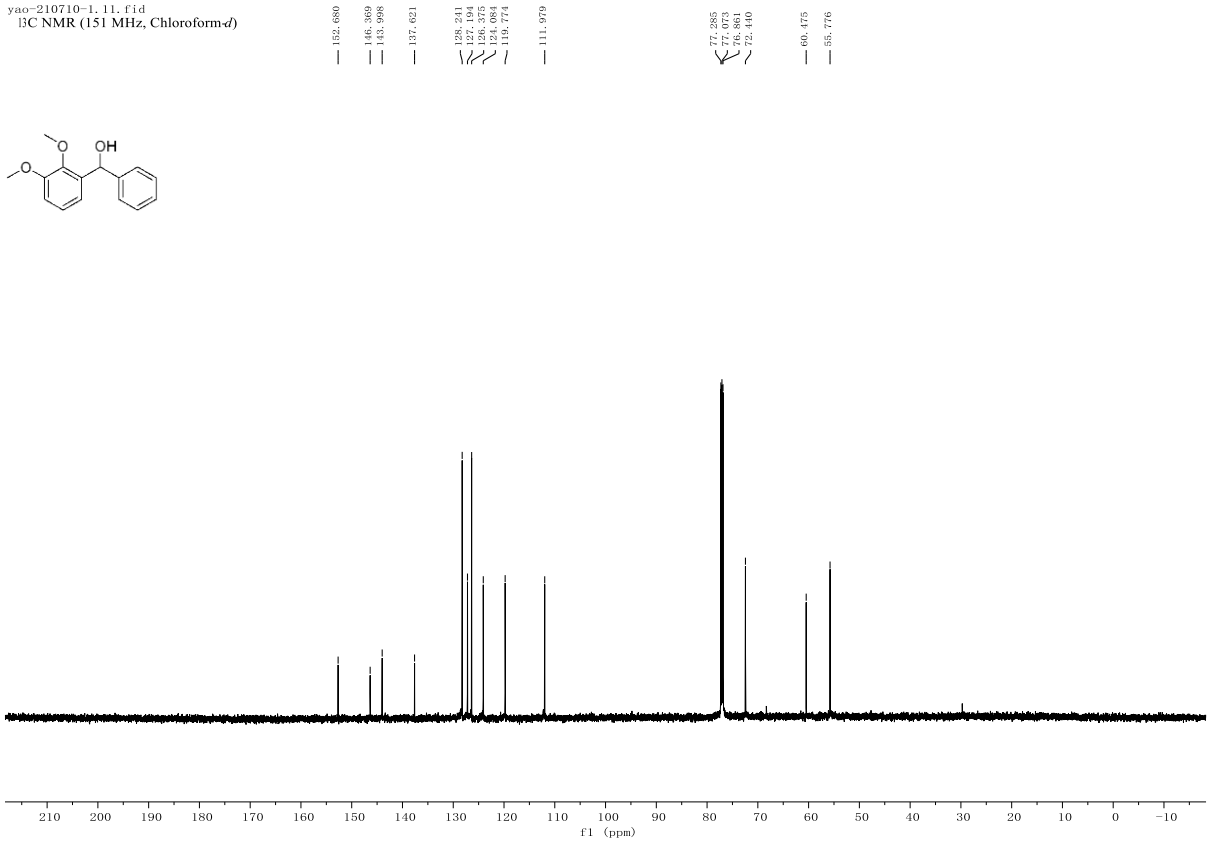
yao-210710-1.11.fid
13C NMR (151 MHz, Chloroform-d)
152.680
146.369
143.998
137.621
128.241
127.194
126.375
124.084
119.774
111.979
77.285
77.073
76.861
72.440
60.475
55.776
f1 (ppm)

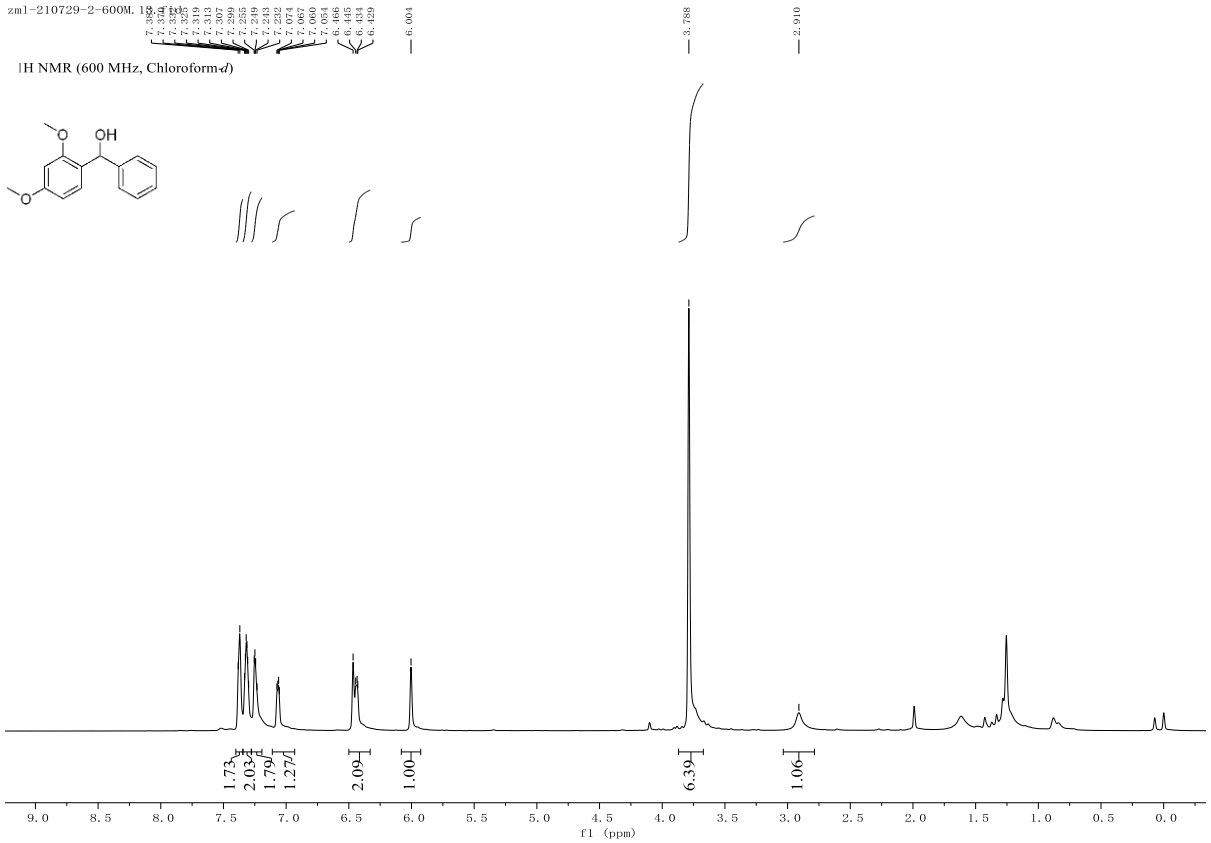
zm1-210729-2-600M.13.fid
1H NMR (600 MHz, Chloroform-d)
7.384
7.374
7.342
7.325
7.319
7.313
7.307
7.299
7.255
7.249
7.241
7.232
7.074
7.067
7.060
7.054
6.446
6.445
6.434
6.429
6.004
3.788
2.910
OH
1.73
2.03
1.79
1.27
2.09
1.00
6.39
1.06
f1 (ppm)

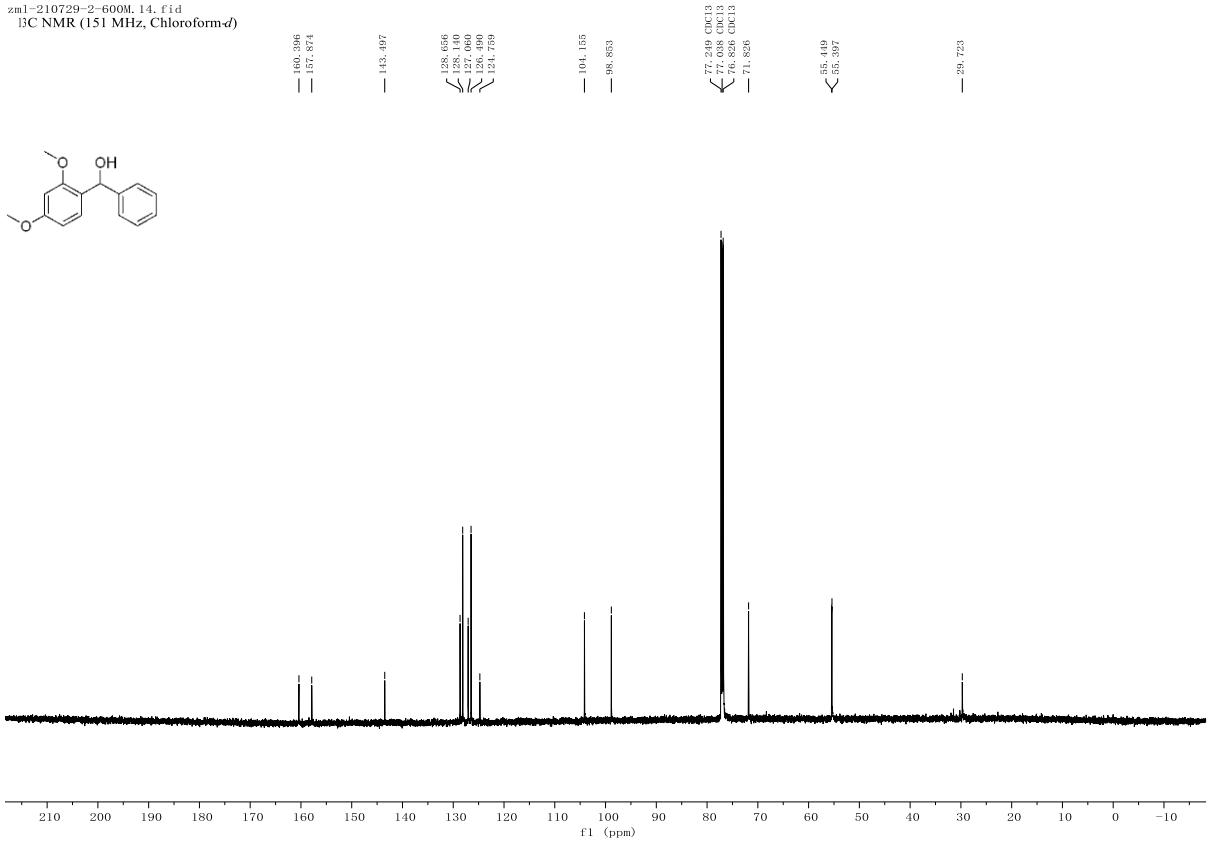
zm1-210729-2-600M.14.fid
13C NMR (151 MHz, Chloroform-d)
160.396
157.874
143.497
128.656
128.140
127.060
126.490
124.759
104.155
98.853
77.249 CDCl3
77.038 CDCl3
76.826 CDCl3
71.826
55.449
55.397
29.723
OH
f1 (ppm)

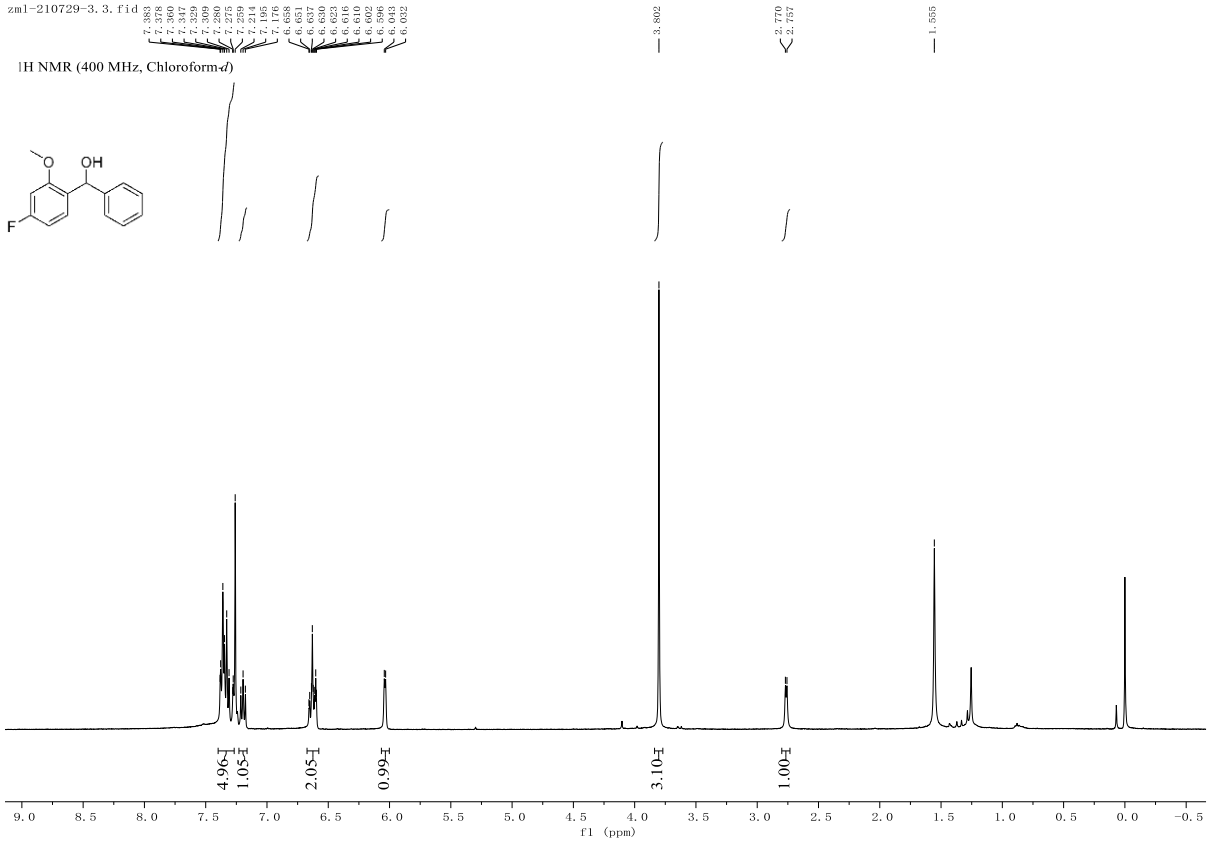
zml-210729-3.3.fid
1H NMR (400 MHz, Chloroform-d)
7.383
7.378
7.360
7.347
7.329
7.309
7.280
7.275
7.259
7.214
7.195
7.176
6.658
6.651
6.637
6.630
6.623
6.616
6.610
6.602
6.596
6.041
6.032
3.802
2.770
2.757
1.555
OH
O
F
4.96
1.05
2.05
0.99
3.10
1.00
f1 (ppm)

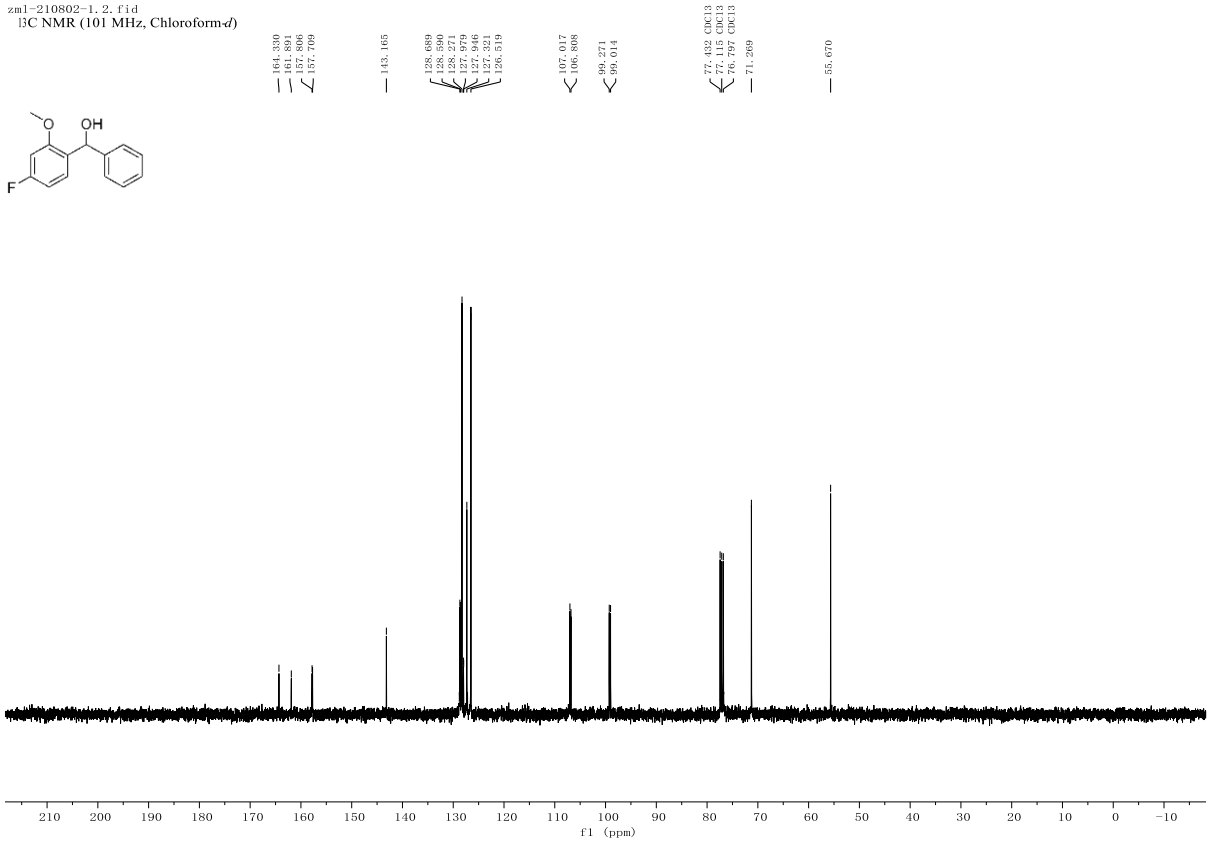
zml-210802-1.2.fid
13C NMR (101 MHz, Chloroform-d)
164.330
161.891
157.806
157.709
143.165
128.689
128.590
128.271
127.979
127.946
127.321
126.519
107.017
106.868
99.271
99.014
77.432 CDCl3
77.115 CDCl3
76.797 CDCl3
71.269
55.670
OH
O
F
f1 (ppm)

yao-210710-4-new.8.fid
^{19}F NMR (376 MHz, Chloroform-*d*)

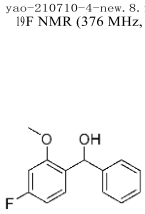

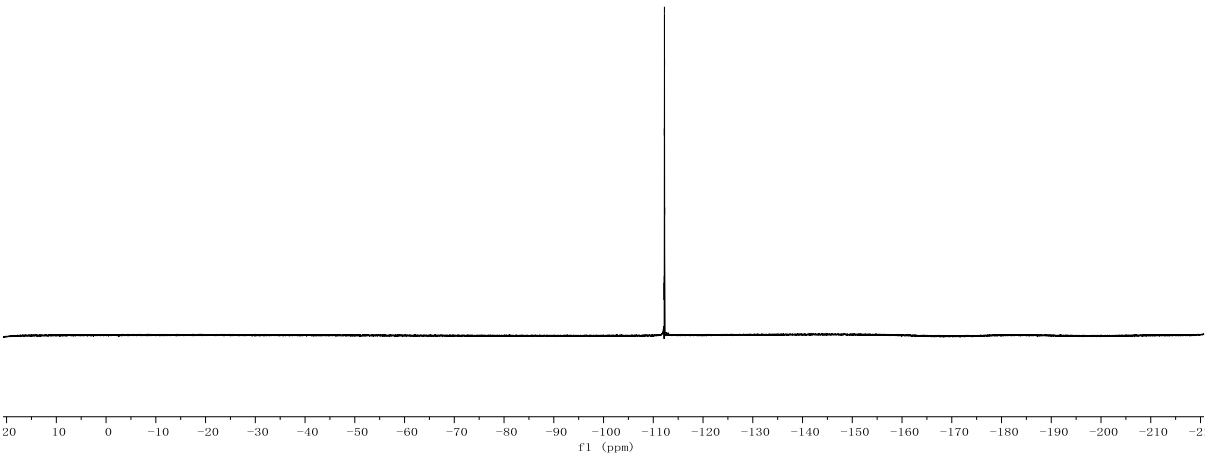

zm1-210729-4-600M.4.fid
^{1}H NMR (600 MHz, Chloroform-*d*)

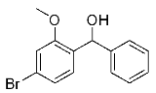

zml-210729-4-600M.5.fid

13C NMR (151 MHz, Chloroform-*d*)

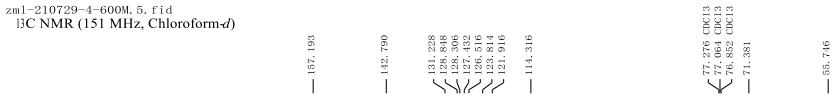

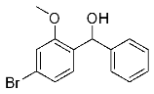

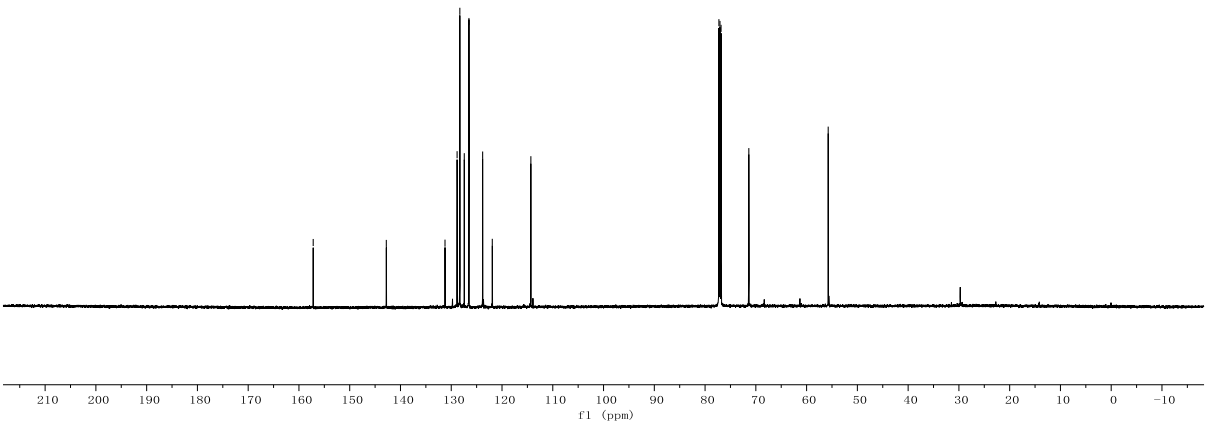

yao-210710-5-fl

1H NMR (400 MHz, Chloroform-*d*)

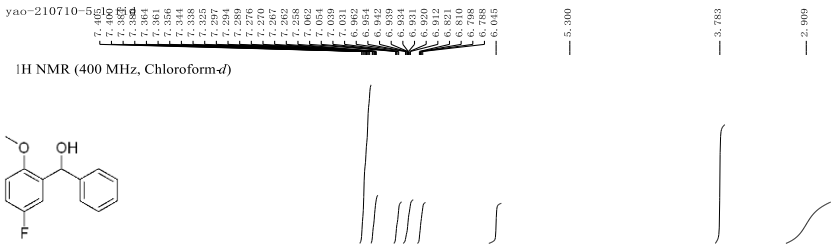

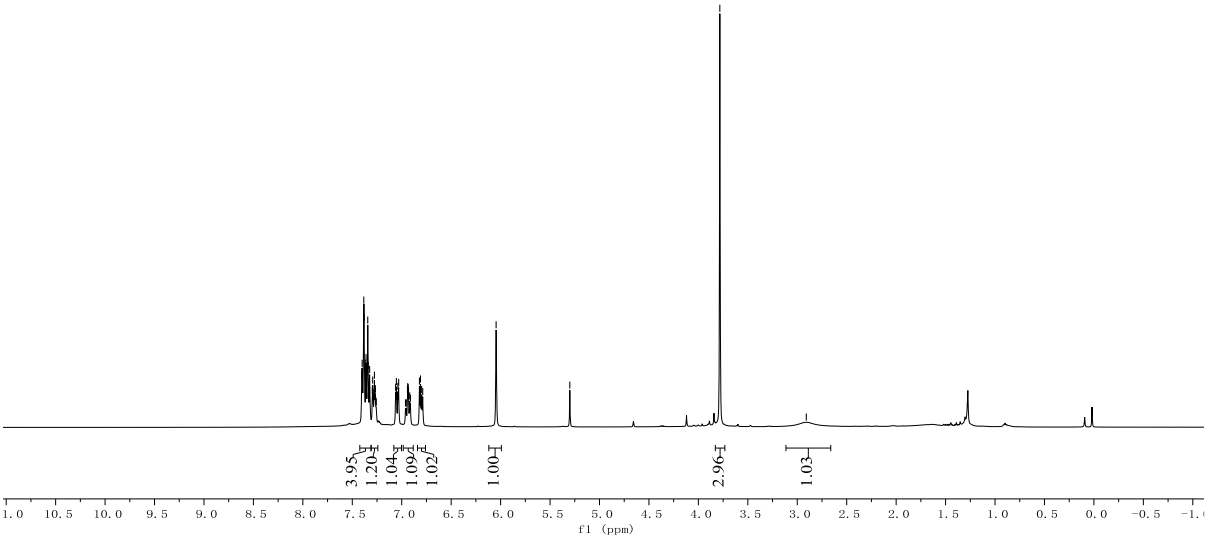

yao-210710-5.3.fid
13C NMR (101 MHz, Chloroform-d)

158.379
156.006
152.679
152.662
142.649
133.857
133.791
128.336
127.512
126.867
114.717
114.473
114.241
111.666
111.685
77.364 CDCl3
77.047 CDCl3
76.729 CDCl3
71.469
55.977

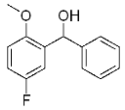

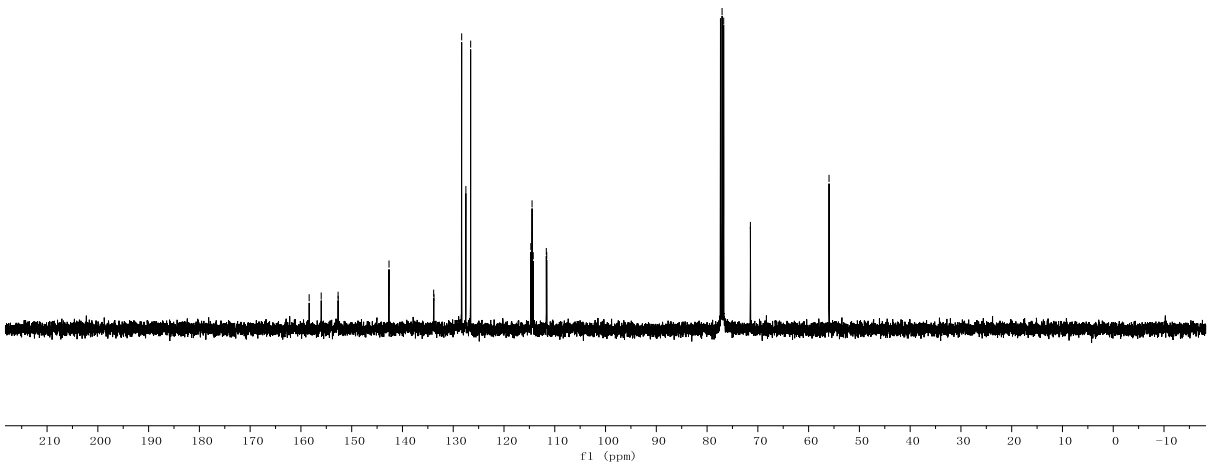

yao-210710-5.2.fid
19F NMR (376 MHz, Chloroform-d)

−123.050
−123.062
−123.073
−123.084
−123.095
−123.107

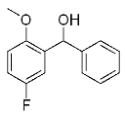

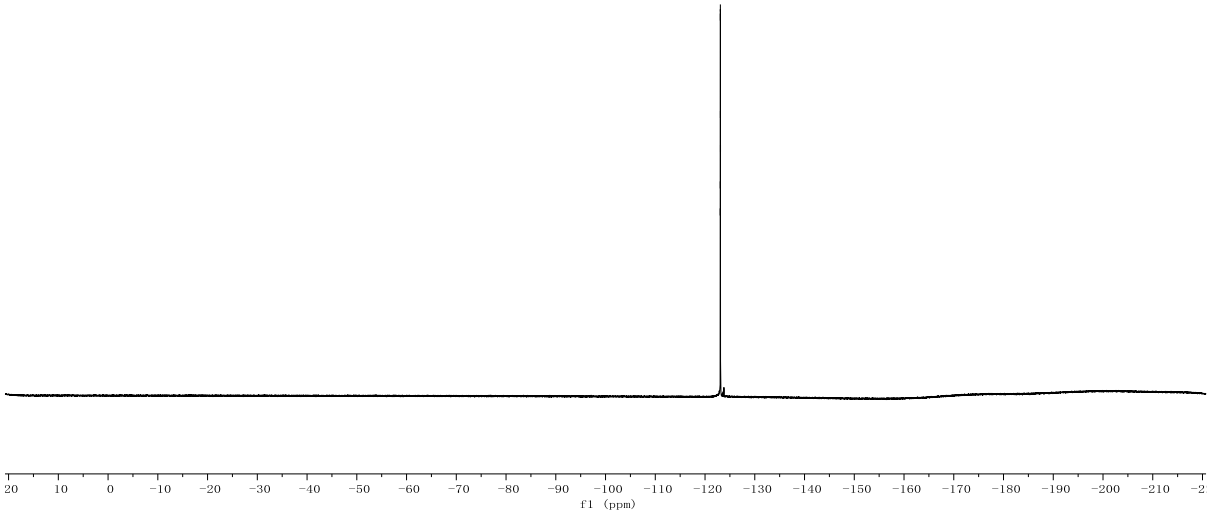

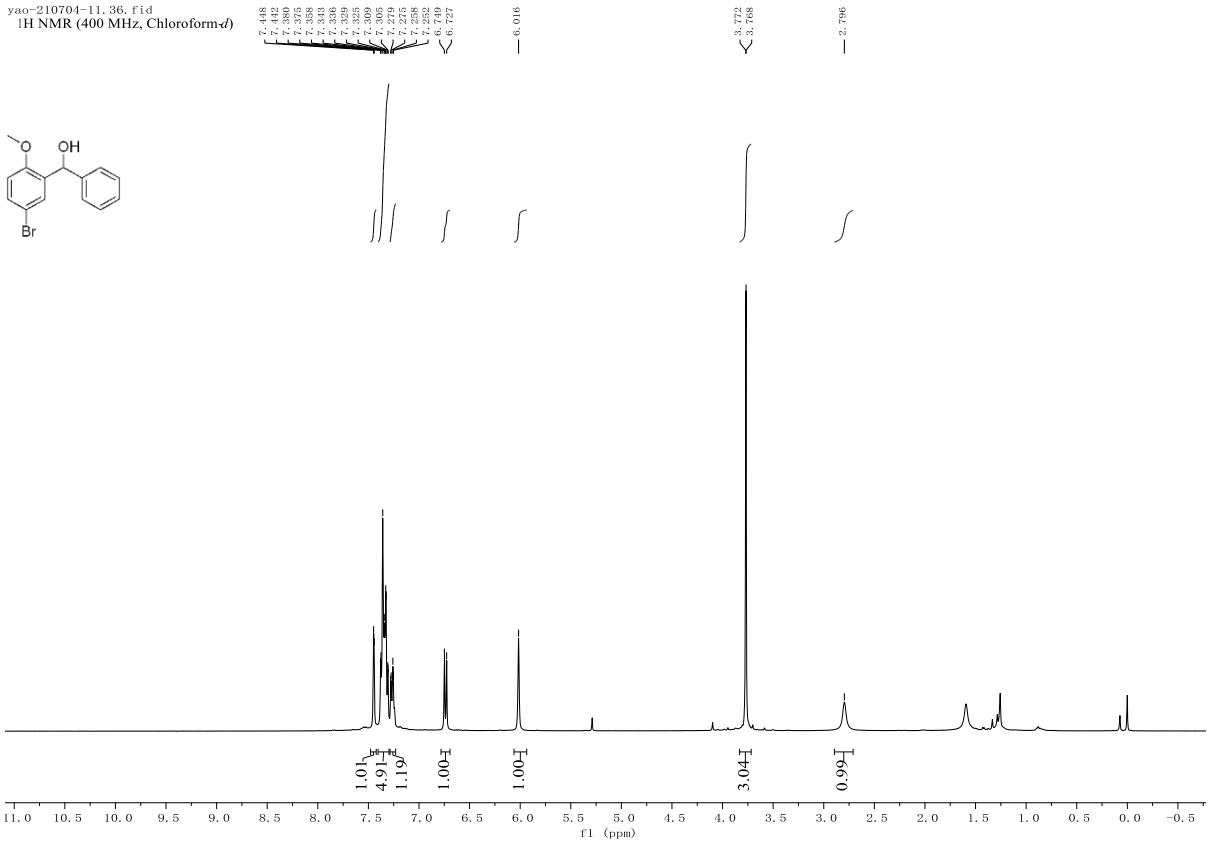
yao-210704-11.36.fid
1H NMR (400 MHz, Chloroform-d)
7.448
7.442
7.380
7.375
7.338
7.334
7.336
7.329
7.309
7.295
7.279
7.275
7.258
7.252
6.749
6.727
6.016
3.772
3.768
2.796
O
OH
Br
1.01
4.91
1.19
1.00
1.00
3.04
0.99
11.0 10.5 10.0 9.5 9.0 8.5 8.0 7.5 7.0 6.5 6.0 5.5 5.0 4.5 4.0 3.5 3.0 2.5 2.0 1.5 1.0 0.5 0.0 -0.5
f1 (ppm)

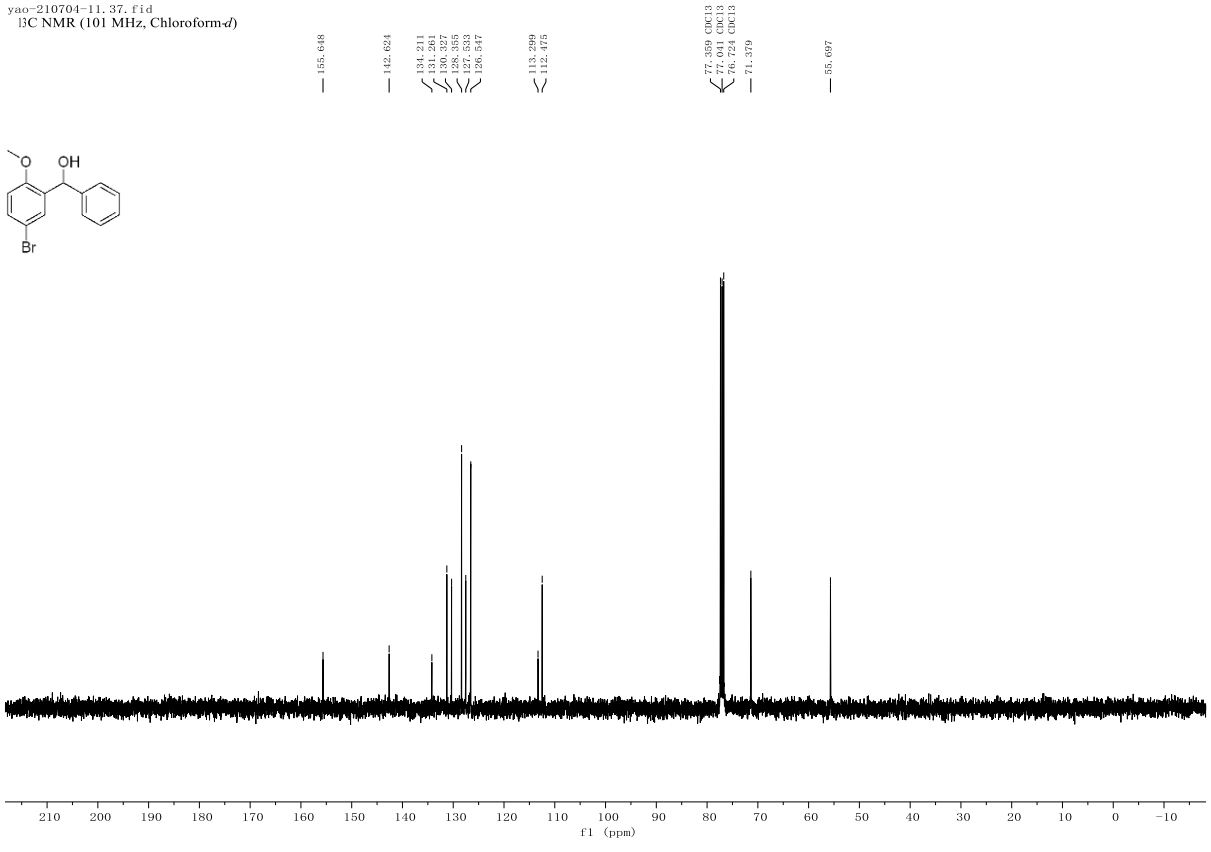
yao-210704-11.37.fid
13C NMR (101 MHz, Chloroform-d)
155.648
142.624
134.211
131.261
130.327
128.355
127.533
126.547
113.299
112.475
77.359 CDCl3
77.041 CDCl3
76.724 CDCl3
71.379
55.697
O
OH
Br
210 200 190 180 170 160 150 140 130 120 110 100 90 80 70 60 50 40 30 20 10 0 -10
f1 (ppm)

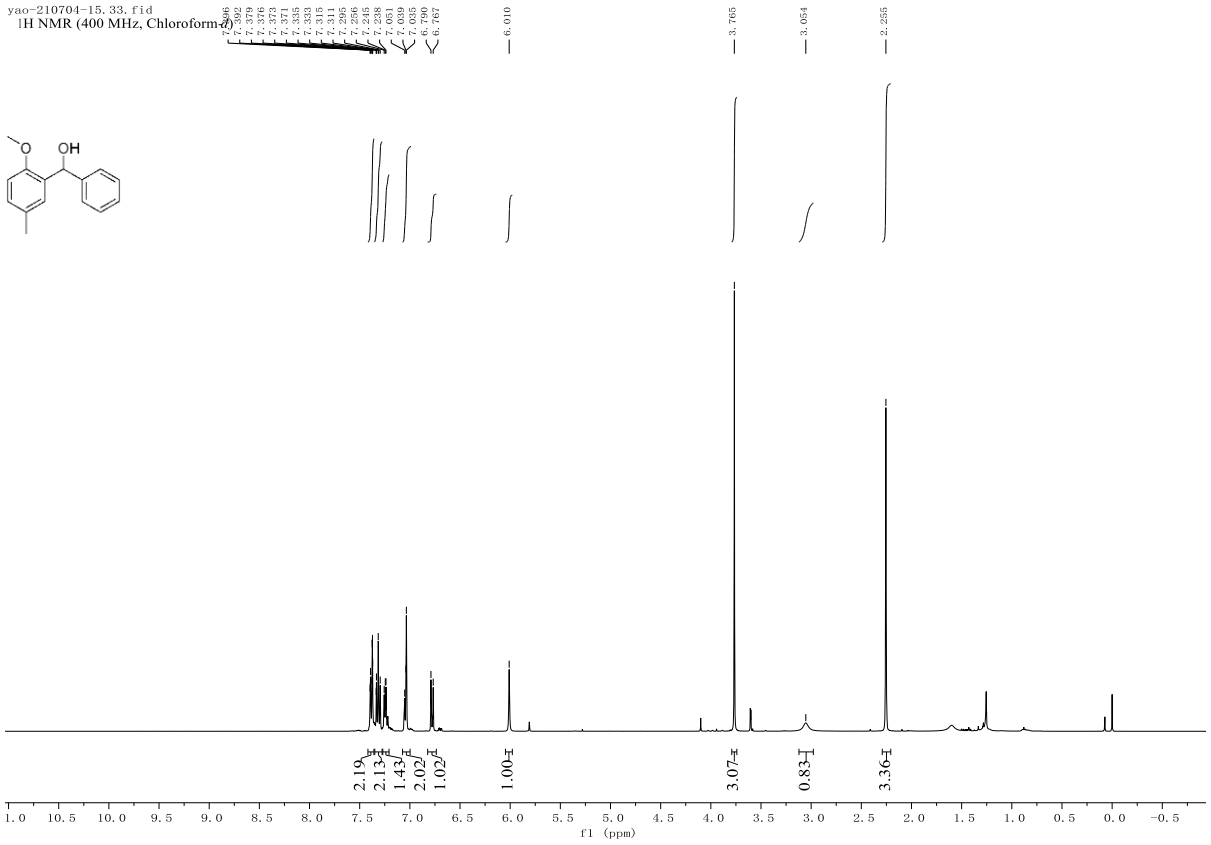
yao-210704-15.33.fid
1H NMR (400 MHz, Chloroform-d)
7.398
7.392
7.379
7.376
7.373
7.371
7.335
7.333
7.315
7.311
7.295
7.258
7.248
7.238
7.051
7.039
7.035
6.790
6.767
6.010
3.765
3.054
2.255
O
OH
2.19
2.13
1.43
2.02
1.02
1.00
3.07
0.83
3.36
f1 (ppm)

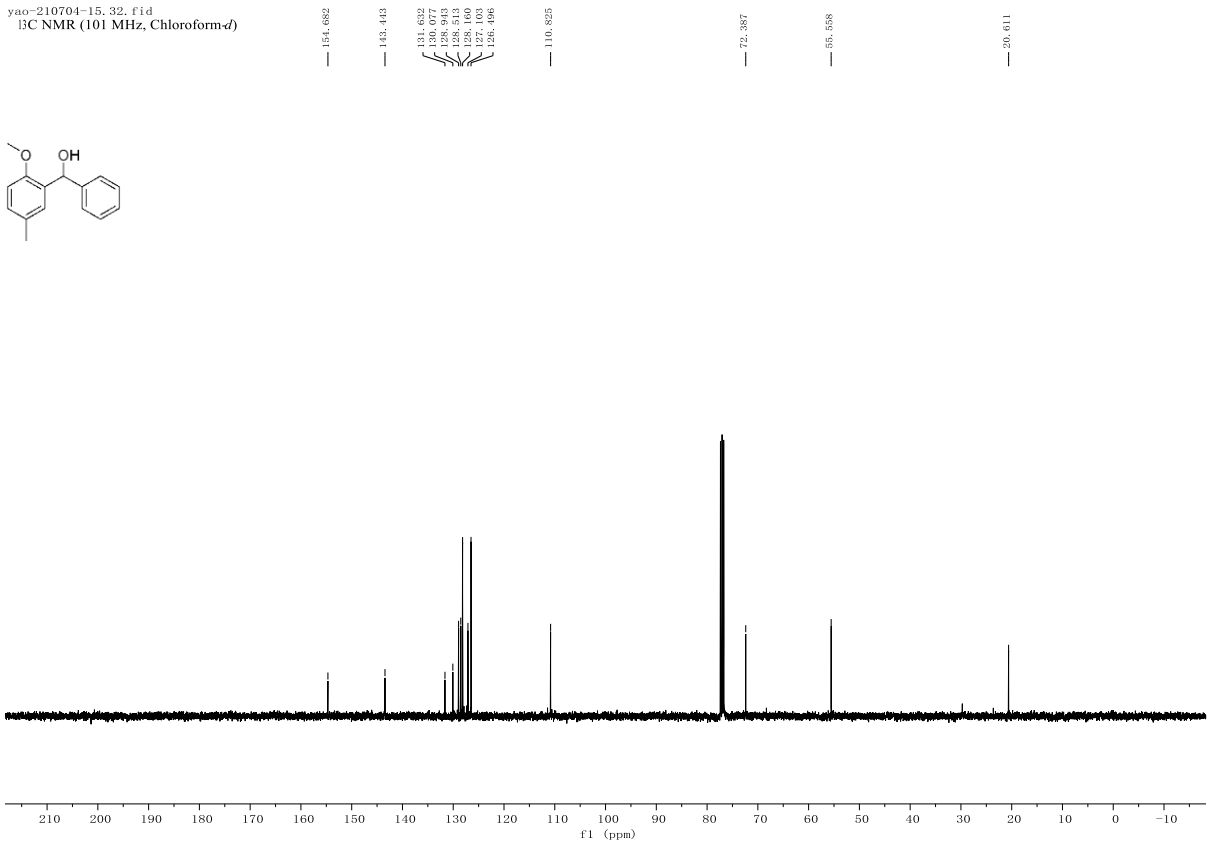
yao-210704-15.32.fid
13C NMR (101 MHz, Chloroform-d)
154.682
143.443
131.632
130.077
128.943
128.513
128.160
127.103
126.496
110.825
72.387
55.558
20.611
O
OH
f1 (ppm)

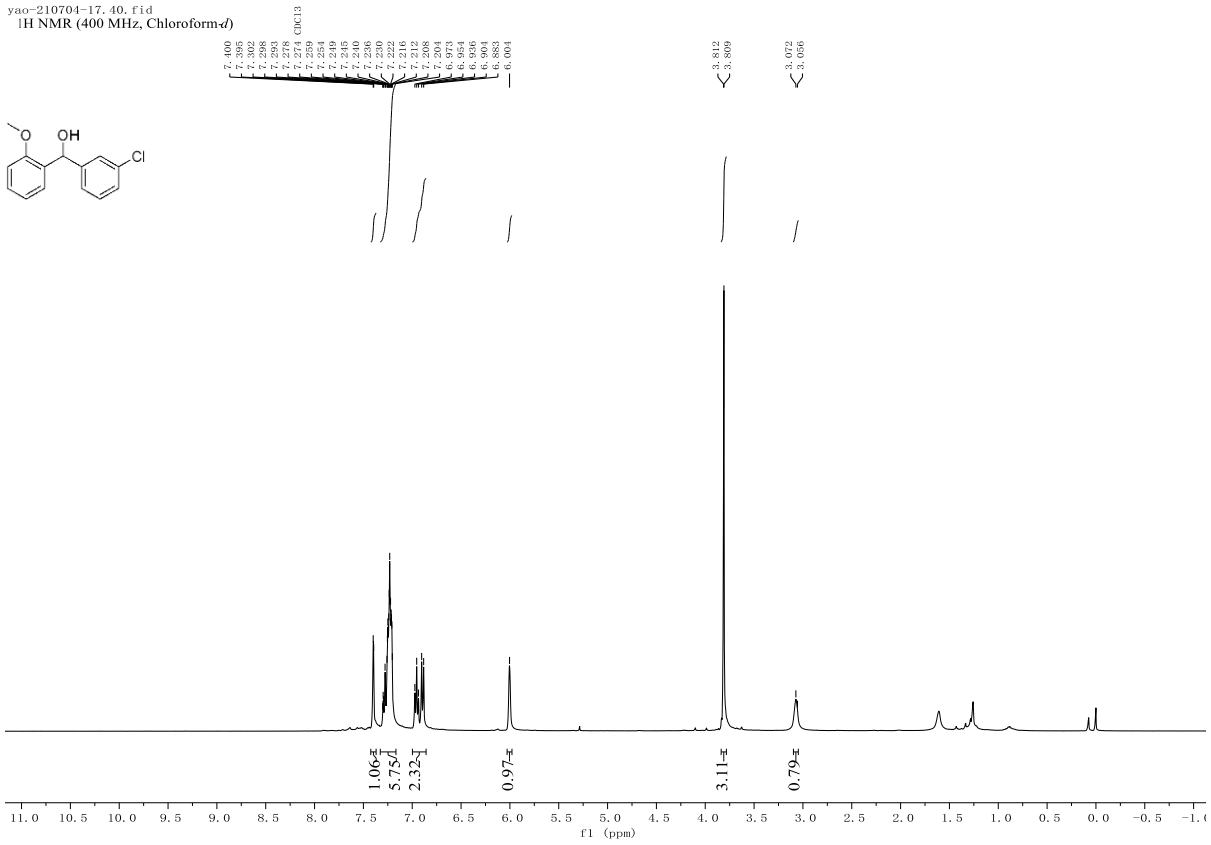
yao-210704-17.40.fid
1H NMR (400 MHz, Chloroform-d)
7.400
7.395
7.392
7.298
7.293
7.278
CDCl3
7.274
7.259
7.254
7.249
7.245
7.240
7.236
7.229
7.222
7.216
7.212
7.208
7.204
6.973
6.953
6.936
6.904
6.883
6.004
3.812
3.809
3.072
3.056
OH
O
Cl
1.06
5.75
2.32
0.97
3.11
0.79
f1 (ppm)

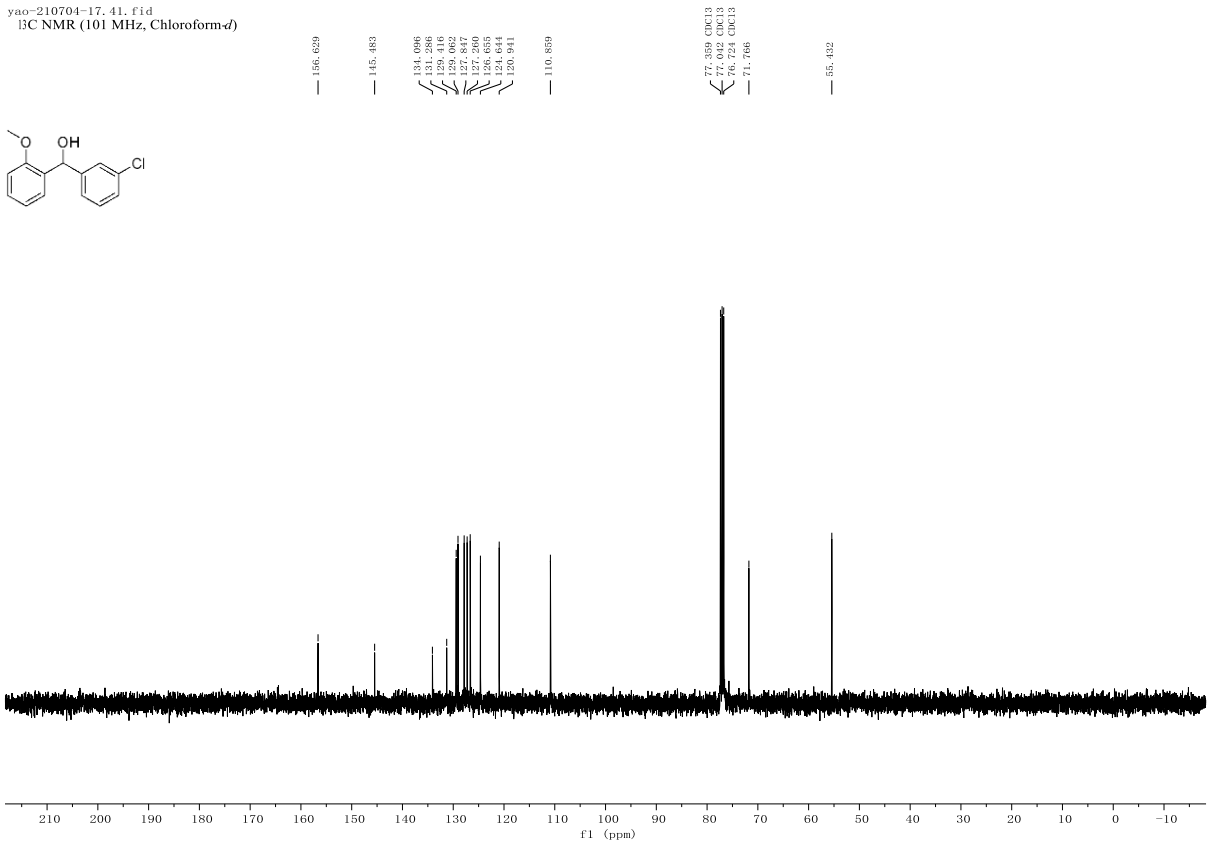
yao-210704-17.41.fid
13C NMR (101 MHz, Chloroform-d)
156.629
145.483
134.096
131.286
129.416
129.062
127.847
127.200
126.655
124.644
120.941
110.859
77.359
CDCl3
77.042
CDCl3
76.724
CDCl3
71.766
55.432
OH
O
Cl
f1 (ppm)

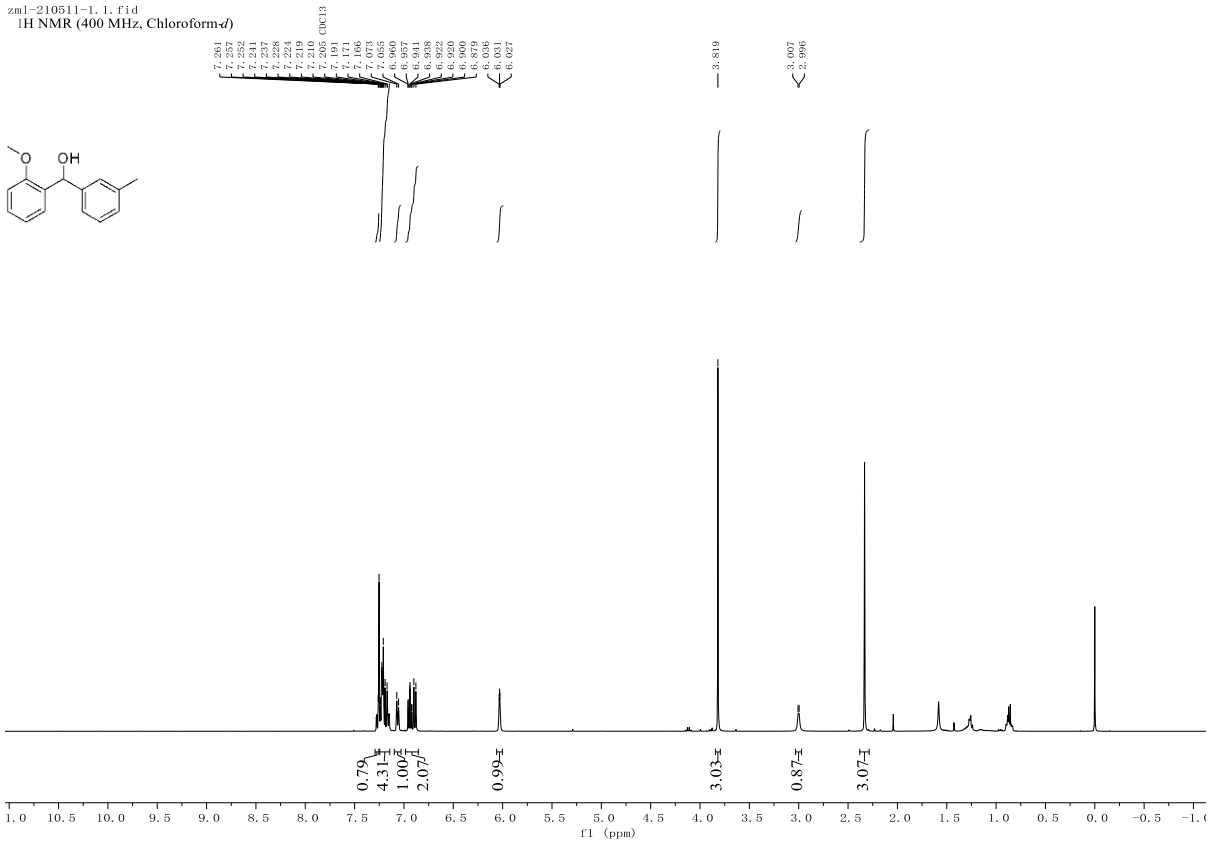
zml-210511-1.1.fid
1H NMR (400 MHz, Chloroform-d)
7.261
7.257
7.252
7.241
7.237
7.228
7.224
7.219
7.210
7.205
CDCl3
7.191
7.171
7.166
7.073
7.065
6.960
6.957
6.941
6.938
6.922
6.920
6.900
6.879
6.036
6.031
6.027
3.819
3.007
2.996
OH
0.79
4.31
1.00
2.07
0.99
3.03
0.87
3.07
f1 (ppm)

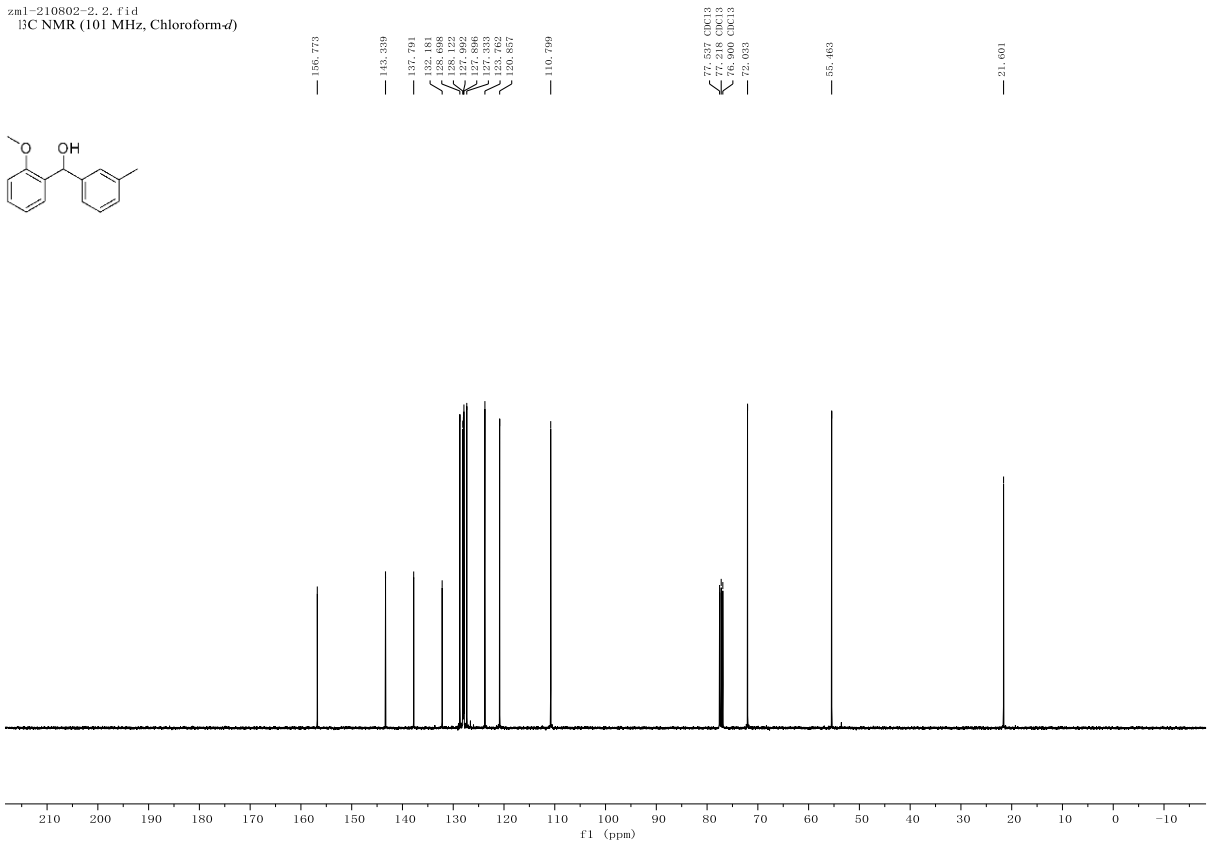
zml-210802-2.2.fid
13C NMR (101 MHz, Chloroform-d)
156.773
143.339
137.791
132.181
128.698
128.122
127.940
127.896
127.333
123.762
120.857
110.799
77.537 CDCl3
77.218 CDCl3
76.900 CDCl3
72.633
55.463
21.601
OH
f1 (ppm)

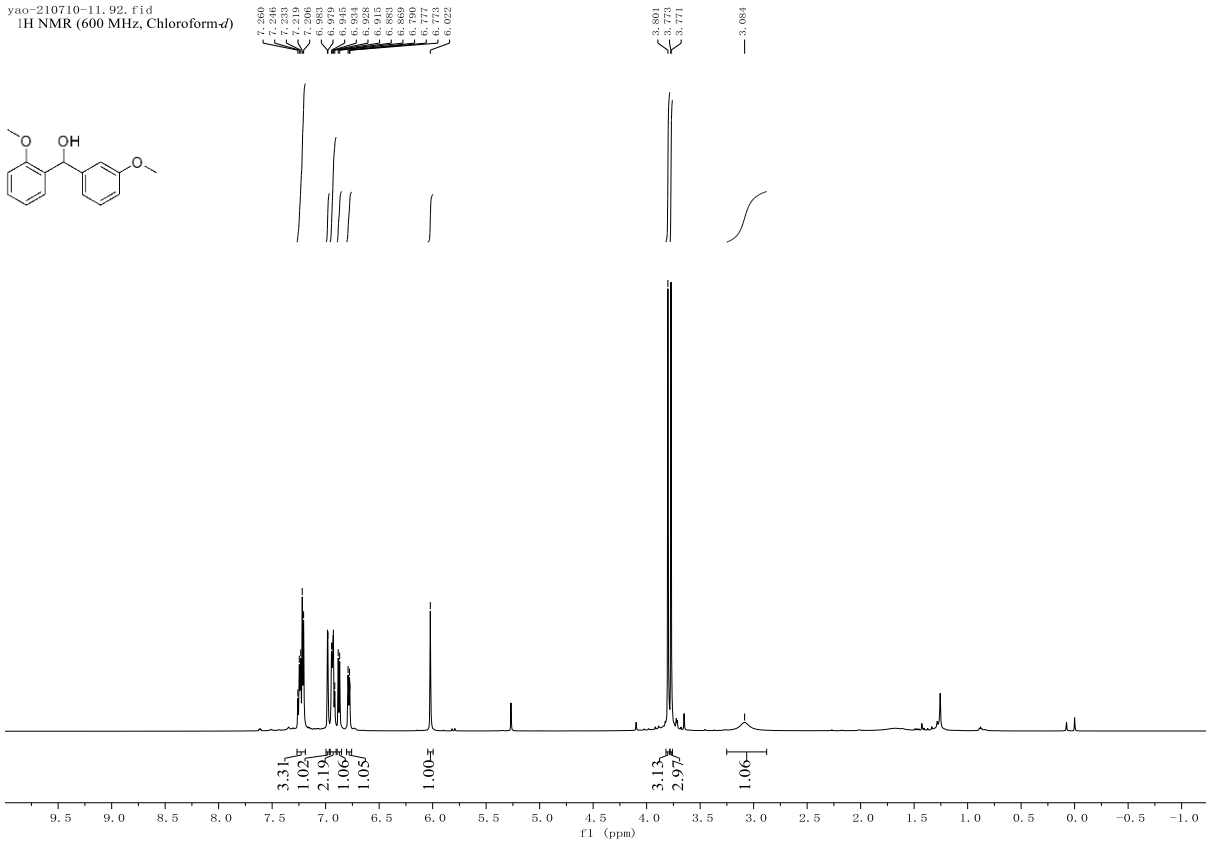
yao-210710-11.92.fid
1H NMR (600 MHz, Chloroform-d)
7.260
7.246
7.233
7.219
7.206
6.983
6.979
6.945
6.934
6.898
6.915
6.883
6.869
6.790
6.777
6.733
6.722
3.801
3.773
3.771
3.084
OH
3.31
1.02
2.19
1.06
1.05
1.00
3.13
2.97
1.06
f1 (ppm)

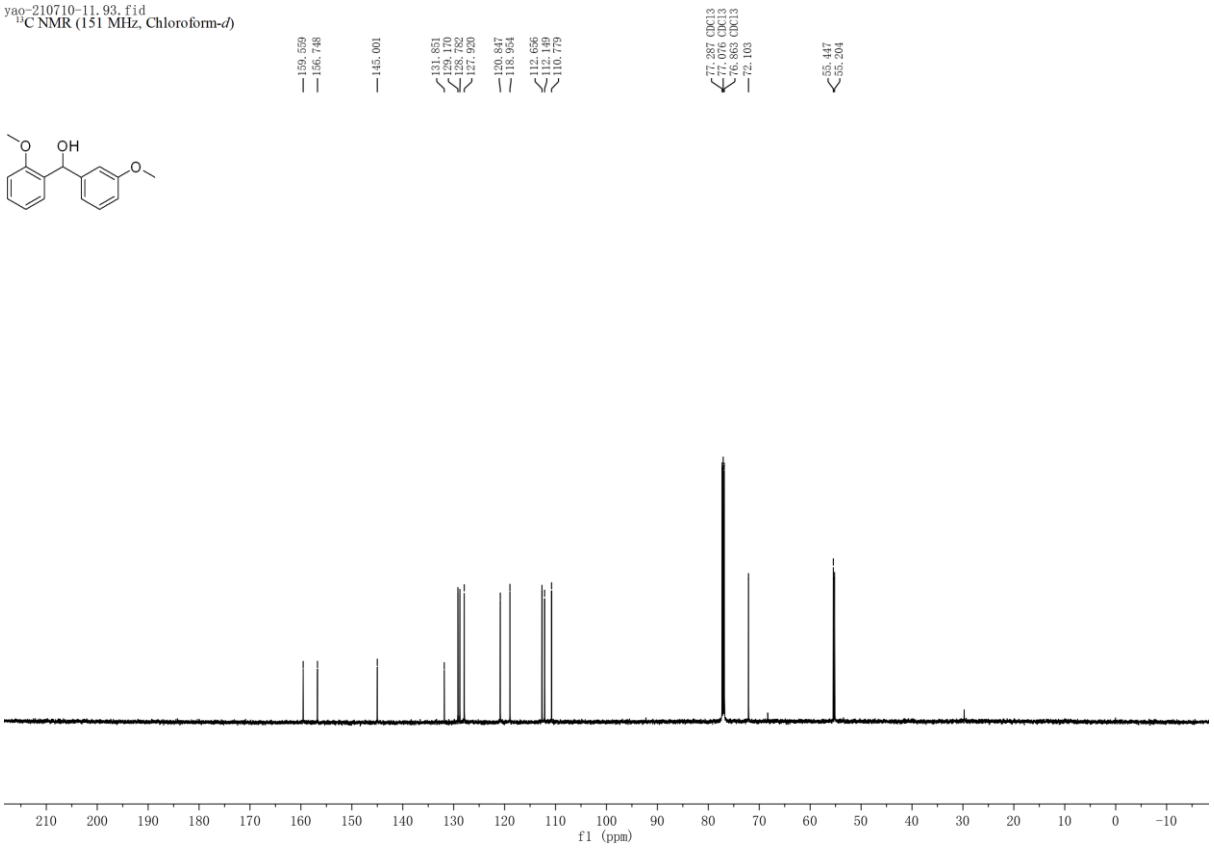
yao-210710-11.93.fid
13C NMR (151 MHz, Chloroform-d)
159.559
156.748
145.001
131.851
129.170
128.782
127.920
120.847
118.954
112.656
112.149
110.779
77.287 CDCl3
77.076 CDCl3
76.863 CDCl3
72.103
55.447
55.204
OH
f1 (ppm)

yao-210710-10.7.fid

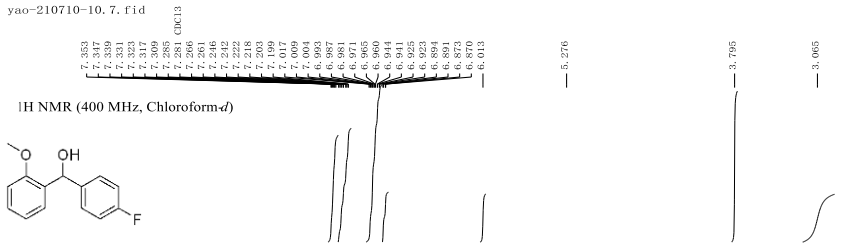

1H NMR (400 MHz, Chloroform-*d*)

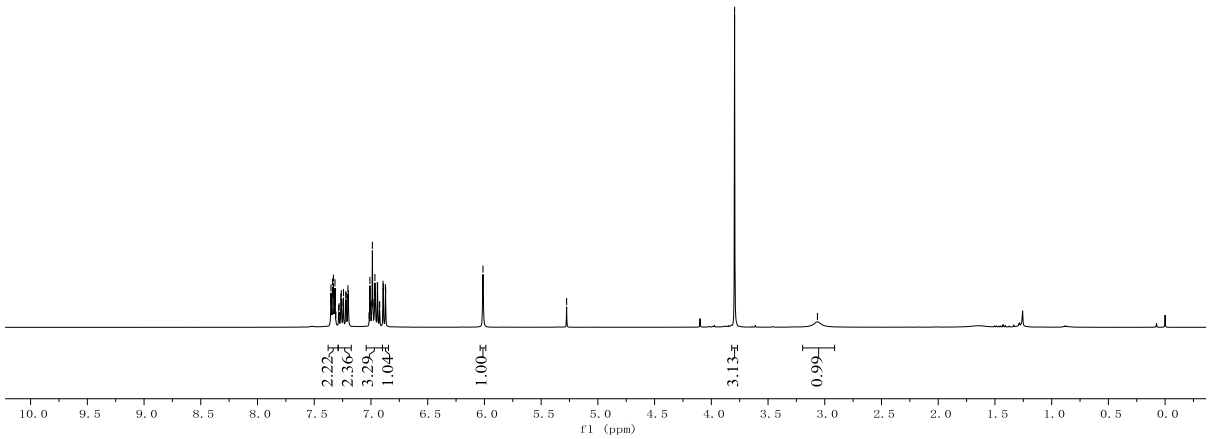

yao-210710-10.6.fid

13C NMR (101 MHz, Chloroform-*d*)

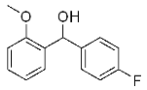

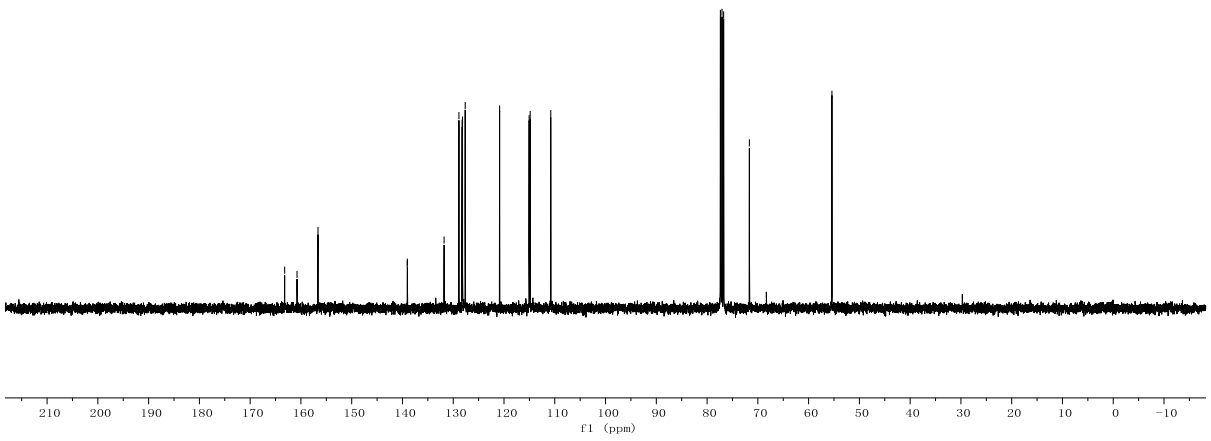

yao-210710-10.8.fid

^{19}F NMR (376 MHz, Chloroform-*d*)

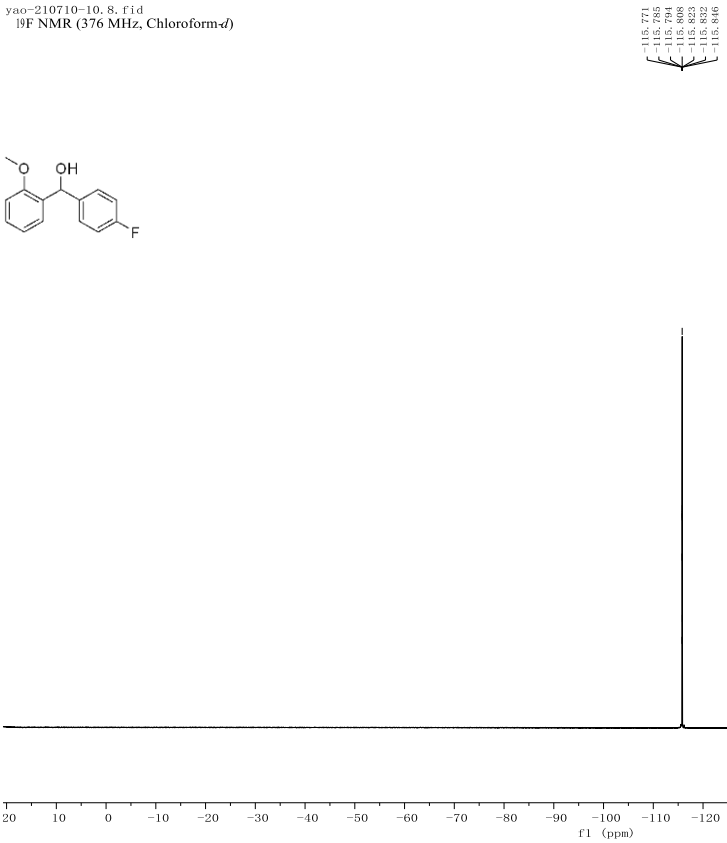

zm1-0401-4.42.fid

^{1}H NMR (600 MHz, Chloroform-*d*)

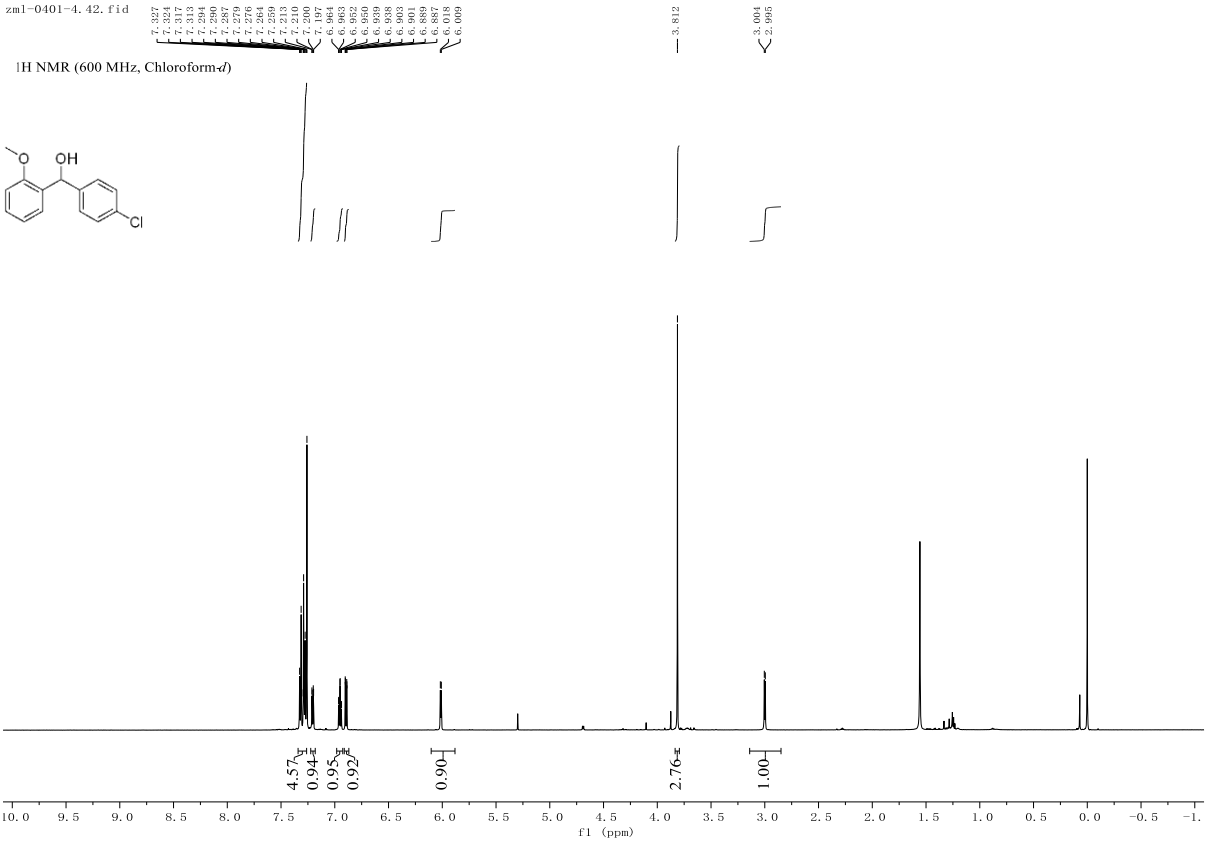

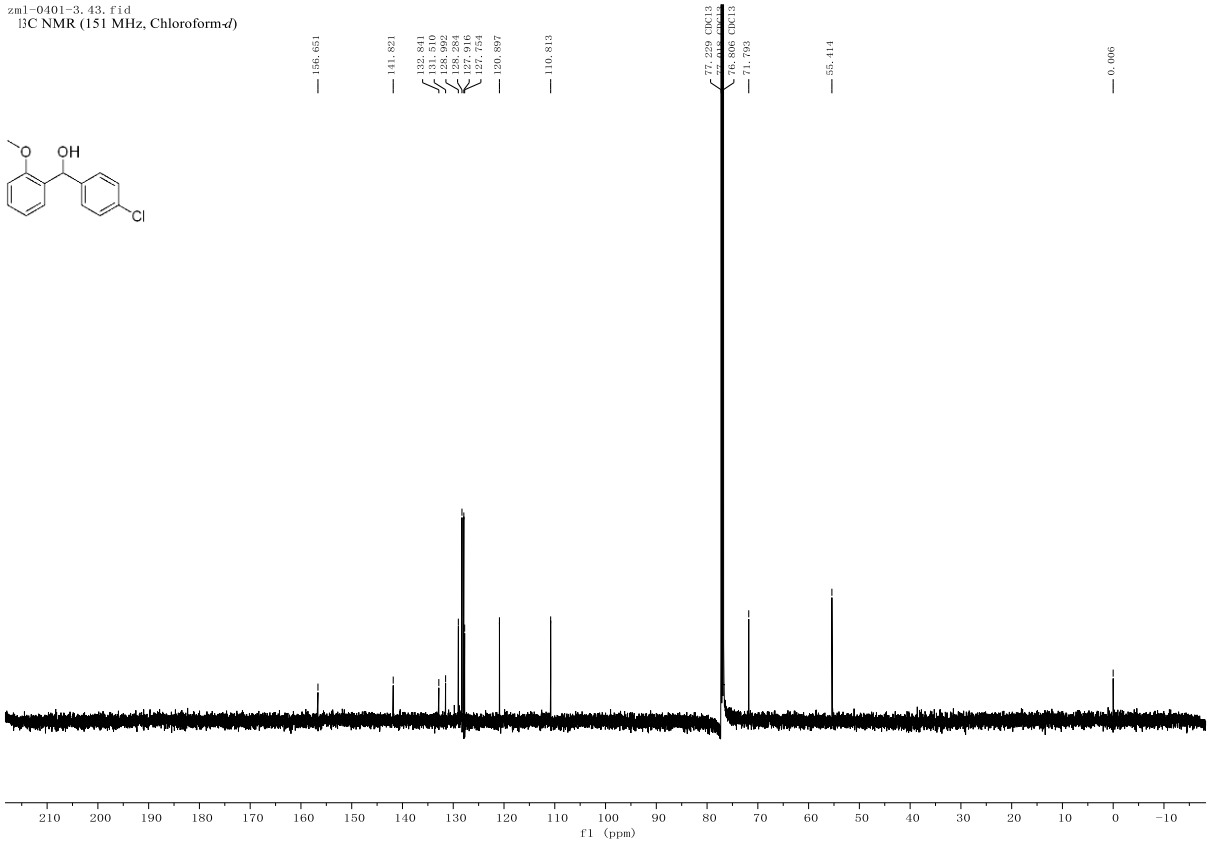
zml-0401-3.43.fid
13C NMR (151 MHz, Chloroform-d)
156.651
141.821
132.841
131.510
128.992
128.284
127.916
127.754
120.897
110.813
77.229 CDCl3
76.806 CDCl3
71.793
55.414
0.006
OH
Cl
f1 (ppm)

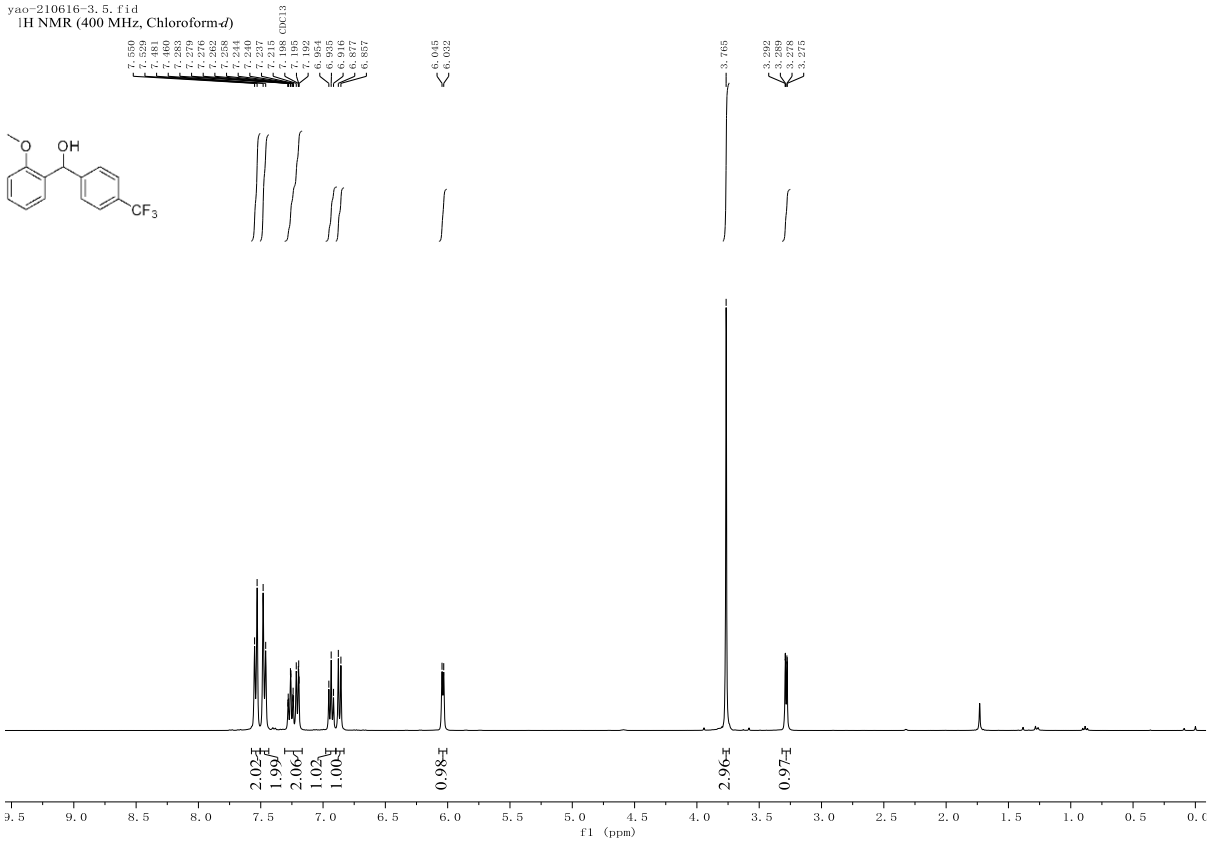
yao-210616-3.5.fid
1H NMR (400 MHz, Chloroform-d)
7.550
7.529
7.481
7.460
7.283
7.279
7.276
7.262
7.258
7.244
7.240
7.237
7.215
7.198
7.195
CDCl3
6.954
6.935
6.916
6.877
6.857
6.045
6.032
3.765
3.292
3.289
3.278
3.275
OH
CF3
2.02
1.99
2.06
1.02
1.00
0.98
2.96
0.97
f1 (ppm)

yao-210616-3-C.1.fid
^{13}C NMR (101 MHz, Chloroform-*d*)

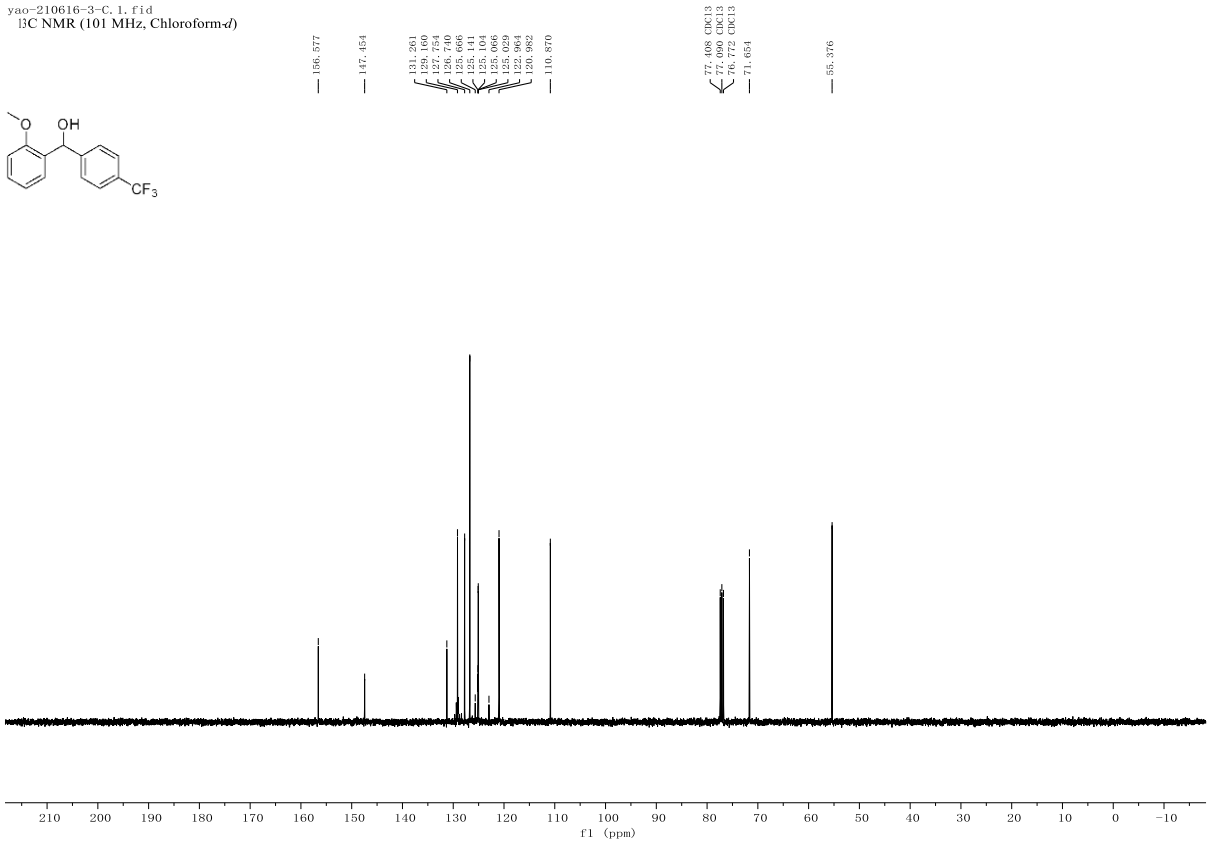

yao-210616-3.7.fid
^{19}F NMR (376 MHz, Chloroform-*d*)

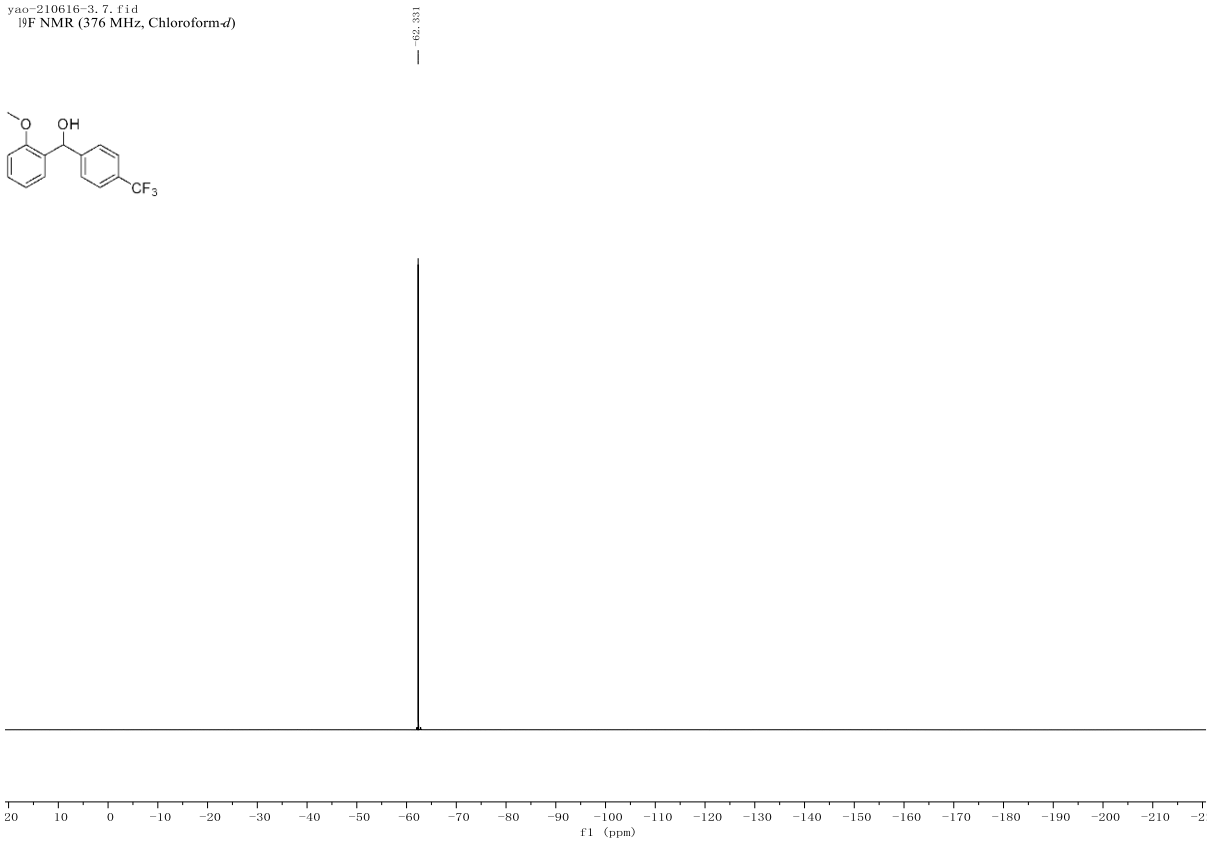

zml-0401-3.32.fid
1H NMR (600 MHz, Chloroform-*d*)

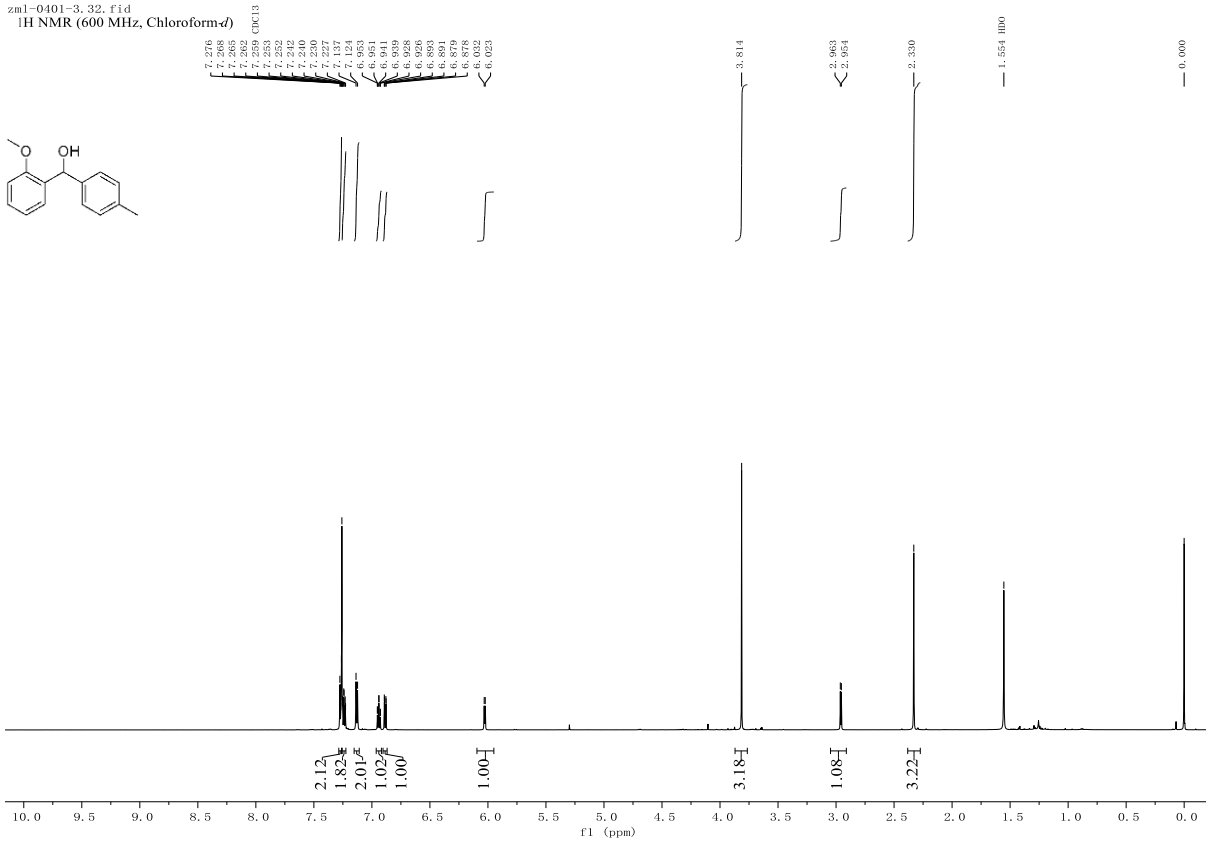

zml-0401-3.33.fid
13C NMR (151 MHz, Chloroform-*d*)

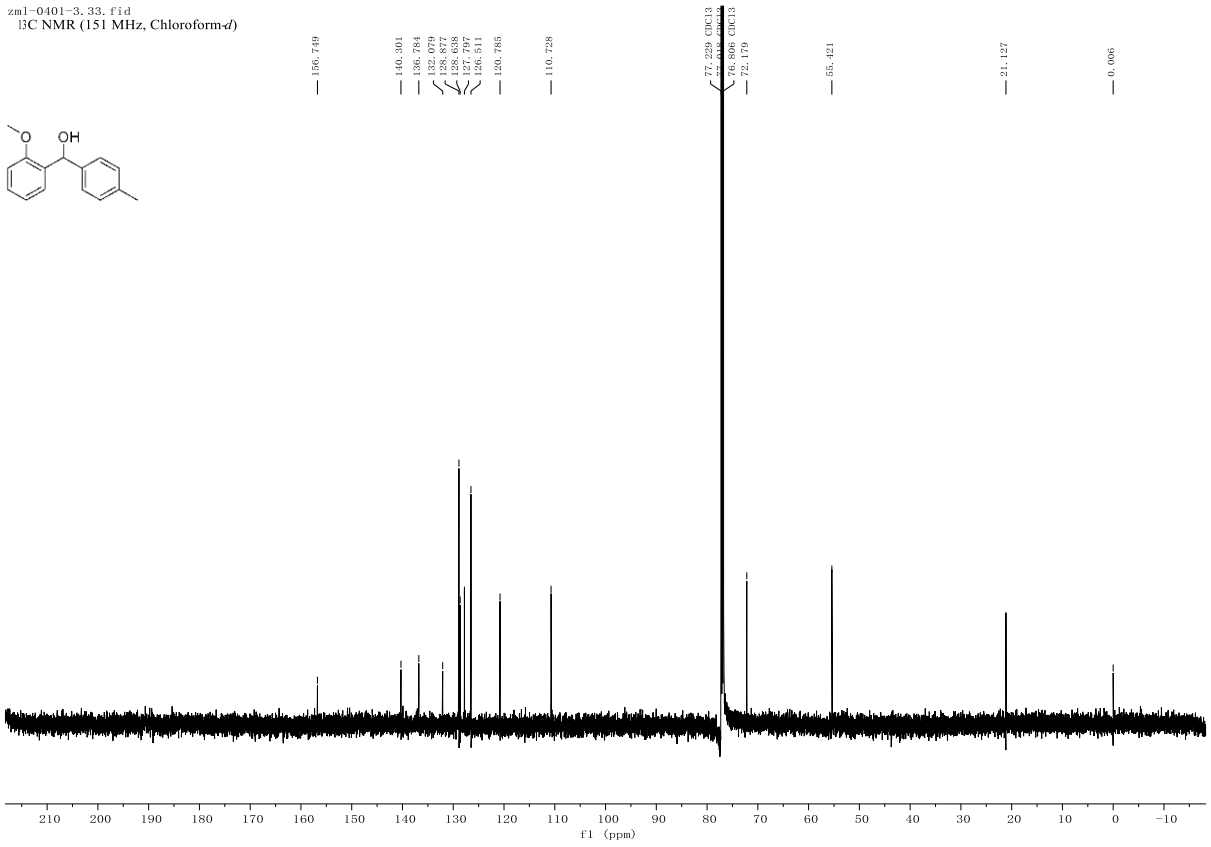

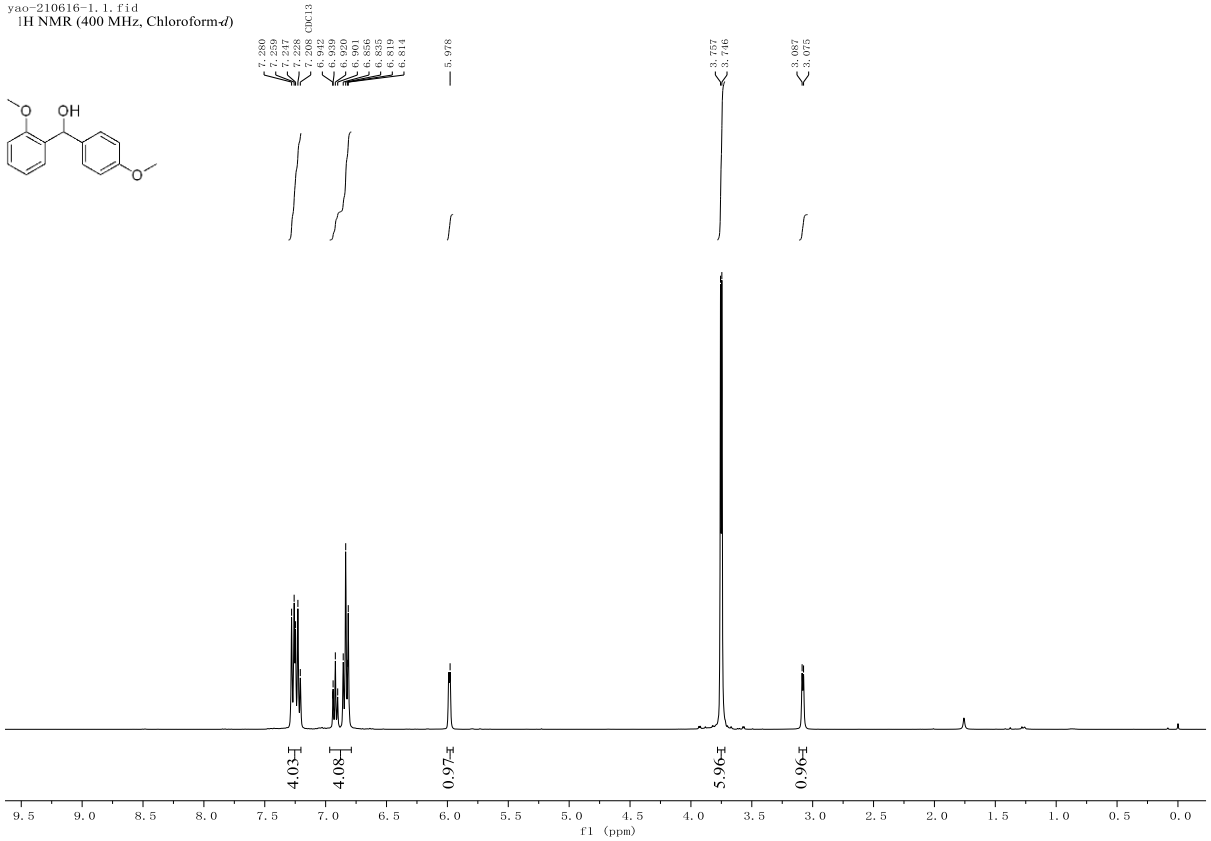
yao-210616-1.1.fid
1H NMR (400 MHz, Chloroform-d)
7.280
7.259
7.247
7.228
7.208
CDCl3
6.942
6.939
6.920
6.901
6.856
6.835
6.819
6.814
5.978
3.757
3.746
3.087
3.075
OH
4.03
4.08
0.97
5.96
0.96
f1 (ppm)

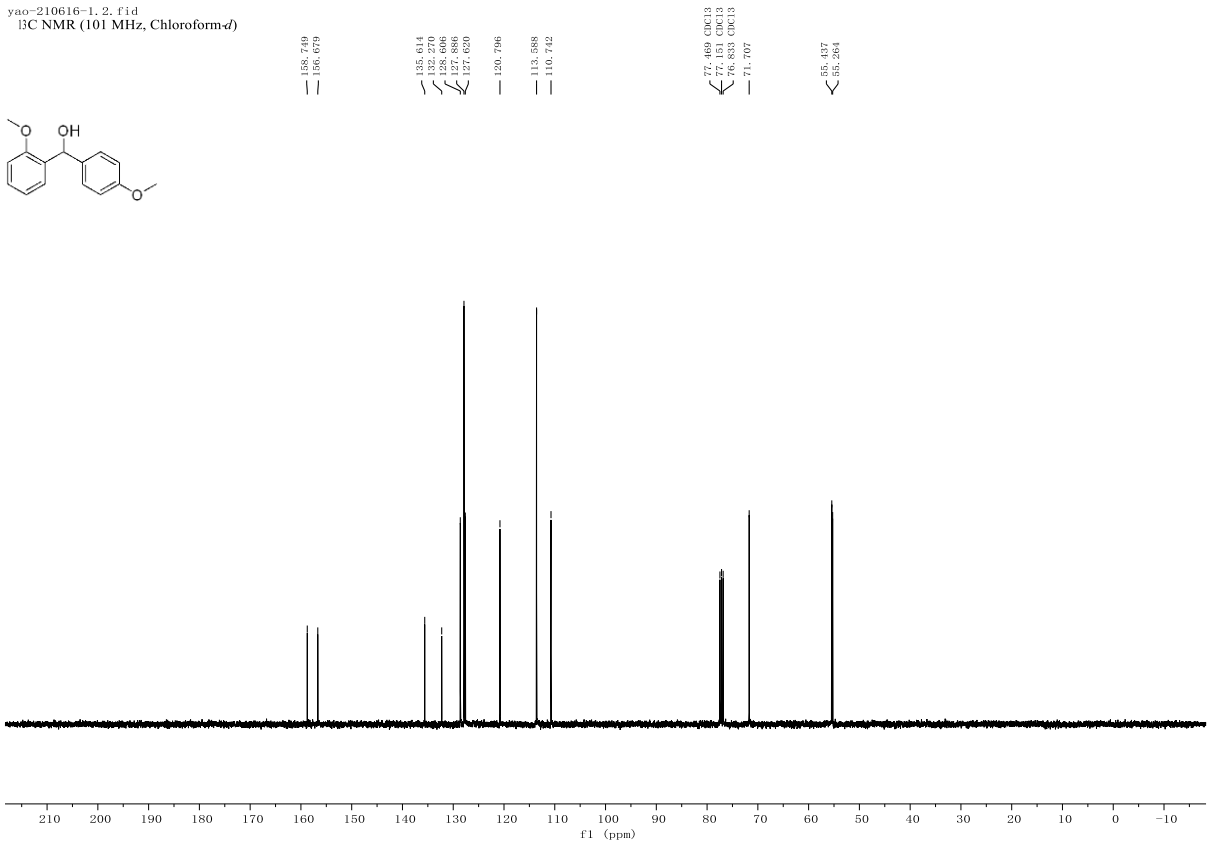
yao-210616-1.2.fid
13C NMR (101 MHz, Chloroform-d)
158.749
156.679
135.614
132.270
128.606
127.886
127.620
120.796
113.588
110.742
77.469 CDCl3
77.151 CDCl3
76.833 CDCl3
71.707
55.437
55.264
OH
f1 (ppm)

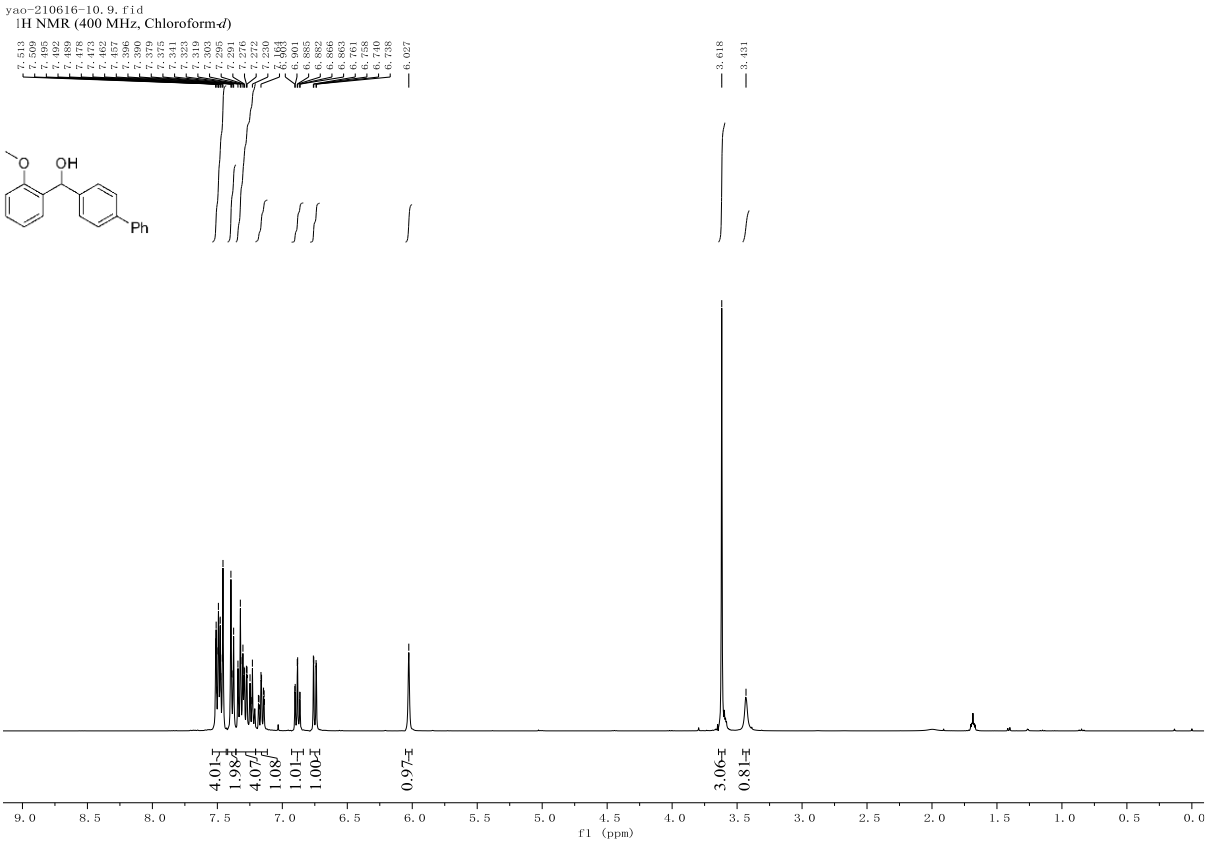
yao-210616-10.9.fid
1H NMR (400 MHz, Chloroform-d)
7.513
7.509
7.495
7.492
7.490
7.478
7.473
7.462
7.457
7.396
7.390
7.379
7.375
7.341
7.323
7.319
7.303
7.295
7.291
7.276
7.272
7.230
6.904
6.901
6.885
6.882
6.866
6.863
6.761
6.758
6.740
6.738
6.027
3.618
3.431
O
OH
Ph
4.01
1.98
4.07
1.08
1.01
1.00
0.97
3.06
0.81
9.0
8.5
8.0
7.5
7.0
6.5
6.0
5.5
5.0
4.5
4.0
3.5
3.0
2.5
2.0
1.5
1.0
0.5
0.0
f1 (ppm)

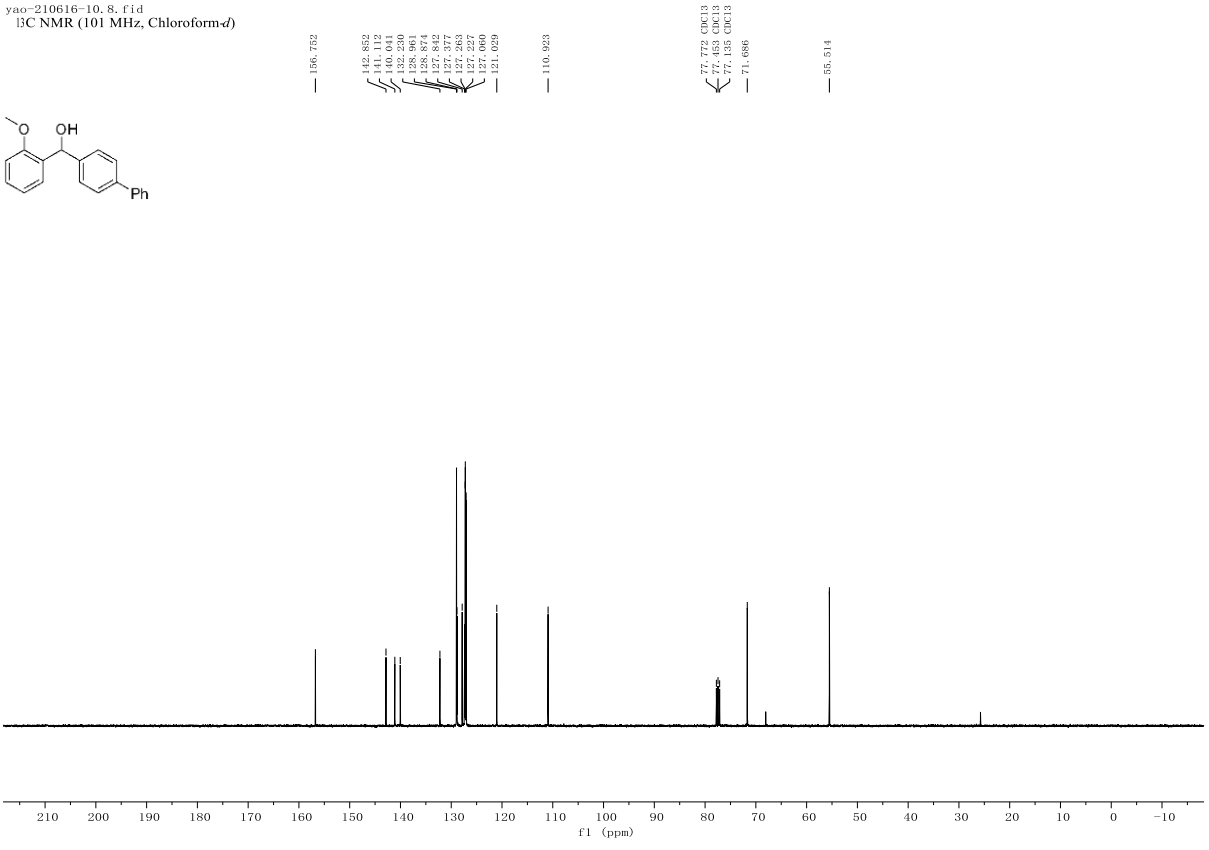
yao-210616-10.8.fid
13C NMR (101 MHz, Chloroform-d)
156.752
142.852
141.112
140.041
132.230
128.961
128.874
127.842
127.377
127.263
127.227
127.060
121.029
110.923
77.772 CDCl3
77.453 CDCl3
77.135 CDCl3
71.686
55.514
O
OH
Ph
210
200
190
180
170
160
150
140
130
120
110
100
90
80
70
60
50
40
30
20
10
0
-10
f1 (ppm)

yao-210616-2.1.fid

1H NMR (400 MHz, Chloroform-*d*)

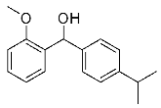

yao-210616-2.2.fid

13C NMR (101 MHz, Chloroform-*d*)

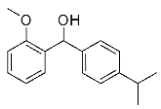

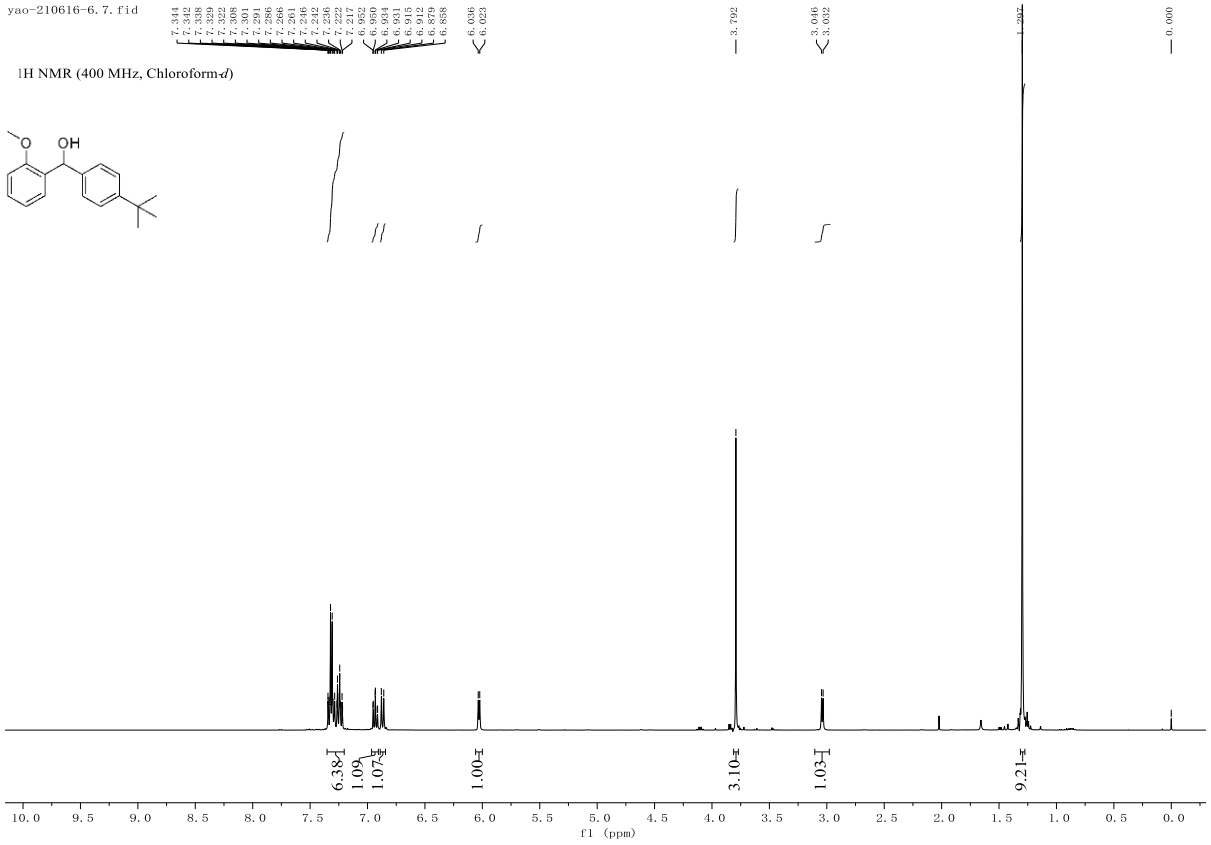
yao-210616-6.7.fid
1H NMR (400 MHz, Chloroform-d)
7.344
7.342
7.338
7.329
7.322
7.308
7.301
7.291
7.286
7.266
7.261
7.246
7.242
7.236
7.222
7.217
6.952
6.950
6.934
6.931
6.915
6.912
6.879
6.858
6.036
6.023
3.792
3.046
3.032
1.297
0.000
OH
6.38
1.09
1.07
1.00
3.10
1.03
9.21
f1 (ppm)

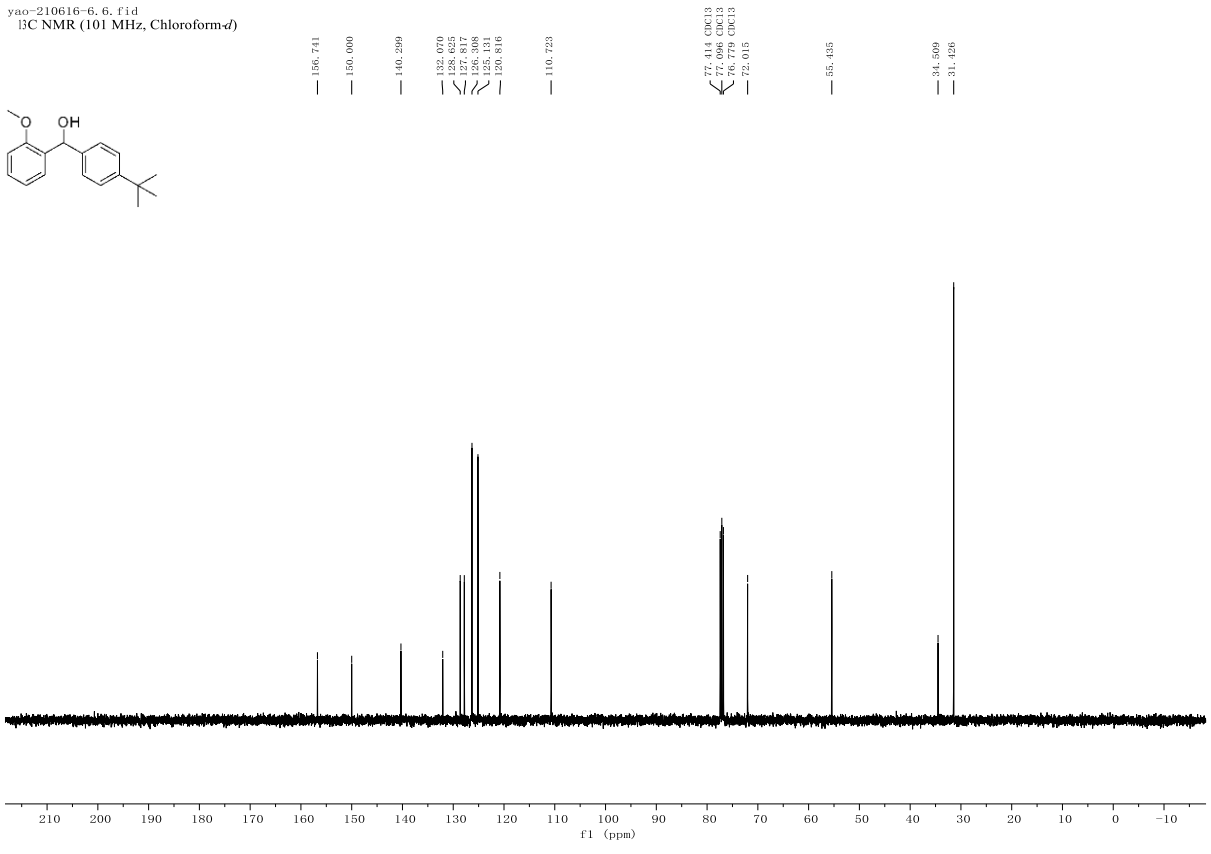
yao-210616-6.6.fid
13C NMR (101 MHz, Chloroform-d)
156.741
150.000
140.299
132.070
128.625
127.847
126.308
125.131
120.816
110.723
77.414 CDCl3
77.096 CDCl3
76.779 CDCl3
72.015
55.435
34.509
31.426
OH
f1 (ppm)

yao-210710-9.72.fid

1H NMR (600 MHz, Chloroform-*d*)

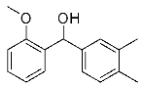

yao-210710-9.73.fid

13C NMR (151 MHz, Chloroform-*d*)

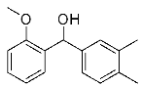

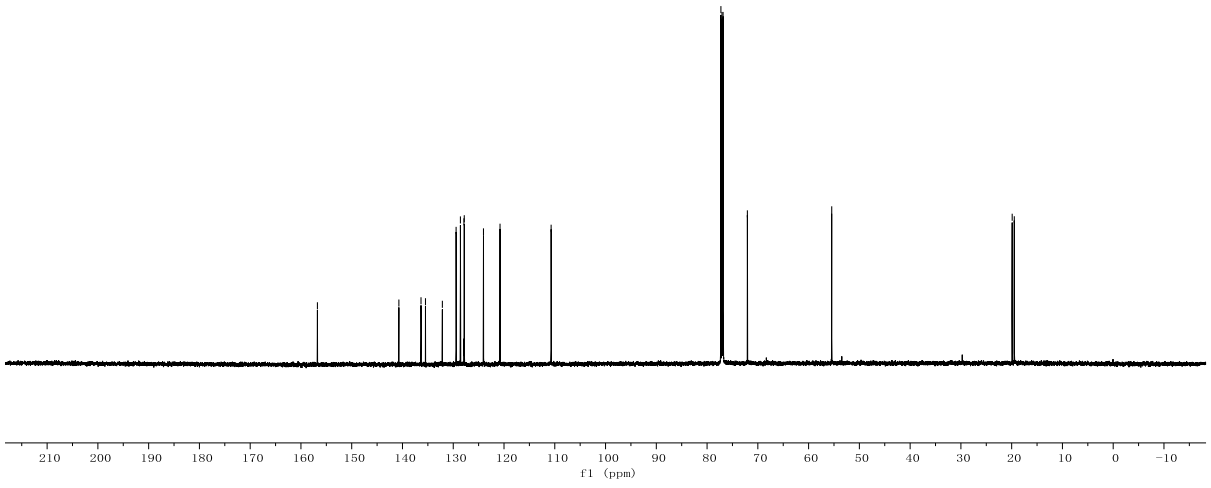

3.7.2 Crystal data

3.7.2.1 Crystal data for Co-1

Table 3.5 Crystal data and structure refinement for **Co-1**

Identification code	**Co-1**
Empirical formula	$C_{49}H_{46}Cl_4CoFe_2OP_3$
Formula weight	1056.20
Temperature/K	100.0
Crystal system	orthorhombic
Space group	P212121
a/Å	11.2324(11)
b/Å	18.0870(18)
c/Å	22.927(2)
α /°	90
β /°	90
γ /°	90
Volume/Å3	4657.8(8)
Z	4
ρ calcg/cm3	1.506
μ /mm-1	1.336
F(000)	2160.0
Crystal size/mm3	0.35 × 0.32 × 0.29
Radiation	MoKα (λ = 0.71073)
2Θ range for data collection/°	4.206 to 61.47
Index ranges	-16 ⩽ h ⩽ 16, -25 ⩽ k ⩽ 25, -32 ⩽ l ⩽ 32
Reflections collected	191102
Independent reflections	14466 [Rint = 0.0621, Rsigma = 0.0297]
Data/restraints/parameters	14466/4/550
Goodness-of-fit on F2	1.031
Final R indexes [I>=2σ (I)]	R1 = 0.0313, wR2 = 0.0691
Final R indexes [all data]	R1 = 0.0397, wR2 = 0.0728
Largest diff. peak/hole / e Å-3	0.79/-1.08
Flack parameter	-0.009(3)

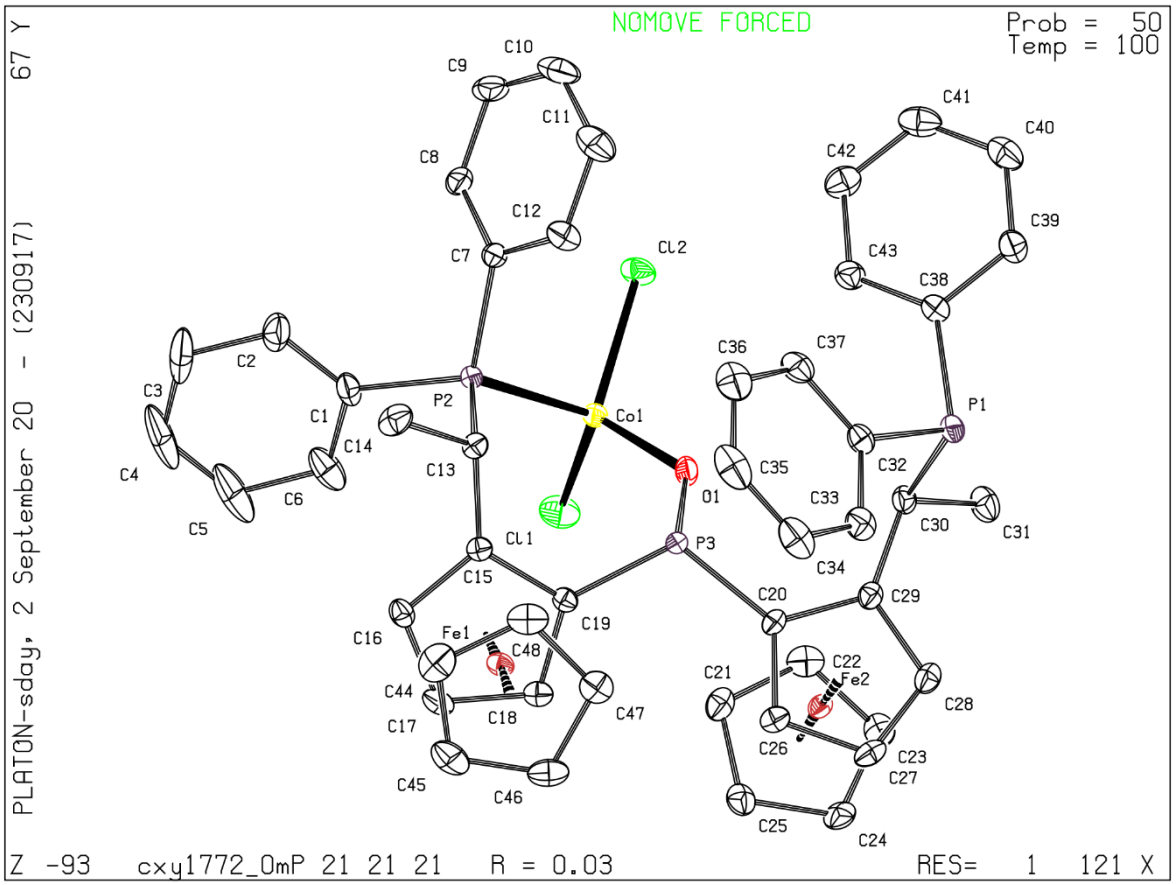

Figure 3.2 Crystal structure of **Co-1** with ellipsoids drawn at the 50% probability level with hydrogen atoms omitted for clarity

3.8 References

[1] J. Wen, F. Wang, X. Zhang, *Chemical Society Reviews* **2021**, *50*, 3211-3237.

[2] Y. Y. Li, S. L. Yu, W. Y. Shen, J. X. Gao, *Acc Chem Res* **2015**, *48*, 2587-2598.

[3] F. Kallmeier, R. Kempe, *Angew Chem Int Ed Engl* **2018**, *57*, 46-60.

[4] R. ter Halle, A. Bréhéret, E. Schulz, C. Pinel, M. Lemaire, *Tetrahedron: Asymmetry* **1997**, *8*, 2101-2108.

[5] E. D. Pan, *Asymmetric Catalytic Reduction of Aromatic Ketones,* Master's Dissertation, Xiamen University **2003**.

[6] D. Zhang, E.-Z. Zhu, Z.-W. Lin, Z.-B. Wei, Y.-Y. Li, J.-X. Gao, *Asian Journal of Organic Chemistry* **2016**, *5*, 1323-1326.

[7] T. Du, B. Wang, C. Wang, J. Xiao, W. Tang, *Chinese Chemical Letters* **2021**, *32*, 1241-1244.

[8] T. Nemoto, T. Matsumoto, T. Masuda, T. Hitomi, K. Hatano, Y. Hamada, *Journal of the American Chemical Society* **2004**, *126*, 3690-3691.

[9] N. V. Dubrovina, A. Börner, *Angewandte Chemie International Edition* **2004**, *43*, 5883-5886.

[10] D. Martin, D. Moraleda, T. Achard, L. Giordano, G. Buono, *Chemistry – A European Journal* **2011**, *17*, 12729-12740.

[11] T. M. Shaikh, C.-M. Weng, F.-E. Hong, *Coordination Chemistry Reviews* **2012**, *256*, 771-803.

[12] X. Tan, W. Zeng, X. Zhang, L. W. Chung, X. Zhang, *Chemical Communications* **2018**, *54*, 535-538.

[13] X.-b. Jiang, A. J. Minnaard, B. Hessen, B. L. Feringa, A. L. L. Duchateau, J. G. O. Andrien, J. A. F. Boogers, J. G. de Vries, *Organic Letters* **2003**, *5*, 1503-1506.

[14] X.-b. Jiang, M. van den Berg, A. J. Minnaard, B. L. Feringa, J. G. de Vries, *Tetrahedron: Asymmetry* **2004**, *15*, 2223-2229.

[15] H. Landert, F. Spindler, A. Wyss, H.-U. Blaser, B. Pugin, Y. Ribourduoille, B. Gschwend, B. Ramalingam, A. Pfaltz, *Angewandte Chemie International Edition* **2010**, *49*, 6873-6876.

[16] P. M. Castro, H. Gulyás, J. Benet-Buchholz, C. Bo, Z. Freixa, P. W. N. M. van Leeuwen, *Catalysis Science & Technology* **2011**, *1*, 401-407.

[17] C. Chen, Z. Zhang, S. Jin, X. Fan, M. Geng, Y. Zhou, S. Wen, X. Wang, L. W. Chung, X.-Q. Dong, X. Zhang, *Angewandte Chemie International Edition* **2017**, *56*, 6808-6812.

[18] J. Chen, C. Chen, C. Ji, Z. Lu, *Org Lett* **2016**, *18*, 1594-1597.

[19] X. Li, G. Zou, *Chemical Communications* **2015**, *51*, 5089-5092.

[20] M. Li, C. Wang, H. Ge, *Organic Letters* **2011**, *13*, 2062-2064.

[21] S. Shi, M. Szostak, *Organic Letters* **2016**, *18*, 5872-5875.

[22] T. Li, X.-L. Yan, Z.-W. Li, Z.-H. Ma, S.-Z. Li, Z.-G. Han, X.-Z. Zheng, J. Lin, *Transition Metal Chemistry* **2018**, *43*, 313-322.

[23] F. Lima, M. Meisenbach, B. Schenkel, J. Sedelmeier, *Organic & Biomolecular Chemistry* **2021**, *19*, 2420-2424.

[24] S.-Y. Moon, S.-H. Jung, U. Bin Kim, W.-S. Kim, *RSC Advances* **2015**, *5*, 79385-79390.

[25] S. K. Chittimalla, T.-C. Chang, T.-C. Liu, H.-P. Hsieh, C.-C. Liao, *Tetrahedron* **2008**, *64*, 2586-2595.

[26] H. Neumann, A. Brennführer, M. Beller, *Chemistry – A European Journal* **2008**, *14*, 3645-3652.

[27] H. Wang, Y. Zhang, T. Yang, X. Guo, Q. Gong, J. Wen, X. Zhang, *Organic Letters* **2020**, *22*, 8796-8801.

[28] F. Ling, S. Nian, J. Chen, W. Luo, Z. Wang, Y. Lv, W. Zhong, *The Journal of Organic Chemistry* **2018**, *83*, 10749-10761.

[29] L. Zhang, Y. Tang, Z. Han, K. Ding, *Angewandte Chemie International Edition* **2019**, *58*, 4973-4977.

[30] L. Qian, X. Tang, Y. Wang, G. Liu, Z. Huang, *Chinese Journal of Chemistry* **2022**, *n/a*.

[31] W. Liu, J. Guo, S. Xing, Z. Lu, *Organic Letters* **2020**, *22*, 2532-2536.

[32] H. I. Pérez, H. Luna, N. Manjarrez, A. Solís, M. A. Nuñez, *Tetrahedron: Asymmetry* **2000**, *11*, 4263-4268.

[33] E. Brown, A. Penfornis, J. Bayma, J. Touet, *Tetrahedron: Asymmetry* **1991**, *2*, 339-342.

[34] Y. Yamamoto, K. Kurihara, N. Miyaura, *Angewandte Chemie International Edition* **2009**, *48*, 4414-4416.

[35] Z. Zhu, J. Xiao, M. Li, Z. Shi, *Angewandte Chemie International Edition* **2022**, *n/a*, e202201370.

[36] S.-J. Chang, S. Zhou, H.-M. Gau, *RSC Advances* **2015**, *5*, 9368-9373.

Chapter 4 Ligand Design towards Transition Metal-Catalysed Asymmetric Hydrogenation

4.1 Introduction

As reviewed in Chapter 1, thousands of chiral phosphine ligands have been developed in the transition metal-catalysed AH for a great variety of unsaturated substrates,[1] providing some products with up to extremely high reactivities (up to 4,550,000 TON) and ideal enantioselectivities (up to 99.9% ee).[2] However, there are still many significant challenges in this field, with there being a lack of effective chiral ligands for the AH of certain challenging substrates (e.g. dialkyl ketones and oxime), for working at industrial scales and for catalysis using earth-abundant metals. The development of novel efficient chiral ligands is still a major strategy to solve these ongoing problems, with ligand design for AH being a core topic in the Zhang group for a number of years. Empirically, four principles concerning the design of chiral ligands are summarised as follows - high rigidity, new ligand scaffolds, the opportunity to electronically and sterically fine-tune reactivity, and ease of synthesis.

This chapter introduces two strategies for ligand design towards transition metal-catalysed hydrogenations, including noncovalent interaction-assisted ferrocenyl phosphine ligands and multidentate phosphine ligands. Noncovalent interactions (such as Van der Waals forces, π interactions, electrostatic interactions, and hydrogen bonds) contribute towards lowering the kinetic barriers of reactions by binding substrates and stabilizing transition states, leading to the rate acceleration and selectivity.[3-4] And chiral multidentate phosphine ligands enable active metal intermediates to be stabilized, avoiding catalyst deactivation caused by ligand dissociation or exchange, and providing deep chiral pockets for enantio-induction.

4.2 Noncovalent interaction-assisted ferrocenyl phosphine ligands

4.2.1 Bis-Zhaophos

Bis-Zhaophos is the C_2-symmetric version of **Zhaophos**,[5] a chiral ferrocenyl bisphosphine-thiourea ligand developed in the Zhang group (Figure 4.1). In the design of **Zhaophos**, H-bond donor properties of the thiourea group were found to improve both the acidity and rigidity of the ligand. This noncovalent ligand-substrate interaction endowed **Zhaophos** with excellent reactivities and enantioselectivities in the Rh- and Ir-catalyzed AH of a broad range of substrates, including C=C bonds of neutral substrates, C=N bonds of ionic substrates and carbocations. [4] Based on this strategy, **bis-Zhaophos** was accordingly designed to further improve catalytic efficiency through doubling the H-bond donor properties compared to **Zhaophos**.

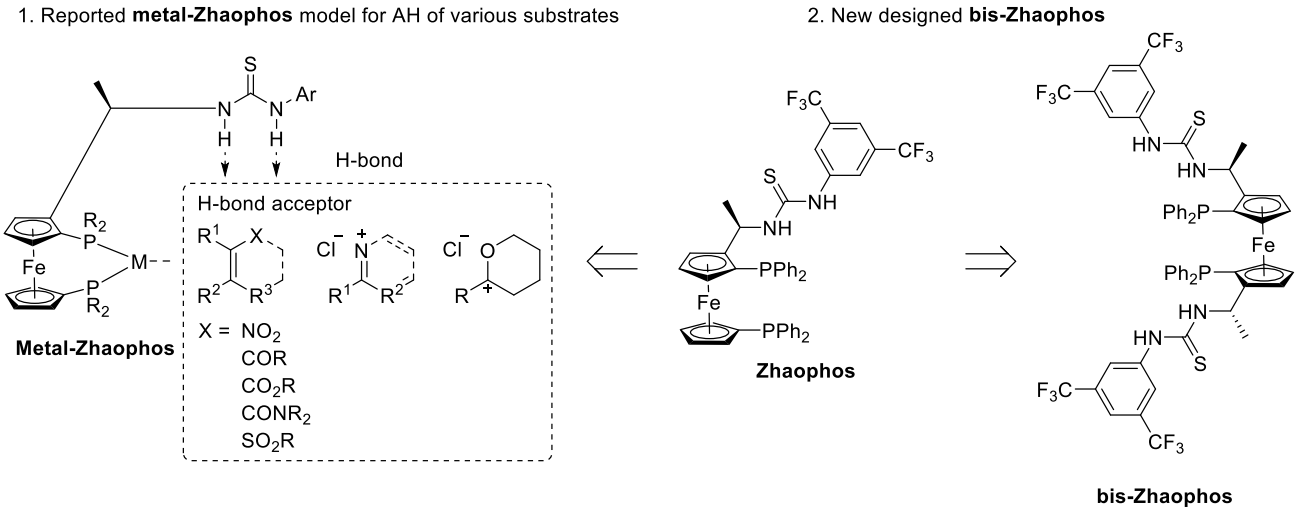

Figure 4.1 Catalyst design for **Zhaophos** and **bis-Zhaophos**

Bis-Zhaophos was successfully prepared via a modification of Zhang's previously reported route towards **Zhaophos** (Scheme 4.1), and characterized using NMR spectroscopy and mass spectrometry.

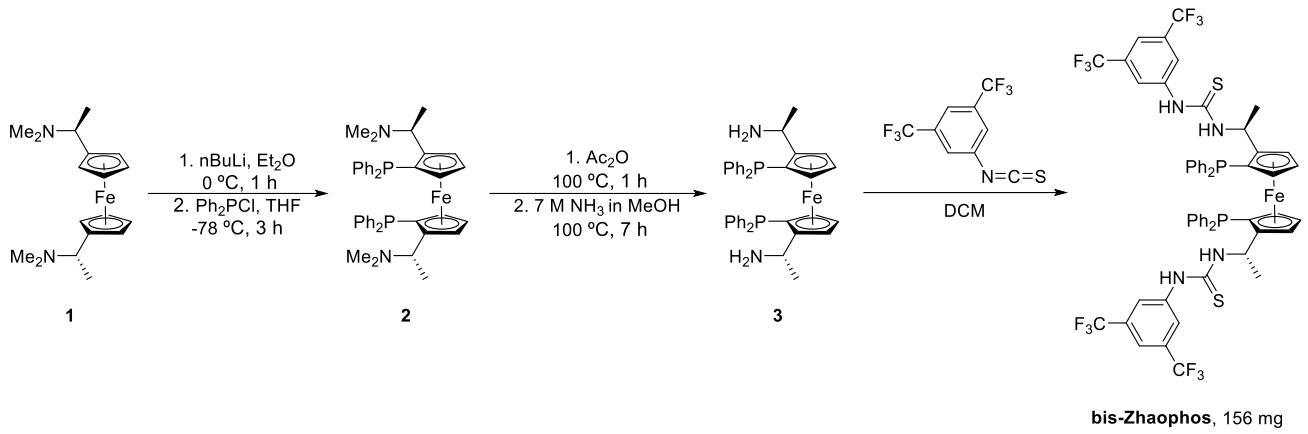

Scheme 4.1 Synthesis of **bis-Zhaophos**

The catalytic performance of **bis-Zhaophos** was studied. Unfortunately, it was found to be inactive in the AH of unsaturated cyclic lactams and *β,β*-disubstituted nitroalkenes, while the presence of **Zhaophos** provided good reactivities and excellent enantioselectivities under the same conditions (Scheme 4.2).[5-6] While adding H-bonding sites would be expected to increase rigidity by increasing the number of interactions between catalyst and substrate, their close proximity to the catalytic centre may also increase the steric hindrance and reduce reactivity. In the future, **bis-Zhaophos** will be used for AH of C_2-symmetric substrates.

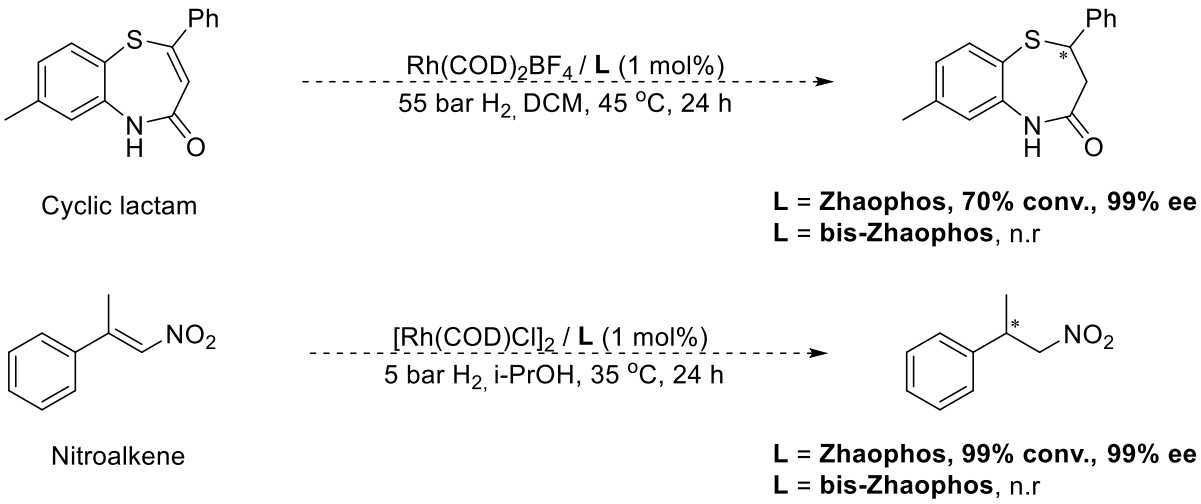

Scheme 4.2 Comparison of catalytic reactivities in AH between **Zhaophos** and **bis-Zhaophos**

4.2.2 Naphth ligand

Naphth ligand was a preliminary attempt to introduce π interactions between catalyst and substrate. This ligand was successfully synthesized, albeit in low yield (Scheme 4.3), and its $^{31}P\{^{1}H\}$ NMR spectrum gave two single peaks at -17.76 ppm and -26.47 ppm (Figure 4.2). This ligand will be tested for the AH of aromatic substrates in the future.

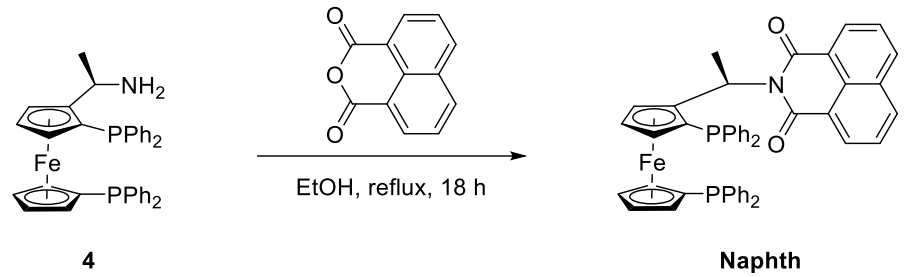

4 **Naphth**

Scheme 4.3 Synthesis of **Naphth** ligand

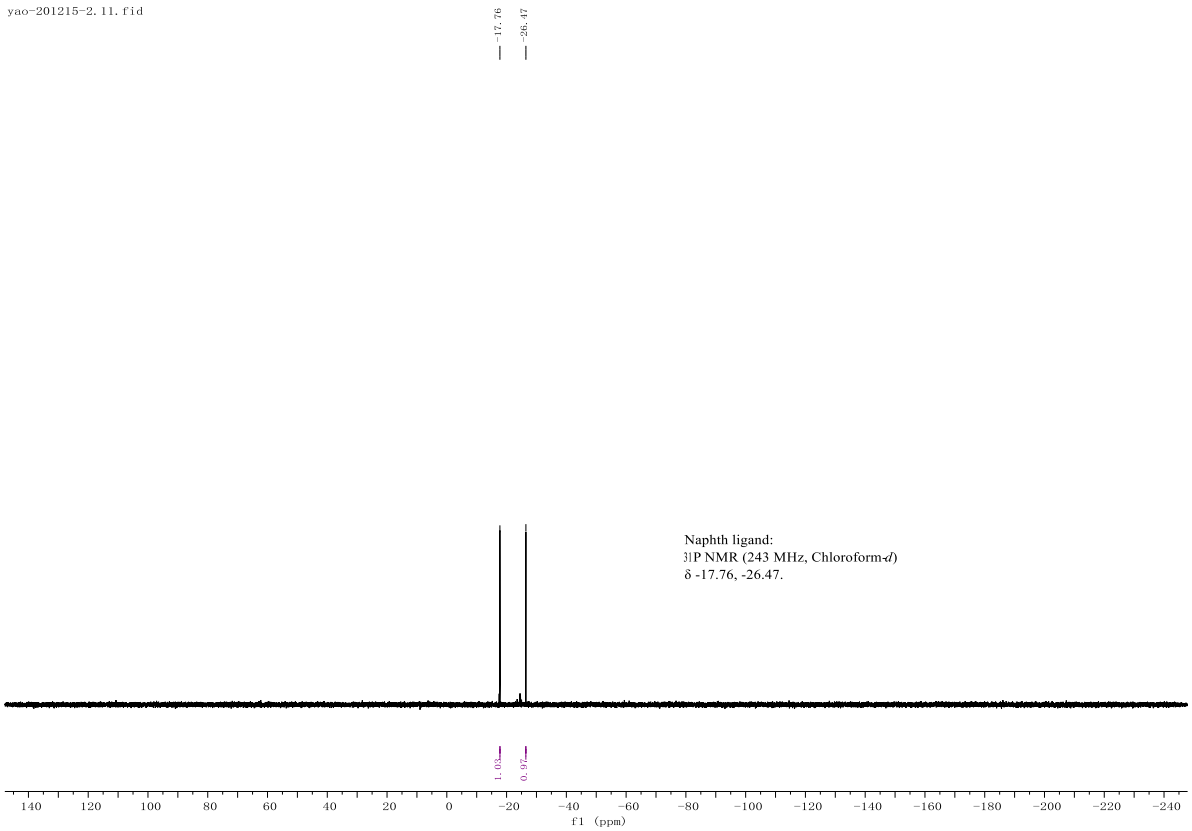

Figure 4.2 $^{31}P\{^{1}H\}$ NMR spectrum of **Naphth** ligand

4.3 Multidentate phosphine ligands

4.3.1 PNP ligand

The **PNP** ligand developed in Chapter 2 has proven to be very efficient for manganese-catalysed AH of simple ketones.[7] Herein, the manganese complex **PNP-Mn** was also found to be active in aldehyde hydrogenation but surprisingly inactive for various other unsaturated substrates (Scheme 4.4). The narrow range of substrates rather limits its further application as a general AH catalyst.

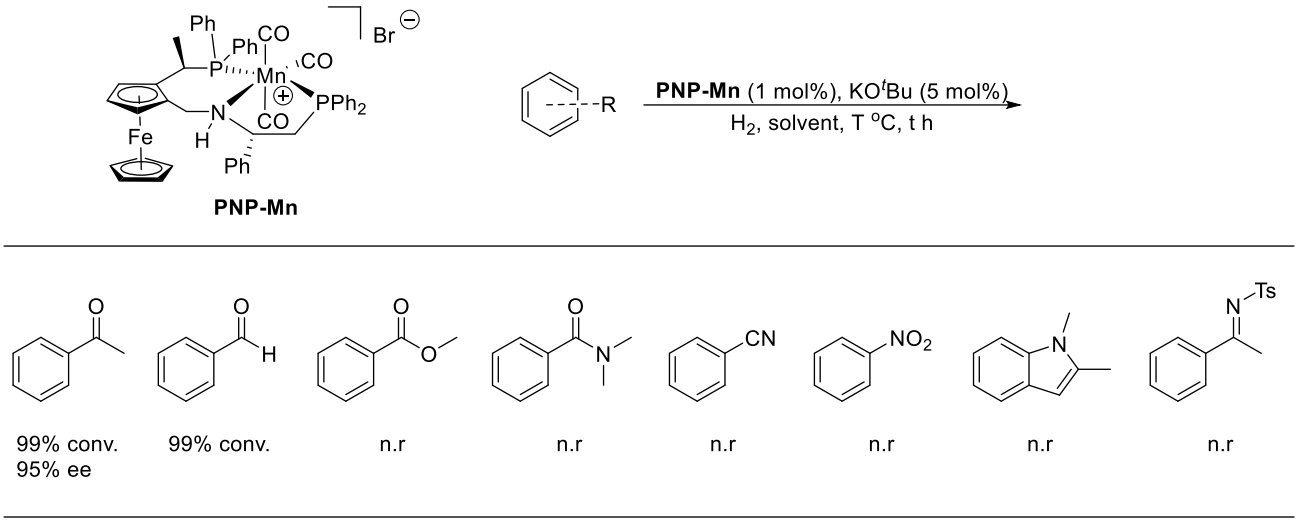

Scheme 4.4 **PNP-Mn**-catalysed hydrogenation of unsaturated substrates

In addition to manganese catalysis, the **PNP** ligand was also probed for the hydrogenation of ketones catalysed by other transition metals such as Fe, Co, Ni, Cu and Ag. However, interestingly, only the cobalt complex **PNP-Co** was found to generate catalytic reactivity with moderate enantioselectivity (Scheme 4.5). It is likely that this chiral tridentate ligand suitable for octahedral Mn(I) complexes is not applicable for the trigonal bipyramidal, square pyramidal and tetrahedral geometries favoured by Co(II), Ni(II) or Cu(I) complexes.

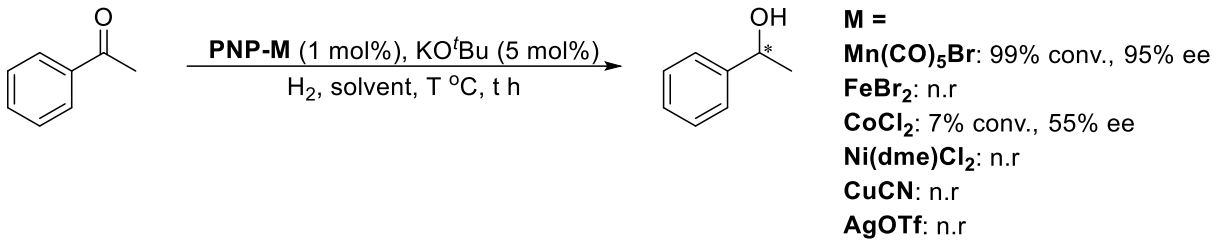

Scheme 4.5 Hydrogenation of acetophenone catalysed by various PNP metal complexes

However, there could be another problem with iron catalysis in this case. A mixture of the **PNP** ligand and $FeBr_2$ under CO atmosphere was expected to generate the iron complex **PNP-Fe-1**, before the treatment with $NaHBEt_3$ at low temperature to give the hydride complex **PNP-Fe-2** (Scheme 4.6).

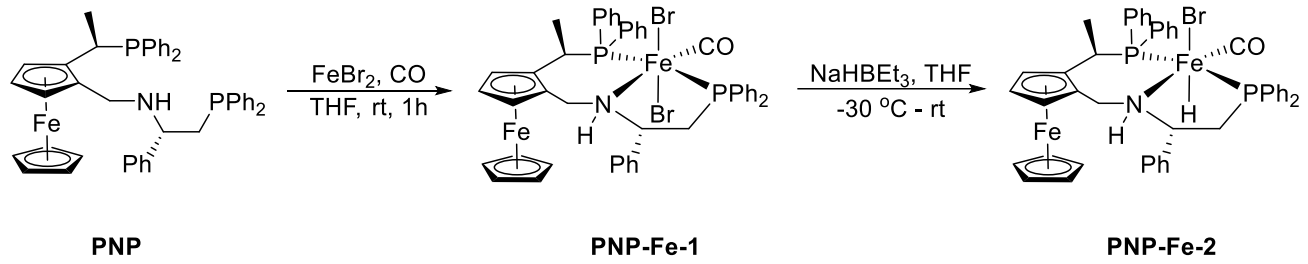

Scheme 4.6 Intended preparation of PNP iron complexes

Unfortunately, no hydride peak of **PNP-Fe-2** was observed in the high field (ca. -15 – 0 ppm) of ^{1}H NMR spectrum, indicating a failure to form the expected iron hydride complex. The $^{31}P\{^1H\}$ NMR spectrum of **PNP-Fe-2** has free ligand peaks (at 7.3 ppm and -22.9 ppm), many unknown peaks and two doublet peaks (at 89.3 ppm, J = 32.1 Hz and 68.9 ppm, J = 32.1 Hz) (Figure 4.3). These two doublet peaks indicate the presence of a PNP iron complex, but its precise structure can not be determined. These unknown iron compounds were not effective for the AH of acetophenone, although this does not prove the inactivity of the expected iron complexes. In the future, the desired PNP iron complexes will be prepared under modified conditions.

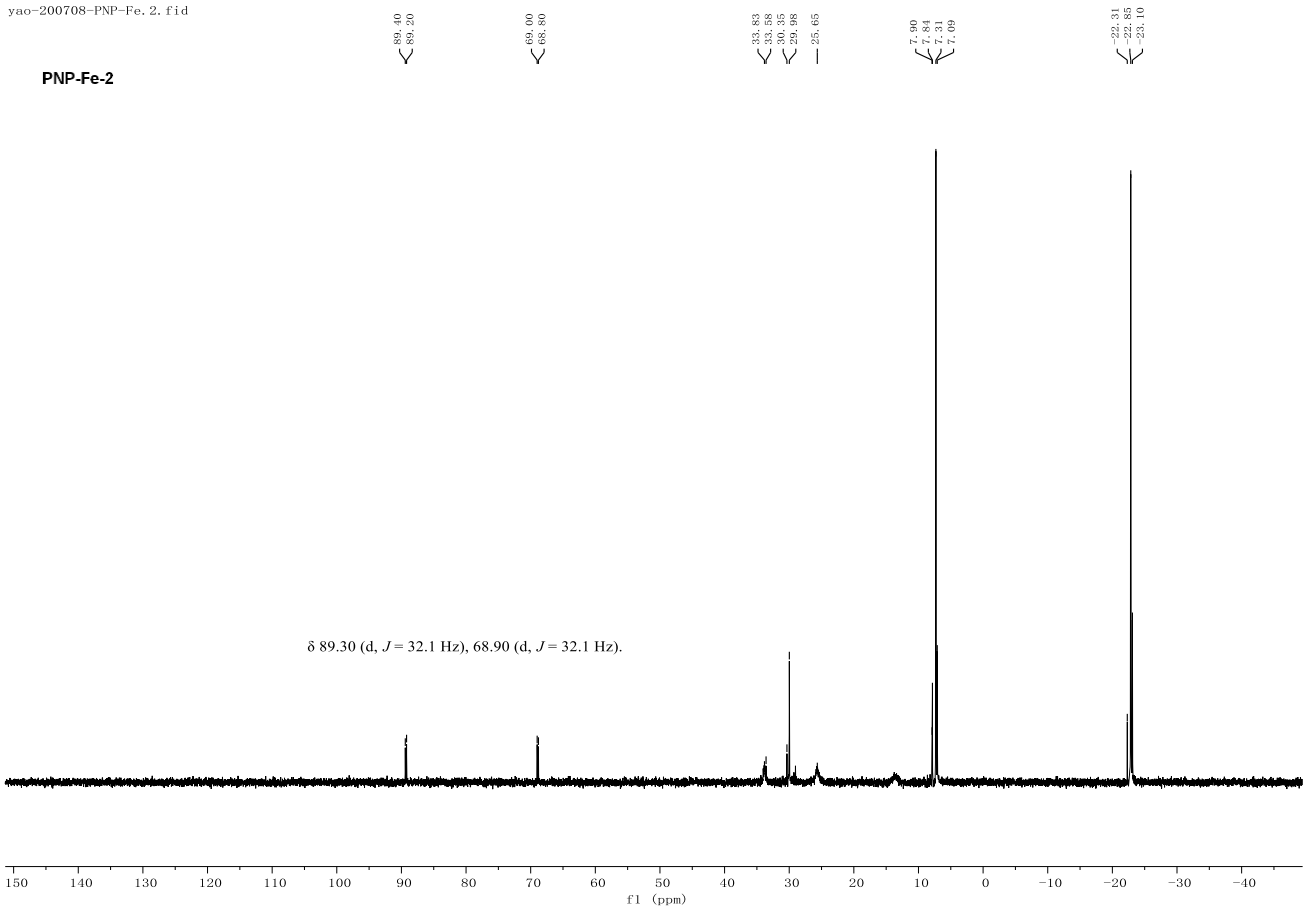

Figure 4.3 $^{31}P\{^{1}H\}$ NMR spectrum of **PNP-Fe-2**

Notably, silver-catalysed hydrogenation reactions have only been reported very rarely. [8] Mixing AgOTf and the **PNP** ligand in DCM for 1 h at RT gave the silver complex **PNP-Ag** as a yellow solid in high yield. Unfortunately, the **PNP-Ag** was inactive in the hydrogenation of ketones but it did give 25% conversion for benzaldehyde hydrogenation under unoptimized conditions (Scheme 4.7).

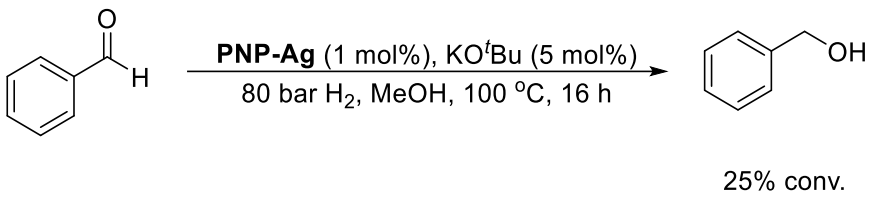

Scheme 4.7 **PNP-Ag**-catalysed hydrogenation of benzaldehyde

The $^{31}P\{^{1}H\}$ NMR spectrum of **PNP-Ag** is very interesting, including two peaks at 28.13 ppm (ddd, *J* = 558.0, 94.6, 39.7 Hz) and -3.35 ppm (ddd, *J* = 462.5, 94.8, 33.1 Hz) (Figure 4.4).

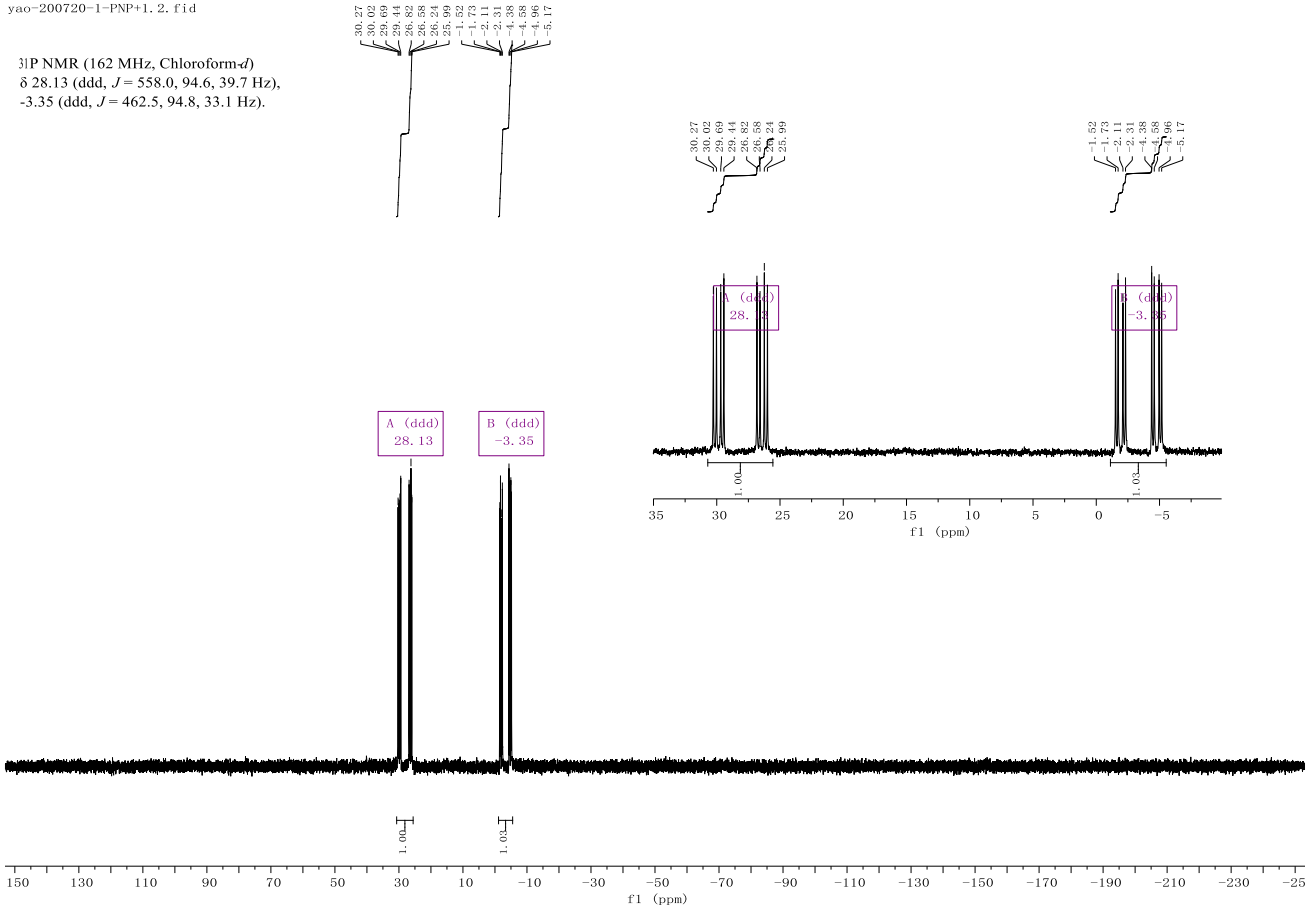

Figure 4.4 $^{31}P\{^{1}H\}$ NMR spectrum of **PNP-Ag**

4.3.2 Bis-Fc-PNP ligand

Bis-ferrocene PNP ligand (**bis-Fc-PNP**) was designed to improve the ligand rigidity and as a result was expected to provide better chiral control for hydrogenation products. It was based on the **PNP** ligand, and could be successfully prepared in low yield via a synthetic pathway similar to that followed for the **PNP** ligand (Scheme 4.8).

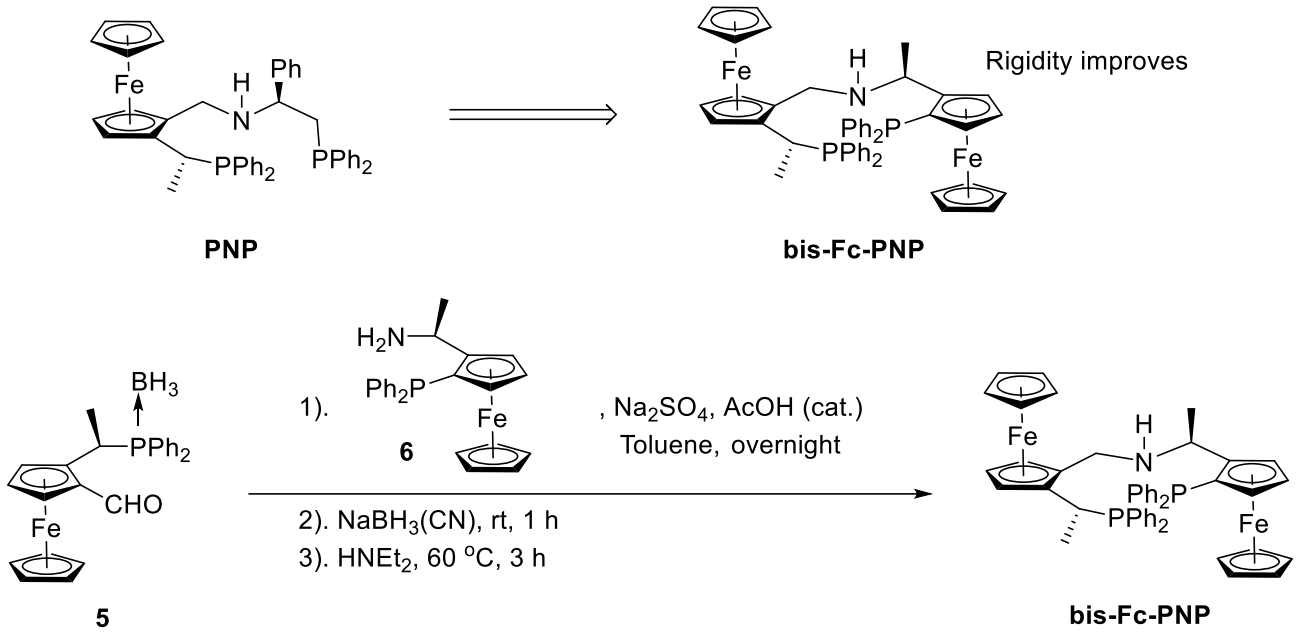

Scheme 4.8 Design and synthesis of **bis-Fc-PNP**

Mixing the **bis-Fc-PNP** ligand with $Mn(CO)_5Br$ in boiling toluene produced the manganese complex **bis-Fc-PNP-Mn** in high yield. The $^{31}P\{^1H\}$ NMR spectrum of **bis-Fc-PNP-Mn** shown in Figure 4.5 has two peaks at 60.4 ppm and 45.2 ppm, which are significantly shifted compared to the corresponding free ligand, which has signals at 6.5 ppm and -24 ppm (for details, see experimental).

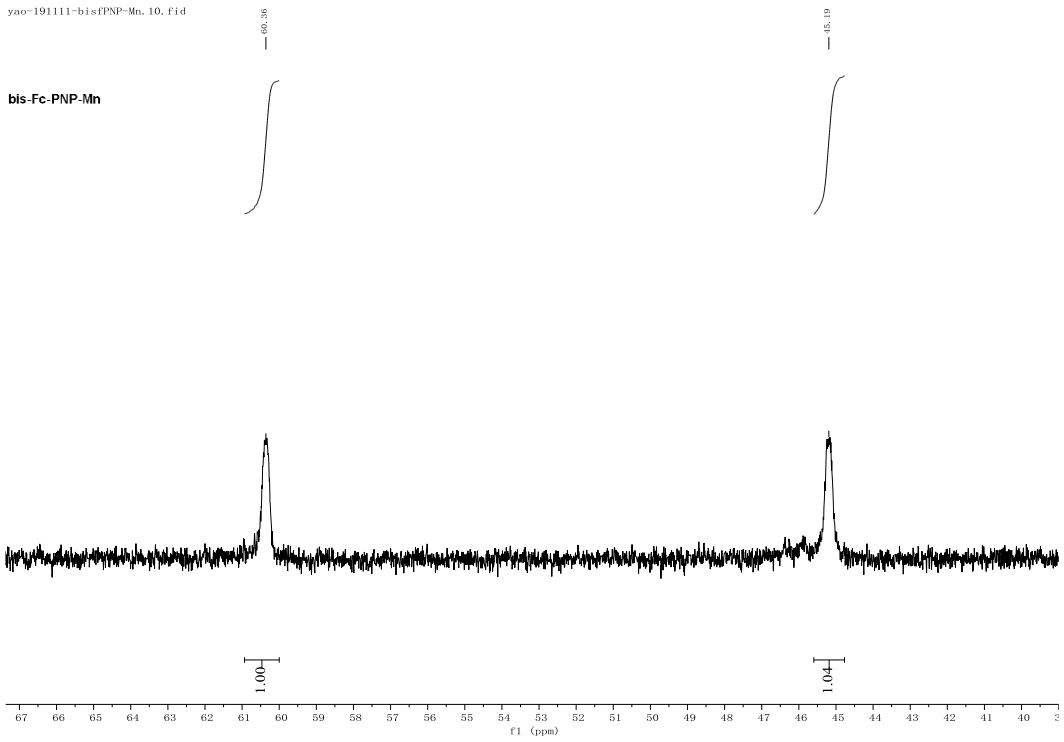

Figure 4.5 $^{31}P\{^{1}H\}$ NMR spectrum of **bis-Fc-PNP-Mn**

The pre-generated manganese complex **bis-Fc-PNP-Mn** and *in-situ* generated cobalt and nickel complexes were used in the hydrogenation of ketones, imines and indoles. Unfortunately, these complexes were found to be inactive in all reactions (Scheme 4.9). It appears that the introduction of an additional ferrocene unit has significant effects on the catalytic reactivities of these metal complexes.

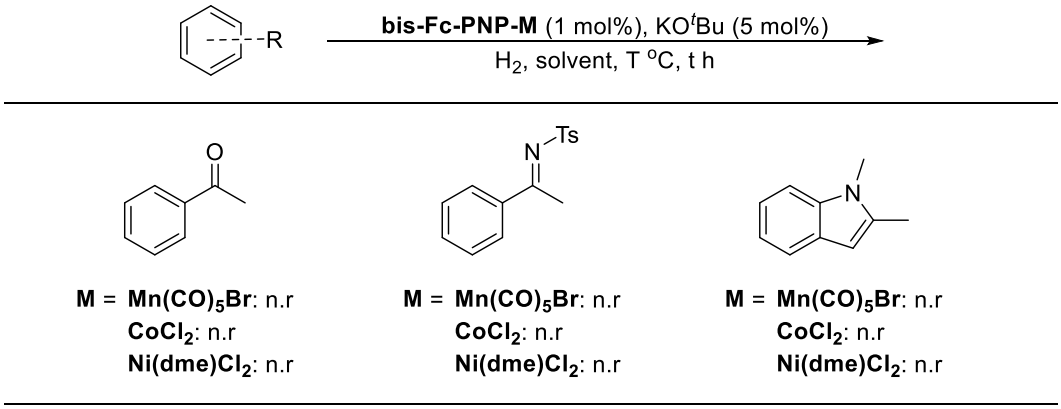

Scheme 4.9 Applications of bis-Fc-PNP in metal-catalysed hydrogenation

4.3.3 Fang-PNP ligand

Fang-PNP ligand was synthesized by Dr Wei Fang of the Zhang group. It was decided to explore its applications in earth-abundant metal-catalysed AH of ketones. The manganese complex **Fang-PNP-Mn** was found to be inefficient in the hydrogenation of acetophenone under different solvent conditions, while the cobalt complex **Fang-PNP-Co** could provide high reactivity (92% conv.) and moderate enantioselectivity (51% ee) using HFIP as solvent (Scheme 4.10). Dr Wei Fang has prepared a family of **Fang-PNP** ligands bearing different substituents on both phosphine groups, and it is likely that a promising catalyst system for cobalt-catalysed AH of ketones will be developed in the future.

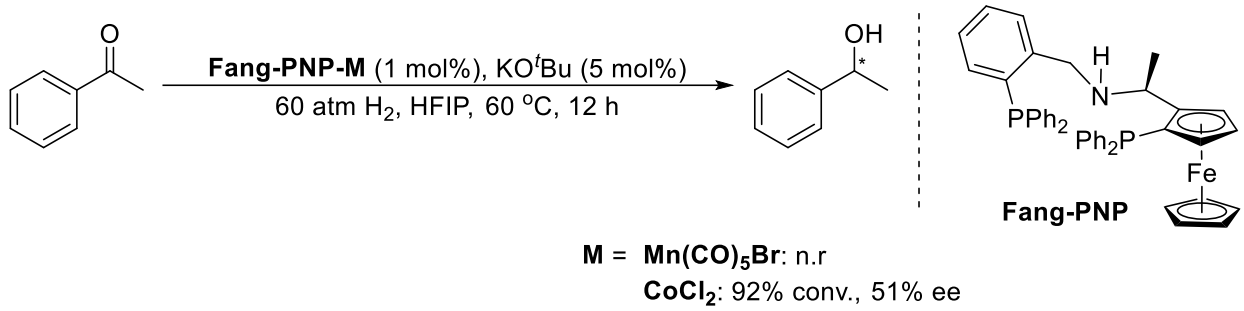

Scheme 4.10 Applications of **Fang-PNP** ligand in metal-catalysed hydrogenation of acetophenone

4.3.4 Fc-SPO ligand

The **Fc-SPO** ligand developed in Chapter 3 was shown to be efficient for cobalt-catalysed AH of diarylketones. Herein, its cobalt complex **Fc-SPO-Co** was also found to be active in aldehyde hydrogenation but inactive for various other unsaturated substrates (Scheme 4.11). Low efficiency and narrow substrate range limits its further application in hydrogenation reactions.

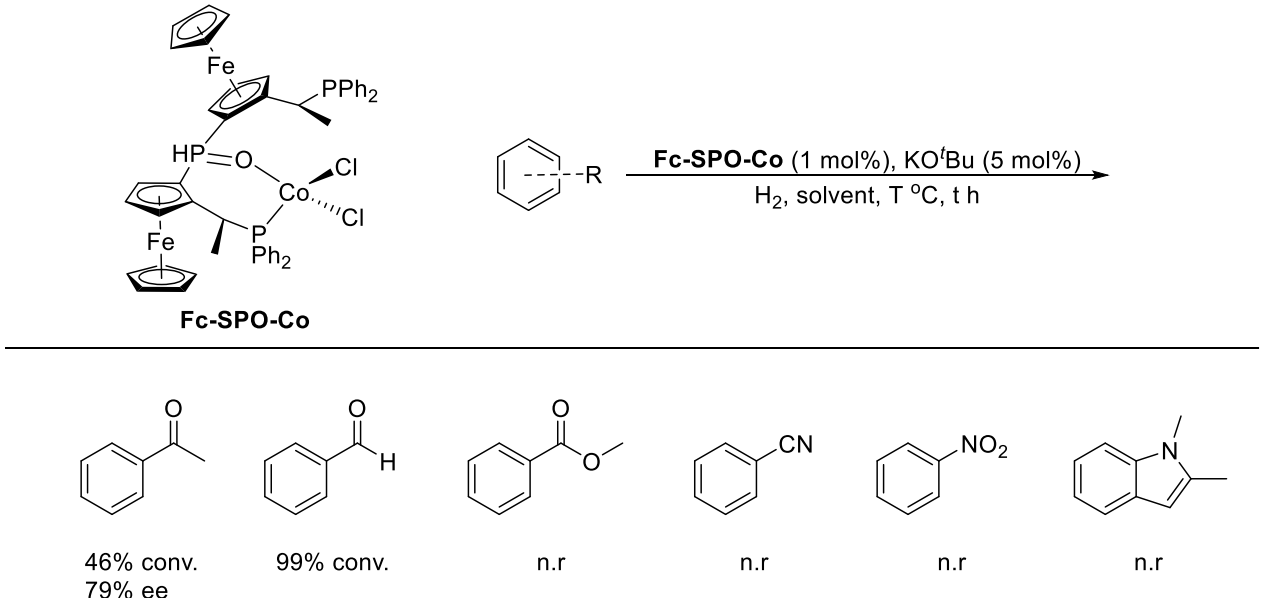

Scheme 4.11 **Fc-SPO-Co**-catalysed hydrogenation of unsaturated substrates

In addition to cobalt catalysis, the **Fc-SPO** ligand was also used in the AH of ketones, catalysed by other earth-abundant metals such as Mn, Ni and Cu. Mixing the **Fc-SPO** ligand with $Mn(CO)_5Br$ in boiling toluene produced the manganese complex **Fc-SPO-Mn** in high yield. The $^{31}P\{^1H\}$ NMR spectrum of **Fc-SPO-Mn** shown in Figure 4.6 has three peaks at 122.06 ppm (dt, J = 255.0, 61.1 Hz, phosphine), 78.73 ppm (dt, J = 239.1, 55.9 Hz, phosphine) and 72.15 ppm (dt, J = 475.6, 56.9 Hz, phosphine oxide), which are noticeably different to the corresponding free ligand peaks at 19.85 ppm (d, J = 10.8 Hz, phosphine), 11.13 ppm (s, phosphine oxide) and 8.86 ppm (d, J = 10.6 Hz, phosphine) (for details, see Chapter 3). The **Fc-SPO** ligand has three different phosphorus atoms despite a

seemingly C_2-symmetric structure, and peak splittings in the NMR are only apparent for the phosphine P atoms and not the phosphine oxide P atom. The $^{31}P\{^1H\}$ NMR spectrum of **Fc-SPO-Mn** is even more intriguing. It is likely that the formation of the tridentate manganese complex brings three phosphorus atoms into close proximity, facilitating further peak splittings that result from coupling between phosphine P atoms and also between phosphine and phosphine oxide P atoms.

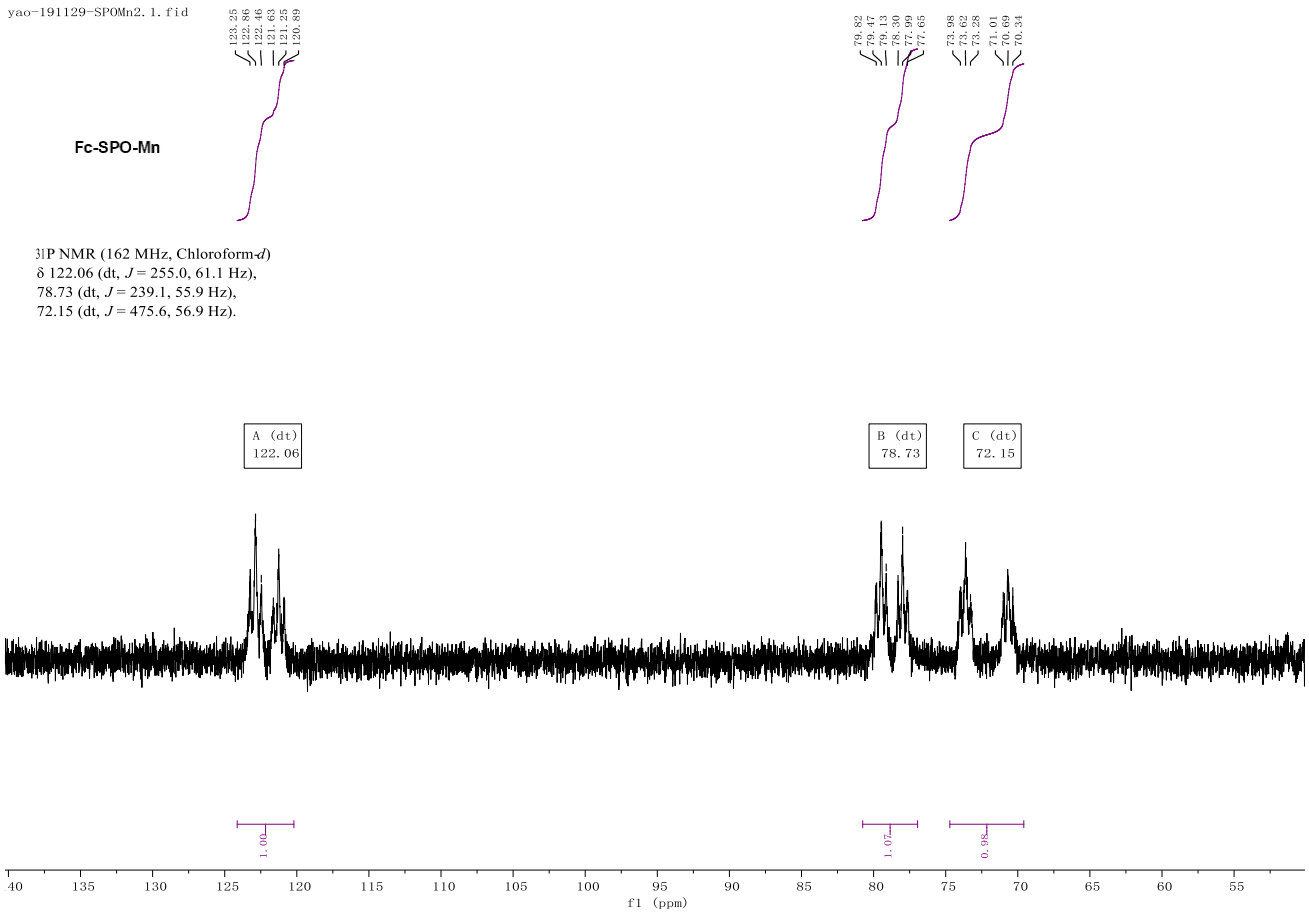

Figure 4.6 $^{31}P\{^1H\}$ NMR spectrum of **Fc-SPO-Mn**

The pre-generated manganese **Fc-SPO-Mn** and *in-situ* generated nickel and copper complexes were used in the hydrogenation of acetophenone. However, these complexes were found to be inefficient for this reaction (Scheme 4.12). This bis-ferrocene, with a second phosphine oxide ligand, showed poor catalytic reactivities for earth-abundant metal-catalysed AH of ketones.

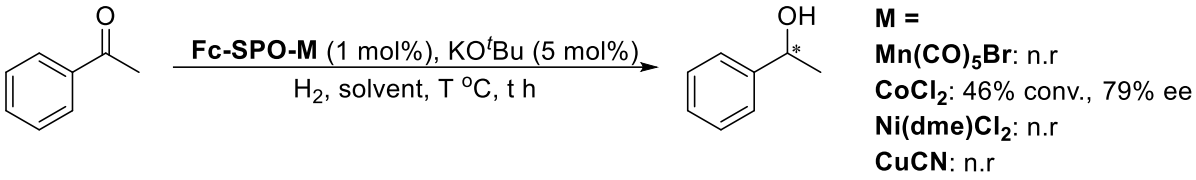

Scheme 4.12 Hydrogenation of acetophenone catalysed by various Fc-SPO metal complexes

4.3.5 SPO-PPP ligand

The ligand **SPO-PPP** was developed by Dr Xuefeng Tan of the Zhang group.[9] Its application in manganese-catalysed hydrogenation of aldehydes was therefore explored. Crystals of **SPO-PPP-Mn** suitable for X-Ray crystallography were grown from an NMR tube in $CDCl_3$. The expected *fac*-geometry was confirmed, where three carbonyl groups are respectively distributed on the opposite positions of three phosphorus atoms (Scheme 4.13). **SPO-PPP-Mn** was found to be highly reactive in the hydrogenation of benzaldehyde, providing a TON of 5,000 in initial attempts using EtOH as solvent. This manganese complex is therefore a promising catalyst for aldehyde hydrogenation.

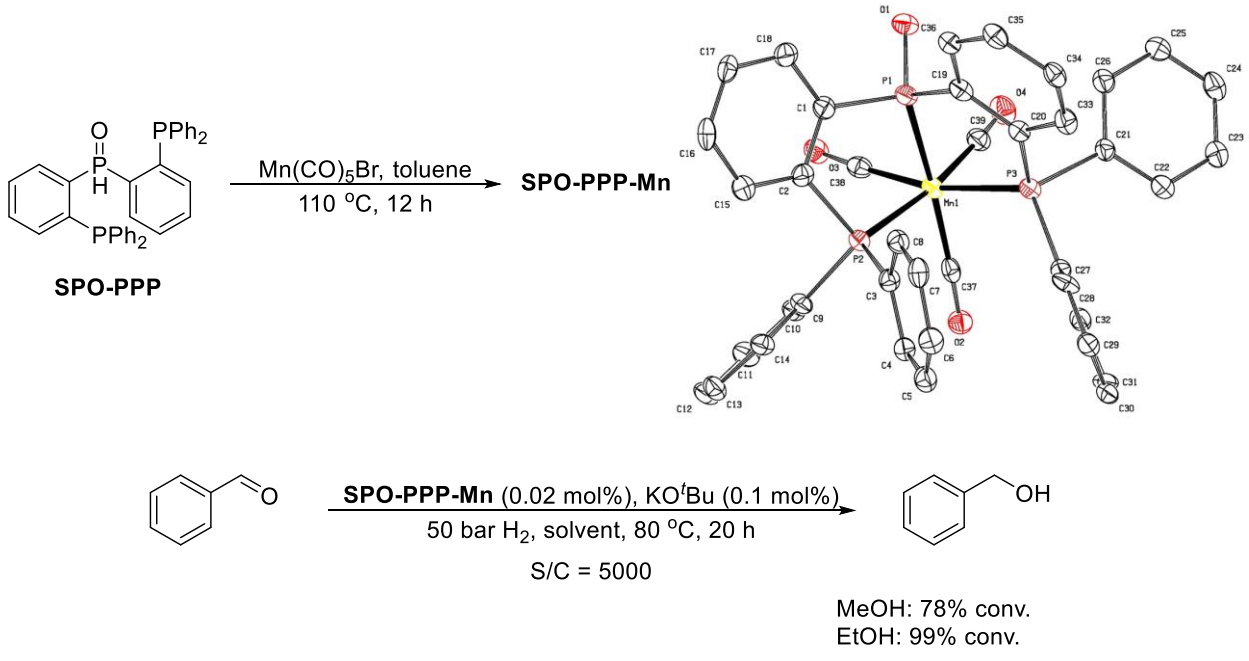

Scheme 4.13 **SPO-PPP-Mn**-catalyzed hydrogenation of benzaldehyde, and crystal structure of **SPO-PPP-Mn** with ellipsoids drawn at the 50% probability level with hydrogen atoms omitted for clarity.

Compared with the **Fc-SPO-Mn** complex discussed above, the **SPO-PPP-Mn** complex has a simpler $^{31}P\{^{1}H\}$ NMR spectrum with two doublet peaks at 89.95 ppm (d, J = 41.3 Hz) and 86.50 ppm (d, J = 35.6 Hz) (Figure 4.7). Splittings of the phosphorus signals in the NMR only appear to result from coupling between phosphine and phosphine oxide P atoms and not between two phosphine P atoms. It is likely that the 5,5-fused ring structure leads to a shorter distance between phosphines.

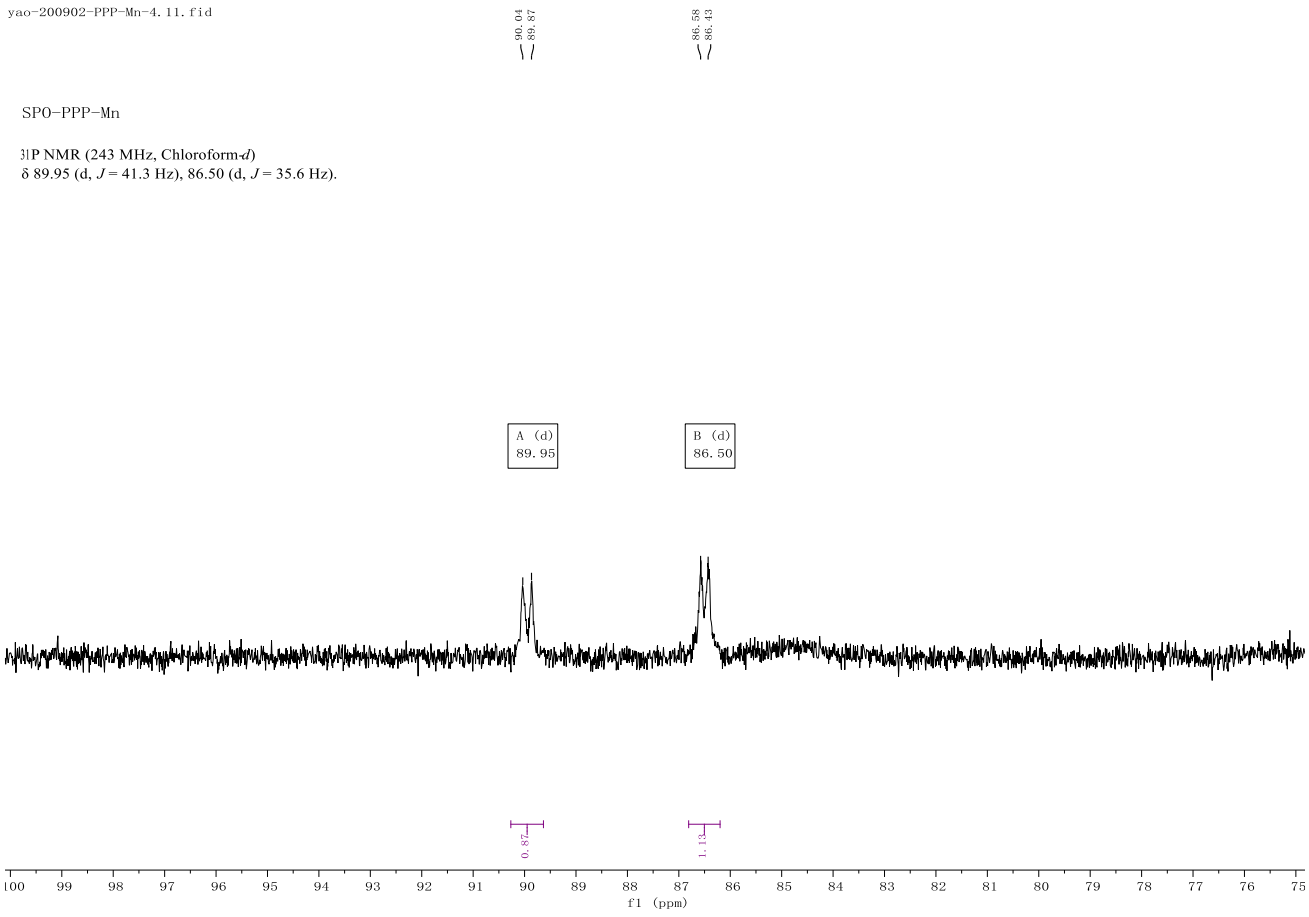

Figure 4.7 $^{31}P\{^{1}H\}$ NMR spectrum of **SPO-PPP-Mn**

4.3.6 PNN ligand

PNN bearing a similar tridentate structure to the **PNP** ligand developed in Chapter 2 was synthesized successfully in high yield (Scheme 4.14).

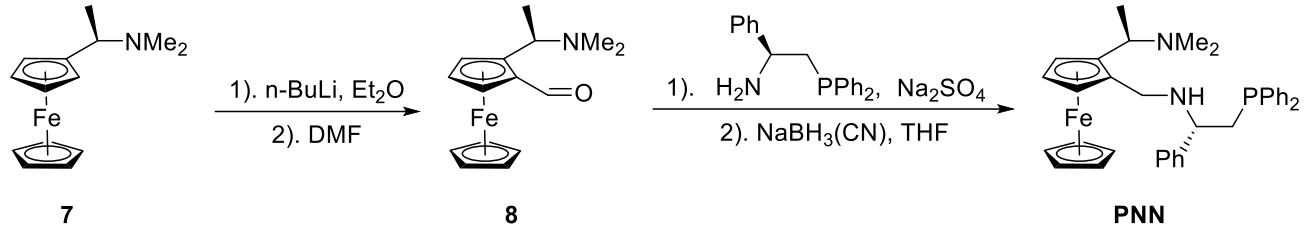

Scheme 4.14 Synthesis of **PNN**

Mixing the **PNN** ligand with $Mn(CO)_5Br$ in boiling toluene produced the manganese complex **PNN-Mn** in high yield, which unfortunately gave low reactivities and enantioselectivities for the AH of acetophenone (Scheme 4.15). Compared with the **PNP** ligand, the **PNN** ligand has a NMe_2 group near the ferrocene unit instead of a PPh_2 group. Clearly this structural change has a significant effect on the catalytic activity and enantioselectivity of the manganese complex. Presumably this is a result of poorer electro-donating properties and lower steric hindrance, which are both detrimental to controlling stereochemistry of the product.

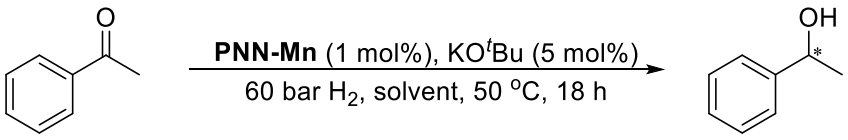

^{i}PrOH: 65% conv., 7% ee
Tol: 23% conv., 4% ee

Scheme 4.15 **PNN-Mn**-catalysed AH of acetophenone

4.3.7 F-amphox ligand

F-amphox ligand was developed by the Zhang group, exhibiting extremely high reactivities (up to 1,000,000 TON) and enantioselectivities (up to 99.9% ee) for iridium-catalysed AH of ketones.[10] Mn-catalysed AH of ketones was therefore attempted. High reactivities and moderate enantioselectivities (up to 62% ee) were obtained in the AH of acetophenone (Table 4.1).

Table 4.1 Solvent screening for **f-amphox-Mn**-catalyzed AH of acetophenone

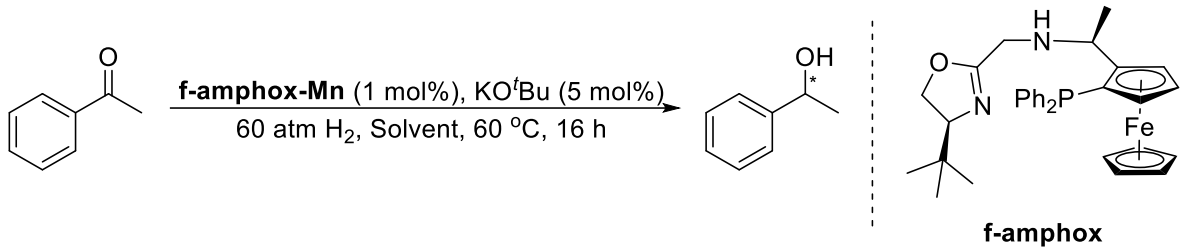

Entry[a]	Solvent	Conversion (%)[b]	Ee (%)[b]
1.	MeOH	34	5
2.	EtOH	86	49
3.	*i*-PrOH	99	42
4.	TFE	0	-
5.	HFIP	0	-
6.	*t*-BuOH	44	49
7.	THF	99	26
8.	Toluene	99	58
9.	DCE	20	63
10.	Hexane	99	62

[a] Reaction conditions: 0.1 mmol of acetophenone, 0.001 mmol of **f-amphox-Mn** (1 mg), 0.005 mmol KO^{t}Bu, 0.5 ml of solvent. [b] Conversions and ee values were determined by ^{1}H-NMR and chiral HPLC, respectively.

The AH of various ketones such as *ortho*-substituted acetophenone, 1-tetralone and diaryl ketone was next investigated, which also gave moderate enantioselectivities (Scheme 4.16). However, the high reactivities observed still make the manganese complex **f-amphox-Mn** a promising catalyst for AH of ketones, because its enantio-induction performance can be modified by the replacement of phenyl groups on phosphine using other substituents.

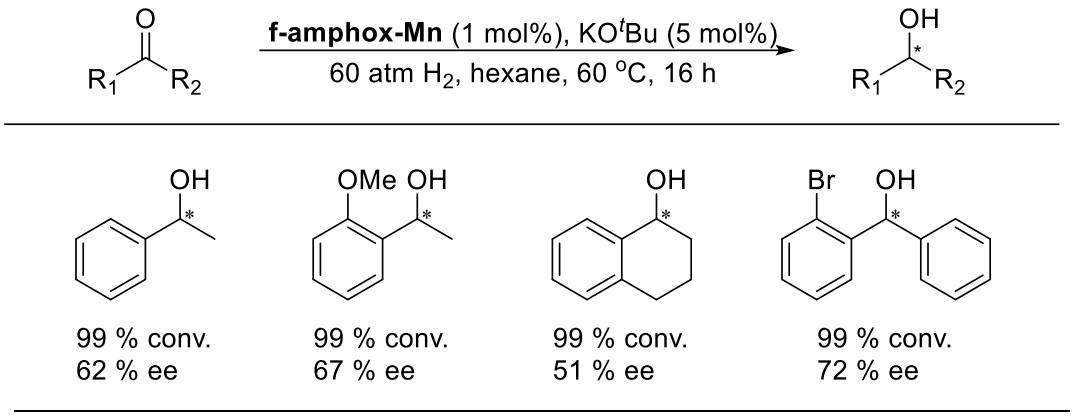

Scheme 4.16 **F-amphox-Mn**-catalysed AH of various ketones

4.3.8 PNNN ligand

In addition to the above tridentate ligands, there was also an attempt to develop novel tetradentate ligands. The ligand **PNNN** was accordingly designed and synthesised for manganese catalysis (Scheme 4.17). However, subsequent DFT calculations could not give the expected tetradentate structure for the manganese complex, with a tridentate PNN-Mn complex possible but an additional pyridine group remaining unbound.

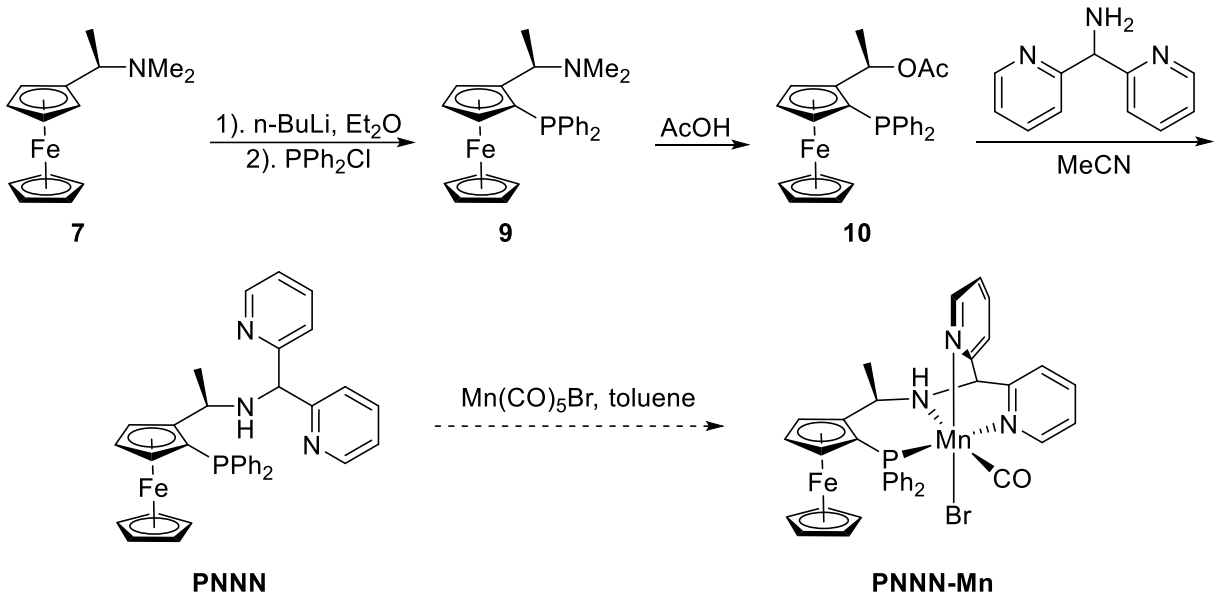

Scheme 4.17 Synthesis of **PNNN** and expected **PNNN-Mn**

4.3.9 PN-bipy ligand

An alternative approach to forming a tetradentate complex is a "2+2" strategy, which involves combining two (different) bidentate ligands onto one metal centre. A preliminary attempt to do this to form the manganese complex **PN-bipy-Mn** was performed (Scheme 4.18). However, the $^{31}P\{^{1}H\}$ NMR spectrum of the supposed product was the same as that of the **PN** ligand, indicating that no reaction had occurred.

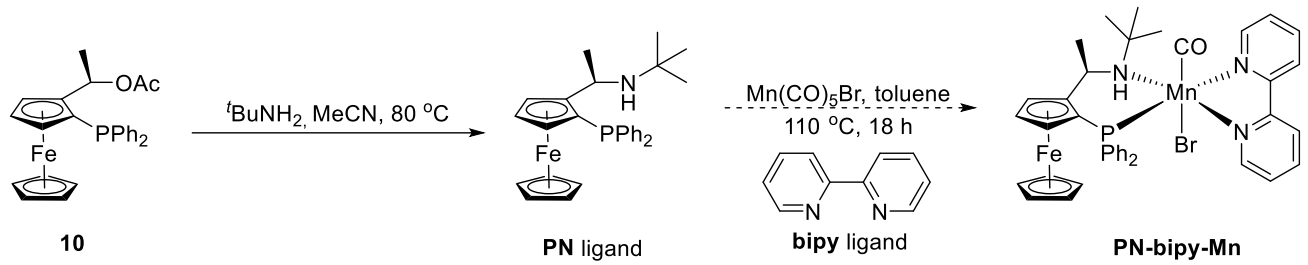

10 **PN** ligand **bipy** ligand **PN-bipy-Mn**

Scheme 4.18 Intended synthesis of **PN-bipy-Mn**

4.3.10 PNP-bipy ligand

Pentadentate ligands are arguably the most difficult ligands to design for octahedral metal complexes, requiring perfect simultaneous alignments for all five binding sites. Just like a tetradentate ligand using the "2+2" strategy, a pentadentate ligand can be designed via a "3+2" strategy. Accordingly, the manganese complex **PNP-bipy-Mn** was designed to improve catalytic turnover numbers of the **PNP-Mn** in the AH of ketones, resulting from the replacement of carbonyl groups with a bipyridine ligand, which would prevent catalyst decomposition (Scheme 4.19). However, the $^{31}P\{^{1}H\}$ NMR and ^{1}H NMR spectra of the supposed product were the same as those of the **PNP-Mn**, indicating that a bipyridine ligand could not replace the carbonyl groups under these conditions.

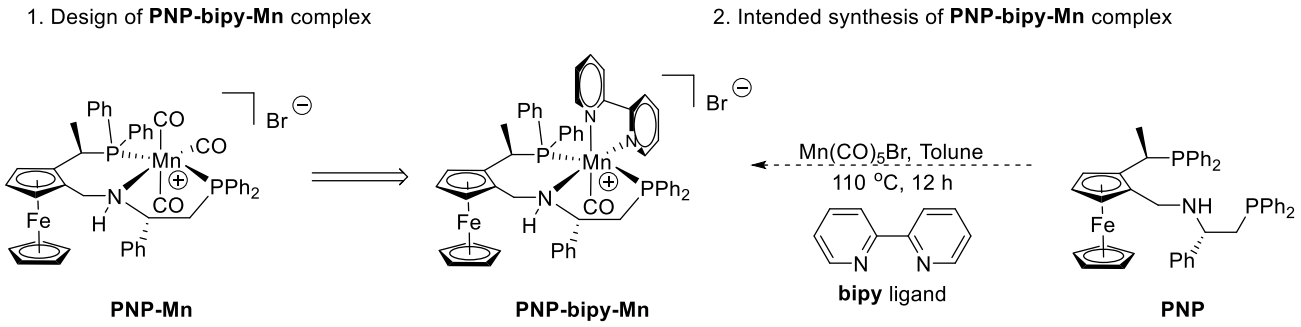

Scheme 4.19 Design and intended synthesis of **PNP-bipy-Mn**

4.4 Conclusion

There are many ligand design strategies for transition metal-catalysed AH. In these projects described here, strategies have included noncovalent interaction-assisted ferrocenyl phosphine ligands and multidentate phosphine ligands. The former approach is highly dependent on noncovalent interactions between catalyst and substrate under specific conditions (solvent, concentration, temperature etc), which to some extent limits wide applications of one ligand. Weak noncovalent interactions can lead to low catalytic efficiencies in this kind of system, and also cause difficulty in the design of suitable ligands. However, noncovalent interactions are ubiquitous in nature and responsible for high reactivities and selectivities in enzyme catalysis.[11-13] It is therefore likely that eventually highly efficient ligand and catalyst systems can be developed in the field of noncovalent interaction-assisted transition metal catalysis.

Multidentate phosphine ligands have attracted widespread attention in transition metal catalysis.[14] In the Zhang group, the focus has been on the development of chiral ferrocenyl multidentate phosphine ligands for earth-abundant metal-catalysed AH. Many tridentate, tetradentate and pentadentate ligands have been designed and synthesized, but only few of them were found to be efficient for AH. Here is a brief summary of my personal experience on ligand design towards earth-abundant metal-catalysed AH.

Firstly, reasonable enantio-induction is the key to the design of chiral ligands. Various chiral scaffolds or chiral moieties can be used as multidentate chiral ligands to control the chirality of products. Secondly, it is necessary to define the spatial structures of chiral ligands and their metal complexes to design and modify novel chiral ligands. The spatial structures can be obtained via Chem3D software or DFT calculation. Thirdly, after the synthesis of a novel chiral ligand, its catalytic capacity can be quickly tested manually by high-throughput screening, involving the AH of various unsaturated

substrates using different metal precursors under different conditions. Fourthly, different metal centres with different d electrons require different ligand design to reach a stable geometry. The philosophy of chiral ligand design for octahedral Mn(I) and Fe(II) complexes is often not applicable for the trigonal bipyramidal, square pyramidal and tetrahedral geometries favoured by Co(II), Ni(II) or Cu(I) complexes. Finally, it remains difficult to precisely predict the catalytic reactivity of any given metal complex, because it is difficult to quantify the exact contribution that a ligand might make to a metal centre in terms of electronics and sterics. However, according to crystal field theory, strong field ligands (phosphine, CN^-, CO etc) are usually required for $3d^6$ metals [e.g. Mn(I) and Fe(II)] and $3d^7$ metals [e.g. Co(II)] to achieve sufficient crystal field stabilization energies, and as a result to form stable metal catalysts for AH. Consequently, phosphine ligands are set to continue to be ligands of choice in the design of efficient catalytic systems for AH catalysed by earth-abundant metals such as Mn, Fe and Co.

4.5 Experimental: synthesis of novel phosphine ligands

4.5.1 Bis-Zhaophos

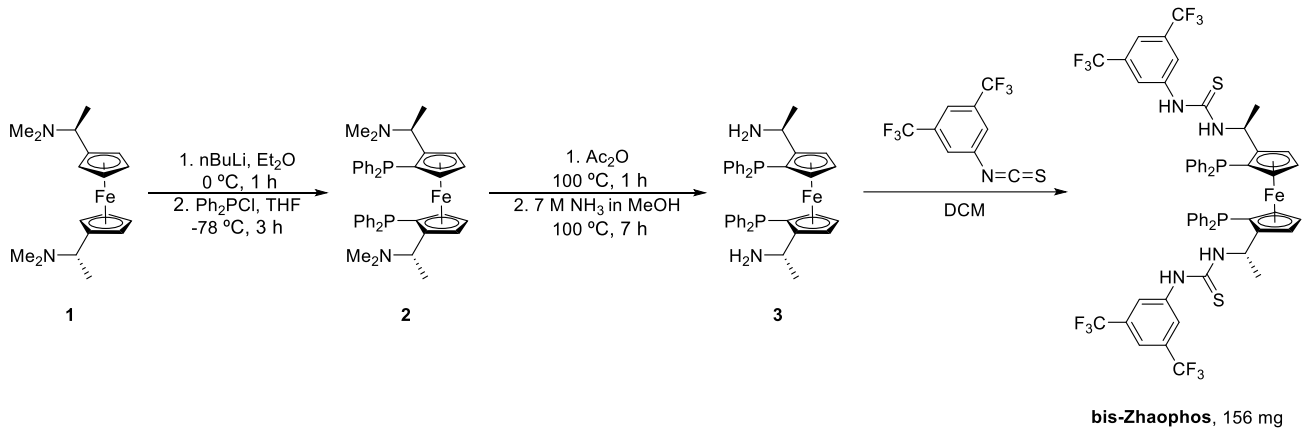

Scheme 4.20 Syntheis of **bis-Zhaophos**

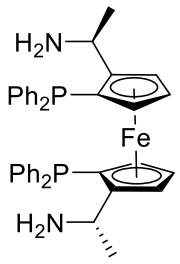

(*S*,*R*$_p$,*S*,*R*$_p$)-**3.** Novel compound. A suspension of (*S*,*R*$_p$,*S*,*R*$_p$)-**2** (1 mmol, 697 mg) in acetic anhydride (1 ml) was heated at 100 ^{o}C for 1 h under argon. The reaction mixture was cooled to RT, before removing remained acetic anhydride under vacuum. The orange residue was purified by recrystallization in hexane (5 ml) and then used for the next step. A suspension of this residue in 7 M NH_3 in MeOH (6 ml) was heated at 100 ^{o}C for 7 h under argon. After cooled to RT, the mixture was concentrated under vacuum. The crude product was purified by column chromatography on silica gel (DCM/MeOH/Et_3N, 90/10/1) to give 200 mg (31% yield for two steps) of (*S*,*R*$_p$,*S*,*R*$_p$)-**3** as an orange solid. ^{1}H NMR (400 MHz, Chloroform-*d*) δ 7.31 – 7.14 (m, 16H), 7.11 (ddd, *J* = 9.6, 4.6, 3.1 Hz, 4H), 4.42 – 4.33 (m, 4H), 4.11 (qd, *J* = 6.7, 2.0 Hz, 2H), 3.07 (dt, *J* = 2.4, 1.1 Hz, 2H), 1.98 (s, 4H), 1.44 (d, *J* = 6.7 Hz, 6H). ^{31}P NMR (162 MHz, Chloroform-*d*) δ -25.43.

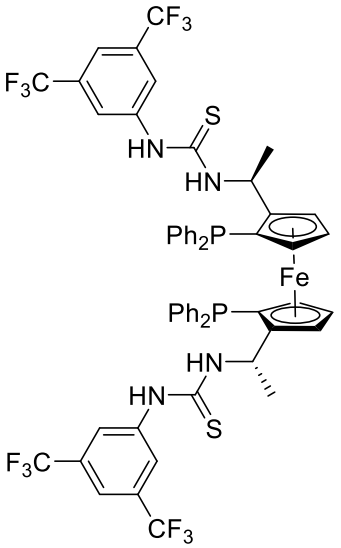

bis-Zhaophos

(S,R_p,S,R_p)-**bis-Zhaophos**. Novel compound. A solution of (S,R_p,S,R_p)-**3** (0.2 mmol, 129 mg) and 1-isothiocyanato-3,5-bis(trifluoromethyl)benzene (0.5 mmol, 0.091 ml) in dry DCM (1 ml) was stirred at RT for 6 h under argon. Then the mixture was concentrated under vacuum. The residue was purified by column chromatography on silica gel (PE/EtOAc, 10/1~4/1) to give 156 mg (66 % yield) of (S,R_p,S,R_p)-**bis-Zhaophos** as a yellow solid. ^{1}H NMR (400 MHz, Chloroform-*d*) δ 7.73 (s, 6H), 7.43 (s, 2H), 7.19 (q, *J* = 4.8 Hz, 10H), 7.09 (t, *J* = 7.3 Hz, 4H), 6.96 (td, *J* = 7.5, 1.8 Hz, 4H), 6.86 (d, *J* = 7.3 Hz, 4H), 5.61 (s, 2H), 4.69 (s, 2H), 4.28 (s, 2H), 2.85 (s, 2H), 1.49 (d, *J* = 5.1 Hz, 6H). ^{31}P NMR (162 MHz, Chloroform-*d*) δ -25.42. **HRMS** (ESI) m/z: $[M+H]^+$ Calcd for $C_{56}H_{45}F_{12}FeN_4P_2S_2^+$ = 1183.1713; Found: 1183.1702.

4.5.2 Naphth ligand

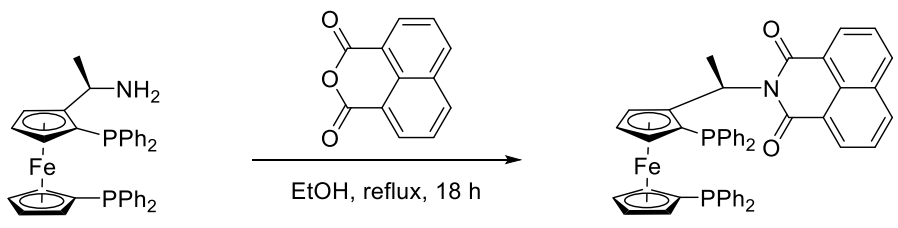

4 **Naphth**

Scheme 4.21 Synthesis of **Naphth** ligand

Naphth ligand. Novel compound. A suspension of (*R*,*S*$_P$)-**4** (1 mmol, 597 mg) and 1,8-Naphthalic anhydride (1 mmol, 198 mg) in dry EtOH (5 ml) was refluxed for 18 h under argon. After cooled to RT, the mixture was concentrated under vacuum. The residue was purified by column chromatography on silica gel (PE/EtOAc, 10/1~4/1) to give 200 mg (26 % yield) of (*R*,*S*$_P$)-**Naphth** as a yellow solid. ^{1}H NMR (600 MHz, Chloroform-*d*) δ 8.39 (dd, *J* = 7.3, 1.1 Hz, 1H), 8.16 – 8.11 (m, 1H), 7.99 (t, *J* = 7.8 Hz, 2H), 7.59 (t, *J* = 7.7 Hz, 1H), 7.53 (t, *J* = 7.7 Hz, 1H), 7.34 – 7.27 (m, 8H), 7.26 – 7.17 (m, 6H), 6.68 – 6.62 (m, 2H), 6.58 – 6.51 (m, 1H), 6.11 (td, *J* = 7.5, 1.5 Hz, 2H), 6.00 (t, *J* = 7.3 Hz, 1H), 4.89 (dd, *J* = 2.8, 1.5 Hz, 1H), 4.60 (d, *J* = 3.1 Hz, 1H), 4.27 (td, *J* = 2.4, 1.2 Hz, 1H), 4.24 (td, *J* = 2.5, 1.2 Hz, 1H), 4.12 (t, *J* = 2.6 Hz, 1H), 3.70 (p, *J* = 1.4 Hz, 1H), 3.46 (dt, *J* = 2.5, 1.1 Hz, 1H), 1.84 (d, *J* = 7.0 Hz, 3H). ^{31}P NMR (243 MHz, Chloroform-*d*) δ -17.76, -26.47.

4.5.3 Bis-Fc-PNP ligand

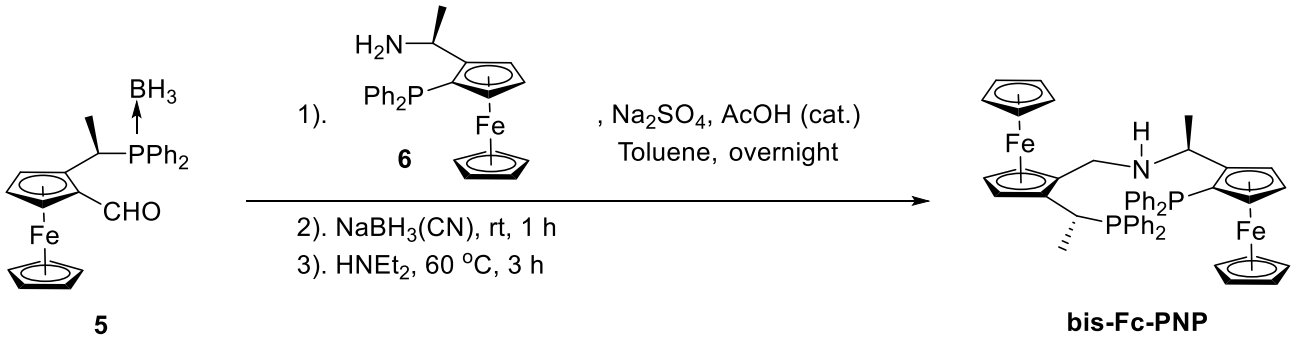

Scheme 4.22 Synthesis of **bis-Fc-PNP**

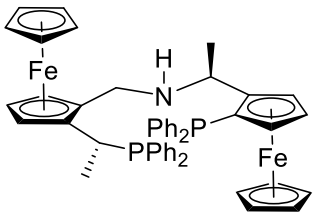

bis-Fc-PNP

(*R*, *Rp*, *S*, *Rp*)-**bis-Fc-PNP**. Novel compound. A suspension of (*R*, *Rp*)-**5** (0.5 mmol, 220 mg), (*S*, *Rp*)-**6** (0.5 mmol, 206 mg), Na_2SO_4 (200 mg) and catalytic amount of acetic acid in degassed toluene (2

mL) was stirred overnight at RT under argon. $NaBH_3(CN)$ (1.5 mmol, 94 mg) was added and the reaction mixture was stirred for 1 h. Then the reaction was quenched by the addition of water (2 mL), extracted with DCM (3*2 mL) and the combined organic layers were dried over anhydrous Na_2SO_4 and concentrated under vacuum. The residue was redissolved in degassed diethylamine (2 mL) under argon and the mixture was heated at 60 °C for 3 h. After cooled to RT, the mixture was concentrated under vaccum. The crude product was purified by flash chromatography on silica gel (PE/EtOAc, 20/1~4/1) to give 170 mg (41 % yield) of (*R*, *Rp*, *S*, *Rp*)-**bis-Fc-PNP** as a yellow solid. ^{1}H NMR (400 MHz, Chloroform-*d*) δ 7.66 – 7.57 (m, 2H), 7.49 – 7.32 (m, 8H), 7.26 – 7.12 (m, 8H), 7.07 – 6.97 (m, 2H), 4.45 (td, *J* = 2.3, 1.3 Hz, 1H), 4.31 (t, *J* = 2.6 Hz, 1H), 3.98 (qd, *J* = 6.5, 2.6 Hz, 1H), 3.95 – 3.90 (m, 1H), 3.89 (s, 5H), 3.86 – 3.78 (m, 7H), 3.63 (dd, *J* = 2.5, 1.4 Hz, 1H), 3.27 (qd, *J* = 7.0, 3.6 Hz, 1H), 2.90 (d, *J* = 12.6 Hz, 1H), 2.60 (d, *J* = 12.6 Hz, 1H), 1.38 (dd, *J* = 12.3, 6.9 Hz, 6H). ^{31}P NMR (162 MHz, Chloroform-*d*) δ 6.48, -24.00.

4.5.4 PNN ligand

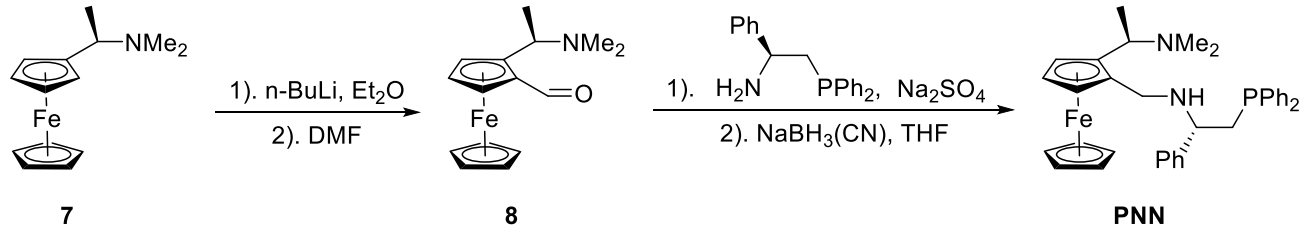

7 **8** **PNN**

Scheme 4.23 Synthesis of **PNN**

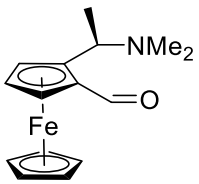

(*R, Sp*)-**8**. Known compound.[15] To a solution of the starting material *R*-Ugi amine **7** (40 mmol, 8.4 mL) dissolved in dry Et_2O (100 mL), *n*-BuLi (44 mmol, 18.3 mL, 2.4 M in hexane) was added dropwise at 0 °C under argon. Warmed to RT, the reaction mixture was stirred for 1 h. Before DMF (80 mmol,

6.2 mL) was added, the red solution was cooled to -78 °C. After the addition of DMF, the reaction mixture was allowed to warm to RT and stirred for further 3 h. Then the reaction was quenched by the addition of aqueous saturated $NaHCO_3$ solution (30 mL), extracted with ethyl acetate (3*30 mL) and the combined organic layers were dried over anhydrous Na_2SO_4 and concentrated under vacuum. The residue was purified by column chromatography on silica gel (PE/EtOAc/Et_3 N, 95/5/1~80/20/1) to give 7.2 g (63 % yield) of (*R, Sp*)-**8** as a dark brown solid. ^{1}H NMR (400 MHz, Chloroform-*d*) δ 10.11 (s, 1H), 4.80 (dd, *J* = 2.7, 1.4 Hz, 1H), 4.58 (t, *J* = 2.7 Hz, 1H), 4.54 (dd, *J* = 2.7, 1.4 Hz, 1H), 4.22 (s, 5H), 4.14 (q, *J* = 6.9 Hz, 1H), 2.07 (s, 6H), 1.47 (d, *J* = 6.9 Hz, 3H).

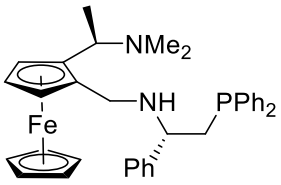

(*R, Sp, S*)-**PNN**. Novel compound. A suspension of (*R, Sp*)-**8** (1.5 mmol, 428 mg), (*S*)-2-(diphenylphosphino)-1-phenylethanamine (1.8 mmol, 550 mg) and Na_2SO_4 (171 mg) in degassed DCM (15 mL) was stirred for 18 h at RT under argon. $NaBH_3(CN)$ (4.5 mmol, 283 mg) was added and the reaction mixture was stirred for 1 h. Then the reaction was quenched by the addition of water (10 mL), extracted with DCM (3*5 mL) and the combined organic layers were dried over anhydrous Na_2SO_4 and concentrated under vacuum. The residue was purified by flash chromatography on silica gel (PE/EtOAc/Et_3 N, 90/10/1~80/20/1) to give 140 mg (54 % yield) of (*R, Sp, S*)-**PNN** as a yellow solid. ^{1}H NMR (400 MHz, Chloroform-*d*) δ 7.36 – 7.28 (m, 6H), 7.28 – 7.18 (m, 9H), 4.07 (dd, *J* = 2.5, 1.5 Hz, 1H), 4.03 – 3.99 (m, 2H), 3.94 (s, 5H), 3.81 (q, *J* = 6.7 Hz, 1H), 3.66 (q, *J* = 7.1 Hz, 1H), 3.56 (d, *J* = 13.3 Hz, 1H), 3.05 (d, *J* = 13.4 Hz, 1H), 2.36 (dd, *J* = 7.1, 2.0 Hz, 2H), 2.03 (s, 6H), 1.22 (d, *J* = 6.7 Hz, 3H). ^{31}P NMR (162 MHz, Chloroform-*d*) δ -23.41.

4.5.5 PNNN ligand

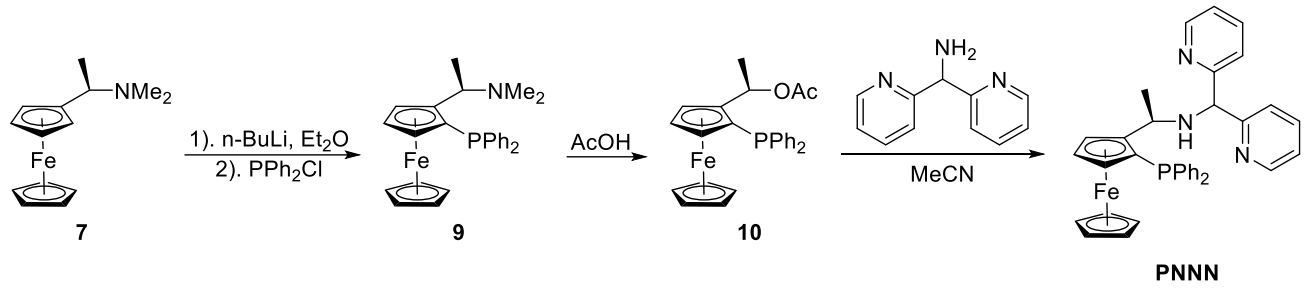

Scheme 4.24 Synthesis of **PNNN**

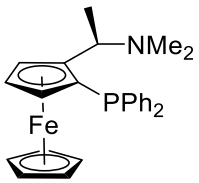

(*R, Sp*)-**9.** Known compound.[16] To a solution of the starting material *R*-Ugi amine **7** (40 mmol, 8.4 mL) dissolved in dry Et_2O (100 mL), *n*-BuLi (44 mmol, 18.3 mL, 2.4 M in hexane) was added dropwise at 0 °C under argon. After warmed to RT, the reaction mixture was stirred for 1 h. Before chlorodiphenylphosphine (80 mmol, 14.3 mL) was added, the red solution was cooled to -78 °C. After the addition of chlorodiphenylphosphine, the reaction mixture was allowed to warm to RT and stirred for further 3 h. Then the reaction was quenched by the addition of aqueous saturated $NaHCO_3$ solution (30 mL), extracted with ethyl acetate (3*30 mL) and the combined organic layers were dried over anhydrous Na_2SO_4 and concentrated under vacuum. The residue was purified by column chromatography on silica gel (PE/EtOAc/Et_3N, 98/2/1~90/10/1) to give 11.5 g (65 % yield) of (*R, Sp*)-**9** as an orange-red solid. ^{1}H NMR (400 MHz, Chloroform-*d*) δ 7.64 – 7.55 (m, 2H), 7.36 (tdd, *J* = 4.9, 3.3, 1.8 Hz, 3H), 7.25 – 7.14 (m, 5H), 4.37 (q, *J* = 1.9 Hz, 1H), 4.25 (t, *J* = 2.5 Hz, 1H), 4.15 (qd, *J* = 6.8, 2.6 Hz, 1H), 3.95 (s, 5H), 3.88 – 3.82 (m, 1H), 1.77 (s, 6H), 1.26 (d, *J* = 6.7 Hz, 3H). ^{31}P NMR (162 MHz, Chloroform-*d*) δ -22.96.

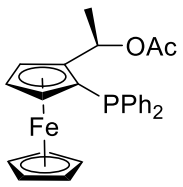

(*R, Sp*)-**10.** Known compound.[17] A suspension of (*R, Sp*)-**9** (20 mmol, 8.8 g) in acetic anhydride (10 mL) was heated at 100 °C for 1 h under argon. The reaction mixture was cooled to RT, before removing remained acetic anhydride under vacuum. The orange residue was purified by recrystallization in hexane and then used for the next step.

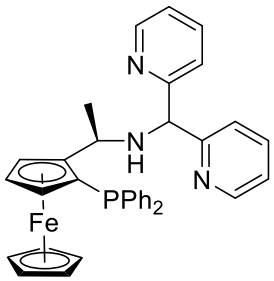

(*R, Sp*)-**PNNN**. Novel compound. A suspension of (*R, Sp*)-**10** (1 mmol, 456.3 mg) and di(pyridin-2-yl)methanamine (2.1 mmol, 390 mg) in degassed acetonitrile (3 mL) was heated at 80 °C for 18 h under argon. After cooled to RT, the mixture was concentrated under vaccum. The residue was purified by column chromatography on silica gel (PE/EtOAc/Et_3N, 90/10/1~80/20/1) to give 349 mg (60 % yield) of (*R, Sp*)-**PNNN** as a brown solid. ^{1}H NMR (600 MHz, Chloroform-*d*) δ 8.45 – 8.41 (m, 1H), 8.32 – 8.28 (m, 1H), 7.51 (td, *J* = 7.9, 6.5, 3.5 Hz, 2H), 7.46 (tt, *J* = 7.7, 1.5 Hz, 1H), 7.41 – 7.33 (m, 4H), 7.27 – 7.19 (m, 5H), 7.11 – 7.03 (m, 3H), 6.96 (ddt, *J* = 7.4, 4.9, 1.3 Hz, 1H), 5.13 (s, 1H), 4.54 (q, *J* = 1.6 Hz, 1H), 4.29 (d, *J* = 2.6 Hz, 1H), 3.99 – 3.93 (m, 6H), 3.77 (dd, *J* = 2.5, 1.2 Hz, 1H), 2.58 (s, 1H), 1.44 (d, *J* = 6.5 Hz, 3H). ^{31}P NMR (243 MHz, Chloroform-*d*) δ -24.58.

4.6 Appendix

4.6.1 NMR Spectra

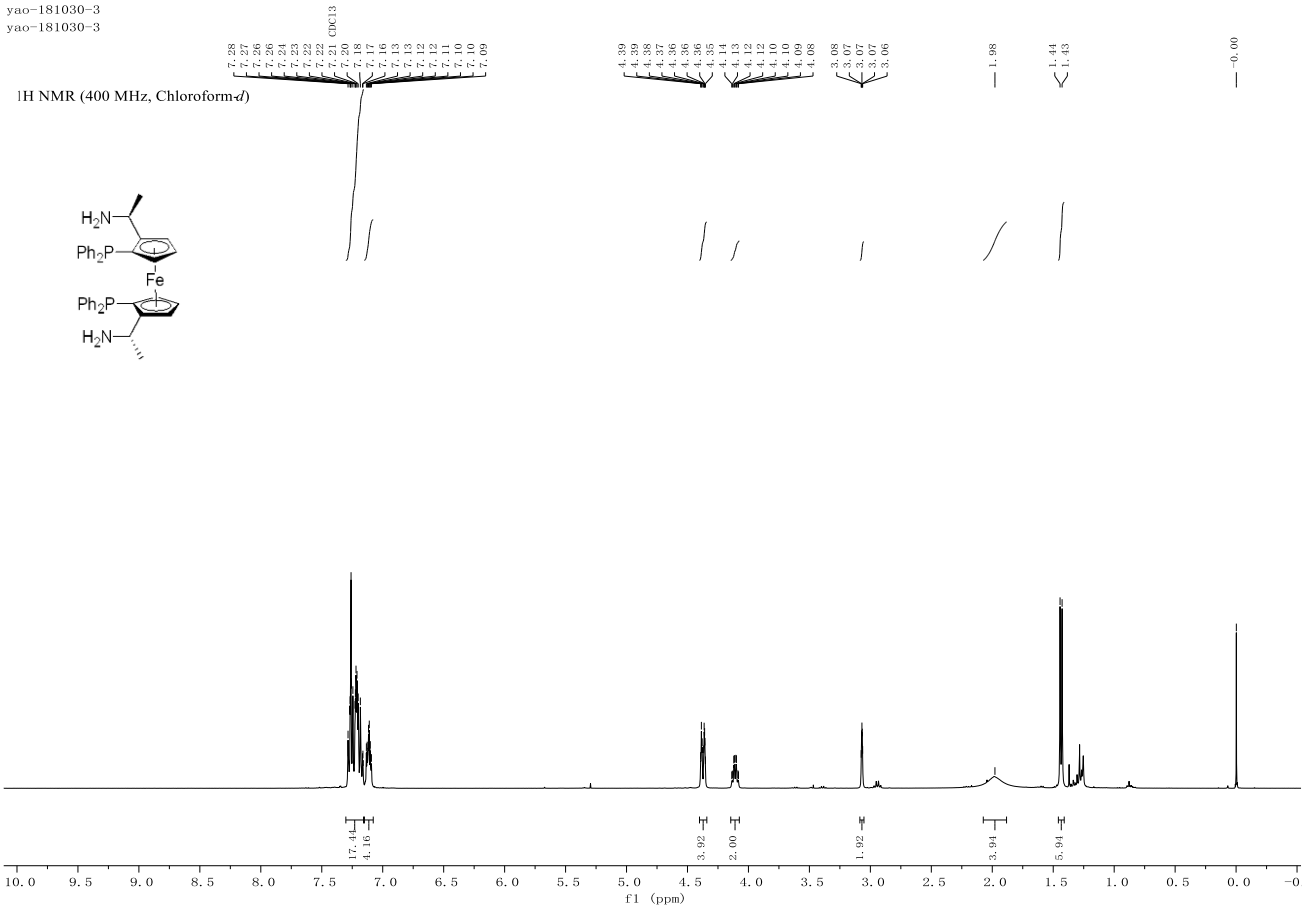

yao-181030-3-P
yao-181030-3-P

31P NMR (162 MHz, Chloroform-*d*)

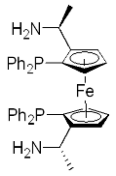

yao-181031-1
yao-181031-1

1H NMR (400 MHz, Chloroform-*d*)

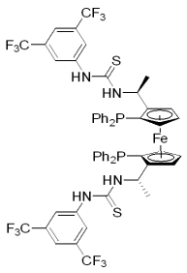

yao-181031-1-P. 1. fid
yao-181031-1-P

31P NMR (162 MHz, Chloroform-*d*) δ -25.42.

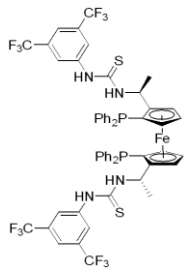

yao-201215-2. 10. fid

1H NMR (600 MHz, Chloroform-*d*)

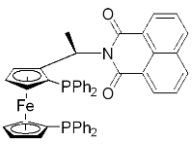

yao-201215-2.11.fid

31P NMR (243 MHz, Chloroform-*d*)

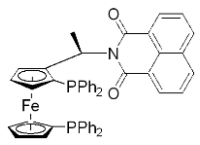

yao-190306-1.2.fid

1H NMR (400 MHz, Chloroform-*d*)

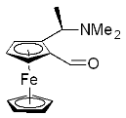

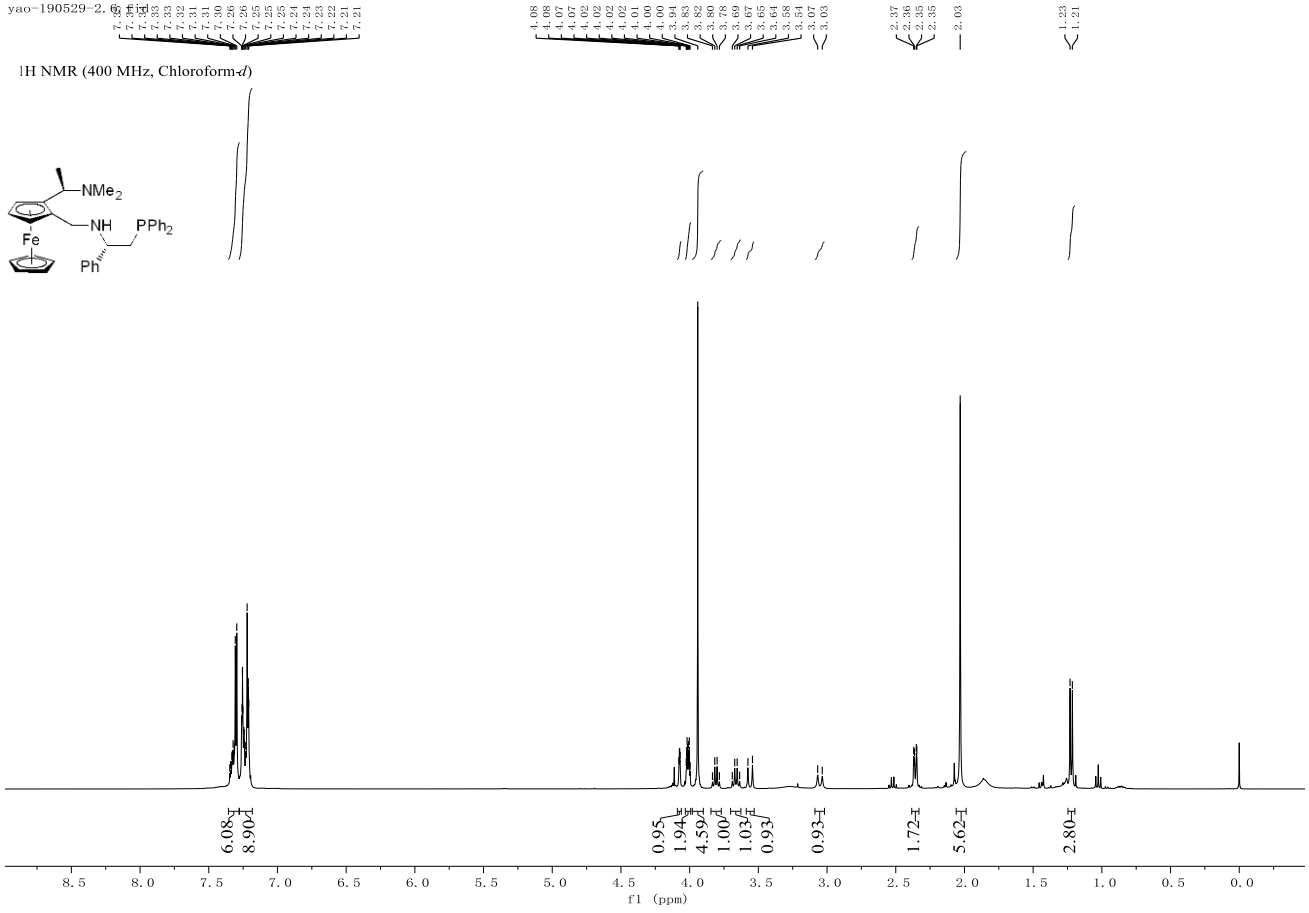
yao-190529-2.6.fid
1H NMR (400 MHz, Chloroform-d)
NMe2
NH
PPh2
Fe
Ph
6.08
8.90
0.95
1.94
4.59
1.00
1.03
0.93
0.93
1.72
5.62
2.80
f1 (ppm)

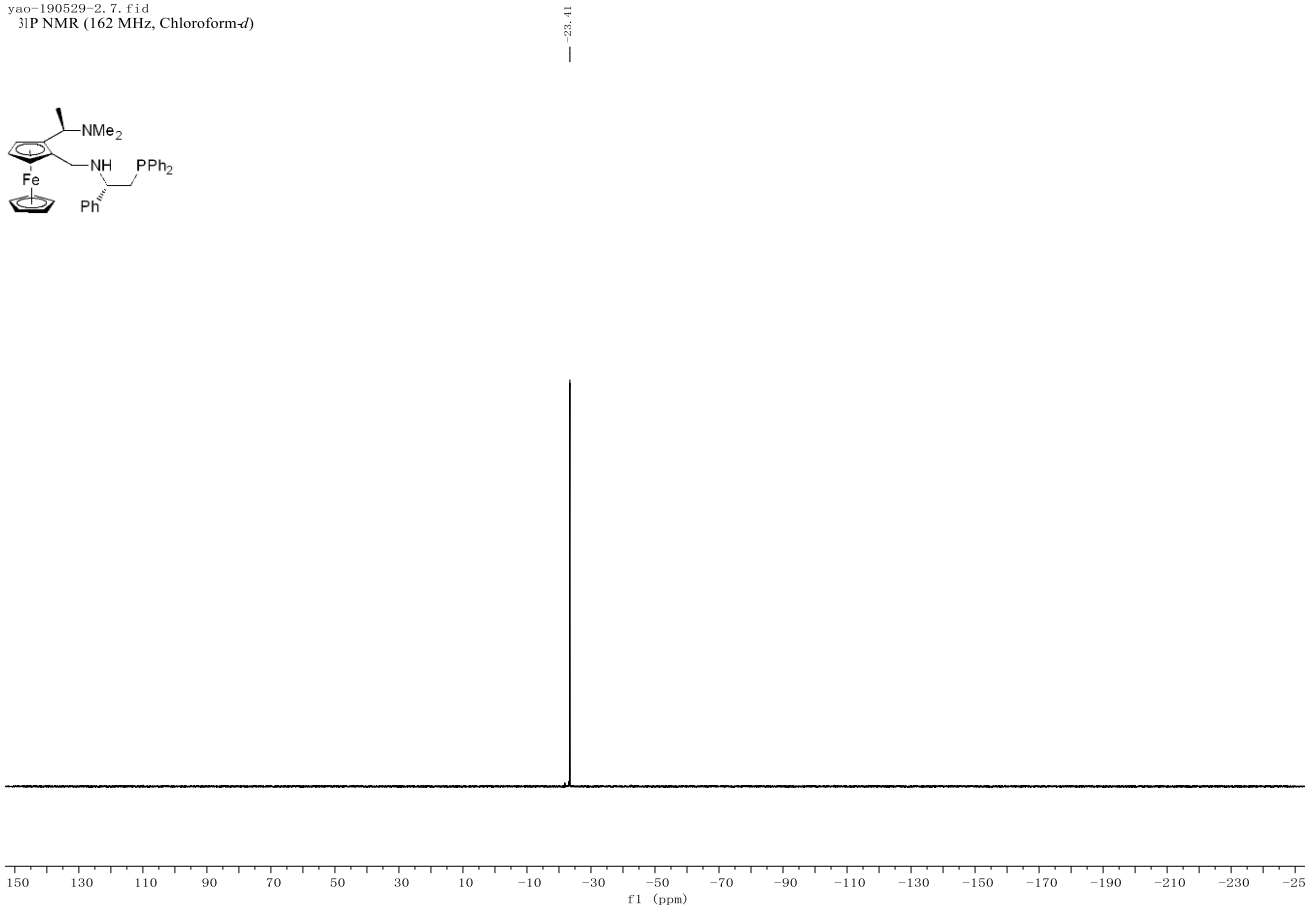
yao-190529-2.7.fid
31P NMR (162 MHz, Chloroform-d)
-23.41
NMe2
NH
PPh2
Fe
Ph
f1 (ppm)

yao-190307-1.1.fid

1H NMR (400 MHz, Chloroform-*d*)

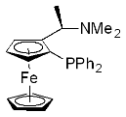

yao-190307-1.2.fid

31P NMR (162 MHz, Chloroform-*d*)

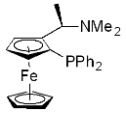

yao-190425-4.10.fid

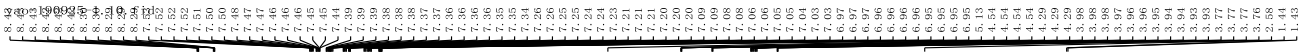

1H NMR (600 MHz, Chloroform-*d*)

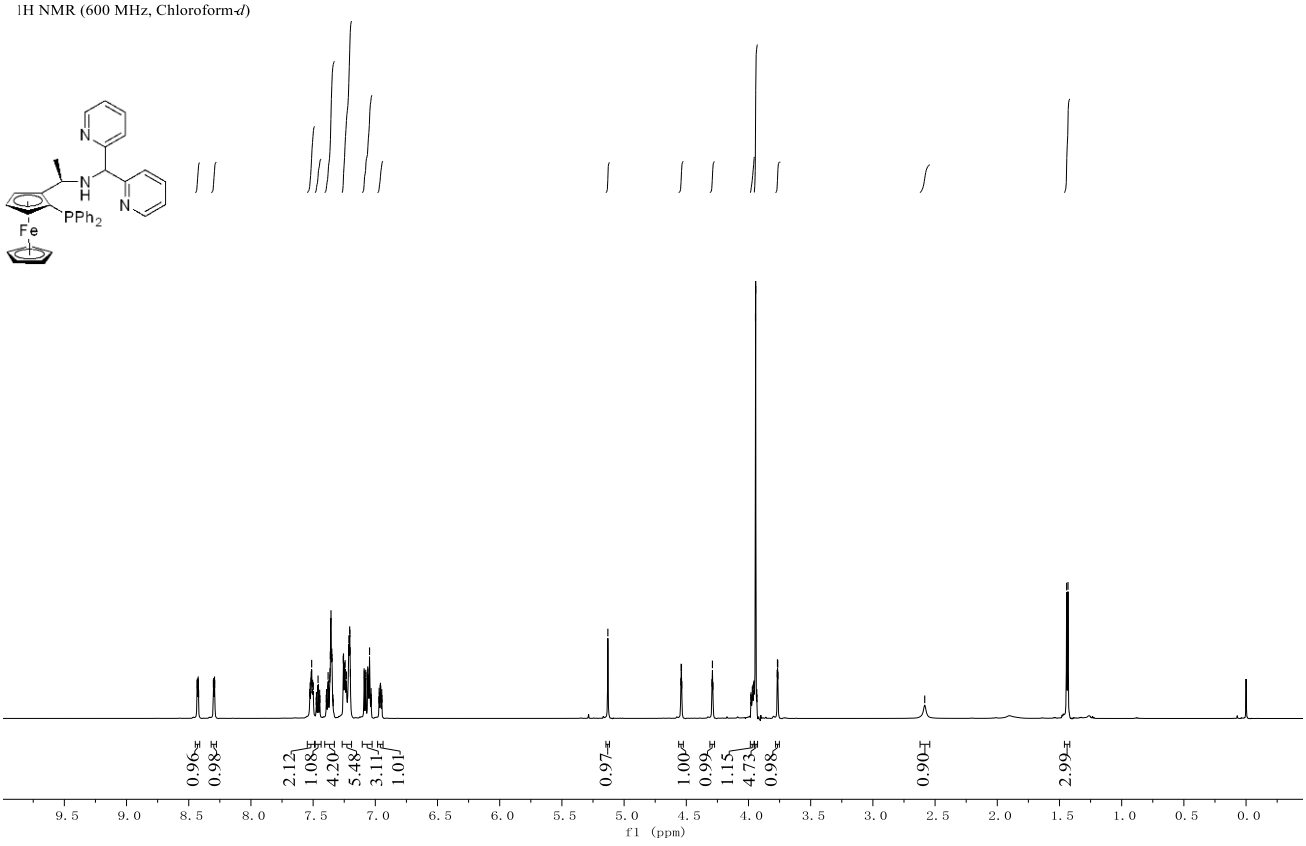

yao-190425-4.11.fid

31P NMR (243 MHz, Chloroform-*d*)

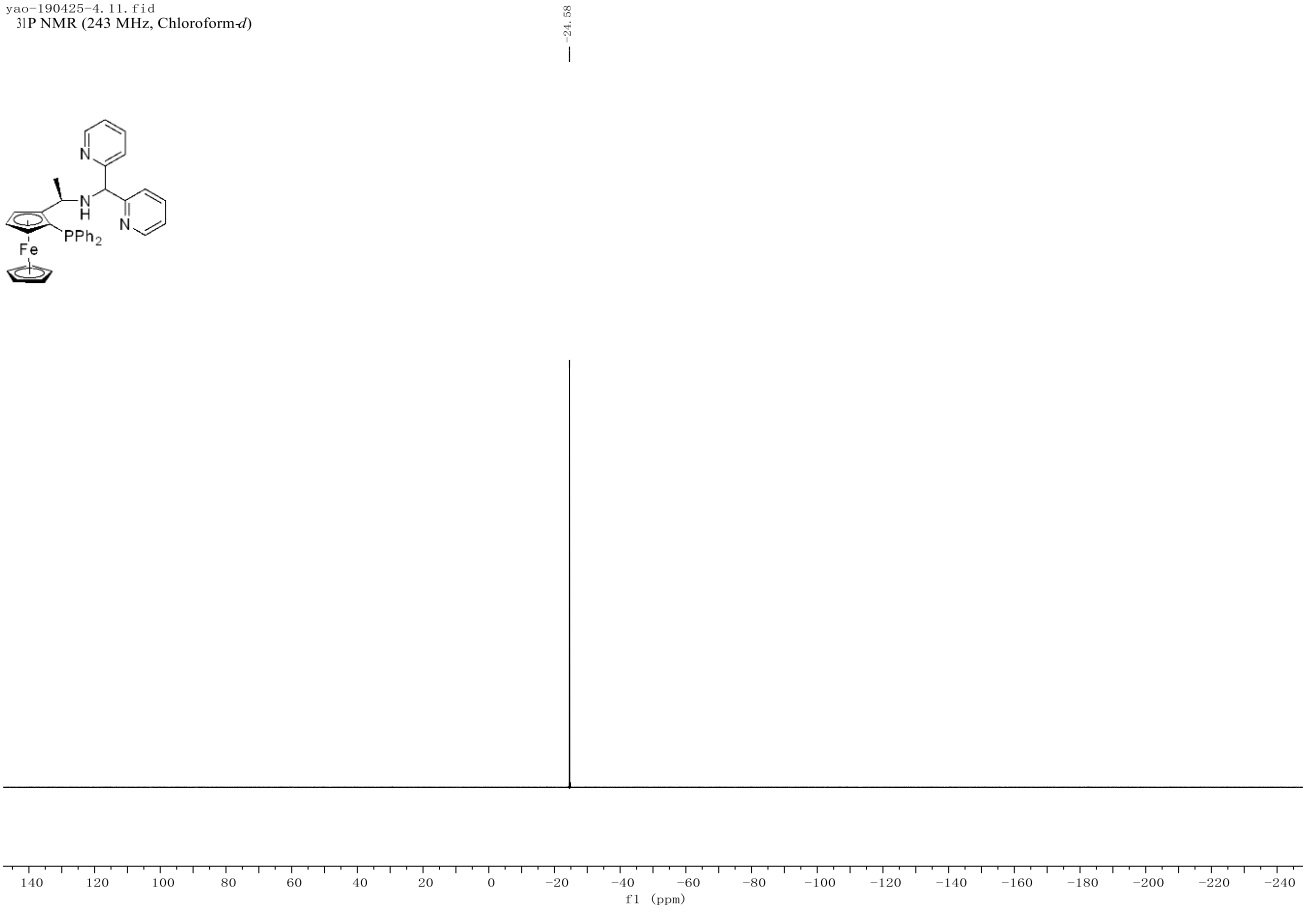

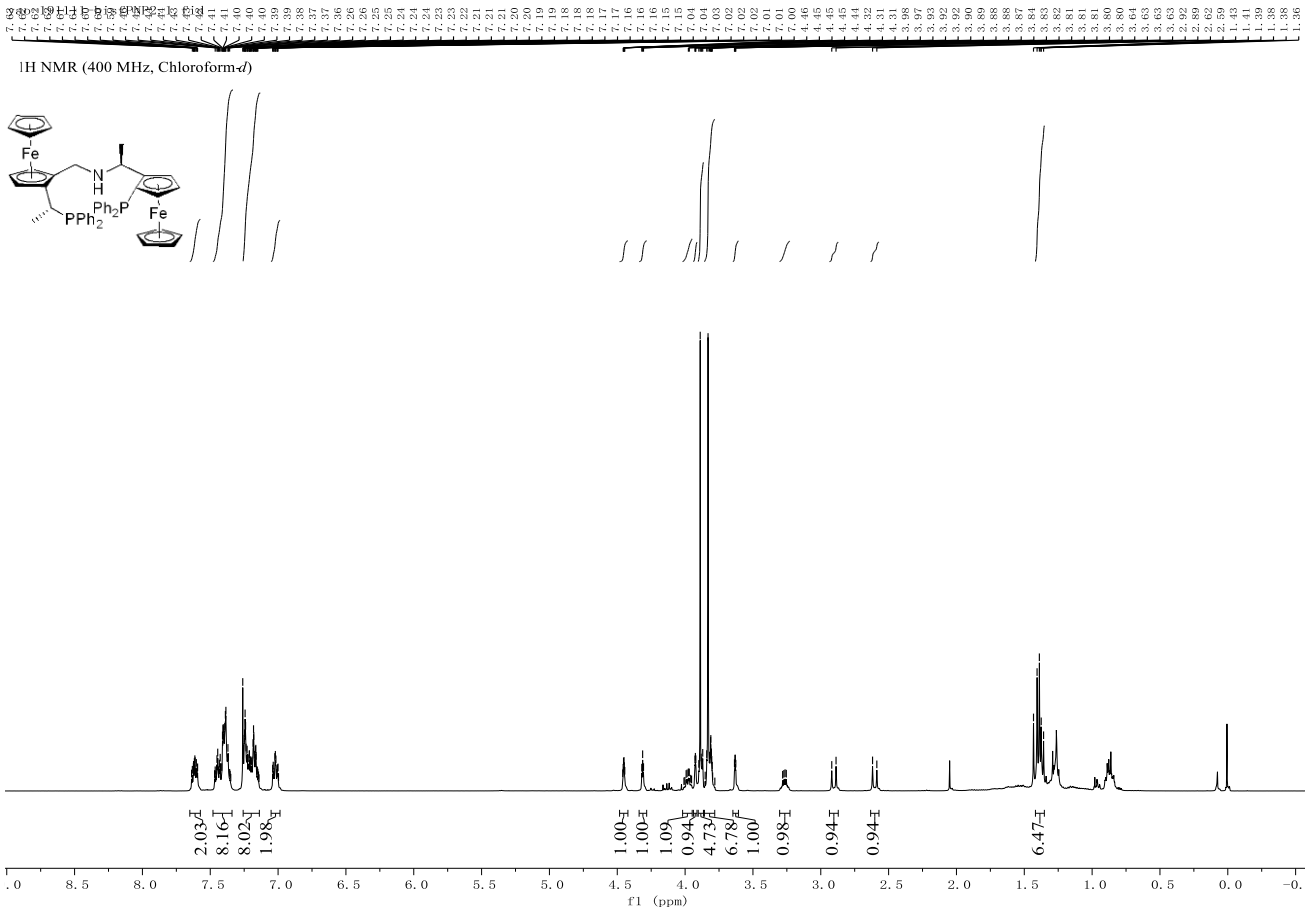
1H NMR (400 MHz, Chloroform-d)
Fe
N
H
Ph2P
PPh2
Fe
2.03
8.16
8.02
1.98
1.00
1.00
1.09
0.94
4.73
6.78
1.00
0.98
0.94
0.94
6.47
f1 (ppm)

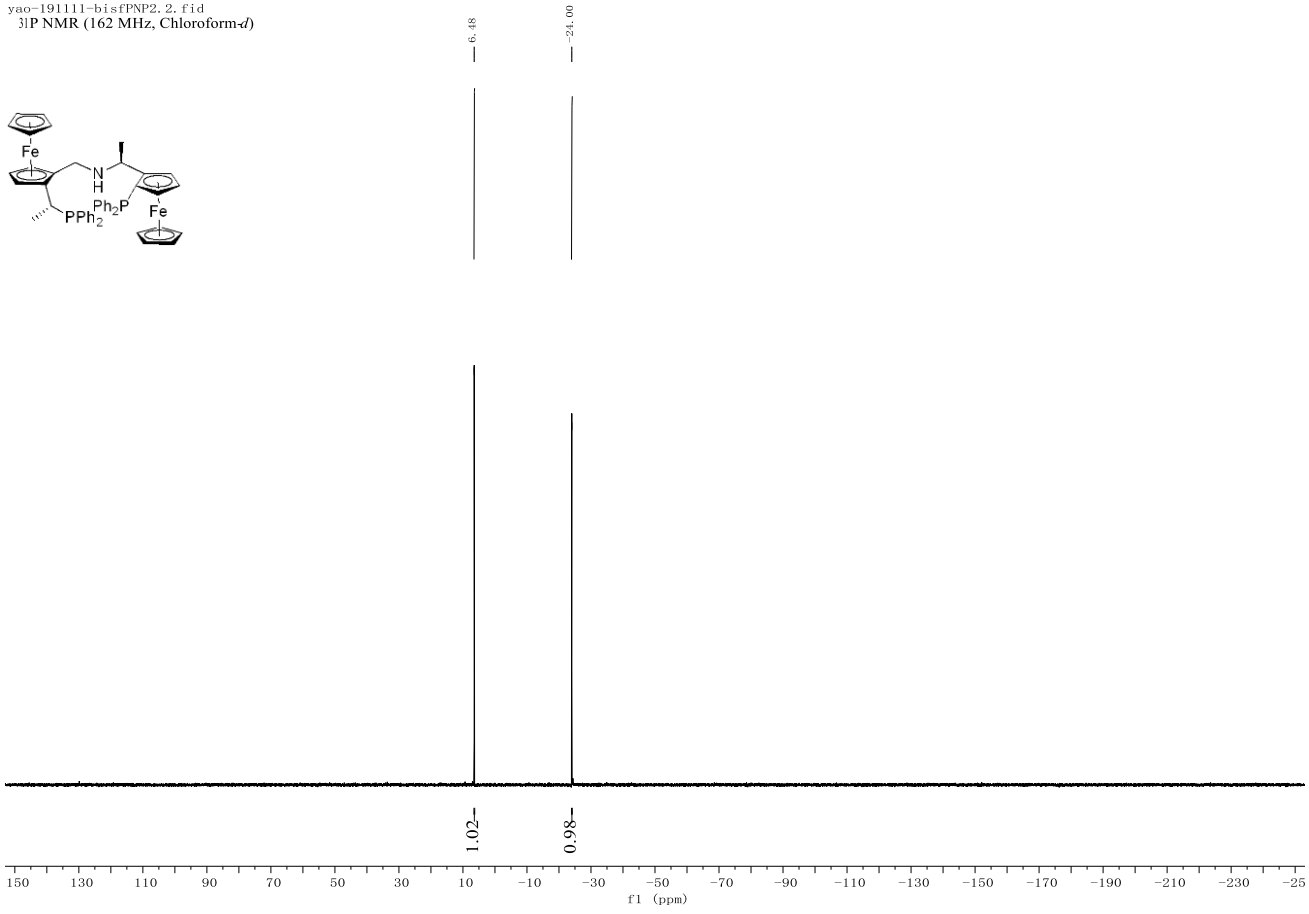
yao-191111-bisfPNP2.2.fid
31P NMR (162 MHz, Chloroform-d)
6.48
-24.00
Fe
N
H
Ph2P
PPh2
Fe
1.02
0.98
f1 (ppm)

4.6.2 Crystal data

4.6.2.1 Crystal data for SPO-PPP-Mn

Table 4.2 Crystal data and structure refinement for **SPO-PPP-Mn**

Identification code	**SPO-PPP-Mn**
Empirical formula	$C_{88}H_{68}BrCl_9Mn_2O_8P_6$
Formula weight	1948.08
Temperature/K	100
Crystal system	monoclinic
Space group	$P2_1/c$
a/Å	22.7589(7)
b/Å	18.4804(6)
c/Å	21.5840(7)
α/°	90
β/°	110.2550(10)
γ/°	90
Volume/Å^3	8516.7(5)
Z	4
ρ_{calc}g/cm^3	1.519
μ/mm^{-1}	7.084
F(000)	3952.0
Crystal size/mm^3	0.26 × 0.25 × 0.18
Radiation	CuKα (λ = 1.54178)
2Θ range for data collection/°	6.326 to 137.166
Index ranges	? ≤ h ≤ ?, ? ≤ k ≤ ?, ? ≤ l ≤ ?
Reflections collected	15662
Independent reflections	15662 [R_{int} = 0.0746, R_{sigma} = 0.0439]
Data/restraints/parameters	15662/3/1044
Goodness-of-fit on F^2	1.076
Final R indexes [I>=2σ (I)]	R_1 = 0.0938, wR_2 = 0.2508
Final R indexes [all data]	R_1 = 0.1011, wR_2 = 0.2566
Largest diff. peak/hole / e Å^{-3}	1.80/-0.94

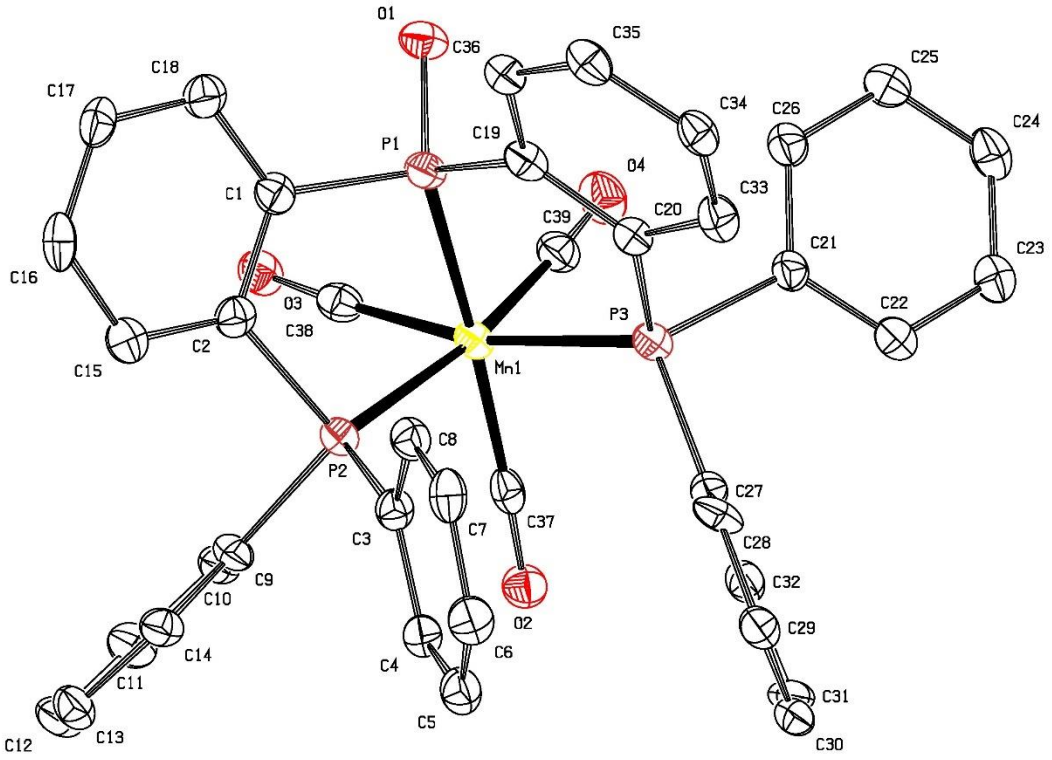

Figure 4.8 Crystal structure of **SPO-PPP-Mn** with ellipsoids drawn at the 50% probability level with hydrogen atoms omitted for clarity

4.7 References

[1] W. Tang, X. Zhang, *Chemical Reviews* **2003**, *103*, 3029-3070.

[2] J. H. Xie, X. Y. Liu, J. B. Xie, L. X. Wang, Q. L. Zhou, *Angew Chem Int Ed Engl* **2011**, *50*, 7329-7332.

[3] R. R. Knowles, E. N. Jacobsen, *Proc. Natl. Acad. Sci. U. S. A* **2010**, *107*, 20678-20685.

[4] Q. Zhao, C. Chen, J. Wen, X. Q. Dong, X. Zhang, *Acc Chem Res* **2020**, *53*, 1905-1921.

[5] Q. Zhao, S. Li, K. Huang, R. Wang, X. Zhang, *Organic Letters* **2013**, *15*, 4014-4017.

[6] C. Yin, T. Yang, Y. Pan, J. Wen, X. Zhang, *Organic Letters* **2020**, *22*, 920-923.

[7] L. Zeng, H. Yang, M. Zhao, J. Wen, J. H. R. Tucker, X. Zhang, *ACS Catalysis* **2020**, *10*, 13794-13799.

[8] Z. Jia, F. Zhou, M. Liu, X. Li, A. S. C. Chan, C.-J. Li, *Angewandte Chemie International Edition* **2013**, *52*, 11871-11874.

[9] X. Tan, W. Zeng, X. Zhang, L. W. Chung, X. Zhang, *Chemical Communications* **2018**, *54*, 535-538.

[10] W. Wu, S. Liu, M. Duan, X. Tan, C. Chen, Y. Xie, Y. Lan, X. Q. Dong, X. Zhang, *Org Lett* **2016**, *18*, 2938-2941.

[11] J.-M. Lehn, *Supramolecular Chemistry: Concepts and Perspectives*, Weinheim Cambridge, **1995**.

[12] A. Warshel, P. K. Sharma, M. Kato, Y. Xiang, H. Liu, M. H. M. Olsson, *Chemical Reviews* **2006**, *106*, 3210-3235.

[13] H.-J. Schneider, *Angewandte Chemie International Edition* **2009**, *48*, 3924-3977.

[14] H. Wang, J. Wen, X. Zhang, *Chemical Reviews* **2021**, *121*, 7530-7567.

[15] A. Sondenecker, J. Cvengroš, R. Aardoom, A. Togni, *European Journal of Organic Chemistry* **2011**, *2011*, 78-87.

[16] I. R. Butler, W. R. Cullen, *Organometallics* **1986**, *5*, 2537-2542.

[17] T. Hayashi, T. Mise, M. Fukushima, M. Kagotani, N. Nagashima, Y. Hamada, A. Matsumoto, S. Kawakami, M. Konishi, K. Yamamoto, M. Kumada, *Bulletin of the Chemical Society of Japan* **1980**, *53*, 1138-1151.

Chapter 5 Mn-PNP Complex as a Novel Redox-Switchable Catalyst for Asymmetric Hydrogenation of acetophenone

5.1 Introduction

The ferrocenyl phosphine manganese complex (**Mn-PNP**) developed in Chapter 2 has been applied successfully in the asymmetric hydrogenation of simple ketones. This chapter describes further research on redox-switchable catalysis (RSC) using the **Mn-PNP** complex, based on the redox properties of ferrocene. Transition metal-catalysed reactions essentially attribute to their activity to the reactivity of the metal centre, which results from the interaction between the metal centre and its bound ligands. [1] Redox-active centres near the catalytic site can have a significant effect on the reactivity of a metal complex, giving so-called redox-switched catalysis (RSC), a phenomenon which has emerged as an intriguing component of homogeneous catalysis in recent years.[2-8] Changing the redox-state of such a centre, which typically comprises an organometallic group such as ferrocene, can affect the catalytic reactivity of the metal by affecting its electron density. Such a switchable catalytic process can be achieved through either chemical or electrochemical redox switching of the centre (Scheme 5.1).

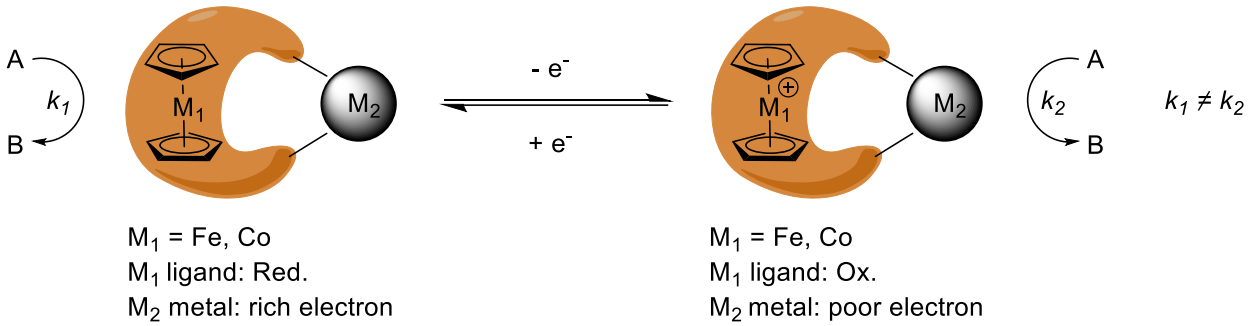

Scheme 5.1 General scheme for RSC. A = reactant, B = product; k_1, k_2 = rate constants.

In 1995, Wrighton et al. reported that the catalytic reactivity of a rhodium(I) diphosphino-cobaltocene complex was controlled by the charge state of the ferrocene ligand (Scheme 5.2).[9] The oxidized cobaltocenium complex **Wrighton-2** was a faster hydrosilation catalyst, while the neutral cobaltocene precursor **Wrighton-1** was a better hydrogenation catalyst. The reduced cobaltocene complex

catalysed the hydrogenation of cyclohexane at 3.5 mM min^{-1} while the oxidized complex at 0.23 mM min^{-1}. More importantly, the *in-situ* switching of catalytic reactivity of the rhodium catalyst was achieved by switching different cobalt oxidation states by treatment with chemical oxidant Fc^*PF_6 or reductant $CoCp_2$.

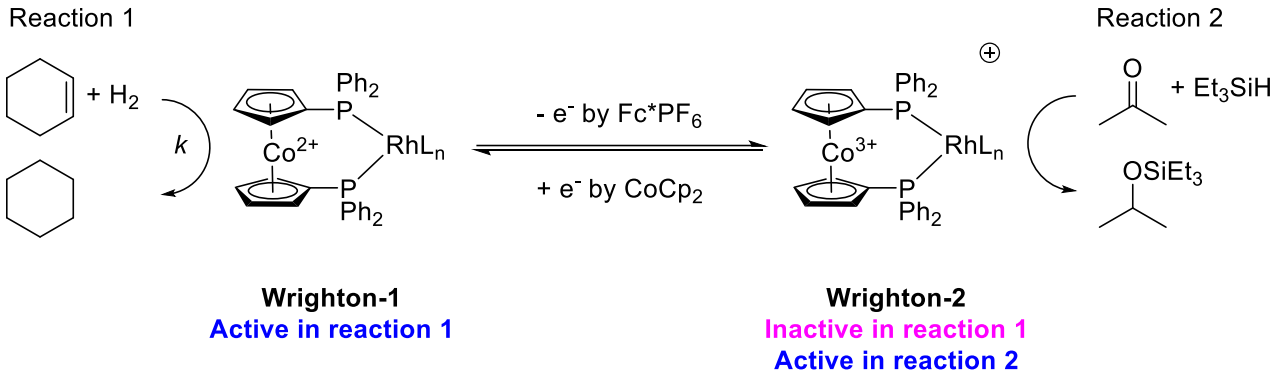

Scheme 5.2 The first RSC reported by Wrighton et al.

Since this pioneering work, RSC has gone through tremendous development over the past two decades, with various redox-switchable catalysts now developed for homogeneous catalysis.[10-21] In 2006, Gibson and Long et al. developed the first redox-modulated polymerization catalyst based on a Ti(IV)-salen complex bearing two conjugated ferrocenyl units, which was used in the ring-opening polymerization of *rac*-lactide (Scheme 5.3).[22] The reactivity of the Ti(IV)-salen catalyst could be altered by changing the ferrocenyl oxidation states. It was found that ring-opening polymerization with the neutral ferrocene-containing complex **Gibson-1** was 30 times faster than with its oxidised ferrocenium-containing version **Gibson-2** under the same conditions. The catalytic reactivity could be controlled well through *in-situ* treatment using the chemical oxidant AgOTf or reductant $FeCp^*_2$.

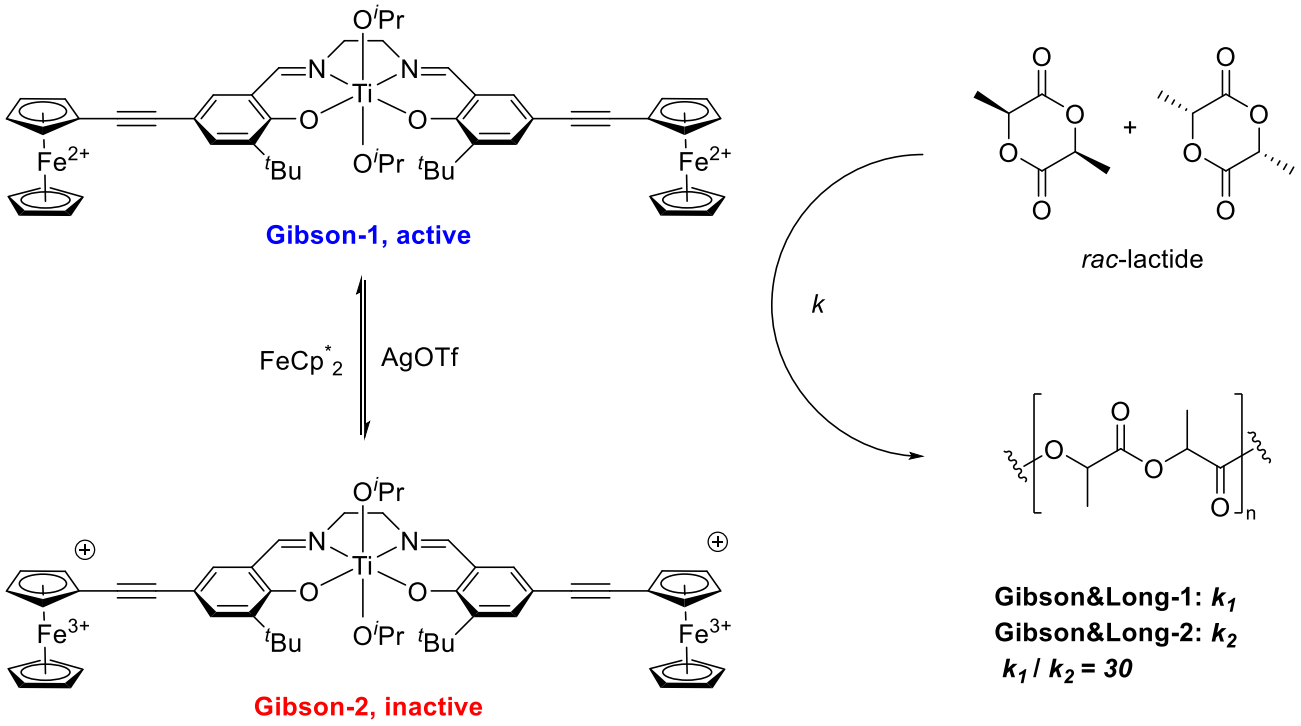

Scheme 5.3 Ti(IV)-salen complex as a redox-switchable catalyst in the ring-opening polymerization of *rac*-lactide

Based on a similar strategy, Diaconescu et al. developed ferrocenyl yttrium(III)[23] and indium(III) alkoxide complexes as redox-switchable catalysts for the ring-opening polymerization of L-lactide and trimethylene carbonate, respectively (Scheme 5.4). The ferrocenyl unit was reversibly oxidised with $FcBAr^{F}_{4}$ (ferrocenium tetrakis[3,5-bis-(trifluoromethyl)phenyl]borate) and reduced with $CoCp_2$. The neutral yttrium(III) complex **Diaconescu-Y-1** catalysed the ring-opening polymerization of L-lactide with 74% conversion after 3 h, while its oxidised form **Diaconescu-Y-2** was inactive. Therefore full *in situ* switching of the catalytic activity (i.e. on to off) was fully realized. However, replacing yttrium(III) with indium(III) resulted in opposite catalytic reactivity. The oxidized indium(III) complex **Diaconescu-In-2** reached 49% conversion for the ring-opening polymerization of trimethylene carbonate, while the reduced indium(III) complex **Diaconescu-In-1** gave only 2% conversion after 1 day. Using the similar ligand system, the same group also reported redox-switchable zirconium(IV)

complexes and titanium(IV) complexes towards the ring-opening polymerization of L-lactide and ε-caprolactone.

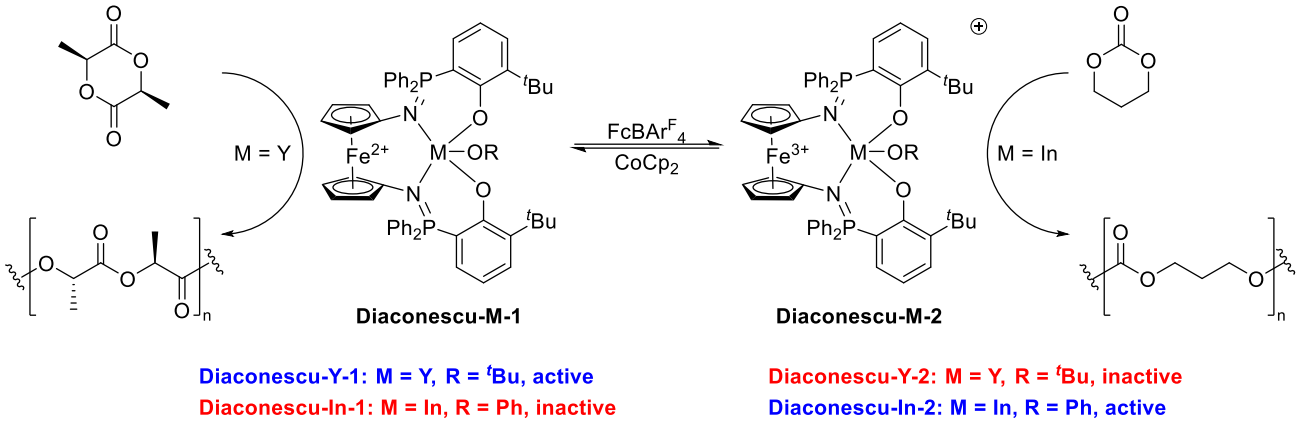

Scheme 5.4 Yttrium(III) and indium(III) complexes as redox-switchable catalysts in the ring-opening polymerization of *L*-lactide and trimethylene carbonate, respectively

In 2013, Bielawski et al. reported the first redox-switchable Ru(II)-NHC catalysts for ring-closing olefin metathesis (Scheme 5.5).[12, 14] Reversible oxidation and reduction of the ferrocene unit was realized using $FcBF_4$ (ferrocenium tetrafluoroborate) and $FeCp^*_2$ (decamethylferrocene), respectively. The initial neutral Ru(II) complex **Bielawski-1** catalyzed the ring-closing metathesis of diethyl diallylmalonate with a rate constant (k_{obs}) of 4.5×10^{-5} s $^{-1}$, and the oxidised form **Bielawski-2** reduced the rate constant to 0.86×10^{-5} s $^{-1}$. After the subsequent addition of $FeCp^*$, the *in situ* generated reduced Ru(II) complex recovered more than 94% of the catalytic activity (k_{obs} = 4.25×10^{-5} s $^{-1}$).

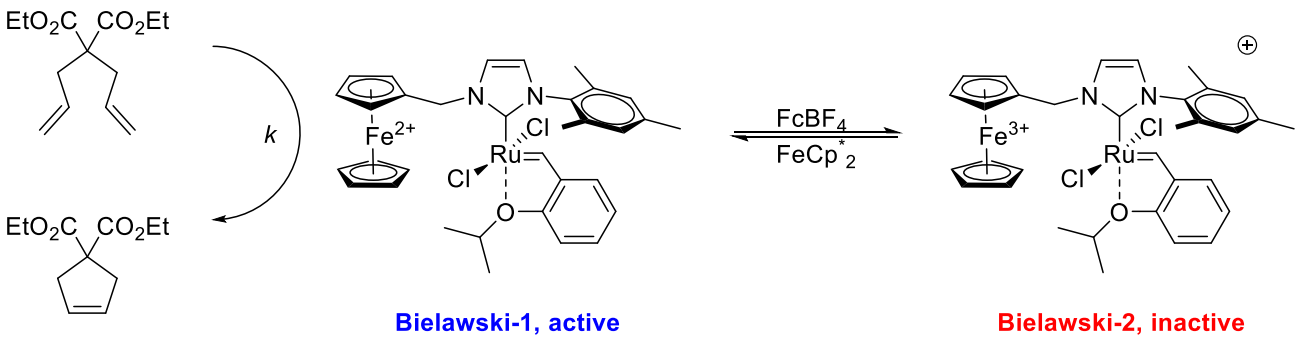

Scheme 5.5 Ru(II)-NHC complex as a redox-switchable catalyst in the ring-closing metathesis of diethyl diallylmalonate

Subsequently, the concept of RSC has been expanded to some other reactions.[24] Sarkar et al. introduced a series of ferrocenyl mesoionic carbene gold(I) complexes for the synthesis of heterocycles: oxazoline, furan and phenol (Scheme 5.6).[25-27] The ferrocenyl unit was reversibly oxidized with [FcOAc]BF_4 and reduced with $FeCp^*_2$. In this case, the catalytic reactivity of the oxidised ferrocenium gold(I) complex **Sarkar-2** was triggered on, while the reduced form **Sarkar-1** was off for the formation of heterocycles. This simple redox-induced strategy allowed for efficient cyclization reactions without using any additives such as silver (I) and copper(II), which were commonly required in the area of gold(I) catalysis.

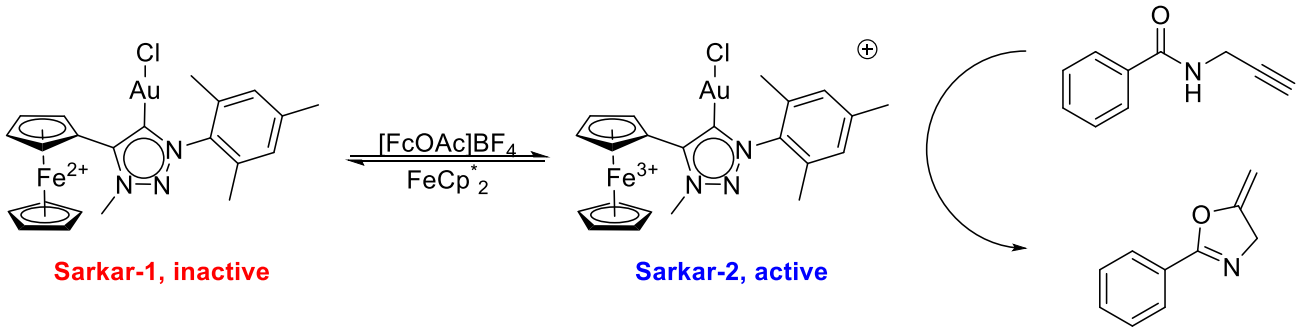

Scheme 5.6 Au(I)-NHC complex as a redox-switchable catalyst for synthesis of heterocycles

In 2016, Diaconescu et al. described redox-switchable hydroalkoxylation of styrenes using a tetrahedral cobalt(II) catalyst containing a ferrocenyl salicylimine ligand (Scheme 5.7).[28] Reversible oxidation and reduction of the ferrocene unit was realized using [FcOAc] [BAr^F_4] and $CoCp_2$, respectively. The neutral ferrocenyl cobalt(II) complex **Diaconescu-Co-1** was highly reactive towards the hydroalkoxylation of a family of olefin substrates, while its oxidised ferrocenium species **Diaconescu-Co-2** was inactive. Furthermore, the hydroalkoxylation reactivity could be switched on or off *in situ*.

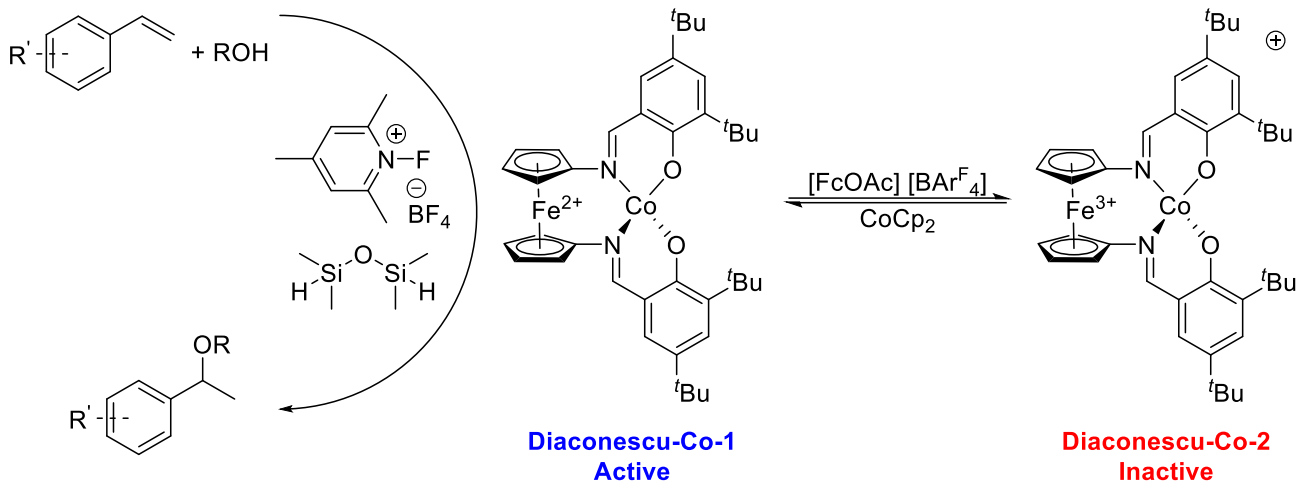

Scheme 5.7 Tetrahedral cobalt(II) complex as a redox-switchable catalyst in the hydroalkoxylation of styrenes

In 2016, Poyatos and Peris et al. developed a ferrocenyl-benzo-fused imidazolylidene Ru(II) complex for redox-switchable transfer hydrogenation of ketones and imines (Scheme 5.8).[29] The ferrocenyl unit was reversibly oxidized with [FcOAc]BF_4 and reduced with $CoCp_2$. In the case of ketone hydrogenations, the neutral ferrocenyl Ru(II) complex **Peris-1** was very active, while its oxidised ferrocenium form, **Peris-2,** gave low reactivity, with once again, *in situ* switching of the process possible. In the case of imine hydrogenation, both the neutral and oxidised Ru(II) complexes gave good and similar yields. Using the same ferrocenyl ligand, they also reported redox-switchable gold(I)-catalyzed cyclization of alkynes with furans.

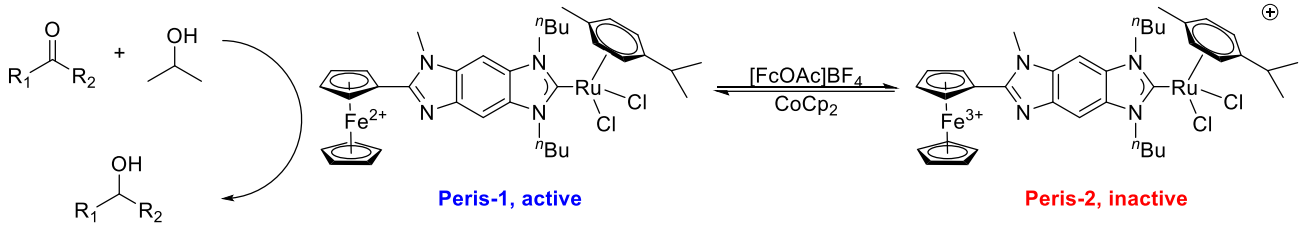

Scheme 5.8 Ferrocenyl-benzo-fused imidazolylidene Ru(II) complex for redox-switchable transfer hydrogenation of ketones

Recently, Hey-Hawkins et al. reported the redox-switchable asymmetric transfer hydrogenation of acetophenone, catalysed by a P-chiral dendritic ferrocenyl phosphine Ru(II) complex (Scheme 5.9),[30] itself based on their previous achiral dendritic complex design.[31] Reversible oxidation and reduction of the ferrocene unit was realized using $[FcOAc]BF_4$ and $FeCp^*_2$, respectively. The neutral ferrocenyl monomeric and dendritic Ru(II) complexes **Hawkins-1** were active, while the oxidised ferrocenium forms **Hawkins-2** gave low reactivity. The catalytic reactivities of the Ru(II) complexes were reversibly switched off or on *in situ*, but only low enantioselectivities were obtained for these asymmetric transfer hydrogenations.

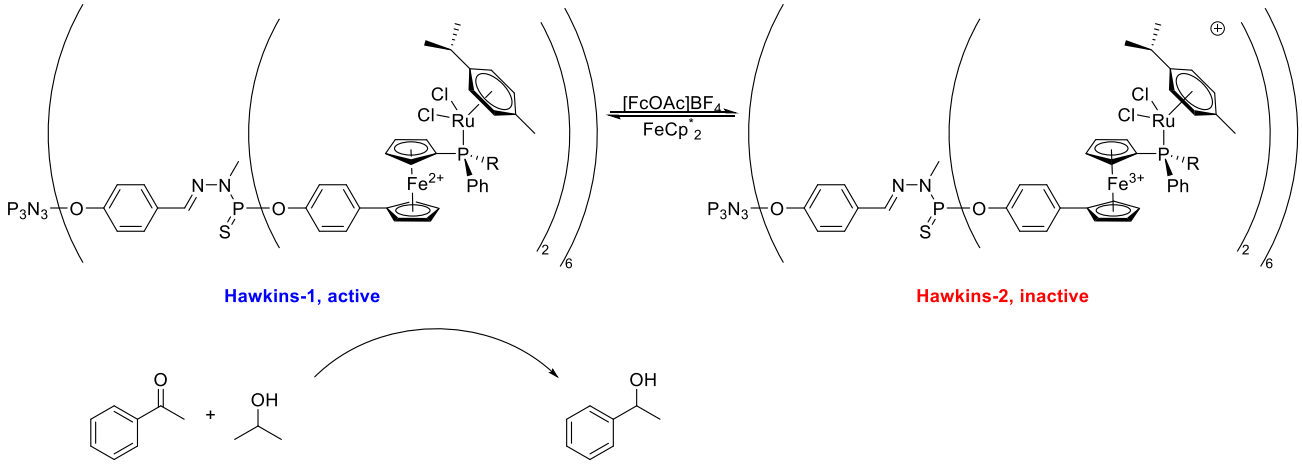

Scheme 5.9 P-chiral dendritic ferrocenyl phosphine Ru(II) complex for redox-switchable asymmetric transfer hydrogenation of acetophenone

5.2 Chapter Aims

As described in Chapter 2, the **Mn-PNP** complex is an excellent catalyst precursor for the asymmetric hydrogenation of aryl-alkyl ketones, affording high reactivities and excellent enantioselectivities. Its great performance is attributed to the enhancement of the rigidity of the backbone by introducing a 7-membered ring with a planar chiral ferrocene moiety in a fixed conformation. Ferrocene plays an important role in this ligand design with its unique steric and electronic contributions. Herein, the aim was to explore the effect on the catalytic reactivity of the manganese complex in the asymmetric hydrogenation of acetophenone as a function of the different oxidation states of ferrocene. Upon oxidation of the ferrocene, it was anticipated that the more electron withdrawing ferrocenium unit would make the manganese centre of **Mn-PNP+** less electron rich, possibly resulting in lower reactivity in the hydrogenation of ketones. In contrast, after reduction to reform the ferrocene unit, the reactivity of the manganese complex would be recovered (Scheme 5.10).

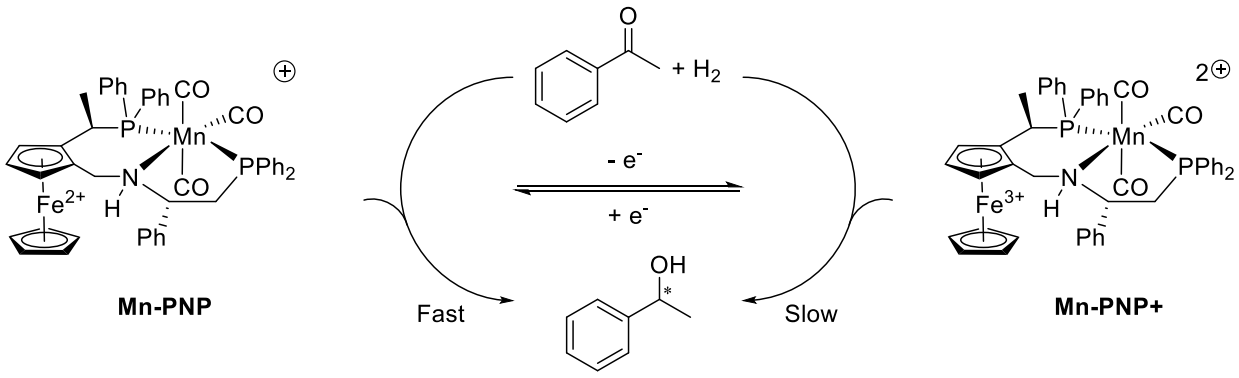

Scheme 5.10 Design of novel RSC using Mn-PNP complex

However before redox-switched catalysis was probed, it was first important to establish that the ferrocene unit could give a sufficiently stable oxidized product. Therefore a further aim was to explore the redox properties of **PNP** and **Mn-PNP** and to compare their properties with another ferrocene system **Fc-SPO** and its cobalt complex **Co-0**. The ligand **PNP** and its manganese complex **Mn-1** were described in Chapter 2. Likewise the ligand **Fc-SPO** and its cobalt complex **Co-0** were described in

Chapter 3. It was decided to study their electrochemical properties using cyclic voltammetry (CV) in acetonitrile.

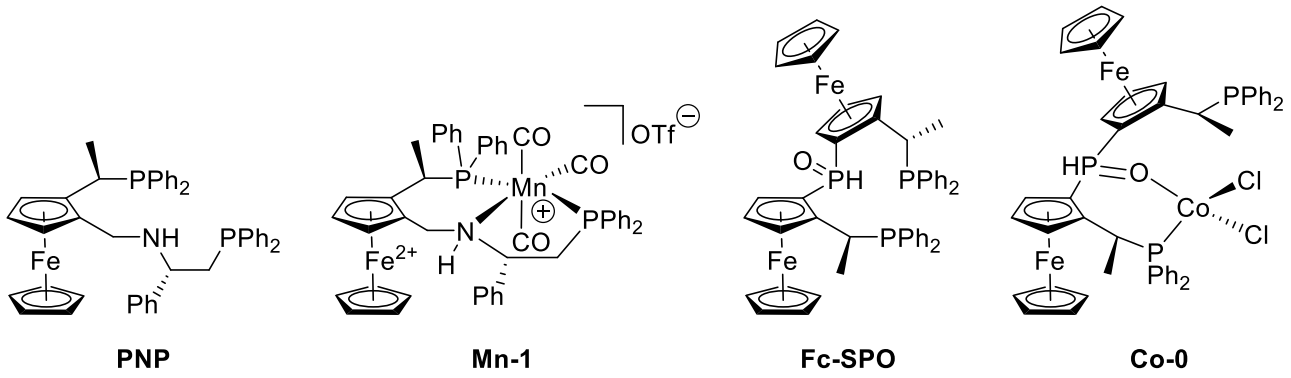

Figure 5.1 Ligands and their metal complexes selected to be characterized by CV

The $E_{1/2}$ values for the ferrocene units of **PNP** and **Mn-1** were found to be +465 mV and +715 mV, respectively (Figure 5.2). The coordination of manganese with **PNP** ligand increased oxidation potential of the ferrocene unit. This behaviour has been reported previously in the literature[32] and is consistent with metal cation complexation making oxidation of the ferrocene unit more thermodynamically unfavourable. Most importantly, the CV curves of both the **PNP** ligand and the **Mn-1** complex displayed reversible chemical and electrochemical behaviour, which indicated the suitability of the manganese complex to be employed in redox-switchable catalysis.

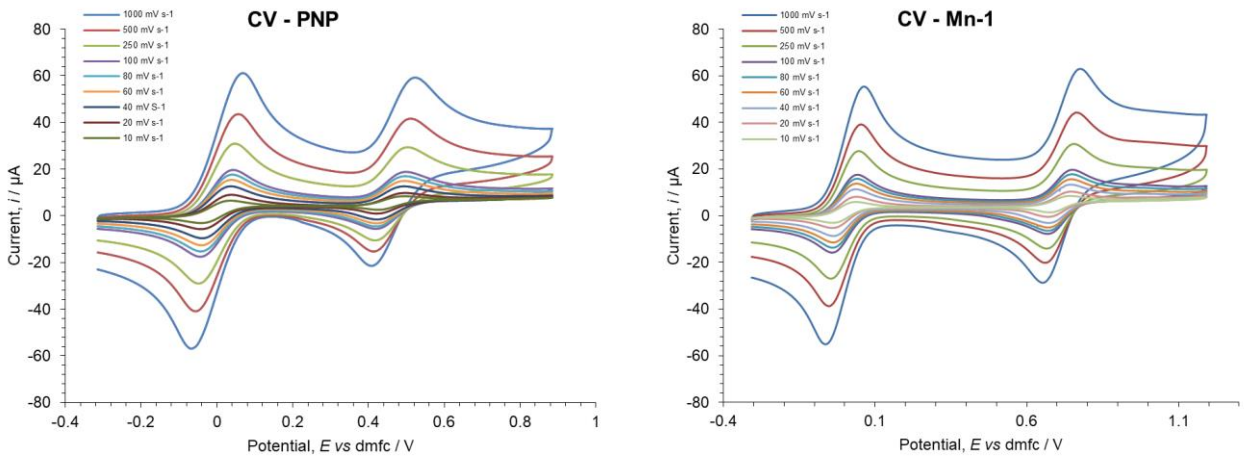

Figure 5.2 CV of the PNP ligand (1.0 mM) and Mn-1 (1.0 mM) at various scan rates wrt dmfc (1.0 mM) in dry acetonitrile with an electrolyte of $TBAPF_6$ (0.1 M)

The **Fc-SPO** ligand and the **Co-0** complex have two ferrocene units, which potentially increases the complexity of their electrochemical properties. Furthermore, the $^{31}P\{^{1}H\}$ NMR spectrum of **Fc-SPO** shows three peaks at 19.85 ppm (d, J = 10.8 Hz), 11.13 ppm (s) and 8.86 ppm (d, J = 10.6 Hz) (details in Chapter 3), which indicates that these two phosphine groups (and therefore each ferrocene) are not in identical environments. Indeed two $E_{1/2}$ values were observed for the two ferrocene units of **Fc-SPO** at +676 mV and +1044 mV, which shifted to +768 mV and +1216 mV respectively for its cobalt complex **Co-0** (Figure 5.3). However, the reduction waves of both ferrocene units within **Fc-SPO** were much smaller than their oxidation waves, indicating irreversible behaviour. The same effect was seen for **Co-0**, albeit at more positive potentials. This irreversible behaviour indicated that the ligand **Fc-SPO** and its cobalt complex were much less suitable for redox-switchable catalysis compared to the ligand **PNP** and its manganese complex.

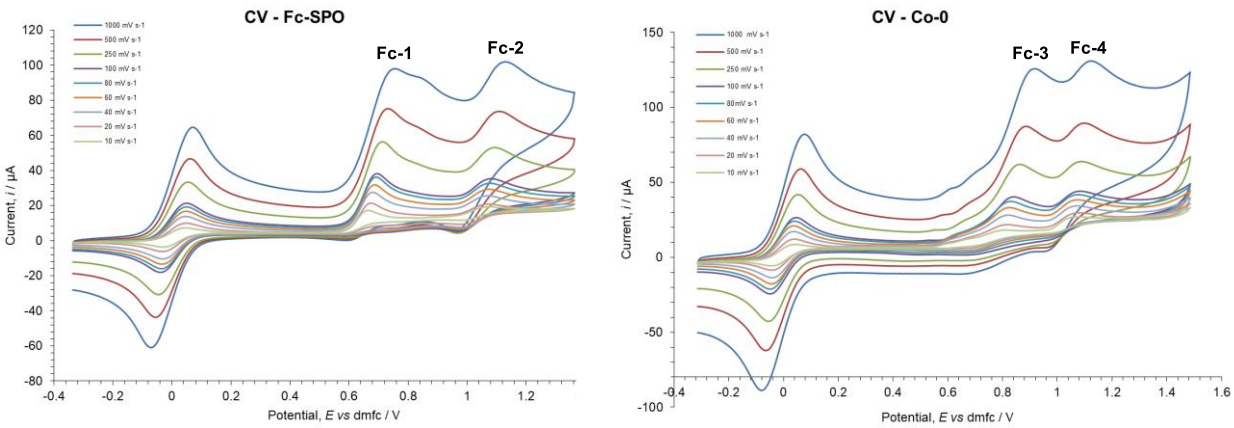

Figure 5.3 CV of the Fc-SPO ligand (1.0 mM) and Co-0 (1.0 mM) at various scan rates wrt dmfc (1.0 mM) in dry acetonitrile with an electrolyte of $TBAPF_6$ (0.1 M)

5.3 Results and discussion

5.3.1 Synthesis of the redox-switchable complexes

The routes for the synthesis of the redox-switchable manganese complexes are shown in Scheme 5.11. The procedures for the **PNP** ligand and its manganese(I) complex **Mn-0** were previously described in Chapter 2. To begin with the precursor to the ferrocenium species, **Mn-1**, was prepared in which the Br^- anion in **Mn-0** was exchanged for trifluoromethanesulfonate (OTf^-). It could be formed in two ways. The first was through the addition of 1eq. of AgOTf in CH_2Cl_2. The byproduct AgBr could be easily removed by filtration. The second method was via formation of the silver complex **Ag-1**, which was then reacted with $Mn(CO)_5Br$ in toluene. **Ag-1** was found to be highly air stable, probably because of the strong interaction of the soft acid (Ag) with the phosphine and amine donor atoms, which enabled purification using column chromatography with silica gel. The paramagnetic ferrocenium manganese complex **Mn-2** was then generated by the oxidation of **Mn-1** with 1eq. of AgOTf. Its structure was confirmed by X-Ray crystallography from dark green crystals grown from DCM/hexane (Figure 5.4). The reduction process was achieved by the addition of 1 mol eq. of decamethylferrocene ($FeCp^*_2$) to give the product **Mn-1-red.**

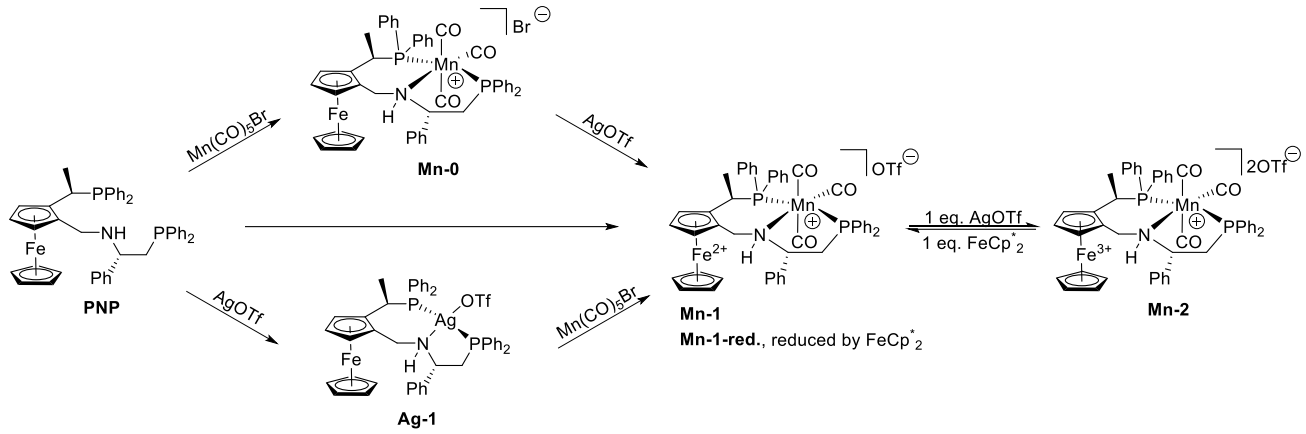

Scheme 5.11 Synthesis of the ferrocene- and ferrocenium-based Mn-PNP complexes

A meridional geometry for the oxidised ferrocenium manganese complex **Mn-2** was apparent, where two phosphorus atoms P1 and P2 are on the opposite sites of Mn01 atom.

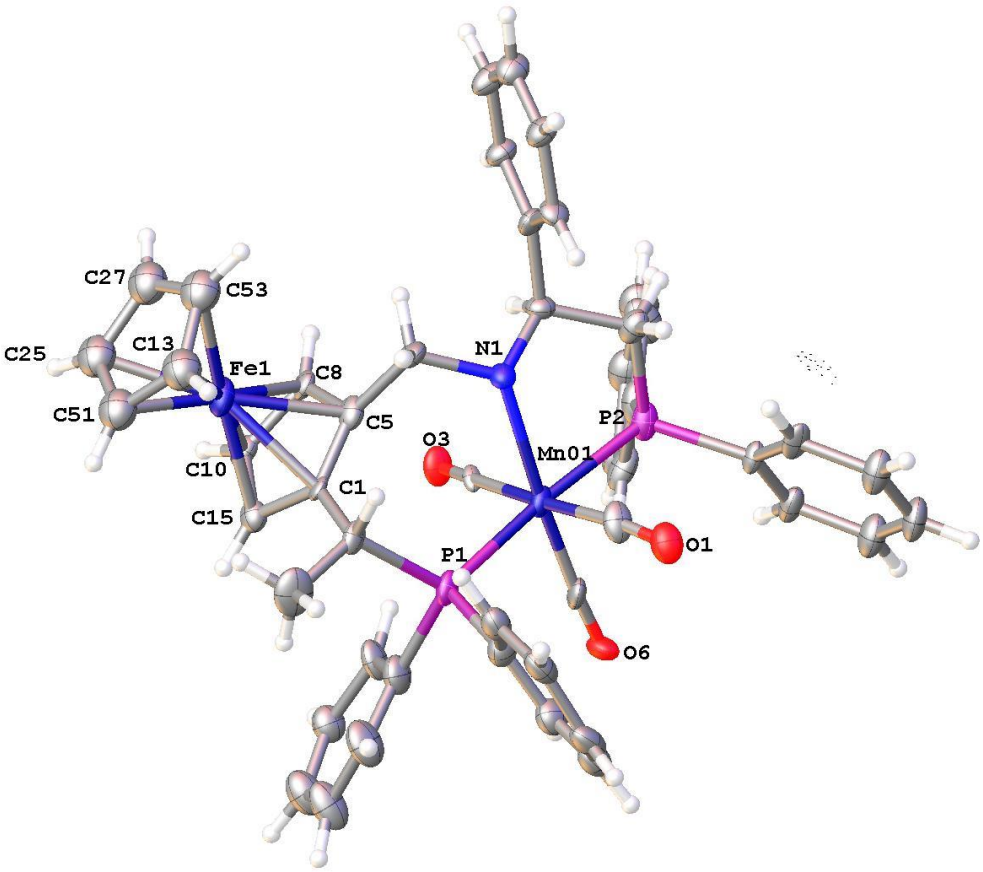

Figure 5.4 Crystal structure of Mn-2 without showing counter ions, with ellipsoids drawn at the 50% probability level

The bond lengths from the Cp carbons to the Fe1 atom are shown in Table 5.1. The ten Fe-C bonds in ferrocene have identical lengths (see X-Ray of **Fc-SPO-Co** in Chapter 3), while here the Fe-C bonds are significantly different. This indicates a distorted Fe-Cp structure within the ferrocenium moiety.

Table 5.1 Bond lengths for Fe1 atom with its surrounding carbon atoms of Mn-2

Atom	Atom	Length/Å
Fe1	C1	2.114(19)
Fe1	C5	2.12(2)
Fe1	C8	2.06(2)
Fe1	C10	2.07(2)
Fe1	C15	2.16(2)
Fe1	C25	2.09(3)
Fe1	C51	2.01(3)
Fe1	C13	2.03(3)
Fe1	C53	2.13(3)

5.3.2 NMR analysis of the redox-switchable complexes

5.3.2.1 Silver complexes

The silver complex **Ag-1** generated by treating **PNP** with 1 mol. eq. of AgOTf in CH_2Cl_2 gave two unique $^{31}P\{^1H\}$ NMR signals at 28.13 ppm (ddd) and -3.35 ppm (ddd). (for details, see experimental) Figure 5.5 shows this $^{31}P\{^1H\}$ NMR spectrum, as well as the effect of treating **Ag-1** with one further molar equivalent of AgOTf, which resulted broadened single peaks at 5.23 ppm and 2.69 ppm. However, the original signals could be regenerated following the addition of 1 mol eq. of the reducing agent $FeCp^*_2$.

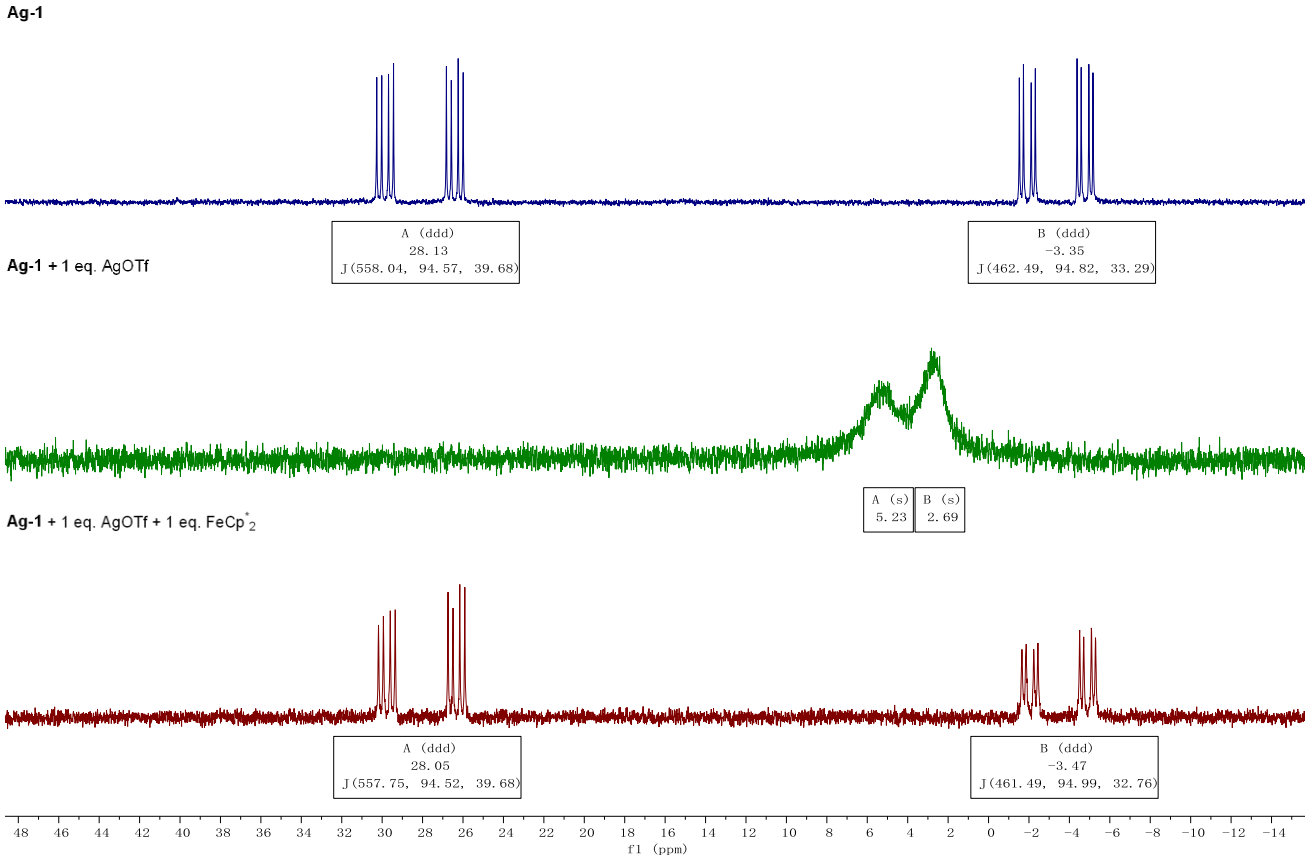

Figure 5.5 Changes in the $^{31}P\{^{1}H\}$ NMR spectra of the silver complexes in $CDCl_3$ induced by the redox cycling process (AgOTf and $FeCp^*_2$)

5.3.2.2 Manganese complexes

The $^{31}P\{^{1}H\}$ NMR spectra of the manganese complexes underwent similar changes to those of the silver complexes (Figure 5.6). The original orange complex **Mn-1** gave two doublet peaks at 65.73 ppm and 65.19 ppm in $CDCl_3$. The addition of 1 mol eq. of AgOTf yielded a green compound with a single peak at 66.03 ppm, consistent with the formation of the oxidized complex **Mn-2**. This compound was then treated with 1 mol eq. of $FeCp^*_2$ to reduce the complex back to **Mn-1**, which was renamed **Mn-1-red** in order to distinguish the two neutral ferrocenyl manganese complexes. Furthermore, a different reducing reagent $CoCp_2$ was also found to give a similar result. However, excess $CoCp_2$ gave some unknown effects on the $^{31}P\{^{1}H\}$ NMR spectra (for details, see experimental). Therefore it was better to employ $FeCp^*_2$ as the reducing reagent in the redox process.

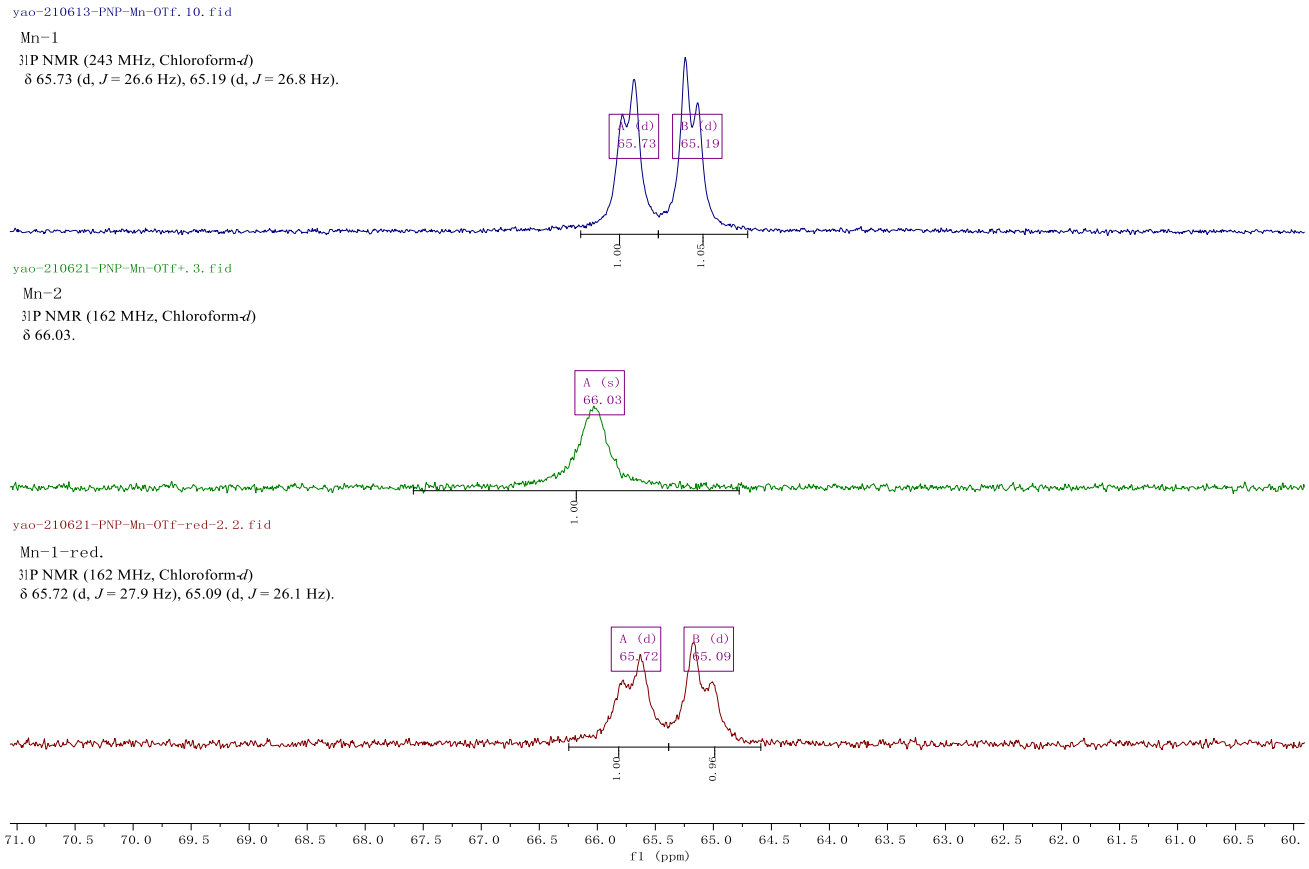

Figure 5.6 Changes in the $^{31}P\{^{1}H\}$ NMR spectra of the manganese complexes in $CDCl_3$ induced by the redox cycling process (AgOTf and $FeCp^*_2$).

5.3.3 Catalysis results

The catalytic activities of these manganese complexes in the asymmetric hydrogenation of acetophenone were investigated (Table 5.2). **Mn-1** was found to be less active than **Mn-0** at 25 °C (entry 2), but afforded high reactivities and excellent enantioselectivities at higher temperatures (entry 3 and 4). Using 2 mol% of KOH at 70 °C gave similar results (entry 5). The oxidized complex **Mn-2** was not active at all using 1 mol% of KOH (entry 6). However with 2 mol% of KOH, the conversion increased to 31%, while the enantioselectivity was almost as high (entry 7). The reduced complex **Mn-1-red** recovered almost the same original reactivities and the same enantioselectivities under the same conditions (entries 8 and 9) These results indicate that the oxidation of the ferrocene unit has a significant effect on the reactivity of the manganese complex, but a limited effect on enantioselectivity.

The lower reactivity can be explained by the more electron withdrawing ferrocenium unit making the manganese centre of Mn-2 less electron rich. Regarding the lack of change in enantioselectivity, it would appear that even though the redox process does affect the ferrocene structure to some extent (see X-ray in Figure 5.4), this does significantly affect the arrangement of the chiral ligand backbone around the catalytic centre.

Regarding the large differences in reactivities for **Mn-2** as a function of KOH loading (entries 5 and 6), possible explanation is that there are interactions between the generated ferrocenium cation and OH^- anions from the base (KOH). The positive charge could attract the OH^- group into close proximity, resulting in the catalyst precursor not being activated by the free base until sufficient amounts of KOH are present (it has previously been shown in Chapter 2 that the conversion for **Mn-0** was only 29% in the absence of KOH).

Table 5.2 Asymmetric hydrogenation of acetophenone catalyzed by Mn complexes

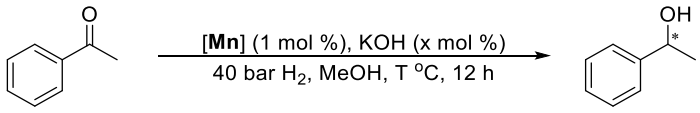

Entry[a]	[**Mn**]	KOH (x mol%)	T (°C)	Conversion (%)[b]	ee (%)[b]
1	**Mn-0**	1	25	88	94
2	**Mn-1**	1	25	26	95
3	**Mn-1**	1	60	76	92
4	**Mn-1**	1	70	99	91
5	**Mn-1**	2	70	99	91
6	**Mn-2**	1	70	1	-
7	**Mn-2**	2	70	31	89

8	**Mn-1-red**	1	70	79	91
9	**Mn-1-red**	2	70	99	91

[a] Reaction conditions: acetophenone (0.2 mmol), cat.(0.002 mmol), MeOH (0.4 mL), 40 bar of H_2, 12 h. [b] Conversions and ee values were determined by ^{1}H-NMR and chiral HPLC, respectively.

5.4 Conclusion

In summary, we report the ferrocene-based manganese complexes **Mn-PNP** as novel redox-switchable catalysts for the asymmetric hydrogenation of acetophenone. Switching between two iron oxidation states of the ferrocene unit was found to have a significant effect on the catalytic reactivity, with the process chemically reversible. Notably, little or no effect was found on AH enantioselectivity, presumably since oxidation has a limited effect on the chiral ligand backbone. Further work will explore other catalytic processes (e.g hydroformylation) where oxidation to a more electron-withdrawing ligand environment would expect to enhance reactivity rather than diminish it.

5.5 Experimental

5.5.1 Synthesis of the redox-switchable complexes

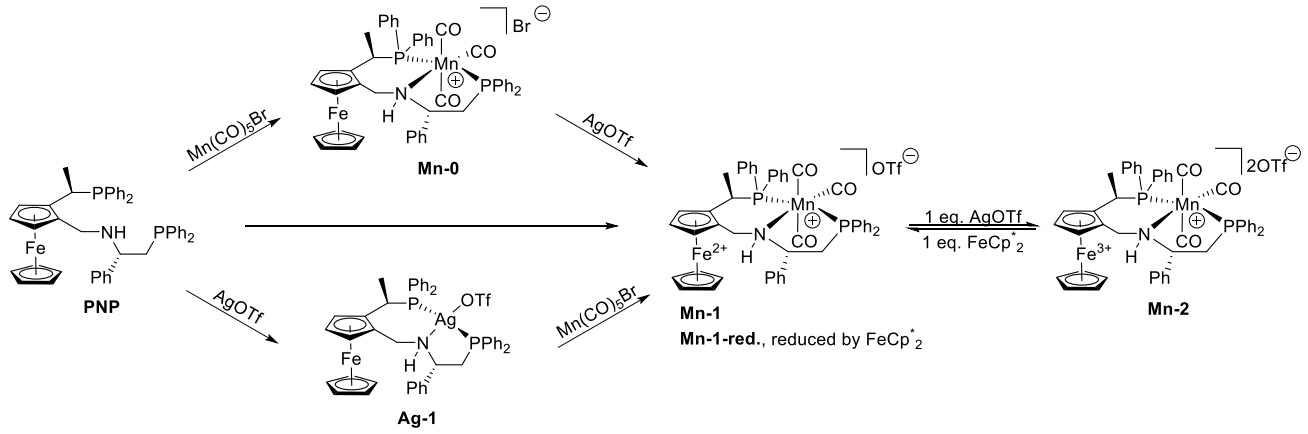

Scheme 5.12 Synthesis of the redox-switchable manganese complexes

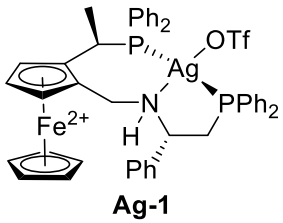

Ag-1

Ag-1. Novel compound. The **PNP** ligand (0.6 mmol, 429 mg) and AgOTf (0.6 mmol, 154 mg) were added to dry DCM (5 mL) in a glovebox. After stirred at rt for 1 h, the reaction mixture was concentrated under vacuum and purified by column chromatography on silica gel (PE/EtOAc, 2/1) to yield 510 mg (87%) of **Ag-1** as an orange solid. ^{1}H NMR (600 MHz, Chloroform-*d*) δ 7.73 – 7.67 (m, 2H), 7.57 – 7.47 (m, 6H), 7.46 – 7.35 (m, 13H), 7.35 – 7.27 (m, 4H), 4.43 (dd, J = 13.4, 5.5 Hz, 1H), 4.16 (dd, J = 13.8, 5.4 Hz, 1H), 3.99 – 3.95 (m, 2H), 3.94 (s, 5H), 3.87 (q, J = 7.0 Hz, 1H), 3.66 (td, J = 12.4, 7.0 Hz, 1H), 3.37 (dt, J = 14.4, 2.3 Hz, 1H), 3.17 – 3.11 (m, 1H), 2.71 (t, J = 13.6 Hz, 1H), 2.57 (t, J = 13.5 Hz, 1H), 1.54 (dd, J = 9.8, 7.1 Hz, 3H). ^{13}C NMR (101 MHz, Chloroform-*d*) δ 141.8, 141.7, 137.0 (d, J = 3.1 Hz), 136.8 (d, J = 3.0 Hz), 133.9 (d, J = 2.3 Hz), 133.7 (d, J = 2.4 Hz), 132.7 (d, J = 1.7 Hz), 132.5 (d, J = 1.8 Hz), 132.1, 132.0, 131.6, 131.1, 130.2, 129.8, 129.3, 129.2, 129.1, 129.0, 129.0, 128.9, 128.8, 128.3, 128.2, 127.9, 126.8, 89.3 (d, J = 15.1 Hz), 82.3 (d, J = 2.5 Hz), 70.7, 69.2,

67.5, 66.8, 56.6 (d, J = 6.5 Hz), 43.5, 38.6 (d, J = 15.5 Hz), 31.2 (d, J = 11.8 Hz), 15.8. ^{19}F NMR (376 MHz, Chloroform-*d*) δ -77.87. ^{31}P {^{1}H} NMR (162 MHz, Chloroform-*d*) δ 28.1 (ddd, J = 558.0, 94.6, 39.7 Hz), -3.3 (ddd, J = 462.5, 94.8, 33.1 Hz). **HRMS** (ESI) m/z: $[M\text{-}OTf]^+$ Calcd for $C_{45}H_{43}AgFeNP_2^+$ = 822.1266; Found: 822.1259.

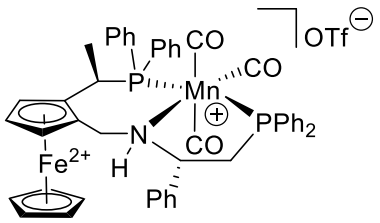

Mn-1

Route 1: **Mn-0** (0.1 mmol, 93 mg) and AgOTf (0.1 mmol, 26 mg) were added to dry DCM (1 mL) in a glovebox. After stirred at rt for 1 h, the reaction mixture was filtered to remove generated AgBr. The residue was concentrated under vacuum and washed with hexane to yield 90 mg (90%) of **Mn-1** as an orange solid.

Route 2: **Ag-1** (0.5 mmol, 486 mg) and $Mn(CO)_5Br$ (0.5 mmol, 137 mg) were added to dry toluene (10 mL) in a glovebox. After stirred at 110 ^{o}C for 10 h, the reaction mixture was filtered to remove generated AgBr. The residue was concentrated under vacuum and washed with hexane to yield 480 mg (96%) of **Mn-1** as an orange solid.

Mn-1. Novel compound. ^{1}H NMR (600 MHz, Chloroform-*d*) δ 7.97 (t, J = 8.6 Hz, 2H), 7.67 (d, J = 7.6 Hz, 2H), 7.64 – 7.41 (m, 16H), 7.36 (s, 3H), 7.27 (q, J = 6.7, 6.1 Hz, 1H), 7.17 (dd, J = 15.3, 7.5 Hz, 1H), 5.69 (d, J = 9.0 Hz, 1H), 4.36 (s, 1H), 4.21 (s, 1H), 4.03 (s, 1H), 3.92 (s, 5H), 3.88 (s, 1H), 3.77 (q, J = 12.5, 12.0 Hz, 1H), 3.71 (d, J = 14.7 Hz, 2H), 3.23 (t, J = 14.6 Hz, 1H), 2.90 – 2.76 (m, 1H), 1.34 (dd, J = 11.3, 6.6 Hz, 3H). ^{13}C NMR (151 MHz, Chloroform-*d*) δ 211.1 (t, J = 18.3 Hz), 136.9, 136.8, 132.3, 132.3 (d, J = 8.2 Hz), 132.1, 131.7 (d, J = 3.9 Hz), 131.4, 130.9 (d, J = 8.7 Hz),

130.3 (d, J = 9.6 Hz), 130.0 – 129.8 (m), 129.7 (d, J = 2.4 Hz), 129.4 (d, J = 2.1 Hz), 128.4 (d, J = 8.9 Hz), 128.3 (d, J = 9.7 Hz), 128.1, 128.1, 128.0, 127.2, 127.1 (d, J = 8.9 Hz), 124.3, 89.2 (d, J = 11.9 Hz), 79.3 (d, J = 3.7 Hz), 70.4, 68.4, 66.6 (dd, J = 9.7, 2.7 Hz), 66.5 (d, J = 4.3 Hz), 47.3, 35.3 (d, J = 18.0 Hz), 32.3 (d, J = 8.0 Hz), 20.4, 13.3 (d, J = 6.5 Hz). ^{31}P {^{1}H} NMR (243 MHz, Chloroform-*d*) δ 65.74 (d, J = 27.1 Hz), 65.16 (d, J = 27.4 Hz). **HRMS** (ESI) m/z: $[M\text{-}OTf]^+$ Calcd for $C_{48}H_{43}FeMnNO_3P_2^+$ = 854.1443; Found: 854.1434. IR absorptions (C=O): 1966, 1922, 1852.

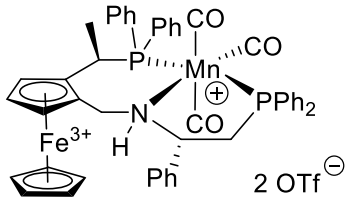

Mn-2

Mn-1 (0.15 mmol, 150 mg) and AgOTf (0.15 mmol, 39 mg) were added to dry DCM (1 mL) in a glovebox. The reaction mixture became green suspension in seconds. After stirred at rt for 1 h, the reaction mixture was filtered to remove generated Ag. The residue was concentrated under vacuum and washed with hexane to yield 150 mg (87%) of **Mn-2** as a deep green solid. ^{31}P {^{1}H} NMR (162 MHz, Chloroform-*d*) δ 66.03. IR absorptions (C=O): 1965, 1920.

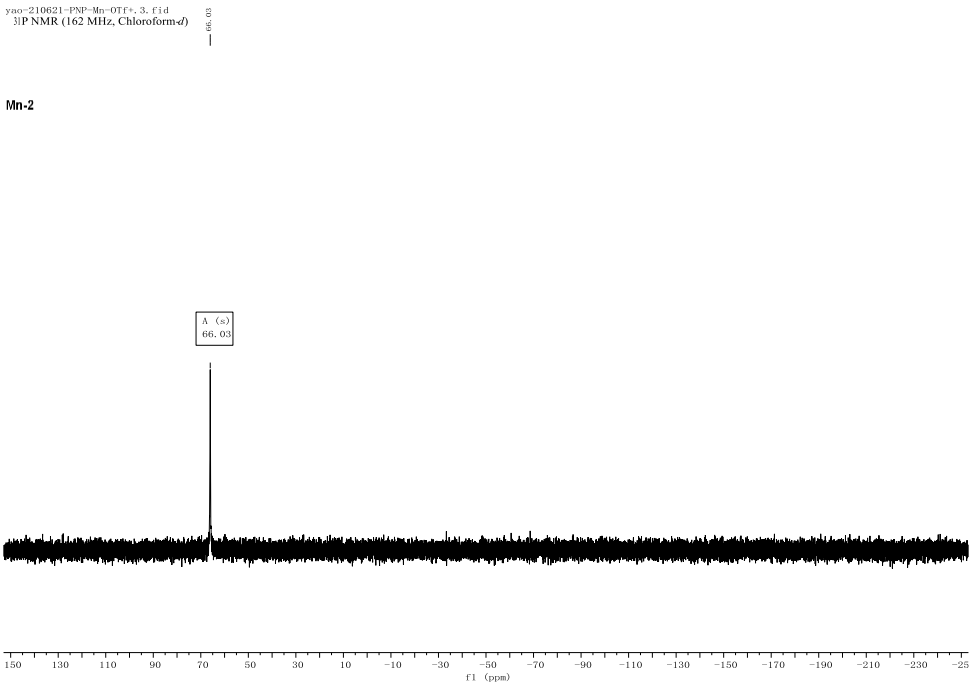

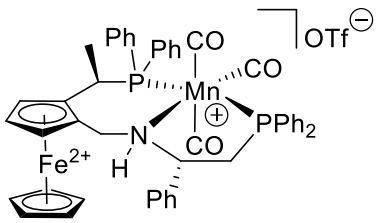

Mn-1-red

Mn-2 (0.02 mmol, 23 mg) was dissolved in dry DCM (0.5 mL), and $CoCp_2$ (0.02 mmol, 4 mg) or $FeCp^*_2$ (0.02 mmol, 7 mg) was added into the green solution. After stirred at rt for 1 h, the mixture was filtered, concentrated under vacuum, and washed with hexane. The addition of $CoCp_2$ generated the brown suspension **Mn-1-red (CoCp2)**, while $FeCp^*_2$ gave the green solid **Mn-1-red**, both in quantitative yields.

^{31}P {^1H} NMR (243 MHz, Chloroform-d) for **Mn-1-red (CoCp2)**: δ 65.60, 64.93 (bad splitting).

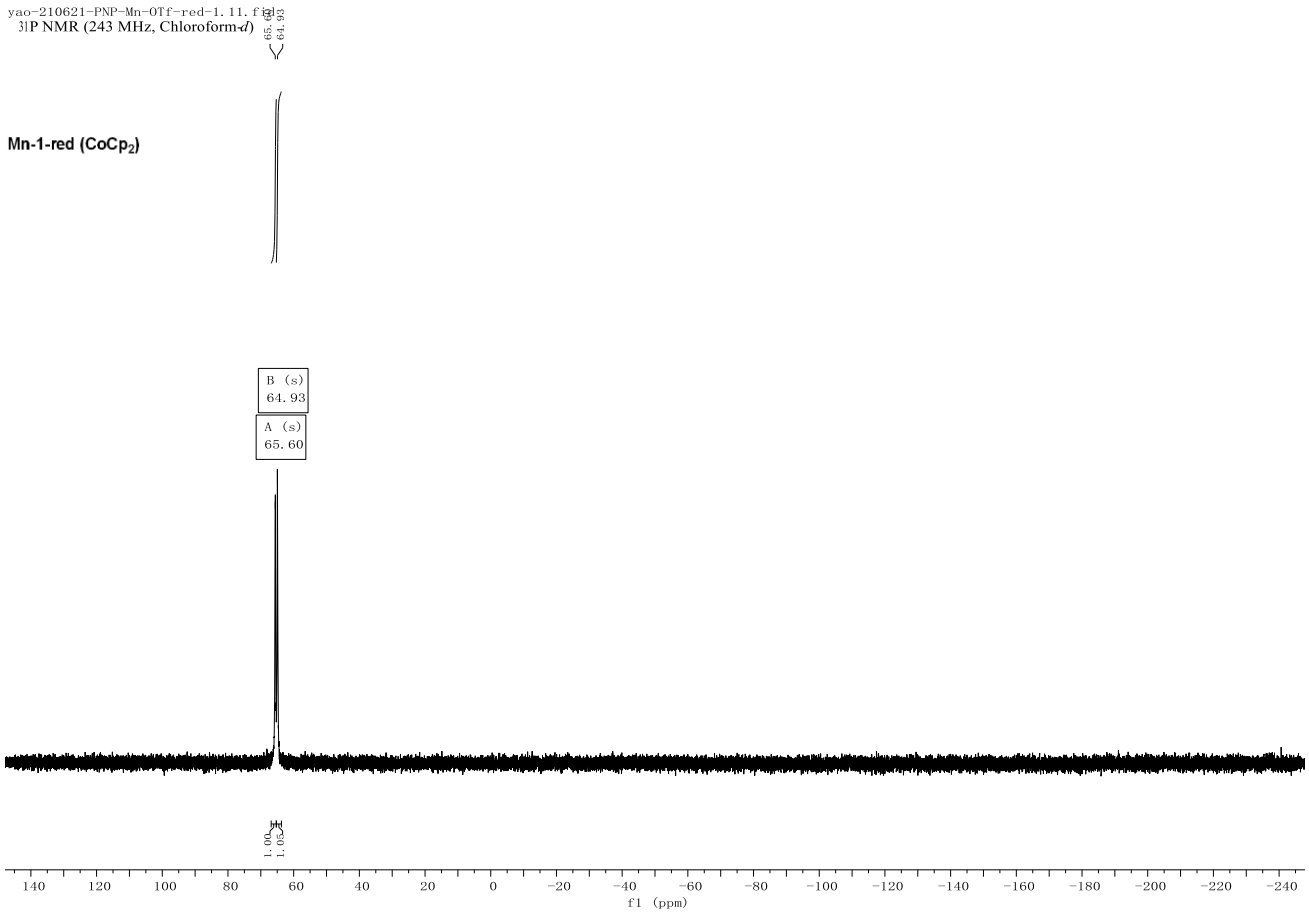

^{31}P {^{1}H} NMR (243 MHz, Chloroform-d) for **Mn-1-red**: δ 65.71 (d, J = 26.0 Hz), 65.10 (d, J = 27.3 Hz).

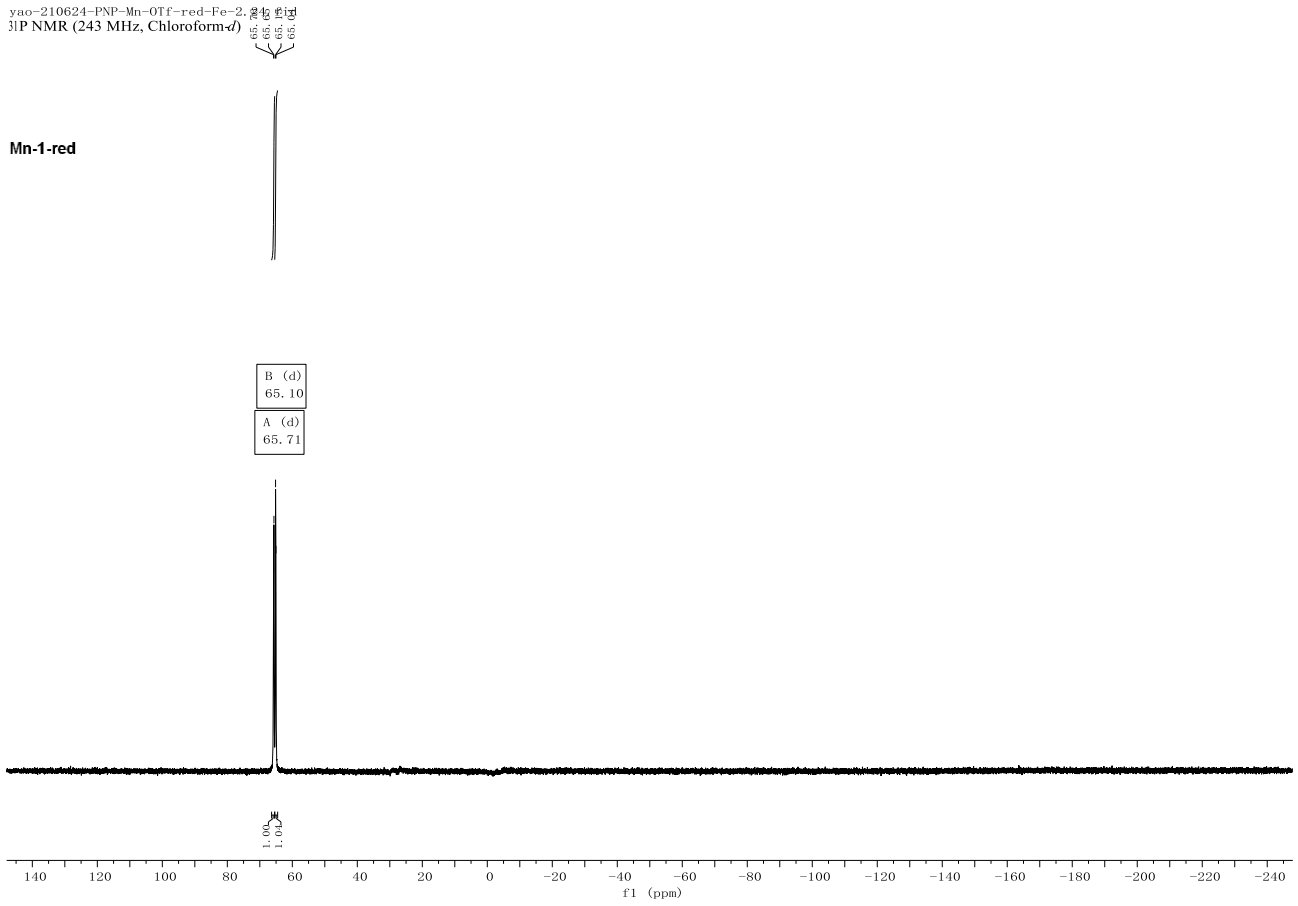

5.5.2 NMR analysis of the redox-switchable complexes

5.5.2.1 Silver complexes

The silver complex **Ag-1** (0.015 mmol, 15 mg) was treated with 1 eq. of AgOTf (0.015 mmol, 4 mg) in $CDCl_3$ (0.5 mL) in the glovebox. After stirred at rt for 1 h, the green suspension was filtered into a Youngtube for the NMR analysis before transferred back into the glovebox. Then 1 eq. of $FeCp^*_2$ (0.015 mmol, 5 mg) was added. The reaction mixture was still green. After shaken for 1 h, the green suspension was resubmitted for the NMR.

5.5.2.2 Manganese complexes

The manganese complex **Mn-1** (0.01 mmol, 10 mg) was treated with 1 eq. of AgOTf (0.01 mmol, 3 mg) in $CDCl_3$ (0.5 mL) in the glovebox. After stirred at rt for 1 h, the green suspension **Mn-2** was transferred into a Youngtube for the NMR analysis, before transferred back into the glovebox. Then 1 eq. of $CoCp_2$ (0.01 mmol, 2 mg) or $FeCp^*_2$ (0.01 mmol, 4 mg) was added into the reactions in parallel, generating the reduced manganese complex **Mn-1-red ($CoCp_2$)** or **Mn-1-red**, respectively. The addition of $CoCp_2$ turned the reaction mixture to be brown suspension, while $FeCp^*_2$ had no obvious effect on the color of the reaction mixture. After shaken for 1 h, the manganese complexes **Mn-1-red ($CoCp_2$)** and **Mn-1-red** were resubmitted for the NMR analysis. The procedures of adding 1 eq. of $CoCp_2$ (0.01 mmol, 2 mg) or $FeCp^*_2$ (0.01 mmol, 4 mg) into the reactions and submitting the Youngtubes for the NMR were carried out for twice, and the changes of the ^{31}P NMR of the corresponding manganese complexes were recorded.

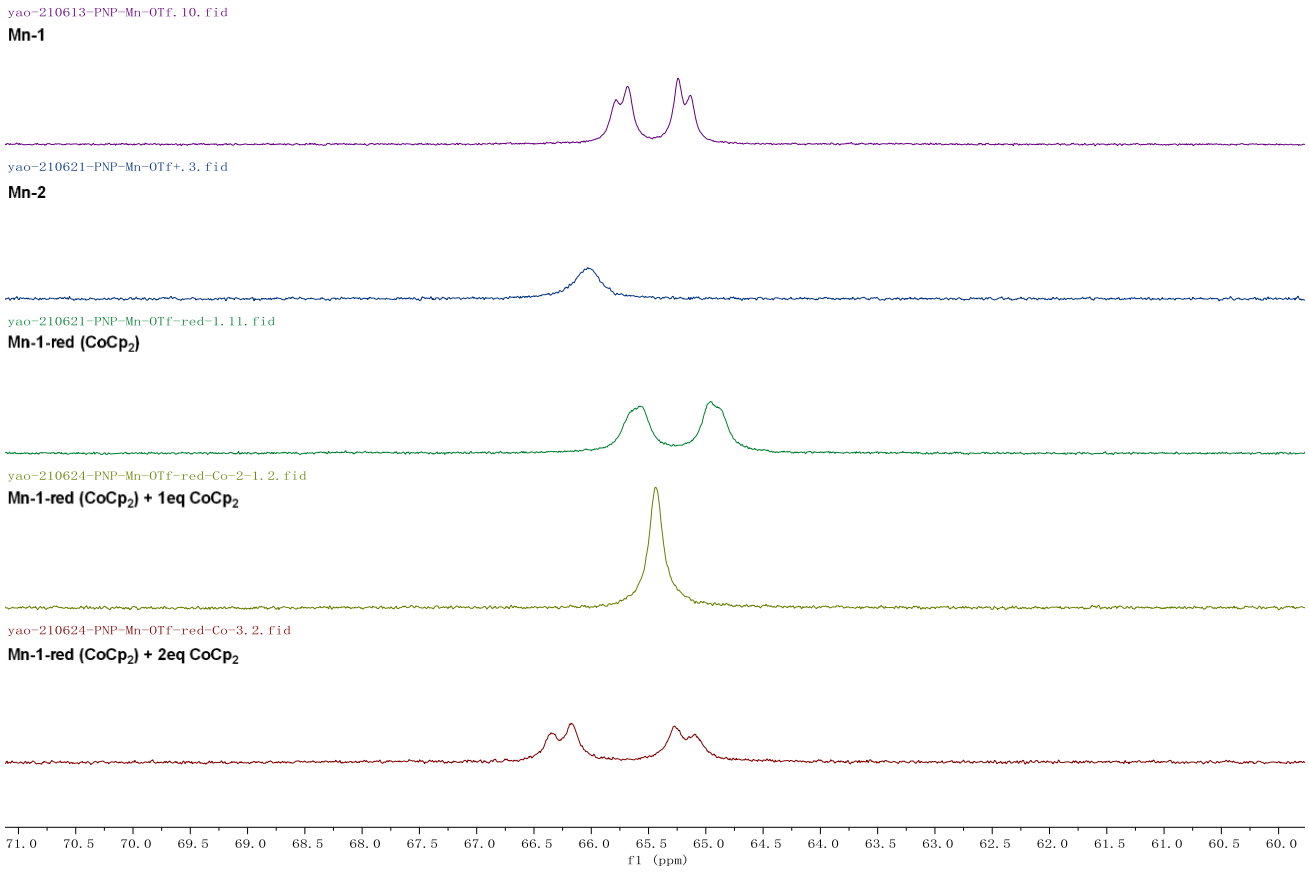

Figure 5.7 $^{31}P\{^{1}H\}$ NMR spectra of the manganese complexes reduced by $CoCp_2$

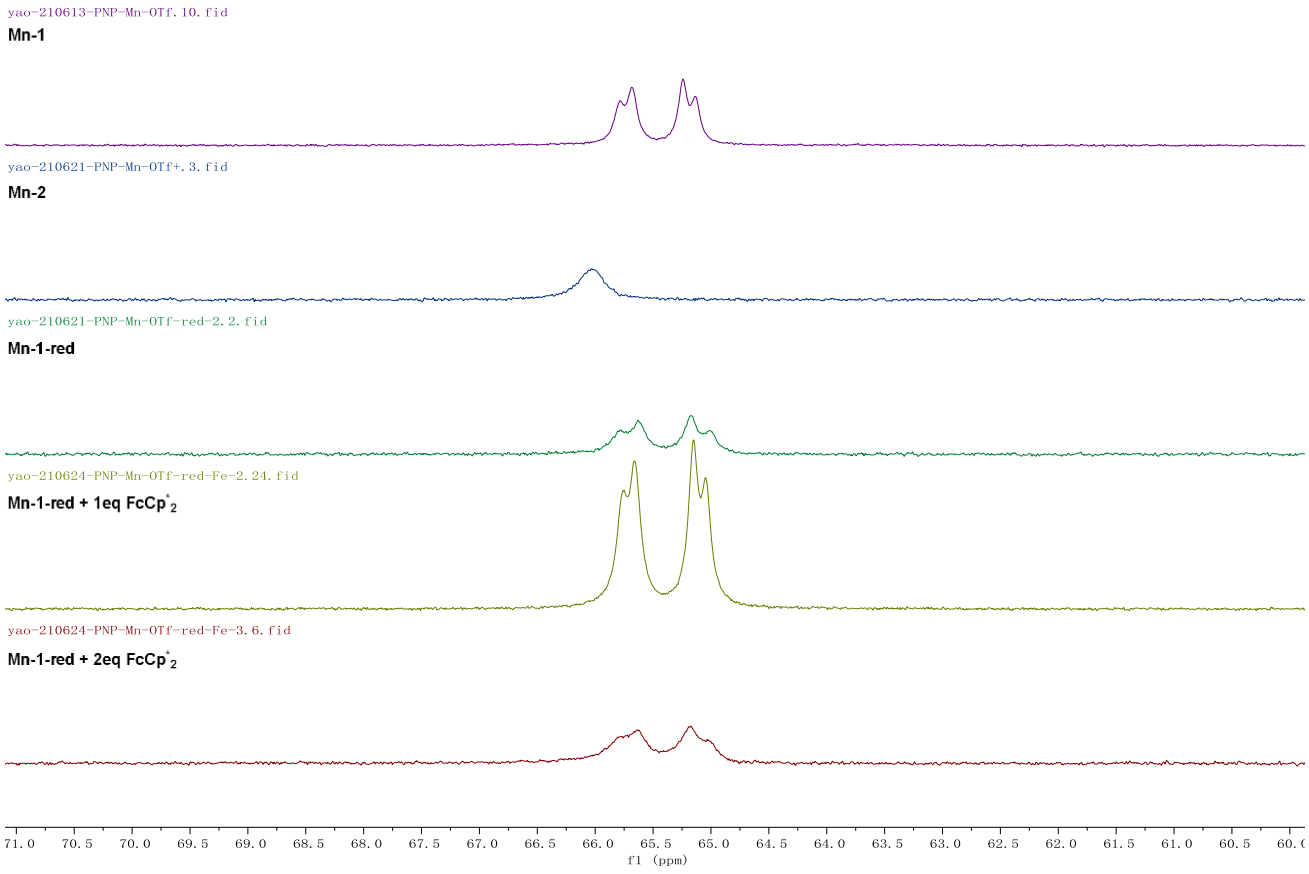

Figure 5.8 $^{31}P\{^{1}H\}$ NMR spectra of the manganese complexes reduced by $FeCp^{*}_{2}$

5.5.3 Asymmetric hydrogenation of acetophenone

In a glove box, to a vial (3 mL) was charged with the manganese complexes (1 mol %, 2 mg), KOH (2 mol %, 40 uL, 0.1 M in MeOH), substrate (0.2 mmol) and MeOH (0.4 mL). The vial was placed into the autoclave. The autoclave was sealed and purged three times with hydrogen gas, then pressurized to 40 bar and stirred at specific temperatures for 12 h. Afterwards, the vessel was vented carefully in a hood and the reaction mixture was concentrated *in vacuo*. The residue was purified by flash chromatography on silica (PE/EtOAc, 10/1) to remove the metal complex. The conversion was determined by ^{1}H-NMR and enantiomeric excess (ee) was determined by HPLC on a chiral stationary phase.

5.5.4 Electrochemistry

Cyclic voltammetry (CV) measurements were obtained for **PNP**, **Mn-1, Fc-SPO** and **Co-0** by using a BioAnalytical Systems Inc. (West Lafayette, IN) EC Epsilon potentiostat with a traditional three-electrode set-up, including a glassy carbon electrode as a W.E, a platinum wire as a C.E and a Ag/AgCl/3 M KCl electrode as a R.E. Before use, the platinium electrode was flamed, the Ag/AgCl/3 M KCl electrode was washed with dry MeCN and the carbon electrode was polished with alumina slurry (1.0 μm, 0.5 μm and 0.05 μm). The measurements were performed under standard CV conditions using 1.0 mM of ferrocenyl compounds and 1.0 mM of an internal reference dmfc in dry and degassed MeCN with a base electrolyte of 0.1 M tetrabutylammonium hexafluorophosphate ($TBAPF_6$) at rt. Molecular sieves and an argon balloon were employed to maintain the experiment under dry and argon conditions.

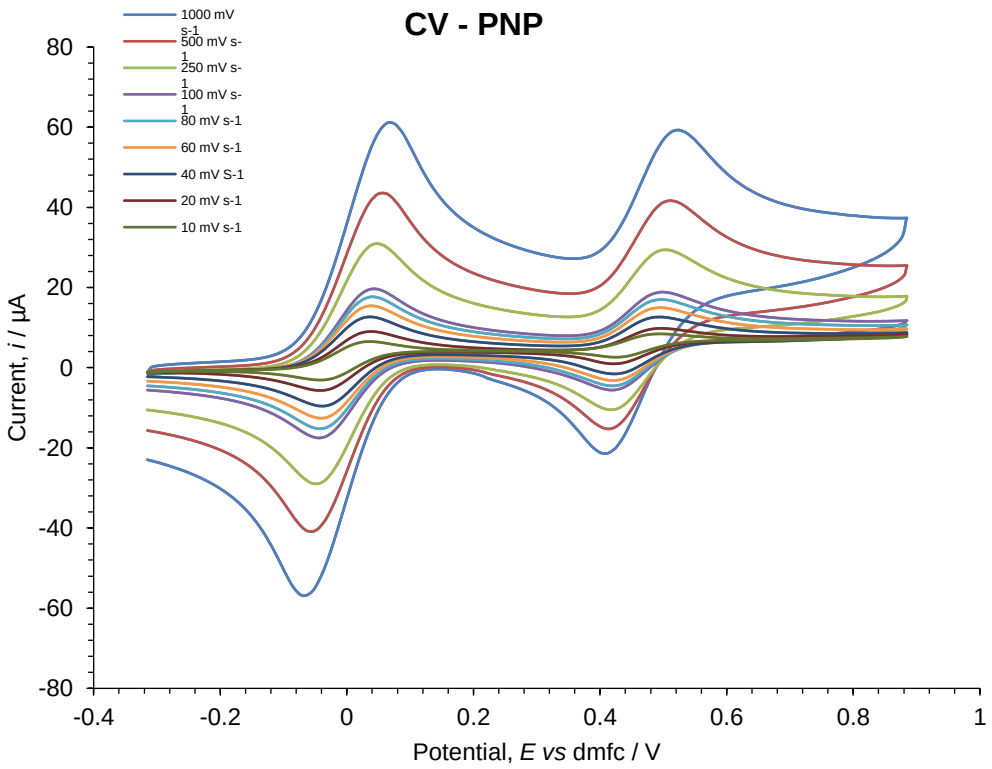

Figure 5.9 CV of **PNP** (1.0 mM) at various scan rates wrt dmfc (1.0 mM) in dry acetonitrile with an electrolyte of $TBAPF_6$ (0.1 M)

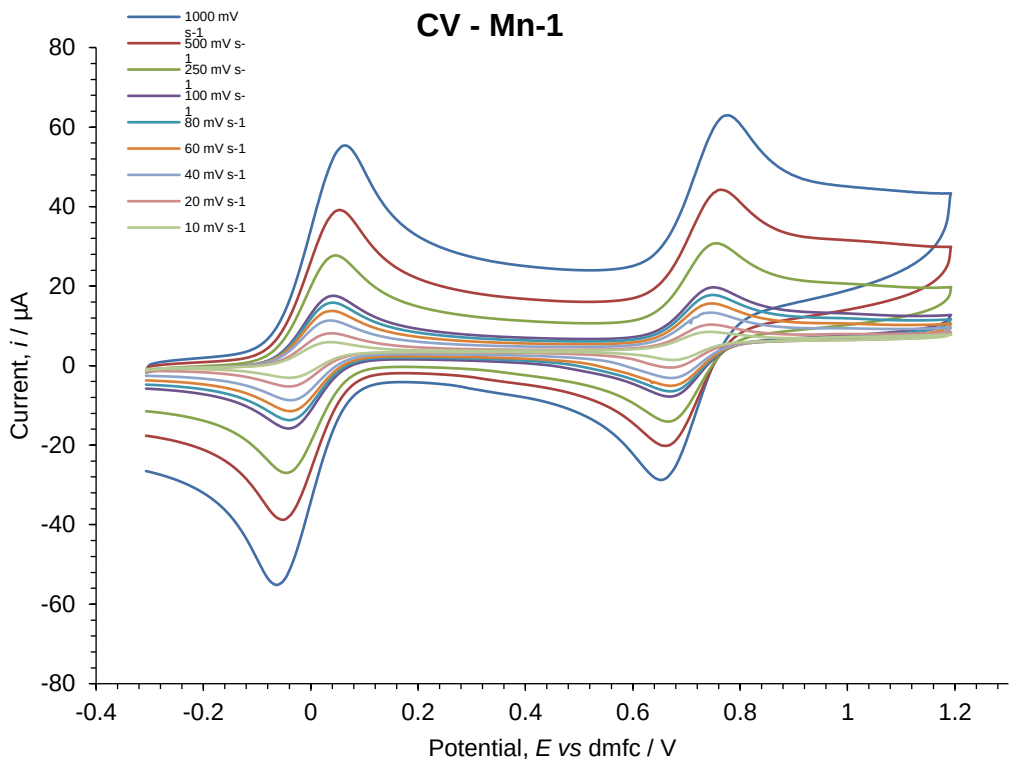

Figure 5.10 CV of **Mn-1** (1.0 mM) at various scan rates wrt dmfc (1.0 mM) in dry acetonitrile with an electrolyte of $TBAPF_6$ (0.1 M)

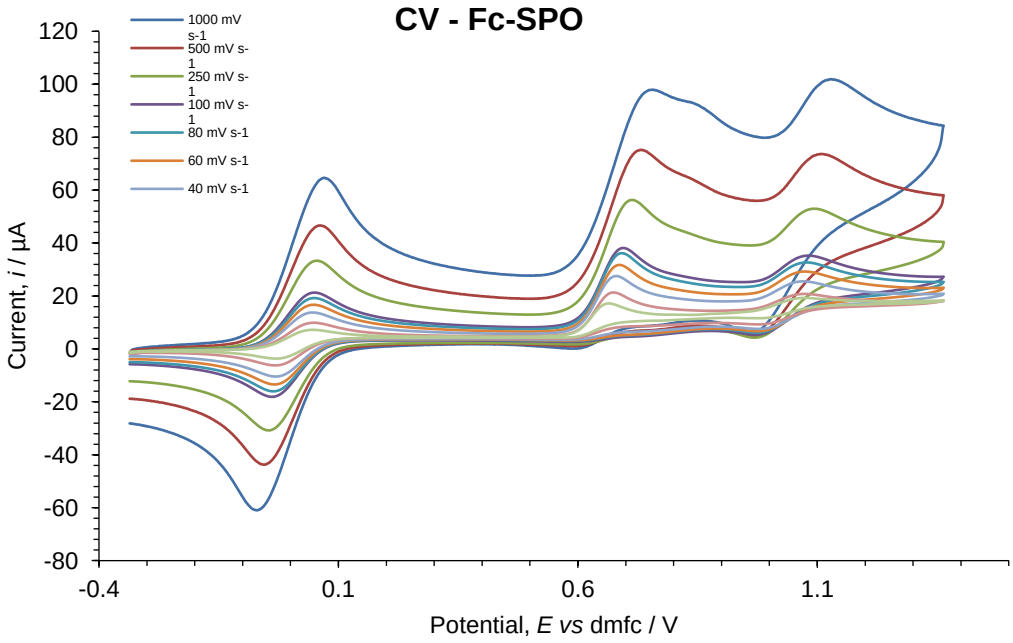

Figure 5.11 CV of **Fc-SPO** (1.0 mM) at various scan rates wrt dmfc (1.0 mM) in dry acetonitrile with an electrolyte of $TBAPF_6$ (0.1 M)

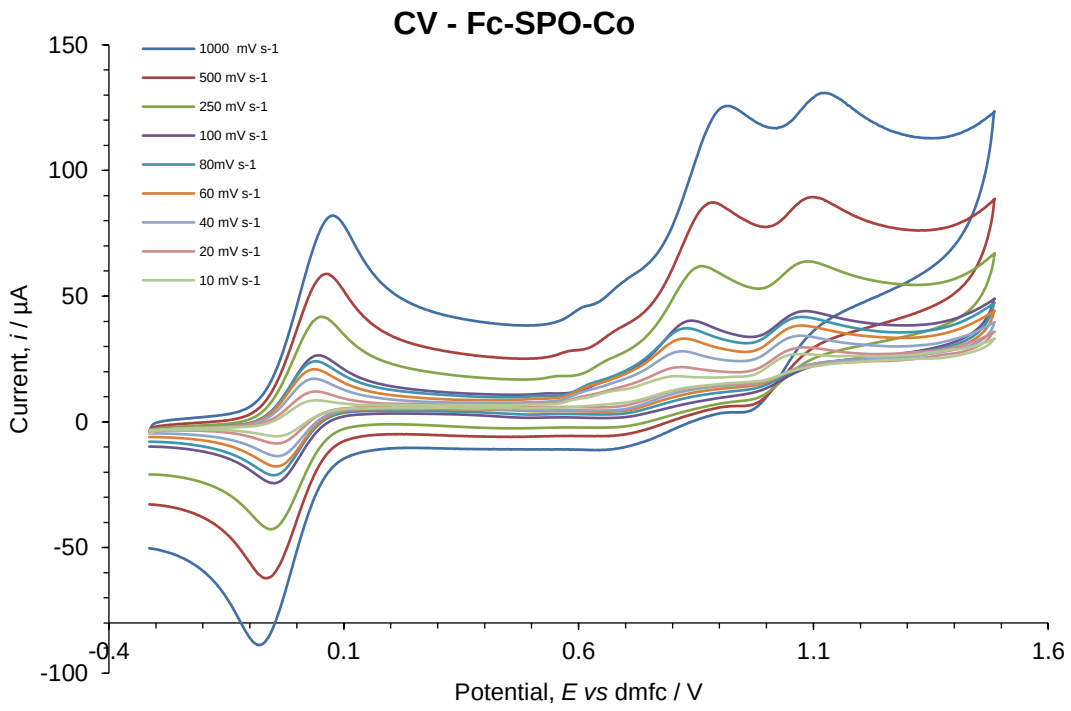

Figure 5.12 CV of **Co-0** (1.0 mM) at various scan rates wrt dmfc (1.0 mM) in dry acetonitrile with an electrolyte of $TBAPF_6$ (0.1 M)

5.6 Appendix

5.6.1 NMR spectra

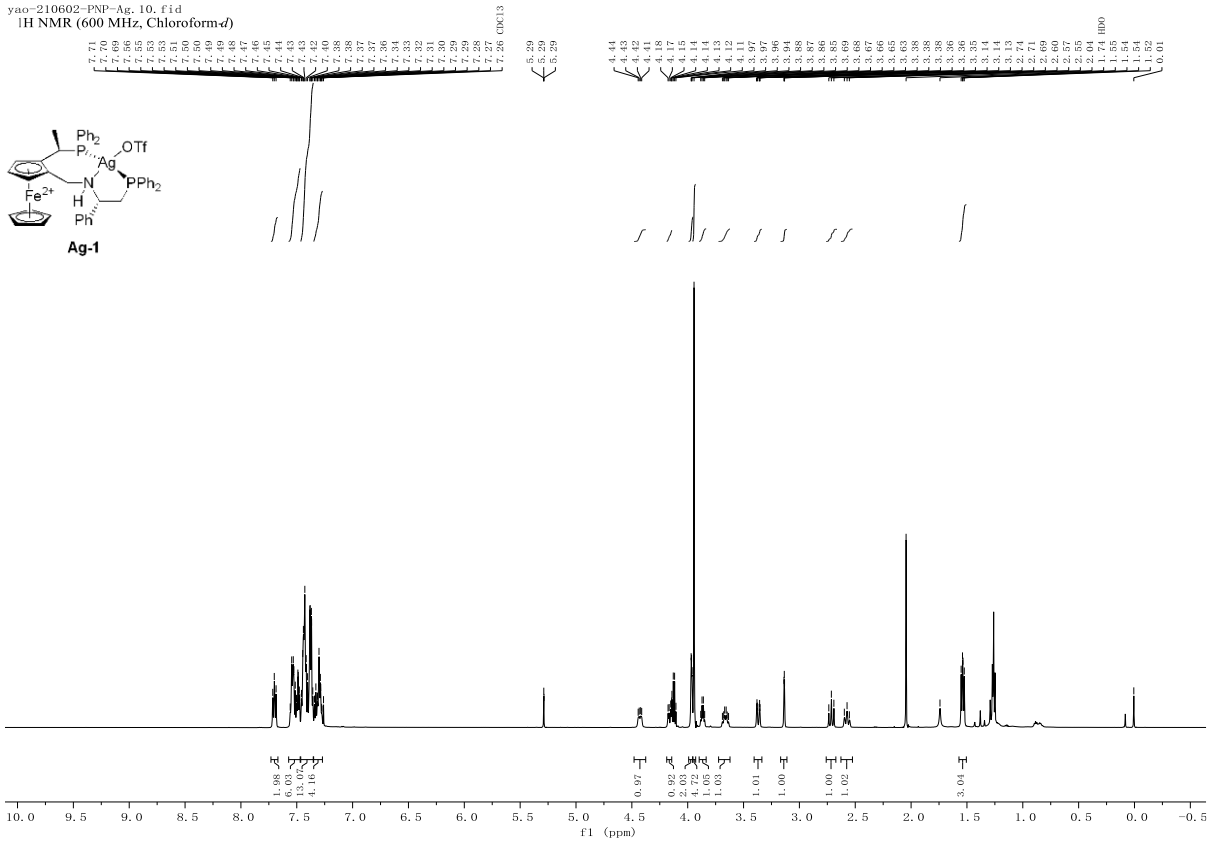

yao-200720-1-PNP+1.4.fid
^{13}C NMR (101 MHz, Chloroform-*d*)

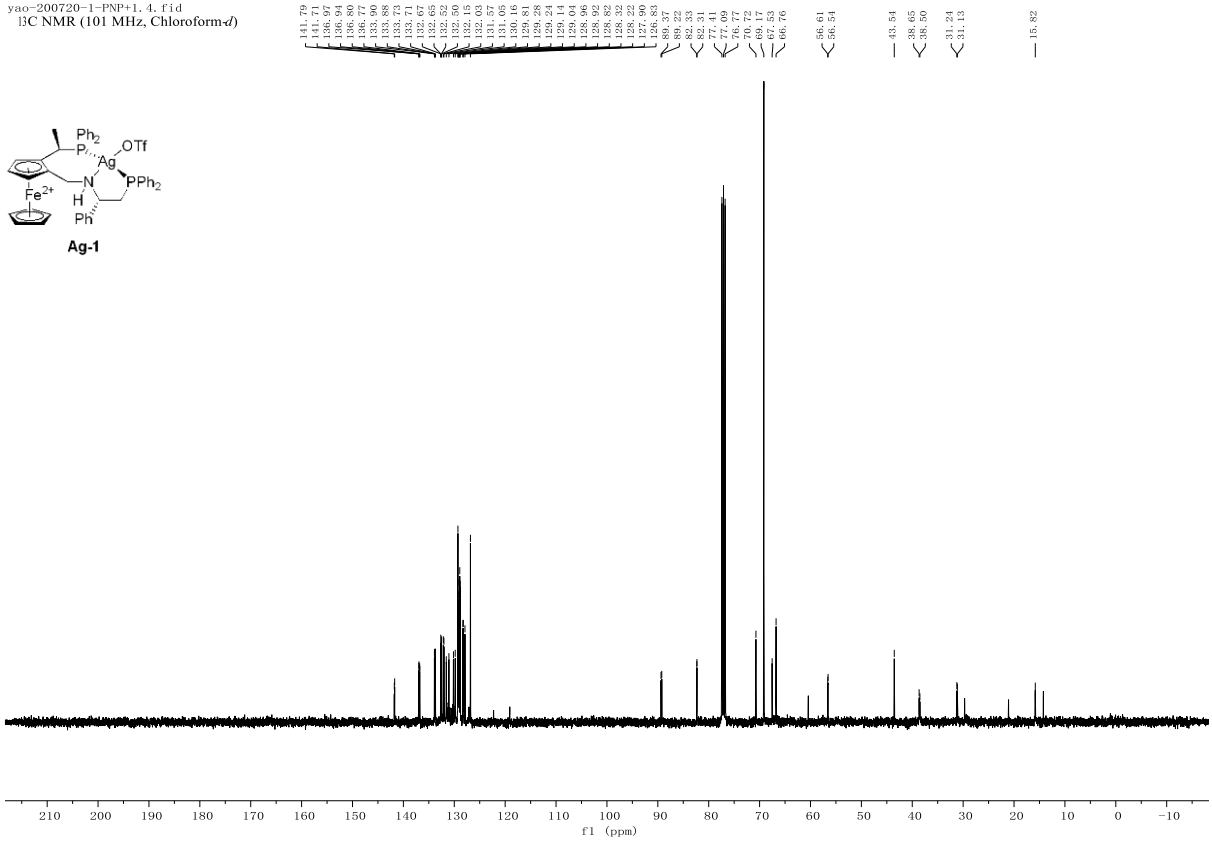

yao-200720-1-PNP+1.3.fid
^{19}F NMR (376 MHz, Chloroform-*d*)

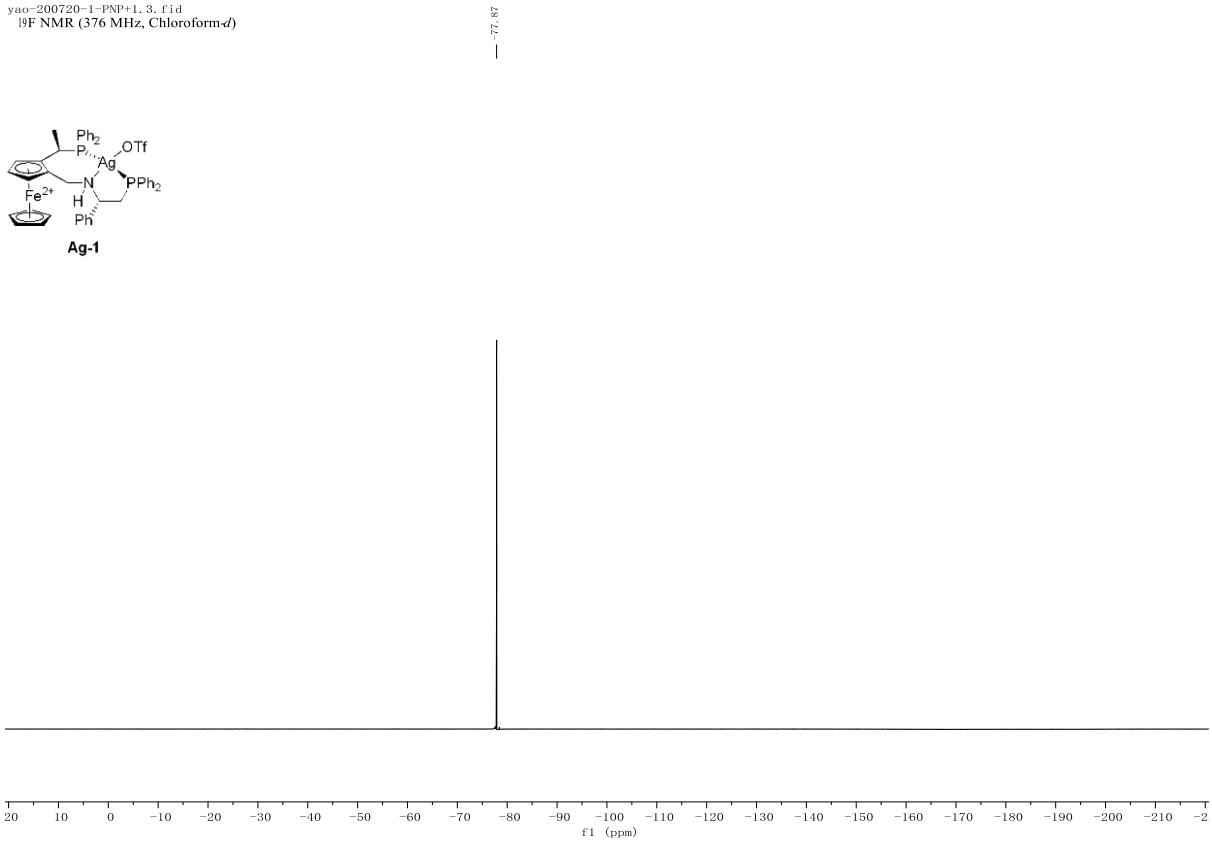

yao-200720-1-PNP+1.2.fid

31P NMR (162 MHz, Chloroform-*d*)

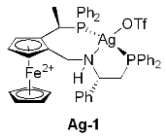

Ag-1

yao-210802-PNP-Mn-OTf.10.fid

1H NMR (600 MHz, Chloroform-*d*)

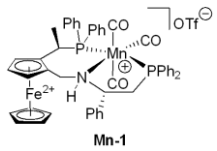

Mn-1

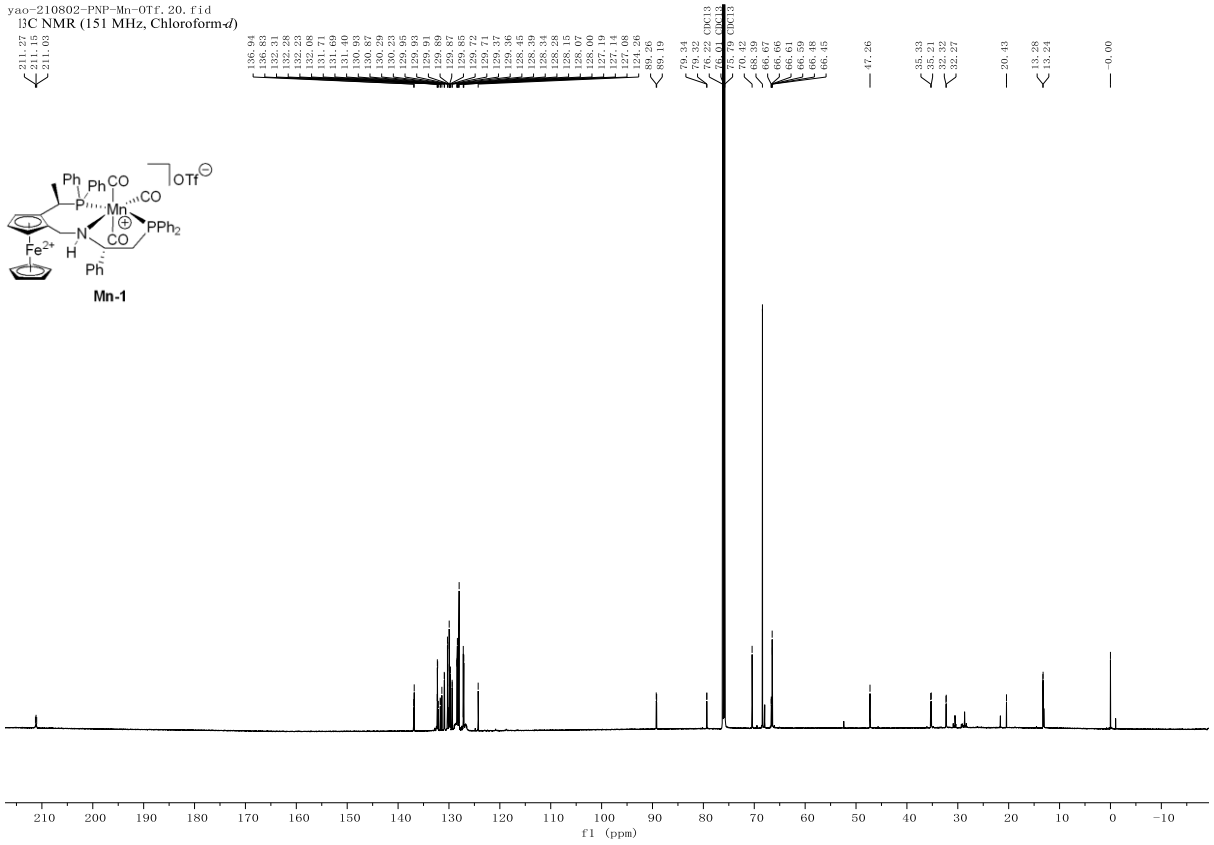
yao-210802-PNP-Mn-OTf. 20. fid
13C NMR (151 MHz, Chloroform-d)
211.27
211.15
211.03
136.94
136.83
132.31
132.28
132.23
132.08
131.71
131.69
131.40
130.93
130.87
130.39
130.23
129.95
129.93
129.91
129.89
129.87
129.85
129.72
129.71
129.37
129.36
128.45
128.39
128.34
128.28
128.15
128.09
127.19
127.14
127.08
124.26
89.26
89.19
79.34
79.32
76.22
CDCl3
75.79
75.47
CDCl3
68.39
66.67
66.66
66.61
66.59
66.48
66.45
47.26
35.33
35.21
32.32
32.27
20.43
13.28
13.24
0.00
Mn-1
210
200
190
180
170
160
150
140
130
120
110
100
90
80
70
60
50
40
30
20
10
0
−10
f1 (ppm)

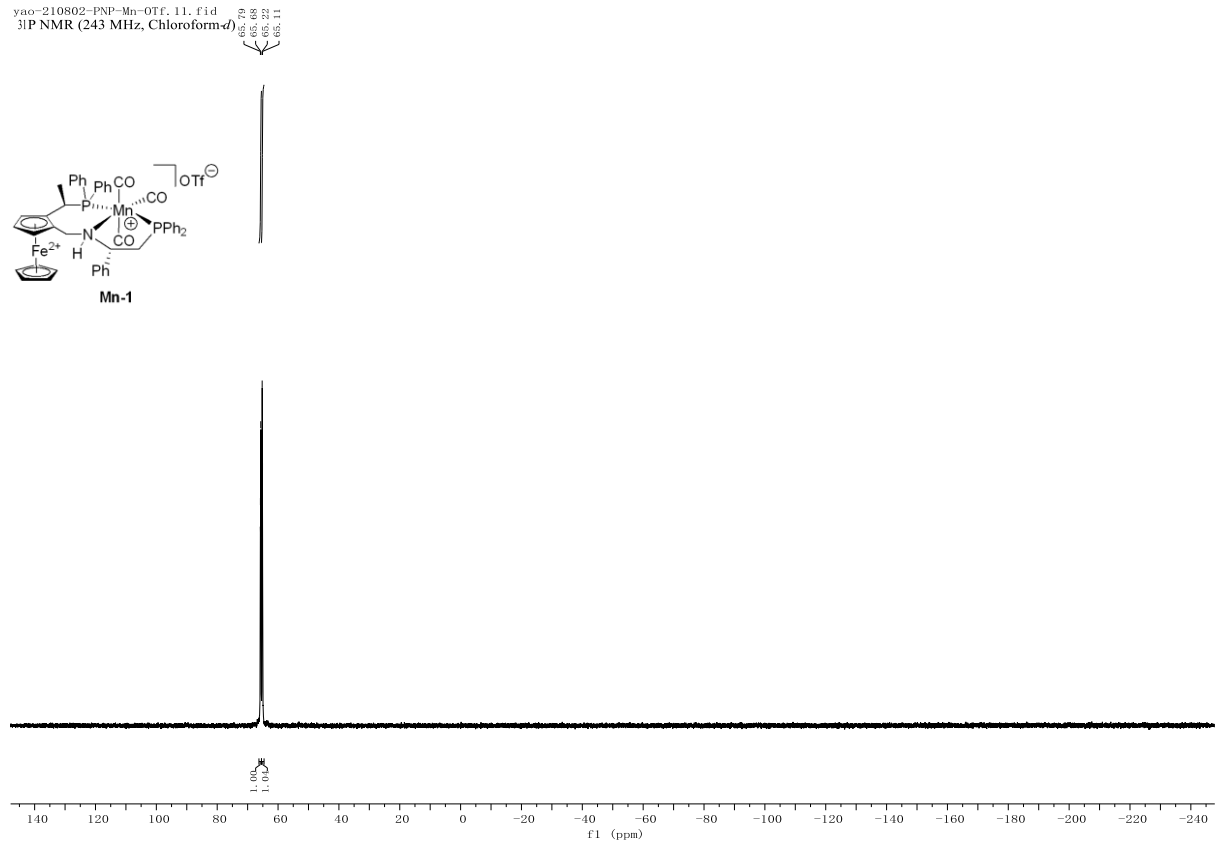
yao-210802-PNP-Mn-OTf. 11. fid
31P NMR (243 MHz, Chloroform-d)
65.79
65.68
65.22
65.11
Mn-1
1.00
1.00
140
120
100
80
60
40
20
0
−20
−40
−60
−80
−100
−120
−140
−160
−180
−200
−220
−240
f1 (ppm)

5.6.2 Crystal data

5.6.2.1 Crystal data for Mn-2

Table 5.3 Crystal data and structure refinement for **Mn-2**.

Identification code	**Mn-2**
Empirical formula	$C_{51}Cl_2F_6FeH_{46}MnNO_{11}P_2S_2$
Formula weight	1270.64
Temperature/K	100.0
Crystal system	orthorhombic
Space group	$P2_12_12_1$
a/Å	10.2293(4)
b/Å	12.9870(6)
c/Å	41.9708(15)
α/°	90
β/°	90
γ/°	90
Volume/Å^3	5575.7(4)
Z	4
ρ_{calc}g/cm^3	1.514
μ/mm^{-1}	6.736
F(000)	2592.0
Crystal size/mm^3	0.35 × 0.31 × 0.24
Radiation	CuKα (λ = 1.54178)
2Θ range for data collection/°	4.21 to 137.362
Index ranges	$-12 \leq h \leq 12$, $-15 \leq k \leq 15$, $-37 \leq l \leq 50$
Reflections collected	54727
Independent reflections	10271 [R_{int} = 0.0987, R_{sigma} = 0.0654]
Data/restraints/parameters	10271/680/604
Goodness-of-fit on F^2	1.071
Final R indexes [I>=2σ (I)]	R_1 = 0.1622, wR_2 = 0.3699
Final R indexes [all data]	R_1 = 0.1647, wR_2 = 0.3715
Largest diff. peak/hole / e Å^{-3}	1.61/-1.70
Flack parameter	0.19(2)

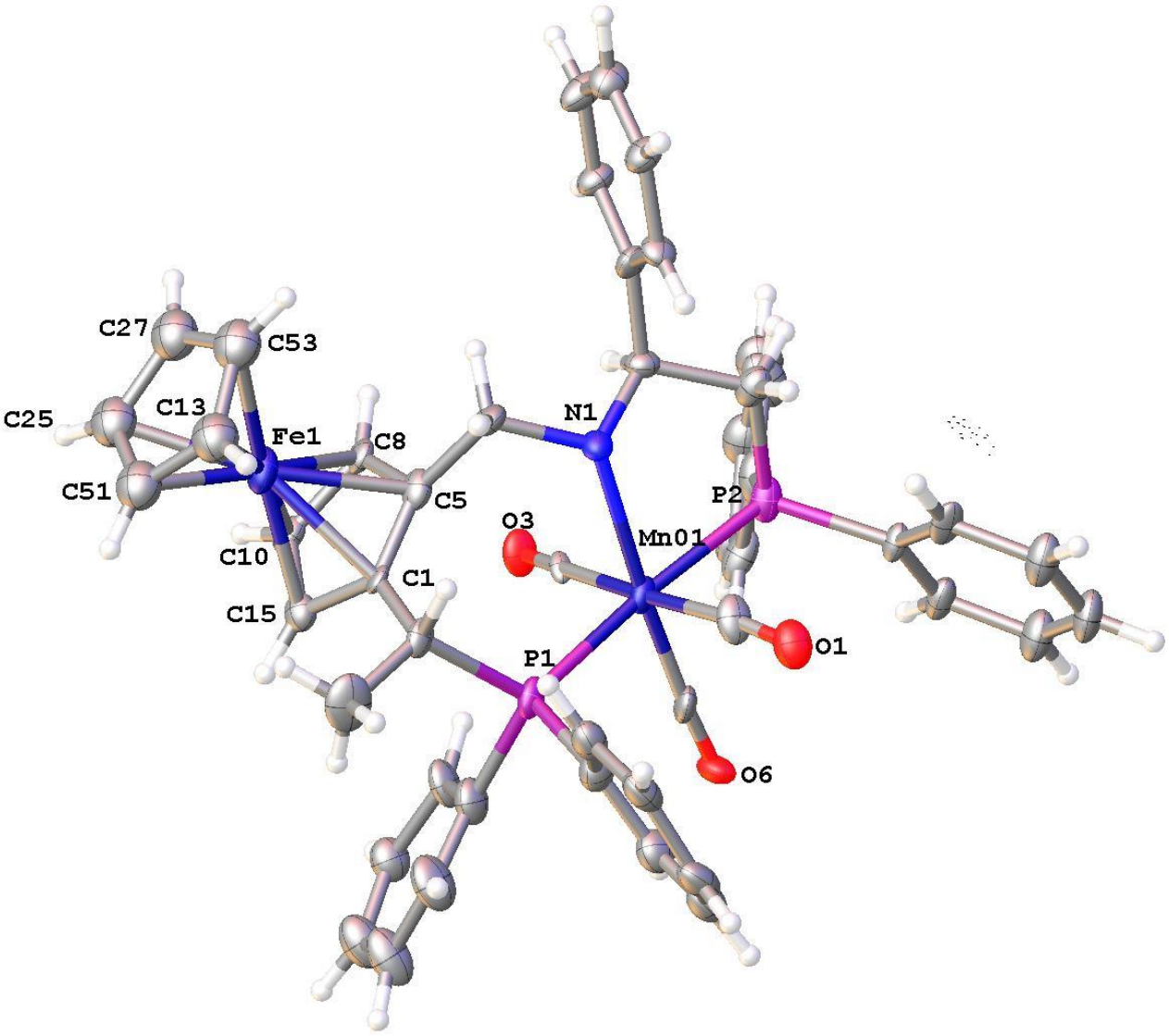

Figure 5.13 Crystal structure of **Mn-2** without showing counter ions, with ellipsoids drawn at the 50% probability level

5.7 References

[1] H. Grützmacher, *Angewandte Chemie International Edition* **2008**, *47*, 1814-1818.

[2] V. Lyaskovskyy, B. de Bruin, *ACS Catalysis* **2012**, *2*, 270-279.

[3] O. R. Luca, R. H. Crabtree, *Chem Soc Rev* **2013**, *42*, 1440-1459.

[4] V. Blanco, D. A. Leigh, V. Marcos, *Chem Soc Rev* **2015**, *44*, 5341-5370.

[5] J. Choudhury, *Tetrahedron Letters* **2018**, *59*, 487-495.

[6] E. Peris, *Chem Rev* **2018**, *118*, 9988-10031.

[7] Y. Ryu, G. Ahumada, C. W. Bielawski, *Chem Commun (Camb)* **2019**, *55*, 4451-4466.

[8] B. L. Thompson, C. R. Simons, Z. M. Heiden, *Chem Commun (Camb)* **2019**, *55*, 11430-11433.

[9] I. M. Lorkovic, R. R. Duff, M. S. Wrighton, *Journal of the American Chemical Society* **1995**, *117*, 3617-3618.

[10] M. Sussner, H. Plenio, *Angew Chem Int Ed Engl* **2005**, *44*, 6885-6888.

[11] G. Liu, H. He, J. Wang, *Advanced Synthesis & Catalysis* **2009**, *351*, 1610-1620.

[12] K. Arumugam, C. D. Varnado, Jr., S. Sproules, V. M. Lynch, C. W. Bielawski, *Chemistry* **2013**, *19*, 10866-10875.

[13] R. Savka, S. Foro, M. Gallei, M. Rehahn, H. Plenio, *Chemistry* **2013**, *19*, 10655-10662.

[14] C. D. Varnado, Jr., E. L. Rosen, M. S. Collins, V. M. Lynch, C. W. Bielawski, *Dalton Trans* **2013**, *42*, 13251-13264.

[15] S. M. Guillaume, E. Kirillov, Y. Sarazin, J. F. Carpentier, *Chemistry* **2015**, *21*, 7988-8003.

[16] A. J. Teator, D. N. Lastovickova, C. W. Bielawski, *Chem Rev* **2016**, *116*, 1969-1992.

[17] A. Feyrer, F. Breher, *Inorganic Chemistry Frontiers* **2017**, *4*, 1125-1134.

[18] M. Zhao, C. Chen, *ACS Catalysis* **2017**, *7*, 7490-7494.

[19] C. Chen, *ACS Catalysis* **2018**, *8*, 5506-5514.

[20] J. Wei, P. L. Diaconescu, *Acc Chem Res* **2019**, *52*, 415-424.

[21] A. M. Doerr, J. M. Burroughs, N. M. Legaux, B. K. Long, *Catalysis Science & Technology* **2020**, *10*, 6501-6510.

[22] C. K. Gregson, I. J. Blackmore, V. C. Gibson, N. J. Long, E. L. Marshall, A. J. White, *Dalton Trans* **2006**, 3134-3140.

[23] E. M. Broderick, P. S. Thuy-Boun, N. Guo, C. S. Vogel, J. Sutter, J. T. Miller, K. Meyer, P. L. Diaconescu, *Inorg Chem* **2011**, *50*, 2870-2877.

[24] P. Veit, C. Volkert, C. Forster, V. Ksenofontov, S. Schlicher, M. Bauer, K. Heinze, *Chem Commun (Camb)* **2019**, *55*, 4615-4618.

[25] L. Hettmanczyk, S. Manck, C. Hoyer, S. Hohloch, B. Sarkar, *Chem Commun (Camb)* **2015**, *51*, 10949-10952.

[26] L. Hettmanczyk, L. Suntrup, S. Klenk, C. Hoyer, B. Sarkar, *Chemistry* **2017**, *23*, 576-585.

[27] S. Klenk, S. Rupf, L. Suntrup, M. van der Meer, B. Sarkar, *Organometallics* **2017**, *36*, 2026-2035.

[28] S. M. Shepard, P. L. Diaconescu, *Organometallics* **2016**, *35*, 2446-2453.

[29] S. Ibáñez, M. Poyatos, E. Peris, *ChemCatChem* **2016**, *8*, 3790-3795.

[30] J. Popp, A. M. Caminade, E. Hey‐Hawkins, *European Journal of Inorganic Chemistry* **2020**, *2020*, 1654-1669.

[31] P. Neumann, H. Dib, A. M. Caminade, E. Hey-Hawkins, *Angew Chem Int Ed Engl* **2015**, *54*, 311-314.

[32] J. D. Carr, S. J. Coles, M. B. Hursthouse, M. E. Light, E. L. Munro, J. H. R. Tucker, J. Westwood, *Organometallics* **2000**, *19*, 3312-3315.

Chapter 6 DNA-Organometallic Scaffolds for Asymmetric Catalysis

6.1 Introduction

Metalloenzymes often provide high efficiencies and selectivities for challenging reactions under mild conditions.[1] This is largely attributed to the second coordination sphere comprised of various functional groups, which generates supramolecular interactions (e.g. Van der Waals forces, π interactions, electrostatic interactions and hydrogen bonds) to activate substrates and stabilize transition states.[2-6] This reaction model provides a considerable inspiration for the development of new synthetic catalysts. Artificial metalloenzymes[7-8] have been designed by incorporating catalytically active transition-metal complexes into biomolecular scaffolds, such as proteins[9-15] and DNA[16-18], affording promising efficiencies for a series of asymmetric reactions. As an elegant example of chirality in nature, double helical DNA has become an attractive chiral biomolecular scaffold for hybrid catalysts for asymmetric catalysis.[19-24] The major and minor grooves of its secondary structure are involved in the second coordination sphere interactions, providing unique chiral microenvironments for anchoring transition metal complexes and substrates. [8, 17] Furthermore, the high water-solubility of DNA makes it ideal for reactions in water, which is a very important consideration in green chemistry.[25]

6.1.1 Supramolecular anchoring

In 2005, Feringa and Roelfes reported the first example of DNA-based asymmetric catalysis, using the chirality of DNA to control stereoselectivity for a metal-catalysed reaction.[19] They described the asymmetric Diels-Alder reaction of cyclopentadiene with aza chalcone in water catalysed by the Cu-DNA hybrid catalysts, combining an achiral 9-aminoacridine copper complex with chiral salmon testes DNA (st-DNA) via supramolecular self-assembly through acridine intercalation (Scheme 6.1). Up to 53% for the major (endo) isomer and up to 90% for the minor (exo) isomer products were obtained. Shortly thereafter, they used the same catalyst system with ligand 4,4′-dimethyl-bipyridine (dmbipy)

instead of 9-aminoacridine compounds to achieve excellent regioselectivity (up to >99% endo) and enantioselectivity (up to >99% ee) for the same Diels-Alder reaction.[26]

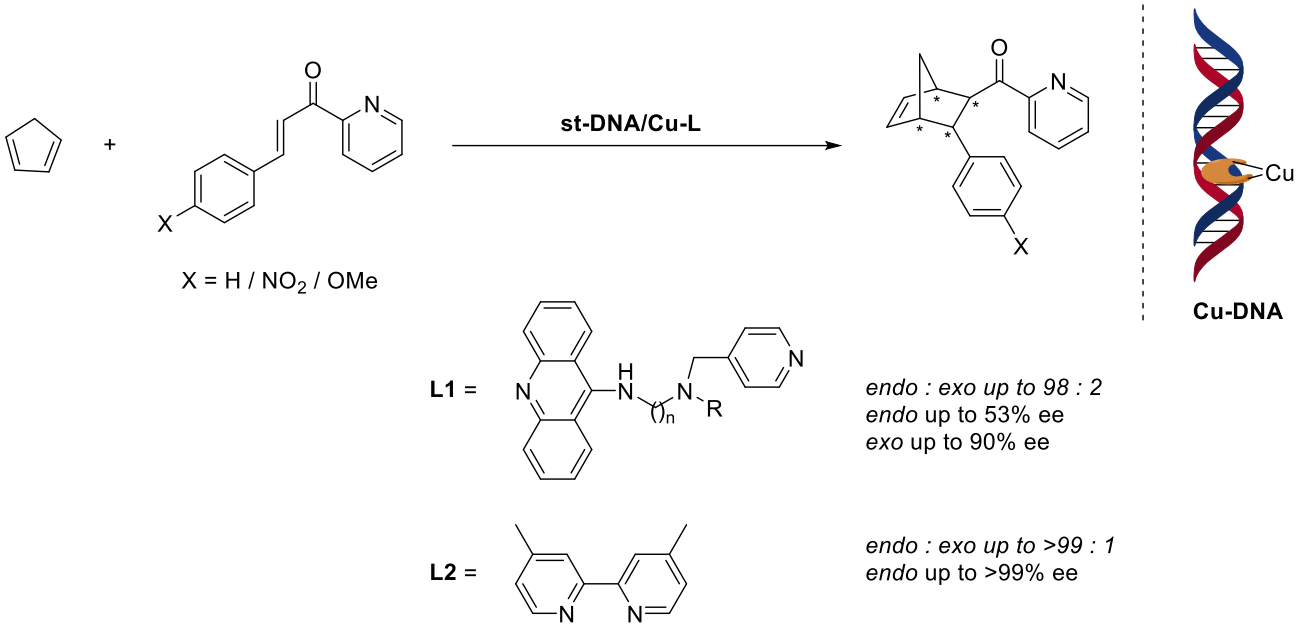

Scheme 6.1 DNA-based hybrid catalysts for asymmetric Diels-Alder reaction of cyclopentadiene with aza chalcone

Since this pioneering work, DNA-based hybrid catalysts through a supramolecular anchoring strategy have aroused considerable attention in the field of asymmetric catalysis. This approach has been applied successfully to varieties of enantioselective reactions. In 2007, Feringa and Roelfes et al reported that unsaturated 2-acyl imidazoles could be used as alternative and practical dienophiles for the enantioselective Diels-Alder reaction in water catalysed by the **st-DNA/Cu-dmbipy** catalyst, giving the products with high enantioselectivities (up to 98% ee) (Scheme 6.2).[27]

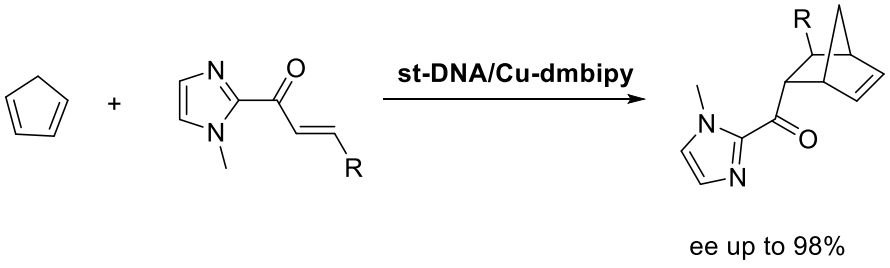

Scheme 6.2. Enantioselective Diels-Alder reaction of cyclopentadiene with α, β -unsaturated 2-acyl imidazoles

Feringa and Roelfes et al also found that unsaturated 2-acyl imidazoles could act as Michael acceptors in the asymmetric Michael addition in water catalysed by the **st-DNA/Cu-dmbipy** catalyst, achieving up to 99% ee with dimethyl malonate or nitromethane as the nucleophile (Scheme 6.3).[28] A notable fact is that the previous best result of the catalytic asymmetric Michael additions in water was up to 86% ee for the products, using a Pd–BINAP complex as the catalyst.[29]

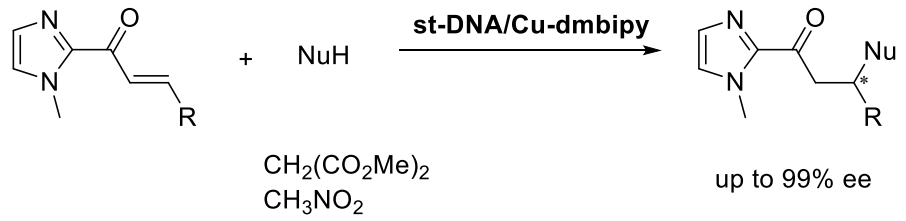

Scheme 6.3. Asymmetric Michael addition of α, β -unsaturated 2-acyl imidazoles

In 2009, Feringa and Roelfes et al reported the first asymmetric Friedel–Crafts reaction catalysed by the **st-DNA/Cu-dmbipy** catalyst in water, using unsaturated 2-acyl imidazoles as electrophiles to react with 5-methoxyindole under aqueous conditions, resulting in up to 93% ee for the corresponding products (Scheme 6.4).[30]

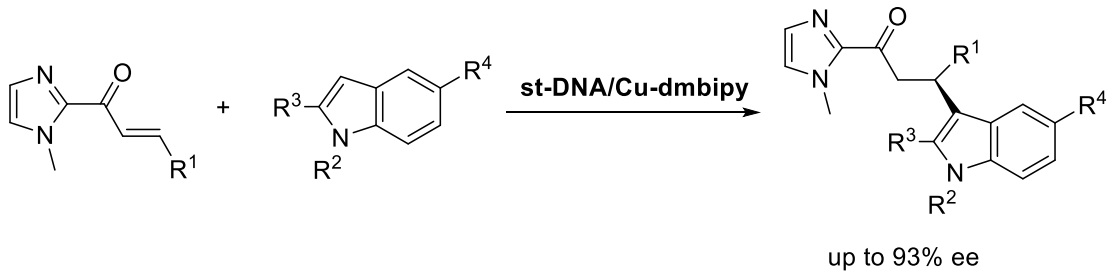

Scheme 6.4. Asymmetric Friedel-Crafts reaction of α, β -unsaturated 2-acyl imidazoles

Wang and Arseniyadis et al reported that the use of unnatural left-handed DNA could provide the opposite enantiomers of the products for the Diels-Alder, Michael addition, and Friedel-Crafts reaction catalysed by the **st-DNA/Cu-dmbipy** catalyst.[31]

In addition to the carbon-carbon bond-forming reactions, carbon-heteroatom bond-forming reactions were achieved by the Toru group in the form of electrophilic fluorination reactions.[32] By using the **st-DNA/Cu-dmbipy** catalyst, fluorination of indanone ketoesters with selectfluor worked in an aqueous buffer, giving up to 74% ee for the products (Scheme 6.5).

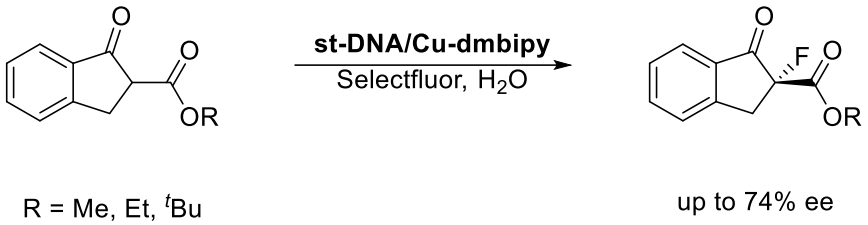

Scheme 6.5 Enantioselective C-F bond formation.

In 2010, Feringa and Roelfes et al exhibited the first example of enantioselective *syn* hydration of α,β-unsaturated ketones catalysed by **st-DNA/Cu-L** catalysts, giving β-hydroxy ketone products with up to 82% ee (Scheme 6.6).[33]

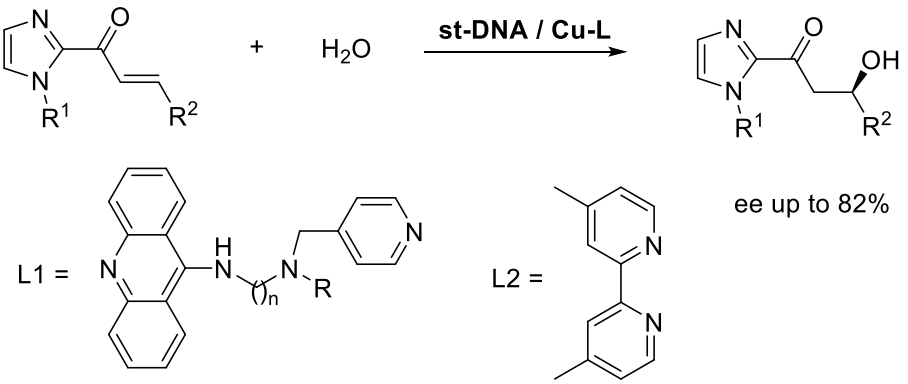

Scheme 6.6 Enantioselective hydration of a,ß-unsaturated ketones

In 2013, the Roelfes group reported the first copper-catalysed asymmetric cyclopropanation in water, known as the first example of DNA-based organometallic catalysis in water.[34] By using **st-DNA/Cu(II)-dppz** catalyst, the asymmetric intramolecular cyclopropanation of sulfones in water was achieved with up to 84% ee for the products (Scheme 6.7).

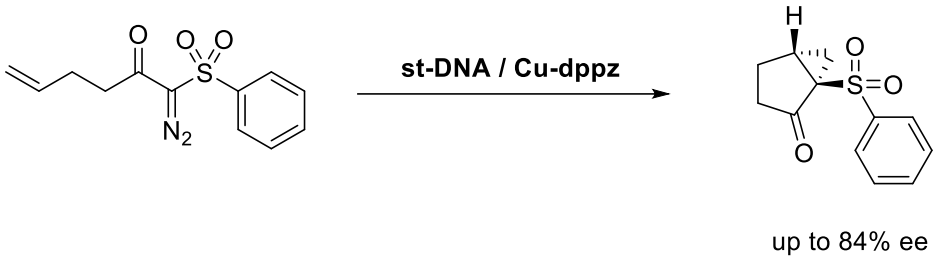

Scheme 6.7 Asymmetric intramolecular cyclopropanation of α-diazo- β -keto sulfone

In 2016, the Roelfes group reported that a catalytic carbene-transfer reaction such as enantioselective cyclopropanation of styrene derivatives was carried out in water, under mild conditions and an ambient atmosphere.[35] It was catalysed by a **st-DNA/ Fe(III)-porphyrin** hybrid catalyst, providing promising ee values for the corresponding cyclopropanation products (Scheme 6.8).

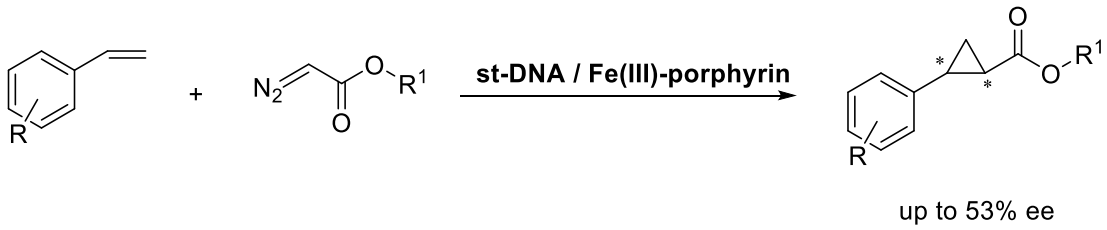

Scheme 6.8 Enantioselective cyclopropanation of styrene derivatives

6.1.2 Covalent anchoring

In most of these reactions, DNA has a double role, transferring its chirality to the products and accelerating the reaction rates. The supramolecular anchoring approach using intercalators and groove binders has allowed for quick testing and optimization in identifying the best hybrid catalysts.[20] However, the existence of multiple binding positions in DNA gives less control over altering and optimising the local (e.g base) environment to affect and improve catalytic efficiencies. Based on this issue, a more controllable anchoring approach involving covalent attachment to DNA has also been reported in the literature,[36-42] via either pre- or post-synthetic modification. Such modifications can be achieved by covalently binding or replacing a ligand to the nucleobase or phosphate ester of the

DNA. In principle, this approach would enable more precise control over the active site for catalysis, with the immediate DNA base environment having a more direct role, but of course at the expense of a more time-consuming and complicated approach to the scaffold design.[1, 20]

In 2007, Jaschke et al. reported the introduction of phosphine groups on nucleobases.[39] In this example, DNA bases were functionalized post-synthetically with a series of phosphines via amide linker (Scheme 6.9). However, phosphine oxidation caused a considerable issue. Subsequently, they developed other DNA-based hybrid ligands based on the same system using diene-modified instead of phosphine-modified DNA bases, providing only up to 28% ee for iridium(I)-catalysed asymmetric allylic amination of phenyl allyl acetate in aqueous medium.[40]

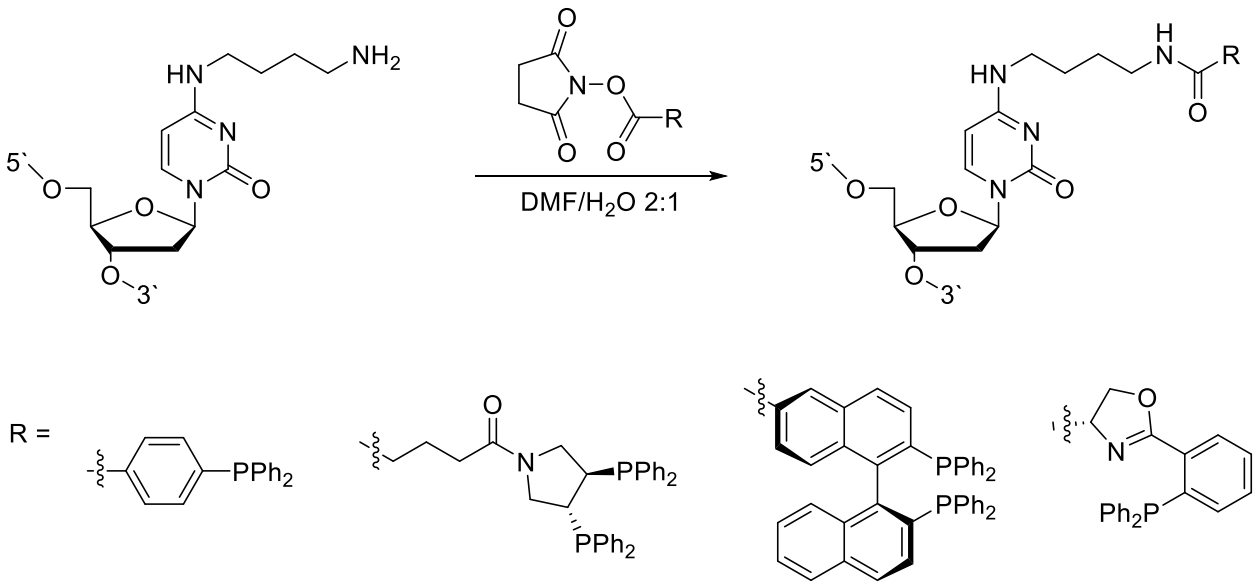

Scheme 6.9 Post-synthetically functionalized DNA bases with phosphines

In 2008, the Roelfes group introduced the design and synthesis of a covalently anchored DNA-Cu hybrid catalyst,[41] starting with the functionalization of terminally amino-modified oligonucleotide ODN1, and following with the hybridization of ODN1, ODN2 and a template oligonucleotide in the presence of a metal ion. ODN1 was commercially available or prepared through solid-phase synthesis,

and the template oligonucleotide was complementary to both ODN1 and ODN2. The **DNA-Cu** catalyst afforded up to 93% ee values for the asymmetric Diels–Alder reaction of aza-chalcone with cyclopentadiene in water (Scheme 6.10).

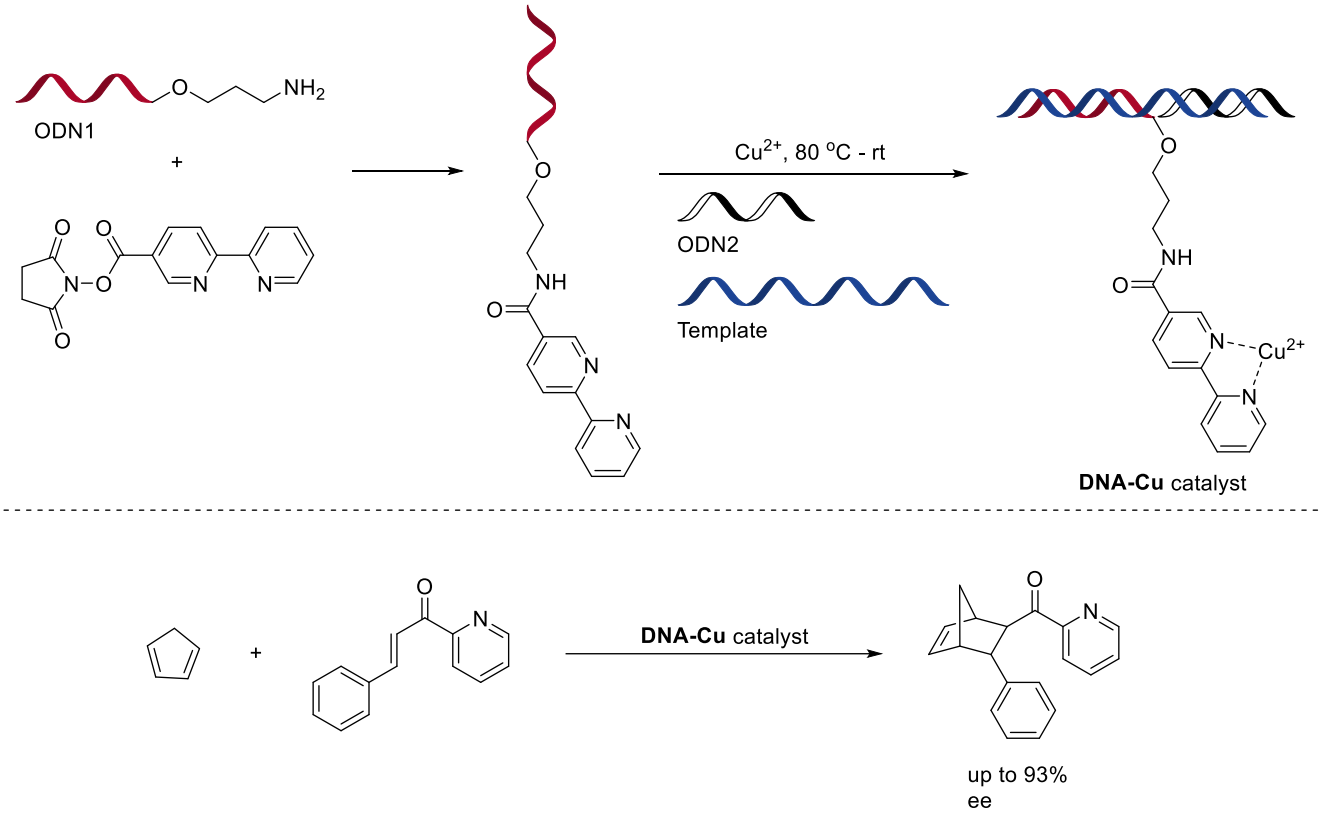

Scheme 6.10 Asymmetric Diels–Alder reaction of aza-chalcone with cyclopentadiene

In 2014, Sugiyama et al. developed a new class of DNA-based hybrid catalysts by directly incorporating a bipyridine ligand into the DNA phosphate backbone.[43] The hybrid catalysts were applied for asymmetric intramolecular Friedel-Crafts alkylations, affording the products with up to 84% ee (Scheme 6.11).

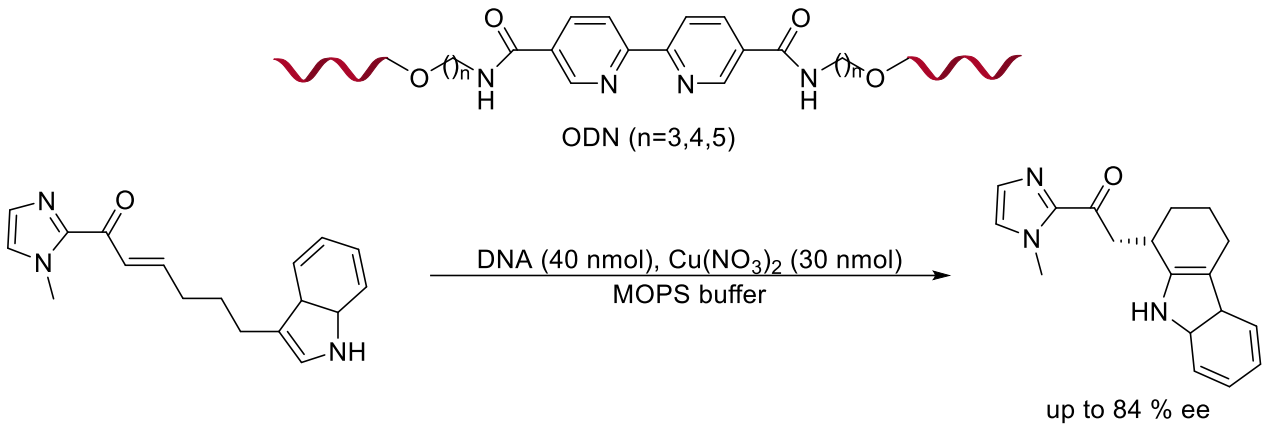

Scheme 6.11 Asymmetric intramolecular Friedel-Crafts alkylations

6.2 Project aim

There is extensive literature on ferrocenyl phosphine metal catalysis, which has been reviewed in detail in Chapter 1. It is considerable to incorporate such systems into DNA. At the same time, examples of ferrocene in DNA have been reported. In 2012, Tucker and co-workers successfully demonstrated ferrocene as a substitute of the sugar-phosphate backbone in a nucleic acid.[44] However, could we make heterobimetallic DNA systems (Fe and catalysis metal)? Inspired by Tucker's work, we designed a novel type of DNA-based hybrid catalysts by directly incorporating a ferrocenyl phosphine ligand into the DNA phosphate backbone (Scheme 6.12).

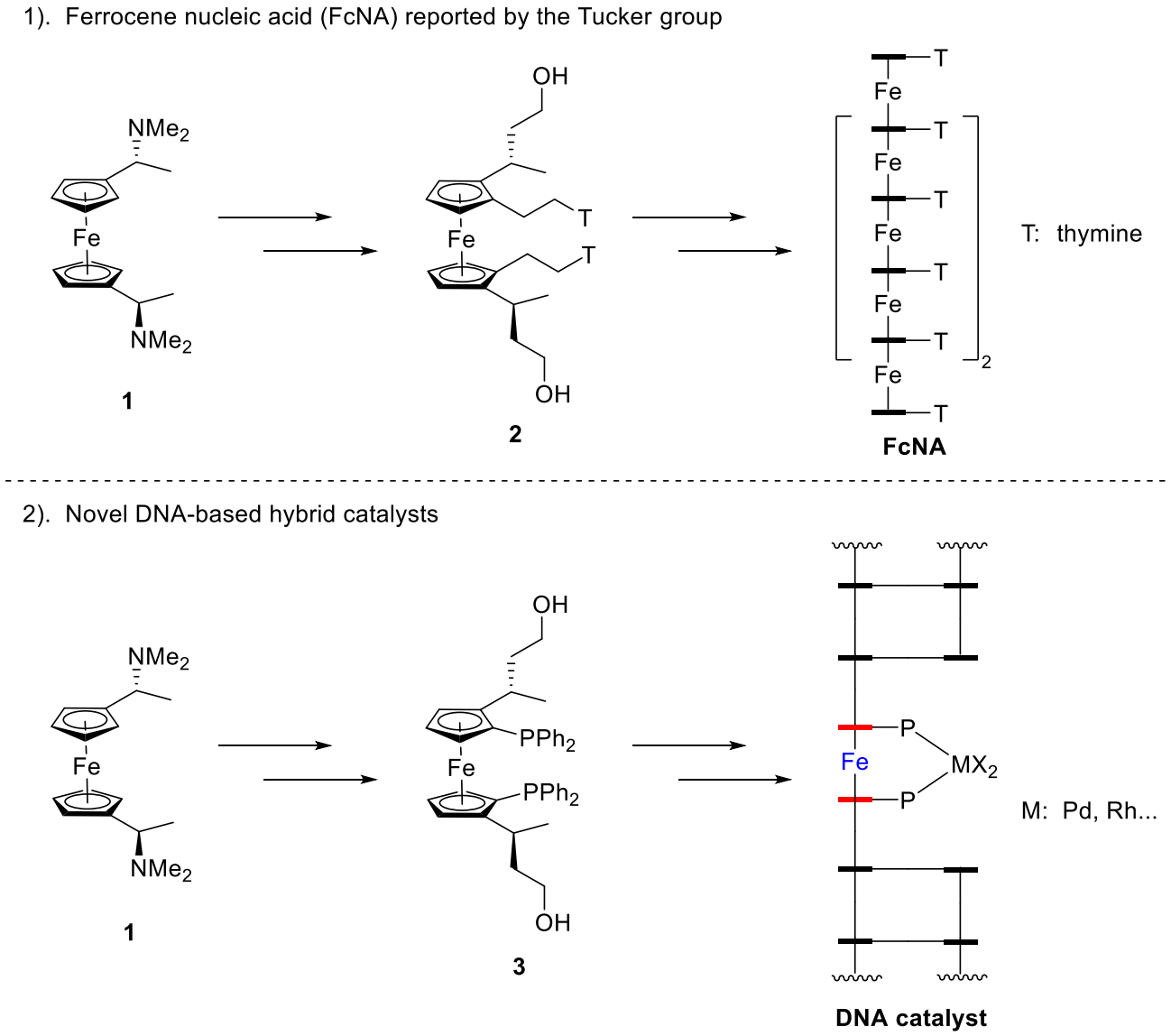

Scheme 6.12 Design of the novel DNA-based hybrid catalysts

6.3 Results and discussion

6.3.1 Synthesis of the ferrocenyl phosphine monomers

The ferrocenyl phosphine monomer was successfully prepared via a modification of Tucker's previously reported route[44] towards chiral tetrasubstituted ferrocences (Scheme 6.13).

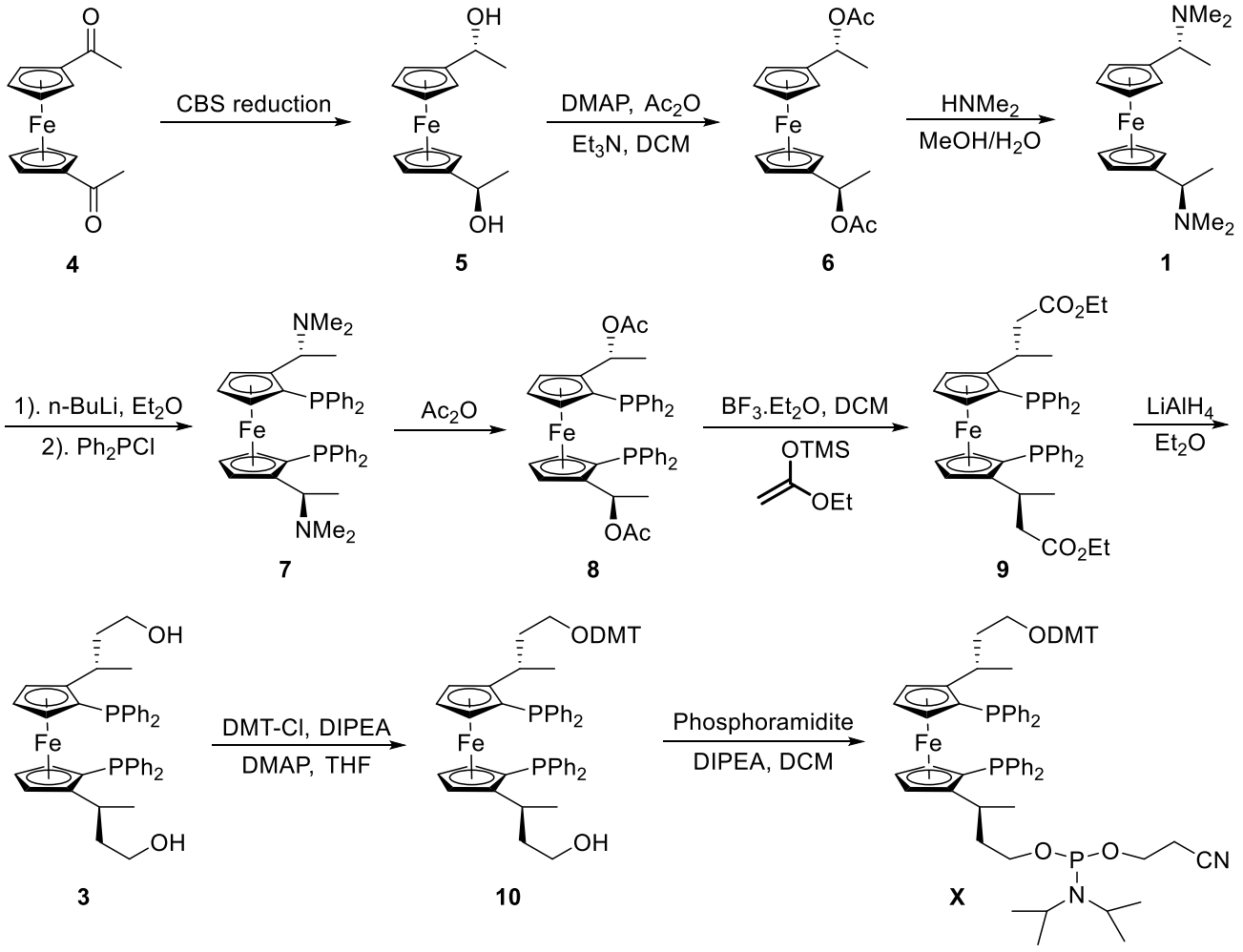

Scheme 6.13 Synthesis route of ferrocenyl phosphine monomer X

The starting material 1,1′-diacetylferrocene compound **4** was supplied from the undergraduate teaching laboratories and purified. Compound **5** was obtained through the asymmetric hydrogenation of 1,1′-diacetylferrocene, catalysed by f-ampha/Ir catalyst developed by the Zhang group.[45] However, the commercially available CBS catalyst enabled the reaction to be performed on a large scale under relatively safe conditions without flammable hydrogen gas.[46] The first challenge came with the synthesis of compound **7** (also called Mandyphos) via ortho-lithiation and followed by phosphination of compound **1** (named bis-Ugi amine) using PPh_2Cl. Frustratingly, compound **7** could not be successfully made on a small (100 mg) scale even after more than ten attempts at different temperatures (e.g., room temperature, 0 ^oC or -78 ^oC). Using fresh n-BuLi, dry Et_2O, distilled PPh_2Cl brought no

improvement to the reaction. However, the reaction subsequently worked on a 1 g or larger scale, providing compound **7** in more than 30% yield. Another problem was phosphorus oxidation in the reduction of compound **9** to compound **3**. When DIBAL-H was initially used as the reductant in Et_2O, although the ester moiety of compound **9** could be reduced to the desired alcohol, the phosphine was always oxidized to the phosphine oxide. Changing the reducing agent to $LiAlH_4$ resulted the expected product in a quantitative yield. After the successful synthesis of the ferrocenyl phosphine diol compound **3**, compound **X** was generated by first tritylation and then phosphitylation of the symmetrical hydroxyl groups. In this way, both enantiomers (**X_1, X_2**) of the ferrocenyl monomer **X** could be obtained with 81 mg and 237 mg, respectively (Figure 6.1). The next step was to incorporate the monomers into the oligonucleotides (ODN) via solid-phase synthesis.

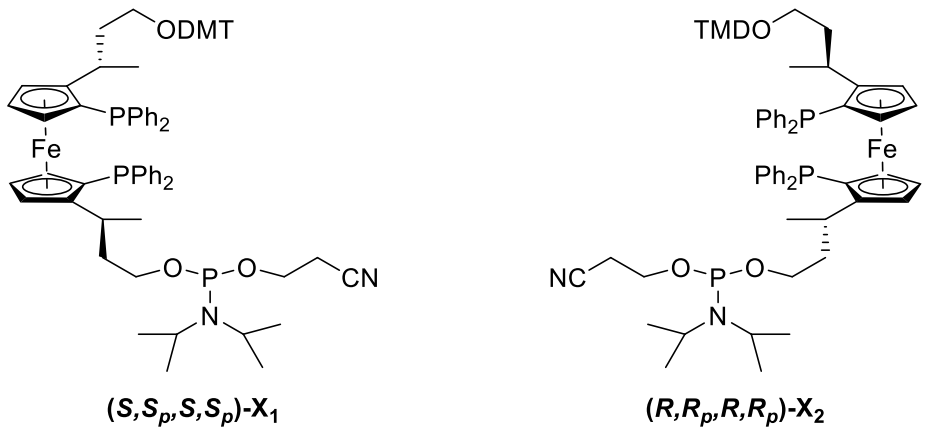

(S,S_p,S,S_p)-X_1 **(R,R_p,R,R_p)-X_2**

Figure 6.1 Both enantiomers (X_1, X_2) of ferrocenyl phosphine monomer X

6.3.2 Oligonucleotides

Oligonucleotides were synthesised using the solid-phase phosphoramidite strategy developed by Beaucage and Caruthers in 1981,[47] which was performed on an Applied Biosystems ABI 394 DNA/RNA synthesiser. The synthesis cycle is shown in Scheme 6.14.

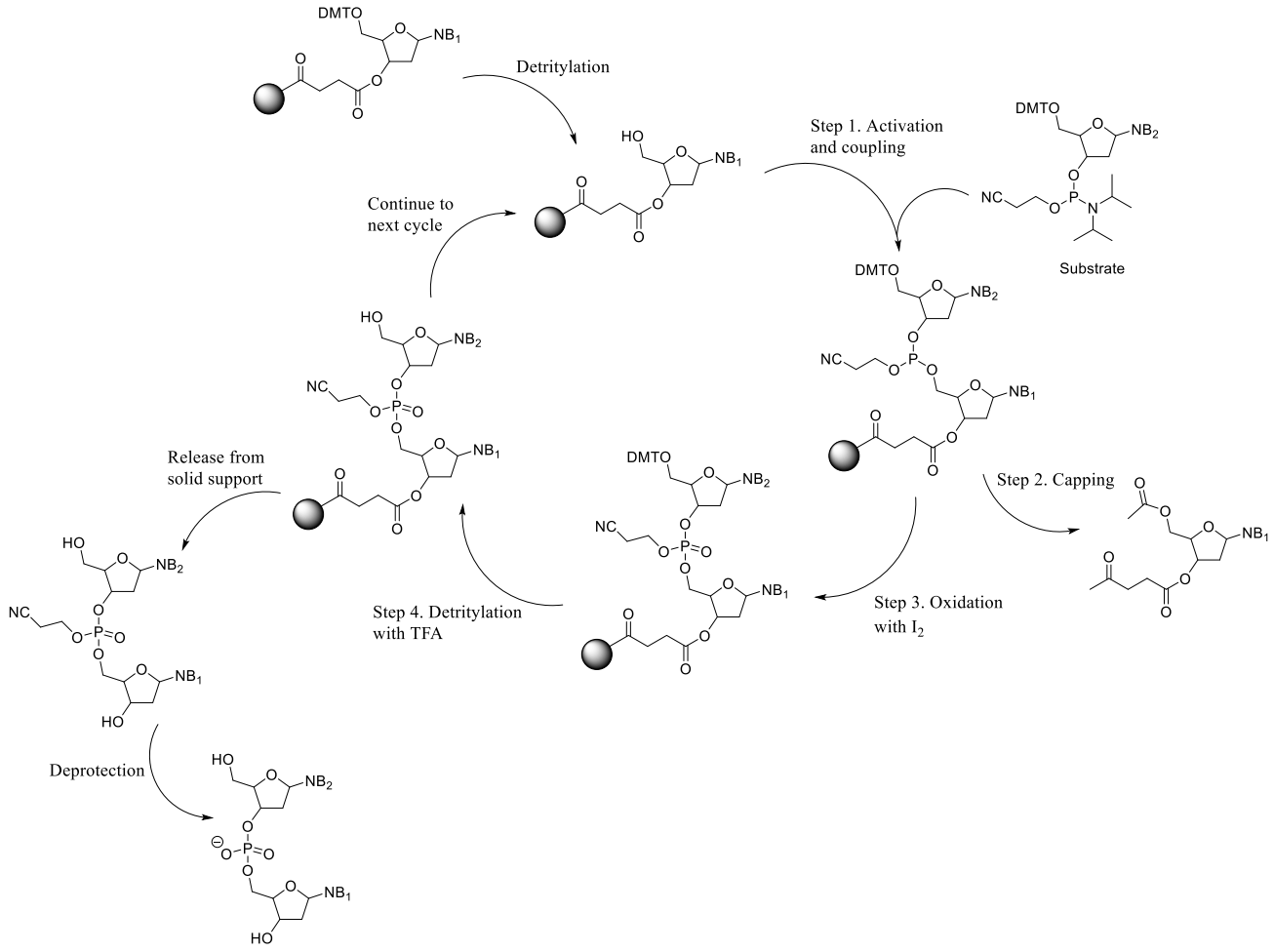

Scheme 6.14 Solid-phase oligonucleotide synthesis developed by Beaucage and Caruthers

Substrates protected with specific functional groups, a DMT group at the 5′-hydroxyl and a phosphoramidite at the 3′-hydroxyl position, are prepared prior to the oligonucleotide synthesis. The first step is the coupling between the phosphoramidite of a substrate with the 5′-hydroxyl group of a detritylation nucleoside attached to a solid support, followed with a capping step using a mixture of acetic anhydride and *N*-methylimidazole in THF to remove unreacted 5′-hydroxyl groups. The growing oligonucleotide is then oxidised by iodine to result a phosphotriester, before the DMT deprotection step with TFA. The resulting oligonucleotide continues to the next cycle, and various nucleosides are added according to the pre-programmed sequence. The synthesis finishes after the releasing from solid support and removal of the cyanoethyl protecting group.

Solid-phase synthesis using the standard conditions gave the DNA oligonucleotides in good yields. **ODN2042** and **ODN2065** were the modified strands, with the ferrocenyl phosphine ligand **X** incorporated into the 13-mer Sugiyama oligonucleotides 5′-GCA TGG **X**C ACG GT-3′.[42] Four complementary strands (**ODN2011**, **ODN2018**, **ODN2020**, and **ODN2056**) of the modified oligonucleotides were also prepared to allow us to consider the effect of all four bases (G, A, C, and T) opposite the ferrocene on the corresponding DNA duplexes. The crude oligonucleotides were readily purified by reversed-phase HPLC with good separation from other impurities. Analytical reversed-phase HPLC confirmed the excellent purity of the modified strands (Figure 6.2).

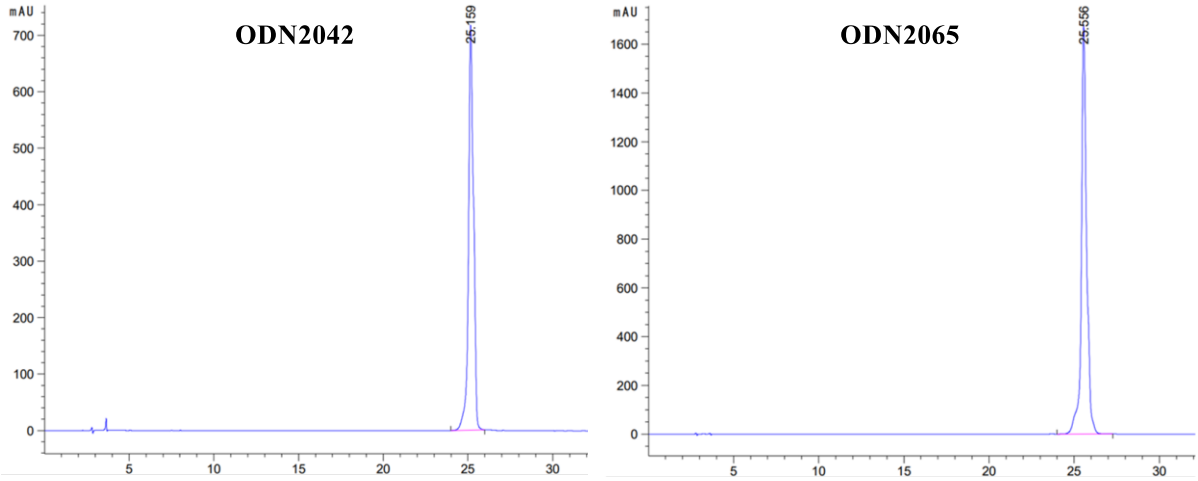

Figure 6.2 Analytical HPLC of ODN2042 and ODN2065

However, when the products were subjected to ES MS analysis, the expected masses were not obtained in the case of the modified strands, with each being 32 mass unit too high (Table 6.1Table 6.1). In fact, this was also found to be the case for the crude samples prior to HPLC. The extra mass indicated that these two phosphine-modified strands had been oxidised to give the corresponding strands with phosphine oxide groups.

Table 6.1 Sequence and MS of oligonucleotides

Entry	Sequences (5′-3′)	**Calc. MS**	**ES MS**
ODN2042	GCA TGG **X_1**C ACG GT	4444.83	4476.84
ODN2065	GCA TGG **X_2**C ACG GT	4444.83	4476.83
ODN2011	CGT ACC GGG TGC CA	4262.75	4262.74
ODN2018	CGT ACC AAG TGC CA	4230.76	4230.75
ODN2020	CGT ACC CCG TGC CA	4182.73	4182.74
ODN2056	CGT ACC TTG TGC CA	4212.73	4212.74

To confirm this, the strand **ODN2065** was dissolved in D_2O and submitted for ^{31}P NMR analysis (Figure 6.3). The chemical shift at ca. -1.1 ppm was ascribed to the phosphate backbone of the oligonucleotide.[48] However, two additional peaks at 34.9 ppm and 34.4 ppm did indeed indicate the presence of two phosphine oxide peaks. By contrast, ferrocenyl phosphine peaks would be more upfield (ca. -25 ppm, see experimental). It is likely that oxidation occurred either during ODN synthesis (I_2 oxidation) or immediately afterwards during the workup procedure. We found ferrocenyl phosphine compound **8** did not give any obvious change in its ^{31}P NMR spectrum after stirring in the presence of excess I_2 in THF/pyridine/H_2O (78/20/2) overnight. Thus, the oxidation could well have been caused by using standard ODN work-up conditions by the treatment with K_2CO_3 in methanol, acetic acid and MilliQ water which were not oxygen-free.

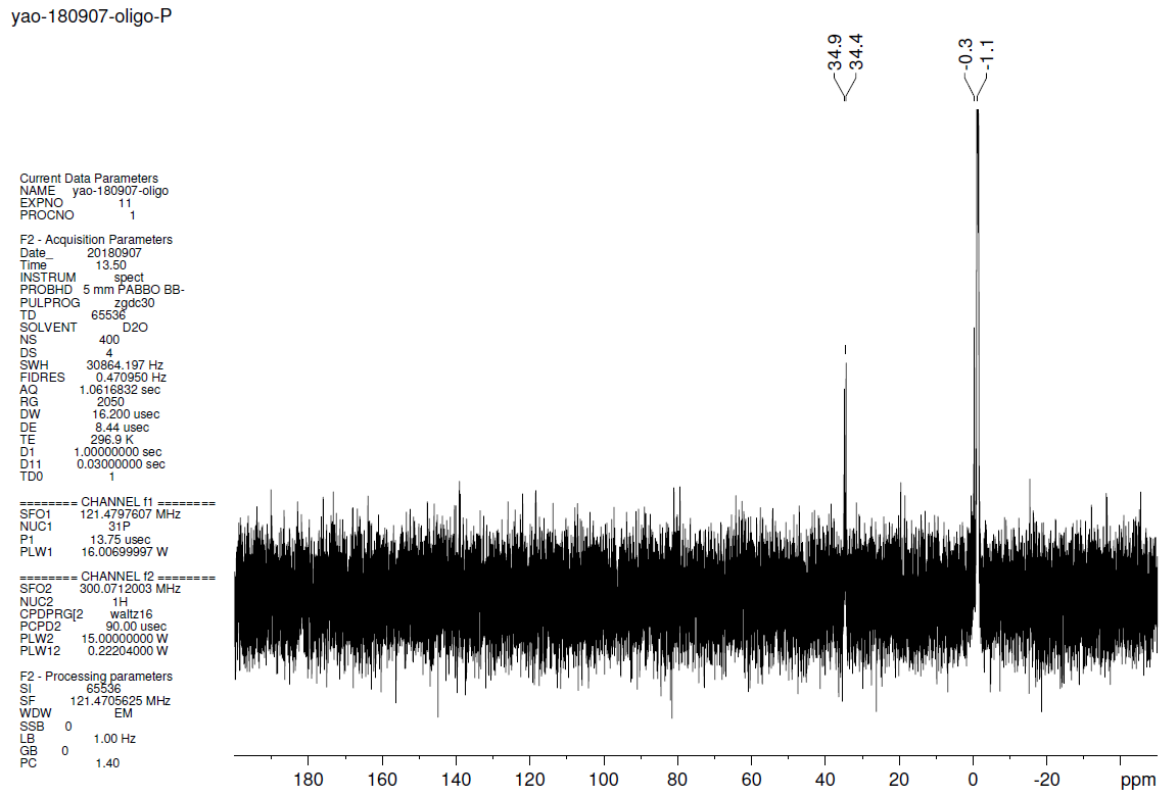

Figure 6.3 ^{31}P {^{1}H} NMR spectrum for ODN2065 in D_2O

6.3.3 DNA duplexes

Although the ferrocenyl phosphine-modified oligonucleotides had been oxidized, which precluded metal binding and catalytic experiments, nevertheless DNA duplexes formation studies were still undertaken first using VT UV/vis and then gel electrophoresis studies. For the VT studies, equimolar amounts (20 μM) of each duplex forming strand were made up in buffer (sodium phosphate and NaCl in water, pH 7), and heated at 85 °C for 5 min, then cooled down and kept at RT for 2 h, before being left in a fridge overnight before starting the study. The resulting thermal melting temperature (T_m) data of the DNA duplexes is summarized in Table 6.2. It was found that the **X₁**-modified DNA duplexes had higher T_m values than the **X₂**-modified DNA, indicating that **X₁** enantiomer could accommodate duplex formation more than **X₂** enantiomer.

Table 6.2 DNA duplexes and their T_m values

Entry	DNA	Sequences	T_m
1	**42FcGG**	5′-GCA TGG **X$_1$**C ACG GT-3′ (**ODN2042**) 3′-CGT ACC GGG TGC CA-5′ (**ODN2011**)	42 ºC
2	**42FcAA**	5′-GCA TGG **X$_1$**C ACG GT-3′ (**ODN2042**) 3′-CGT ACC AAG TGC CA-5′ (**ODN2018**)	47 ºC
3	**42FcCC**	5′-GCA TGG **X$_1$**C ACG GT-3′ (**ODN2042**) 3′-CGT ACC CCG TGC CA-5′ (**ODN2020**)	44 ºC
4	**42FcTT**	5′-GCA TGG **X$_1$**C ACG GT-3′ (**ODN2042**) 3′-CGT ACC TTG TGC CA-5′ (**ODN2056**)	45 ºC
5	**65FcGG**	5′-GCA TGG **X$_2$**C ACG GT-3′ (**ODN2065**) 3′-CGT ACC GGG TGC CA-5′ (**ODN2011**)	39 ºC
6	**65FcAA**	5′-GCA TGG **X$_2$**C ACG GT-3′ (**ODN2065**) 3′-CGT ACC AAG TGC CA-5′ (**ODN2018**)	44 ºC
7	**65FcCC**	5′-GCA TGG **X$_2$**C ACG GT-3′ (**ODN2065**) 3′-CGT ACC CCG TGC CA-5′ (**ODN2020**)	41 ºC
8	**65FcTT**	5′-GCA TGG **X$_2$**C ACG GT-3′ (**ODN2065**) 3′-CGT ACC TTG TGC CA-5′ (**ODN2056**)	42 ºC

The gel-loading dye purple (6X) was used in gel electrophoresis. It contains two different dyes (bromophenol blue and xylene cyanol FF) for visual tracking of DNA migration during electrophoresis. Two gels containing DNA single strands (ssDNA) and duplexes (dsDNA) were obtained (Figure 6.4). In the lanes proceeding, from left to right, the samples were as follows: **2042(1)-2011(2)-2018(3)-2020(4)-2056(5)-42FcGG(6)-42FcAA(7)-42FcCC(8)-42FcTT(9)** for gel 1 and **2065(1)-2011(2)-2018(3)-2020(4)-2056(5)-65FcGG(6)-65FcAA(7)-65FcCC(8)-65FcTT(9)** for gel 2. The dye gave two bands, as shown in Lanes Y and Z. In both gels, the bottom bands indicated ssDNA, and the four more slowly moving bands on the right indicated the duplexes. In gel 1, **42FcAA(7)** and **42FcTT(9)** remained less in the gel, which might be stronger duplexes and have higher T_m, in accord with the observed T_m data.

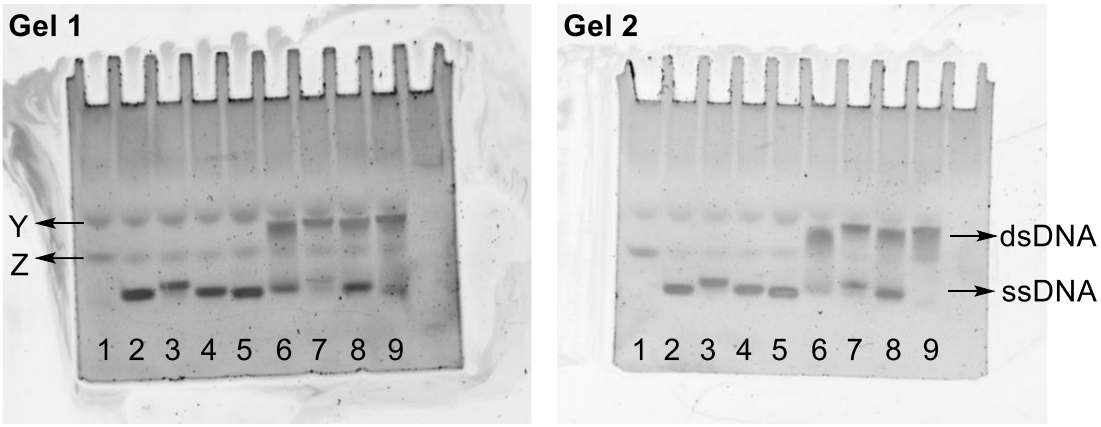

Figure 6.4 Two gels. (From left to right) Gel 1. 2042(1)-2011(2)-2018(3)-2020(4)-2056(5)-42FcGG(6)-42FcAA(7)-42FcCC(8)-42FcTT(9); Gel 2. 2065(1)-2011(2)-2018(3)-2020(4)-2056(5)-65FcGG(6)-65FcAA(7)-65FcCC(8)-65FcTT(9)

CD spectra showed that the $\mathbf{X_1}$- and $\mathbf{X_2}$-modified DNA duplexes had significantly different absorptions in the wavelength range 200 nm to 225 nm (Figure 6.5). Opposite absorption peaks occurred at ca. 210 nm. On the other hand, all the DNA duplexes had similar absorptions profiles in the wavelength range 225 nm to 300 nm.

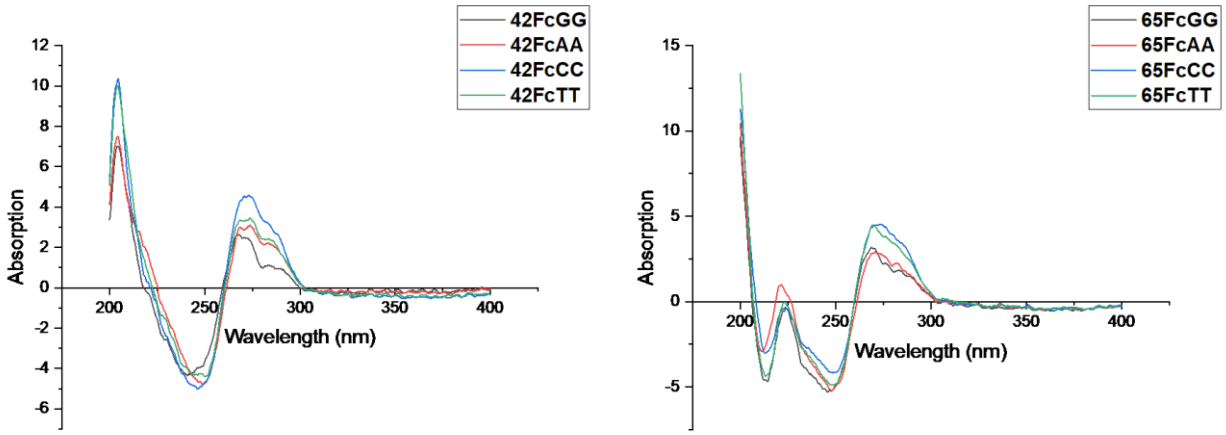

Figure 6.5 CD spectra for DNA duplexes

6.4 Conclusion

In summary, this work involved efforts to develop a new type of DNA-organometallic hybrid scaffold for asymmetric catalysis. Both enantiomers of the ferrocenyl phosphine monomer were successfully synthesized and incorporated into DNA strands. Unfortunately, the resulting hybrid DNA ligands were oxidized, probably at the work-up stage due to the presence of oxygen. However, the resulting ferrocenyl phosphine oxide-modified strands could still successfully form duplexes, which at least widens the range of bio-organometallic nucleic acid systems that can be made. In the future, the desired phosphine-modified DNA strands will be prepared and subjected to work up in oxygen-free conditions to allow metal-binding studies and catalysis to be performed.

6.5 Experimental

6.5.1 Synthesis of the ferrocenyl phosphine monomers

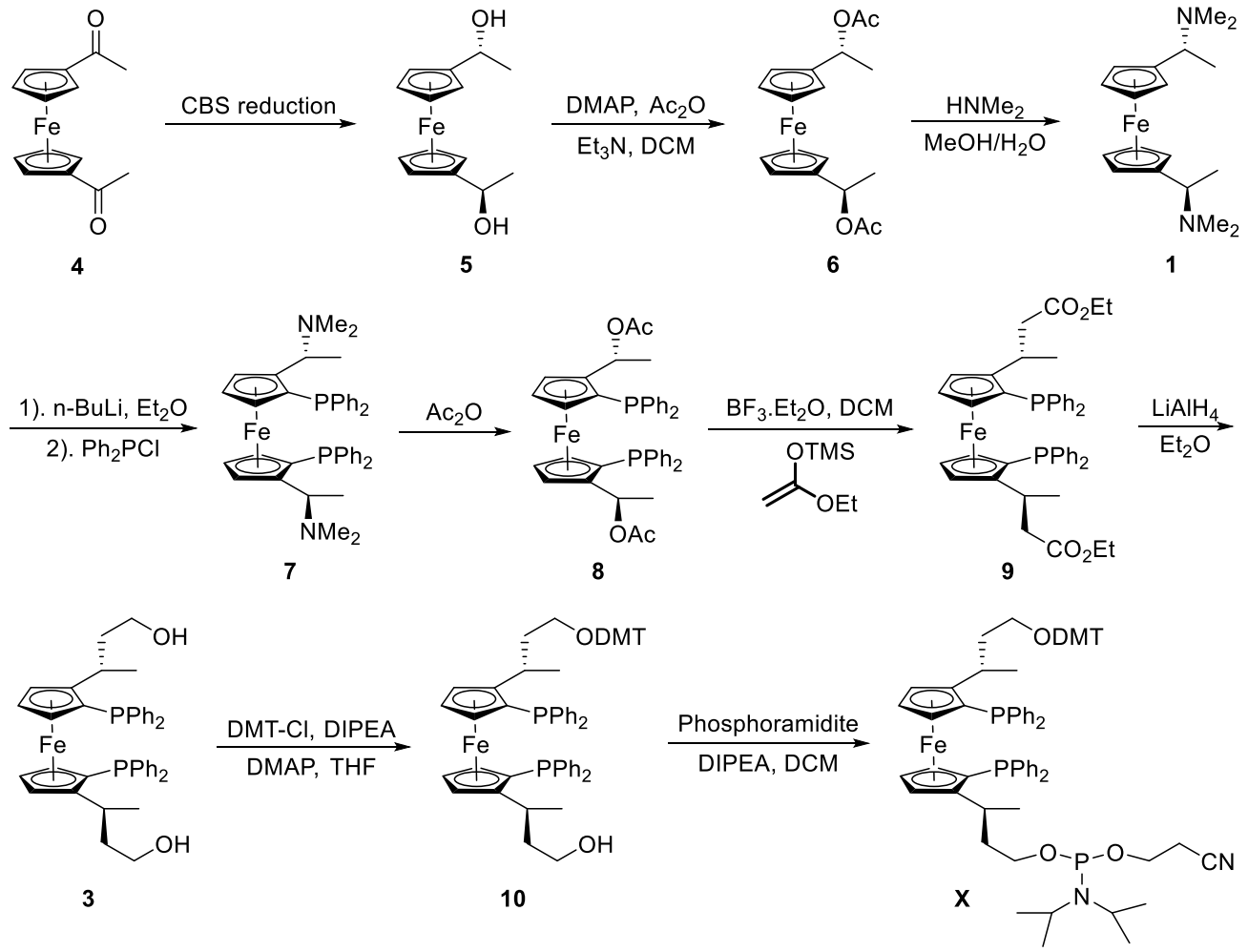

Scheme 6.15 Synthesis of the ferrocenyl phosphine monomer X

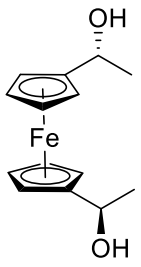

(*R, R*)-**5.** Known compound.[49] The (S)-(−)-2-Methyl-CBS-oxazaborolidine (1.66 g, 6 mmol) was dissolved in dry THF (60 mL) and cooled to 0 °C under argon. From a syringe charged with $BH_3{\cdot}SMe_2$

(2 M in THF, 10 mL), 20% of the final amount (2 mL) was added to the catalyst solution. After 5 min stirring, the remaining $BH_3 \cdot SMe_2$ and a solution of the starting material **4** (2.7 g, 10 mmol) in THF (25 mL) were added simultaneously within 20 min. The colour of the stirring solution turned to yellow from red on reduction. After 30 min stirring at 0 °C, the excess $BH_3 \cdot SMe_2$ was quenched by dropwise addition of methanol (10 mL). Then the mixture was poured into saturated aqueous NH_4Cl (100 mL) and extracted with ether (2*100 mL). After washed with water (100 mL) and brine (100 mL), the organic layer was dried over Na_2SO_4, and concentrated to give the compound (*R, R*)-**5** as an oil in vacuo used for the next step without further purification.

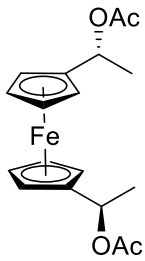

(*R, R*)-**6.** Known compound.[49] The starting material **5** and DMAP (0.012 g, 0.1 mmol) were dissolved in dry DCM (50 mL) under argon. After 5 min stirring, trimethylamine (3.46 mL, 25 mmol) and acetic anhydride (2.36 mL, 25 mmol) were added sequentially to the solution. After stirring for 5 h at room temperature, the reaction mixture was poured into saturated aqueous $NaHCO_3$ (50 mL) and extracted with DCM (2*50 mL). After washed with water (100 mL) and brine (100 mL), the organic layer was dried over Na_2SO_4, and concentrated to give the compound (*R, R*)-**6** as an oil in vacuo used for the next step without further purification.

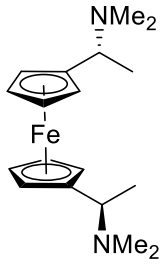

(*R, R*)-**1.** Known compound.[49] The starting material **6** was dissolved in MeOH (15 mL). Then an excess of the dimethylamine (40% in water, 25 mL, 200 mmol) was added. After stirring overnight at room temperature, the reaction mixture was poured into saturated aqueous NH_4Cl (50 mL) and extracted with ether (2*50 mL). After washed with water (50 mL) and brine (50 mL), the organic layer was dried over Na_2SO_4, and concentrated to give an oil in vacuo. The crude was purified via column chromatography with a gradient eluent system of 0-10% MeOH in DCM with 5% TEA to yield the compound (*R, R*)-**1** as a yellow solid (1.88 g, 57.3% yield of three steps). ^{1}H NMR (300 MHz, Chloroform-*d*) δ 4.05 (tdt, *J* = 4.0, 2.2, 1.4 Hz, 8H), 3.58 (q, *J* = 6.9 Hz, 2H), 2.07 (s, 12H), 1.43 (d, *J* = 6.9 Hz, 6H).

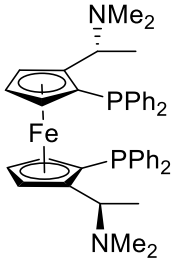

(*R, Sp, R, Sp*)-**7.** Known compound.[49] The diamine **1** (1.36 g, 4.15 mmol) was dissolved in dry Et_2O (20 mL) under argon, and the n-BuLi (2.5 M in hexanes, 6.64 mL, 16.6 mmol) was added dropwise at room temperature. After 2 min stirring the colour changed from yellow to red. After stirring for 1 h, the solution was cooled to -78 ^oC by use of a dry ice/acetone bath, and then a solution of diphenylchlorophosphine (5.22 mL, 29.05 mmol) in THF (5 mL) was added dropwise. After the addition was complete, the reaction was allowed to warm to room temperature by removing the bath. And the reaction suspension was stirred for 1 h before hydrolysed by the saturated aqueous $NaHCO_3$

(40 mL). After extraction with Et_2O (3*50 mL), the combined organic layers were dried over $MgSO_4$, and concentrated to give an oil, which was purified by column chromatography without delay. The crude was purified with a gradient eluent system of 0-20% ethyl acetate in hexanes with 5% TEA to yield the compound (*R, Sp, R, Sp*)-**7** as a yellow solid (870 mg, 30% yield). ^{1}H NMR (300 MHz, Chloroform-*d*) δ 7.29 (td, *J* = 7.8, 1.6 Hz, 4H), 7.23 – 7.01 (m, 16H), 4.34 (t, *J* = 2.5 Hz, 2H), 4.14 (q, *J* = 1.9 Hz, 2H), 4.06 (qd, *J* = 6.7, 2.5 Hz, 2H), 3.02 (dt, *J* = 2.3, 1.1 Hz, 2H), 1.70 (s, 12H), 1.26 (d, *J* = 6.7 Hz, 6H). ^{13}C NMR (101 MHz, Chloroform-*d*) δ 140.96 (d, *J* = 7.0 Hz), 138.37 (d, *J* = 9.5 Hz), 134.83 (d, *J* = 21.9 Hz), 132.08 (d, *J* = 18.7 Hz), 128.52, 127.85 (d, *J* = 7.7 Hz), 127.17 (d, *J* = 6.7 Hz), 126.89, 98.29 (d, *J* = 23.4 Hz), 76.81, 72.73 (d, *J* = 6.2 Hz), 72.58 (d, *J* = 4.4 Hz), 70.82 (d, *J* = 3.9 Hz), 56.66 (d, *J* = 7.0 Hz), 38.79, 8.96. ^{31}P NMR (121 MHz, Chloroform-*d*) δ -23.81.

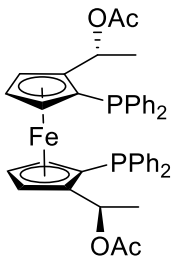

(*R, Sp, R, Sp*)-**8.** Known compound.[50] The starting material **7** was dissolved in acetic anhydride (5 mL) and heated to 95 °C. After stirring for 1 h at that temperature, the reaction mixture was cooled to room temperature, and poured into saturated aqueous $NaHCO_3$ (20 mL) and extracted with DCM (2*20 mL). After washed with water (50 mL) and brine (50 mL), the organic layer was dried over $MgSO_4$, and concentrated to give an oil. The crude was purified via column chromatography with a gradient eluent system of 0-20% ethyl acetate in hexanes with 5% TEA to yield the compound (*R, Sp, R, Sp*)-**8** as a yellow solid (730 mg, 37% yield). ^{1}H NMR (300 MHz, Chloroform-*d*) δ 7.28 – 7.10 (m, 16H), 7.09 – 7.00 (m, 4H), 6.12 (qd, *J* = 6.4, 2.7 Hz, 2H), 4.61 (t, *J* = 2.5 Hz, 2H), 4.42 (dt, *J* = 2.8, 1.5 Hz, 2H), 3.08 (dt, *J* = 2.3, 1.1 Hz, 2H), 1.64 (d, *J* = 6.4 Hz, 6H), 1.16 (s, 6H). ^{13}C NMR (101 MHz, Chloroform-*d*) δ 169.68, 139.36 (d, *J* = 9.6 Hz), 136.07 (d, *J* = 8.3 Hz), 134.77 (d, *J* = 21.9 Hz), 132.42

(d, *J* = 18.4 Hz), 129.28, 128.12 (d, *J* = 8.0 Hz), 127.92 (d, *J* = 5.9 Hz), 127.81, 93.20 (d, *J* = 24.8 Hz), 77.71 (d, *J* = 11.7 Hz), 73.54 (d, *J* = 4.4 Hz), 72.41 (dd, *J* = 11.7, 4.3 Hz), 67.84 (d, *J* = 9.5 Hz), 46.29, 19.97, 18.64, 11.68. ^{31}P NMR (121 MHz, Chloroform-*d*) δ -26.11.

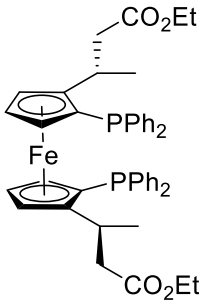

(*S, Sp, S, Sp*)-**9.** Novel compound. The starting material **8** (640 mg, 0.88 mmol) was dissolved in dry DCM (8 mL) and cooled to -78 °C under argon. The silane (5 mL) was added stirring for 30 min before dropwise addition of $BF_3{\cdot}Et_2O$ (0.24 mL, 1.94 mmol), and the reaction mixture was stirred for 3 h at -78 °C. Then the solution was allowed to warm to room temperature with stirring a further 1 h, before quenched by saturated aqueous $NaHCO_3$ (20 mL) and extracted with DCM (2*20 mL). After washed with water (50 mL) and brine (50 mL), the organic layer was dried over $MgSO_4$, and concentrated to give an oil. The crude was purified via column chromatography with a gradient eluent system of 0-10% ethyl acetate in hexanes with 5% TEA to yield the compound (*S, Sp, S, Sp*)-**9** as a yellow oil (360 mg, 52% yield). ^{1}H NMR (300 MHz, Chloroform-*d*) δ 7.26 (tt, *J* = 7.4, 1.7 Hz, 6H), 7.21 – 7.13 (m, 10H), 7.12 – 7.03 (m, 4H), 4.46 (t, *J* = 2.5 Hz, 2H), 4.31 (q, *J* = 2.1 Hz, 2H), 3.99 (q, *J* = 7.1 Hz, 4H), 3.31 (ddp, *J* = 10.2, 6.9, 3.4 Hz, 2H), 2.94 (dt, *J* = 2.3, 1.1 Hz, 2H), 2.16 (dd, *J* = 14.9, 3.5 Hz, 2H), 2.00 (dd, *J* = 14.9, 9.8 Hz, 2H), 1.40 (d, *J* = 6.9 Hz, 6H), 1.15 (t, *J* = 7.1 Hz, 6H). ^{13}C NMR (101 MHz, Chloroform-*d*) δ 171.90, 139.91 (d, *J* = 9.0 Hz), 136.82 (d, *J* = 8.4 Hz), 134.84 (d, *J* = 22.1 Hz), 132.48 (d, *J* = 18.4 Hz), 128.97, 128.12 (d, *J* = 8.1 Hz), 127.97 (d, *J* = 6.1 Hz), 127.83, 100.65 (d, *J* = 25.6 Hz), 74.43 (d, *J* = 9.6 Hz), 72.15 (d, *J* = 4.8 Hz), 71.56 (d, *J* = 4.6 Hz), 71.44 (d, *J* = 4.1 Hz), 59.98, 43.82 (d, *J* = 2.8 Hz), 29.19 (d, *J* = 9.9 Hz), 20.14, 14.20. ^{31}P NMR (121 MHz, Chloroform-*d*) δ -26.02.

HRMS (ESI) m/z: $[M+H]^+$ Calcd for $[C_{46}H_{49}FeO_4P_2]^+$ = 783.2450; Found: 783.2457. IR (neat): 3051, 2978, 2933, 1728, 1585, 1433, 1368, 1342, 1299, 1262, 1173, 1092, 1029, 828, 740, 696 cm^{-1}.

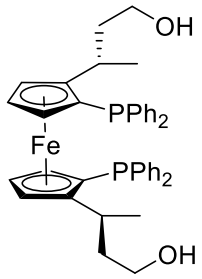

(*S, Sp, S, Sp*)-**3.** Novel compound. The starting material **9** (630 mg, 0.80 mmol) was dissolved in dry Et_2O (10 mL) and cooled to 0 °C under argon. Diisobutylaluminium hydride (2 mL, 2 mmol, 1.0 M in THF) was added dropwise and the reaction mixture was stirred at 0 °C for 10 min before quenched by cold water (5 mL) and extracted with DCM (2*10 mL). After washed with water (10 mL) and brine (10 mL), the organic layer was dried over $MgSO_4$, and concentrated to give an oil. The crude was purified via column chromatography with 50% ethyl acetate in hexanes to yield the compound (*S, Sp, S, Sp*)-**3** as a yellow solid. (602 mg, 99% yield) ^{1}H NMR (400 MHz, Chloroform-*d*) δ 7.32 – 7.24 (m, 4H), 7.23 – 7.16 (m, 12H), 7.13 (ddd, *J* = 6.1, 3.8, 2.3 Hz, 4H), 4.44 (t, *J* = 2.2 Hz, 2H), 4.29 (s, 2H), 3.34 (dt, *J* = 11.7, 6.7 Hz, 4H), 3.01 (tt, *J* = 6.8, 3.3 Hz, 2H), 2.95 (s, 2H), 1.41 (d, *J* = 6.9 Hz, 6H), 1.36 (td, *J* = 7.5, 3.8 Hz, 2H), 1.32 – 1.23 (m, 2H), 0.76 (s, 2H). ^{13}C NMR (101 MHz, Chloroform-*d*) δ 140.08 (d, *J* = 8.5 Hz), 136.77 (d, *J* = 7.7 Hz), 134.88 (d, *J* = 22.2 Hz), 132.50 (d, *J* = 18.5 Hz), 128.98, 128.19, 128.09 (d, *J* = 4.4 Hz), 127.97 (d, *J* = 6.2 Hz), 102.23 (d, *J* = 25.7 Hz), 73.95 (d, *J* = 8.2 Hz), 71.74 (d, *J* = 4.7 Hz), 71.31, 71.23 (d, *J* = 4.9 Hz), 60.60, 42.42 (d, *J* = 2.5 Hz), 28.32 (d, *J* = 10.2 Hz), 20.13. ^{31}P NMR (121 MHz, Chloroform-*d*) δ -26.02. **HRMS** (ESI) m/z: $[M+H]^+$ Calcd for $[C_{42}H_{45}FeO_2P_2]^+$ = 699.2239; Found: 699.2253. M.p. 90-91 °C. IR (neat): 3358, 3051, 2930, 1584, 1477, 1433, 1372, 1265, 1166, 1043, 827, 738, 696 cm^{-1}.

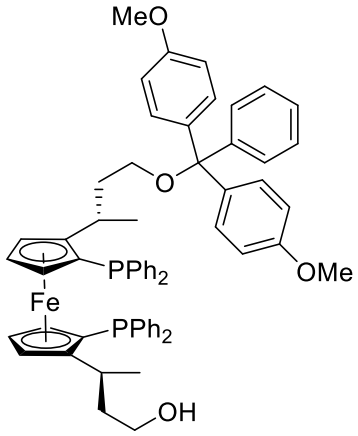

(*S, Sp, S, Sp*)-**10.** Novel compound. To a suspension of the ferrocene diol **3** (203 mg, 0.29 mmol), DMT-Cl (98.3 mg, 0.29 mmol) and DMAP (7.1 mg, 0.058 mmol) dissolved in dry THF (5 mL) was added DIPEA (0.051 mL, 0.29 mmol) under argon. The reaction mixture was stirred overnight at room temperature before quenched by saturated aqueous $NaHCO_3$ (5 mL) and extracted with DCM (2*5 mL). The combined organic layers were dried over $MgSO_4$ and concentrated to give an oil. The crude was purified via column chromatography with a gradient eluent system of 20 - 60% ethyl acetate in hexanes to yield the compound (*S, Sp, S, Sp*)-**10** as a yellow solid (100 mg, 34% yield). ^{1}H NMR (300 MHz, Chloroform-*d*) δ 7.35 – 7.04 (m, 29H), 6.81 – 6.70 (m, 4H), 4.46 (t, *J* = 2.4 Hz, 1H), 4.39 (t, *J* = 2.4 Hz, 1H), 4.29 (dt, *J* = 3.4, 1.6 Hz, 1H), 4.19 (td, *J* = 2.4, 1.2 Hz, 1H), 3.77 (d, *J* = 1.5 Hz, 6H), 3.32 (tdd, *J* = 10.7, 9.0, 6.2 Hz, 2H), 3.15 – 2.94 (m, 3H), 3.00 – 2.92 (m, 2H), 2.90 (dt, *J* = 2.3, 1.1 Hz, 1H), 2.78 (ddq, *J* = 23.1, 8.8, 5.0 Hz, 2H), 1.64 (tdd, *J* = 9.0, 6.2, 2.8 Hz, 2H), 1.37 (d, *J* = 6.9 Hz, 4H), 1.38 – 1.24 (m, 5H), 1.19 (d, *J* = 6.9 Hz, 4H), 0.76 (s, 1H). ^{31}P NMR (121 MHz, Chloroform-*d*) δ -25.50, -25.87.

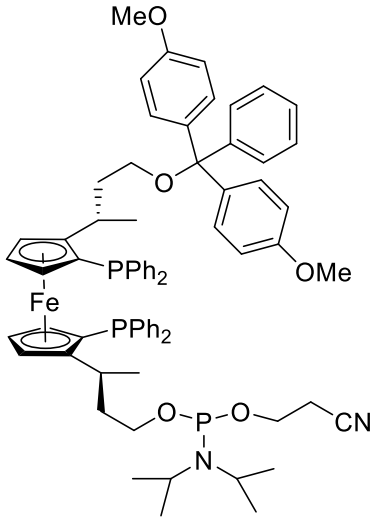

(*S, Sp, S, Sp*)-**X**. Novel compound. The starting material **10** (140 mg, 0.14 mmol) azetroped with DCM (2*10 mL) was redissolved in dry DCM (5 mL) under argon. DIPEA (0.49 mL, 2.8 mmol) and (0.045 mL, 0.20 mmol) were added, and the reaction mixture was stirred for 3.5 h before degassed ethyl acetate (5 mL) was added. The mixture was washed with degassed saturated aqueous $NaHCO_3$ (5 mL) and brine (5 mL). The organic layer was dried over $MgSO_4$, and concentrated to give an oil. The crude was purified with a gradient eluent system of 10 - 50% ethyl acetate in hexanes with 1% TEA to yield the compound (*S, Sp, S, Sp*)-**X** as a yellow solid (81 mg, 48% yield). ^{1}H NMR (300 MHz, Chloroform-*d*) δ 7.36 – 6.97 (m, 30H), 6.82 – 6.70 (m, 4H), 4.45 (q, *J* = 2.3 Hz, 1H), 4.37 (q, *J* = 2.4 Hz, 1H), 4.29 (d, *J* = 2.1 Hz, 1H), 4.20 (dt, *J* = 4.3, 2.2 Hz, 1H), 3.79 (d, *J* = 1.4 Hz, 6H), 3.72 – 3.58 (m, 2H), 3.59 – 3.30 (m, 4H), 2.96 (t, *J* = 2.6 Hz, 1H), 2.88 – 2.83 (m, 1H), 2.77 (ddt, *J* = 17.9, 9.1, 4.7 Hz, 2H), 2.64 – 2.42 (m, 4H), 1.38 (d, *J* = 6.9 Hz, 3H), 1.20 (d, *J* = 6.8 Hz, 3H), 1.15 – 1.04 (m, 14H). ^{31}P NMR (121 MHz, Chloroform-*d*) δ 146.71, -25.49, -25.55.

6.5.2 Oligonucleotide Solid-Phase Synthesis

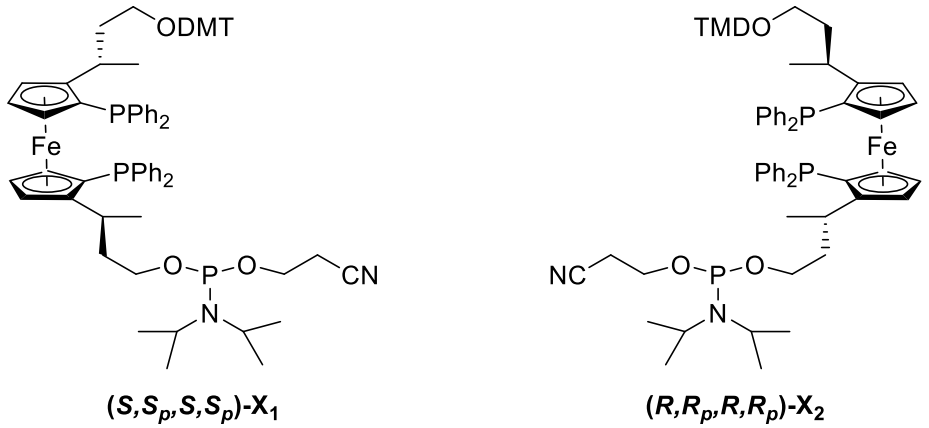

(S,S_p,S,S_p)-$\mathbf{X_1}$ (R,R_p,R,R_p)-$\mathbf{X_2}$

Figure 6.6 Both enantiomers (X_1 and X_2) of ferrocenyl phosphine monomer X

Ferrocenyl phosphine phosphoramadites (S,S_p,S,S_p)-$\mathbf{X_1}$ **(**81 mg**)** and (R,R_p,R,R_p)-$\mathbf{X_2}$ (210 mg) were dissolved in anhydrous acetonitrile, filtered through a syringe filter, and then made 0.1 M in dry acetonitrile (0.67 mL and 1.75 mL, respectively). The solution of $\mathbf{X_1}$ in MeCN was dispensed into 3 vials (**2041, 2042, 2043**), and the solution of $\mathbf{X_2}$ into 9 vials (**2059, 2060, 2061, 2062, 2063, 2064, 2065, 2065, 2067**). These vials were fitted to DNA synthesiser (Applied Biosystems 394 DNA/RNA synthesiser). The solid-phase synthesis was carried out on a 1.0 μM scale. The standard conditions were applied, using 0.5 M ETT in acetonitrile as the activator, 10% acetic anhydride in THF and 10% methylimidazole in THF as capping agents, 0.02 M iodine in water as the oxidising agent, and 3% trichloroacetic acid in DCM as the detritylation agent. After the completion of automated synthesis, the crude product was removed from the solid support by treatment with 1 mL of K_2CO_3 solution in methanol at rt for 1 h, followed by heating at 55 ^oC for 3 h before putting on a shaker overnight. The residue was concentrated on a speed vac, purified by C18 RP-HPLC, and desalted using a NAP 10 column. As a result, these strands were synthesized successfully in high yields except for **2041**. Furthermore, four complementary oligonucleotides (**2011, 2018, 2020, 2056**) were also prepared using the same synthesis method.

6.5.3 Analytical HPLC of oligonucleotides

ODN2042

Data File C:\Chem32\3\Data\Francia\Francia 2018-08-13 11-11-09\2042.D
Sample Name: 2042

```
    ======================================================================
    Acq. Operator   : SYSTEM                        Seq. Line :  50
    Acq. Instrument : LC-FC                         Location :   42
    Injection Date  : 15-Aug-18 1:22:10 AM               Inj :   1
                                                  Inj Volume : 20.000 µl
    Method          : C:\Chem32\3\Data\Francia\Francia 2018-08-13 11-11-09\FcNA Anth.M (Sequence
                      Method)
    Last changed    : 07-Feb-18 4:44:52 PM by SYSTEM
    Additional Info : Peak(s) manually integrated
```

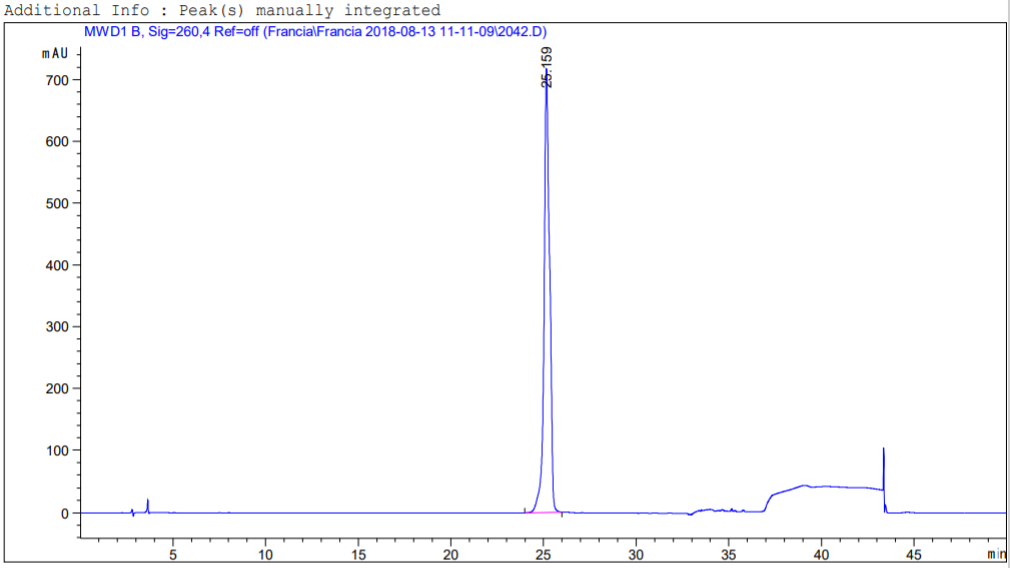


```
    ============================================================================
                              Fraction Information
    ============================================================================
    No Fractions found.
    ============================================================================
    ============================================================================
    ======================================================================
                             Area Percent Report
    ======================================================================

    Sorted By             :      Signal
    Multiplier            :      1.0000
    Dilution              :      1.0000
    Do not use Multiplier & Dilution Factor with ISTDs


    Signal 1: MWD1 B, Sig=260,4 Ref=off

    Peak RetTime Type  Width     Area      Height     Area
      #   [min]        [min]   [mAU*s]     [mAU]       %
    ----|-------|----|-------|----------|----------|--------|
       1  25.159 BB    0.2936 1.49664e4   716.85443 100.0000

    Totals :                  1.49664e4   716.85443
```

ODN2065

Data File C:\Chem32\3\Data\Francia\Francia 2018-08-13 11-11-09\2065.D
Sample Name: 2065

```
======================================================================
Acq. Operator   : SYSTEM                        Seq. Line :  58
Acq. Instrument : LC-FC                          Location :   50
Injection Date  : 15-Aug-18 8:16:31 AM               Inj :   1
                                               Inj Volume : 20.000 µl
Method          : C:\Chem32\3\Data\Francia\Francia 2018-08-13 11-11-09\FcNA Anth.M (Sequence
                  Method)
Last changed    : 07-Feb-18 4:44:52 PM by SYSTEM
Additional Info : Peak(s) manually integrated
```

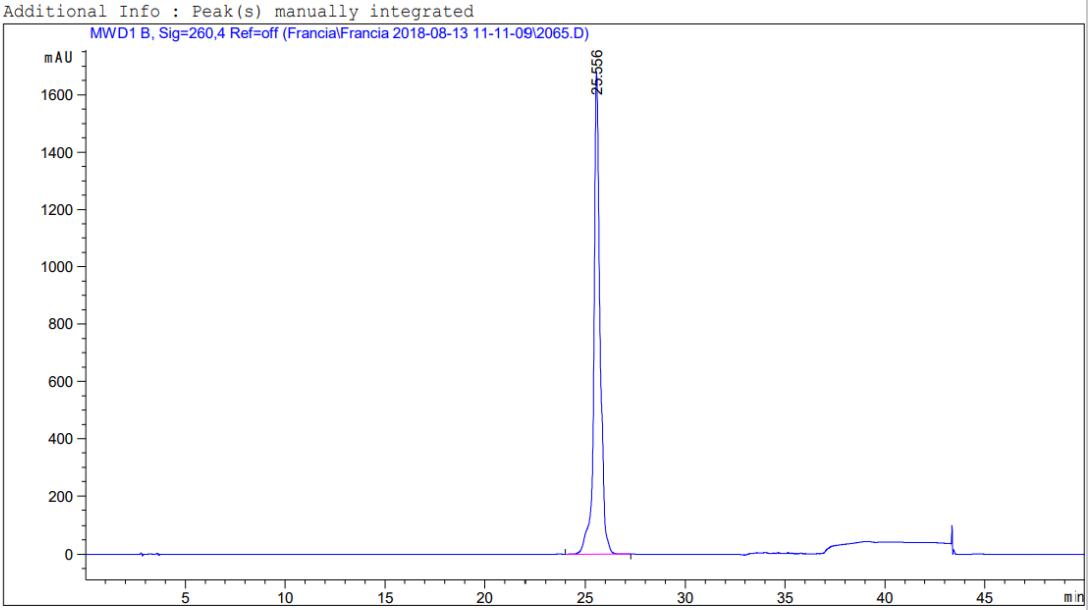


```
================================================================================
                          Fraction Information
================================================================================
No Fractions found.
================================================================================
================================================================================
======================================================================
                        Area Percent Report
======================================================================

Sorted By             :      Signal
Multiplier            :      1.0000
Dilution              :      1.0000
Do not use Multiplier & Dilution Factor with ISTDs


Signal 1: MWD1 B, Sig=260,4 Ref=off

Peak RetTime Type  Width     Area      Height     Area
  #   [min]        [min]   [mAU*s]     [mAU]       %
----|-------|----|-------|----------|----------|--------|
   1  25.556 BB    0.3163 3.62055e4  1674.03284 100.0000

Totals :                  3.62055e4  1674.03284
```

ODN2011

Data File C:\Chem32\3\Data\Francia\Francia 2018-08-13 11-11-09\2011.D
Sample Name: 2011

```
    ==================================================================
    Acq. Operator   : SYSTEM                       Seq. Line :  62
    Acq. Instrument : LC-FC                         Location :  53
    Injection Date  : 15-Aug-18 11:38:02 AM              Inj :  1
                                                  Inj Volume : 20.000 µl
    Acq. Method     : C:\Chem32\3\Data\Francia\Francia 2018-08-13 11-11-09\Short Oligo.M
    Last changed    : 19-Apr-18 10:04:25 AM by SYSTEM
    Analysis Method : C:\Chem32\3\Data\Francia\Francia 2018-08-13 11-11-09\Short Oligo.M (
                      Sequence Method)
    Last changed    : 16-Aug-18 10:31:36 AM by SYSTEM
                      (modified after loading)
    Additional Info : Peak(s) manually integrated
```

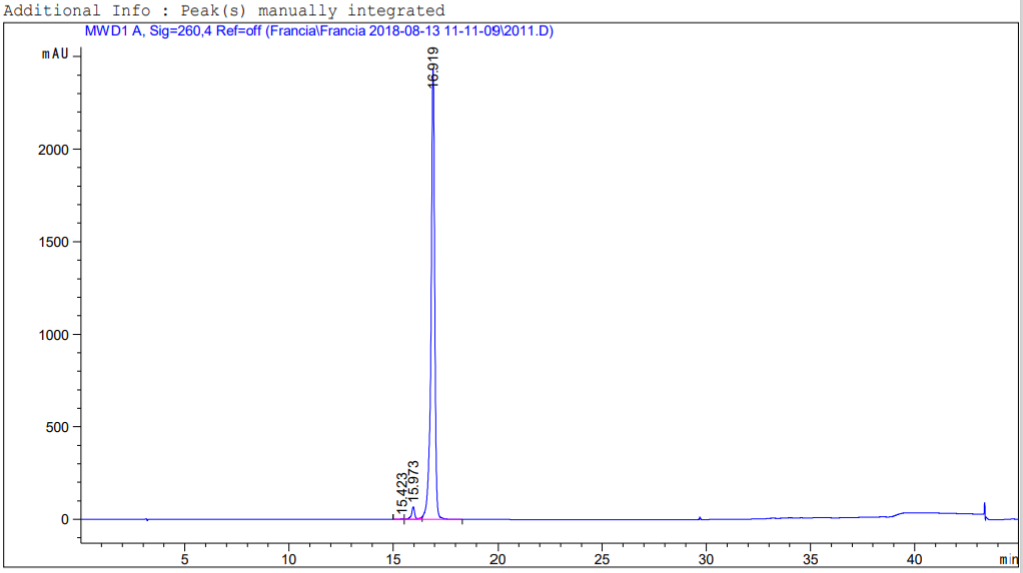


```
    ================================================================================
                               Fraction Information
    ================================================================================
    No Fractions found.
    ================================================================================
    ================================================================================
    ================================================================
                            Area Percent Report
    ================================================================

    Sorted By             :      Signal
    Multiplier            :      1.0000
    Dilution              :      1.0000
    Do not use Multiplier & Dilution Factor with ISTDs
```

ODN2018

Data File C:\Chem32\3\Data\Francia\Francia 2018-08-13 11-11-09\2018.D
Sample Name: 2018

```
==================================================================
Acq. Operator   : SYSTEM                       Seq. Line :  64
Acq. Instrument : LC-FC                         Location :  55
Injection Date  : 15-Aug-18 1:11:25 PM              Inj :  1
                                               Inj Volume : 20.000 µl
Acq. Method     : C:\Chem32\3\Data\Francia\Francia 2018-08-13 11-11-09\Short Oligo.M
Last changed    : 19-Apr-18 10:04:25 AM by SYSTEM
Analysis Method : C:\Chem32\3\Data\Francia\Francia 2018-08-13 11-11-09\Short Oligo.M (
                  Sequence Method)
Last changed    : 16-Aug-18 10:31:36 AM by SYSTEM
                  (modified after loading)
Additional Info : Peak(s) manually integrated
```

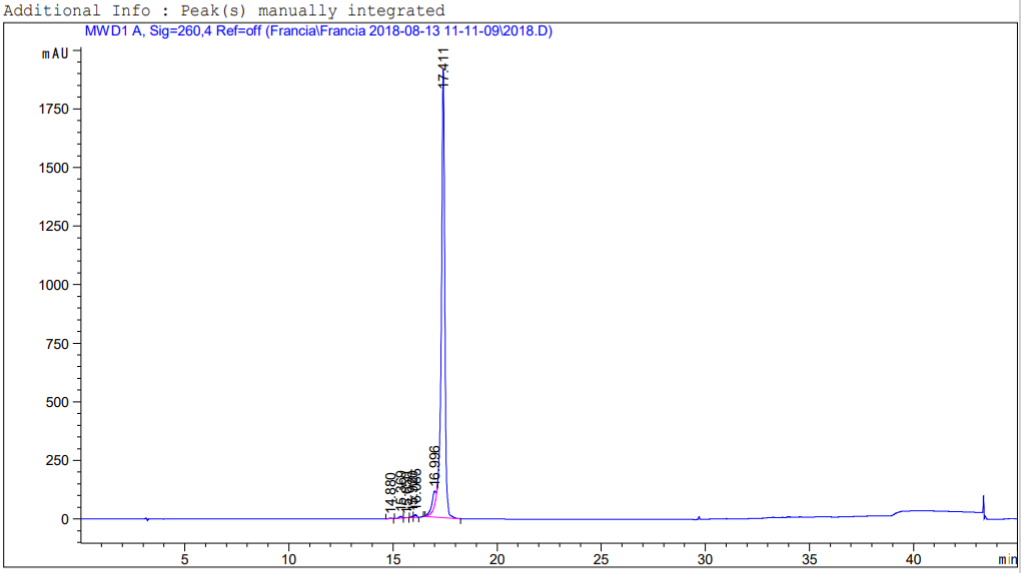


```
==========================================================================
                        Fraction Information
==========================================================================
No Fractions found.
==========================================================================
==========================================================================
==================================================================
                      Area Percent Report
==================================================================

Sorted By             :      Signal
Multiplier            :      1.0000
Dilution              :      1.0000
Do not use Multiplier & Dilution Factor with ISTDs
```

ODN2020

Data File C:\Chem32\3\Data\Francia\Francia 2018-08-13 11-11-09\2020.D
Sample Name: 2020

```
==================================================================
Acq. Operator   : SYSTEM                       Seq. Line :  63
Acq. Instrument : LC-FC                        Location :   54
Injection Date  : 15-Aug-18 12:24:44 PM             Inj :   1
                                              Inj Volume : 20.000 µl
Acq. Method     : C:\Chem32\3\Data\Francia\Francia 2018-08-13 11-11-09\Short Oligo.M
Last changed    : 19-Apr-18 10:04:25 AM by SYSTEM
Analysis Method : C:\Chem32\3\Data\Francia\Francia 2018-08-13 11-11-09\Short Oligo.M (
                  Sequence Method)
Last changed    : 16-Aug-18 10:31:36 AM by SYSTEM
                  (modified after loading)
Additional Info : Peak(s) manually integrated
```

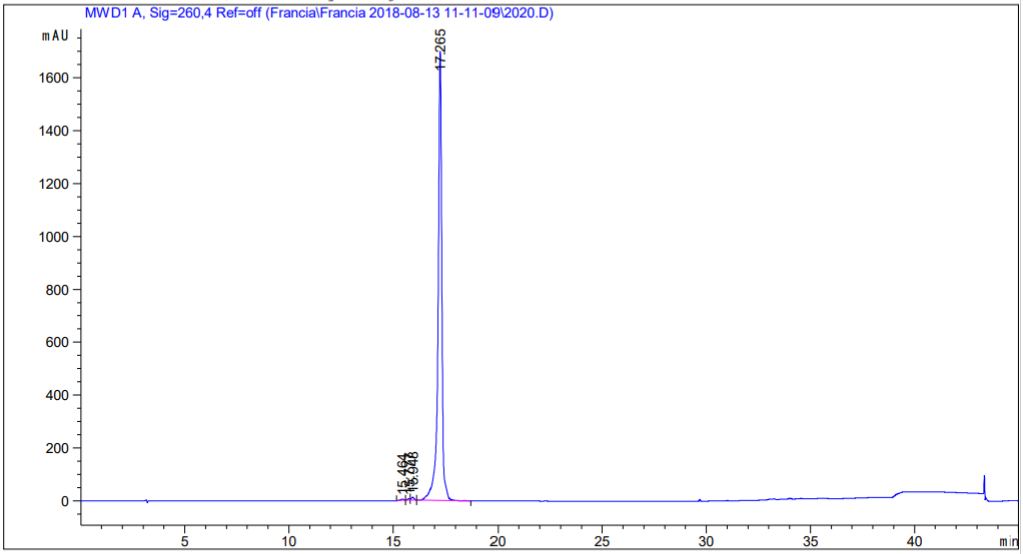


```
================================================================================
                          Fraction Information
================================================================================
No Fractions found.
================================================================================
================================================================================
==========================================================
                       Area Percent Report
==========================================================

Sorted By             :      Signal
Multiplier            :      1.0000
Dilution              :      1.0000
Do not use Multiplier & Dilution Factor with ISTDs
```

ODN2056

Data File C:\Chem32\3\Data\Francia\Francia 2018-08-13 11-11-09\2056.D
Sample Name: 2056

```
    ======================================================================
    Acq. Operator   : SYSTEM                       Seq. Line :  65
    Acq. Instrument : LC-FC                        Location :   56
    Injection Date  : 15-Aug-18 1:58:06 PM              Inj :   1
                                                  Inj Volume : 20.000 µl
    Acq. Method     : C:\Chem32\3\Data\Francia\Francia 2018-08-13 11-11-09\Short Oligo.M
    Last changed    : 19-Apr-18 10:04:25 AM by SYSTEM
    Analysis Method : C:\Chem32\3\Data\Francia\Francia 2018-08-13 11-11-09\Short Oligo.M (
                      Sequence Method)
    Last changed    : 16-Aug-18 10:31:36 AM by SYSTEM
                      (modified after loading)
    Additional Info : Peak(s) manually integrated
```

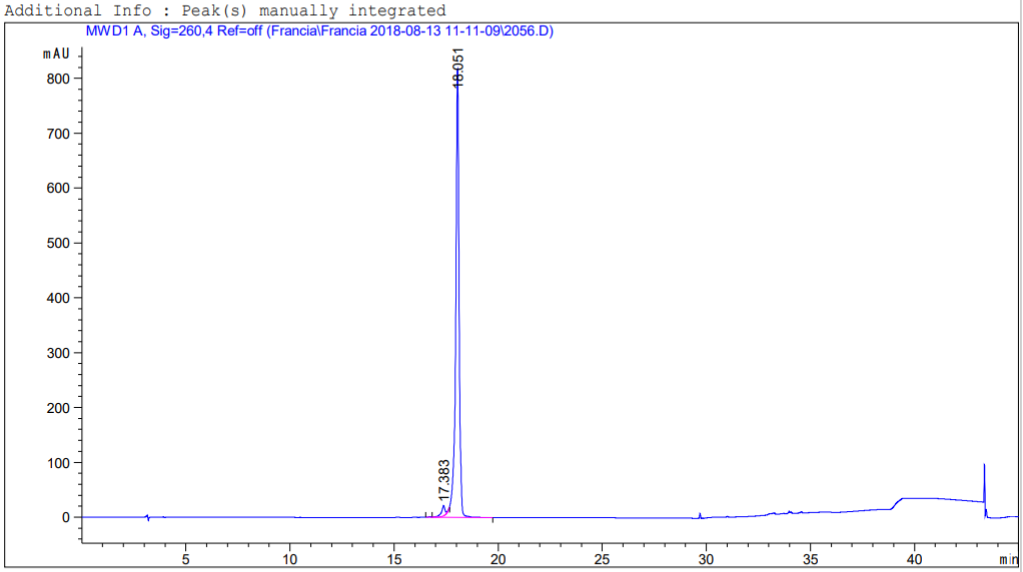


```
    ============================================================================
                              Fraction Information
    ============================================================================
    No Fractions found.
    ============================================================================
    ============================================================================
    ======================================================================
                            Area Percent Report
    ======================================================================

    Sorted By             :      Signal
    Multiplier            :      1.0000
    Dilution              :      1.0000
    Do not use Multiplier & Dilution Factor with ISTDs
```

6.5.4 ES MS of oligonucleotides

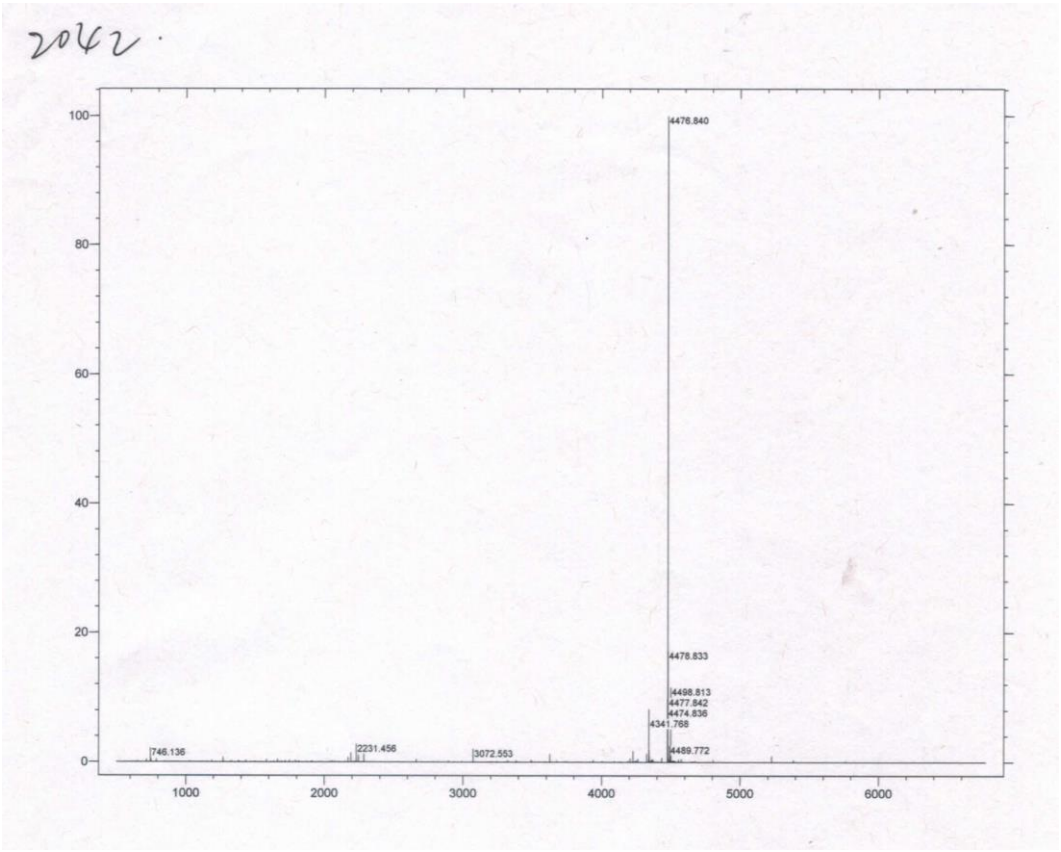

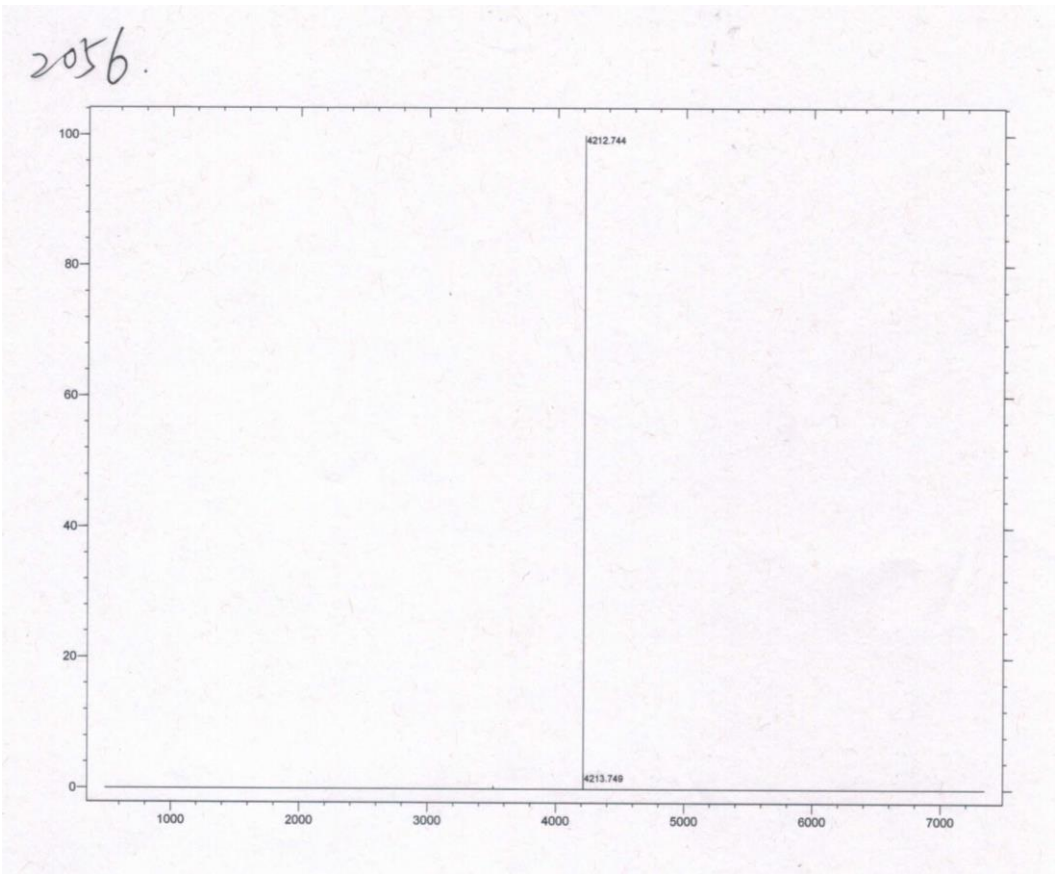

2011.

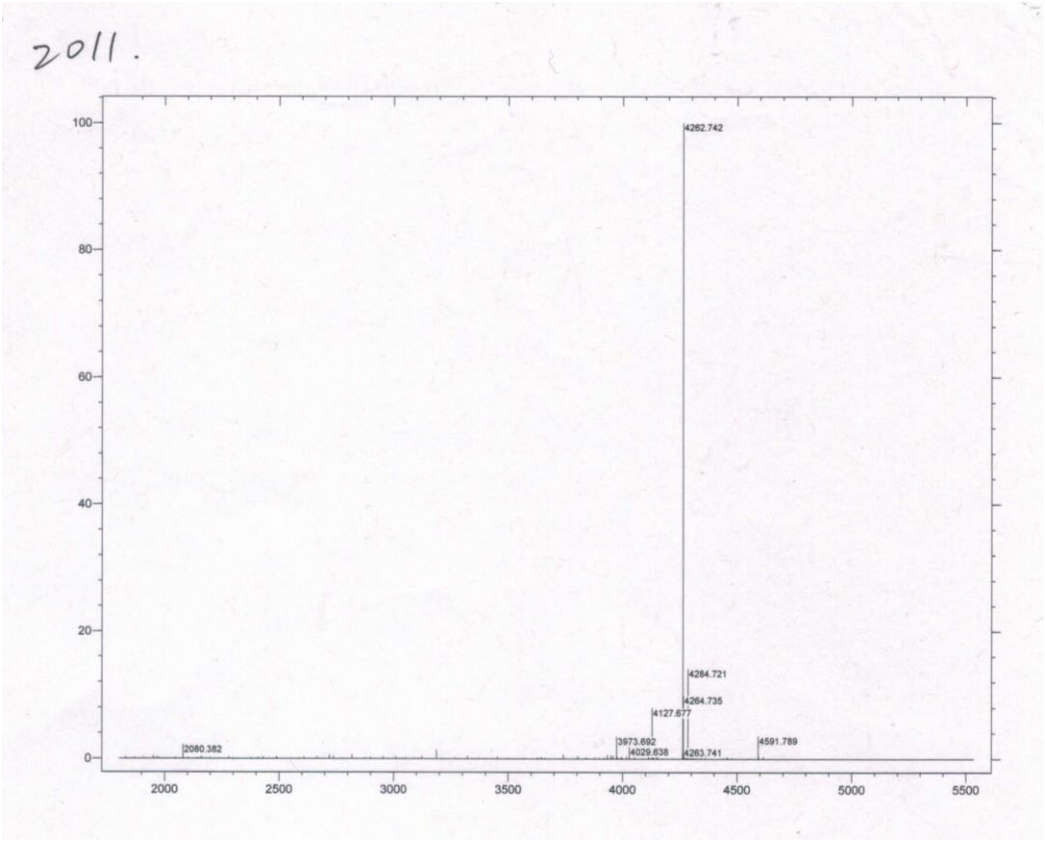
4262.742
4284.721
4264.735
4127.677
3973.692
4029.638
4263.741
4591.789
2080.382
100
80
60
40
20
0
2000
2500
3000
3500
4000
4500
5000
5500

2018.

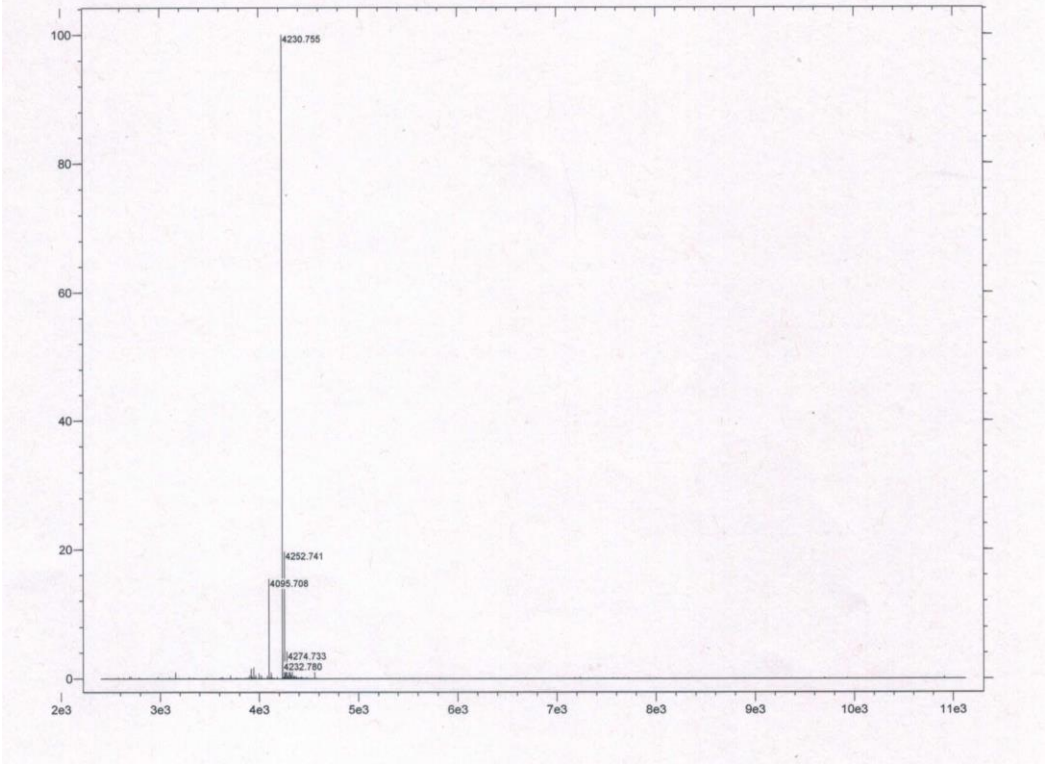
4230.755
4252.741
4095.708
4274.733
4232.780
100
80
60
40
20
0
2e3
3e3
4e3
5e3
6e3
7e3
8e3
9e3
10e3
11e3

2020.

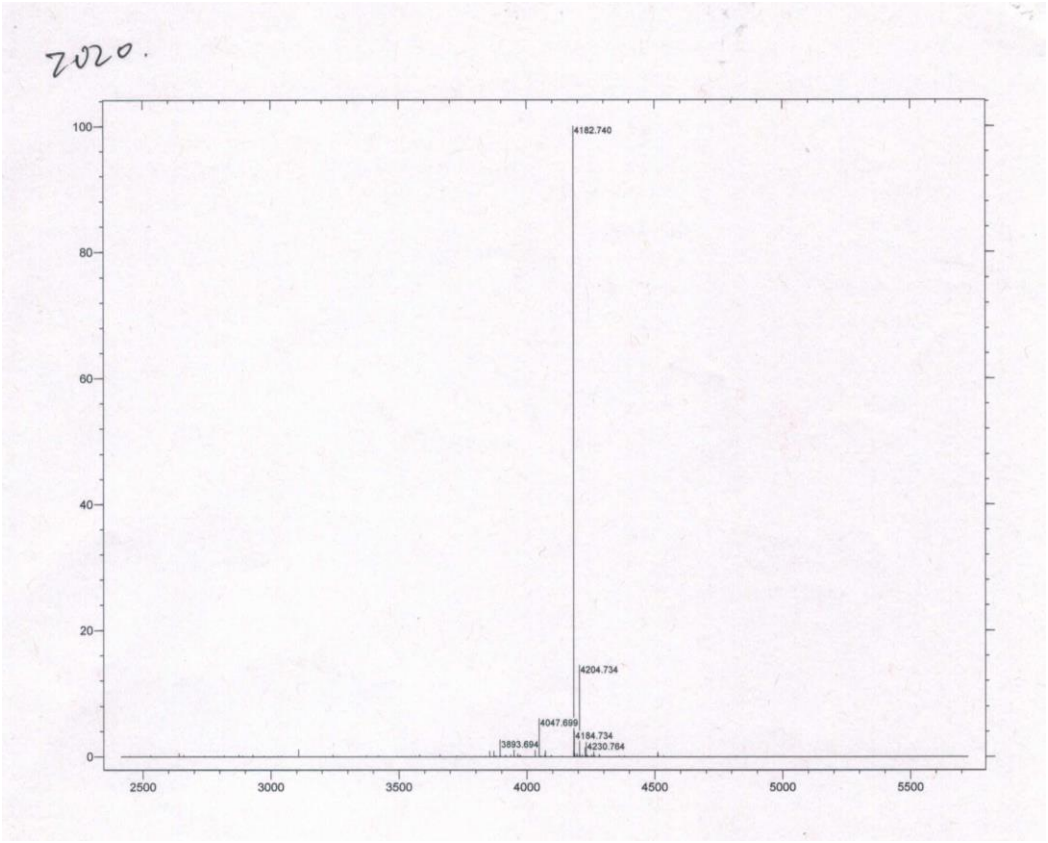
100
80
60
40
20
0
2500
3000
3500
4000
4500
5000
5500
4182.740
4204.734
4047.699
4184.734
3893.694
4230.764

2065.

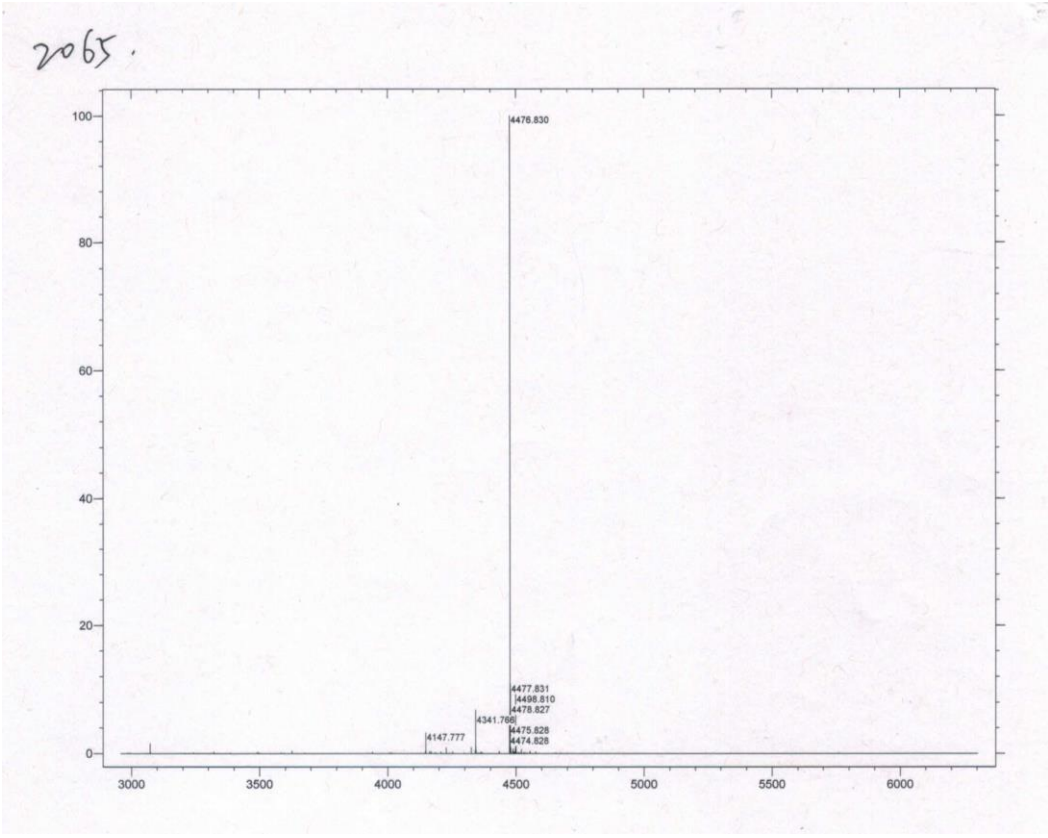
100
80
60
40
20
0
3000
3500
4000
4500
5000
5500
6000
4476.830
4477.831
4488.810
4478.827
4341.766
4475.828
4474.828
4147.777

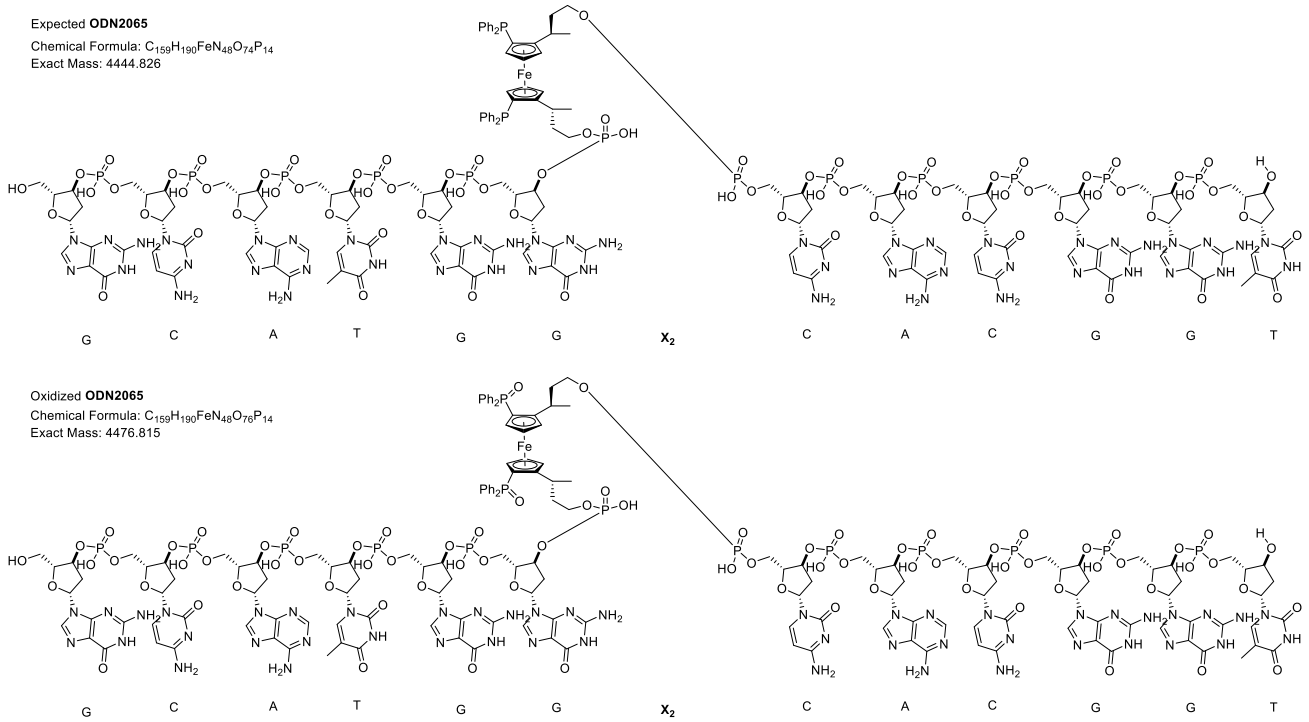

Figure 6.7 Sequence and MS of expected and oxidized ODN2065

6.5.5 Thermal Melting Experimental

Thermal melting studies were performed using a Cary 5000 UV/vis spectrophotometer combined with with a peltier temperature controller. The absorbance was measured at 260 nm with temperature rising from 20 °C to 95 °C at a rate of 0.5 °C/min.

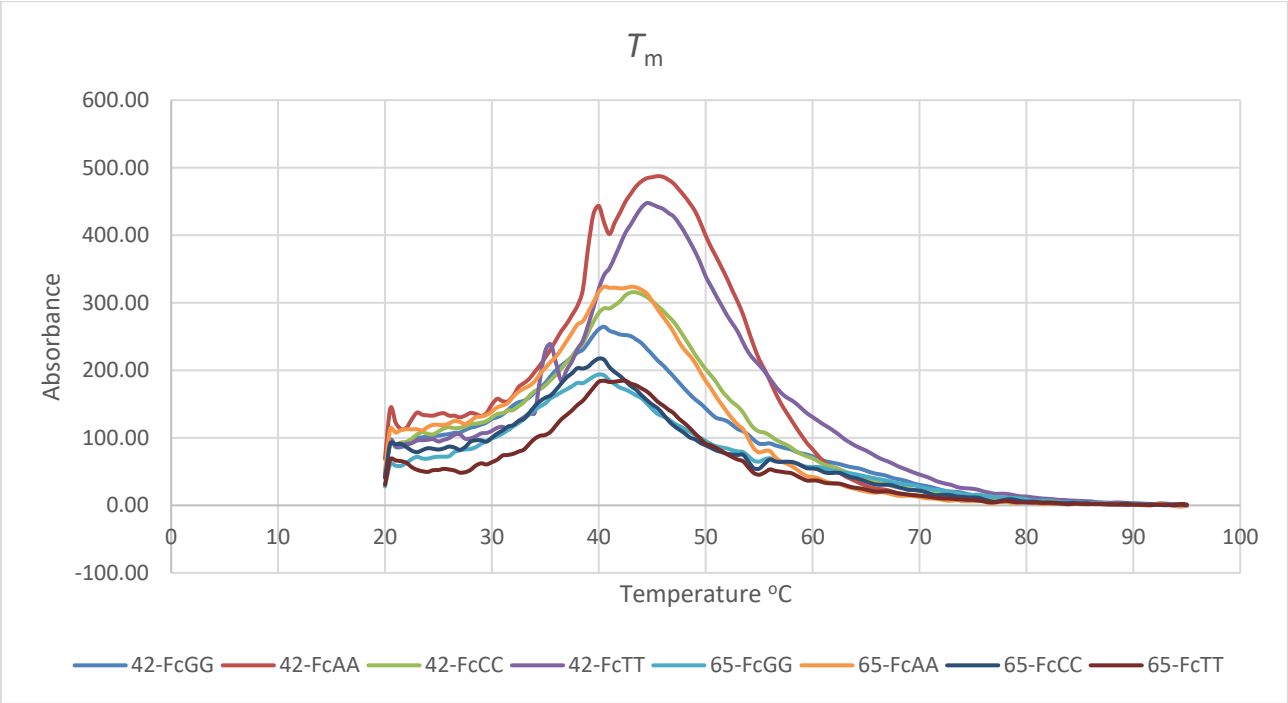

Figure 6.8 T_m of DNA duplexes

6.6 Appendix

6.6.1 NMR spectra

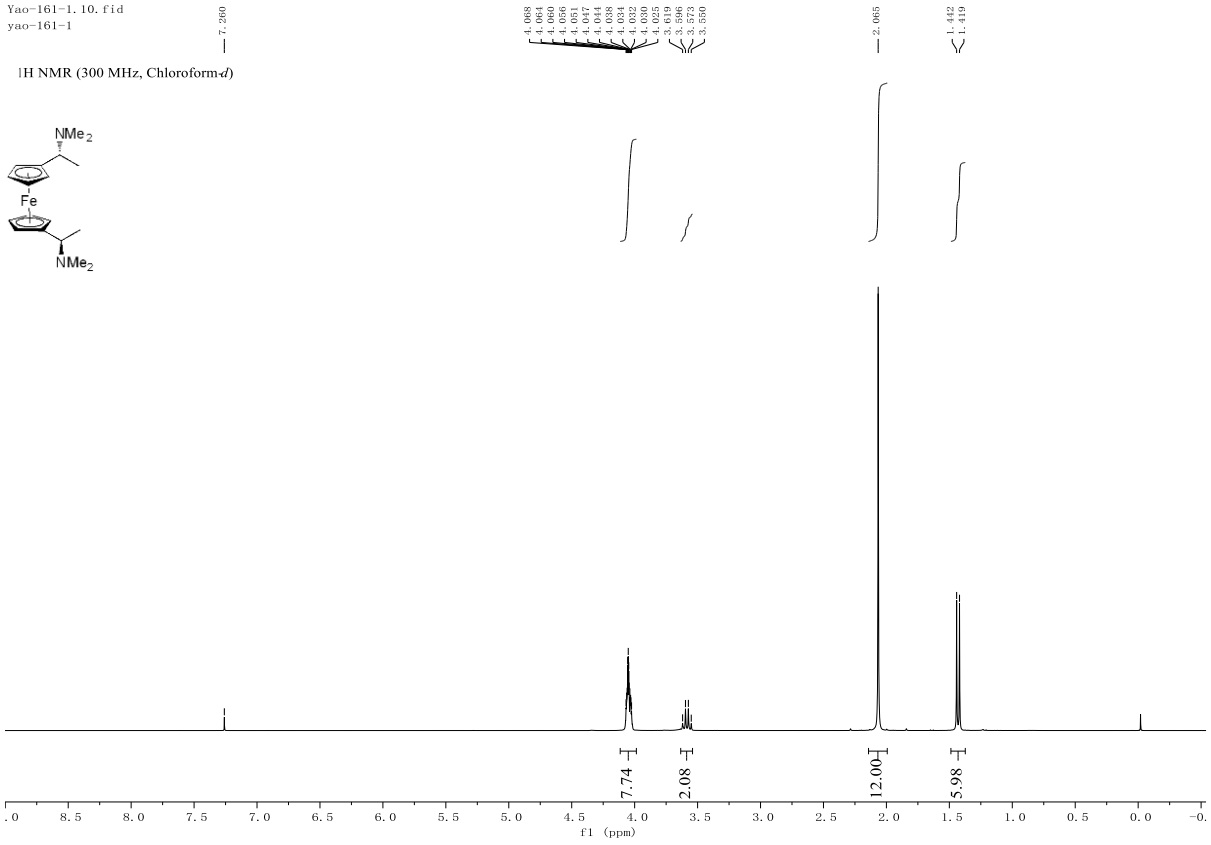

yao-179-1.10.fid
yao-179-1-H

1H NMR (300 MHz, Chloroform-*d*)

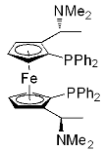

yao-179-1.12.fid
yao-179-1-C

13C NMR (101 MHz, Chloroform-*d*)

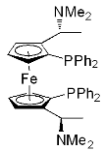

yao-179-1.11.fid
yao-179-1-P

31P NMR (121 MHz, Chloroform-*d*)

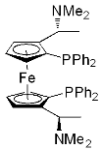

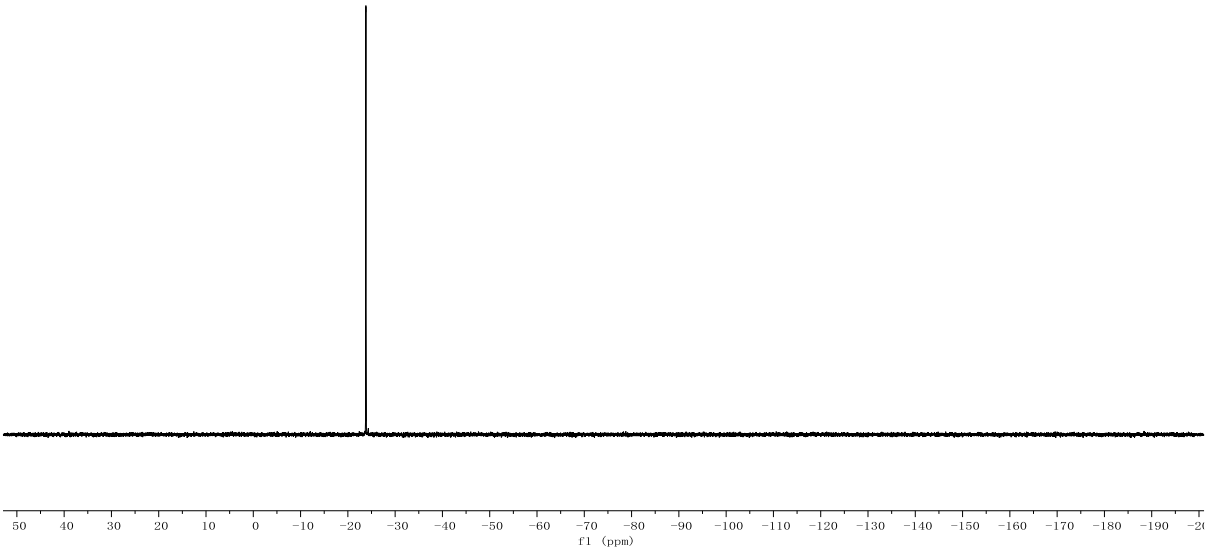

1H NMR (300 MHz, Chloroform-*d*)

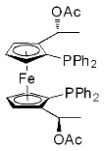

yao-181-1.12.fid
yao-181-1-C

169.659
139.392
139.297
136.099
136.015
134.859
134.642
132.999
132.315
129.261
128.150
128.070
127.957
127.875
127.791
93.310
93.063
77.755
77.639
77.418
77.101
76.782
73.559
73.512
72.490
72.406
72.363
72.323
67.882
67.787
46.285
19.962
18.644
11.677

^{13}C NMR (101 MHz, Chloroform-*d*)

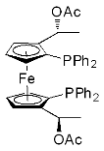

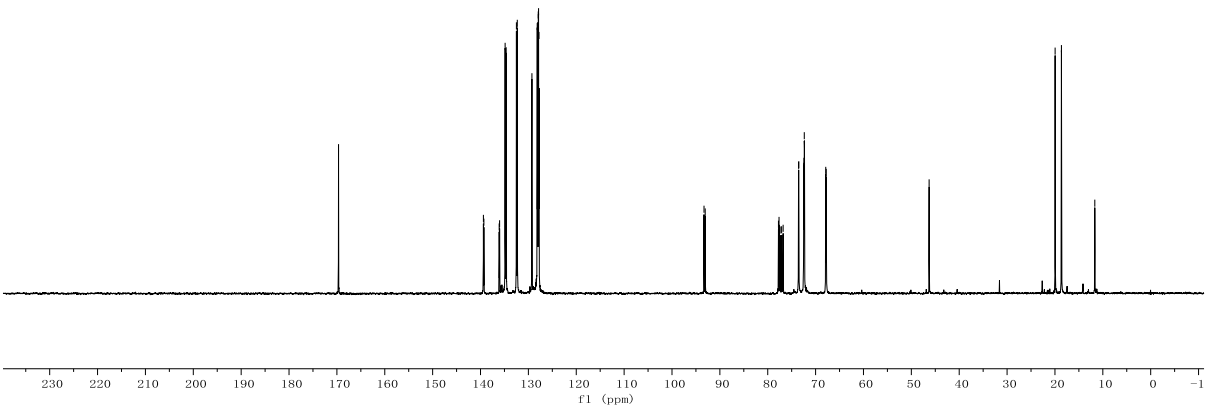

yao-181-1
yao-181-1-C

169.68
139.41
139.31
136.11
136.03
134.87
134.66
132.51
132.33
129.28
128.16
128.08
127.95
127.849
127.81
93.32
93.07
77.76
77.65
77.43
77.11
76.79
73.57
73.52
72.49
72.45
72.37
72.33
67.89
67.79
46.29
19.97
18.64
11.68

^{13}C NMR (101 MHz, Chloroform-*d*)

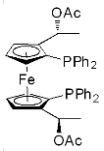

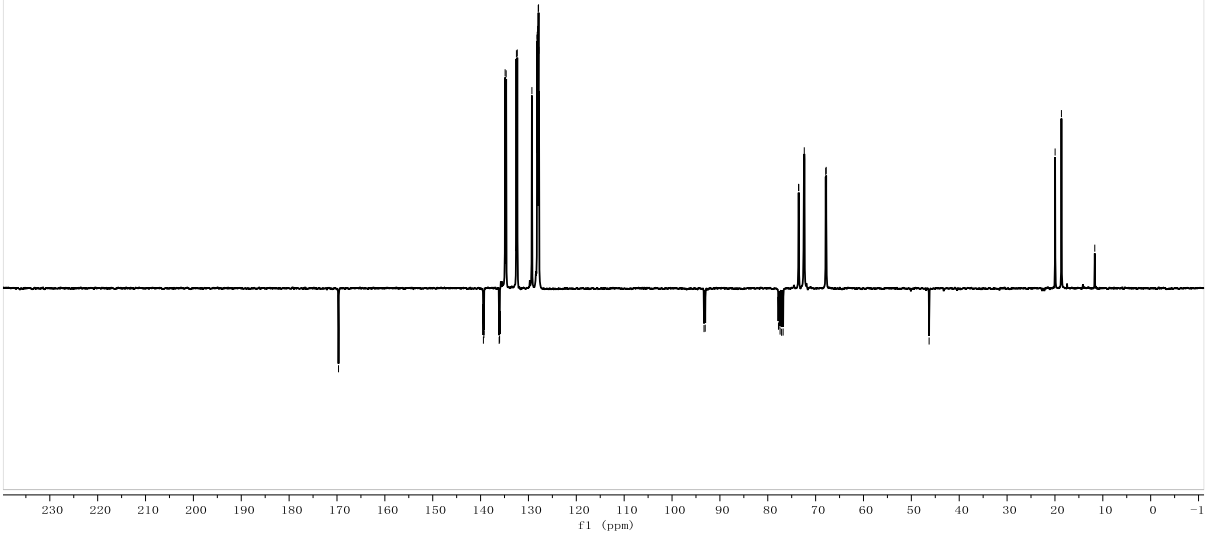

yao-181-1.21.fid
yao-181-1-P

31P NMR (121 MHz, Chloroform-*d*)

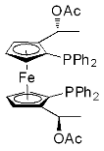

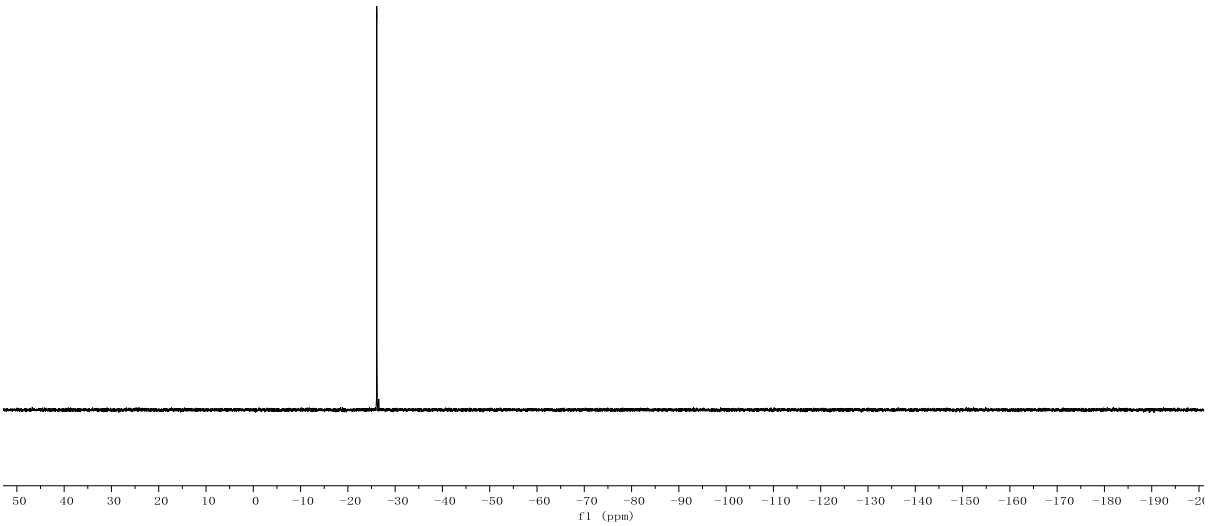

yao-182-1.10.fid
yao-182-1-H

1H NMR (300 MHz, Chloroform-*d*)

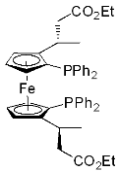

yao-180405-5.11.fid
yao-180405-5-C

^{13}C NMR (101 MHz, Chloroform-*d*)

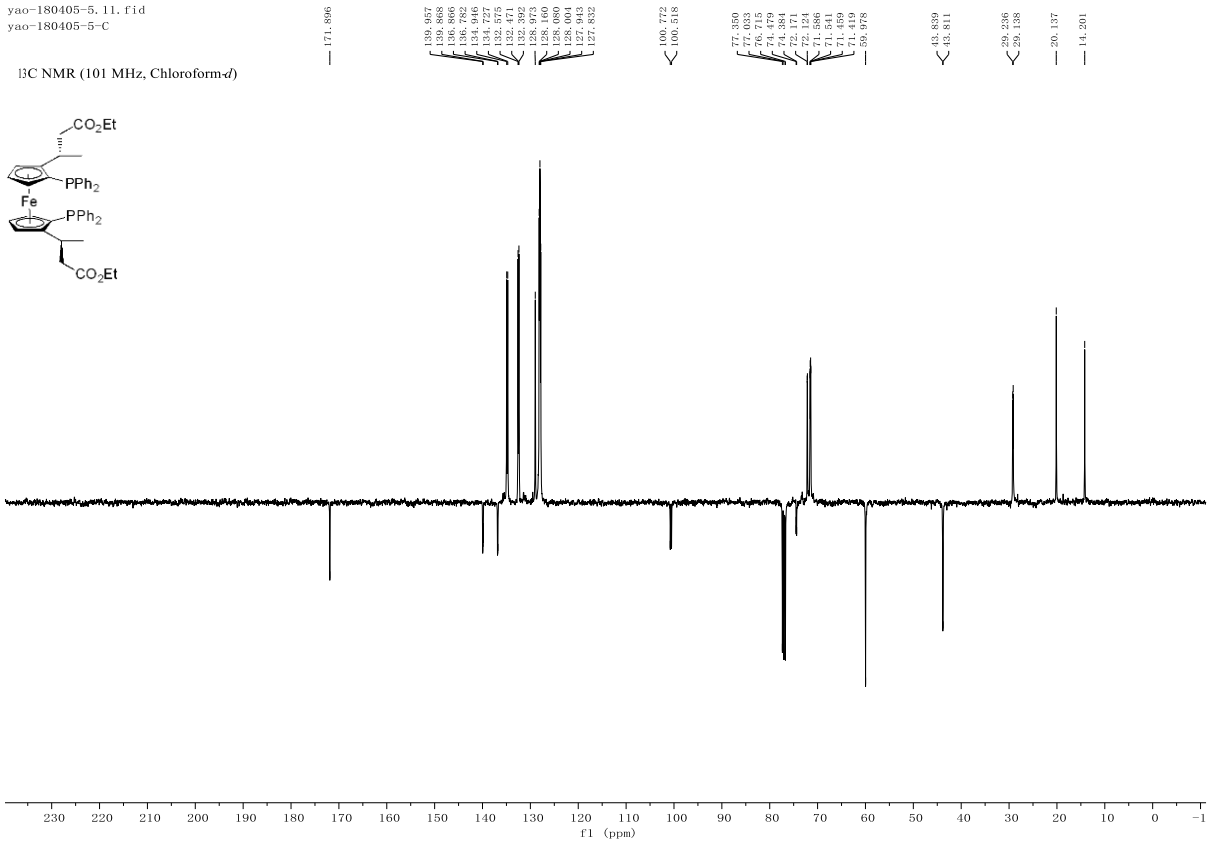

yao-182-1.11.fid
yao-182-1-P

^{31}P NMR (121 MHz, Chloroform-*d*)

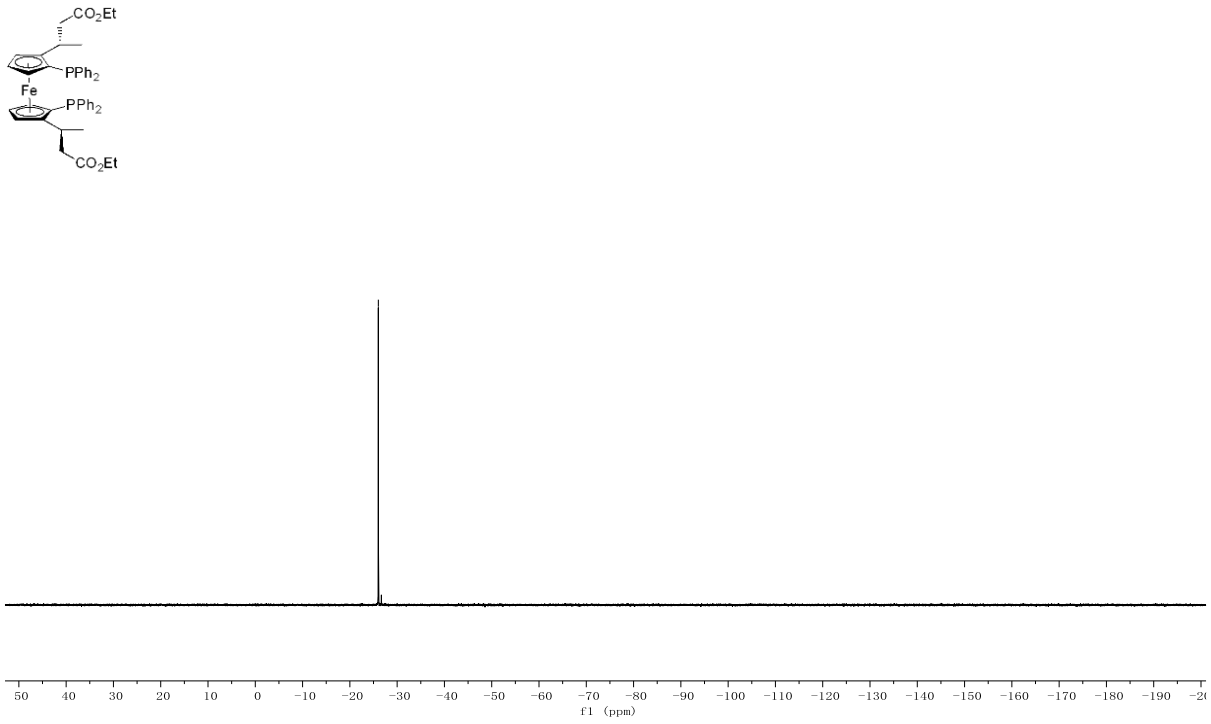

yao-180326-1
yao-180326-1-H

1H NMR (400 MHz, Chloroform-*d*)

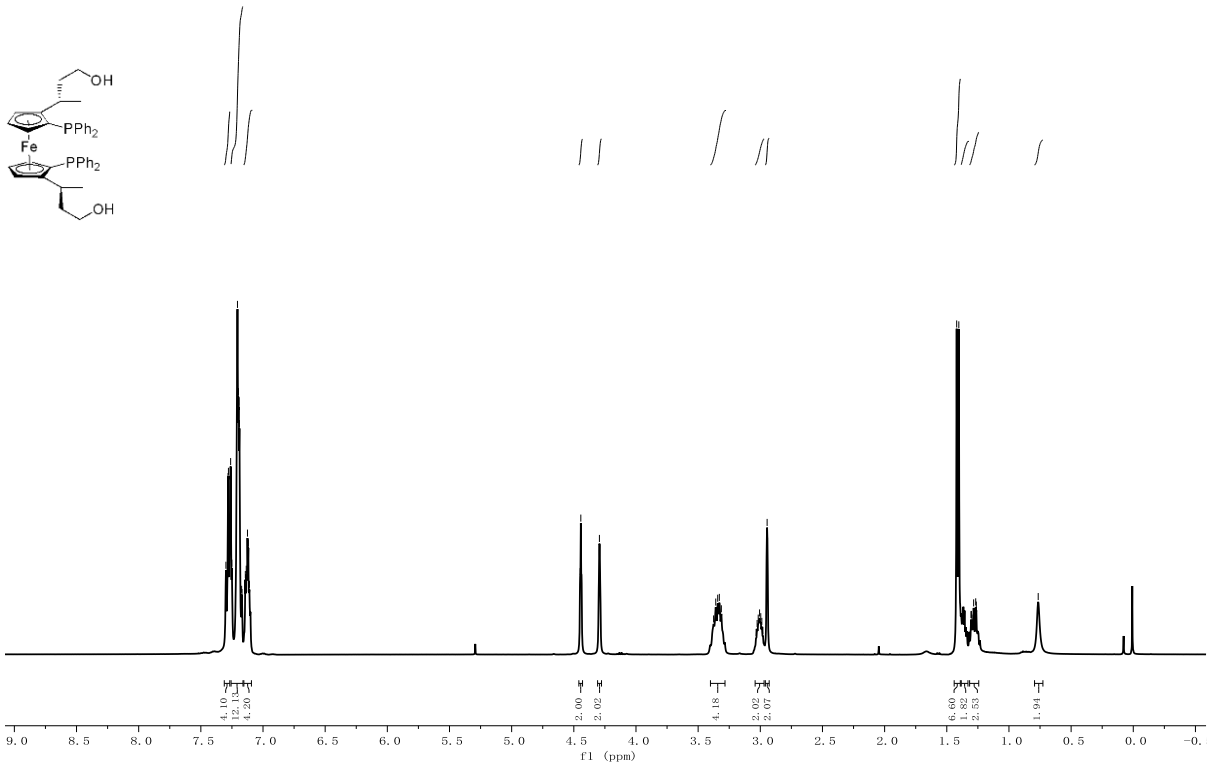

f1 (ppm)

yao-180326-1.14.fid
yao-180326-1-C

13C NMR (101 MHz, Chloroform-*d*)

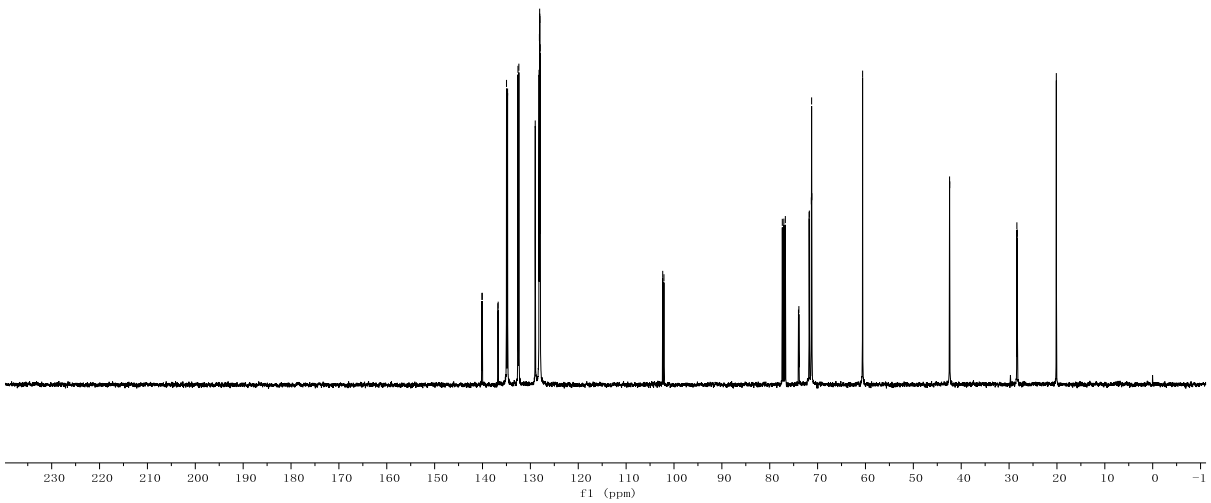

f1 (ppm)

yao-180326-1
yao-180326-1-C

13C NMR (101 MHz, Chloroform-*d*)

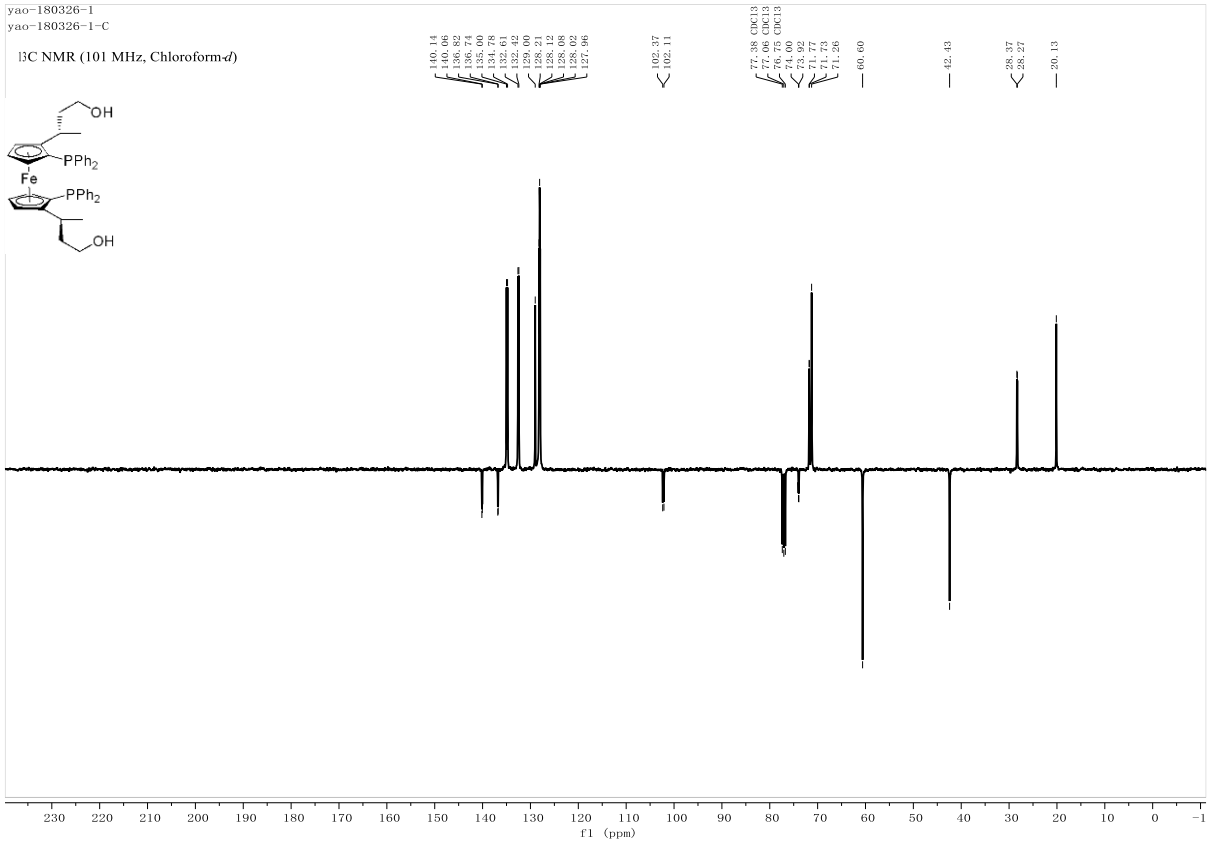

yao-180326-1.11.fid
yao-180326-1-P

31P NMR (121 MHz, Chloroform-*d*)

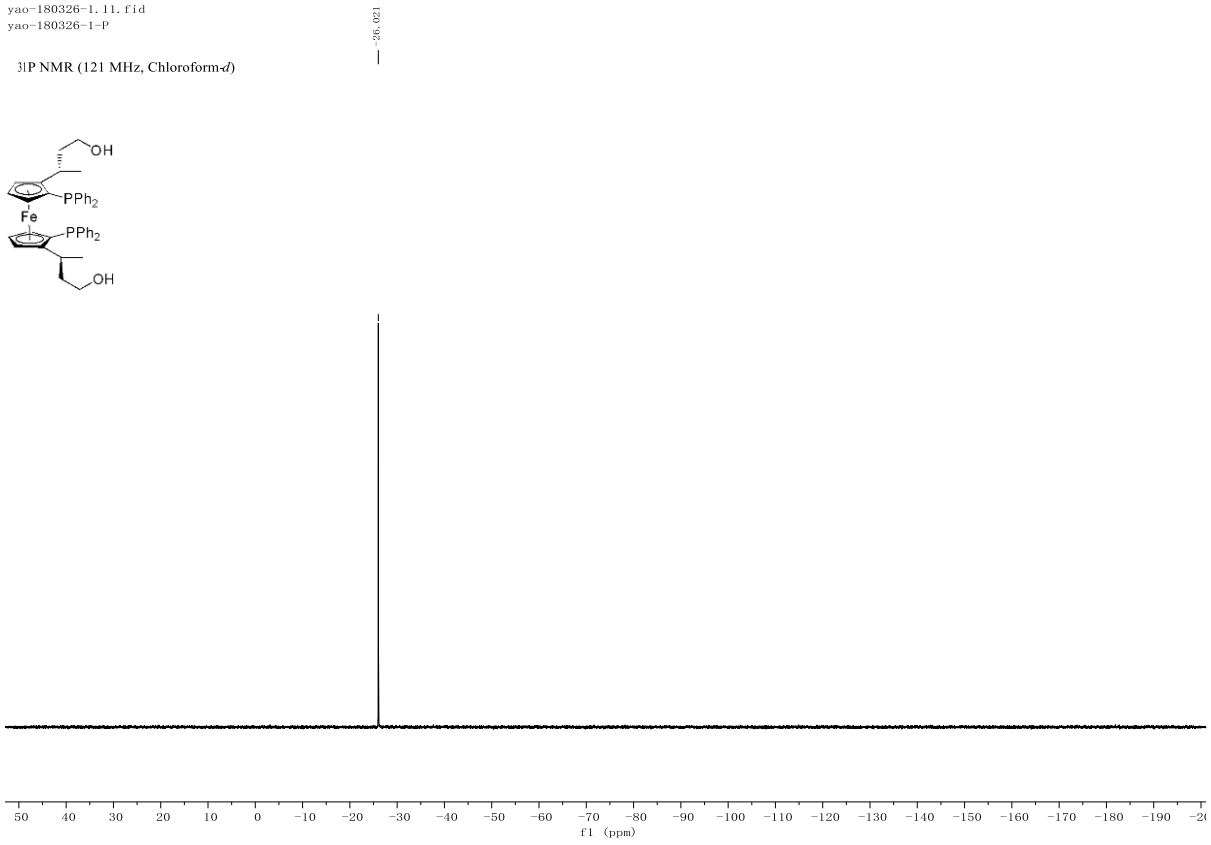

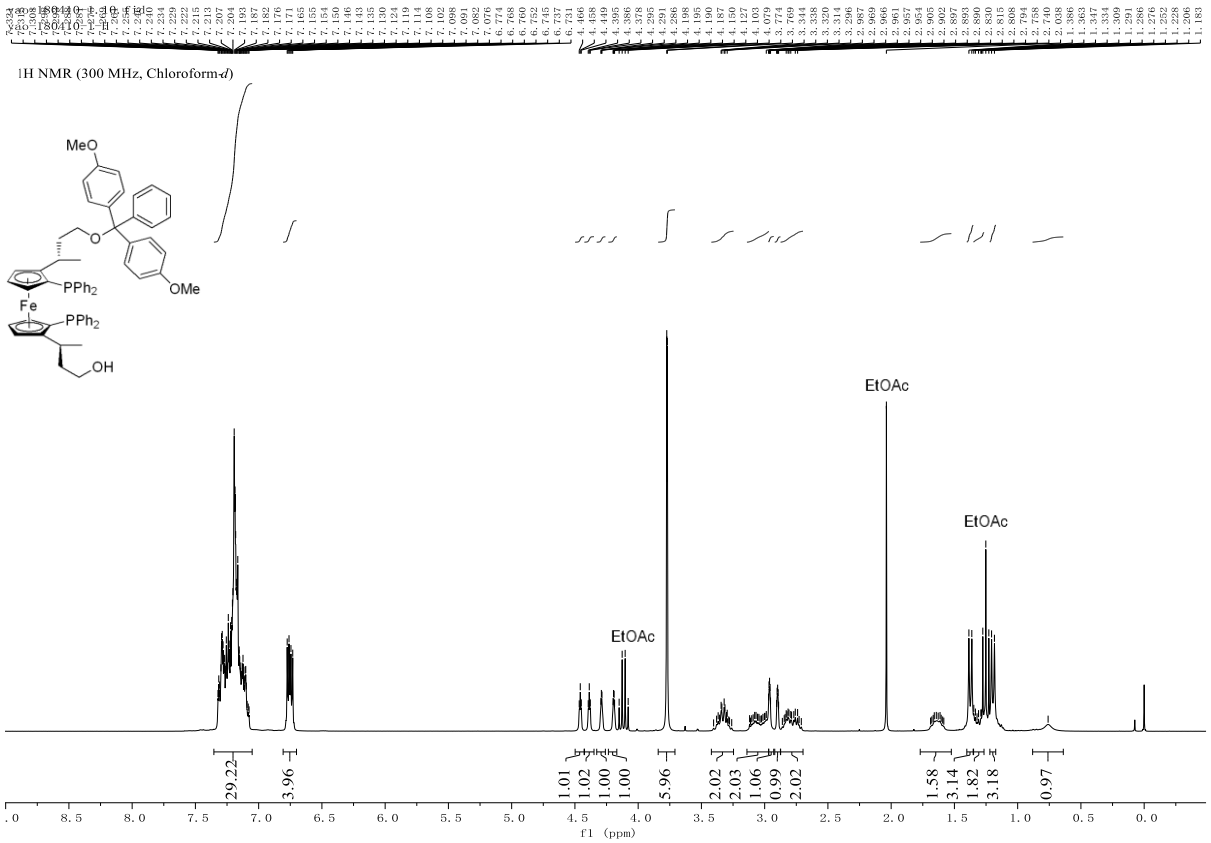
1H NMR (300 MHz, Chloroform-d)
MeO
OMe
PPh2
Fe
PPh2
OH
EtOAc
EtOAc
EtOAc
29.22
3.96
1.01
1.02
1.00
1.00
5.96
2.02
2.03
1.06
0.99
2.02
1.58
3.14
1.82
3.18
0.97
f1 (ppm)

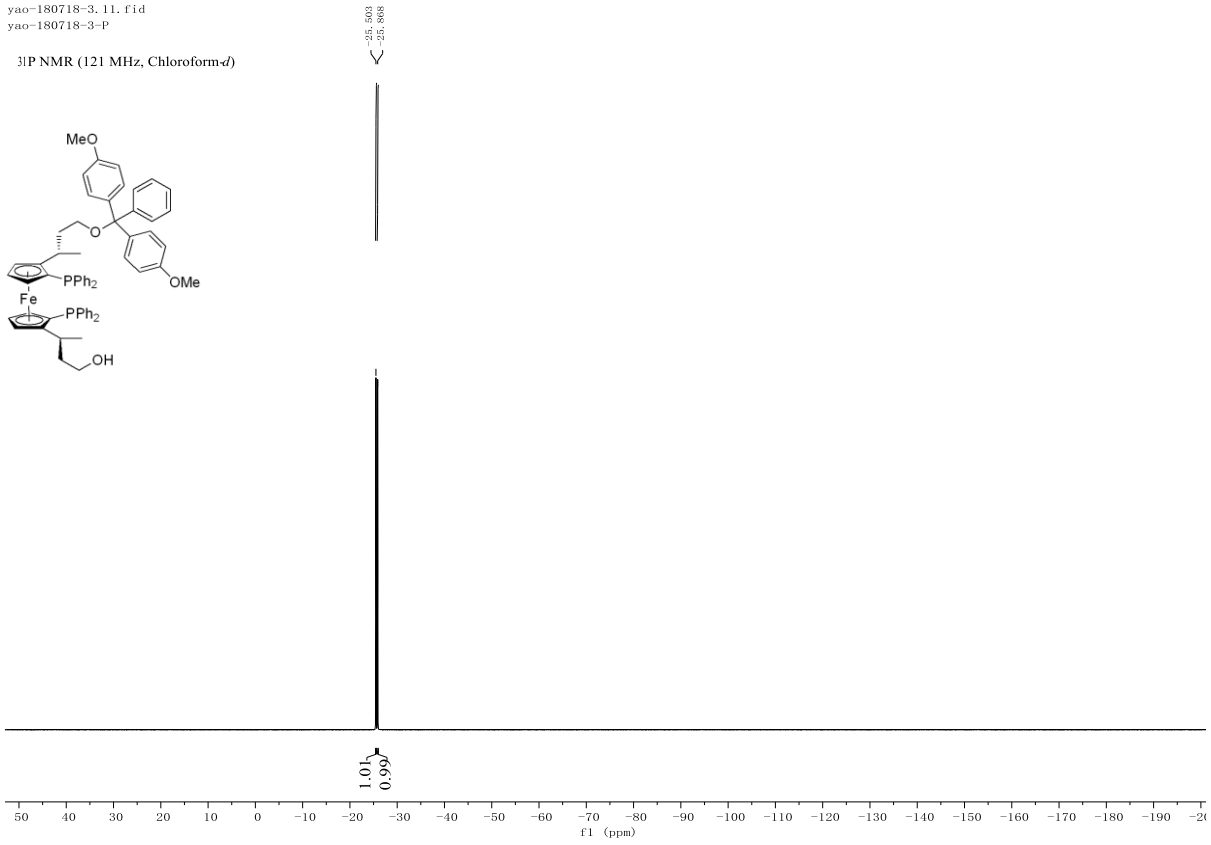
yao-180718-3.11.fid
yao-180718-3-P
31P NMR (121 MHz, Chloroform-d)
25.503
25.868
MeO
OMe
PPh2
Fe
PPh2
OH
1.01
0.99
f1 (ppm)

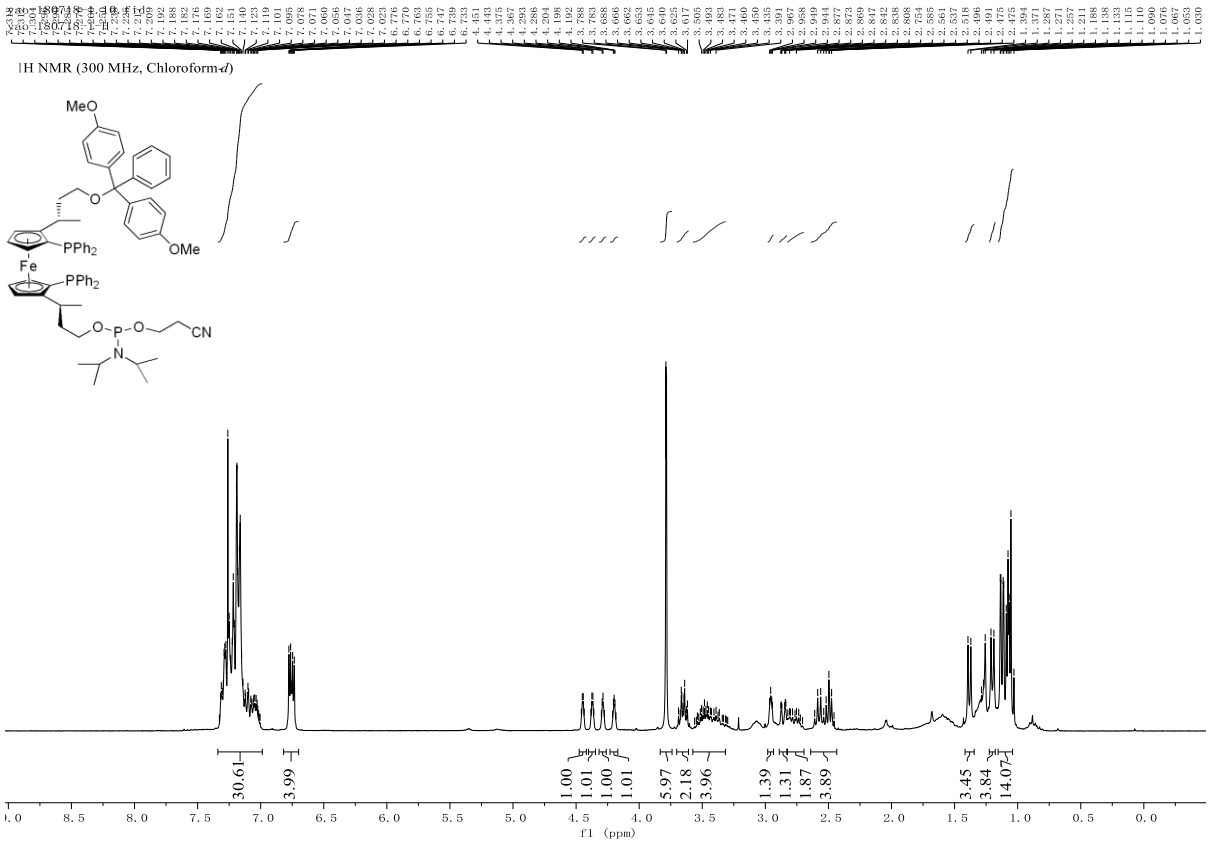
1H NMR (300 MHz, Chloroform-d)
MeO
OMe
PPh2
Fe
PPh2
O
P
O
CN
N
30.61
3.99
1.00
1.01
1.00
1.01
5.97
2.18
3.96
1.39
1.31
1.87
3.89
3.45
3.84
14.07
f1 (ppm)

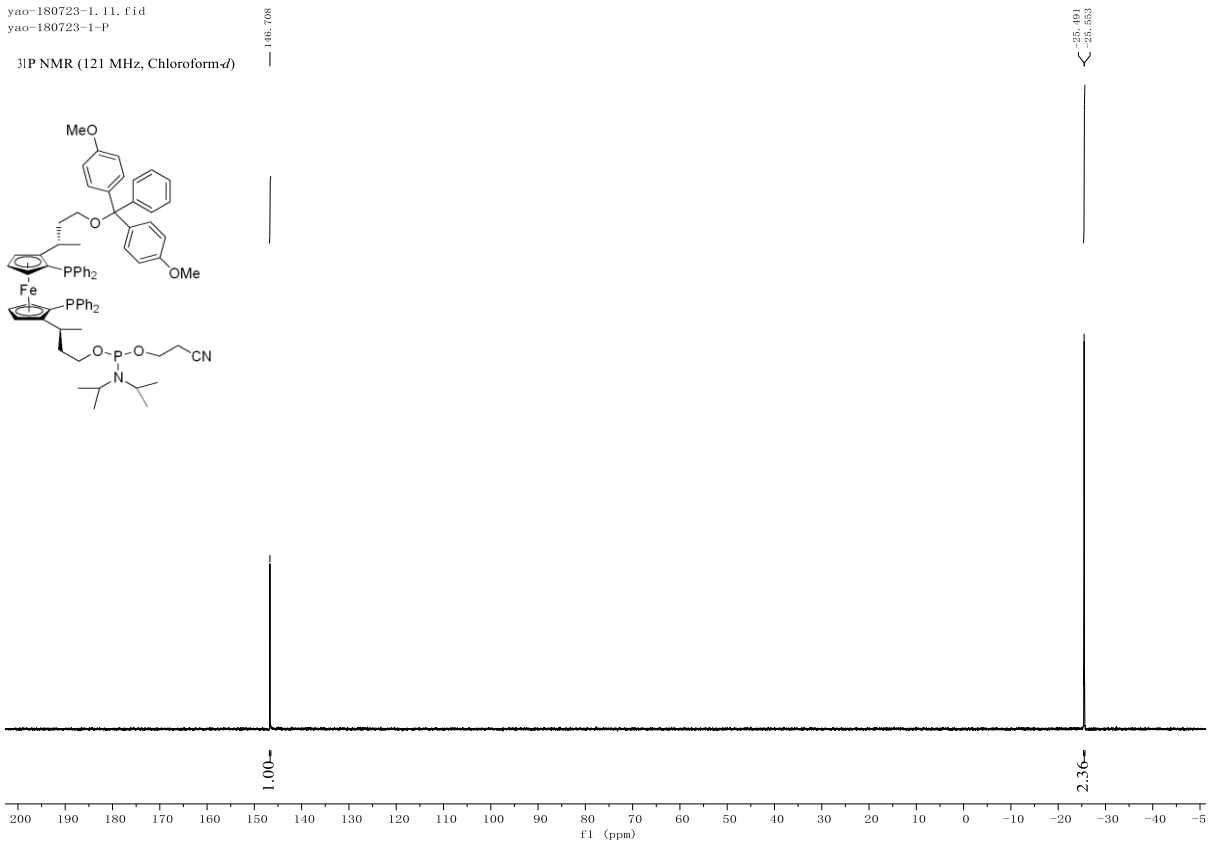
yao-180723-1.11.fid
yao-180723-1-P
31P NMR (121 MHz, Chloroform-d)
146.708
-25.491
-25.553
MeO
OMe
PPh2
Fe
PPh2
O
P
O
CN
N
1.00
2.36
f1 (ppm)

6.7 References

[1] S. Park, H. Sugiyama, *Angew Chem Int Ed Engl* **2010**, *49*, 3870-3878.

[2] J.-M. Lehn, *Supramolecular Chemistry: Concepts and Perspectives*, Weinheim Cambridge, **1995**.

[3] M. S. Taylor, E. N. Jacobsen, *Angewandte Chemie International Edition* **2006**, *45*, 1520-1543.

[4] A. Warshel, P. K. Sharma, M. Kato, Y. Xiang, H. Liu, M. H. M. Olsson, *Chemical Reviews* **2006**, *106*, 3210-3235.

[5] H.-J. Schneider, *Angewandte Chemie International Edition* **2009**, *48*, 3924-3977.

[6] R. R. Knowles, E. N. Jacobsen, *Proc. Natl. Acad. Sci. U. S. A* **2010**, *107*, 20678-20685.

[7] F. Rosati, G. Roelfes, *ChemCatChem* **2010**, *2*, 916-927.

[8] I. Drienovská, G. Roelfes, *Israel Journal of Chemistry* **2015**, *55*, 21-31.

[9] J. Collot, J. Gradinaru, N. Humbert, M. Skander, A. Zocchi, T. R. Ward, *Journal of the American Chemical Society* **2003**, *125*, 9030-9031.

[10] M. T. Reetz, J. J. P. Peyralans, A. Maichele, Y. Fu, M. Maywald, *Chemical Communications* **2006**, 4318-4320.

[11] C. Letondor, A. Pordea, N. Humbert, A. Ivanova, S. Mazurek, M. Novic, T. R. Ward, *Journal of the American Chemical Society* **2006**, *128*, 8320-8328.

[12] G. Klein, N. Humbert, J. Gradinaru, A. Ivanova, F. Gilardoni, U. E. Rusbandi, T. R. Ward, *Angewandte Chemie International Edition* **2005**, *44*, 7764-7767.

[13] A. Fernández-Gacio, A. Codina, J. Fastrez, O. Riant, P. Soumillion, *ChemBioChem* **2006**, *7*, 1013-1016.

[14] M. T. Reetz, N. Jiao, *Angewandte Chemie International Edition* **2006**, *45*, 2416-2419.

[15] R. S. Roy, B. Imperiali, *Protein Engineering, Design and Selection* **1997**, *10*, 691-698.

[16] G. Roelfes, *Mol Biosyst* **2007**, *3*, 126-135.

[17] S. K. Silverman, *Angew Chem Int Ed Engl* **2010**, *49*, 7180-7201.

[18] J. J. Marek, U. Hennecke, *Chemistry – A European Journal* **2017**, *23*, 6009-6013.

[19] G. Roelfes, B. L. Feringa, *Angewandte Chemie International Edition* **2005**, *44*, 3230-3232.

[20] A. J. Boersma, R. P. Megens, B. L. Feringa, G. Roelfes, *Chem Soc Rev* **2010**, *39*, 2083-2092.

[21] A. García-Fernández, G. Roelfes, in *Interplay between Metal Ions and Nucleic Acids* (Eds.: A. Sigel, H. Sigel, R. K. O. Sigel), Springer Netherlands, Dordrecht, **2012**, pp. 249-268.

[22] H. Zhao, K. Shen, *RSC Advances* **2014**, *4*, 54051-54059.

[23] A. Rioz-Martínez, G. Roelfes, *Current Opinion in Chemical Biology* **2015**, *25*, 80-87.

[24] M. Smietana, S. Arseniyadis, *CHIMIA International Journal for Chemistry* **2018**, *72*, 630-634.

[25] U. M. Lindström, *Chemical Reviews* **2002**, *102*, 2751-2772.

[26] G. Roelfes, A. J. Boersma, B. L. Feringa, *Chemical Communications* **2006**, 635-637.

[27] A. J. Boersma, B. L. Feringa, G. Roelfes, *Organic Letters* **2007**, *9*, 3647-3650.

[28] D. Coquière, B. L. Feringa, G. Roelfes, *Angewandte Chemie International Edition* **2007**, *46*, 9308-9311.

[29] Y. Hamashima, D. Hotta, N. Umebayashi, Y. Tsuchiya, T. Suzuki, M. Sodeoka, *Advanced Synthesis & Catalysis* **2005**, *347*, 1576-1586.

[30] A. J. Boersma, B. L. Feringa, G. Roelfes, *Angewandte Chemie International Edition* **2009**, *48*, 3346-3348.

[31] J. Wang, E. Benedetti, L. Bethge, S. Vonhoff, S. Klussmann, J.-J. Vasseur, J. Cossy, M. Smietana, S. Arseniyadis, *Angewandte Chemie International Edition* **2013**, *52*, 11546-11549.

[32] N. Shibata, H. Yasui, S. Nakamura, T. Toru, *Synlett* **2007**, *2007*, 1153-1157.

[33] A. J. Boersma, D. Coquière, D. Geerdink, F. Rosati, B. L. Feringa, G. Roelfes, *Nature Chemistry* **2010**, *2*, 991-995.

[34] J. Oelerich, G. Roelfes, *Chemical Science* **2013**, *4*, 2013-2017.

[35] A. Rioz-Martínez, J. Oelerich, N. Ségaud, G. Roelfes, *Angewandte Chemie International Edition* **2016**, *55*, 14136-14140.

[36] K. Rohr, S. Vogel, *ChemBioChem* **2006**, *7*, 463-470.

[37] U. Jakobsen, K. Rohr, S. Vogel, *Nucleosides Nucleotides Nucleic Acids* **2007**, *26*, 1419-1422.

[38] L. Ropartz, N. J. Meeuwenoord, G. A. van der Marel, P. W. van Leeuwen, A. M. Slawin, P. C. Kamer, *Chem Commun (Camb)* **2007**, 1556-1558.

[39] M. Caprioara, R. Fiammengo, M. Engeser, A. Jaschke, *Chemistry* **2007**, *13*, 2089-2095.

[40] P. Fournier, R. Fiammengo, A. Jaschke, *Angew Chem Int Ed Engl* **2009**, *48*, 4426-4429.

[41] N. S. Oltra, G. Roelfes, *Chem Commun (Camb)* **2008**, 6039-6041.

[42] S. Park, I. Okamura, S. Sakashita, J. H. Yum, C. Acharya, L. Gao, H. Sugiyama, *ACS Catalysis* **2015**, *5*, 4708-4712.

[43] S. Park, L. Zheng, S. Kumakiri, S. Sakashita, H. Otomo, K. Ikehata, H. Sugiyama, *ACS Catalysis* **2014**, *4*, 4070-4073.

[44] H. V. Nguyen, Z.-y. Zhao, A. Sallustrau, S. L. Horswell, L. Male, A. Mulas, J. H. R. Tucker, *Chemical Communications* **2012**, *48*, 12165-12167.

[45] J. Yu, J. Long, Y. Yang, W. Wu, P. Xue, L. W. Chung, X. Q. Dong, X. Zhang, *Org Lett* **2017**, *19*, 690-693.

[46] J. J. Almena Perea, M. Lotz, P. Knochel, *Tetrahedron: Asymmetry* **1999**, *10*, 375-384.

[47] S. L. Beaucage, M. H. Caruthers, *Tetrahedron Letters* **1981**, *22*, 1859-1862.

[48] X. Li, J. Yong, Y. Zhang, in *The Relationship Between 31P NMR Chemical Shift and the Phosphorus Compounds, Huaxue Tongbao: online edition*, **2001**, pp. 1-6.

[49] L. Schwink, P. Knochel, *Chemistry – A European Journal* **1998**, *4*, 950-968.

[50] T. Hayashi, A. Yamamoto, M. Hojo, K. Kishi, Y. Ito, E. Nishioka, H. Miura, K. Yanagi, *Journal of Organometallic Chemistry* **1989**, *370*, 129-139.

Publications and Presentations

Publications

1. *C_1*-Symmetric PNP Ligands for Manganese-Catalyzed Enantioselective Hydrogenation of Ketones: Reaction Scope and Enantioinduction Model. **Liyao Zeng**, Huaxin Yang, Menglong Zhao, Jialin Wen, James H. R. Tucker, Xumu Zhang. *ACS Catal*. **2020**, 10, 13794.

2. Ir-catalyzed asymmetric hydrogenation of ketones using novel PNO phosphine ligands. Shaoke Zhang, Yanan Duan, **Liyao Zeng,** Jialin Wen, Xumu Zhang. *Chin Sci Bull*. **2021**, 66, 3317.

Presentations

2021 – MSBC PhD/PDRA Seminar, University of Birmingham